Title
Seismic Performance of Reinforced Concrete Bridges Allowed to Uplift During Multi-Directional Excitation

Author
Espinoza, Andres Oscar

Publication Date
2011

Peer reviewed|Thesis/dissertation

Seismic Performance of Reinforced Concrete Bridges Allowed to Uplift During Multi-Directional Excitation

By
Andres Oscar Espinoza

A dissertation submitted in partial satisfaction of the
requirements for the degree of

Doctor of Philosophy
in
Engineering – Civil and Environmental Engineering
in the
Graduate Division
of the
University of California, Berkeley

Committee in charge:

Professor Stephen A. Mahin, Chair
Professor Bozidar Stojadinovic
Professor Douglas S. Dreger

Fall 2011

Seismic Performance of Reinforced Concrete Bridges Allowed to Uplift During Multi-Directional Excitation

Abstract

Seismic Performance of Reinforced Concrete Bridges Allowed to Uplift During Multi-Directional Excitation

by

Andres Oscar Espinoza

Doctor of Philosophy in Engineering - Civil and Environmental Engineering

University of California, Berkeley

Professor Stephen A. Mahin, Chair

The behavior of bridges subjected to recent moderate and large earthquakes has led to bridge design detailed for better seismic performance, particularly through wider bridge foundations to handle larger expected design forces. Foundation uplift, which is not employed in conventional bridge design, has been identified as an important mechanism, in conjunction with structural yielding and soil-structure interaction that may dissipate energy during earthquakes. Preventing uplift through wider foundations looks past the technical and economical feasibility of allowing foundation uplift during seismic events. The research presented in this thesis is part of a larger experimental and analytical investigation to develop and validate design methods for bridge piers on shallow foundations allowed to uplift during seismic events.

Several analytical and some experimental studies have been performed to assess rocking and or uplift of shallow foundation systems, however they have evaluated systems with a limited range of footing dimensions and seismic excitations. As such, there is an uncertainty in the information needed to base a performance evaluation and develop design methods. The purpose of this study is to investigate, through experimental and analytical studies, the seismic performance of uplifting bridge piers on shallow foundations when considering different ground motions and footing dimensions. As well as to identify key differences in performance evaluation criteria for conventional and uplifting bridge pier systems.

The experimental study dynamically tested a single reinforced concrete bridge column specimen with three adjustable footing configurations grouped by footing dimension, and tested for various combinations of one, two, and three components of seismic excitation. Groups one and two evaluated uplifting systems where the column was limited to elastic loading levels while group three considered inelastic column loading levels. All test groups remained stable and exhibited some rocking and or uplift during testing. Analytical models were developed and validated using the experimental testing results to predict local and global footing and column response. Reliable estimates of forces and displacements during elastic and inelastic response were achieved. To assess the seismic performance of a range of bridge pier systems allowed to uplift a parametric investigation

using the validated analytical models was performed in which the column was modeled per conventional design criteria to ensure adequate strength and flexural ductility. The parameters varied include footing width, ground motion excitation, and elastic or inelastic column response. Response of the uplifting bridge pier systems was found to be sensitive to the structural periods, magnitude of excitation, and footing width.

Table of Contents

List of Figures

List of Tables

Acknowledgements

An undertaking such as a dissertation must be an effort of many people if it is to be successfully accomplished. I would first like to thank Professor Stephen Mahin, my adviser and committee chair, whose guidance, patience, and enthusiasm proved invaluable in development of this work. Special thanks are also due to Professor Bozidar Stojadinovic and Professor Douglas Dreger for their support and review of this work.

The work described in this thesis was supported in part by the Earthquake Engineering Research Center and the California Department of Transportation. I would like to thank the staff at the Earthquake Engineering Research Center where much of this research work was performed. In particular Charles James was helpful in the preparation of this work. The experimental test program could not have been completed without the help of Wesley Neighbour, Don Clyde, David Maclam, and Shakhzod Takhirov.

I am grateful to my friends and colleagues during my time at UC Berkeley who provided suggestions, help, and useful discussions. Thanks to Kevin Mackie, for his friendship and support. Thanks also go to Frank McKenna, Michael Scott, Gabriel Hurtado, and Patxi Uriz.

Finally, I would like to thank my wife Anne for all her love, support, and understanding, without which none of this would have been possible.

1 Introduction

1.1 Background

Recent moderate to large earthquakes have caused significant damage to bridge structures around the world. Such examples include the 1989 Loma Prieta, 1994 Northridge, and 1995 Kobe earthquakes. These events subjected many types of bridges to intense ground motions that created a wide range of damage states: from little to no damage, to catastrophic failures in some cases. Newer bridges detailed for better performance during seismic events did particularly well. Nonetheless, the wide range of damage created a need to reevaluate the design and rehabilitation procedures of new and existing structures.

In many cases, bridges are being designed or retrofit to withstand higher seismic design forces, resulting in larger bridge foundations. The inclination to make foundations larger may have overlooked the potential benefits of allowing foundation systems to uplift during seismic events. Foundation rocking has been identified as an important mechanism, along with structural yielding and soil-structure interaction, that may explain why some engineered structures suffer less damage during strong earthquake ground shaking than might be predicted on the basis of elastic methods of dynamic analysis (e.g., Rutenberg, 1982; Werner, 1992).

The California Department of Transportation (Caltrans) has investigated several mechanisms for absorbing and dissipating energy during intense earthquake ground motions. However, to date, rocking of foundations is one of the few for which Caltrans has yet to develop and validate design guidelines. Development of design and analysis guidelines could be very beneficial to the assessment of existing and new construction by identifying situations where allowing the foundation to uplift could improve and at a minimum not degrade, bridge performance during ground shaking.

Following conventional design methods, large and expensive foundations are often required so that a bridge can achieve a "fixed base" condition and dissipate energy during intense earthquake shaking through ductile plastic hinging in the columns. For instance, Caltrans Seismic Design Criteria (Caltrans, 2004) indicates that rigid footing response can be assumed if the width of a regular spread footing on competent soil is 6 or more times the column diameter. Many engineers, and a significant amount of experimental and analytical evidence, suggest that adequate seismic performance can be achieved on competent soil at less cost, if the foundation of the bridge pier is narrower and allowed to uplift. It appears that there may be circumstances under which improved

performance can be obtained by allowing bridge foundations to rock. The lack of information and guidelines related to foundations allowed to uplift leads most engineers to avoid rocking all together through the use of more costly widened spread footings or foundations supported by piles.

The state-of-the-art information on seismic performance of rocking foundations has yet to be integrated and evaluated to determine conditions where rocking might be dependably permitted, or which design procedures might be most appropriate.

The behavior of even simple bridge foundations that are allowed to rock is quite complex and highly nonlinear. There is a worry that bridge piers might become globally unstable and simply overturn if their foundations are allowed to uplift. Some studies suggest that short period structures supported on rocking foundations may not perform as well as conventionally designed structures. However, other studies indicate that the nonlinearity associated with uplift and the energy dissipation added by the supporting soil may be sufficient to improve response compared to a fixed base bridge pier.

A significant concern in the evaluation of rocking foundations is the performance of the supporting soil. If the demand for soil yielding becomes excessive, significant permanent vertical and lateral displacements of the bridge could occur due to permanent deformations of the supporting soil. Thus, assessment of the rocking mechanism and development of reliable design guidelines requires a methodology that carefully integrates structural and geotechnical engineering expertise.

To date most experimental and analytical studies of rocking foundations have considered cases that are simpler than encountered in actual bridges, and analytical models have generally not been validated in terms of experimental data. A concern is thus raised when considering more complex systems. For example when a bridge column is subjected to multiple components of motion or to intense near-fault pulse-like motions, the accuracy of analytical predictions maybe uncertain. Thus, a critical review of the structural and geotechnical engineering issues involved with allowing bridge pier foundations to rock during strong earthquake ground motions is needed.

The performance of systems allowed to uplift has been studied in systems ranging from rigid bodies to deformable systems resting on tension carrying or compression-only media with a wide array of assumptions regarding soil behavior. For example, in an early study, Chopra and Yim analyzed flexible single-degree-of freedom systems subjected to one horizontal component of ground shaking (Chopra and Yim, 1983). In these studies, the model assumed the soil to be elastic and not to resist tension. The soil was modeled as either a two-spring and dashpot or Winkler spring and dashpot model. The benefit of foundation uplift illustrated in this work was a reduction in lateral force acting on the structure. This reduction could be used to effectively reduce the damage to existing structures in seismic events without the need to strengthen or otherwise retrofit. The investigation additionally illustrated the ability to develop appropriate parameters that could be used to objectively identify the distinct conditions where no rocking, rocking and no yielding, or simultaneous rocking and yielding occur during seismic shaking.

Modeling of soil behavior during system uplift is a key aspect of capturing the complexity of soil structure interaction. Many studies have investigated the performance both experimentally and numerically (e.g. Rosebrook, 2001; Harden et al., 2005). The experimental studies have investigated rocking of scale models in centrifuge tests where the supporting soil was sand and saturated clay. Analysis modeling assumptions for foundations on soil have varied from the two-spring model to the Winkler spring model that incorporates a significant number of soil springs. Harden et al. (2005) investigated the nonlinear cyclic response of shallow foundations under building shearwalls. The work done suggested the behavior of soil and foundations during rocking could be reasonably predicted using nonlinear Winkler foundations for a given soil.

To date few analytical or experimental studies have investigated the performance of systems allowed to uplift in more than one-direction. While experimental and analytical predictions have been done for one-dimensional excitation, many concerns remain for multi-directional dynamic response:

1. Modeling of the foundation and underlying soil has been generally limited to one-dimension analytical models. This may be significant when considering non-linear soil behavior, which may be affected by interaction of displacements along the principal directions.
2. The type of input excitation has been limited to one-dimension primarily. There has not been much investigation into behavior of uplifting systems loaded in two- or three-dimensions for a rectangular footing configuration. The effective width of footing is larger when observing the footing along the diagonal axis and may affect the rocking characteristics of the system.
3. Interaction and force redistribution for a system which may uplift and then yield or vice versa.
4. The global performance and residual displacements of a system. Global stability is a concern. Allowances for total displacement demand may be a concern. A system may rock, not yield, yet exceed the allowable displacement and thereby perform negatively.

Tests that assess dynamic behavior of a simple bridge system could be used to identify key characteristic of uplifting systems. In turn the results could be used to identify conditions of incipient rocking, yielding or both. The behavior of these systems under moderate and significant near-fault ground motions could be useful in design of systems in regions of high seismicity.

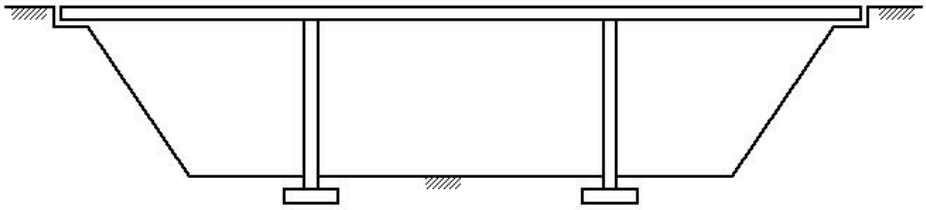

Figure 1-1: Generalized Bridge with Spread Footings

1.2 Research Program Objectives

This work addresses the key aspects involved in assessment of bridge piers allowed to uplift during seismic events. Specifically, single column reinforced concrete bridge piers are considered. The thrust of the research program aims to address knowledge gaps identified on uplifting foundations and has the following specific objectives:

1. Gather and review available information about structural behavior, analysis and design of bridge column foundations that rock and uplift during seismic response.
2. Perform shake table experiments to obtain data to better understand rocking behavior under multiple components of motion and fill in gaps in knowledge.
3. Validate analytic models using experimental results.
4. Perform numerical studies to identify situations where rocking foundations can be utilized dependably with acceptable bridge pier performance expectations.

The scope of this effort is limited to individual bridge piers supported on competent soil using rectangular shallow spread footings. Issues potentially raised concerning marginal soil conditions and the response of complete bridge systems are not addressed herein.

1.3 Organization of Report and Scope

The focus of work was on conducting a series of shaking table tests of moderate-scale bridge piers subject to one-, two-, or three-components of base shaking. Soil behavior is not believed to reduce properly for reduced scale 1-g shaking table tests so the supporting soil for these tests is idealized using an elastomeric sheet. To compare the response of bridge piers with fixed and rocking foundations, test specimens used in these tests were similar to ones previously tested with a fixed base condition (Hachem et al., 2003). In design, Caltrans typically will use a spread footing width of 4 column diameters in plan dimension, and if fixed base conditions are assumed then a footing width of 6 column diameters. To assess impact of smaller than normal footing dimensions the test specimens were chosen to be 3 and 5 times the column diameter.

The following chapters address the assessment, observation, and prediction of spread footing bridge piers allowed to uplift. Each subsequent chapter builds upon the previous one and ultimately develops a knowledge base that may provide the ability to formulate design guidelines for uplifting bridge piers. Chapter 2 discusses the review of literature available for systems allowed to uplift. Also, it discusses current design practices of reinforced concrete bridge columns and their footings. The experimental test program, design and physical test setup are explained in Chapter 3. The experimental results, including global response, and the overall damage state experienced by the specimens, is described in Chapter 4. Chapter 5 presents a comparison of the experimental and analytical results. Simple methods used in design as well as refined inelastic dynamic analyses are used to compare the observed and predicted response. Based on the analytic models of Chapter 5, ranges of parametric analyses are performed in Chapter 6. The analyses present the effects of varying physical dimensions and loading conditions of uplifting bridge piers. Conclusions and recommendations are summarized in Chapter 7.

Also included are several appendices, which present further information obtained in the investigation. Appendix A explains the experimental test schedule, instrumentation and location associated with testing. Appendix B presents further experimental test data for all the three groups of testing. Appendix C includes the code used to represent uplifting foundations in the simulation software.

2 Literature Review

2.1 Introduction

Much research has been done to date to investigate the dynamic rocking or uplift of rigid bodies. There has also been research conducted on various types of steel and reinforced concrete bridges allowed to experience unrestrained or controlled uplift. In addition, some studies have investigated simple frame type structures where column uplift relative to the footing is unrestrained or where some type of energy dissipation device has been installed between the column and foundation connection. The studies have indicated in general that allowing a structure to uplift may reduce forces and damage in a structure when compared to a similar structure with a fixed base condition. To date there has been relatively little analytical and even less experimental research on the behavior of deformable bodies resembling bridge piers where the footing is allowed to rock or uplift on the supporting soil.

Some analytical and experimental studies investigating the characteristics and response of structural systems allowed to uplift are described in Section 2.2. Studies that have attempted to determine or validate design-oriented procedures for structural systems, which may rock and or uplift are described in Section 2.3. A summary of conclusions of this review of available literature is presented in Section 2.4.

2.2 Structural Systems with Uplifting Foundation

The studies described here identify the characteristics of rocking and uplifting systems and the effects on structural response, including the global and local response related to deformation, acceleration and force. The types of systems reviewed include: elastic and inelastic columns, shear walls, elastic and inelastic soil response, spread footing foundations, and uni- or multi-directional earthquake input excitation. Analytical only investigations are reviewed in Section 2.2.1 and experimental investigations are described in Section 2.2.2.

2.2.1 Analytical Investigations

Meek (1975) studied the dynamic in-plane response of flexible single degree-of-freedom elastic columns connected to a rigid spread footing supported only at the outer edges (2 locations) and where the soil is being modeled as rigid with elastic impact assumed. Basic equations of motion for a flexible superstructure were developed and used to determine the dynamic response of tipping and fixed base systems. Tipping or

rocking was found to significantly reduce the lateral shear force acting on the structure, especially for large ratios of super structure mass height to footing half width. Tipping or rocking mechanism was found to be a viable option that effectively reduced base shear without having a strong structure. Further clarification was found to be needed for the potential negative effects on nonlinearity of the soil where the footing uplifts and subsequently impacts the ground.

Yim and Chopra investigated a system similar to that by Meek with a simple elastic single- or multiple degree-of-freedom model considered in combination with a more complex soil model. The column foundation was supported on either a two-spring/dashpot model (at each edge) or a Winkler model with springs and dashpots uniformly distributed along the entire width of the footing (Figure 2-1). Nonlinear soil springs were modeled as being elastic in compression only, and with no tension resistance. Additional soil nonlinearity and inelastic impact damping qualities were modeled using viscous dampers.

In general, the peak base shear (in comparison to a fixed base system) is reduced if the foundation uplifts for either foundation model. The most important factors determined to influence structural response were:

- Fixed base period (T_n)
- Structure slenderness (h/b)
- Ratio of foundation weight to superstructure weight ($W/W_{footing}$)
- Vertical period of fixed base system
- Damping ratio of fixed base structure with rigid soil to damping ratio of fixed base structure considering dynamic characteristics of soil.

The authors developed simple equations to predict the critical base shear, which occurs at incipient footing uplift, assuming the soil springs had no tension carrying abilities and were fully elastic in compression. The critical base shear equation (V_c) for the two-spring soil model is given in Equation (2-1) and Equation (2-2) for the Winkler foundation model.

Two-Spring Model:

$$V_c = (m + m_o) g \frac{b}{h} \qquad (2\text{-}1)$$

Winkler Foundation

$$V_c = (m + m_o) g \frac{b}{3h} \qquad (2\text{-}2)$$

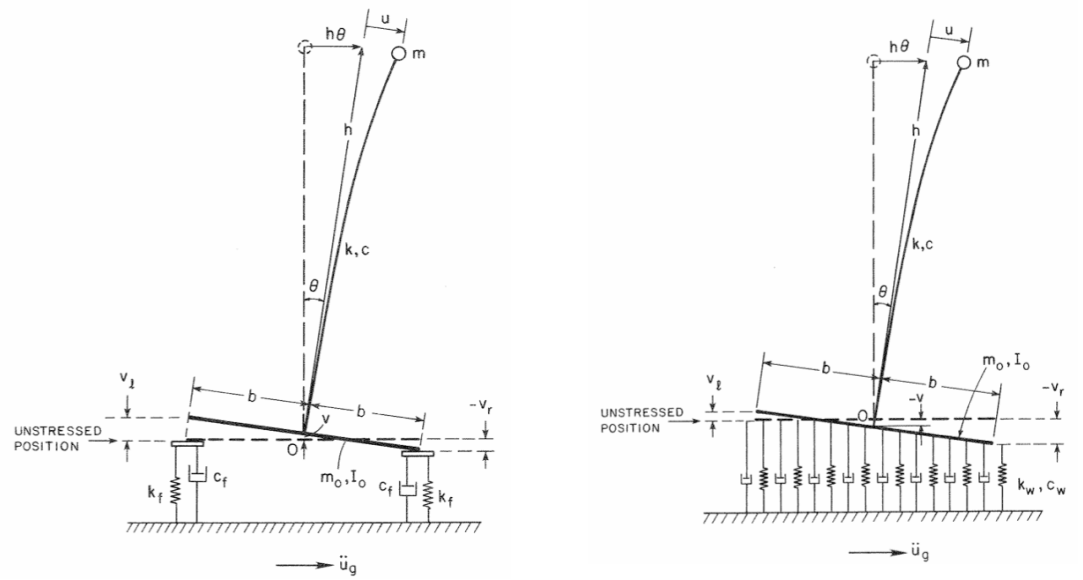

(a) Two Spring Model (b) Winkler Foundation Model

Figure 2-1: Uplifting Elastic Column Models on Spread Footing (Yim and Chopra, 1984)

The lateral force-displacement relation for the system is bi-linear for the two-spring model. In comparison, the Winkler-foundation response differs due to the distribution of vertical springs along the footing length. After initial edge uplift, the base shear continues to increase gradually with applied lateral force as the rotational stiffness of the footing decreases as additional springs lose contact with the uplifting footing. This repeats until only one spring is in contact with the footing at which point the Winkler model calculated base shear has converged on the two-spring model calculation. Rotational flexibility of the uplifting foundation contributes to lengthening the natural period of the system compared to a fixed base system. The critical base shear formulation indicates there is a limited value of base shear which may be induced in a structure which is independent of the applied excitation and dependent only on the structural weight and the geometry of the system (h and b).

Results for the numerical models subjected to several earthquake ground motion records are shown in Figure 2-2 for both foundation types. The Winkler-spring model uplifts earlier than the two-spring model, however in the short period range, where significant uplift is expected, the base shear demand approaches that for the two spring model.

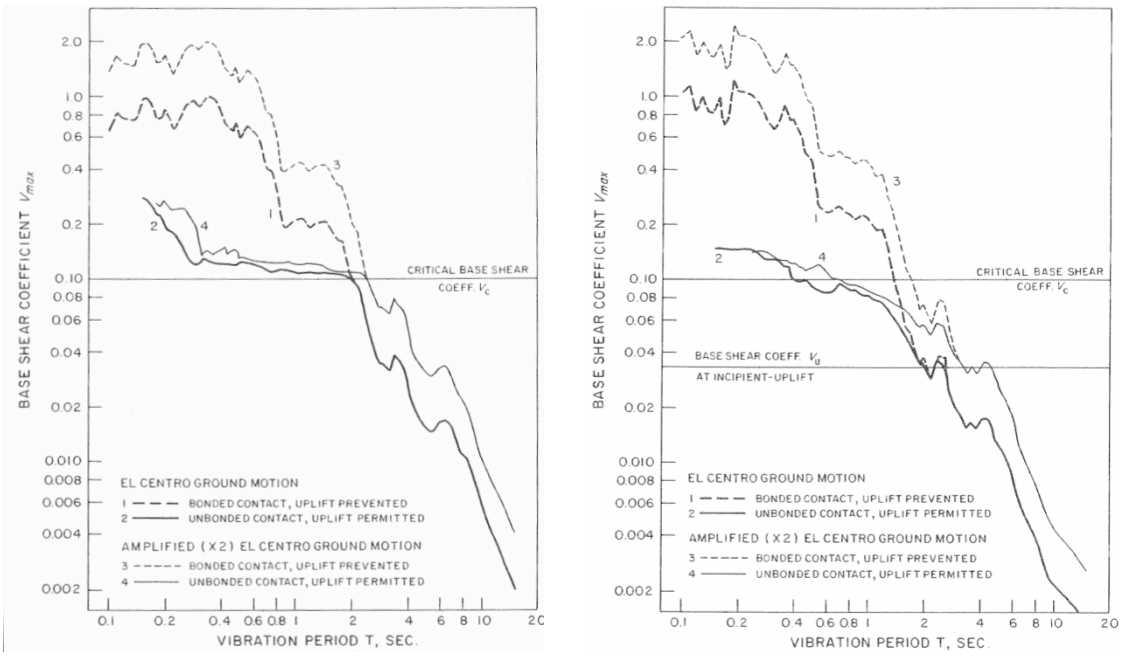

(a) Two Spring Model (b) Winkler Foundation Model

Figure 2-2: Base Shear Spectra Uplifting System with H/B = 10 (Yim and Chopra 1983)

Yim and Chopra developed a simplified two-spring model to represent the behavior exhibited by the Winker model. From these studies, Yim and Chopra reached several conclusions:

1. Base shear in long period range may be equal for structures allowed or prevented from uplifting, due to a seismic demand less than that required to initiate uplift for a given axial load and column height to footing width ratio h/b.
2. Uplift expected in short period range.
3. Base shear for uplifting systems is reduced compared to elastic column fixed base systems.
4. Maximum base shear is relatively independent of the intensity and dynamic characteristics of the ground motion.
5. Uplift is more likely in slender column systems (i.e. large h/b). Results in larger reductions in base shear for columns with narrower foundations.

Yim and Chopra concluded there is no need to prevent uplift, as it has a positive effect on structural deformations and forces and that the critical base shear (Eqn. (2-1)) can be used as a guide in designing a column that would not yield or be damaged in an earthquake. It should be noted that global displacements of systems with fixed or uplifting foundations were not compared in this study nor were the effects of multi-directional ground motions. Lateral displacements of bridge piers are important to estimate P-Δ effects and assess displacement demands at abutments and expansion joints.

Priestley, Evison, and Carr (1978) conducted an experimental and analytical study on rocking and uplifting of a simple cantilever column system. The experimental

program performed a series of small shaking table tests of the system allowed to rock and uplift. A rigid foundation was provided that rested upon a rubber pad supported uniformly or only at the four corners. The analytical investigation estimated peak lateral displacements of the system and the amount of deformation due to column flexibility by utilizing Housner's method developed for rocking of rigid bodies (1963). This modified Housner methodology was also used in subsequent analytical investigations by Priestley and Seible (1991) and Priestely, Seible, and Calvi (1996). Maximum lateral displacement of the rocking system was estimated using a conventional elastic response spectrum and equivalent elastic characteristics of the system allowed to rock.

To determine the maximum lateral displacement, the authors developed an iterative method. This method used an initial prediction of total lateral displacement (Δ_1) with an assumed viscous damping ratio ξ_1 of the rocking system to determine an effective equivalent period T_1. The values T_1 and ξ_1 were used with the elastic response spectrum to determine a new lateral displacement Δ_2. The process was repeated *i* times until the maximum lateral displacement converged on $\Delta_i = \Delta_{total}$. With a converged solution, the computed shear force (Eqn. (2-3)) is used with the lateral stiffness of the fixed base bridge pier to estimate the contribution of column flexural displacement to the total system displacement (Eqn. (2-4)). The rocking displacement was then calculated by subtracting total displacement from column flexural displacement (Eqn. (2-5)).

$$V_{base} = S_A\left(T_i, \xi_i\right)\left(\frac{W}{g}\right) \qquad (2\text{-}3)$$

$$\Delta_{flexure} = \frac{V_{base}}{k_{column}} \qquad (2\text{-}4)$$

$$\Delta_{rock} = \Delta_{total} - \Delta_{flexure} \qquad (2\text{-}5)$$

The methodology proposed by Priestely et al. is susceptible to inaccuracy owing in part to the assumptions of rigid body rocking, perfect inelastic impact, equivalent linearization, etc. The software program WINROCK (2005) has implemented this method despite not being substantially validated by more thorough analytic or experimental methods.

Kawashima and Hoisori (2003) investigated the uplift response of an existing bridge pier system using nonlinear dynamic analysis and found the results indicate the bridge pier system performed well when uplift was allowed. A Takada degrading stiffness model was used to characterize the moment-rotation response of the plastic hinge region of the bridge column along with a nonlinear Winkler spring foundation model based on uplift and elastic properties of the soil properties. The ground motion used was a one-dimensional strong motion near-fault record (1995 Kobe, JMA Observatory).

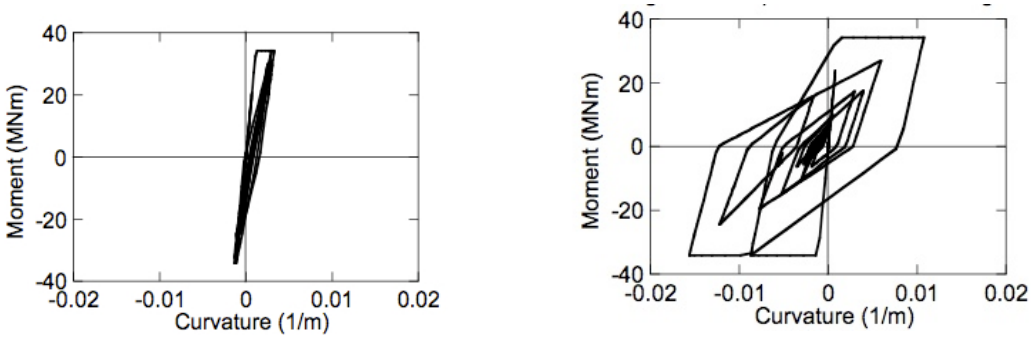

(a) Uplifting System **(b) Fixed Base System**

Figure 2-3: M-ϕ Column Response of RC Bridge Column (Kawashima & Hoisori, 2003)

Kawashima and Hoisori found that allowing uplift significantly reduced the moment-rotation response compared to a fixed base assumption (Figure 2-3). Global displacements increased 27% for the case considered in spite of allowing uplift. However, the contribution of column flexure to total displacement was only 20%, which corresponds with the reduction in inelastic column behavior and damage. No residual displacements were observed when the column was allowed to uplift. The authors concluded that allowing inelastic rocking and uplift essentially created an isolation mechanism that increases as the footing width decreases.

2.2.2 Experimental Studies

Sakellaraki, Watanabe, and Kawashima (2005) performed a shake table test of an idealized bridge column with uplifting foundation. The system was a steel column with a mass at the top and a metal footing resting upon a rubber pad with footing translation prevented. The mass was varied to achieve a system with natural periods (fixed base assumption) ranging from 0.3 to 1.2 sec. Additional analytic studies were performed to gauge rocking response and validate analytic modeling techniques of the experimental tests (Sakellarki, Watanabe, and Kawashima, 2005; Sakellaraki and Kawashima, 2006). The uplifting foundation model consisted of an elastic column and footing resting upon elastic (compression only) Winkler springs.

Rocking was found to affect the system by increasing the effective natural period and viscous damping ratio as the amount of rotation increased. Typically, rocking response increased as the mass increased, footing width decreased, and/or soil stiffness decreased. Specimen performance under rocking and uplifting footing conditions had both positive and negative effects. The column flexural deformation decreased, as did the center of mass accelerations. The acceleration reduction correlates to a reduction in the base shear. However, the total displacement increased due to rocking. Large vertical accelerations were recorded at the footing edges during impact of foundation with the soil.

The recorded vertical accelerations suggested to the authors a risk of soil yielding in actual bridges due to uplifting systems. The inelastic Winkler spring model provided good correlation between predicted and experimental results at small and medium

rotations of the footing, but less so at large values, which indicates the need for an improved numerical model of the foundation springs.

Nagai and Kawashima (2006) built upon this study and performed an analysis on the effect of two-horizontal components of excitation on the behavior of bridge piers on foundations allowed to uplift. A typical bridge on spread footing foundation was analyzed under uni- and bi-directional excitation. The columns were modeled using inelastic behavior assumptions. As previously shown (Sakalleraki et al., 2005, 2006) under unidirectional excitation, foundation rocking significantly reduces the plastic deformation of the column. The authors found that bidirectional excitation increases the uplift of the footing by comparison, but also increases the isolation effect, thereby reducing the potential yielding behavior in the column.

Kawashima, Nagai, and Sakellaraki followed up on their earlier work in 2007 and considered three-directional input excitation. The findings indicate that the soil stress induced at the corners of the foundation significantly increase. In general, they found that foundation rocking provides a positive benefit in seismic design of bridges. However, they express concern that underlying soil may need enhancement at foundation corners to fully realize the benefits of rocking systems.

2.3 Design of Uplifting Foundation Systems

The design-oriented studies reviewed in this section investigate when rocking is an acceptable response mode and determine or assess design guidelines for evaluating new and existing systems allowed to uplift. The evaluation is based on the local response (forces, deformations, etc) and global response (displacements).

An investigation by Alameddine and Imbsen (2002) suggests the iterative solution methodology by Priestley, Seible, and Calvi (1996) may not converge on a total displacement solution that agrees with analyses based on nonlinear dynamic analysis. Comparisons of results of studies of equivalent elastic systems (such as the iterative methodology used), with those from simpler direct methods based on empirically modified elastic response spectrum suggest that comparable accuracy can be obtained in the moderate and long period range. However reliability of the iterative equivalent elastic approach decreases substantially for short period structures (Chopra and Goel, 1999; Miranda and Ruiz-Garcia, 2002). Chopra and Goel (1999) found that iterative methods may not converge or converge on erroneous solutions.

Alameddine & Imbsen (2002) investigated a retrofit strategy for older bridges where columns might have inadequate lap splices in discontinuous reinforcement or inadequate confinement of continuous reinforcement at the column footing connection. They examined the seismic response when the column foundations were allowed to rock. The systems considered all had a footing to column width ratio of 3 and were supported by spread footings on dense soil subjected to low, moderate and high intensity ground motions. Analysis was performed using either WINROCK (2005), based on the iterative method by Priestley and Seible (1991) or a nonlinear dynamic analysis incorporating a Winkler spring model for the soil with a nonlinear beam-column element for modeling

the inelastic response of the column. A total of 24 column systems where subjected to six ground motions.

The nonlinear dynamic analysis model found that for existing columns with relatively high flexural strength and narrow footing widths, allowing uplift resulted in acceptable total lateral displacement and elastic column response for a majority of cases. Columns with weak flexural strength exhibited significant yielding and a 30% increase in total lateral displacement compared to stronger columns. Rocking and uplifting did not significantly contribute to the response of these weaker systems and in some cases no rocking occurred. It was observed that larger ductility demands occurred for columns with larger footing width to column height (b/H) ratios.

A comparison of nonlinear analysis results with results predicted by WINROCK showed large discrepancies. Stronger columns with limited flexural demands due to significant uplift had very different results compared to weaker columns where less rocking and more flexural yielding occurred. For example, the peak ratio (nonlinear analysis to WINROCK) of flexural column displacements predicted by the two methods varied by a factor of 0.71 to 1.95 for each ground motion on average for the stronger column and 0.56 to 4.01 for the weaker column system. Larger discrepancies were found for low footing width to column height ratios. Using both methods they found that rocking and uplifting was not a cause of instability in any of the analyses which led to the conclusion that enlarging the footing as part of a retrofit scheme was not warranted. Some of the weak column systems with little or no rocking collapsed due to inadequate flexural ductility.

Design guidelines, based on the nonlinear dynamic analyses, identifying acceptable conditions of rocking and uplifting systems were developed for new design and existing column retrofit by Alameddine & Imbsen. The criteria for allowing rocking in the design process is primarily based on the calculated ratio of overturning moment to restoring moment β. The overturning moment is defined as the column axial load P times the center of column mass displacement (Δ_{demand}). The restoring moment is calculated as the minimum of the factored column plastic moment capacity (1.2Mp) or the moment resisting uplift calculated as the total structure and soil weight (W_t) times the distance from the centroid of W_t to the centroid of the soil force generated by uplift. Figure 2-4 is a schematic of the forces developed in the uplifting and deforming system. Relationships between β and drift, ductility and column width to height ratios (D/H) were developed to identify acceptable response criteria.

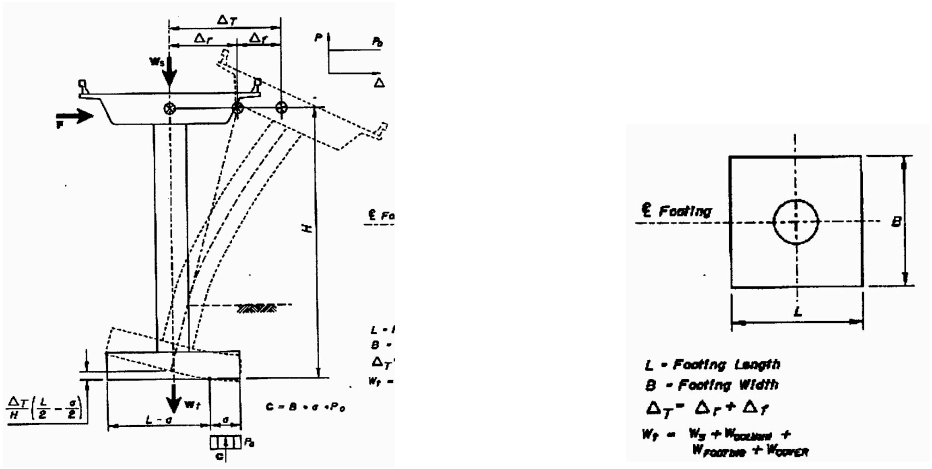

Figure 2-4: Uplifting Column Model (Alameddine & Imbsen, 2002)

To evaluate the acceptability of rocking the authors developed a decision making flowchart with β as the primary decision variable. They then determined the footing dimension required by service loading or the minimum footing width of 3 column diameters and estimated the lateral flexural displacement of the column (Δ_{demand}) using WINROCK (2005), although alternative methods could have been used. The overturning and restoring moments were then determined and these were used to evaluate β (Eqn. (2-6)). Based on the analysis conducted, Alameddine & Imbsen determined acceptable values of β for design based on the column fixed base ductility (Eqn. (2-7)). When β was larger than $\beta_{allowable}$ they re-evaluated the design process using a larger footing dimensions. They iterated on the footing dimensions until an acceptable value of β was achieved.

$$\beta = \frac{P \cdot \Delta_{demand}}{\min\left(1.2M_p, W_t(L-a)/2\right)} \qquad (2\text{-}6)$$

Criteria for accepting rocking in design:

$$\begin{aligned} \mu < 6 \qquad & \beta_{allowable} \le 0.3 \\ \mu = 6 - 8 \qquad & \beta_{allowable} \le 0.2 \end{aligned} \qquad (2\text{-}7)$$

In the design procedure, the column is required to be ductile regardless of the amount of rocking. This is to prevent against column failure in the event of modeling uncertainty or an unanticipated increase in footing strength (e.g. additional soil surcharge). While the study is very useful it only considers a limited number of soil conditions, does not include damping effects of the soil and foundation (which means elastic rebound would occur upon contact), and limits the seismic excitation to one-direction.

Harden et al. (2005) studied methods for numerical modeling of nonlinear cyclic response of shallow foundations similar to those used for shear walls in building structures. Using the developed numerical modeling methods the authors investigated the ability of several design-oriented analysis procedures to predict lateral displacements and

bases shears of uplifting systems. A simple method was developed based on a refined FEMA 356 prediction methodology that could be used to estimate peak displacements and base shears. They concluded by performing a case study of a shear wall and highlighting accuracy between the methods as wells as the benefits in allowing uplift.

Work done by Rosebrook (2001) and Phalen (2003) was reviewed by Harden et al. to develop their numerical models. The works reviewed investigated the effect of foundation rocking on the inelastic behavior of soils and overall dynamic response of structures on rocking and uplifting foundations. Rosebrook summarized tests of small-scale pairs of coupled walls supported on sand and saturated clay. Phalen summarized tests of single strips footings on dry sand having different sizes and design vertical factors of safety.

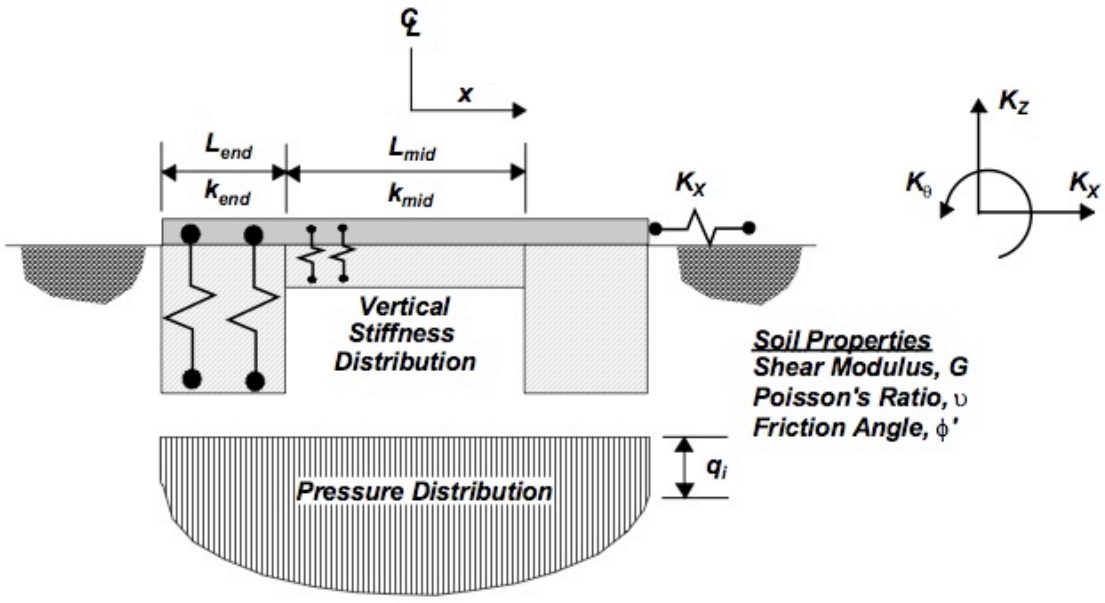

Figure 2-5: Nonlinear Winkler Foundation (Harden et al., 2005)

Based on the recent quasi-static and dynamic tests, Harden et al. developed a nonlinear Winkler foundation to model the underlying soil of a shear wall on a strip footing. The primary input parameters are shown in Figure 2-5. Three types of material models were used for the supporting springs: elastic-perfectly plastic combined with gap elements, general hysteretic materials, and the QzSimple1 material model developed by Boulanger et al. (1999). Dashpots were excluded since Wang et al. (1998) previously showed that including rate-dependent damping in parallel with hysteretic spring elements overestimates the damping force.

In the investigation of the design analysis procedures ability to predict lateral displacements and bases shears of uplifting systems the authors compared their numerical models to four simplified analysis methods included in FEMA 356 (2000). The design methods were evaluated for three foundation assumptions: elastic springs with tension

allowed, inelastic springs with uplift (no tension) allowed, and a fixed base assumption which ignored soil-structure interaction. The four simplified methods included the Capacity Spectrum approach, a method similar to Priestley and Seible (1991), the Nonlinear Static Procedure (method of coefficients) and the time history method.

The subsequent investigation of the simplified methods improved on the parameter C1 used in the Nonlinear Static Procedure. C1 is the ratio of predicted peak displacements for the nonlinear time history analysis using inelastic spring models with uplift to that of a similar system with elastic springs with elastic tension/compression springs where uplift is prevented. The estimation of C1 depends on the period of the elastic structure (on a Winkler foundation) and the Harden et al. parameter R. R is defined as the ratio of base shear developed for the structure if the foundation remained elastic (uplift prevented) to the base shear at incipient uplift (Eqn. (2-2)). This definition provides an upper bound on R. In the cases considered, the supported structures had yielding forces much larger than those required to cause uplift of the foundation.

Harden et al. investigated directly measured values of C1 for preselected R values using an elastic cantilever column structure model on Winkler foundation. The foundation was modeled as nonlinear soil with uplift allowed and entirely elastic without uplift. Figure 2-6 shows the simulation data points, best-fit curves and FEMA 356 recommended values of C1. Inspection shows that for structural periods greater than T_s, C1 is typically around 1 (i.e. no amplification in lateral displacements due to soil model) but increases for structural periods less than or equal to T_s. Especially with increasing values of R. By comparison FEMA 356 limits C1 to 1.5 in the short period range which is unconservative for all the cases shown, except R=1.5. As another example, the Newmark & Rosenblueth (1971) energy conserved method for calculating C1 gives a value of 2.13 when R=4.0 for a structural period of approximately $T_s/2$. A lower value of R might be warranted since the footing strength incrementally increases as it continues to uplift.

Harden et al. also investigated the peak structural lateral displacements and base shears predicted by their model using inelastic time history analysis with uplift to the simplified methods in FEMA 356. The structural system used was a reinforced concrete shear wall on a shallow strip footing supported on soil with a bearing capacity factor of safety of 4. The seismic hazard level was selected as 10% probability of exceedance in 50 years with a site specific characteristic period T_s = 0.367 sec. The structural period was 0.03 sec for a fixed base assumption and 0.44 sec on an elastic Winkler foundation. The computed R value was 3.97. The results for peak lateral displacement and base shear are given in Table 2.1 and Table 2.2.

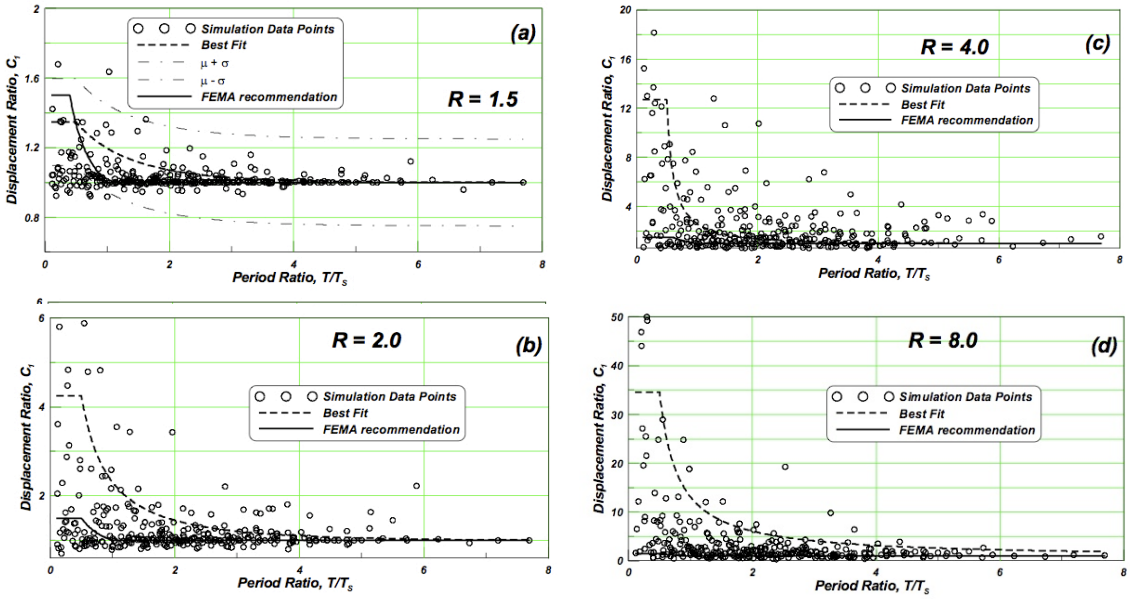

Figure 2-6: C1 Ratio of Max. lateral displacement with/without footing uplift (Harden et al., 2005)

Comparing the displacements shows that the simplified methods all underestimate the peak response. The least accurate method is the Nonlinear Static Procedure with C1 defined by FEMA 356 (2000), followed by the modified Housner model, and the Capacity Spectrum method. Using the C1 defined by the best fit curve in Figure 2-6 the peak displacement is slightly over-estimated using the more complex inelastic time history analysis. Base shear results have much less scatter than the peak lateral displacements. The modified Housner method and the capacity spectrum method over-estimate the base shear by 70% and 25%, respectively. The Nonlinear Static Procedure with the FEMA 356 or Harden et al. calculation of C1 predict a base shear within 5% of that from the inelastic time history analyses. The design shear for a fixed base system is 7.9 times larger than the case allowing uplift.

The improved calculation of C1 for the nonlinear static procedure shows much larger displacements than predicted by the simplified methods, which advocates against allowing uplift. However, typically displacements for short period structures are very small so a large percentage increase still may be a small displacement. The reinforced concrete shear wall investigation shows that allowing uplift significantly reduces base shear but increase global displacements of the system. For the shear wall, assuming the system could accommodate increased displacements, allowing foundation uplift would be very beneficial because there would be a significant reduction in base shear and deformation of the wall. The studies by Harden et al. are promising, but do not directly address the concerns of longer period structures like bridges where bi-directional bending is also of greater concern.

	Soil Structure Interaction (SSI) Included			*SSI Not Included*
	Uplift Allowed		*Elastic*	*Fixed Base*
	Nonlinear Soil Springs	*Elastic Soil Springs*	*Method 1*	
Natural Period, T (sec)	0.555	0.424	0.424	0.033
Analysis Method	u_{top} (mm)	u_{top} (mm)	u_{top} (mm)	u_{top} (mm)
LDP (Capacity Spectrum)	280	178	38	0.14
Housner Model	206	202	202	0.16
FEMA NSP - C_1 defined by FEMA 356 (2000)	91	57	57	0.27
FEMA NSP - C_1 based on uplifting foundation (values from this study)	414	308	62	0.27
Time History Method (envelope of three ground motions)	385	102	237	0.0003

Table 2.1: Lateral Displacement Comparison of Shear Wall Model Using Various Methods (Harden et al., 2005)

	Soil Structure Interaction (SSI) Included			*SSI Not Included*
	Uplift Allowed		*Elastic*	*Fixed Base*
	Nonlinear Soil Springs	*Elastic Soil Springs*	*Method 1*	
Natural Period, T (sec)	0.555	0.424	0.424	0.033
Analysis Method	V (kN)	V (kN)	V (kN)	V (kN)
LDP (Capacity Spectrum)	211	331	1181	728
Housner Model	284	291	291	723
FEMA NSP - C_1 defined by FEMA 356 (2000)	162	240	1024	793
FEMA NSP - C_1 based on uplifting foundation (values from this study)	170	265	1108	793
Time History Method (envelope of three ground motions)	169	251	4245	1341

Table 2.2: Base Shear Comparison of Shear Wall Model Using Various Methods (Harden et al., 2005)

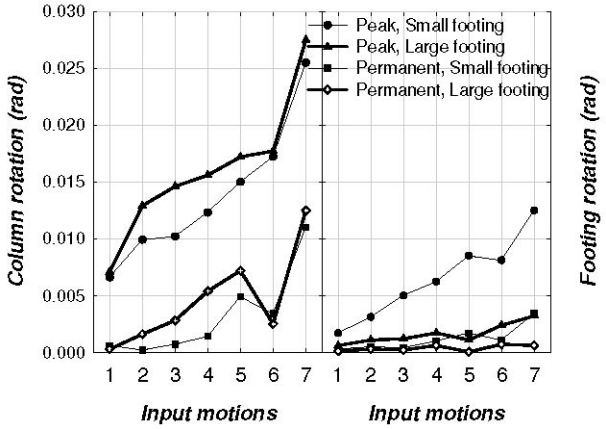

Figure 2-7: Two Column Bridge Bent Column and Footing Rotations (Deng et al., 2010)

Algie et al. (2008) performed dynamic centrifuge testing of rocking bridge spread footing foundations with cantilevered columns allowed to yield and variable footing dimensions. Experimental results found footing moment-capacity could be reliably predicted when allowed to rock. The results also identified a reduction in column plastic rotation demand that was consistent with a reduction in foundation moment-capacity which highlights a potential design benefit.

Deng et al. (2010) utilized methods similar to those by Algie et al. to predict foundation moment-capacity and perform dynamic centrifuge modeling of a bridge system with rocking footings. The experimental testing validated a design method which allows rocking of bridge spread footings to protect columns from excessive ductility demands. Two 2 column bents systems, with columns designed to Caltrans standards and pinned at the top, and small or large footings were evaluated. They were designed such that one bent (small footings) had less moment-capacity than the column and the other (large footing) had more moment-capacity than the column. Column peak and permanent rotations of the smaller footing with yielding soil were typically less, for the seven input motions considered, relative to the larger footing with column yield and little rocking, which had little soil yield (Figure 2-7). Soil yielding caused settlements that may cause permanent rotation of the system not related to column yielding. Algie et al. also identified soil settlement as a potential negative effect when allowing rocking.

Deng and Kutter (2011) investigated through centrifuge testing the settlements associated with bridge piers on spread footings allowed to rock on dry sand. The aim was to mitigate settlements due to rocking foundations while still allowing rocking to reliably dissipate energy through soil structure interaction. Placement of localized concrete pads beneath footing edges was found to reduce settlements associated with rocking, but still allow the foundations to reliably rock. One of the important factors found for acceptable combination of energy dissipation and re-centering (minimized soil yielding) ability was the ratio of footing length to critical length required to support axial loads only (L_f/L_c). The studies by Algie et al., Deng et al., and Deng and Kutter are encouraging and provide an example of the benefits of allowing bridge piers to rock during seismic events and the potential negative effects rocking piers might have on re-centering abilities post-seismic event. However they do not consider a large sample of bridge column dimensions and footings sizes or seismic excitations.

2.4 Summary

From the review of analytical and experimental studies there appears to be a large share of evidence that suggests that soil-structure interaction and uplifting of a spread foundation from the supporting soil can significantly diminish the base shear of a bridge column when compared to a fixed based elastic structure. Inelastic deformation and shear force demands on the column can be significantly reduced when competent soil is provided and the foundation restoring capacity is smaller than the column strength. Force demands on columns supported on uplifting foundations can be reasonably estimated from existing relationships.

Reliably estimating total displacement of the column supported on an uplifting foundation and the contribution of uplift to total displacement is much less certain. The approximate simplified methods, suitable for design, for estimating displacements are less well developed and appear to vary significantly compared to nonlinear dynamic analyses. More robust numerical models have been used, but they have limited experimental data to calibrate the material and kinematic properties. Additional research is warranted related to the behavior of bridge columns supported on foundations that can rock and uplift during severe earthquake ground motions.

3 Experimental Test Program

3.1 Introduction

A review of available literature on rocking columns revealed the need for better physical understanding of uplifting reinforced concrete columns. Sakellaraki, Watanabe, and Kawashima (2005) performed experimental testing and analysis of a small-scale elastic column that experienced no inelastic loading during shaking. Representative modeling of elastic soil was done via a rubber pad. The testing did not explore the behavior of uplifting systems when there is a transition to inelastic response of the supporting column. A study presented by Nagai and Kawashima (2006) assessed the effect of two-horizontal components of excitation on the behavior of piers supported on foundations allowed to rock. The work illustrated analytically that foundation rocking significantly reduced the plastic deformation of the column for one component of excitation and even more when considering two components of excitation. However, to date there has been little work published on the experimental testing of uplifting reinforced concrete columns resting on spread footings. Better understanding of the characteristics of uplifting systems would identify when the already known potential benefits of rocking systems would occur and under what conditions allowing a system to uplift could be detrimental to performance. There are several response modes to consider for uplifting bridge piers: rocking on flexible soil without uplift and elastic column response, rocking and uplift on the flexible soil with elastic column response, rocking without uplift and inelastic column response, and the simultaneous occurrence of rocking, uplift and inelastic column response.

The specimen presented herein investigates the seismic performance of a conventional reinforced concrete bridge column with varying footing widths under near-field forward-directivity strong ground motion excitations through a series of earthquake simulator tests. A single specimen was tested for three different types of footing width and axial load combination. The prototype column used as the basis of the test specimen is described in Section 3.2. The design of the specimen including scaling laws, column, footing, elastic soil representation, steel brackets and mass blocks are described in Section 3.3. The construction sequence is described in Section 3.4. Measured material properties for elastomeric pad, concrete, and steel are described in Section 3.5. The test setup for investigating uplifting columns is described in Section 3.6. The instrumentation, data acquisition system and test documentation is described in Sections 3.7, 3.8, and 3.9, respectively. Grounds motions used in testing are describe in Section 3.10. Finally, the testing sequence for all runs of the specimen is described in Section 3.11.

3.2 Prototype Column

To simplify the investigation, a cantilever reinforced concrete bridge column considered in previous shaking table studies at UC Berkeley (Hachem, Mahin, and Moehle, 2003; Sakai and Mahin, 2006; Jeong et al., 2008) was selected as the prototype. The prototypical column is shown in Figure 3-1. The column was designed in accordance with the Caltrans Seismic Design Criteria (2004). The prototype column used in design of the test specimen had a circular cross-section diameter of 6 ft. In order to achieve a target aspect ratio of 6, the column was specified as 36 ft high. Measured from the bottom of the column to the center-of-mass of the superstructure. The axial load was taken to be $0.10\ f'_{co}A_g$ based on a typical nominal strength of unconfined concrete of 3.25 ksi.

The prototype column was reinforced longitudinally with 48 No. 9 deformed bars, which provided a longitudinal reinforcement ratio (ρ_l) of 1.18%. Confinement of the concrete core was achieved using No. 5 spirals spaced at a 3-in pitch, which resulted in a volumetric ratio (ρ_s) of 0.61%. Nominal yield strength of the longitudinal and spiral reinforcement was considered to be 60 ksi.

Column strength per Caltrans Seismic Design Criteria is independent of the specified footing dimensions. Thus, there is no affect on column strength for varying the footing. Based on typical Caltrans analysis assumptions and procedures (SDC, 2004), the ultimate lateral load capacity of the fixed base column was 290 kip, with a corresponding yield and ultimate displacement of 4.3 in and 22.8 in, respectively. Thus, the column has a displacement ductility capacity of 5.2. The effective natural period of the prototype column is 1.26 sec.

Once the dimensions and geometry of the prototype column were determined, a subsequent analysis was performed to assess the effect of ground motion and footing size on global displacements and local column flexural and shear demands. The prototype was modeled using a detailed fiber element model for the column, nonlinear Winkler beam foundation for soil, and rigid beams for footing elements. Several hundred analyses were

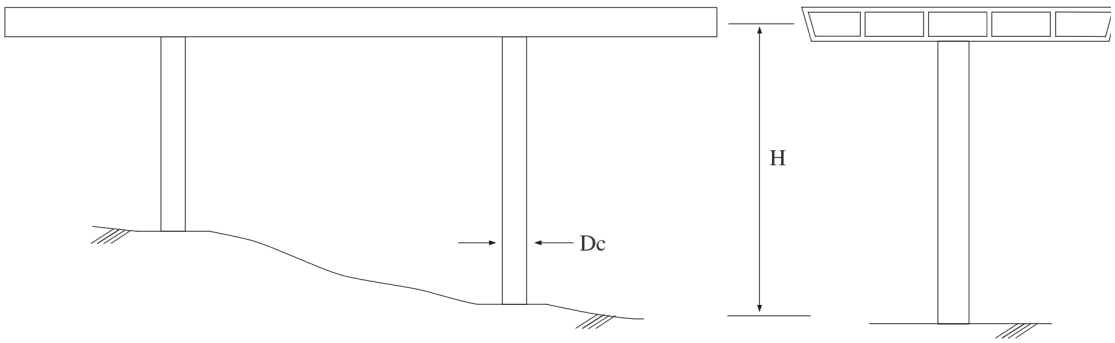

Figure 3-1: Prototype column

run for multiple footing widths, ground motions, and amplitude scales. The results were used to select appropriate footing dimensions and ground motions for consideration in these tests.

3.3 Design of Specimens

Many experimental tests are not conducted at full-scale size due to the lack of equipment available and the relatively high cost of specimens. Additionally, shake table tests are limited by the physical table size and the range of displacement, velocity, and acceleration values the simulator can impose. The combination of these factors, in addition to many others, often requires specimens be built at a reduced scale.

Based on work done by Hachem et al. (2003), described in Section 3.2, the diameter of the column was set at 16 in., which corresponds to a model length scale factor of 4.5. The length scale factor was used as the basis for computing other necessary quantities for scaling of the test specimen.

3.3.1 Model Scaling

Dimensional analysis provides a methodology for how to scale the dimensions, material properties, and loads for the model specimen. The rules of scaling for dynamic tests include time-dependent parameters such as strain rate, velocity, and acceleration in addition to those for statically loaded specimens. Dimensional analysis of the dynamic tests was performed considering the scale-length factor (Eqn. (3-1)), the acceleration of gravity be maintained (Eqn. (3-2)), and the modulus of elasticity of materials be identical (Eqn. (3-3)). By stipulating the acceleration of gravity be maintained, the strains in the test specimen and prototype, are identical. Further, if the same materials are used in the model and prototype then the same stress would be expected for each. Table 3.1 summarizes the dimensional similitude requirements for dynamic test under the condition that acceleration of gravity is maintained. For further discussion of dimensional analyses the reader is referred to Krawinkler and Moncarz (1982).

$$L = 4.5 \tag{3-1}$$

$$LT^{-2} = 1 \tag{3-2}$$

$$ML^{-1}T^{-2} = 1 \tag{3-3}$$

Limitations exist on scaling all quantities properly. For instance very small-scale models are problematic when scaling concrete. Small scale concrete that scales the aggregate and sand dimensions does not have the same mechanical properties as the full sized material. To avoid this phenomenon, typically a regular concrete mix design utilizing slightly reduced aggregate size is employed for moderately reduced scale specimens.

Table 3.1: Similitude Requirements and Scale Factors for Column Test

Quantity	Scale Symbol	Target Scale Factor	Scale Factor Value Used
Length	S_d	S_d	4.50
Time	S_t	$S_d^{1/2}$	2.12
Frequency	S_ω	$S_d^{-1/2}$	0.47
Displacement	S_d	S_d	4.50
Velocity	S_v	$S_d^{1/2}$	2.12
Acceleration	S_a	1	1
Mass Density	S_ρ	S_E/S_d	0.22
Strain	S_ε	1	1
Stress	S_σ	S_E	1
Modulus of Elasticity	S_E	S_E	1
Force	S_F	$S_E S_d^2$	20.25
Moment	S_M	$S_E S_d^3$	91.13
Energy	S_W	$S_E S_d^3$	91.13

3.3.2 Design of Test Specimens

Based on the design of the earlier reinforced concrete bridge column specimens (Hachem, Mahin, and Moehle, 2003; Sakai and Mahin, 2006), a single 16 in. diameter reinforced concrete column specimen was designed. The clear cover to the spiral reinforcement was set at ½ inch. The footing design was altered to investigate the effects of footing width on foundation uplift. The footing was cast monolithically with the column and had square dimensions of 48 in x 48 in that were three times the column diameter ($3D_C$). Horizontally oriented post-tensioning ducts were provided to facilitate the widening of the footing in some tests.

The general specimen design was nearly identical to the design of specimens in previous studies of fixed base columns, except for the footing width and supports provided for supporting the top mass block. To facilitate construction, reusable steel brackets were designed to support the top mass blocks. Reinforced concrete slabs were used as the mass blocks and attached to the top of the column via the steel brackets. Figure 3-2 shows the effective height of the specimen with mass blocks installed to represent the weight and inertial mass of the superstructure.

Normal density hard rock concrete was specified which had a design strength of concrete f_{co} = 5 ksi in order to provide the specimen with representative *in situ* concrete properties. The axial dead load from the combination of steel brackets and three weight

blocks was 54 kip which when combined with the measured column concrete strength of 5.25 ksi resulted in an axial force ratio (α_{DL}= P / $f_{co}A_g$) of 5.7%.

Following the static pushover analysis procedures recommended by the Caltrans SDC (2004), the yield and ultimate displacement capacities and the lateral strength of the specimen were evaluated for a fixed base condition to be 1.02 in, 8.26 in, and 15 kip, respectively. When expressed as a drift ratio (displacement divided by column height measured from bottom of column to center of gravity of mass blocks), the yield and ultimate displacement occur at drift ratios of 1.02% and 8.3% respectively. Using procedures developed by Priestley et al. (1996) the plastic hinge length is calculated as 12.9 in.

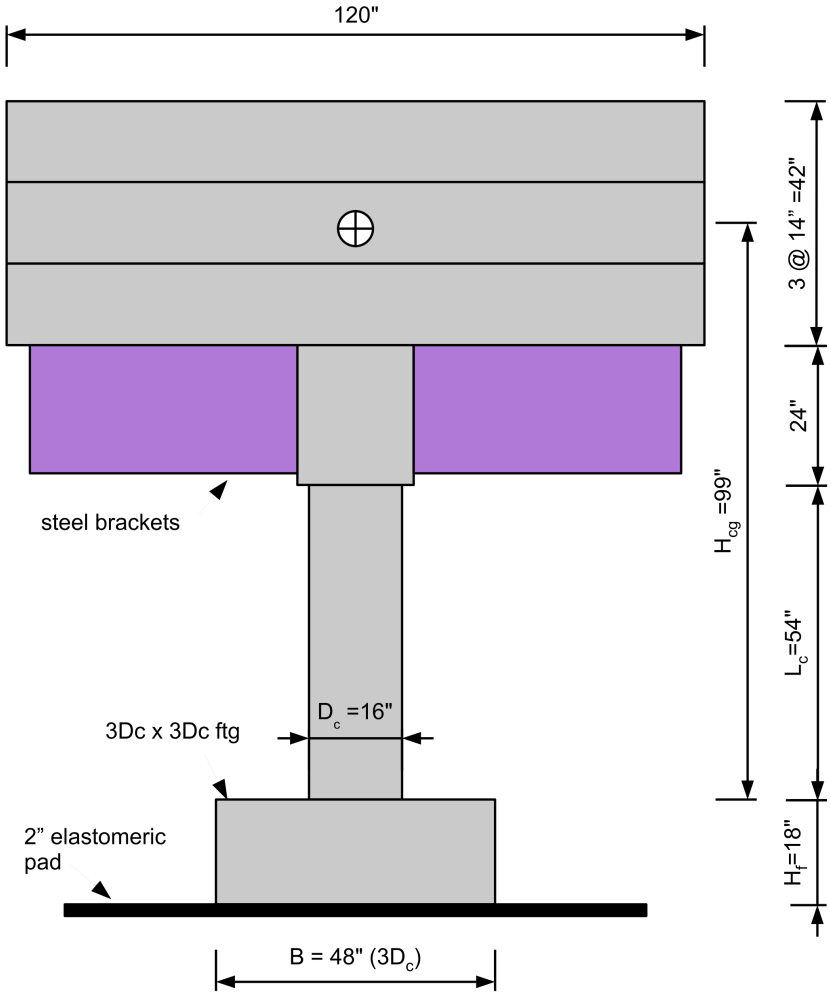

Figure 3-2: Specimen with mass blocks

3.3.2.1 Column Reinforcement

The column was reinforced with 12-No. 4 deformed grade 60 (A706) reinforcing bars. This resulted in a longitudinal reinforcement (ρ_l) ratio of 1.18%. A moment capacity of about 1400 kip-in was calculated for the design axial load. The amount of steel was selected based on satisfaction of the Caltrans Seismic Design Criteria (2004). At footing end of the bar, 90 degree hooks with a bend radius of 6 bar diameters (d_b) were used.

3.3.2.2 Spiral Reinforcement

The prototype column had a diameter of 6 ft that was used to calculate a required volumetric ratio of spiral reinforcement equal to 0.54% (SDC, 2004). However, smooth wire with a diameter small enough to satisfy the volumetric ratio was not available. A larger diameter continuous W3.5 Grade 80 (ASTM 82) smooth wire with d_{sp}= 0.211 in and A_{sp}= 0.035 in^2 was used which resulted in a volumetric ratio of spiral reinforcement (ρ_s) of 0.61%.

3.3.3 Footing

The footing was designed to remain elastic and as rigid as possible during the tests to avoid additional deformation caused by flexure or shear loading in the system. Design forces for the footing were evaluated based on a factory of safety of 4 on the plastic moment capacity of the column when the plastic hinge was fully developed. The Caltrans Bridge Design Specifications (BDS, 2004) require the ability of the footing to develop the full plastic moment capacity of the column. Regulations on footing thickness are limited to the ability to develop the mentioned column capacity. Reinforcement ratios for the designed specimen footing exceed those required (BDS, 2004). The footing was directly connected to the bottom of the column and rested on top of the elastomeric pads that were centered on the earthquake simulator platform.

The footing was 4-ft square and 18-in thick and was reinforced longitudinally with No. 6 deformed bars. Transverse reinforcing consisted of No. 3 stirrup ties. See Figure 3-4 for footing details. To widen the footing from $3D_c$ square to $3D_c$ x $5D_c$, 1-1/8 in. diameter high-strength post-tensioning rods were used to fasten concrete blocks to the existing footing. The blocks were cast from the same concrete batch and had the same height as the existing footing with a plan depth of 1Dc such that when attached to both sides would create a new width of $5D_c$. To expand the footing blocks, which had the same reinforcement ratio as footing, were connected using high strength grout and post-tensioning rods. See Figure 3-5. The weight of the footing was 3.6 kip for the $3D_c$ x $3D_c$ configuration. Expanding the footing to $3D_c$ x $5D_c$ created an additional weight of 2.4 kip for a total of 6.0 kips.

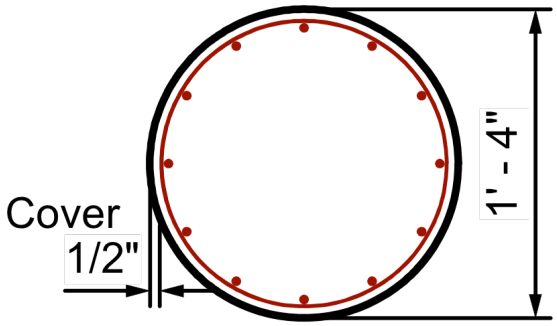

(a) Column cross-section (12 No. 4 Grade 60 longitudinal bars; W3.5 smooth Grade 80 wire spirals with a 1-1/4 in. pitch)

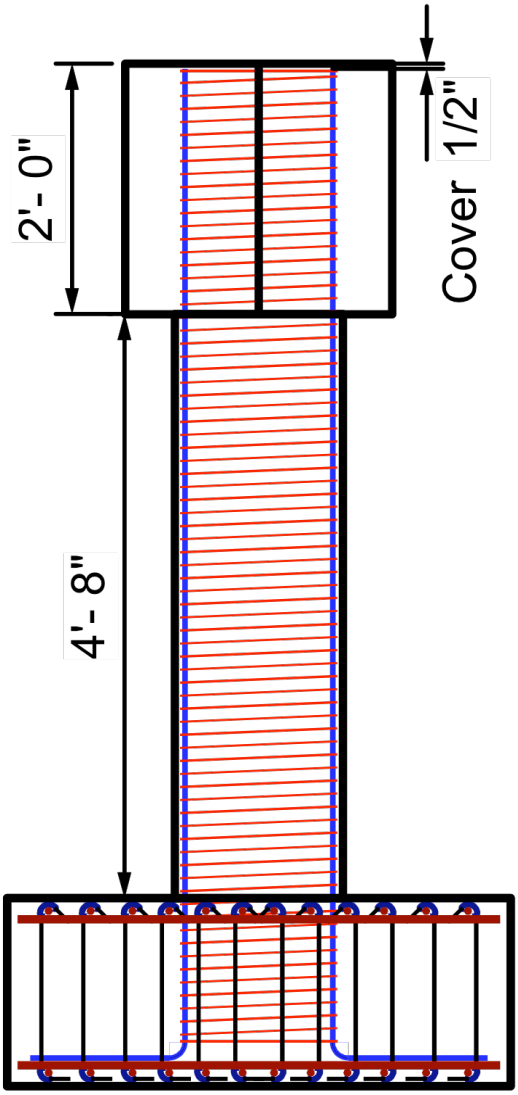

(b) Specimen

Figure 3-3: Column Reinforcement Details

3.3.4 Elastomeric Pad

The elastomeric pad was chosen such that the initial stiffness was similar to that of a competent dense sandy soil. A thorough review of available material types and thickness found that the target properties which best matched the initial stiffness of sand soil were a Commercial Neoprene Duro 80 with a 2-in. thickness which satisfied ASTM D-2000 standards. Single pieces of Duro 80 were not available in the size need to extend beyond the footing edges. Instead, two separate pieces 8 ft x 2 ft-6 in. in size were used to support the 3Dc square footing and the 3Dc x 5Dc footing and still maintain a minimum of 6 in. pad clearance from the footing on all sides (Figure 3-6). Bearing properties of the pad were determined from uniaxial compression tests of a 12-in square sample of the same material. The results are presented in Chapter 4.

3.3.5 Steel Brackets

Four steel brackets connected to the top of the column via 1-1/8 in. high strength post-tensioning rods supported the mass blocks. The steel brackets were checked for bending and shear due to the supported dead load of the weight blocks that included a factor of safety. The steel bracket weight for all four was 1.84 kip. Excluding the mass blocks the total weight of the steel brackets, column, and $3D_c$ square footing was 7.12 kip.

3.3.6 Mass Blocks

Three 10ft x 10ft x 14 in concrete blocks were used to represent the weight and mass of the superstructure of the bridge. The blocks were post-tensioned to the steel brackets via 1-1/8 in high strength steel rods to ensure they acted as a unit. The weight of each block was approximately 17.1 kip, resulting in a total weight of 54 kip for the mass blocks and steel brackets.

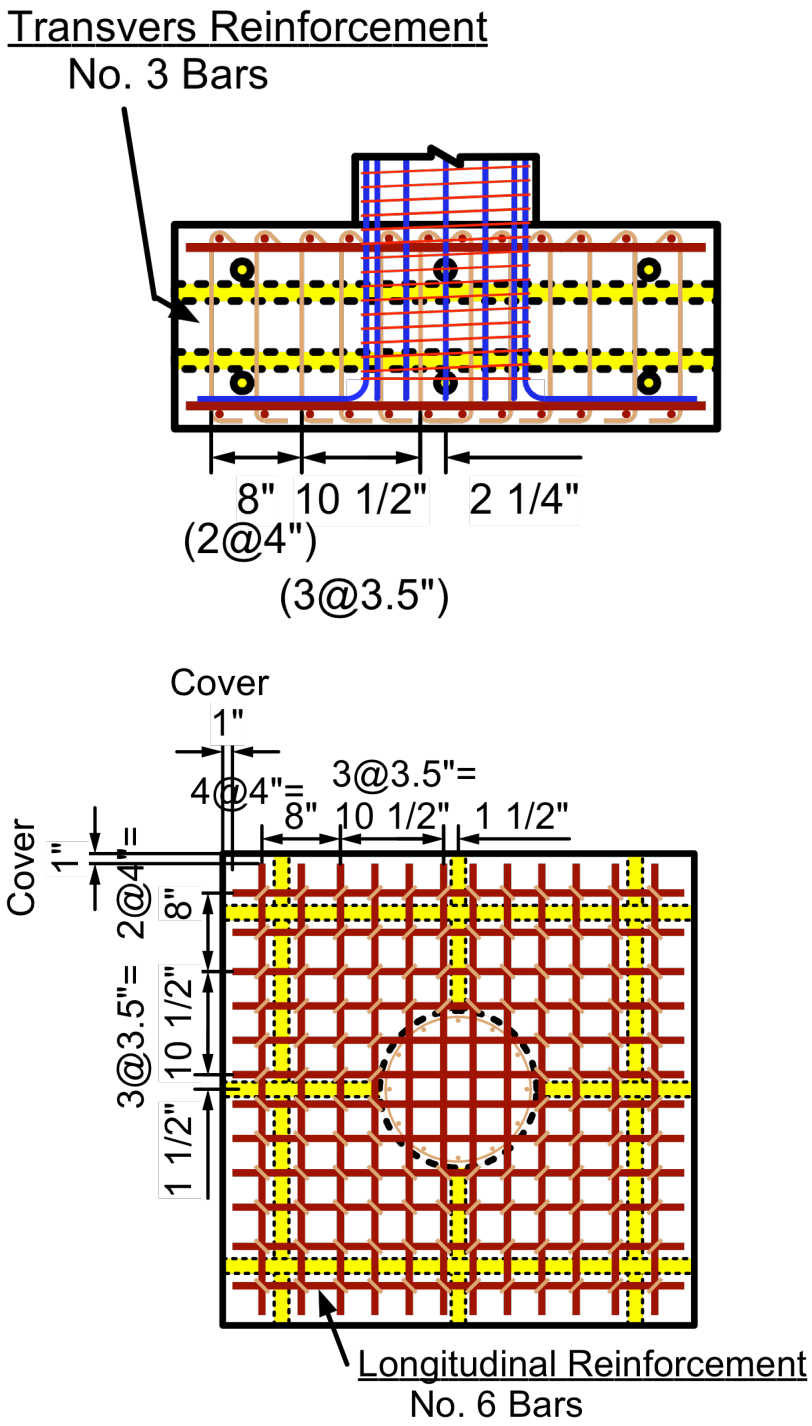

Figure 3-4: Footing Reinforcement Details

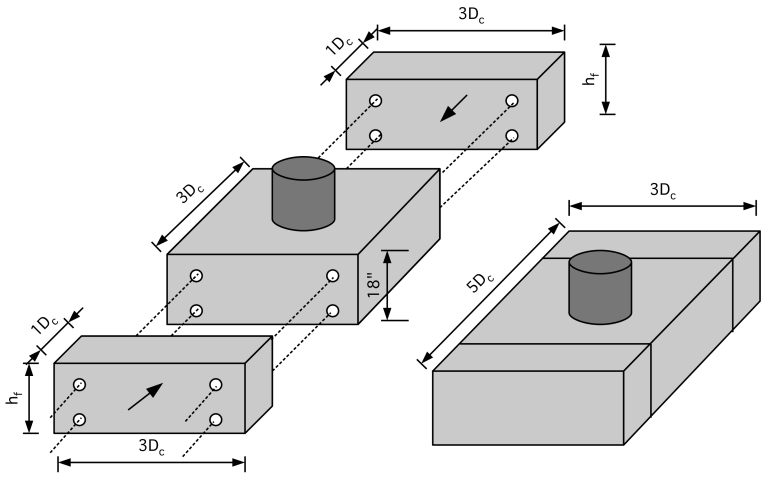

Figure 3-5: Footing Configuration for $3D_c$ x 5 D_c

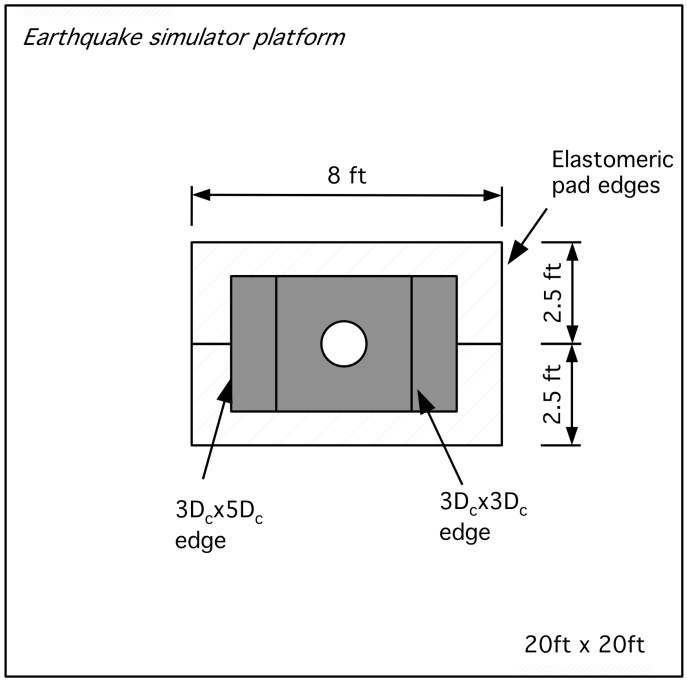

Figure 3-6: Elastomeric Pad and Footing Edges

3.4 Specimen Construction

To model the simple inverted pendulum, several options were considered. The design was governed by several factors including cost, ease of construction and use, safety, and method reusability for future testing of additional single column cantilevers. The design considered options previously erected for shaking table tests (e.g. Hachem et al., 2003) before deciding on a system where steel brackets would be post-tensioned to the top of the column to create a support frame which would support mass blocks to achieve the desired axial stress.

The construction site used an existing level platform, that was cleaned and prepared, as the bottom of the formwork for the test specimen as well as four other single column specimens that were not in the scope of the work presented herein. Formwork was erected for the footing as well as the blocks that would be used to widen the footing during testing (Figure 3-7). During this time the four longitudinal bars that were to have strain gauges were prepared and instrumented. The bottom layer of steel for the footings was placed as well as the steel necessary for the widening blocks of the footing. The column cage was next constructed using 12-No. 4 bars including the four instrumented bars with strain gauges (2 per bar along the bar height for a total of 8 gauges). Next, the cage was spirally reinforced along the column height with W3.5 wire (0.21 in diameter) at a pitch of 1.25 in. At the top of the column where the post-tensioned steel brackets were to connect, the pitch of spiral reinforcing was reduced to 0.5 in. The column cage was installed at the center of the footing and tied to the bottom steel layer (Figure 3-8). The top layer of footing reinforcement as well as the 2-in diameter PVC ducts to be used for widening the footing were then installed. PVC pipes extended along the entire length of the footing in each direction to create a connection for the widening blocks (Figure 3-9). The No 3. hooked bars for transverse reinforcement were then placed and the footing and blocks were ready to be cast.

The specified design strength of the footing was larger than the column, which required the footing and blocks to be cast separately (Figure 3-9). Several 6-in. diameter by 12-in. long cylinders were cast for testing concrete compressive strength at 7 days, 28 days, and the testing date as necessary. The slump of concrete, which had been specified as 5 in., was measured to be 3.5 in for the footing. After casting, the footing and blocks were covered with plastic sheathing and allowed to cure. Following the necessary curing time the joint area at the column-footing interface was sand blasted and cleaned in preparation for casting the column. A circular column form was placed that had holes cut to allow installation of additional instrumentation equipment. Threaded rods ½ inch in diameter were installed transversely through the holes in the column to provide a method of measuring curvature distribution along the column height (Figure 3-11). Wiring necessary for monitoring the strain gauge readings was guided along the longitudinal bars to an exit point at the column mid-height. At the top of the column formwork was added to create the block to which the steel brackets would be connected. PVC ducts and additional No. 3 transverse reinforcement were added as necessary for the design objective. The column and top block were then cast and allowed to cure for 28 days before removal of the formwork (Figure 3-12). Again, several 6 in x 12 in concrete cylinders were cast for measuring the concrete compressive strength at 7 days, 28 days,

and the shake table test date. The specified slump for the column was 5 in and measured as 9.5 in.

Figure 3-7: Footing Forms (Rocking Column at Top Right)

Figure 3-8: Column Cage and Footing Steel

Figure 3-9: Casting footing

Figure 3-10: Footing and Blocks before column casting (rocking column center of specimens)

Figure 3-11: Threaded rods for measuring column curvature

Figure 3-12: Column and Top Block (rocking specimen in center)

3.5 Measured Material Properties

3.5.1 Steel Reinforcement Properties

The column longitudinal steel was specified as ASTM A706, Grade 60 steel. Mechanical properties of the reinforcing bars were determined using tensile tests of sample steel coupons. The average values for three sample coupons for yield strength, ultimate strength, and modulus of elasticity of the No. 4 bars was 69.1 ksi, 90.9 ksi, and 29,090 ksi, respectively. See Figure 3-13.

The spiral reinforcement was specified as ASTM 82, Grade 80. No tensile tests were performed due to the absence of coupons for spiral samples. No certified mill test report was available for the spirals either.

3.5.2 Concrete Properties

The concrete for the columns was specified as normal weight with a 28 day strength of no less than 4 ksi and no more than 5.5 ksi, in order to represent the actual properties of concrete used in modern reinforced concrete bridges. Mix design details are presented in Table 3.2. Twenty seven, 6 in. x 12 in. standard cylinders were prepared at the casting of the column and were used to measure the concrete compressive strength and stress-strain relationship. As the forms from the footing and columns were removed so were the casings of the corresponding cylinders. Compressive strength tests were performed at 8 and 29 days after casting of the footing. Column concrete compressive strength tests were performed at 7, 14, 21, and 28 days after the column casting date. Additional cylinders were tested the day following the shake table test of each group.

At each test date, three cylinders were tested. The column concrete had a 28-day strength of 3.9 ksi, while the footing concrete had a strength of 5.25 ksi. The average strength of column concrete on testing day was about 4.7 ksi. The average tangent and secant modulus of elasticity of concrete for the specimen, which are defined by Eqn. (3-4) and Eqn. (3-5), were calculated to be 2,753 ksi and 2,453 ksi, respectively. Values from testing of the cylinders are presented in Table 3.3.

$$E_{c-\tan} = \frac{f_{c-50}}{\varepsilon_{c-50}} \qquad (3\text{-}4)$$

$$E_{c-\sec} = \frac{f_{c-50} - f_{c-25}}{\varepsilon_{c-50} - \varepsilon_{c-25}} \qquad (3\text{-}5)$$

3.5.3 Elastomeric Pad

The elastomeric pad was tested uniaxially with a cyclically increasing amplitude. The force was compression only. Load behavior was determined first by an initial application of a small force, removal of the load, then application of a larger force. This was repeated until the final load considered had reached a strain value that corresponded to a deflection equal to 7% of the pad thickness. See Figure 3-16. From compression data

the modulus of elasticity (E_{pad}) during the loading phase was calculated to be approximately 3000 psi ($\sigma=E_{pad}\,\varepsilon$) from best fit data (Eqn. (3-6)).

$$E_{pad} = \frac{\sigma_2 - \sigma_1}{\varepsilon_2 - \varepsilon_1} \qquad (3\text{-}6)$$

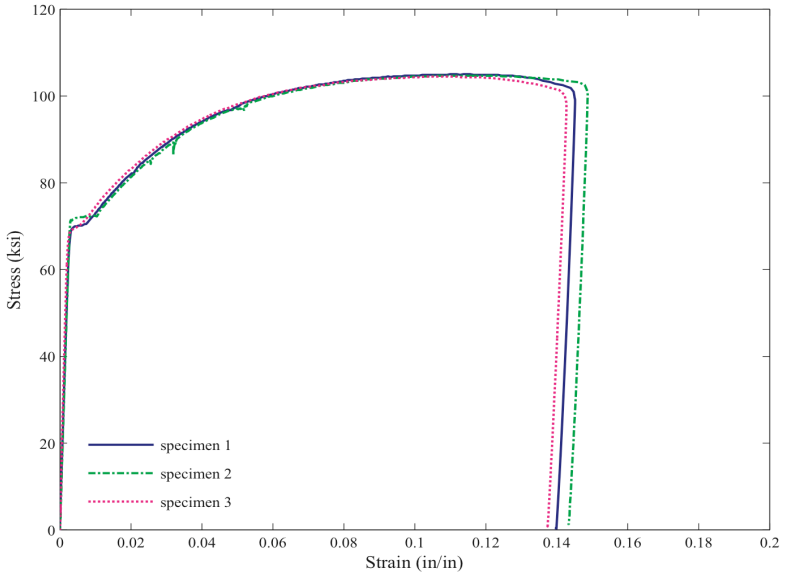

Figure 3-13: Stress-strain curve for grade 60 ASTM 706 bars

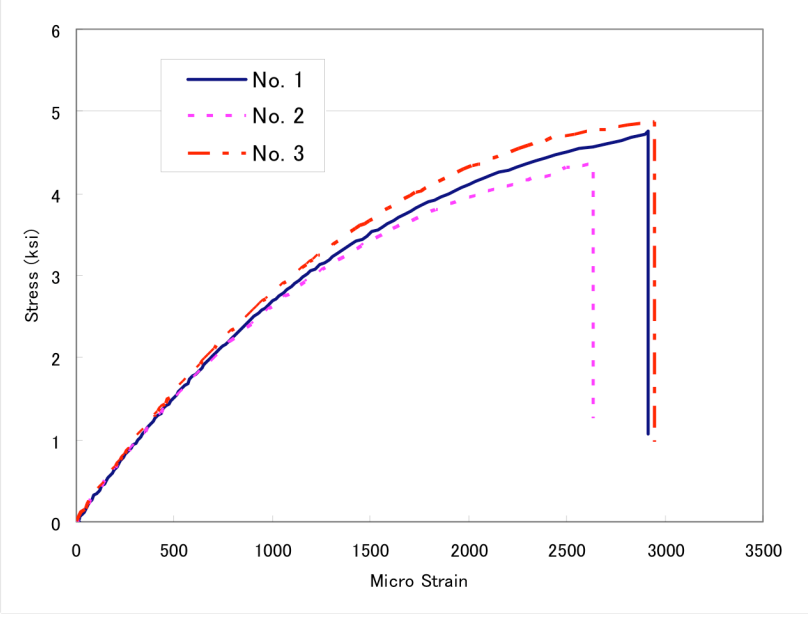

Figure 3-14: Stress-strain curve of concrete cylinders at test date

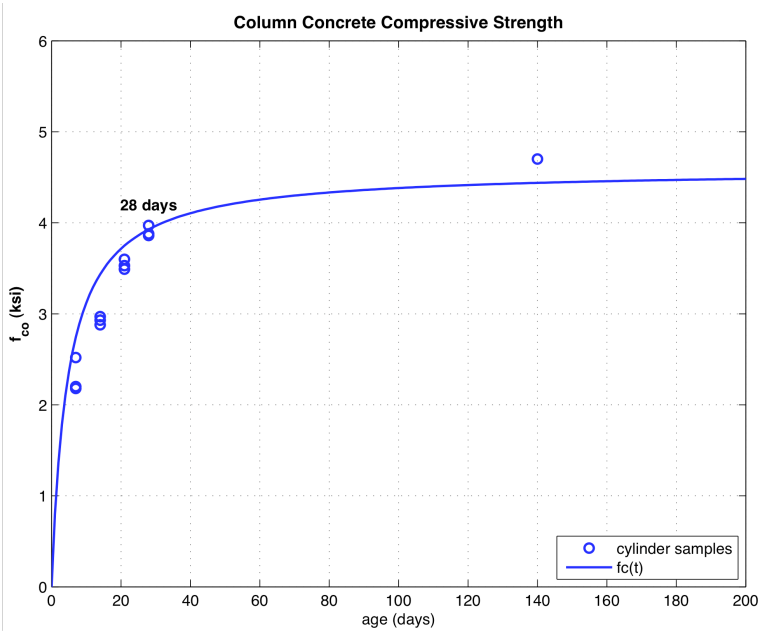

Figure 3-15: Column Concrete Compressive Strength vs. Age

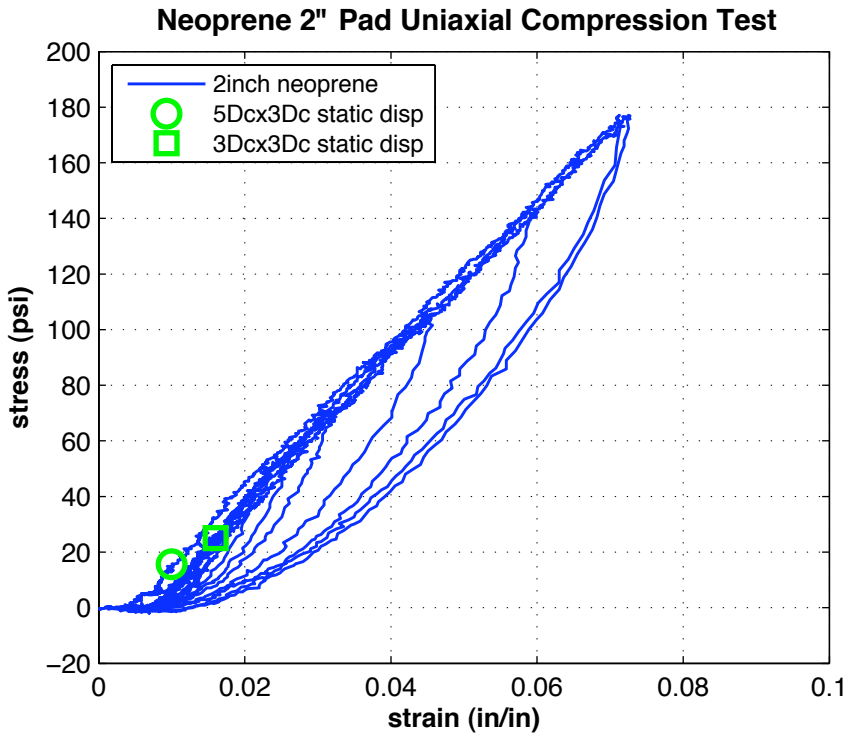

Figure 3-16: Stress-strain curve of compression test of 2-in thick elastomeric pad sample

Table 3.2: Concrete Mix Design

(a) Mix Specifications

Cement	ASTM C-150 TYPE II
Fly ash	ASTM C-618 CLASS F, 15%
Admixture (water reducer)	ASTM C-494 TYPE A
Minimum 28-day strength	3,850 psi
Maximum 28-day strength	4,350 psi
Cementitious sacks/yd^3	5.60
Maximum size aggregate	3/8”
Slump	5”
Water/cement ratio	0.603

(b) Mix Design and Quantities

Material	Specific gravity	Absolute volume	SSD weight
3/8” × #8 gravel	2.68	5.98 ft^3	1,000 lb
Regular top sand	2.67	9.02 ft^3	1,503 lb
SR blend sand	2.60	3.69 ft^3	599 lb
Cement Type II	*3.15*	2.27 ft^3	447 lb
Fly ash	*0.00*	0.55 ft^3	79 lb
Water	1.00	5.08 ft^3	317 lb
Water reducer	-----	0.41 ft^3	26.3 fl oz
Total	-----	27 ft^3	3,945 lb

Table 3.3: Compressive Strength of Column Concrete Cylinders

Day	No. 1 (ksi)	No. 2 (ksi)	No. 3 (ksi)	Average (ksi)
7	2.20	2.52	2.18	2.30
14	2.93	2.88	2.97	2.93
21	3.53	3.60	3.49	3.54
28	3.86	3.88	3.97	3.90

3.6 Test Setup

A series of shaking table tests was performed at the Earthquake Simulation Laboratory, located at the Richmond Field Station of the University of California, Berkeley. Three test group geometric configurations were selected for testing on the earthquake simulator: (1) a footing width of $3D_c$ x $3D_c$ with one weight block with a nominal axial load ratio of $3\%f'_cA_g$, (2) a footing width of $3D_c$ x $3D_c$ with three weight blocks with a nominal axial load ratio of $10\%f'_cA_g$, and (3) a footing width of $3D_c$ x $5D_c$ with three weight blocks with a nominal axial load ratio of $10\%f'_cA_g$. Figure 3-17 shows the specimen set up on the table for the second test group.

To simulate a rocking base at the bottom of the footing, two 8-ft long by 2.5-ft wide elastomeric pads with 2-in thickness were laid down initially side-by-side centered on the platform. No material was placed between the top of the table and the bottom of the pads. The pads were not fastened to the table, instead they were kept in place by utilizing friction from the normal load of the weight blocks, column and footing. Away from the platform, the steel brackets were connected to the specimen at the top of the column. The brackets were placed in pairs along each diagonal direction and fastened to each other using 1-1/8 in. high strength steel rods that passed through the steel connection plate, concrete block at the top of column and through the steel connection plate of the parallel bracket. For each face, a layer of grout was poured between the steel plate and concrete block to ensure uniform bearing stress and prevention of movement during testing. The column and steel brackets were then lifted and placed directly on top of the pads, centered on the table using a 20-kip capacity bridge crane. During transfer to the table care, was taken to prevent any cracking in the column. No material was placed between the top of the pad and the bottom of the footing.

The mass blocks were then placed on top of the steel brackets and connected using 1-1/8 in. high strength post-tensioning rods. Each bracket had a duct that corresponded with holes in the weight blocks and allowed a rod to pass completely through all of the elements. A total of four rods were used to make the weight block to steel bracket connections. At the interface between each block, block and steel bracket, and connection hardware high strength grout was used to ensure a uniform bearing stress and no-slip between the elements.

The initial test group used only one weight block to validate test setup, verify instrumentation and calibrate the analytic models used to plan the subsequent tests. The test set up for test group 1 is shown in Figure 3-20. For test group 2, the same procedure as test group 1was followed for preparing the table and specimen. However, three weight blocks were added to achieve the desired axial load ratio. Figure 3-18 shows the test specimen on the shake table. Upon completion of the second test group all the instrumentation was left in place with the exception of the footing instrumentation. The weight blocks were removed for safety purposes in lifting. The entire specimen was then lifted up 2 in using hydraulic jacks measured from the top of the pad to the bottom of the footing and shored in place for installation of the footing widening blocks. Two blocks measuring $1D_c$ wide by $3D_c$ long and 18 in. thick were connected to opposing footing faces using high strength rods and grout to create a wider footing size of $3D_c$ x $5D_c$. See

Figure 3-19(b). The specimen was then reset back to the original position and the three weight blocks were reinstalled.

To prevent collapse of the specimen during the tests, two steel chains were connected to each corner of the steel brackets. The length of each chain was adjusted to accommodate at least 10 in (10% drift) of lateral column displacement, which corresponds to the maximum displacement of previous fixed based tests. The safety chains were used to prevent overturning of the column and mass blocks. To prevent excessive movement by the footing from "walking" while up uplifting, turnbuckles were used to allow approximately 2 in. of lateral displacement during each test. The details of footing restraint are shown in Figure 3-19 and Figure 3-20.

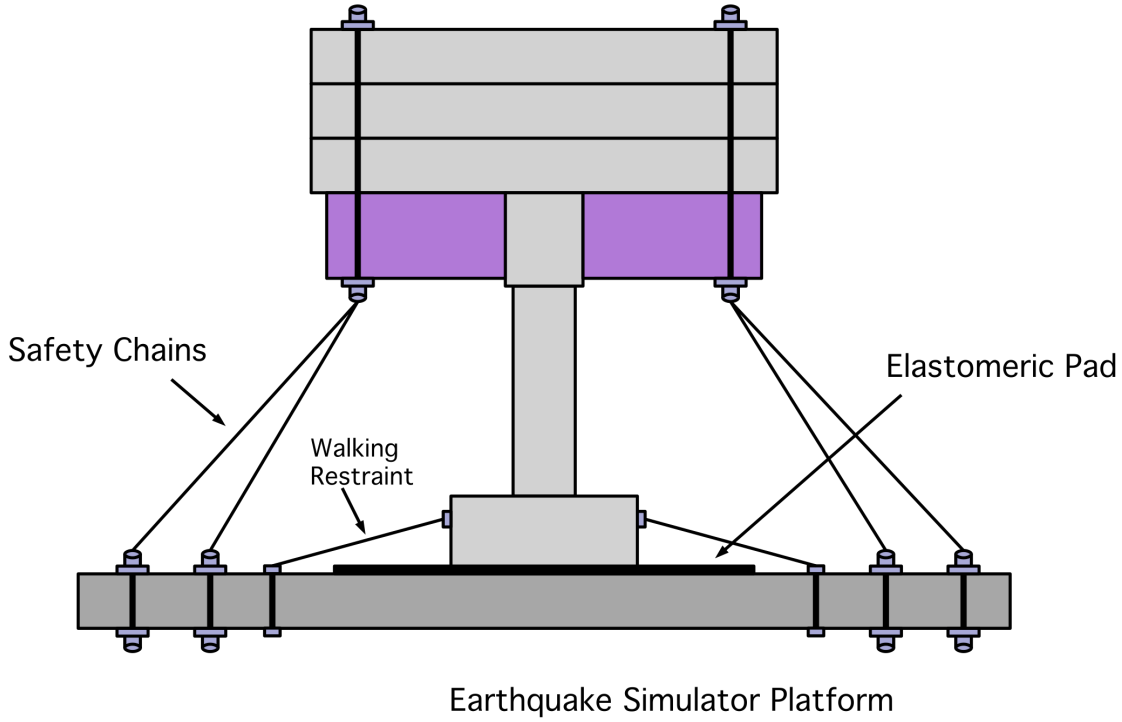

Figure 3-17: Group 2 Specimen Setup

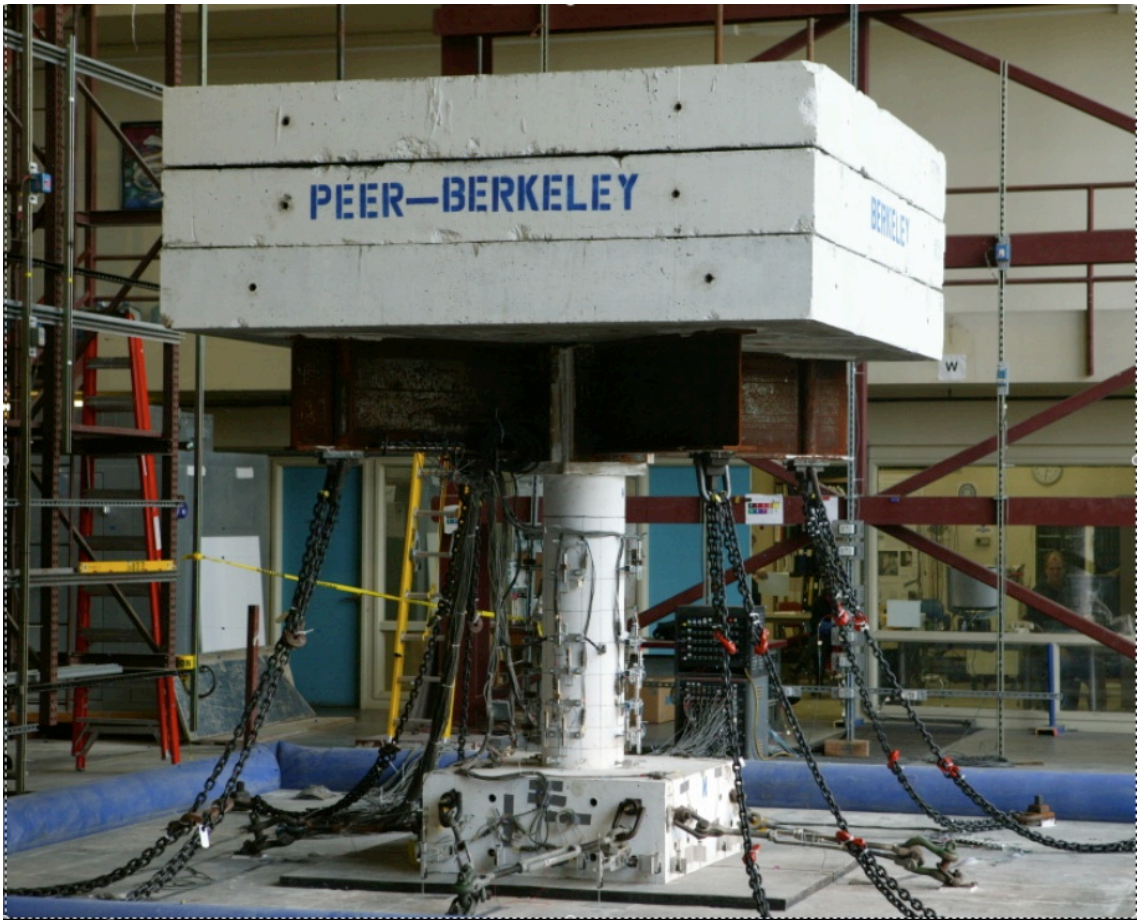

Figure 3-18: Group 2 Specimen

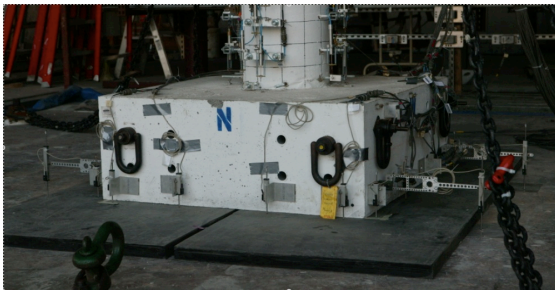

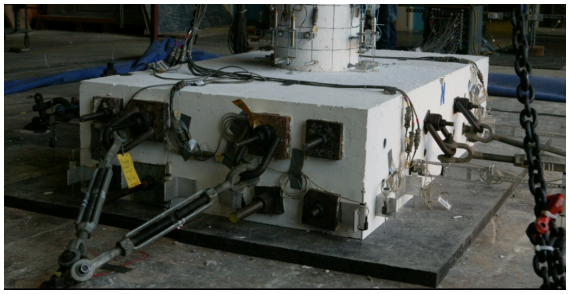

(a) Group 2 – Footing $3D_c$ x $3D_c$ **(b) Group 3 – Footing $3D_c$ x $5D_c$**

Figure 3-19: Footing Configuration with Safety Restraints

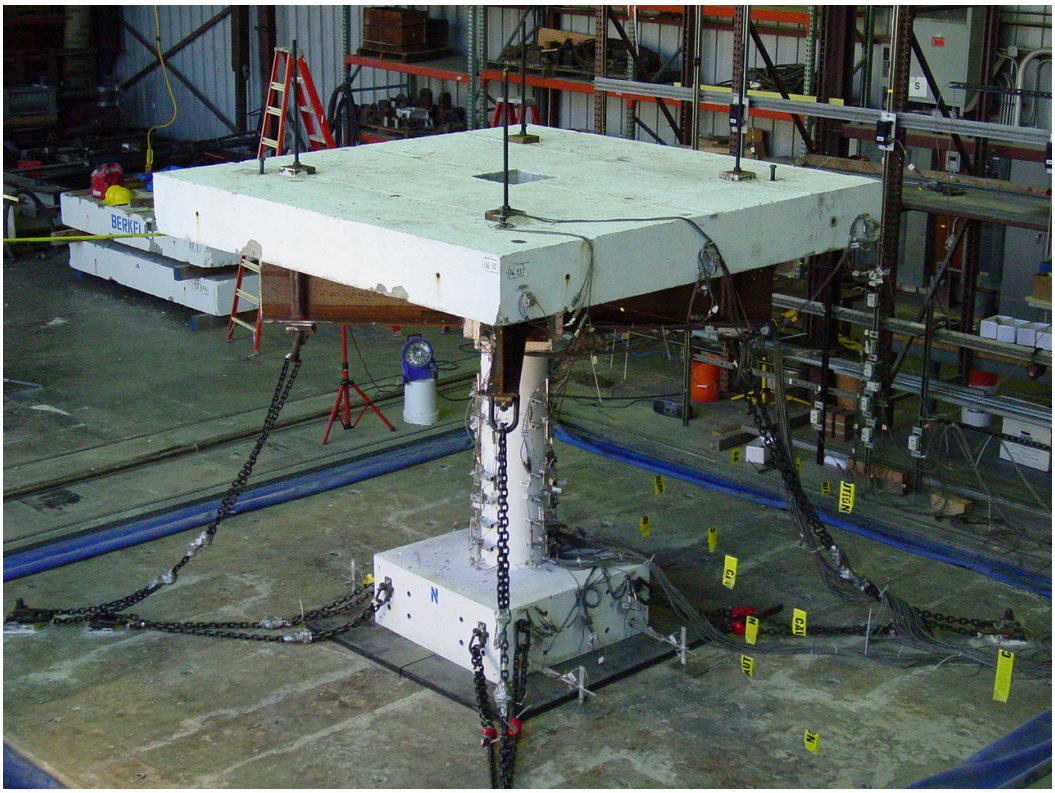

Specimen for Test Group 1

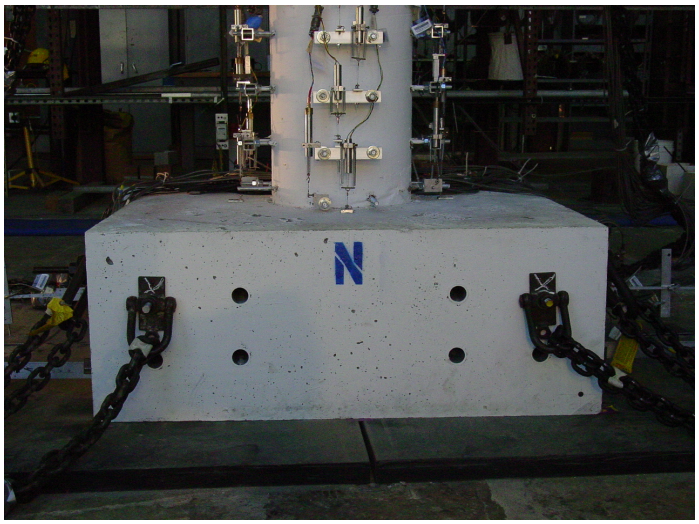

(b) Footing and Elastomeric Pad
Figure 3-20: Specimen Configuration for Test Group 1

3.7 Instrumentation

A vast instrumentation scheme was used to record the global response of the column, footing and local deformations and strain at specific locations. A total of up to 118 channels were used in each of the shaking table tests. The channels were occupied by a variety of instruments for measuring displacements, accelerations, strains and forces. The 118 channels were distributed as follows:

- 16 channels for monitoring the accelerations and displacements of the shaking table;
- 21 channels for accelerometers at weight blocks and footings;
- 28 channels for linear displacement potentiometers (LPs) monitoring global displacement;
- 24 channels for direct current displacement transducers (DCDTs) monitoring local column deformation;
- 8 channels for strain gauges measuring longitudinal reinforcing strain;
- 20 channels for Novotechniks (NOVO) monitoring footing uplift displacement;
- 1 channel for a linear voltage displacement transducer (LVDT) monitoring the displacement at center-of-gravity during free vibration test; and
- 1 channel for load cell monitoring of the pullback force during the pullback test.

A more detailed overview of the distribution on the three test groups is presented herein. The data was sampled at a rate of 200 Hz (0.005 sec). The sign convention for the global system is presented in Figure 3-21: Specimen Global Sign Convention. The origin of the coordinate system was located in the xy-plane at the center of the column. The origin of the z axis was assumed at the bottom of the footing.

3.7.1 Shaking Table Instrumentation

A total of 16 channels are used to capture the movement of the shaking table. Horizontal accelerations and displacements were monitored through four accelerometers placed on the stiffening beams under the table and four displacement transducers acting along the outer horizontal actuators. Vertical accelerations and displacements were monitored through four accelerometers and four displacement transducers placed near the four corners of the table. This instrumentation allows for computation of acceleration and displacement components in all 6 degrees-of-freedom of the shaking table motion. See Figure 3-22 for a diagram of the shake table instrumentation.

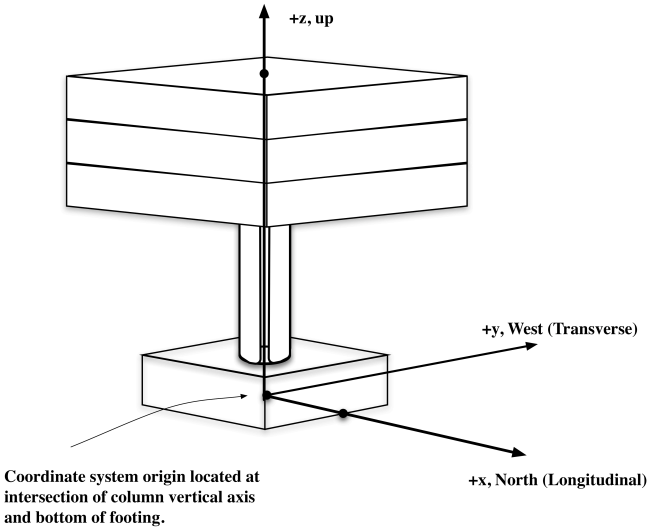

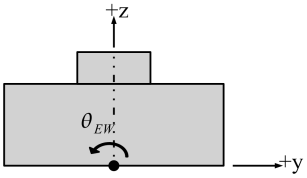

(b) YZ Plane of Footing

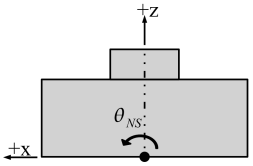

(c) XZ Plane of Footing

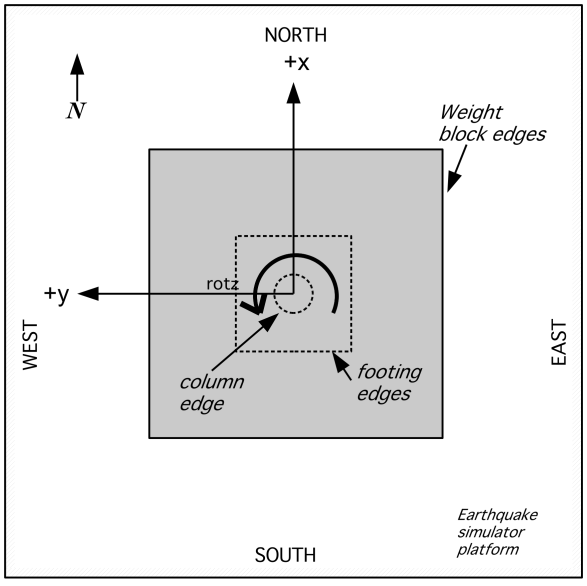

(d) Table in Plan View

Figure 3-21: Specimen Global Sign Convention

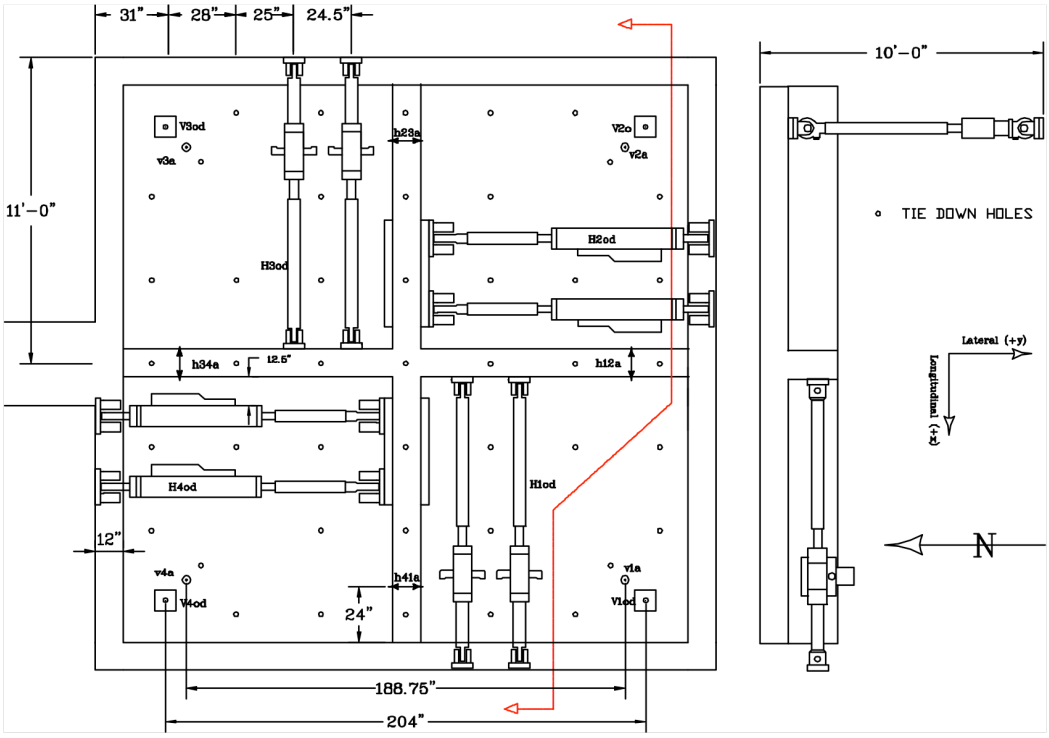

Figure 3-22: Shaking Table Instrumentation

3.7.2 Accelerometers

Accelerations were measured by 21 accelerometers mounted at seven separate locations on the specimen and weight blocks. Each location had a cluster of 3 one-dimensional capable accelerometers that were oriented in the x, y, and z orthogonal directions. Three groups were located on the weight blocks at the center-of-gravity elevation on the West and South faces and on top of the blocks. The remaining four groups were located on the West and South footing faces. See Figure 3-24 through Figure 3-26 for depiction of the accelerometer locations of the three test groups. Each accelerometer group was positioned to coincide with a global displacement measurement using a linear potentiometer.

3.7.3 Linear Potentiometers (LPs)

Global displacements were directly measured by linear potentiometers (LP) that were installed on stiff frames located off the shaking table at the West and South faces. A total of up to 28 potentiometers shown in Figure 3-24 through Figure 3-26 were used for the three test groups. Five potentiometers were used for each face of the weights blocks: one at the center-of gravity of the weight block assembly, two along the top near the corner edges and two more along the bottom near the corner edges. Rotational movement of the weight block assembly was captured by the pairs located near the edges. The movement of footing, including rotation about the vertical axis of the column, was monitored using three potentiometers on each footing face along the top edge: one at the center and two at the outer corners.

Local deformation of the column was captured by six linear potentiometers on the west and south faces. They were used to measure the shape of the column during testing and were located along the center line of each face at heights of 6 in., 12 in., 18 in., 24 in., 38 in., and 44 in. from the bottom of the column.

3.7.4 Direct Current Displacement Transducers (DCDTs)

Twenty-four direct current displacement transducers (DCDTs) were used to measure the relative vertical displacement between different sections along the height of the column. The data was then used to measure the approximate curvature over a region of height h. Figure 3-24 through Figure 3-26 show the locations of the DCDTS along the column height for each of the test groups. Figure 3-23 shows an expanded view of the DCDT typical column configuration.

For DCDT instrumentation implementation, the ½ in. threaded rods installed through the column during construction were used. The rods were located at heights of approximately 1 in., 6 in., 12 in., 18 in., 24 in., and 38 in. The DCDTs were connected to aluminum tubing and fastened to the threaded rod such that they were located approximately 3-1/2 in. from the column surface. Actual horizontal distance between the DCDTs and the column surface, and vertical distance between the rods and the surface of the footing or top slab were measured prior to each test. The readings from the pairs of DCDTs located at the 1 in. and 6 in. heights were used to estimate the amount of rebar pullout from the footing.

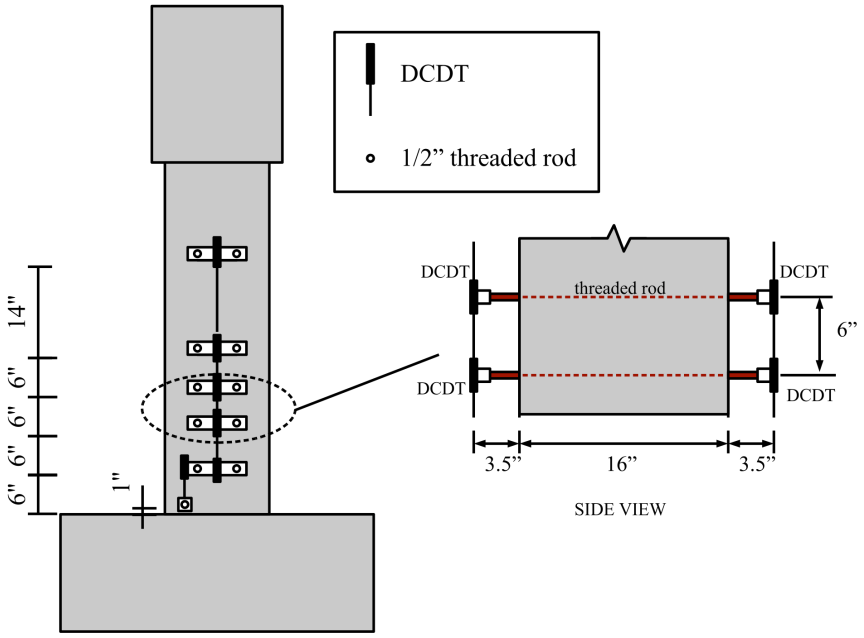

Figure 3-23: DCDT Configuration Along Column Height

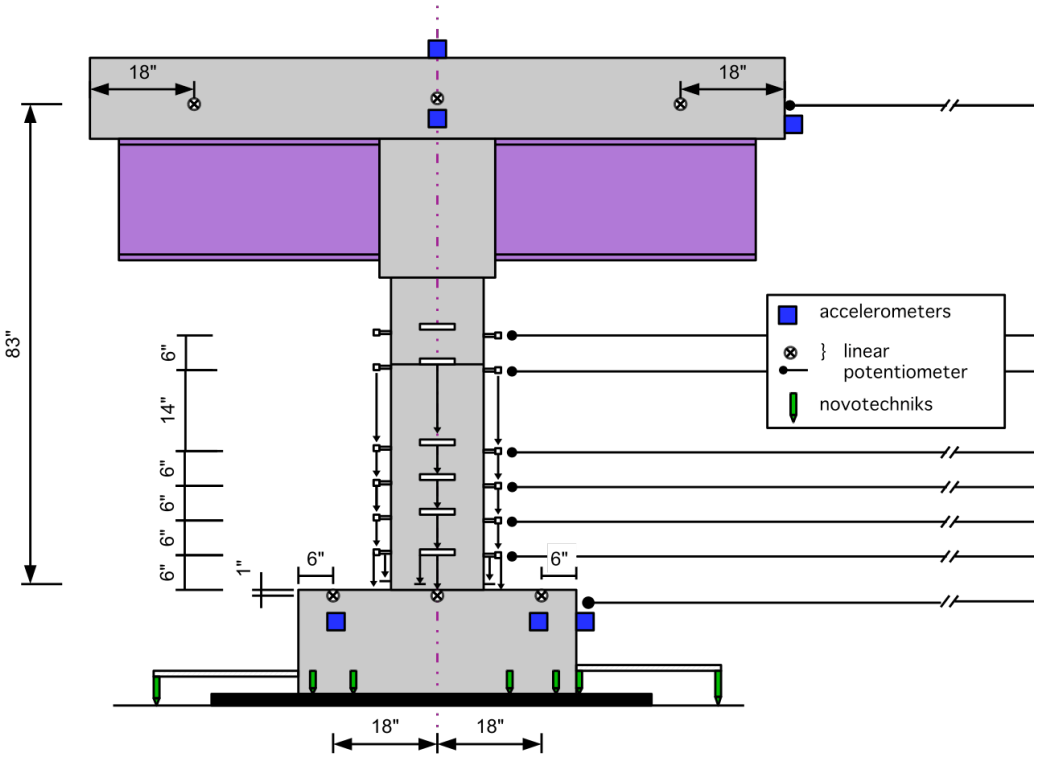

(a) Specimen Instrumentation Elevation Details

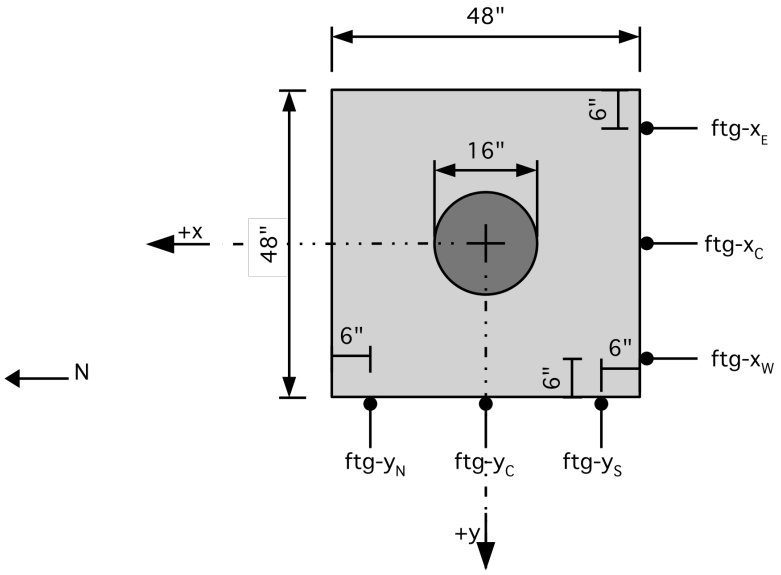

(b) Footing Linear Potentiometer Locations

Figure 3-24: Group 1 ($3D_c$x$3D_c$ Footing) Instrumentation Details

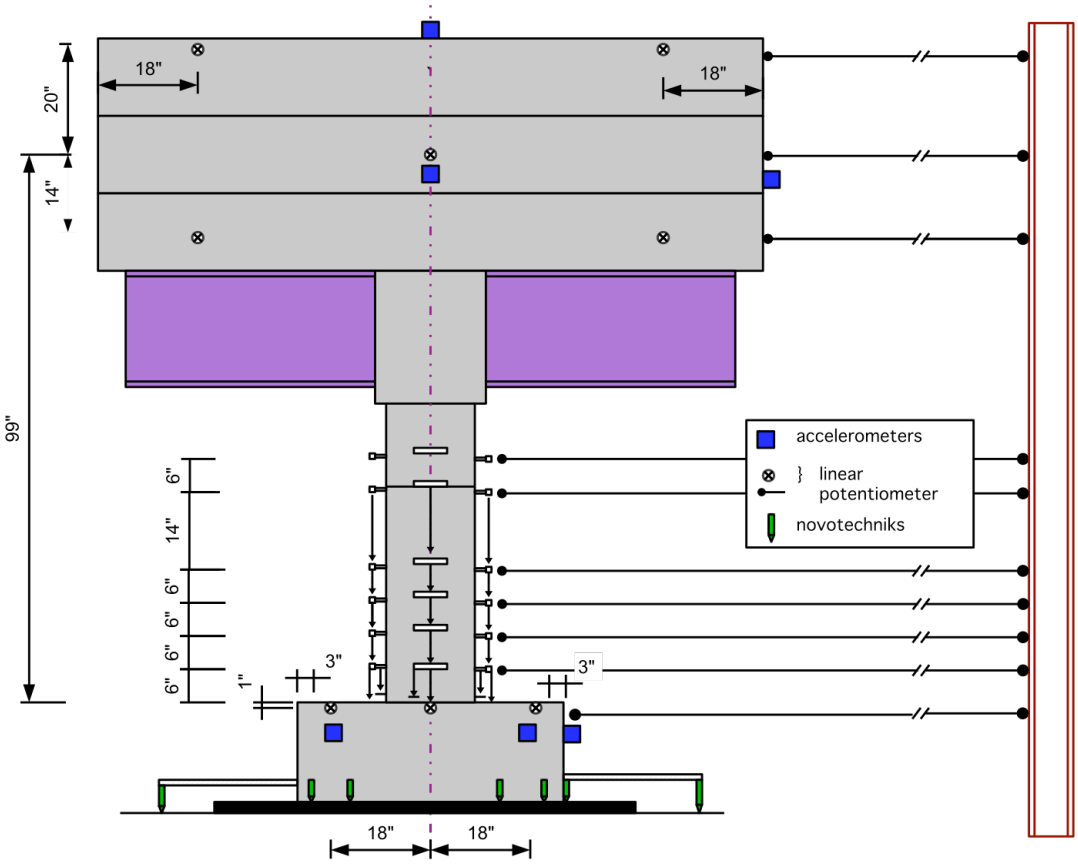

(a) Specimen Instrumentation Elevation Details

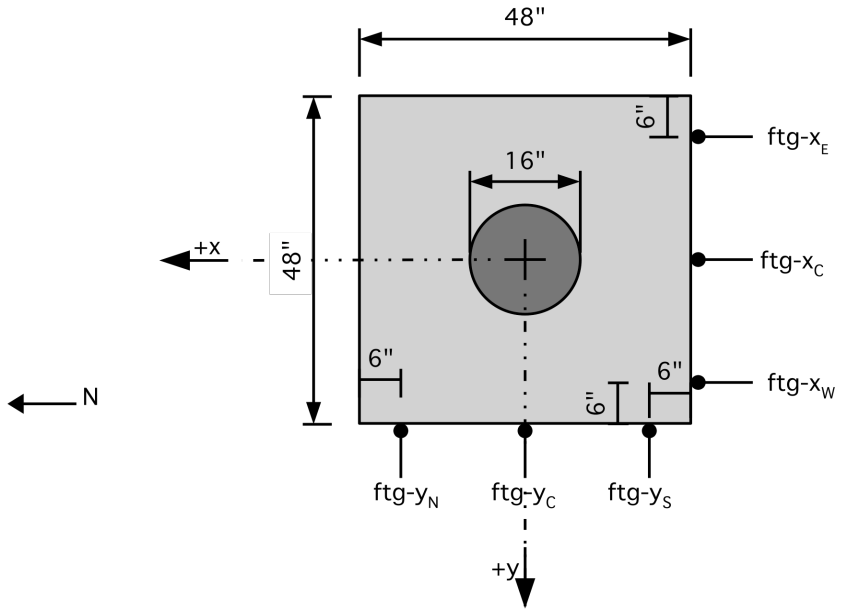

(b) Footing Linear Potentiometer Locations

Figure 3-25: Group 2 (3Dcx3Dc Footing) Elevation of Instrumentation Details

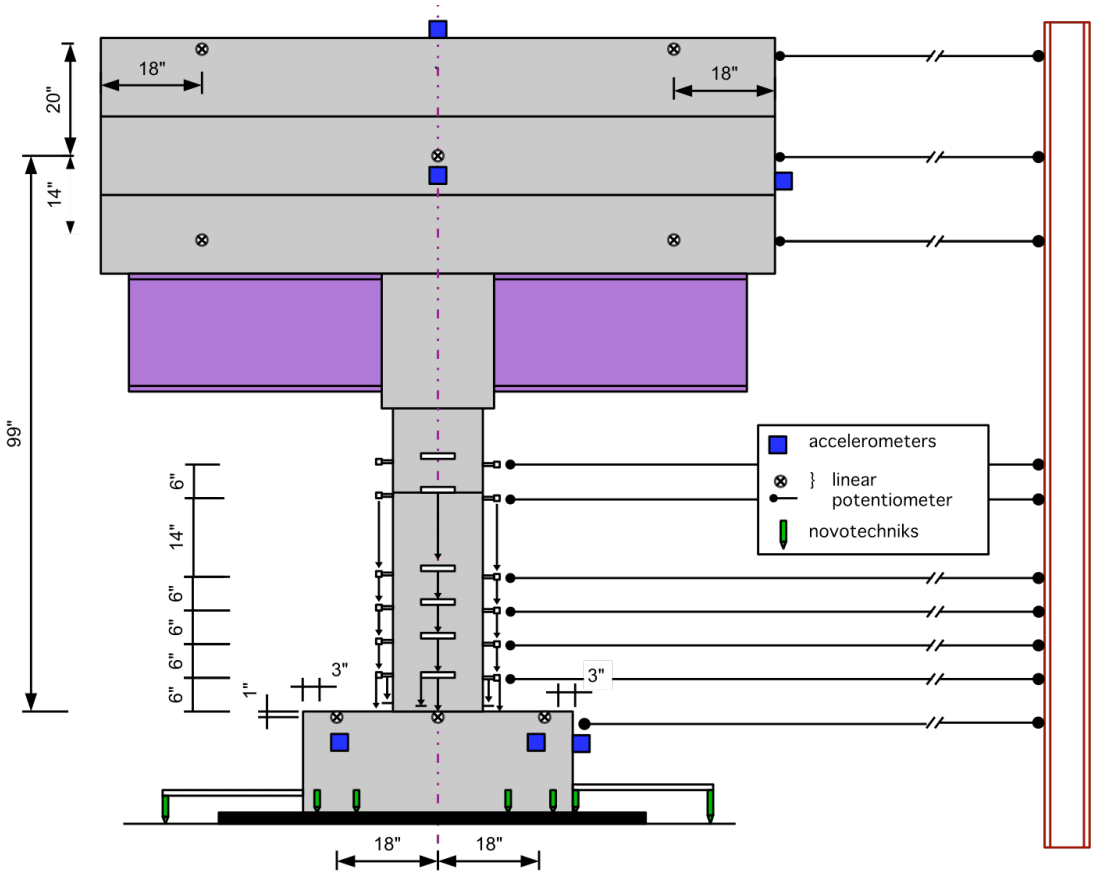

(a) Specimen Instrumentation Elevation Details

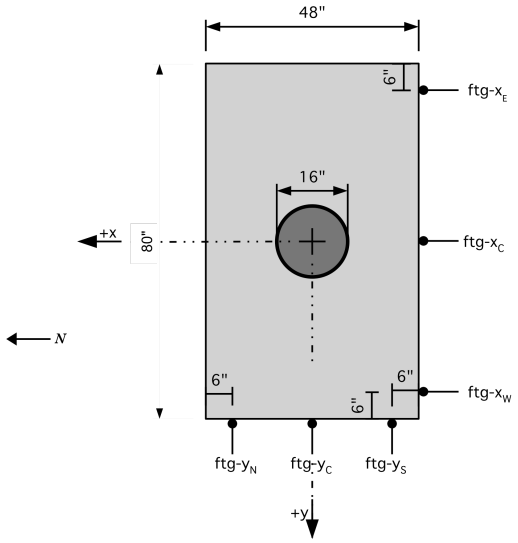

(b) Footing Linear Potentiometer Locations

Figure 3-26: Group 3 (3Dcx5Dc Footing) Elevation of Instrumentation Details

3.7.5 Strain Gauges

A total of 8 strain gauges were used to monitor strain of longitudinal reinforcement in the specimen. Four reinforcing bars, located at the north, east, south, and west sides, were gauged and protected with coating materials prior to construction. The position of the gauges was on the outside face of the rebar. The gauges were located slightly above the top of the footing and 16 in above the top of footing. See Figure 3-27 for the typical strain gauge location. These locations were chosen to approximate the expected plastic hinge length based on methods by Priestly et al. (1996).

3.7.6 Novotechniks (NOVOs)

A total of 20 Novotechniks (NOVOs) were used to monitor uplift displacement of the footing during testing. Measuring uplift during testing was critical to determining the rocking behavior of the system. To do this, four NOVOs were placed on each face of the footing to measure relative displacement between the footing and the pad. In addition, two pairs of outrigger arms were rigidly attached to the footing and used to support NOVOs that measured the relative displacement between the tip of the outrigger and rigid slab of the simulator. Figure 3-28 and Figure 3-29 show the locations of the Novotechniks for each test group and configuration. To accurately capture the pad displacement before each test, snapshot readings were taken as each new load was applied. This information was used to distinguish when the system was simply rocking or also uplifting from the pad.

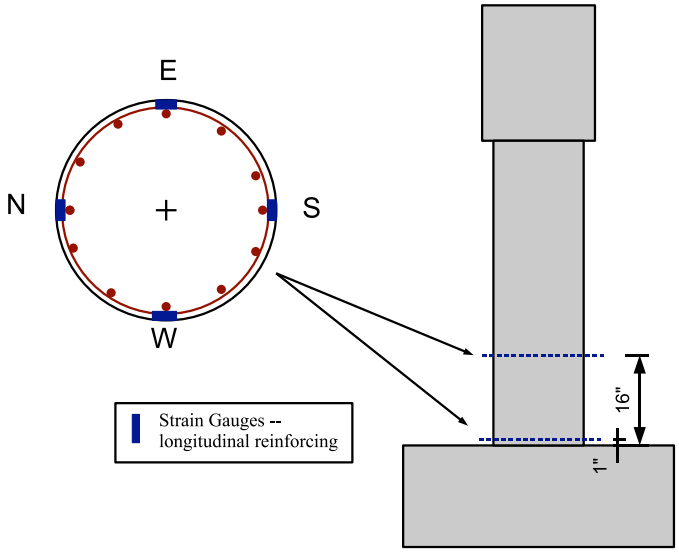

Figure 3-27: Strain Gauge Locations

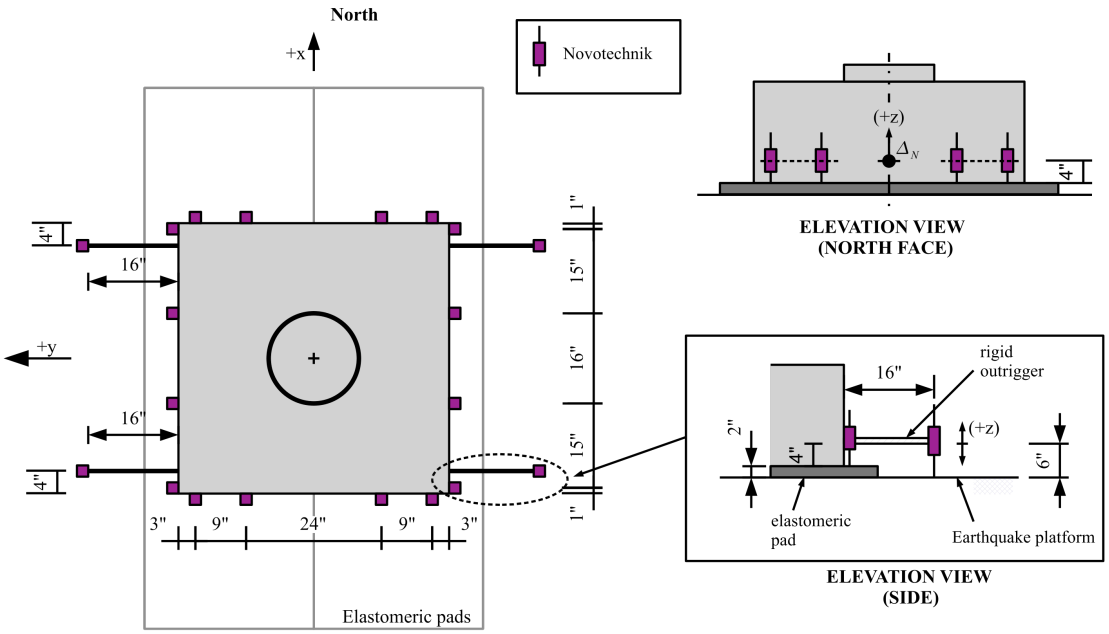

Figure 3-28: Novotechnik Locations (Test Groups 1 & 2)

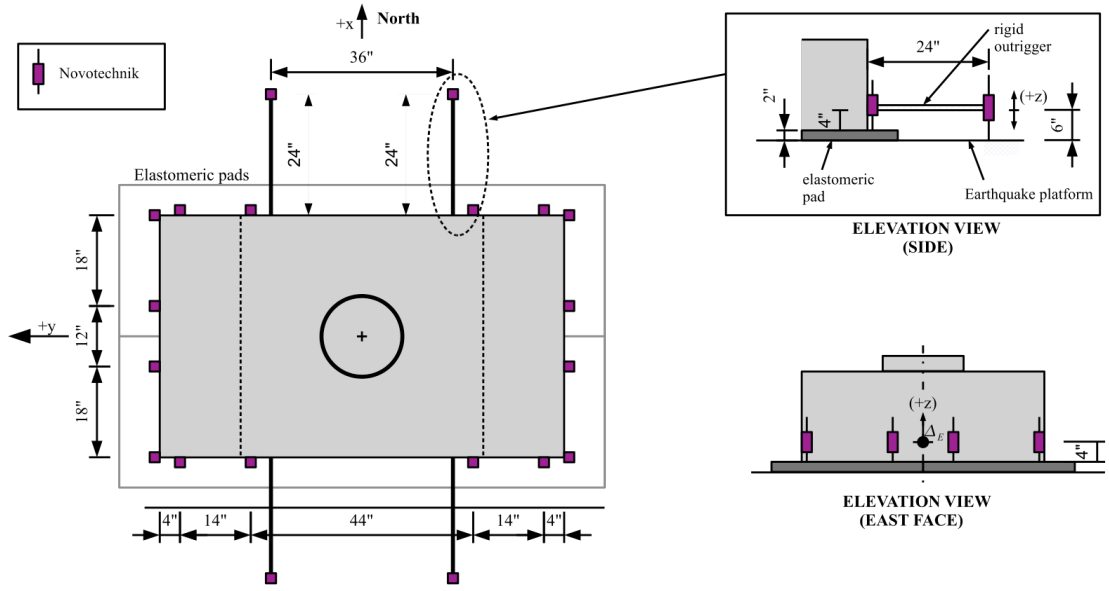

Figure 3-29: Novotechnik Locations (Test Group 3)

3.8 Data Acquisition

During the tests, data was recorded by the shaking table's data acquisition software system. Each instrument of the system was calibrated using distinct cables. Data was recorded at a 200 Hz interval (0.005 sec) and saved to a text file. Each text file began with a header row whose first entry was the date and time stamp followed by a unique column entry for each instrument name. The text file was recorded as a MxN array where M equaled one (for the header row) plus the number of time samples and N equaled one (for the time stamp) plus the number of instruments. Data recording was initiated a few seconds prior to the beginning of each earthquake signal and continued for several seconds following the end of each record to capture the free vibration response.

3.9 Test Specimen Documentation

In addition to the digital data recorded, digital videos were taken during the test to document specimen behavior and the progression of localized damage. Five video cameras were used simultaneously: two focused on the bottom portion of the column – where the plastic hinge was expected to be developed at the east and north faces and capture uplift – and two cameras were used to capture the global response of the specimen from the east and north sides. The last camera was set along the diagonal axis to capture global movements. Digital photographs were taken prior to and after each test to document localized damage of the column. In the interim between tests, new concrete cracks that occurred during the tests were traced by hand and color coded for easy representation.

The specimens were painted white prior to testing and a grid was drawn in black marker on the column to sub-divide and readily identify regions. The grid resolution was drawn by sub-dividing the column into 4-in tall segments, that were approximately 30-degrees wide (~4.2 in). Each footing face, column face, and weight block face were marked with a W, S, E, and N respectively.

3.10 Ground Motions

As mentioned in Section 1.3 two ground motions were used for testing each of the three group configurations. Each test group was subjected to one-, two-, and three-directions of excitations of the two ground motions.

3.10.1 Preprocessing of the recorded motions

Processing was done on both of the records to accommodate the displacement, velocity, and acceleration thresholds that could be delivered by the shake table. The three dimensional components of each record were processed in a similar manner. First, the recorded time step was reduced by the square root of the length scale factor (See Table 3.1). The magnitude of amplitude was left unchanged. Next the ground motion was band passed filtered to remove unwanted frequency components. The frequency characteristics of the band pass filter included two cut-off points and two corner points. Finally the amplitude of acceleration was scaled to meet the desired testing level. The

design level was scaled such that the spectral acceleration of the record matched the target design spectrum at the period of the specimen.

3.10.2 1989 Loma Prieta Earthquake (Loma Prieta record)

Each of the test groups was subjected to a modified version of the Los Gatos (USGS 16 LGPC) record of the 1989 Loma Prieta earthquake. The record was representative of a strong intensity near-fault forward-directivity ground motion. The specific records used were the two horizontal plus vertical components for the NF03 and NF04 motions of the SAC Steel project. The Loma Prieta earthquake had a moment magnitude of M_w=6.9. The Los Gatos records were recorded at a distance of 2.4 miles (3.9 km) from fault rupture and a hypocentral distance of 15.9 miles (25.4 km). The soil conditions were classified as "soft rock" with a shear wave velocity of approximately V_{s30}= 1560 ft/sec (478 m/s). The record peak values were measured as PGA 0.78g, PGV 30.4 in/sec (78 cm/sec) and PGD 16.8 in (42.7 cm). Fault normal and fault parallel components were defined by NF03 and NF04 respectively. The vertical component was from the record NF03_04v. The ground motion was chosen because in preliminary analysis it was shown to cause large permanent displacements. Such a ground motion was considered useful in determining the characteristics of systems allowed to uplift and yield. The records were scaled assuming a length scale factor of 4.5. Thus, the time duration was scaled by √4.5 (~2.12). The original records were band pass filtered using cutoff frequencies of 0.4 Hz and 15 Hz and corner frequencies of 0.5 Hz and 12 Hz.

Figure 3-31 and Figure 3-32 show the horizontal and vertical components before and after band pass filtering. Each figure includes a plot of the (a) Fourier Spectrum, (b) acceleration time history, (c) velocity time history, and (d) displacement time history. For test groups 1 and 2 the fault normal (stronger direction) and fault parallel (weaker direction) components were oriented along +x axis (North-South) and +y axis (East-West) directions, respectively. For test group 3 the orientation of components was rotated 90-degrees to place the strongest ground motion component in-line with the wider footing dimension. The peak ground acceleration, velocity, and displacement of the filtered records are 0.74g, 29.1 in/s and 4.8 in., respectively.

3.10.3 1978 Tabas, Iran Earthquake

Test groups 1 and 2 were subjected to a modified version of the 1978 Tabas, Iran earthquake. The site was located 1.25 miles (2 km) from the epicenter and had a moment magnitude of Mw=7.4. The ground motions used were from the SAC-Steel Project records NF01, NF02, and NF01_02v which were the fault normal, fault parallel, and vertical components, respectively. These records were representative of a strong intensity near-fault forward-directivity ground motion. The soil was described as "rock" and had a shear wave velocity of approximately V_s=2520 ft/sec (770 m/s). The records were scaled assuming a length scale factor of 4.5, thus the time duration was scaled by √4.5 (~2.12). The original records were band pass filtered using cutoff frequencies of 0.1 Hz and 15 Hz and corner frequencies of 0.2 Hz and 14 Hz. The record peak values were measured as PGA 0.84g, PGV 42.5 in/sec (108 cm/sec) and PGD 26.8 in (68 cm).

Figure 3-30 and Figure 3-32 show the horizontal and vertical components before and after band pass filtering. Each figure includes a plot of the (a) Fourier Spectrum, (b)

acceleration time history, (c) velocity time history, and (d) displacement time history. For test groups 1 and 2 the fault normal (stronger direction) and fault parallel (weaker direction) components were oriented along +x axis (North-South) and +y axis (East-West) directions, respectively. The peak ground acceleration, velocity, and displacement of the filtered records are 0.84g, 18.6 in/s and 4.8 in., respectively.

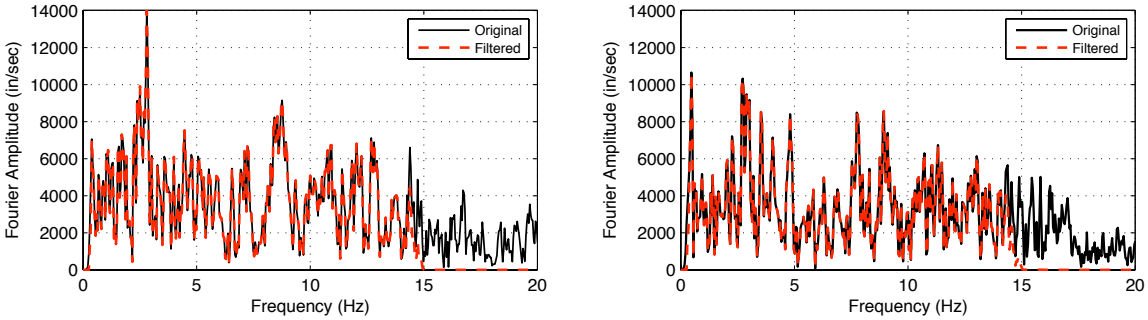

(a) Fourier Spectra

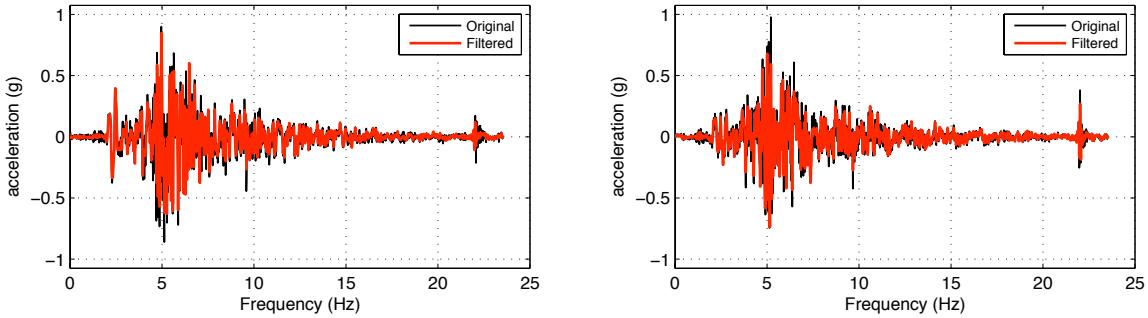

(b) acceleration time history

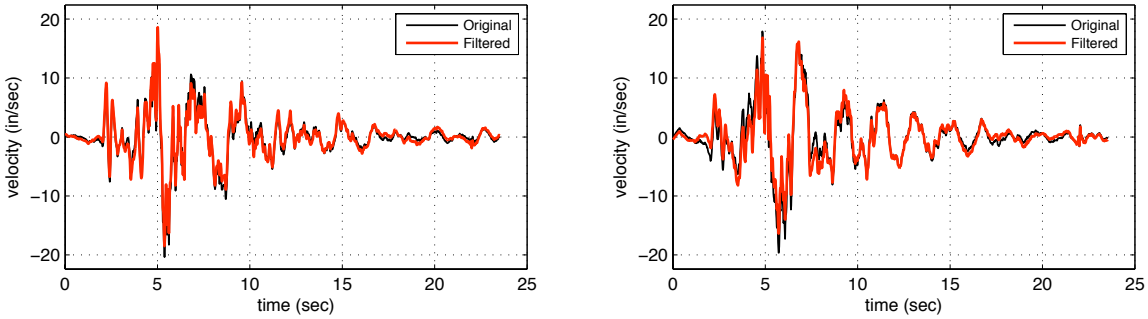

(c) velocity time history

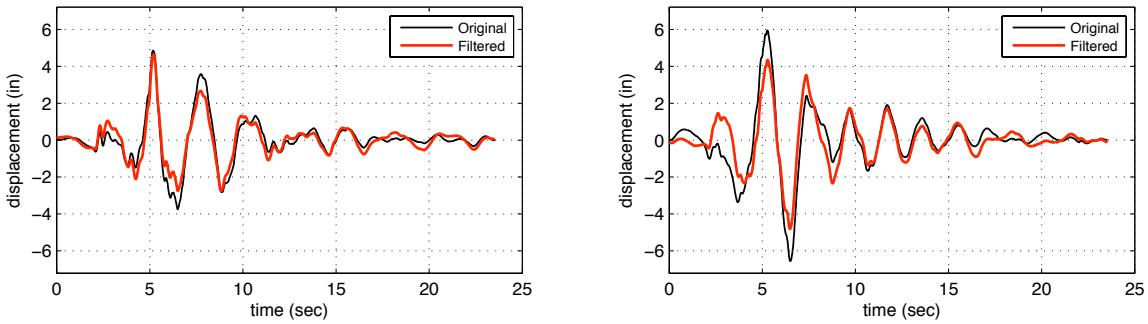

(d) displacement time history

Fault Normal Component Fault Parallel Component

Figure 3-30: NF01 and NF02 Horizontal Filtered Ground Motion

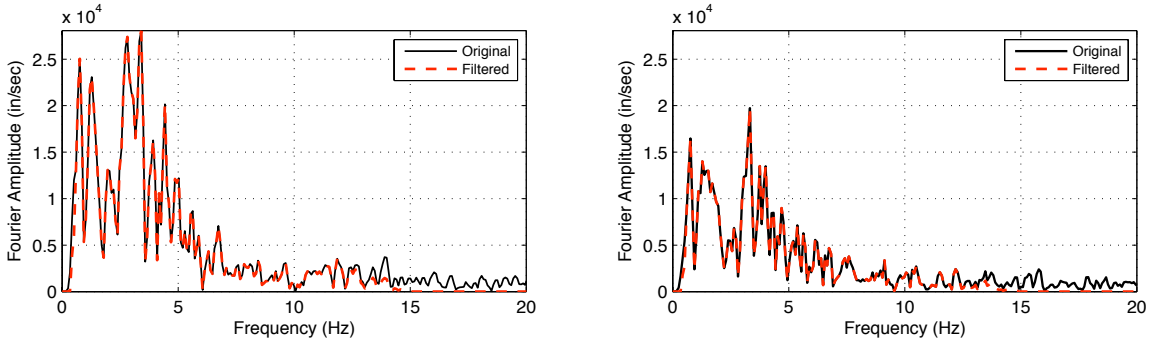

(a) Fourier Spectra

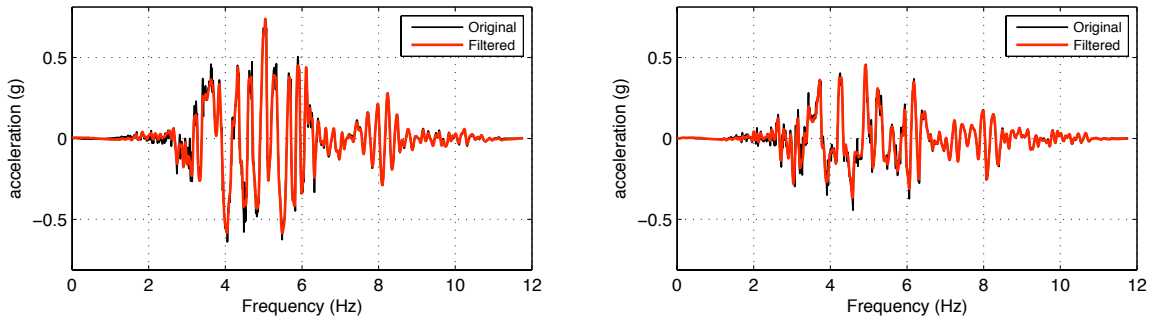

(b) acceleration time history

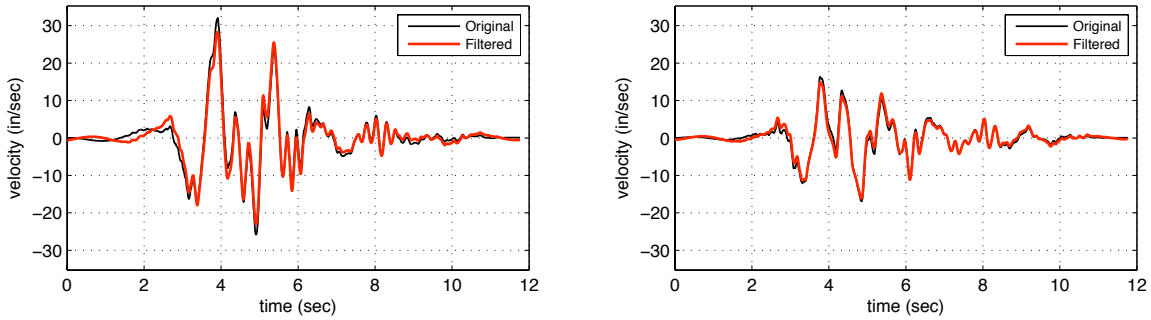

(c) velocity time history

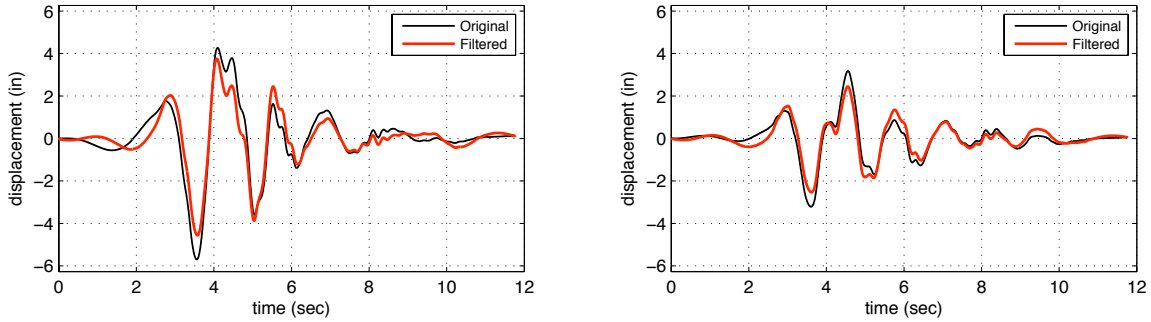

(d) displacement time history

Fault Normal Component Fault Parallel Component

Figure 3-31: NF03 and NF04 Horizontal Filtered Ground Motion

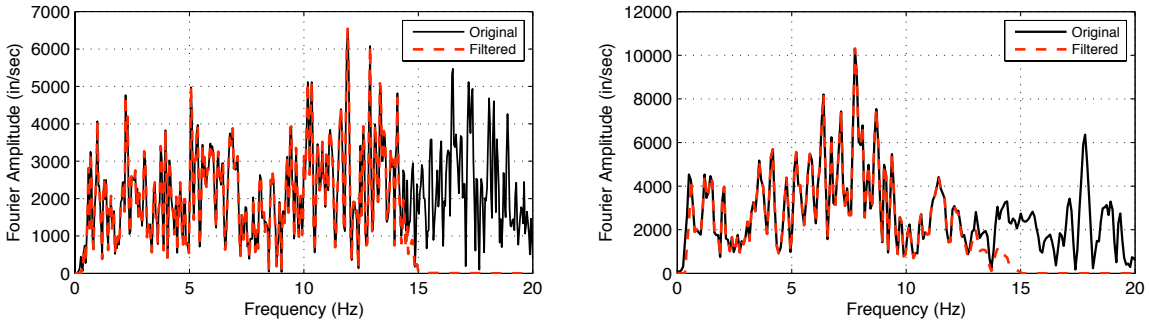

(a) Fourier Spectra

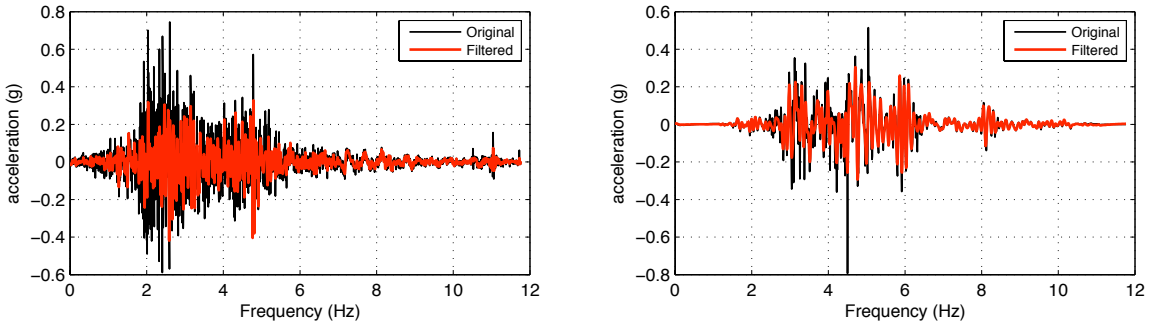

(b) acceleration time history

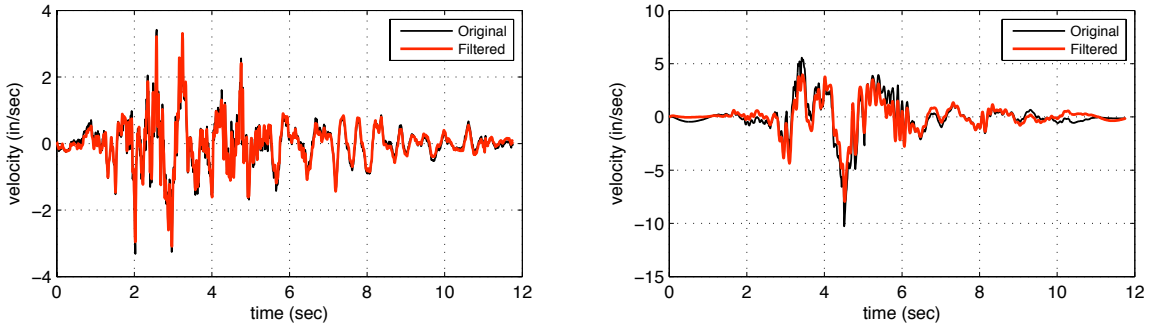

(c) velocity time history

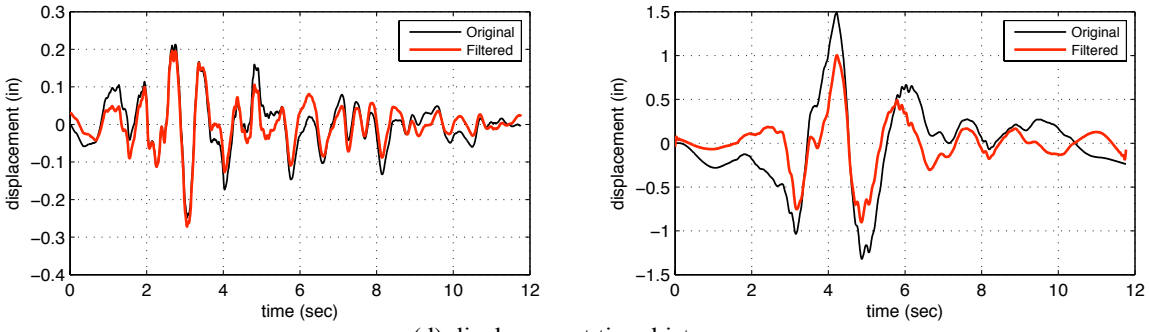

(d) displacement time history

NF01/NF02 Vertical NF03/NF04 Vertical

Figure 3-32: Vertical Filtered Ground Motion

3.11 Test Sequence

3.11.1 Pullback (Free Vibration) Test

Prior to the shaking table tests, each specimen was subjected to pullback tests to investigate dynamic properties of the specimen in the *x* and *y* directions. A cable was attached on both ends at an anchor on the laboratory floor and the center-of-mass of the weight blocks. The cable assembly included a come-along winch for pulling back the specimen and a load cell to measure the corresponding force at the anchor end and a small diameter machine bolt at the other end to be cut. A linear potentiometer was placed at the center-of-mass on the opposing face (connected to the instrumentation frame) to measure displacement. A 1.0 kip force was applied to the mass blocks using the come-along winch and the bolt was then cut to initiate free vibration motion. To prevent the table from moving wood blocks were placed in the gap between the simulator platform and outer edges. Displacement and accelerations were recorded to determine the natural period and damping ratios of the systems.

3.11.2 Shaking Table Test

Following the free vibration test, a series of shake table tests were conducted. There were three test groups selected that varied the footing size, axial load, and earthquake intensity These were presented previously and are shown again in Table 3.4. Each test group varied the input excitation for 1D, 2D, and 3D components of motion. Test groups 1 and 2 were expected to remain elastic during all testing levels. Test Group 1 was an evaluation of the rocking setup and instrumentation, therefore the axial load was one-third the designed for load to avoid damaging the column. The footing dimension was 48 in. x 48 in. ($3D_c$ x $3D_c$). For the two ground motions five earthquake directional combinations were conducted at different earthquake intensity amplitudes: 1D-X, 1D-Y, 2D-X+Y, 2D-X+Z, and 3D-X+Y+Z. In total approximately thirty runs were done for Test Group 1. A complete list of dynamic test runs can be found in Appendix A.

Following group 1 was Test Group 2 for which the footing size remained three times the column diameter ($3D_c$) square. The axial load was increased to 5.7%f'cAg and the column was tested within the elastic range. Similarly to the first group, approximately 5 types of earthquakes were run for five different input excitations. A total of approximately 30 runs were conducted (Appendix A).

Test group 3 was designed to initiate inelastic behavior and rocking/uplifting of the system. The footing was widened to five times the column diameter ($5D_c$) in the strong component loading direction and left at three times the column diameter ($3D_c$) in the opposite direction. The interaction of fixed base behavior in one direction with rocking-uplift behavior was of particular interest. Each of the earthquake runs was a 3D excitation. First the specimen loading was done at an elastic level. Next, the loading was increased to the yield and then design and maximum earthquake (MCE) loading levels. At the conclusion of testing the damaged accrued by the column prevented any further testing. A total of four runs were conducted for test group 3 (Appendix A). Table 3.5 lists the type of earthquakes run for each test group and some of their input characteristics.

Table 3.4: Testing Schedule of Rocking Column

TEST GROUP	Axial Load	Footing Size[1]	Earthquake Loading	Testing Levels[2]	Input Motions
1	Nominal $3\%f'_cA_g$	$3D_c$ x $3D_c$	Los Gatos (1989 Loma Prieta) Tabas, Iran (1977)	Elastic 90% Yield	1D - X 1D - Y 2D-X+Y 2D-X+Z 3D-X+Y+Z
2 Square Footing (S)	Nominal $10\%f'_cA_g$	$3D_c$ x $3D_c$	Los Gatos (1989 Loma Prieta) Tabas, Iran (1977)	Elastic 90% Yield	1D - X 1D - Y 2D-X+Y 2D-X+Z 3D-X+Y+Z
3 Rectangular Footing (R)	Nominal $10\%f'_cA_g$	$5D_c$ x $3D_c$	Los Gatos (1989 Loma Prieta)	Elastic Yield Design MCE	1D - X 1D - Y 2D-X+Y 2D-X+Z 3D-X+Y+Z

[1]multiple of column diameter (D_c)
[2]loading level defined by flexural ductility demands

Table 3.5: Summary of Peak Ground Motion Values for all Test Groups

Run	Record	Level	PGA (g)	PGV (in/sec)	PGD (in)
Test Group 1					
A	Los Gatos	Elastic	0.08	2.4	0.4
B	Los Gatos	Elastic	0.25	8.5	1.3
C	Tabas	Elastic	0.08	7.0	0.3
D	Tabas	Elastic	0.22	10.3	1.3
E	Los Gatos	Elastic	0.15	7.4	1.4
F	Tabas	Elastic	0.30	10.4	1.9
Test Group 2					
AS	Los Gatos	Elastic	0.11	4.0	0.6
BS	Tabas	Elastic	0.20	3.6	0.6
CS	Los Gatos	Elastic	0.20	5.6	0.7
DS	Los Gatos	Elastic	0.30	10.2	1.1
ES	Los Gatos	Elastic	0.28	8.2	1.1
FS	Tabas	Elastic	0.25	6.8	0.8
GS	Tabas	Elastic	0.14	0.14	6.1
HS	Los Gatos	Elastic	0.30	9.1	1.1
Test Group 3					
AR	Los Gatos	Elastic, Yield, Design, MCE	1.1	16.8	4.6

4 Experimental Results

4.1 Introduction

Sample results from the test program described in Chapter 3 are presented in this chapter to illustrate the behavior of bridge piers supported on rectangular spread footings that uplift during seismic response. The results are categorized by global and local response measures. The results of the shaking table specimens are very useful because they provide an indication of the magnitude of response of an uplifting bridge pier and column, which can be compared to previous tests of fixed base bridge piers. The results presented show the response of the test specimen using similar metrics to those used in previous tests (Sakai and Mahin, 2006) and those of importance in designing bridge piers (Caltrans SDC, 2004). Rocking and uplift of the test specimen footing and center mass displacement and rotation is investigated in depth in the following sections.

Several calculations are necessary to efficiently analyze the recorded data. These include the amount of rotation of the footing, translation of the top of the column due to footing uplift, the column base moment, average curvature at various regions along the column and the column shear. These response quantities then are used to develop an index that assesses the likelihood of foundation rocking. The index is described as the ratio of applied moment to restoring moment.

The shaking table test program conducted nearly 70 tests on the single column specimen with variable loads and footing dimensions. Except for the final two test runs, which were expected to undergo inelastic deformations, virtually no damage occurred. Hence, there was negligible change in structural periods or damping during most of the tests. As mentioned previously, each test group was subjected to modified versions of the Los Gatos (1989 Loma Prieta) and Tabas (1977 Iran) ground motions. Test groups 1 and 2 were conducted in the elastic range and had a maximum demand equal to incipient yielding of the column. Test group 3 was designed to test into the inelastic demand range. A total of four runs were conducted for the last group, of which the final two damaged the column as mentioned.

The use of a rectangular footing created interaction between the principal directions and caused rotation of the footing about the vertical axis because of the lack of horizontal restraint. Included are plots that show the amount of rotation compared to the overall displacements.

A complete list of test runs, along with specimen configuration, run identification number, ground motion records and scaling used is provided in Appendix A. A more complete series of plots showing time histories of specimen lateral and uplift displacements and computed column moment-average curvature relations for the tests are available in Appendix B.

4.2 Rocking System Response Quantities

All three of the test groups had similar instrumentation configurations, thus the determination of response was done similarly for all test groups. For each test group minor changes were made to instrumentation position, but the process was not radically altered. For all test runs, displacement and force time histories were calculated as well as force-deformation relationships. To calculate the response, global displacement, local displacement, and acceleration recordings were utilized. The next two sections describe the process for calculating the rocking system response quantities.

4.2.1 Displacements

4.2.1.1 External Displacements

Using the instrumentation described in Chapter 3, the displacement response quantities of interest were calculated. The total relative lateral translation (u_{rel}) in each direction (East-West and North-South) is computed as the difference between the lateral displacement at the center of mass and at the base of the footing in that direction (Eqn. (4-1)).

$$u_{rel} = u_{total} - u_{footing} \qquad (4\text{-}1)$$

The uplift of the footing from the elastomeric pad was measured at four locations offset from the edge of the footing as shown in Figures 3.28 and 3.29. The average vertical displacements from the two vertical displacement transducers on the East side of the footing were subtracted from corresponding value for the transducers on the West side of the footing. Dividing the resultant by the East-West horizontal distance between the pairs of transducers, the base rotation θ_{ftg} of the footing is estimated (4-4). The lateral displacement Δr of the center of the top mass associated with rigid body rotation of the footing is then estimated as the base rotation of the footing times the height of the center mass measured from the center of mass to the bottom of the footing (4-3). Figure 4-1 depicts the displacements of interest of the rocking system. The total relative lateral translation (u_{rel}) is also noted as ΔT for convenience in reporting the results. The total displacement is a combination of the lateral rigid body translation (Δr) due to uplift of the footing and the flexural displacement (Δf) of the column due to input excitation.

$$\Delta T = u_{rel} \qquad (4\text{-}2)$$

$$\Delta r = H \sin\theta \approx H\,\theta \qquad (4\text{-}3)$$

$$\theta_{ftg} = \frac{z_L - z_R}{2B} \qquad (4\text{-}4)$$

The contribution of flexural displacement (Δf) is assumed to include the contribution of flexure, bar pullout, shear and similar internal deformations in the column. At the center of mass the contribution due to flexural displacement is estimated by Equation (4-5) as the total relative displacement minus the rigid body translation. For Test Group 3, where the footing was widened to $3D_c$ x $5D_c$, the outriggers with vertical displacement transducers were shifted to the North-South faces and a similar process was used for calculations.

$$\Delta f = \Delta T - \Delta r \qquad (4\text{-}5)$$

For Test Group 3, where the footing was widened to 3Dc x 5Dc, the outriggers with vertical displacement transducers were shifted to the North-South faces and a similar process was used for calculations.

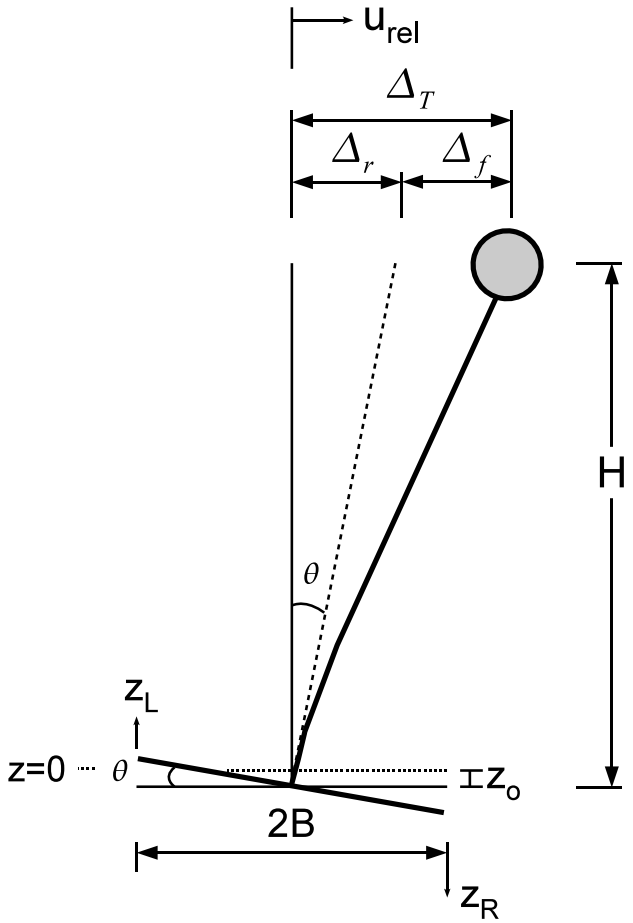

Figure 4-1: Displacement Response Quantities

4.2.1.2 Footing Vertical Uplift

The estimated footing rotation was used to calculate the vertical uplift at any point along the footing. The shear and flexure deformations of the footing were assumed to be negligible by comparison to the footing uplift. Hence the footing was assumed to behave as a rigid block. By assuming rigid motion of the footing the vertical uplift at any point could be estimated using the footing rotation along both principle directions ($\theta_{ftg\text{-}NS}$ and $\theta_{ftg\text{-}EW}$) and the initial displacement (z_o) due to gravity load (Eqn. (4-6)).

$$z_{xy} = (\theta_{ftg\text{-}NS})\, x + (\theta_{ftg\text{-}EW})\, y + z_o \qquad (4\text{-}6)$$

4.2.1.3 Column Curvatures

The DCDT instrumentation along the column height described in Chapter 3 was used to estimate the average curvature along the column. The DCDTs were located on the North, South, East and West column faces and connected to rods running through the column along the North-South and East-West directions. Each instrument was placed a small horizontal distance away from the column face. At each elevation (h_i) the horizontal distance, $S_{N\text{-}S}$, was recorded as the distance between the DCDT instruments on opposing faces. The rotation (θ_i) of each region at each elevation (h_i) was determined by dividing the extension (Δ_i) of the DCDT on each face by the horizontal distance between them (Eqn. (4-7)). The average curvature (ϕ_i) of each region was then estimated by dividing the rotation by the region height measured as the vertical distance between the adjacent set of rods at elevation h_{i-1} (Eqn. (4-8)).

$$\theta_i = \frac{\Delta_S - \Delta_N}{S_{N-S}} \qquad (4\text{-}7)$$

$$\phi_i = \frac{\theta_i}{h_i - h_{i-1}} \qquad (4\text{-}8)$$

4.2.2 Forces and Moments

The shear and moment along the column were estimated using the recorded accelerations and center of mass relative displacements. The shear force was approximated as total acceleration of the mass block times the mass (m) of the block and excluded the contribution from damping. The rotational force was estimated by multiplying the rotational acceleration by the rotational mass (m_R) moment of inertia of the mass block. At the base of the column, moments were determined using equilibrium and neglecting damping forces again. The base column moment is a product of the lateral acceleration, rotational acceleration and the lateral displacement.

Equations (4-9) and (4-10) illustrate the equation of motion for the x direction. The process was similar for the y direction.

$$m\ddot{u}_x + F_{dx} + F_{sx} = -m\ddot{u}_{gx} \quad (4\text{-}9)$$

$$m_R\theta_y + M_{d\theta} + M_{s\theta} = 0 \quad (4\text{-}10)$$

The quantities of interest are:

- m = mass of weight block
- m_R = rotational mass moment of inertia
- $\ddot{u}$ = total relative acceleration of the center of mass
- $\ddot{u}gx$ = table acceleration
- θ_y = rotational acceleration of mass block about y axis
- F_{dx} = damping force
- F_{sx} = hysteretic force
- $M_{d\theta}$ = damping moment about y-axis
- $M_{s\theta}$ = hysteretic moment about y-axis

The total displacement and acceleration can be written as $u_t = u_{rel} + u_g$ and $\ddot{u}_t = \ddot{u}_{rel} + \ddot{u}_g$, respectively, where $\ddot{u}g$ is the ground acceleration. The forces in the system can be determined by rewriting the above equations to solve for the hysteretic force (F_{sx}) in the x direction and the hysteretic moment ($M_{s\theta}$) about the y axis.

$$F_{sx} = -m\ddot{u}_x - m\ddot{u}_{gx} - F_{dx} = -m\ddot{u}_t - F_{dx} \approx -m\ddot{u}_t \quad (4\text{-}11)$$

$$M_{s\theta} = -m_R\theta_y - M_{d\theta} \approx -m_R\theta_y \quad (4\text{-}12)$$

Figure 4-2 depicts the quantities described and calculation of base shear and moment. If we neglect the contribution of damping then $F_{s\theta}$ and $M_{s\theta}$ can be calculated as shown in Equations (4-11) and (4-12). With the shear and moment being known at the center of mass, and using equilibrium, the moment at each point along the column can be calculated. Equation (4-13) shows the calculation for moment at the base of the column. When the damping force is small, the approximation provides a reasonable approximation of the system forces.

$$M_b = (m\ddot{u}_t + F_{dx})H_c - M_{d\theta} - M_{s\theta} + Pu_{rel} \approx F_{sx} * H_c - M_{s\theta} + Pu_{rel} \quad (4\text{-}13)$$

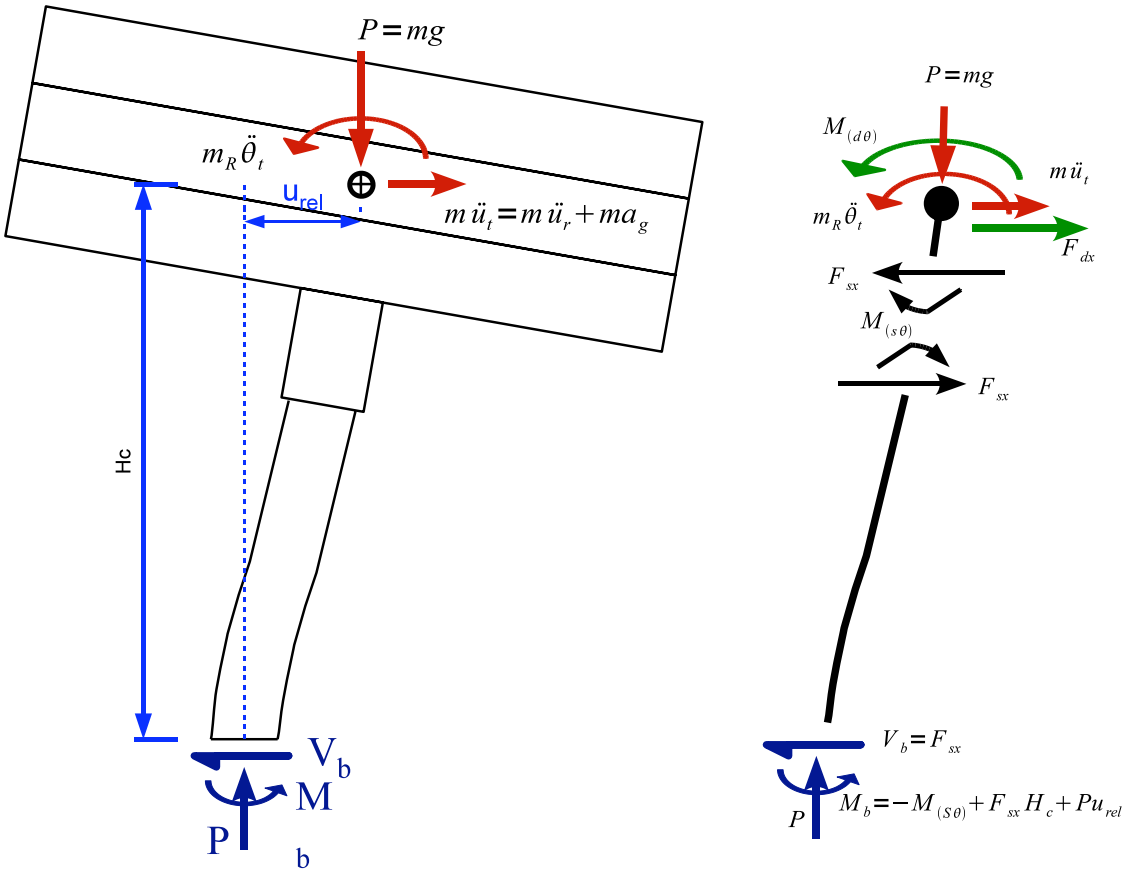

Figure 4-2: Free Body Diagram

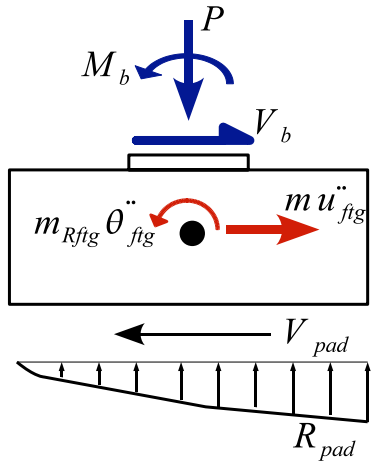

Figure 4-3: Footing Free Body Diagram

The footing free body diagram is shown to illustrate the force transfer at the base of the footing. Instrumentation to clarify the magnitude of compression force developed in the pad was not used. The shear and vertical reaction of the pad can be approximated using the relationships for the base shear and moment already developed. Using equilibrium the shear across the pad is approximated as the base shear plus the total acceleration of the footing. The vertical reaction R_{pad} and its eccentricity from the column center can be determined using equilibrium and the column axial force, shear and moment at the base.

4.3 Observed Column Response

The response of the specimen, with varying footing widths and axial load, to several types of excitation is described in this section. Prior to the start of each test group a pullback and free vibration test were conducted to determine the stiffness, natural period and damping of the system. Except for the final two runs of Test Group 3 all dynamic runs were conducted at a nominal elastic demand level of the column. The final two runs were conducted at the nominal design and maximum levels for the column.

Test groups 1 and 2 were designed to remain elastic so that a large number of tests could be conducted to determine the response of the system to varying footing sizes and axial loads. Test group 3 was designed to cause damage by increasing the amplification of excitation such that the column reached design and maximum loading levels. In general groups 1 and 2 were tested in a similar manner. Typically for each ground motion, amplification scale, and time step combination five runs were conducted which varied the input excitation. The input excitation sequence was usually 2 one-directional excitations (X, Y), 2 two-directional excitations (X+Y, X+Z) and 1 three-directional excitation (X+Y+Z). For example in Appendix A, Test Group 2 Sequence DS lists the five runs for the Los Gatos input signal scaled to 25% of the original amplitude and a modified time step of 0.094 sec.

The principal objective of these rocking tests was to assess the behavior of a system when allowed to simultaneously rock, uplift and deform under typical earthquake loading levels. These loading levels are determined by corresponding systems with the same configuration except for a fixed base assumption that prevents uplift of the footing. Typical performance levels for fixed base bridge systems are design (displacement ductility equal to 4) and maximum credible earthquake (displacement ductility equal to 6-8). Assessing the behavior of uplifting systems allows for a correlation to be drawn between columns of identical design and axial load, and the effect of footing restraint on column performance for seismic loading.

The response of Test Group 1, for low axial load was used for the preliminary analysis of the more relevant system with the design axial load. Prior to dynamic testing the stiffness, natural frequency, and damping of the system were determined using pullback and free vibration tests. Following this a total of 30 runs were conducted to assess the dynamic response. No physical damage resulted in the specimen, including cracking. However the specimen was observed to twist about a vertical axis and translate as shown in Figure 4-4. Table 4.1 summarizes some of the response values for Test

Group 1. The low axial load is not typical of bridge design so its usefulness here is only for characterizing the behavior of rocking systems and modeling of the elastomeric pad of subsequent dynamic analysis.

The total number of dynamic tests for Group 2 was 34. Section 4.5 illustrates some of the important response parameters for the system. During testing, rocking easily occurred for the square footing 3Dc x 3Dc in size. No yielding or damage was noted during the testing. Some cracking was observed however the cracks closed completely at the conclusion of the testing and could not be located. Table 4.2 lists some of the response values for Test Group 2. During testing some rotation of the footing around the vertical axis was observed. Figure 4-5 shows the condition of the specimen following dynamic test D5S. During testing a significant amount of rocking was observed. For the testing of group DS the amount of lateral translation due to rigid body rotation was up to ½ of the total displacement. At the conclusion of Test Group 2 the column had no observable damage and some minor period lengthening from softening of the system after repeated test deformation cycles. Following Test Group 2 the footing of the specimen was widened in the y direction for a new size of 3Dc x 5Dc. The ground motion was rotated 90 degrees also to align the strongest component with the wider footing dimension.

The 4 tests conducted for group 3 (Table 4.3) used all three components of excitation. The yield level test (A2R) was conducted at the same amplitude as test D5S and resulted in less uplift and total displacement than the smaller footing dimension. The footing dimensions clearly have an impact on the total uplift of the system. The design and maximum level tests were scaled to cause inelastic behavior in both directions. The observed response showed there was less relative uplift to total displacement in both directions than the smaller footing size. The column was damaged on the North-West face where spalling occurred during the design and maximum level tests. A plastic hinge was formed over approximately the bottom 16 inches of the column height. Also the large deformations of the center of mass induced a permanent displacement in both direction of the column of about 1 in for the design level and 9 in. and 13 in. for the x and y direction after the maximum level test. At the conclusion of the maximum level tests testing was terminated because the column was deemed to be very damaged and unsafe for any subsequent runs.

Test Group 3 revealed that vertical restraint of the footing was unnecessary to develop the plastic hinge moment of the column and that the desired design goal could be achieved without the restraint. It should be stressed that it is important to detail columns to be ductile, even if they are expected to rock, due to effects of bidirectional bending on the footing and column. Also in the event of accidental restraint being placed on the footing such as by overburden pressures.

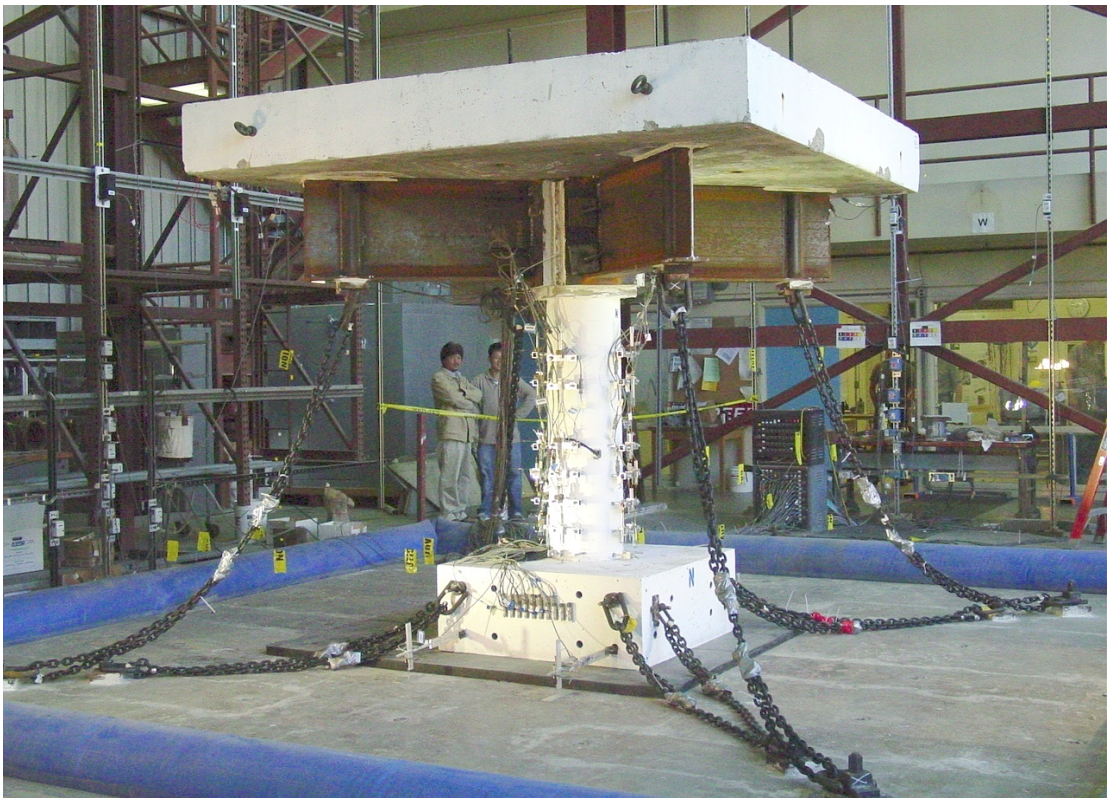

(a) Global View

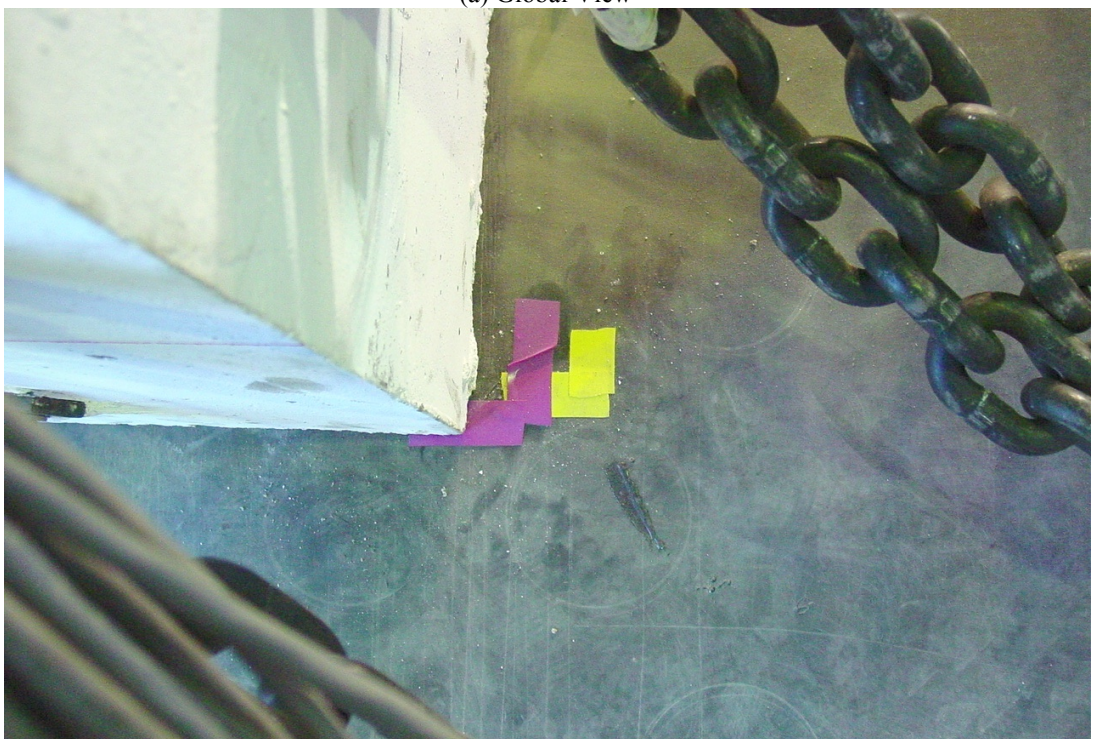

(b) Rotation about vertical axis indicated by distance from tape attached to elastomeric pad

Figure 4-4: Test Group 1 with footing 3Dc x 3Dc and low axial load following final run

(a) Global View

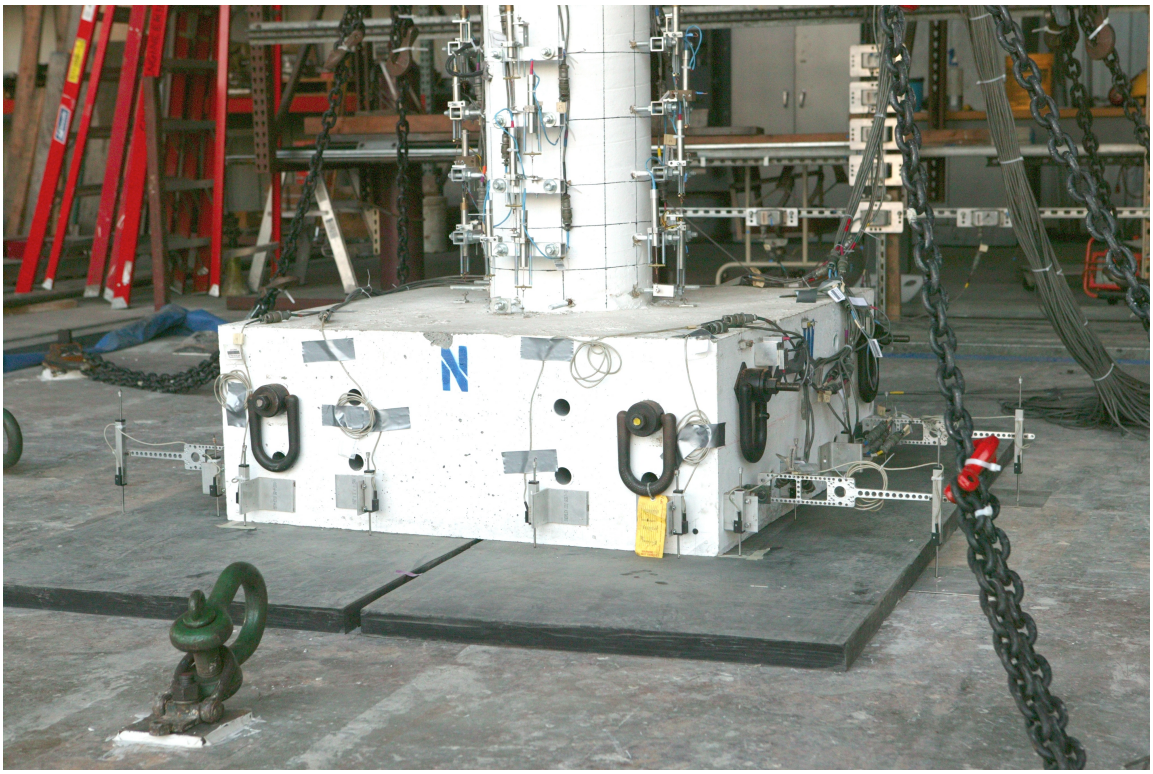

(b) Column Base

Figure 4-5: Specimen Damage Condition with 3Dc x 3Dc footing after run D5S

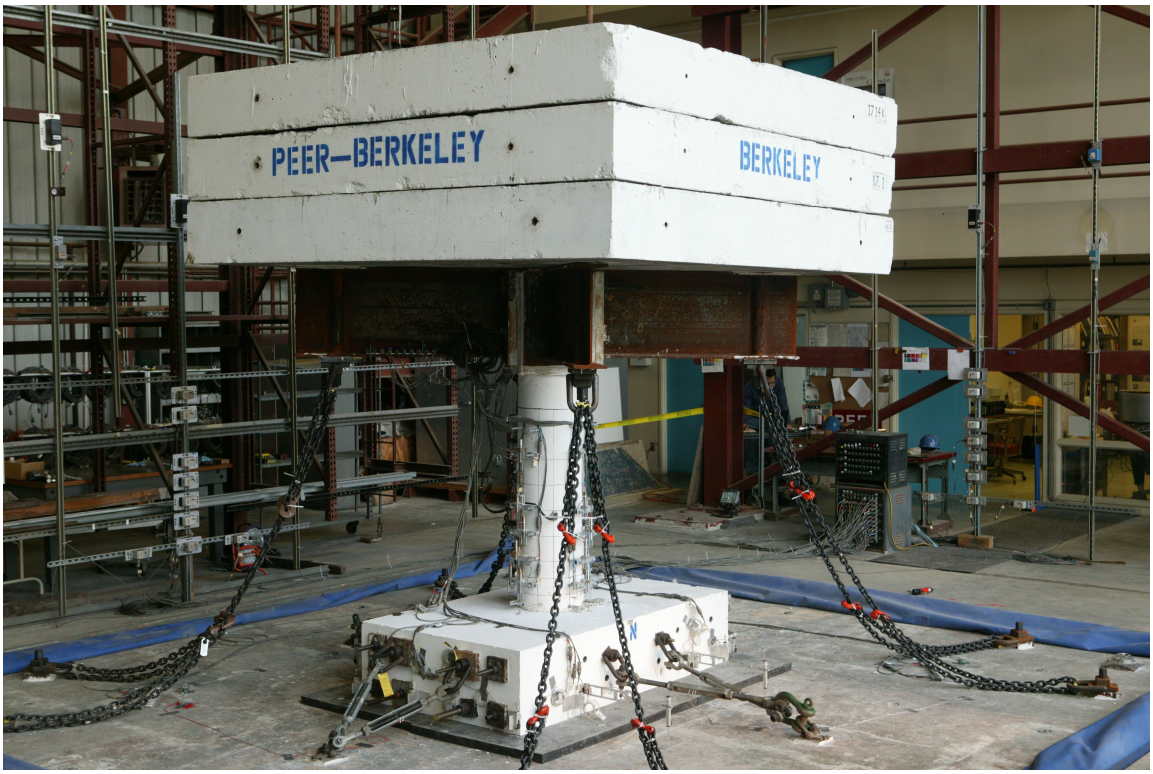

(a) Global View

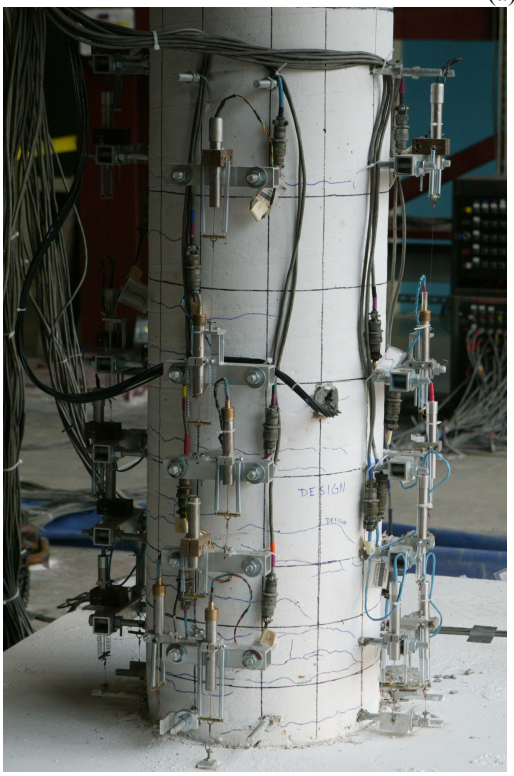

(b) Slight Residual Drift Observed

(c) Local spalling of concrete cover and cracking at NW face

Figure 4-6: Damage Condition of specimen with 3Dc x 5Dc footing following run A3R

(a) Global View – North Direction

(b) Global View – North East Direction

Figure 4-7: Damage condition of specimen with 3Dc x 5Dc footing following Run A4R (safety chains tightened subsequent to testing)

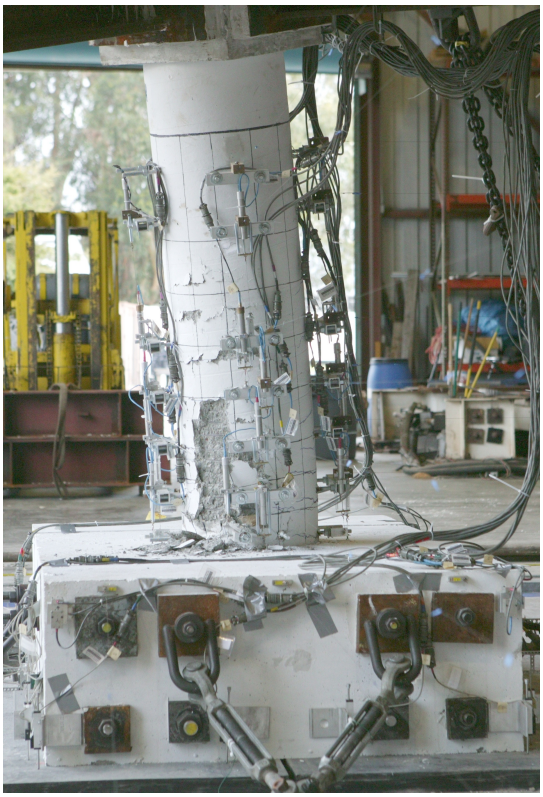

(a) Plastic hinge formation - West side

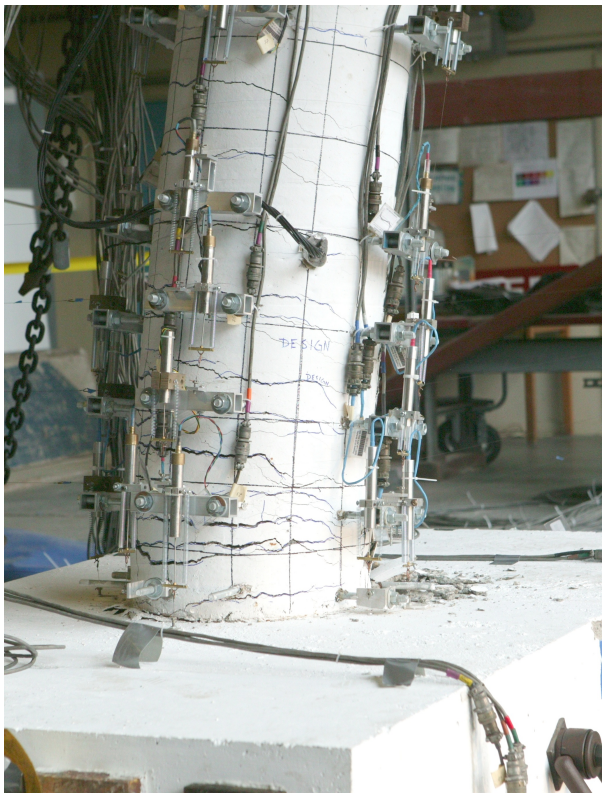

(b) Plastic hinge formation – North-East side

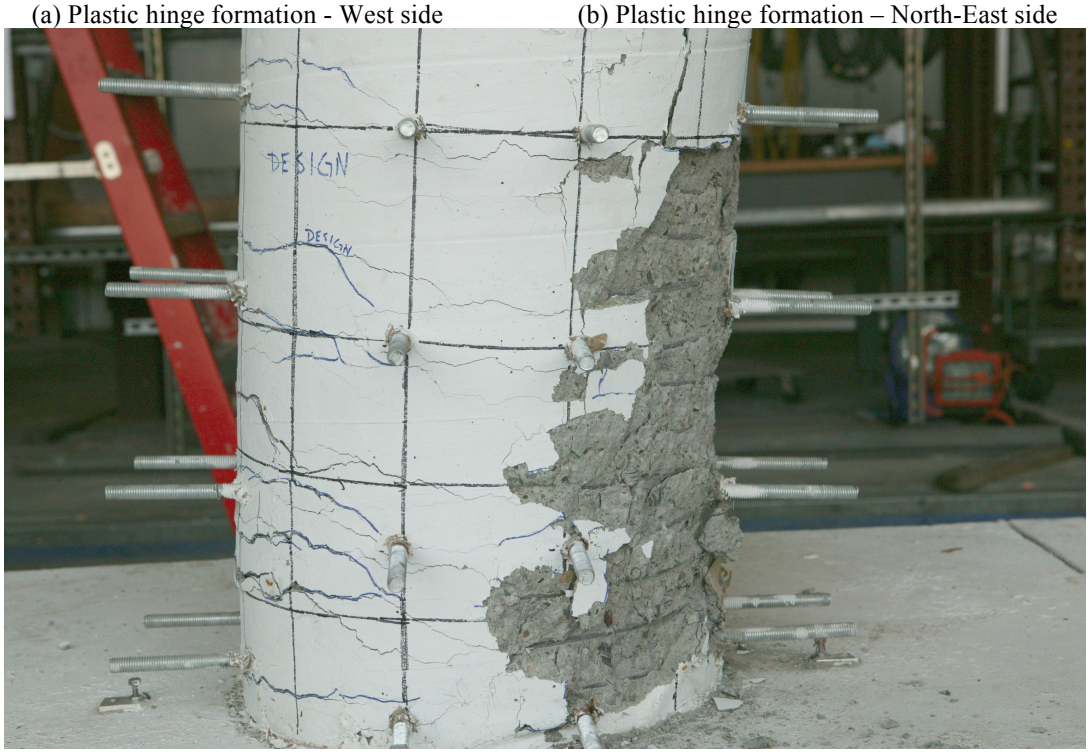

(c) Plastic Hinge formation – North side (after removal of instrumentation)

Figure 4-8: Damage Condition of Specimen with 3Dc x 5Dc footing following Run A4R

Table 4.1: Summary of Test Group 1 Response Footing Size 3Dc x 3Dc with Low Axial Load

Run	Performance Level	Table Acceleration And Displacement				Relative Displacement				Base Shear and Moment				Observations
		u_{gx}	u_{gy}	$\ddot{u}_{gx}$	$\ddot{u}_{gy}$	Peak Lateral		Peak Uplift		Shear		Moment		
		(in)	(in)	(g)	(g)	x (in)	y (in)	θ_y (%)	θ_x (%)	V_{bx} kip	V_{by} kip	M_{by} kip-in	M_{bx} kip-in	
A1	Elastic	0.33	0.00	0.08	0.01	0.16	0.08	0.04	0.11	2.4	1.0	194	84	Stiffness, Free Vibration test Performed prior to dynamic runs.
A3	Elastic	0.33	0.16	0.08	0.04	0.11	0.13	0.02	0.20	2.3	1.4	186	111	
A5	Elastic	0.34	0.16	0.07	0.03	0.12	0.14	0.02	0.20	2.2	1.5	177	121	
B1	Elastic	1.42	0.06	0.23	0.04	0.52	0.32	0.15	0.56	4.4	2.6	359	206	Large amount of uplift and rocking.
B3	Elastic	1.43	0.92	0.23	0.21	1.11	1.14	0.42	2.37	4.6	4.0	365	317	
B5	Elastic	1.46	0.97	0.24	0.20	1.39	1.13	0.54	2.41	4.9	4.1	389	321	
C1	Elastic	0.37	0.00	0.08	0.01	0.09	0.05	0.01	0.04	1.2	0.6	99	48	Little to no uplift.
C3	Elastic	0.36	0.22	0.06	0.02	0.10	0.07	0.01	0.06	1.5	0.9	120	73	
C5	Elastic	0.37	0.22	0.07	0.02	0.09	0.07	0.01	0.07	1.3	0.9	109	74	
D1	Elastic	1.36	0.03	0.23	0.04	0.49	0.28	0.12	0.53	3.7	2.1	300	171	No observed damage.
D3	Elastic	1.36	0.94	0.25	0.09	0.42	0.35	0.10	0.60	3.8	2.8	310	230	
D5	Elastic	1.38	0.97	0.23	0.09	0.42	0.36	0.10	0.60	3.9	2.7	312	221	
E1	Elastic	1.45	0.07	0.17	0.05	0.66	0.44	0.18	0.58	4.5	3.1	364	245	Significant amount of uplift.
E3	Elastic	1.46	0.96	0.18	0.10	0.68	0.63	0.19	1.08	4.4	3.8	356	304	
E5	Elastic	1.46	0.94	0.18	0.10	0.71	0.67	0.19	1.12	4.4	3.8	357	305	
F1	Elastic	1.95	0.06	0.28	0.05	0.74	0.47	0.21	0.81	4.2	2.9	338	236	Significant amount of uplift.
F3	Elastic	2.02	1.42	0.27	0.15	0.70	0.52	0.21	0.97	4.0	3.4	320	272	
F5	Elastic	2.01	1.45	0.25	0.13	0.73	0.52	0.21	1.01	3.9	3.4	318	275	

Table 4.2: Summary of Test Group 2 Response Footing Size 3Dc x 3Dc

Run	Performance Level	Table Acceleration And Displacement				Relative Displacement				Base Shear and Moment				Observations
		u_{gx}	u_{gy}	$\ddot{u}_{gx}$	$\ddot{u}_{gy}$	Peak Lateral		Peak Uplift		Shear		Moment		
		(in)	(in)	(g)	(g)	x (in)	y (in)	θ_y (%)	θ_x (%)	V_{bx} kip	V_{by} kip	M_{by} kip-in	M_{bx} kip-in	
A1S	Elastic	0.68	0.04	0.10	0.02	0.63	0.42	0.13	0.11	5.4	3.0	579	301	Stiffness and free vibration test performed prior to dynamic runs.
A3S	Elastic	0.68	0.36	0.10	0.08	1.02	0.63	0.32	0.25	7.1	3.5	759	359	
A5S	Elastic	0.68	0.35	0.09	0.09	1.10	0.60	0.34	0.25	7.2	3.7	775	380	
B1S	Elastic	0.56	0.02	0.17	0.03	0.65	0.46	0.08	0.07	5.2	3.5	559	353	Negligible amount of uplift.
B3S	Elastic	0.56	0.56	0.16	0.18	0.65	0.70	0.12	0.18	5.4	5.0	557	450	
B5S	Elastic	0.56	0.57	0.17	0.17	0.64	0.67	0.12	0.17	4.9	4.7	543	444	
C1S	Elastic	0.68	0.03	0.14	0.03	1.17	0.51	0.30	0.16	7.2	3.4	847	356	More observable uplift in footing. Footing rotation about vertical axis.
C3S	Elastic	0.68	0.39	0.14	0.12	1.24	0.77	0.40	0.30	7.2	3.9	820	388	
C5S	Elastic	0.70	0.38	0.14	0.12	1.24	0.77	0.40	0.30	7.0	4.2	834	391	
D1S	Elastic	1.16	0.07	0.23	0.07	2.15	0.74	0.98	0.28	9.7	4.1	1078	428	Test reached nominal yield level. Some minor cracks that closed at end of test.
D3S	Elastic	1.15	0.67	0.24	0.15	2.19	1.62	1.06	0.57	9.9	8.3	1047	802	
D5S	Elastic	1.14	0.67	0.27	0.18	2.21	1.87	0.98	0.72	9.8	8.9	1042	858	
E1S	Elastic	0.80	0.02	0.22	0.03	0.97	0.63	0.14	0.09	6.9	3.9	727	411	Frequency content altered small amount of uplift.
E3S	Elastic	0.79	0.77	0.18	0.19	0.91	0.67	0.19	0.16	6.6	4.9	624	411	
E5S	Elastic	0.80	0.76	0.21	0.20	0.91	0.68	0.20	0.17	6.7	5.3	631	409	
F1S	Elastic	0.79	0.01	0.14	0.02	0.53	0.22	0.04	0.03	4.4	1.6	414	146	Frequency content altered small amount of uplift.
F3S	Elastic	0.80	0.75	0.14	0.18	0.40	0.59	0.05	0.09	3.8	4.0	298	379	
F5S	Elastic	0.80	0.77	0.12	0.21	0.41	0.59	0.05	0.09	3.5	3.7	305	370	

Table 4.3: Summary of Test Group 3 Response Footing Size 3Dc x 5Dc

Run	Performance Level	Table Acceleration And Displacement				Relative Displacement				Base Shear and Moment				Observations
		u_{gx}	u_{gy}	$\ddot{u}_{gx}$	$\ddot{u}_{gy}$	Peak Lateral		Peak Uplift		Shear		Moment		
		(in)	(in)	(g)	(g)	x (in)	y (in)	θ_y (%)	θ_x (%)	V_{bx} kip	V_{by} kip	M_{by} kip-in	M_{bx} kip-in	
A1R	Elastic	0.18	0.34	0.10	0.13	0.33	0.70	0.03	0.04	3.3	4.7	287	467	Small amount of uplift. No cracking in column.
A2R	Yield	0.33	0.62	0.13	0.16	0.61	1.28	0.13	0.10	4.9	8.2	495	810	Cracking observed in column. Small uplift recorded.
A3R	Design	1.74	3.16	0.42	0.71	4.31	5.78	0.50	0.16	10.5	14.6	1236	1194	Cracking at column base in plastic hinge zone. Some spalling on NW column face. Residual drift of ~1% in both directions.
A4R	Maximum	2.51	4.54	0.55	1.03	9.86	14.17	0.61	0.27	12.2	18.8	1623	1133	Significant spalling on NW face at plastic hinge zone. Large cracks on SE face. Residual drift of 8% and 12% in x y directions

4.4 Recorded Results

Response histories are presented in Sections 4.5, 4.6, 4.7, and 4.8. The specimen variables of interest are presented for all tests of group 3, and selected results of the elastic runs of test group 2. These include 1D, 2D, and 3D components of excitation comparisons. Appendix B has a more comprehensive review of all the tests conducted.

The response quantities described in Section 4.2 and some simple calculations are presented in the following sections. Each test run includes a description of the following response quantities: (a) relative lateral displacement of center mass and resulting contribution from rocking translation and flexure, (b) amount of footing uplift which includes peak contours and envelopes of displacement, (c) base moment histories, and (d) the hysteretic plots for column base moment vs curvature of the column and rotation of the footing. Additionally, when it is of particular interest the (e) displacement interaction and the (f) footing rotation about a vertical axis are shown.

4.5 Test Specimen with Design Axial Load and 3Dc x 3Dc Footing

For the footing configuration $3D_c$ x $3D_c$, rocking easily occurred during low levels of seismic excitation. No yielding or damage was noted during any of the testing conducted. Cracks may have opened during testing, however they closed completely at the end of the test and their location could not be identified. Appendix A has a complete list of the test runs for Test Group 2. The two ground motions were scaled to meet target objectives for the desired rocking amplitude and or the displacement demand of the column. Interaction between the orthogonal directions was detected even when only one direction of excitation was implemented. During testing it was noted that the specimen would tend to twist about a vertical axis. There was no restraint against horizontal movement of the footing other than friction between the specimen and elastomeric pad.

For theses tests the results showed a linear relationship between the lateral force hysteresis and displacement. However, some inelastic behavior was observed for the moment about the column base and the rotation of the footing due to uplift. The inelastic behavior observed likely produces significant damping for the system.

4.5.1 Global Displacement

Some of the key descriptors of global displacement are shown in Figure 4-9. They include the response quantities described in Section 4.2. The total displacement at which rocking will occur is shown as well as the displacement at which the footing will uplift from the elastomeric pad.

4.5.1.1 Column Response

The test set AS was subjected to a low level seismic excitation intended to be at the onset of uplifting behavior. By analysis it was also determined to be the amplitude that would cause incipient yielding in a similar column and axial load when restrained against uplift. The specimen had a 3Dc x 3Dc footing plan dimension and was subjected to a single component of the Los Gatos record, amplitude scaled to 15% of its initial intensity and time scaled by a factor of $1/\sqrt{4.5}$.

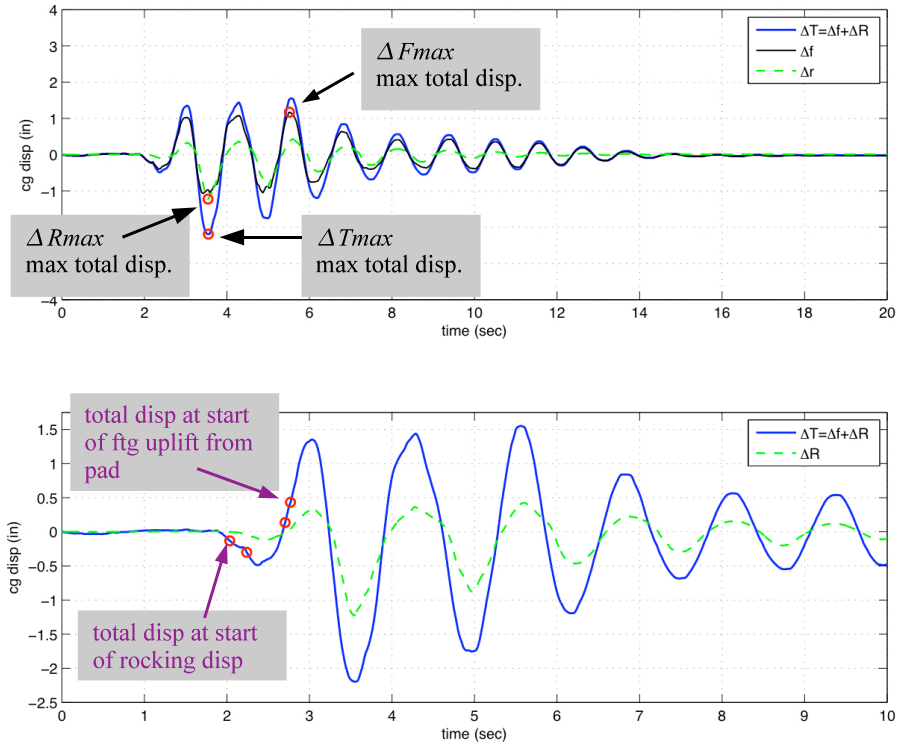

Figure 4-9: Illustration of Terminology Used to Describe Total displacements

Selected results for one horizontal component of excitation are shown in Figure 4-10. These are for test runs A1S and A2S. Also shown is the response of the specimen to two horizontal components of excitation, A3S, and three components of excitation A5S. It can be seen from the time histories of lateral displacement at the center of mass of the top mass blocks that rigid body rotations due to rocking contribute some, but not significantly to the response. The rocking contributions appear to lag behind the overall response. This may be influenced by higher mode response of the specimen.

It is clear that in spite of one direction of only one component of excitation being imposed, the specimen has significant response in the orthogonal direction. This is likely due to two factors: (1) the difficulty of aligning the specimen perfectly with the axis of excitation, and (2) small movements of the table in the direction perpendicular to the direction of specified excitation.

Some selected results from testing set DS are shown, which was for the same Los Gatos ground motion scaled to 25% of the original amplitude, are shown in Figure 4-11. This test sequence was intended to induce about 2/3 of the yield displacement of the column under unidirectional excitation.

The DS test group included 5 different combinations of excitation. Figure 4-11 presents the lateral displacement at the center of mass of the top mass block for runs D1S, D3S, and D5S, which have X, X+Y, and X+Y+Z excitation components. As noted before, there is significant movement in the Y direction during the test, even if excitation is imposed only in the X direction. The basic character of the response in the X direction

does not change when the Y or Y+Z components are added. However, the response for the Y direction increases significantly when the Y-direction excitation is added. It is clear at this level of excitation that the rigid body motion of the specimen associated with rocking and uplift represents ½ or more of the overall response (Figure 4-14).

Results similar to the Los Gatos records are shown in Figure 4-12 for the Tabas record. These records are for test set FS scaled to 25% of the original amplitude and time scaled by a factor of $1/\sqrt{4.5}$. These results indicate that the response is less severe for the test specimen than for the Los Gatos record test set DS, which is associated with the different spectral characteristics of the ground motion. There is interaction between the orthogonal directions even when only one-horizontal component of excitation is applied. When the X direction is excited only (F1S) the Y direction responds with significant motion, including up to 15% of which is due to rocking.

Additional test results are shown in Appendix B.

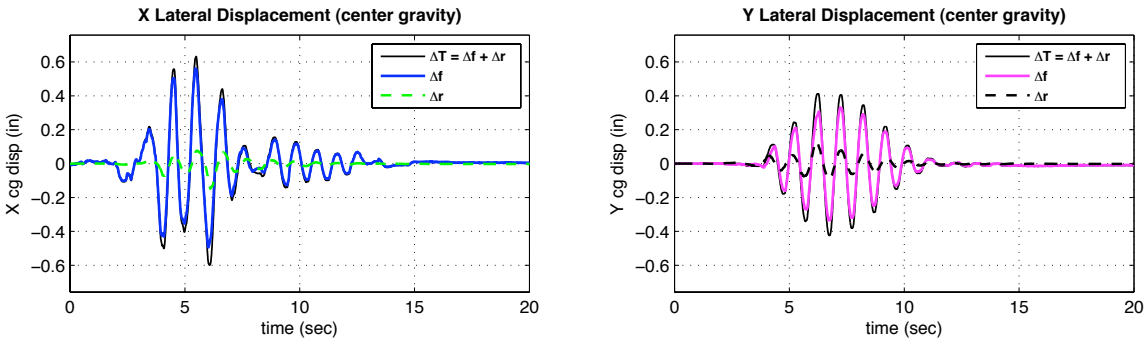

(a) Orthogonal Displacement response for 1D-X input excitation. (Test A1S)

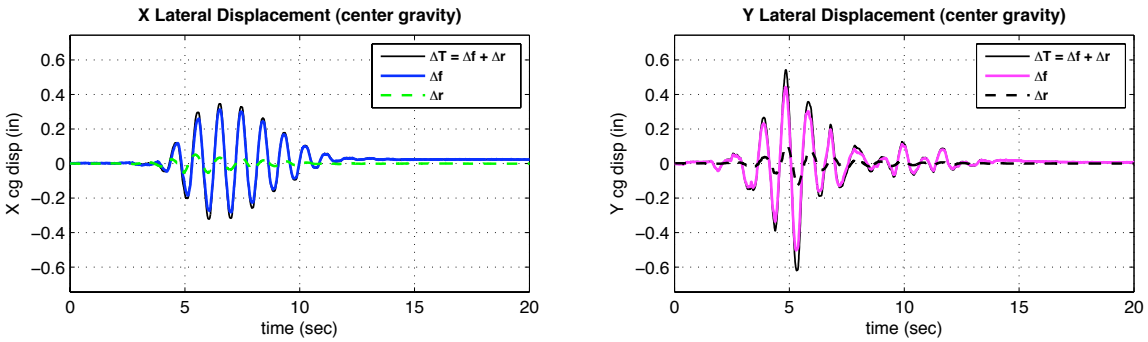

(b) Orthogonal Displacement response for 1D-Y input excitation. (Test A2S)

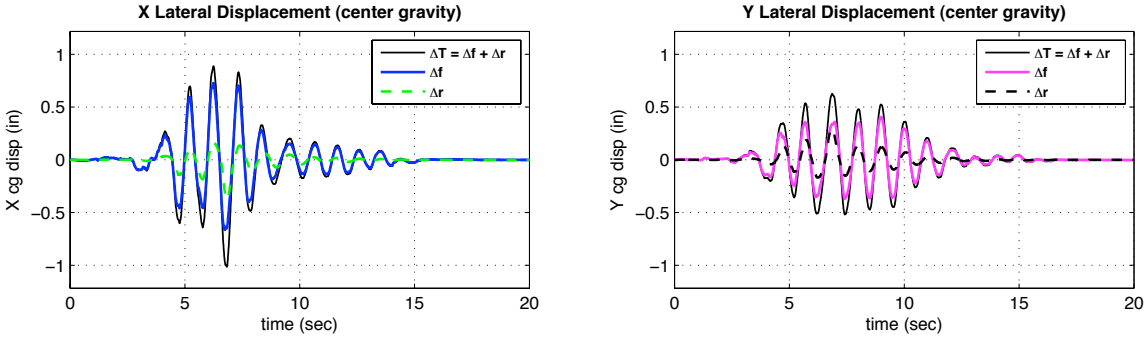

(c) Orthogonal Displacement response for 2D-X+Y input excitation. (Test A3S)

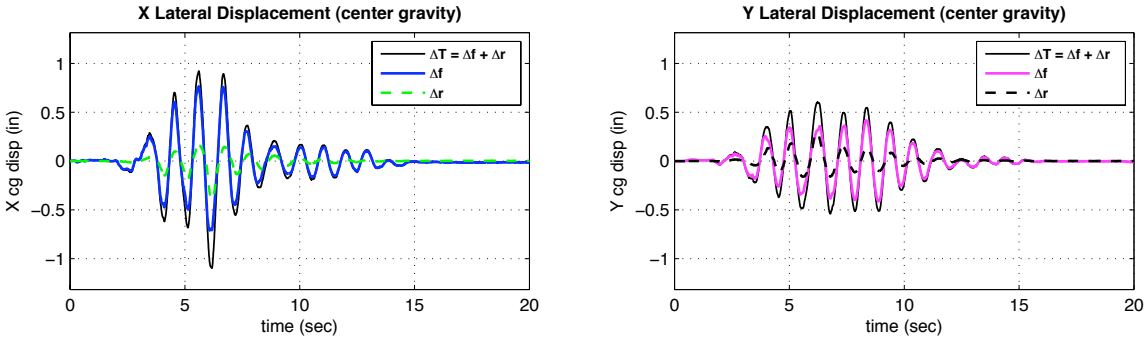

(d) Orthogonal Displacement response for 3D-X+Y+Z input excitation. (Test A5S)

Figure 4-10: Displacement Response: 1 2, 3 Components of Excitation (Test Set AS)

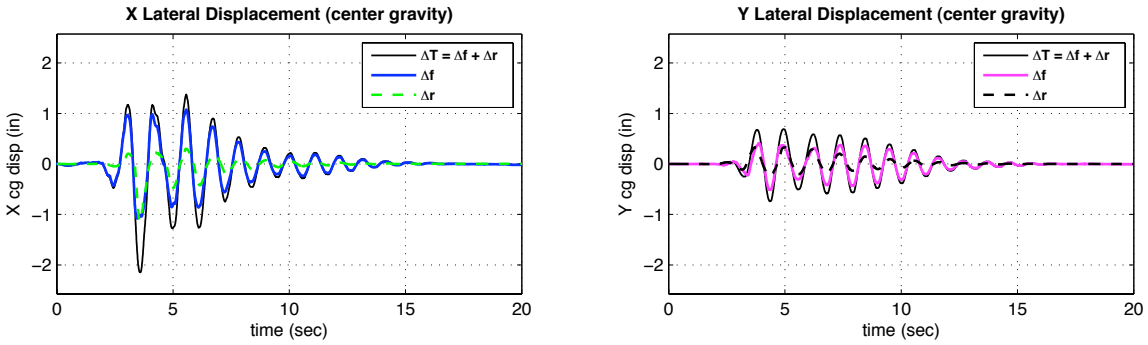

(a) Orthogonal Displacement response for 1D-X input excitation. (Test D1S)

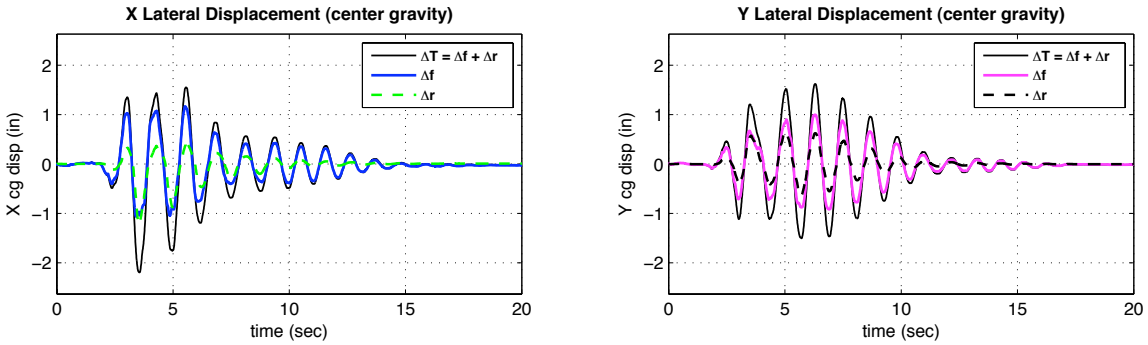

(b) Orthogonal Displacement response for 2D-X+Y input excitation. (Test D3S)

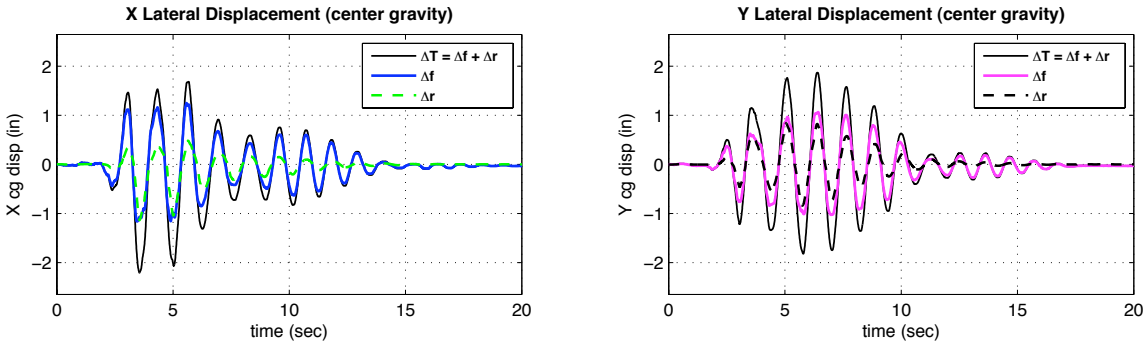

(c) Orthogonal Displacement response for 3D-X+Y+Z input excitation. (Test D5S)

Figure 4-11: Displacement Response: 1 2, 3 Components of Excitation (Test Set DS)

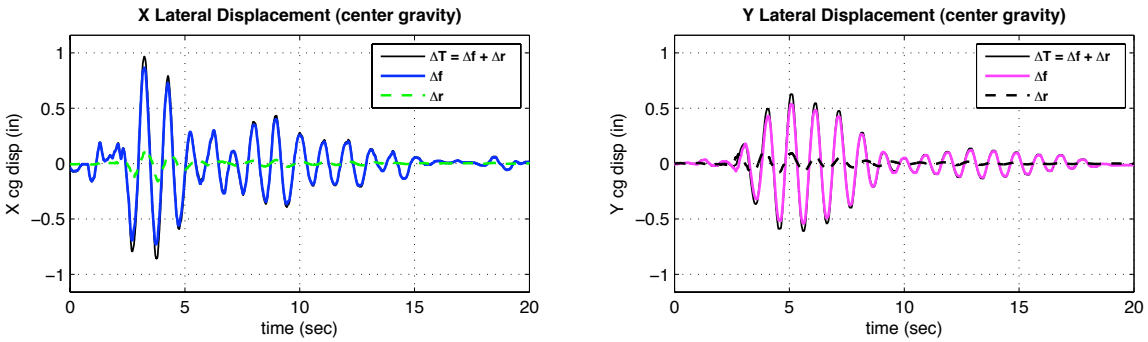

(a) Orthogonal Displacement response for 1D-X input excitation. (Test F1S)

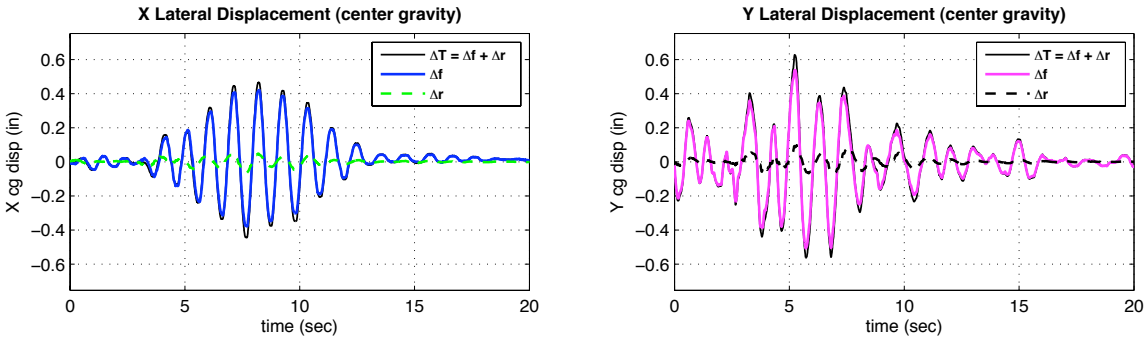

(b) Orthogonal Displacement response for 1D-Y input excitation. (Test F2S)

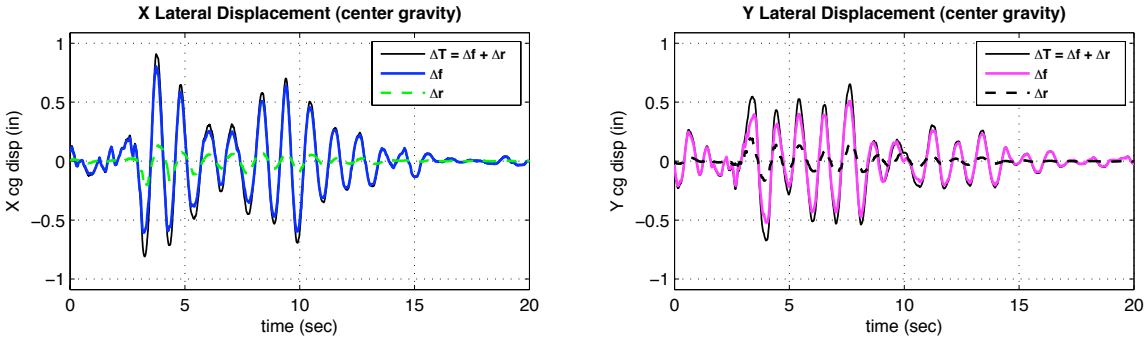

(c) Orthogonal Displacement response for 2D-X+Y input excitation. (Test F3S)

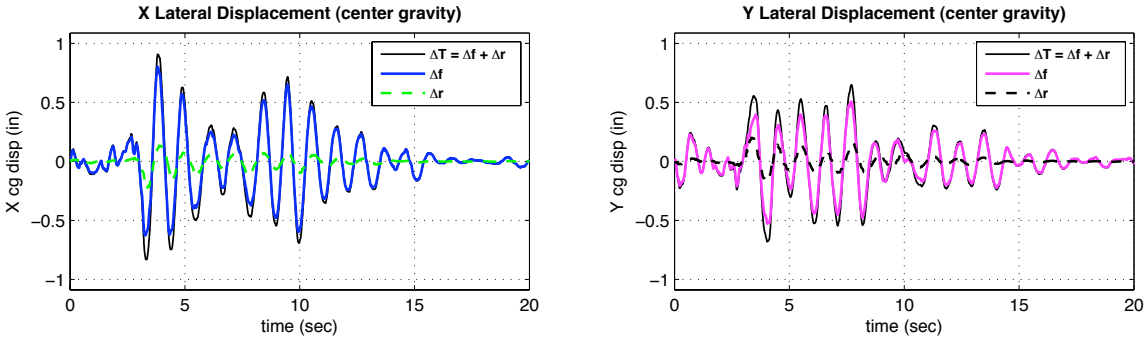

(d) Orthogonal Displacement response for 3D-X+Y+Z input excitation. (Test F5S)

Figure 4-12: Displacement Response: 1 2, 3 Components of Excitation (Test Set FS)

The amount of rocking which comprises the total displacement indicates how susceptible the specimen is to uplift. Inspection of the displacement time histories showed that consistently the peak lateral displacement due to rigid body translation from uplift occurred during the peak total displacement of the system or a fraction of second afterwards (as noted previously by the lag of the overall rocking response). The conclusion can be drawn that essentially the peak rocking displacement occurs at the same moment as the peak total displacement.

The comparison of peak total displacement and the contribution of rocking displacement to the total are shown in Figure 4-13 for test sets AS, DS, FS. These are the amplitude and time scaled records for Los Gatos and Tabas as previously described. The bar on the left is the maximum lateral displacement of the center of mass and the bar on the right is the contribution of rocking to the maximum displacement. The system had a significant contribution from rocking to the total displacement for test sets AS and DS. For these tests, the peaks where upwards of ½ of the total. Test set FS was more resistant to uplift, owing likely to the spectral characteristics of the input excitation.

The ratio of rocking (ΔR) and flexural displacement (ΔF) to the total displacement is calculated by dividing the individual contributions by the total displacement. The assumption is that the peaks for rocking and total displacement occur almost simultaneously and the ratios can be described by $\Delta R_{ti}/\Delta T_{ti}$ and $\Delta F_{ti}/\Delta T_{ti}$ where t_i is time of maximum total displacement. Figure 4-14 shows the described ratios for test sets AS, DS and FS. The first two sets show that rocking displacement comprises up to ½ of the total displacement. For test set FS rocking displacement is no more than 1/5 of the total displacement.

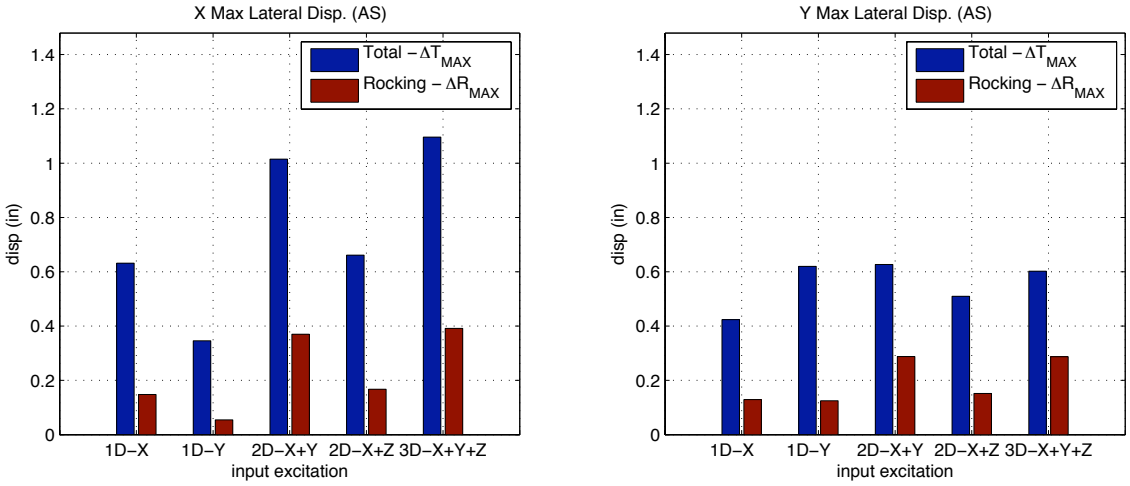

(a) Test Set AS

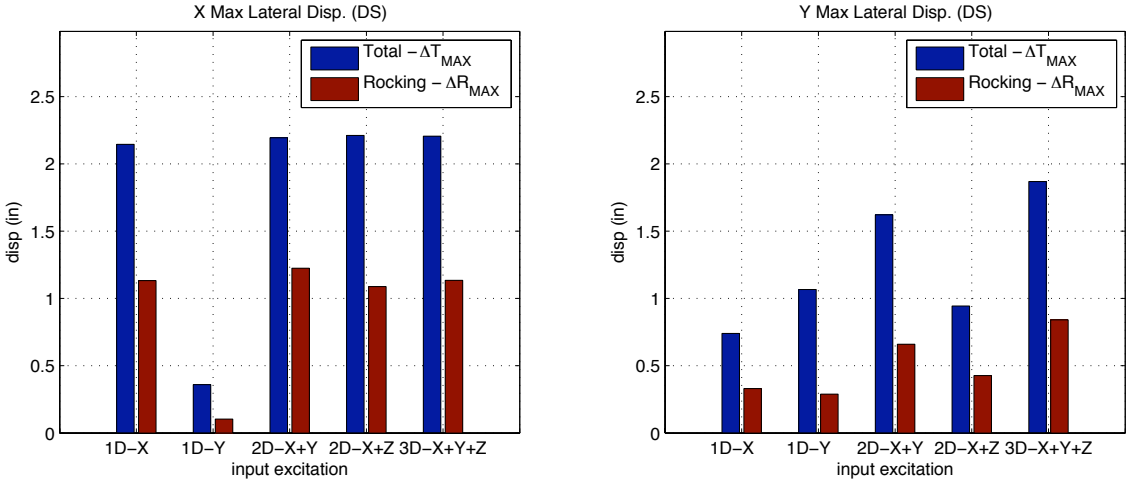

(b) Test Set DS

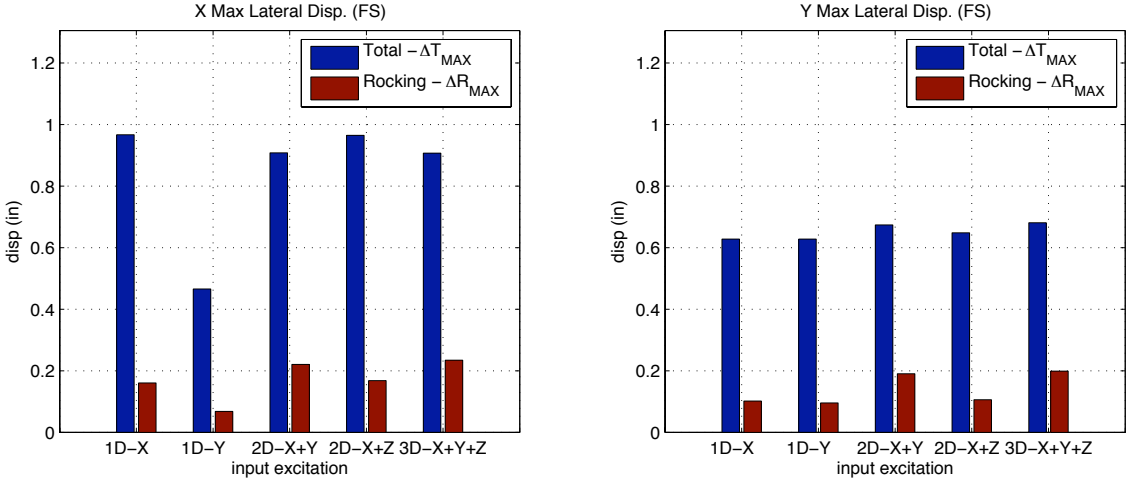

(c) Test Set FS

Figure 4-13: Test Group 2-Rocking Contribution to Max Center Mass Lateral Displacement.

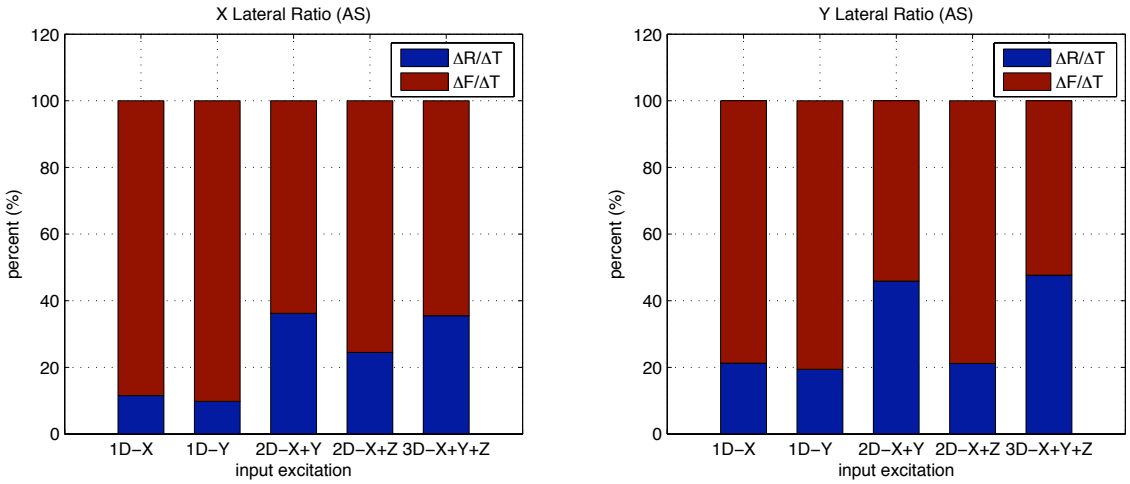

(a) Test Set AS

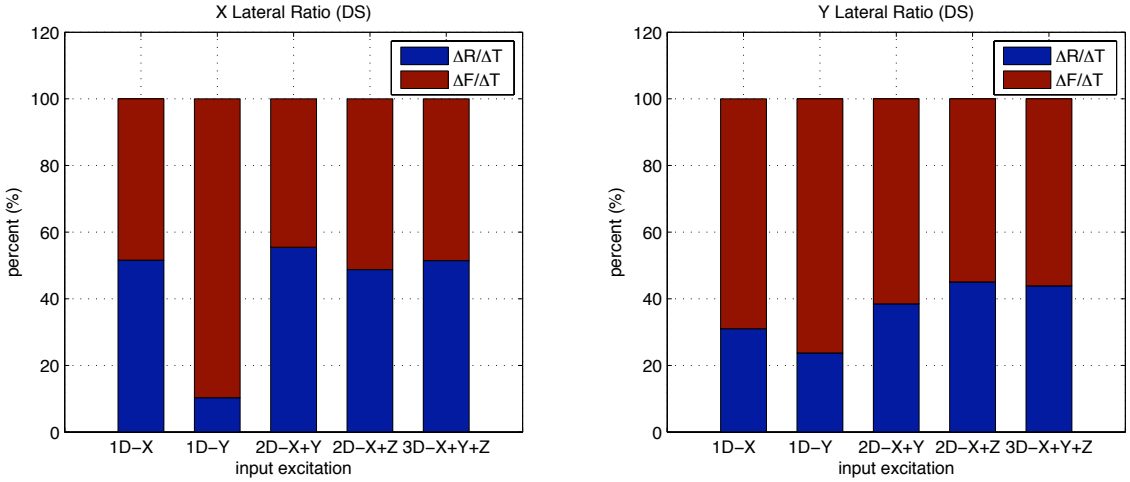

(b) Test Set DS

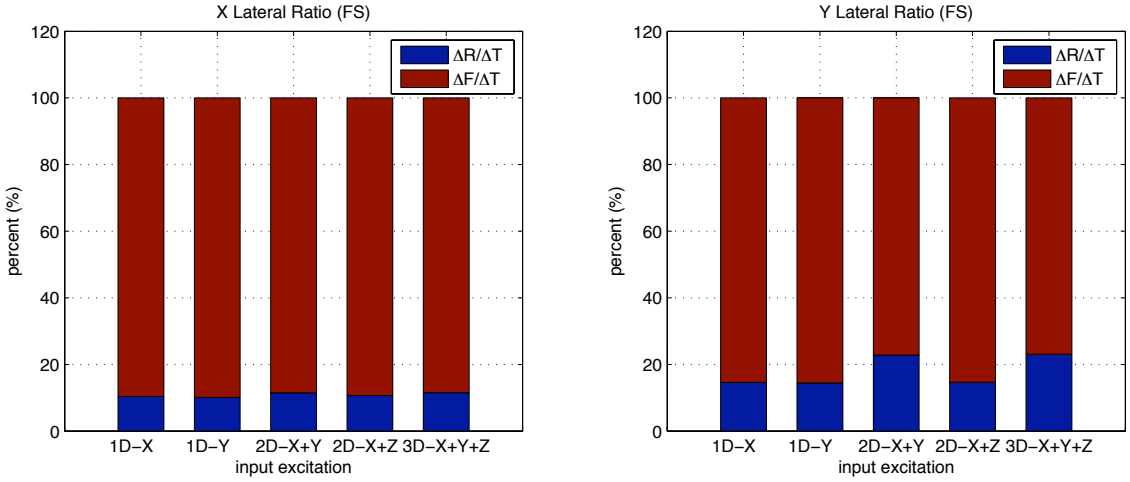

(c) Test Set FS

Figure 4-14: Test Group 2 – Rocking and Flexure Contribution to Peak Lateral Displacement

4.5.1.2 Footing Uplift

The uplift of the footing was determined using the procedures described in Section 4.2.1.2. The initial vertical displacement of the footing was recorded due to axial load and then the dynamic vertical uplift of the footing was determined using the 4 Novotechniks to record the dynamic footing vertical displacement relative to the rigid table surface. The footing vertical displacement was calculated for the entire footing by assuming a rigid body, which was a reasonable approach. The vertical displacement of the footing can be described as uplift when the footing physically separates from the elastomeric pad or rocking when the footing remains in contact with the pad, but rotates due to the flexibility of the pad. Figure 4-15 illustrates the terminology for footing vertical displacement.

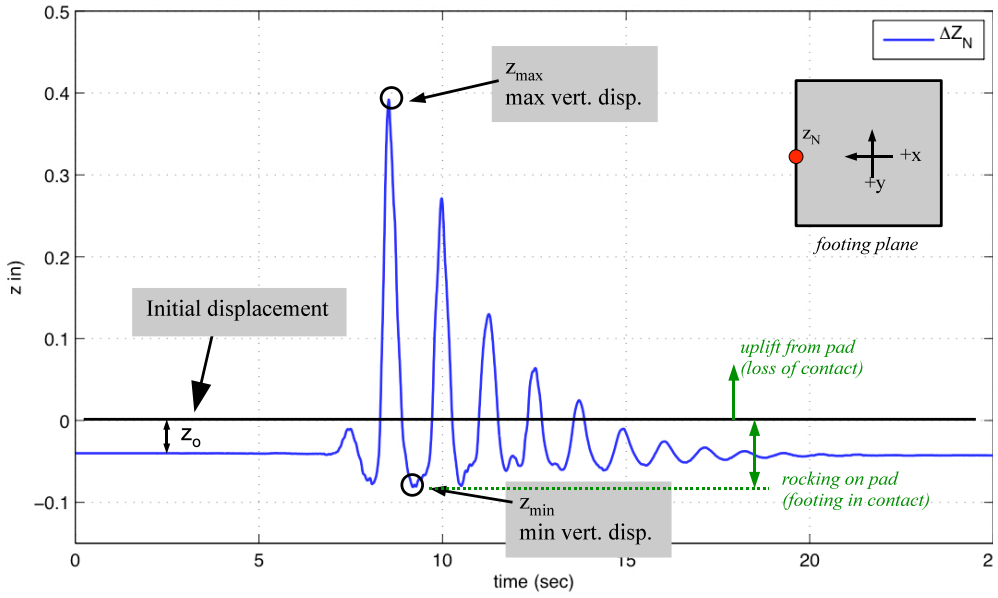

Figure 4-15: Illustration of terminology for footing vertical displacement.

The recorded vertical displacements were used to calculate the rotation about the centerline in the X direction (θ_{NS}) and the Y direction (θ_{EW}). The rotations were then used to calculate the edge vertical displacements along the centerlines in the X direction at the north edge (ΔZ_N) and south edge (ΔZ_S) as Y direction for the east (ΔZ_E) and west (ΔZ_W) edges. A rigid body assumption allowed for calculation of vertical displacements of all locations in the horizontal plane of the footing. The entire footing uplift profile was then used to assess the envelope of displacements along the X and Y directions and the peak contours of vertical displacement for the entire footing.

The measured static displacement due to weight of the top mass, column, and footing was approximately z_o=0.03 inches. The edge displacements for test set AS are shown in Figure 4-16. At this level of excitation the amount of uplift is quite small, on the order of 0.08 inches similar to the amount of indentation on the compression side. This is consistent with the intent of this test.

Selected uplift vertical displacements for tests D1S, D3S, and D5S are shown in Figure 4-17 to Figure 4-19. At this level of excitation the amount of uplift is small about 0.4 inches, but not insignificant. This is consistent with the intent of this test, which was to cause uplift and rocking of the specimen. The envelopes of displacement are presented. Interestingly the peak uplift values take a linear shape and the peak indentation values take a nonlinear shape indicating nonlinear displacement response of the elastomeric pad when compressed. The contours for peak uplift and indentation are also shown for the entire footing. As the column response results illustrated the addition of the Y component of excitation significantly contributes to the uplift in that direction. The additional component increases the peak displacement by approximately 50%.

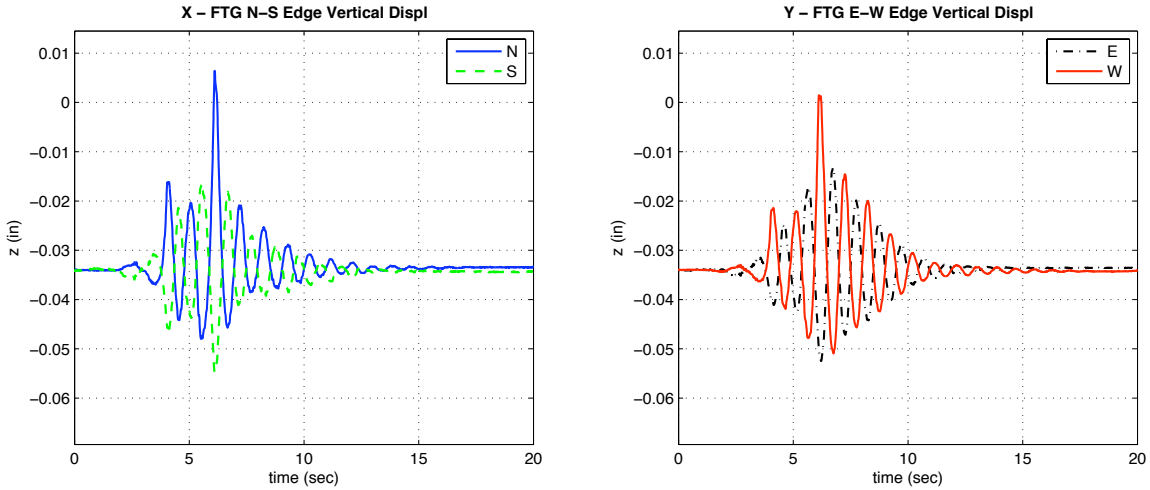

(a) Test Run A1S

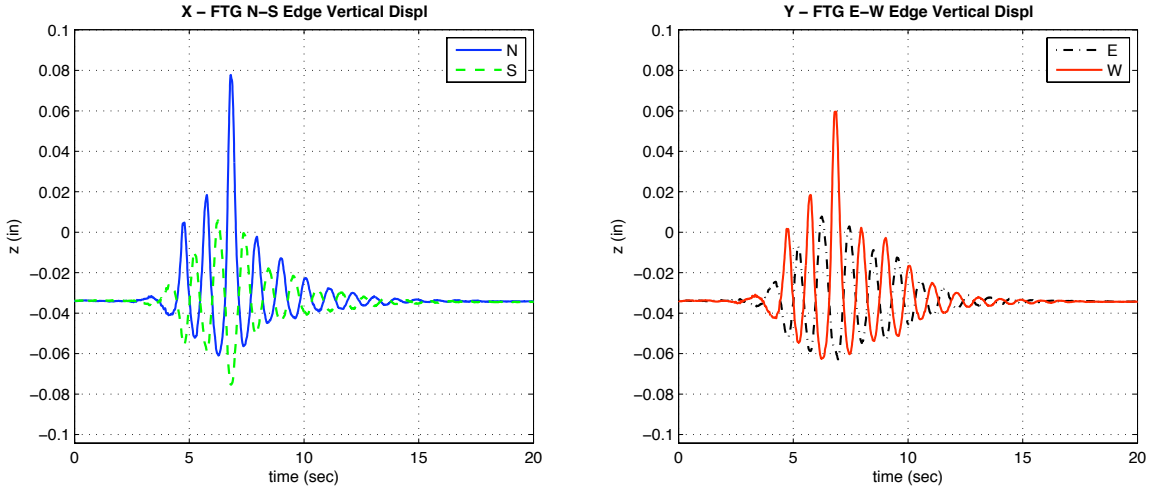

(b) Test Run A3S

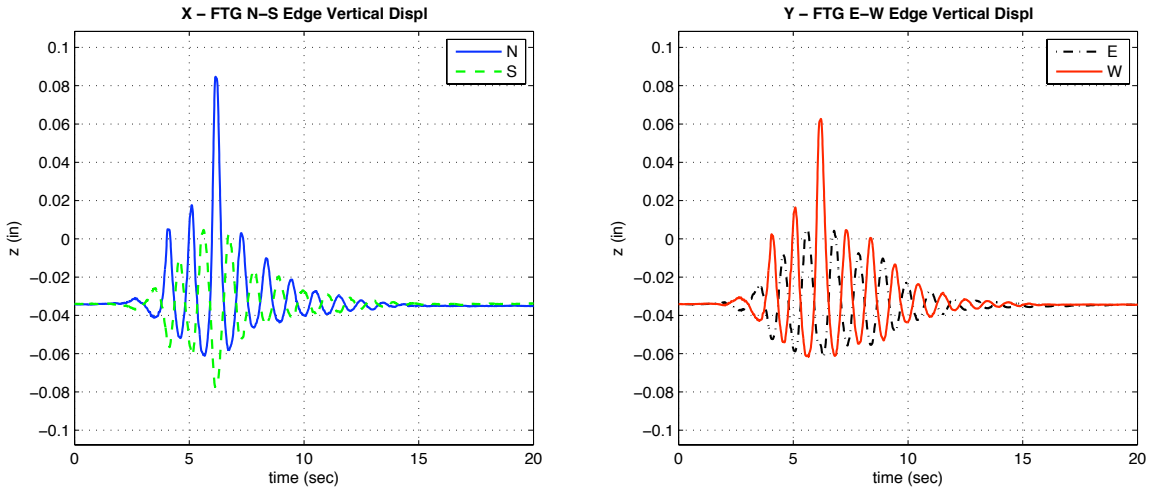

(c) Test Run A5S

Figure 4-16: AS Centerline Edge Footing Uplift Response

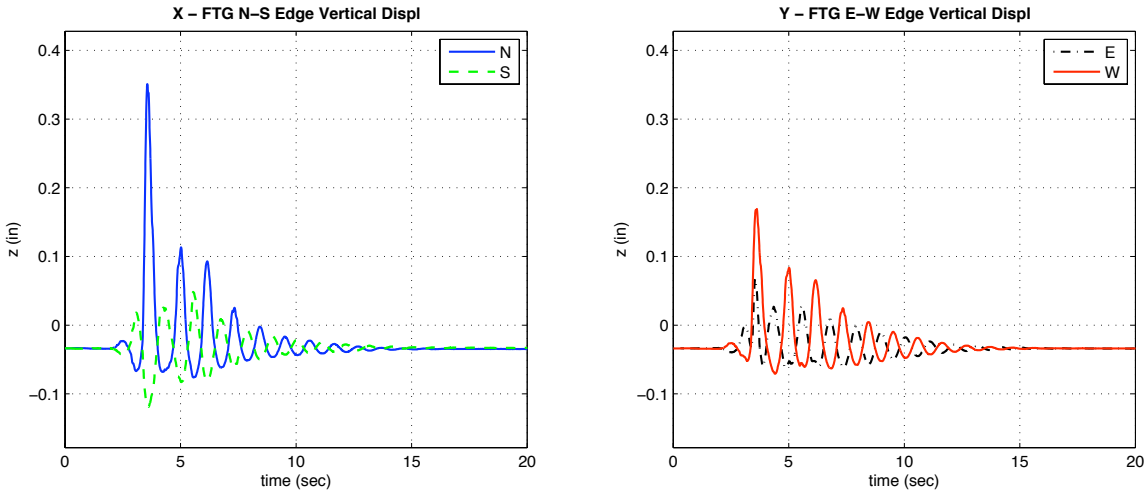

(a) Test Run D1S

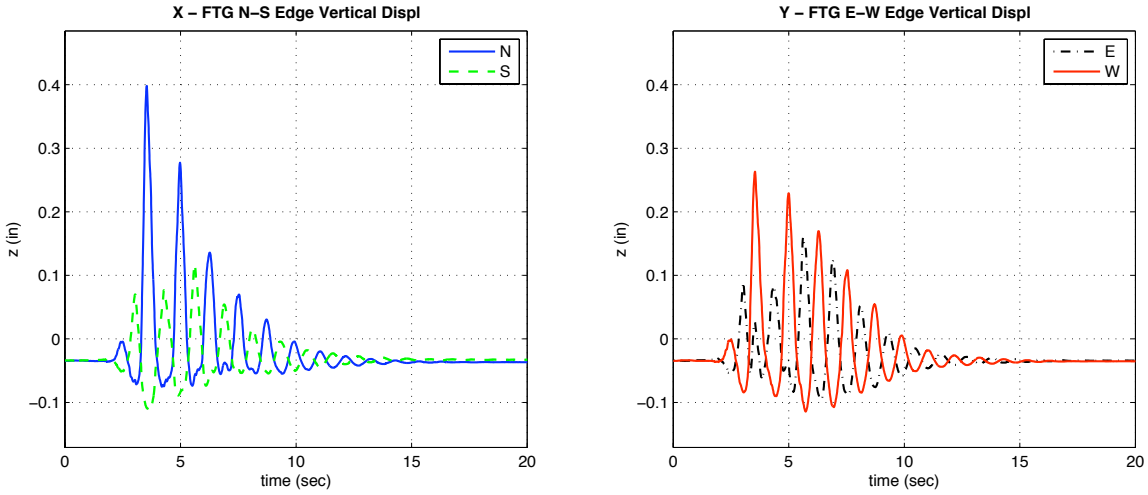

(b) Test Run D3S

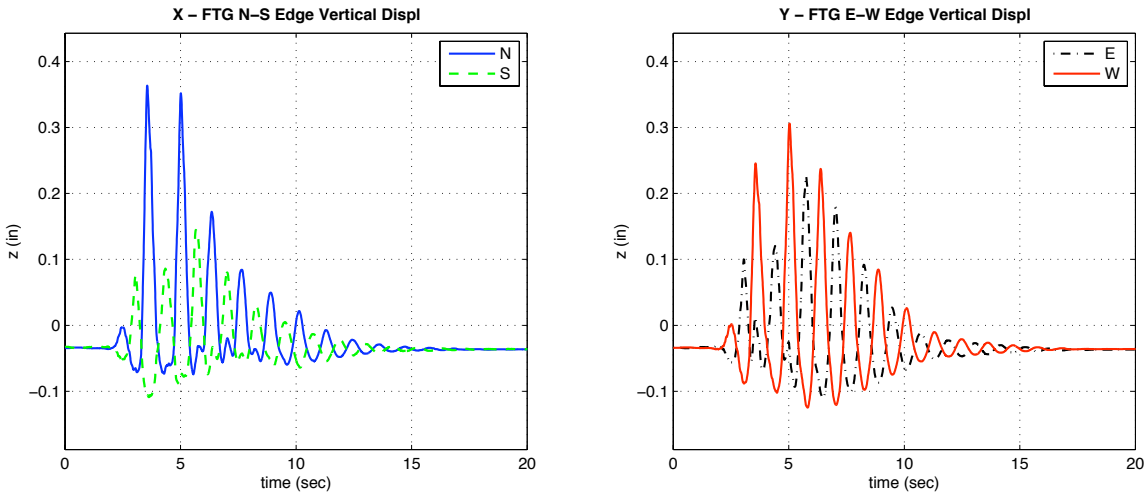

(c) Test Run D5S

Figure 4-17: DS Centerline Edge Footing Uplift Response

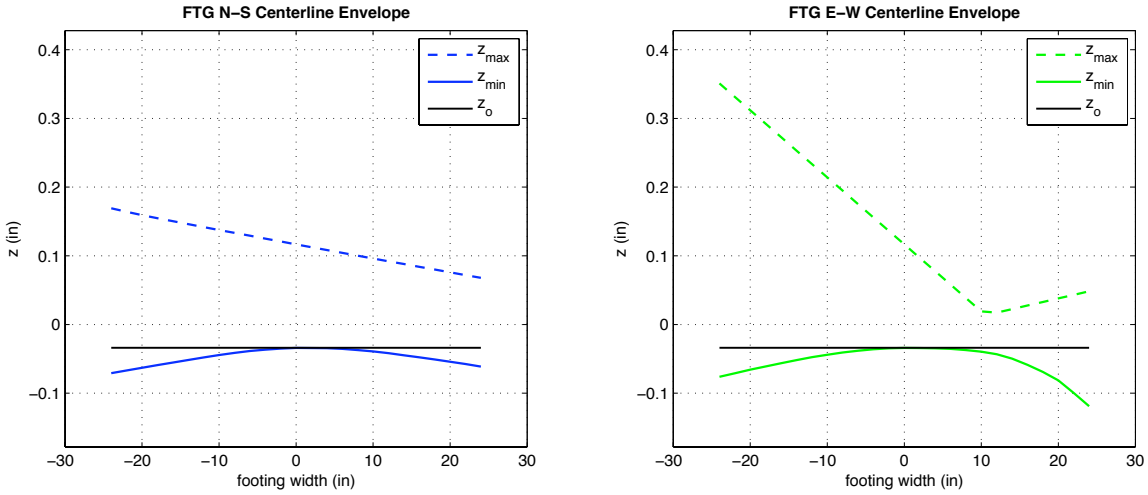

(a) Test Run D1S

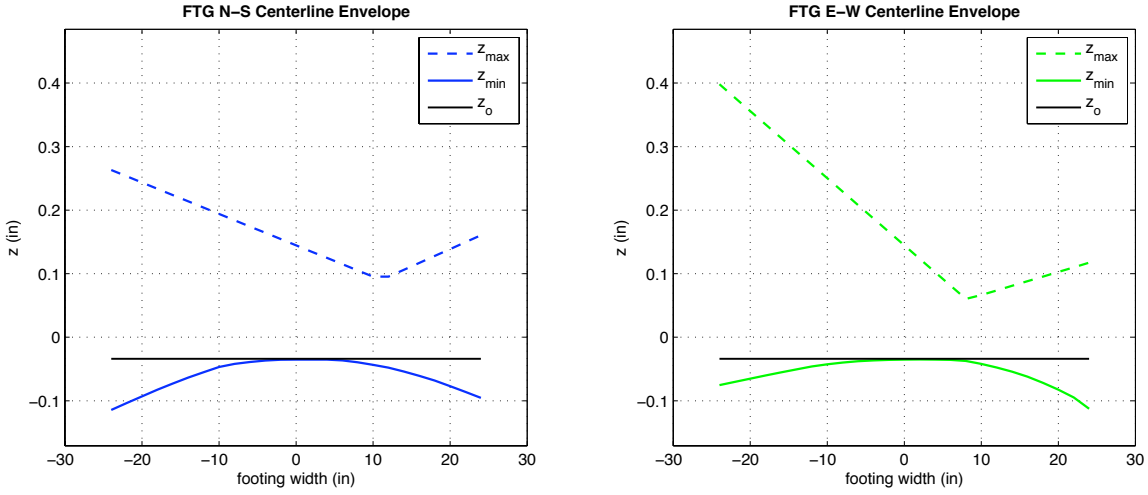

(b) Test Run D3S

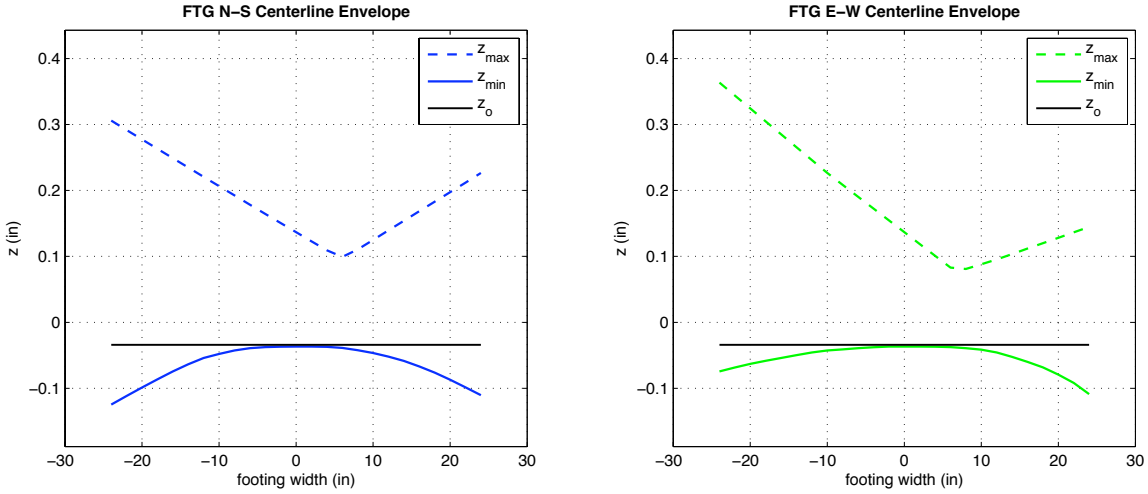

(c) Test Run D5S

Figure 4-18: DS Centerline Envelope Footing Uplift Response

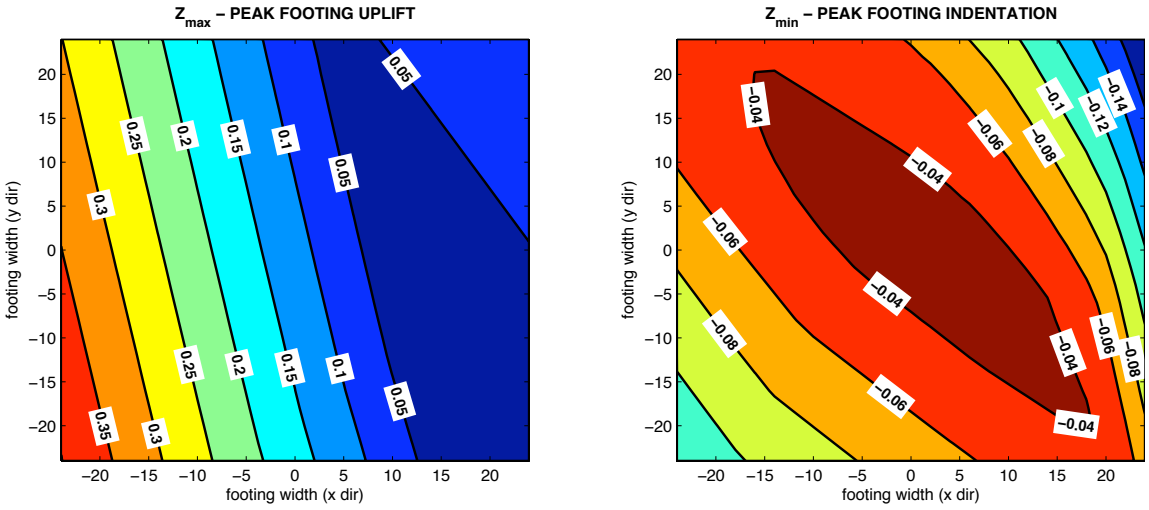

(a) Test Run D1S

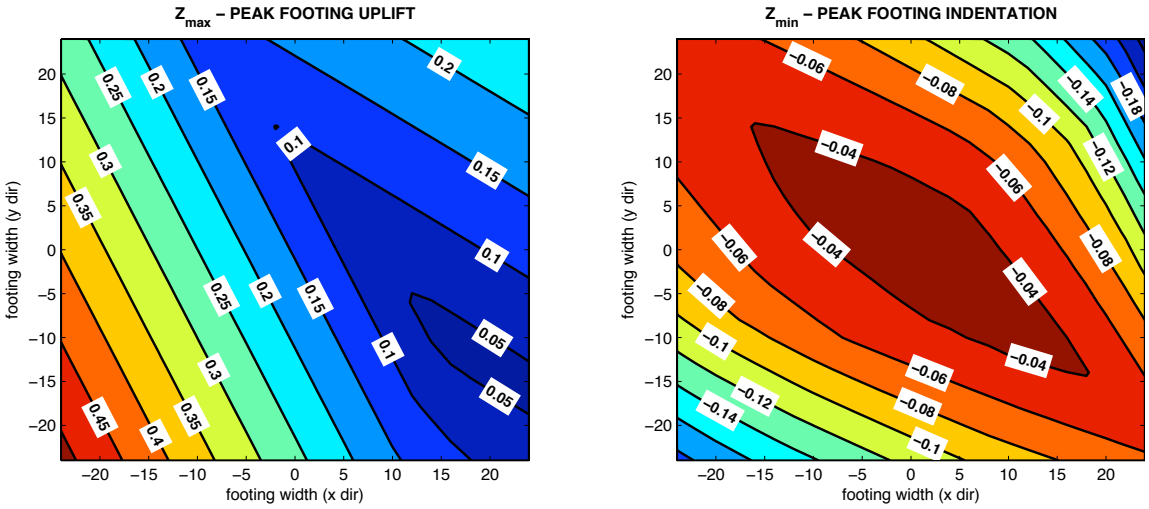

(b) Test Run D3S

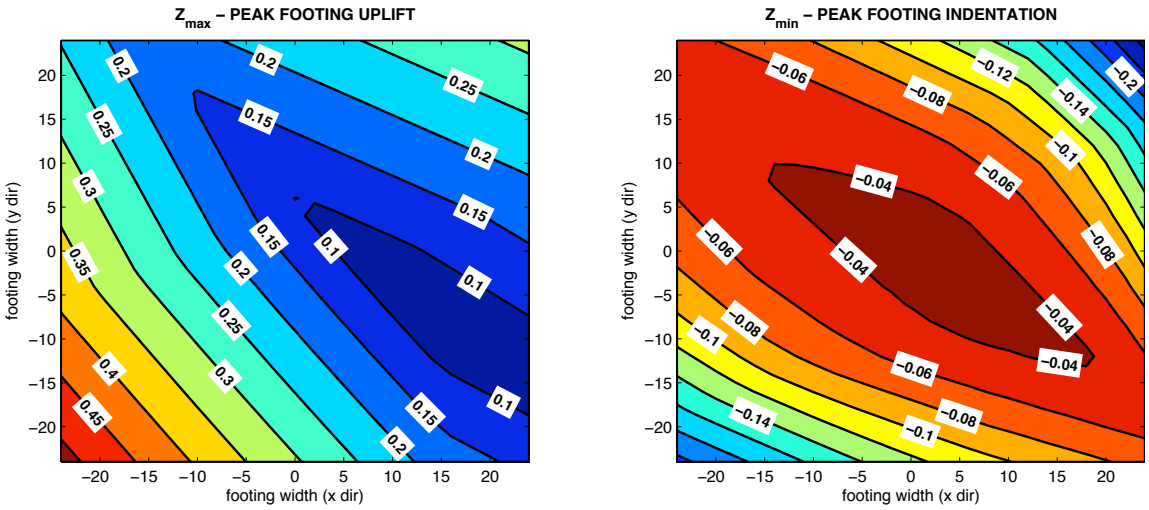

(c) Test Run D5S

Figure 4-19: DS Contour Footing Uplift Response

4.5.1.3 Rotations about Vertical Axis

During testing the unrestrained footing was observed to rotate about a vertical axis especially during strong bidirectional response. The cause of twisting is easy to appreciate considering a situation where the footing is lifting due to excitation in the X direction, and then subjected to an inertial force in the Y direction. Here there is a tendency to rock in the Y direction, and an eccentricity between the center of mass and the center of lateral resistance between the footing and the soil. This eccentricity will tend to twist the specimen, and it tends to pivot around the corner of the footing still in contact with the elastomeric pad.

As a result of repeated occurrences of this phenomenon, a permanent lateral movement in the X and Y directions and rotation about the vertical axis can be seen in the test results. Figure 4-20 shows the results for test sets DS and FS. The cumulative displacement at the conclusion of the test set was 0.5 inches and 0.0 inches, respectively. The amount of uplift for FS was very small as noted, so it would be expected there would be a negligible amount of rotation because of the phenomenon of rotation, which is the case for this test set. In an actual footing, passive pressure of the soil against the sides of the footing and the attachment of the top of the column to the bridge deck would tend to minimize this motion. Because of the high weight of the test specimen relative to the capacity of the laboratory crane, no attempt was made to align the specimen with the principle axes of the table following each test run.

The calculation of rotation about the vertical axis was done using recorded displacement on the corners of one footing face and dividing by the horizontal distance between the locations. Test sets DS and FS had a maximum rotation of approximately 0.012 radians and 0.0015 radians which for the 48 inch square footing is approximately 0.27 inches and 0.03 inches of twists of the corner edges.

4.5.2 Local Response

Measuring curvatures and strains in critical locations provides insight to global response measures and observed damage of the systems. Curvature distributions within the column plastic hinge length are of particular interest as are the strains of reinforcing within this region. Reinforcing slip complicates the analysis of the system and so an attempt is made to quantify the amount of slip in the system. This section describes the average column curvature over several regions of column height, the amount slip or bar pull-out measured at the base of the column and the reinforcing strains in rebar within the plastic hinge zone.

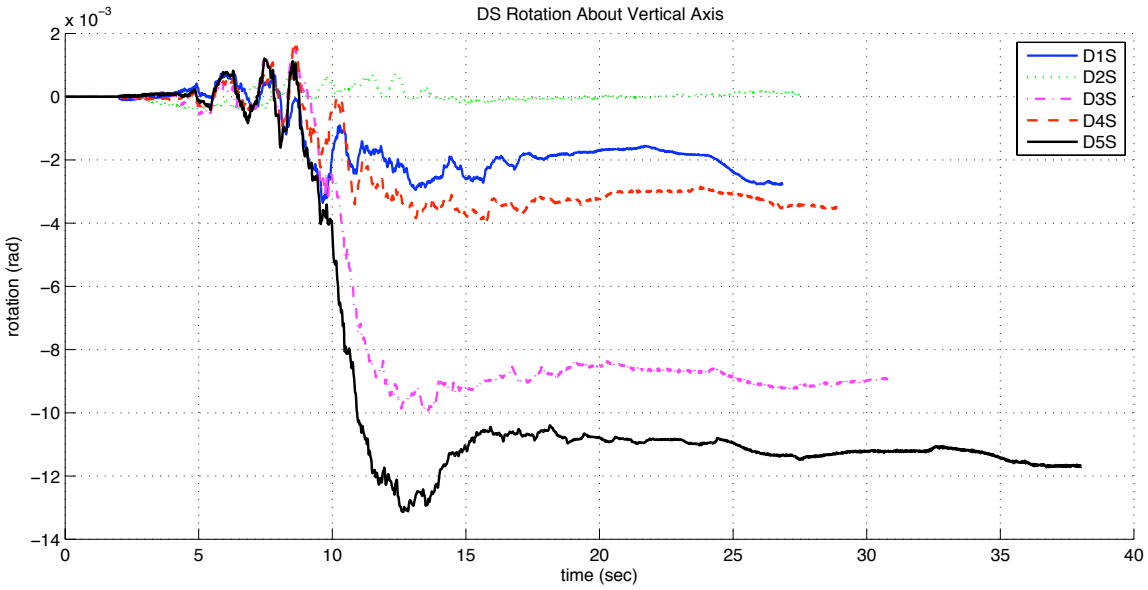

(a) Test Set DS

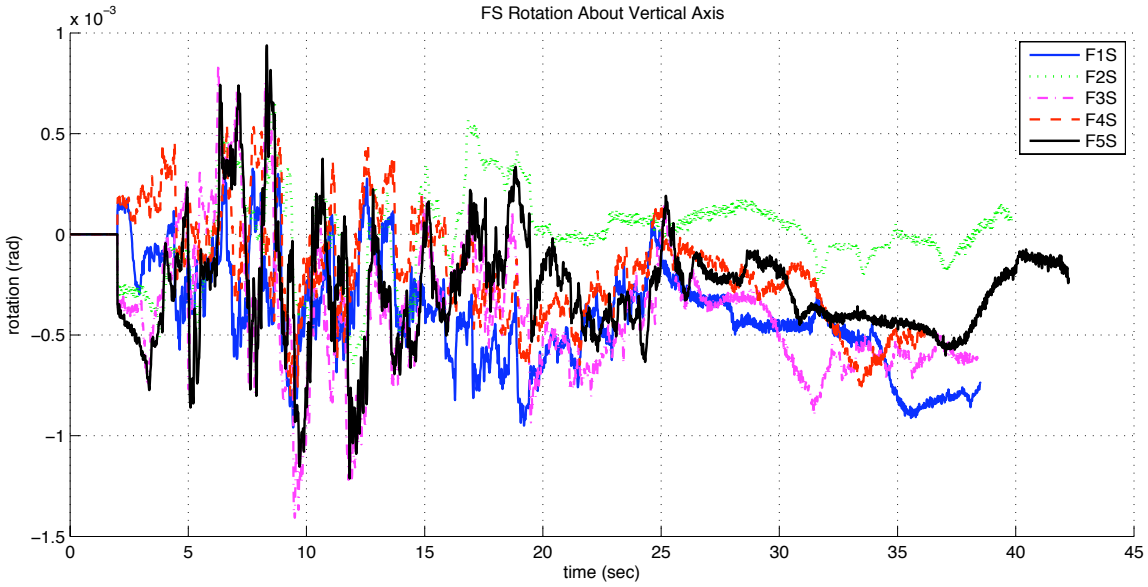

(b) Test Set FS

Figure 4-20: Test Set DS and FS twisting about vertical axis

4.5.2.1 Column Curvature Distribution

Average curvatures were estimated over regions of the column extending between the locations of DCDT instruments attached to the face of column. Section 4.2.1.3 illustrates the method of column curvature calculation and Figure 3.24 highlights the locations of the DCDTs. The curvature recordings for tests D3S and F3S are shown in Figure 4-21. The results show that there was less curvature demand for the FS group which is consistent with global displacements measures shown in Figure 4-11 and Figure 4-12.

Region 1 and 2 are used to determine bar pullout measuring elongation at the same column height to distinct locations at or above the footing. Pullout of the longitudinal reinforcing from the footing was measured using a similar method to the curvature calculations. At the region adjacent to the footing (for each face), a pair of DCDTs was connected 6 inches above the footing. One of the pair measured elongation between the connection and the footing and the other measured elongation between the connection and a rod attached to the column approximately ½ inch above the footing. The difference between the two readings is an estimate of the pullout the bar for that face. Using the same process for the opposing face the slip rotation could be calculated and the displacement of the center of mass due to anchorage slip could be determined. On average for Test Group 2 the amount of slip measured was between 20-30% of the total flexural displacement of the column.

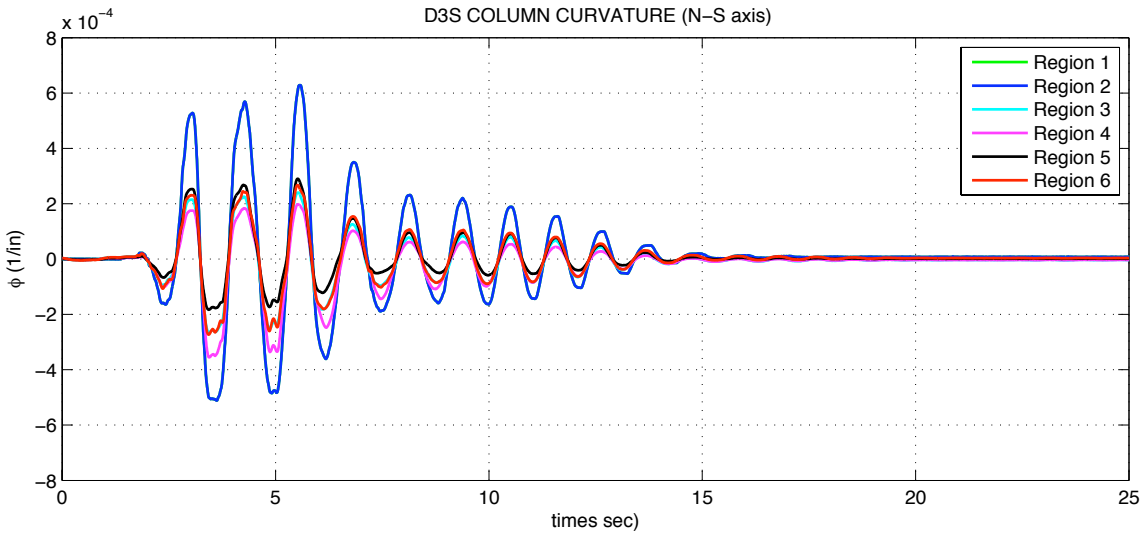

(a) D3S Column Curvature

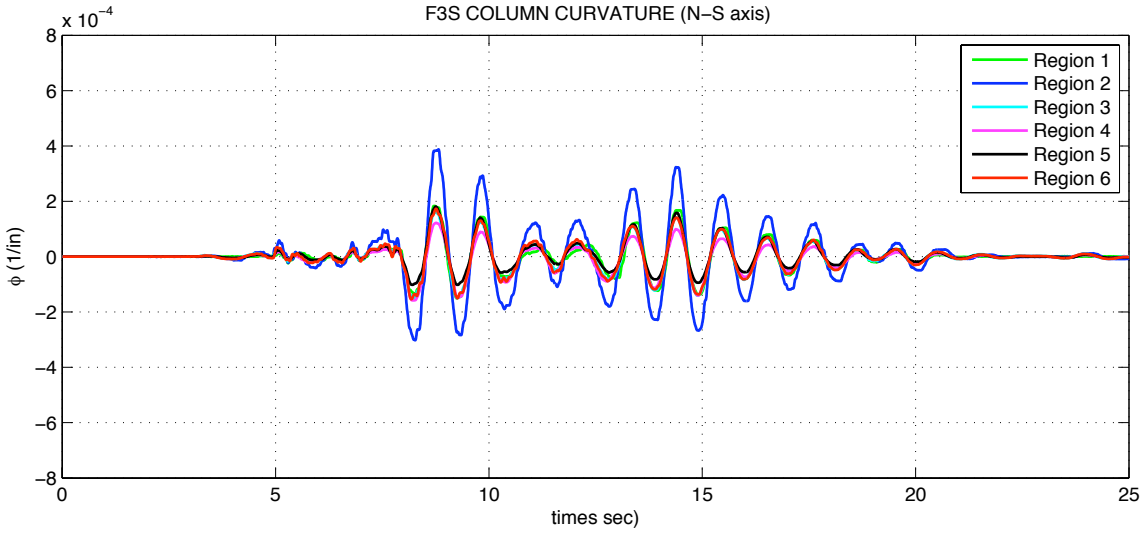

(b) F3S Column Curvature

Figure 4-21: Recorded column curvatures along column height

4.5.2.2 Strains

Strain gauges were mounted on four of the twelve longitudinal reinforcing bars. The measured strains provide insight into the behavior to the bars during loading, in particular, when the strains in the reinforcement reach the inelastic demand level. The four locations of strain measurement were the bars that coincided with the North, South, East and West column faces. The gauges were mounted on the outer face of the reinforcement and were located at two elevation points that corresponded to the top and bottom of the plastic hinge zone. The information from the gauges is very useful to determine when yielding begins, but beyond that the information they provide can be unreliable because the gauges often fail when strains reach excessive demands. Such as those from large deformations and rotations of the column.

Figure 4-22 shows the strains on the South most reinforcing bar for test D5S which is a 3D input excitation. The peak value of tensile strain is 1200 μS which is approximately 60% of the yield strain. Clearly, the strains did not reach an inelastic level. The two locations of recording were at the base (0" height) and the top of the expected plastic hinge zone (16" height) above the base. The cumulative time history for test set DS is shown in Figure 4-23 for the South and East reinforcing steel. The time history is for the strain gauge at the bottom of the column.

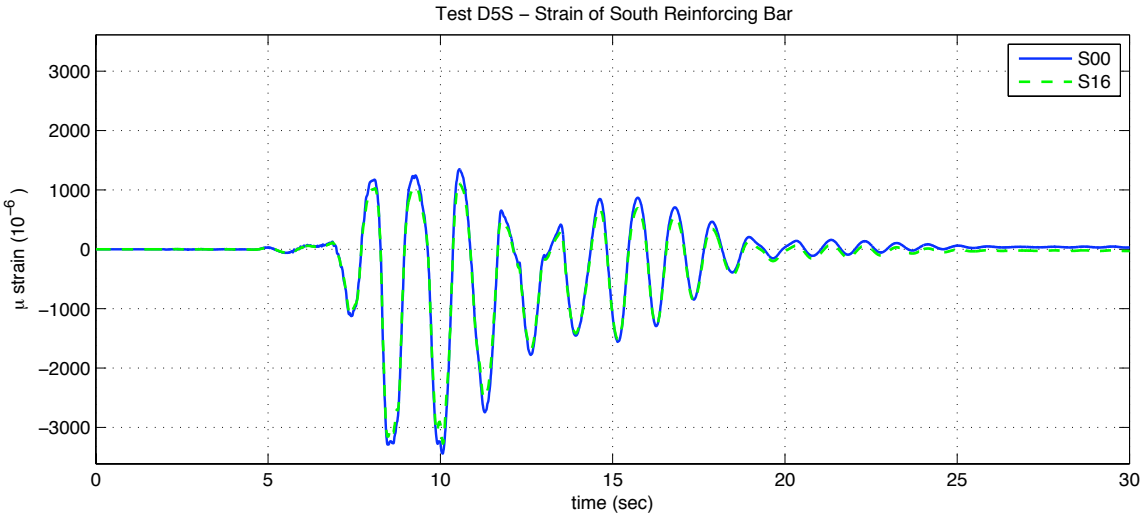

Figure 4-22: Reinforcing steel strain for South rebar (Test D5S)

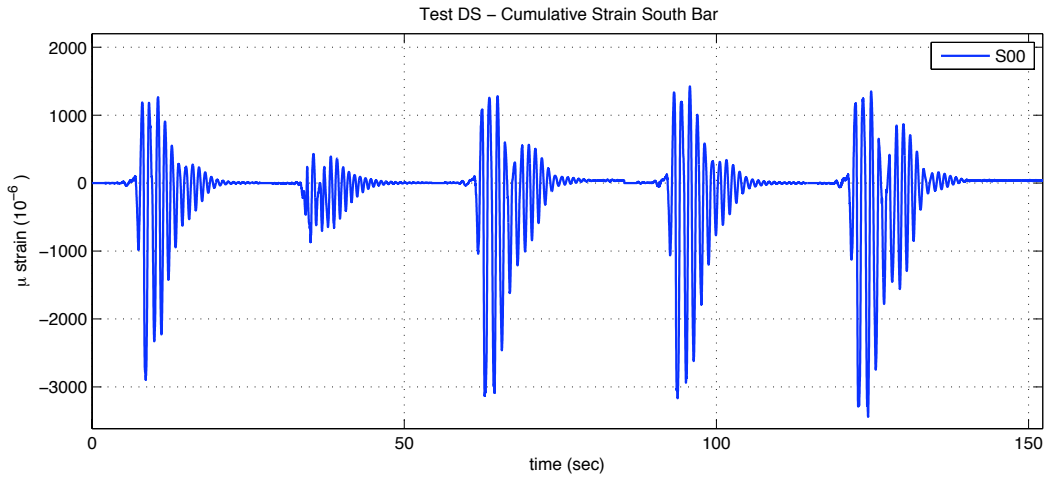

(a) South Bar Strain Gauge @ 0" Height

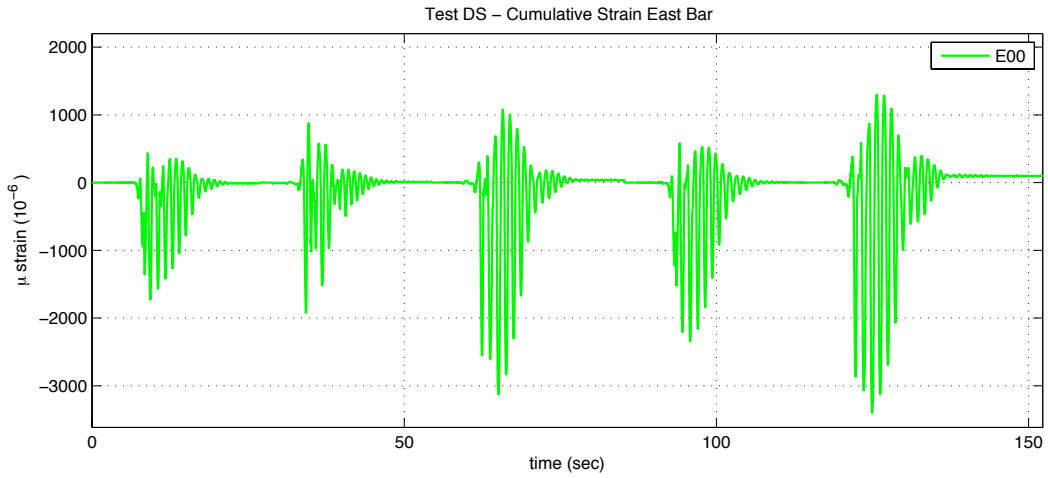

(b) East Bar Strain Gauge @ 0" Height

Figure 4-23: Cumulative Strain Time History Test D5S

4.5.3 Force-Displacement Hysteresis Curves

The force-displacement relationships of the specimen highlight the behavior during shaking and provide particular insight into how the specimen behaves when allowed to uplift. When a well-confined reinforced concrete column is restrained from uplift at the base the moment-curvature relationship at the base of the column is essentially linear until the point where inelastic demands are reached and exceeded. Significant energy dissipation occurs due to nonlinear behavior associated with yielding of the reinforcement and concrete crushing. The inclusion of an uplifting foundation with flexible supporting medium adds considerable hysteretic energy dissipation from uplift and interaction of the soil. The addition of this energy dissipation mode may draw away some of the energy dissipated by the deformation along the column height.

The force-displacement relationships of particular interest of uplifting footings are the base moment-column curvature and the base moment vs. footing rotation. This section illustrates the magnitude of response for both of these relationships.

Calculations of the moment time histories were done by the methods described in Section 4.2.2. Figure 4-24 shows the calculated base moment time histories for test D1S, D3S, and D5S. The results between the two and three components of excitation are similar, but not exact owing to the inclusion of the vertical component of excitation. As the number of input excitations increased the response at the 8 sec. mark became out of phase, more so for each component of excitation. This may owe to a lengthening of the natural period due to softening during testing. More likely, it is caused by the interaction between orthogonal directions when considering additional excitations. For comparison the moment time history of test F1S, F3S, and F5S are shown in Figure 4-25, which had less demand at the column base than the DS test set. The test F1S is not out of phase as it appears, but in reality it is time shifted to start earlier.

The peak moment for tests DS was calculated as 1078 kip-in, 1047 kip-in, and 1041 kip-in for the DS tests shown. The approximate ratio between peak moments was approximately 1. For FS the peak moments are 726 kip-in, 624 kip-in, and 631 kip-in, respectively. It is interesting to note the larger demand for the one component of excitation, which is approximately 115% greater.

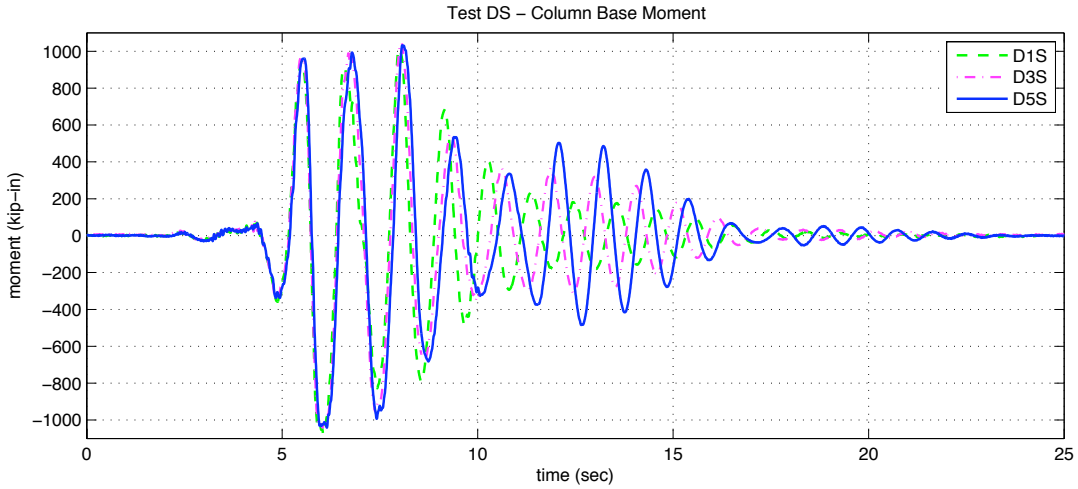

Figure 4-24: DS Column Base Moment Time History

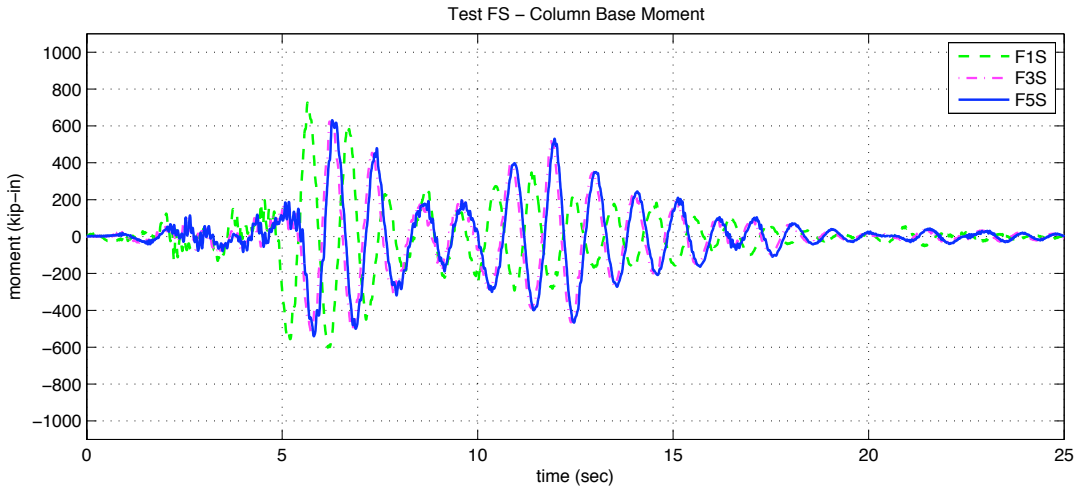

Figure 4-25: FS Column Base Moment Time History

The lateral force versus lateral displacement hysteresis of the column base shear and center-of-mass of the top block is shown in Figure 4-26 for tests AS, DS, and FS whose displacements are shown in Figure 4-10 through Figure 4-12. No significant nonlinear behavior was observed which was consistent with the testing objective. High frequency response is observable in the shears. Hachem et al. (2003) discussed this occurrence and found that it was related to high mode vibrations of the specimen involving rotation of the center of mass about the local horizontal axes.

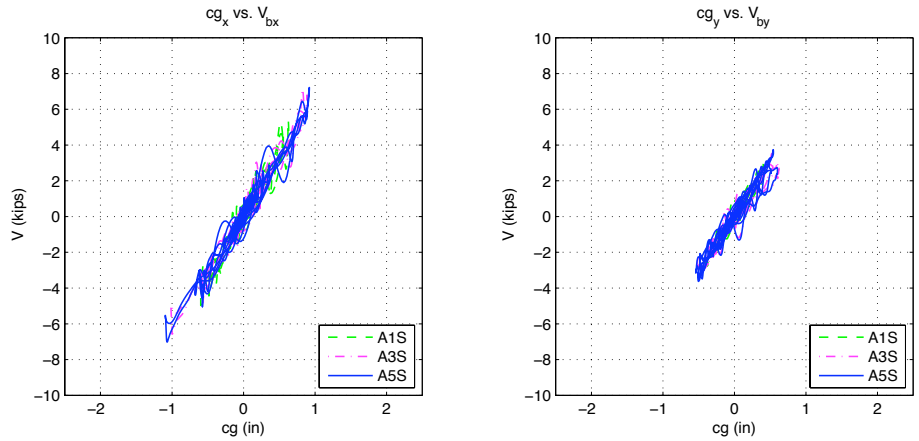

(a) AS – 1D-X, 2D-X+Y, 3D-X+Y+Z

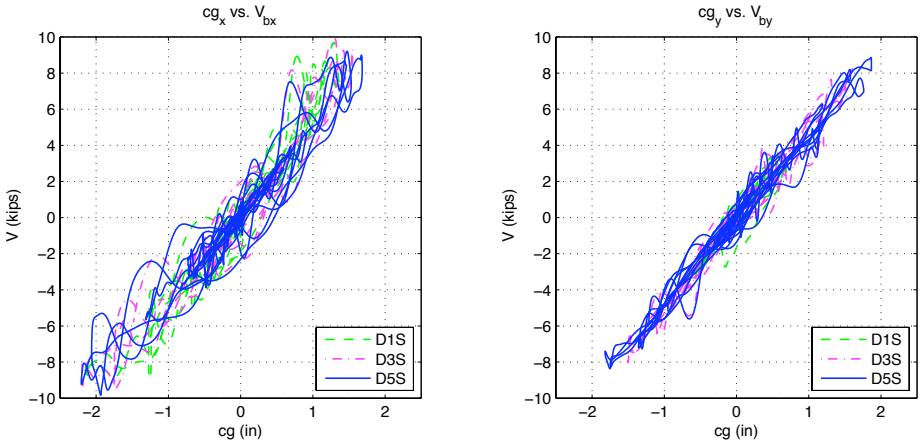

(b) DS – 1D-X, 2D-X+Y, 3D-X+Y+Z

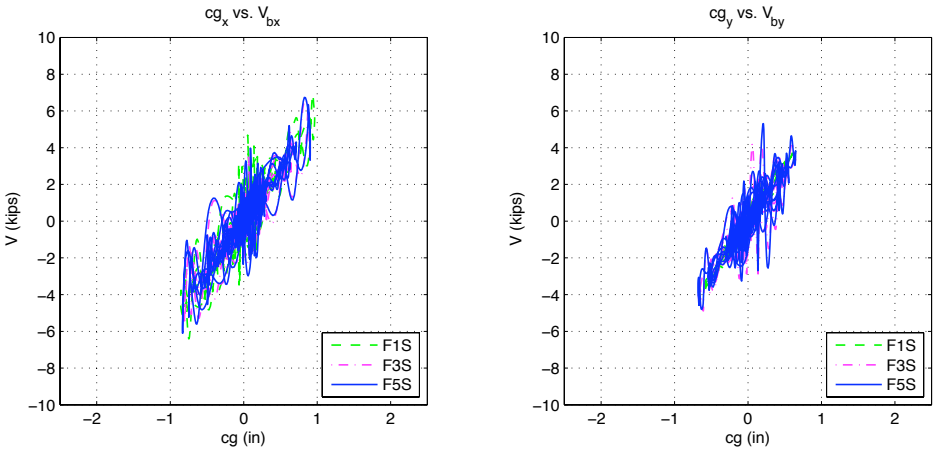

(c) FS – 1D-X, 2D-X+Y, 3D-X+Y+Z

Figure 4-26: Lateral Force vs. Lateral Displacement (Tests AS, DS, FS)

4.5.3.1 Moment-Curvature Column Response

Average column curvatures at the base are plotted here against the calculated column base moment. The average curvatures are those shown in Figure 4-21. A highly linear relationship exists between the moment and curvature, which indicates that the specimens behaved as desired. Figure 4-29 shows the average curvature vs. column moment for tests AS, DS, and FS. In Figure 4-29(b) it should be observed that the stiffness of the system as described by the slope of the curvature-moment plot seems to be more gradual than the other plots. This may be an anomaly due to loading or recording instruments because the subsequent test FS seems to match well with the others.

4.5.3.2 Moment-Rotation Footing Response

The column moment-footing rotation relationship indicates the relationship of rocking and uplift on energy dissipation via hysteresis. Figure 4-27 illustrates some of the important characteristics of a rocking and/or uplifting footing. For low levels of excitation it is likely that the relationship would be essentially linear while rocking and that as uplift occurred the behavior would become nonlinear. At the value of moment the footing loses contact with the pad the response softens indicating an essentially linear response while rocking and nonlinear elastic response while rocking and uplifting. Literature reviews (Chapter 2) indicate that there is likely a value of overturning moment at which point the footing response to applied moment softens and essentially behaves as a bilinear curve with smaller overturning post-yield stiffness.

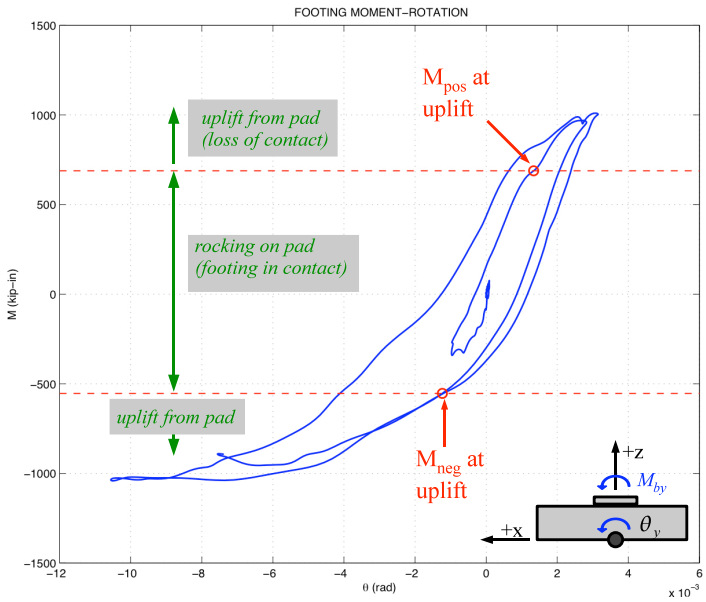

Figure 4-27: Moment-Footing Rotation Characteristics

The footing uplift described in Section 4.5.1.2 was used to calculate rotation along the centerline for both the North-South Axis and the East-West axis. Rotations were calculated by subtracting the relative uplift between opposing footing edges and dividing by the footing width (Equation (4-4)). A sample of the calculated rotation for test D3S is shown in Figure 4-28 for each direction. Figure 4-30 shows the footing rotation vs. column moment for tests AS, DS, and FS

The values for moment at which uplift from the footing and rotation about the outer edge would occur were the same for each direction and were measured to be approximately M_{upNS}=M_{upEW} = 600 kip-in and M_{rotNS}=M_{rotEW}=1100 kip-in, respectively.

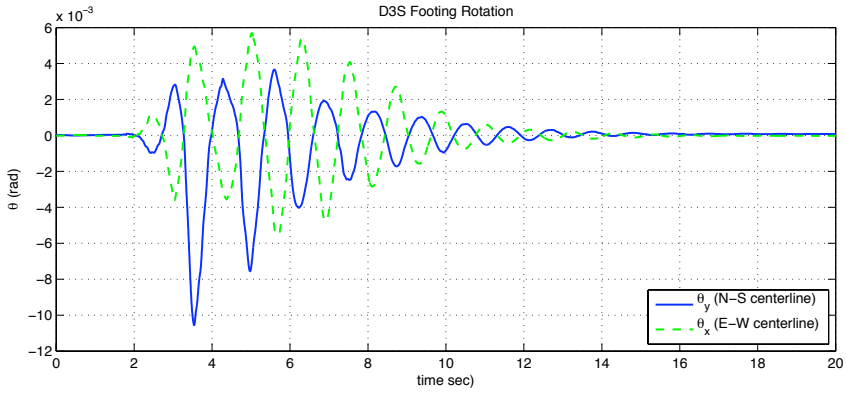

Figure 4-28: D3S Footing Rotation

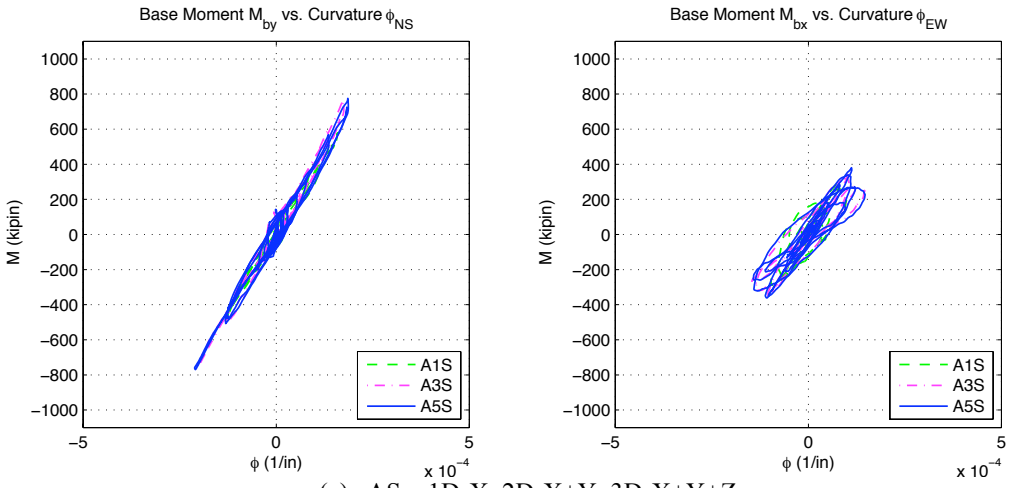

(a) AS – 1D-X, 2D-X+Y, 3D-X+Y+Z

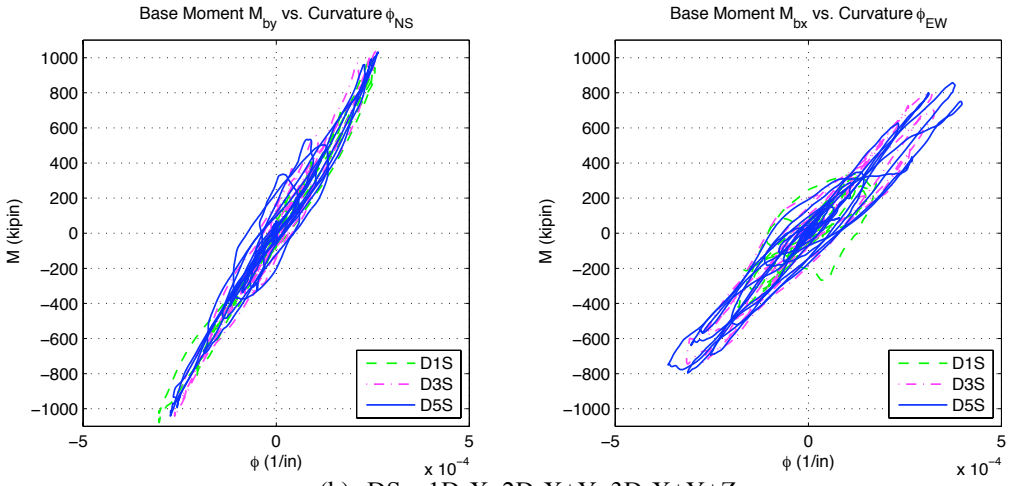

(b) DS – 1D-X, 2D-X+Y, 3D-X+Y+Z

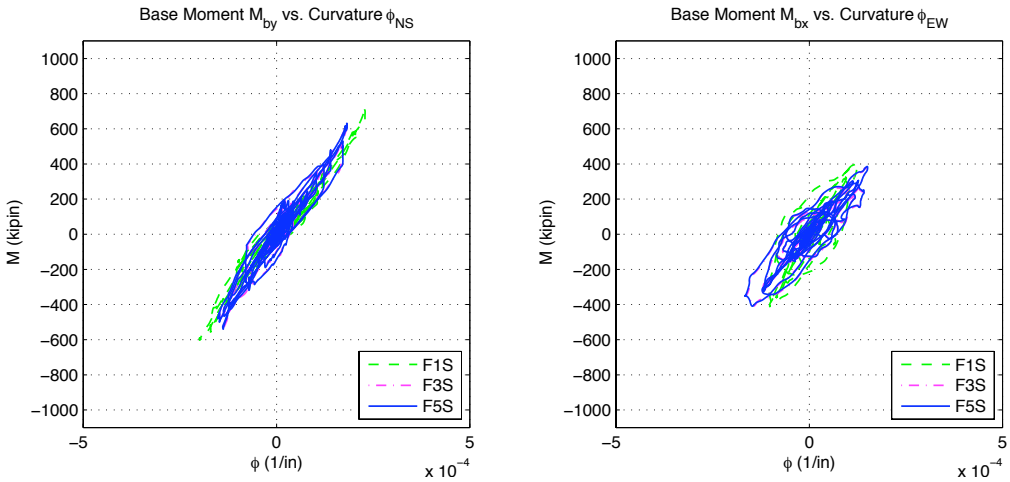

(c) FS – 1D-X, 2D-X+Y, 3D-X+Y+Z

Figure 4-29: Column Base Moment Curvature Response (Tests AS, DS, FS)

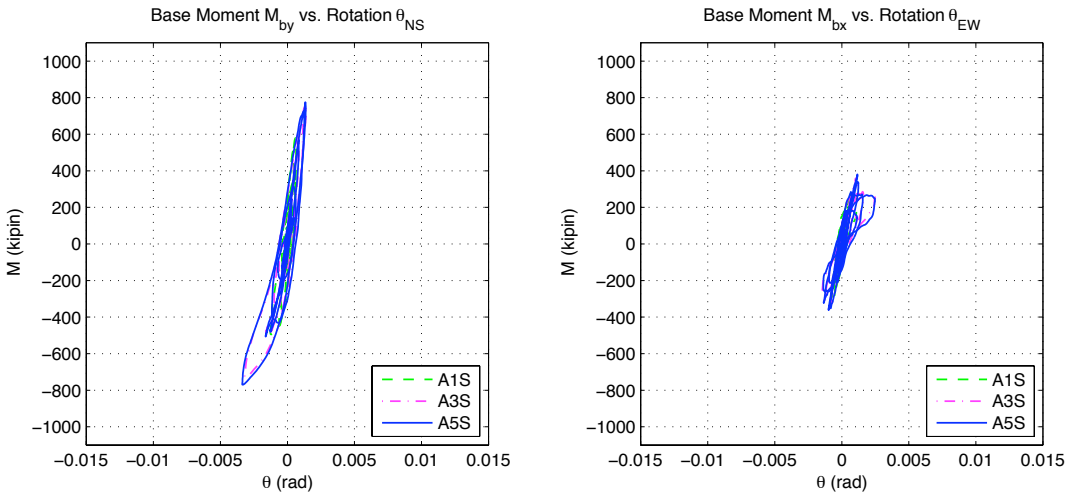

(a) AS – 1D-X, 2D-X+Y, 3D-X+Y+Z

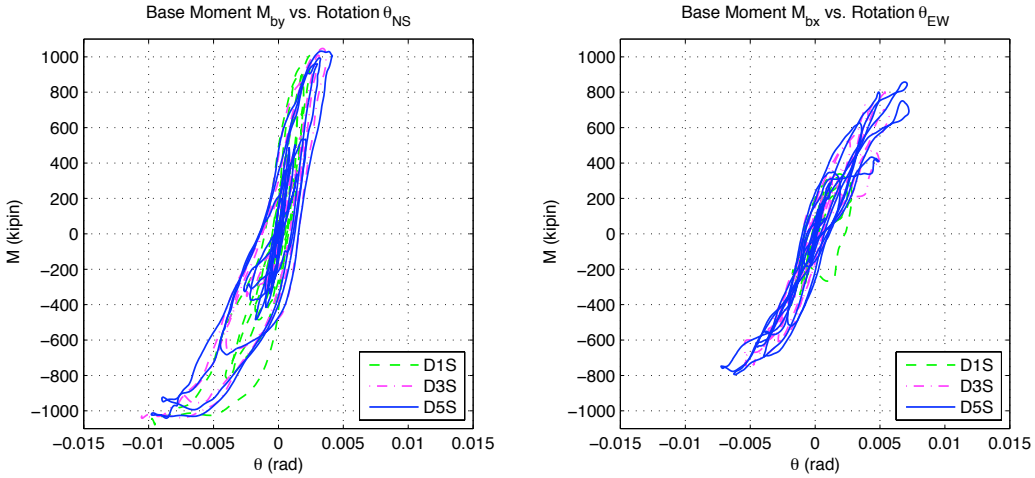

(b) DS – 1D-X, 2D-X+Y, 3D-X+Y+Z

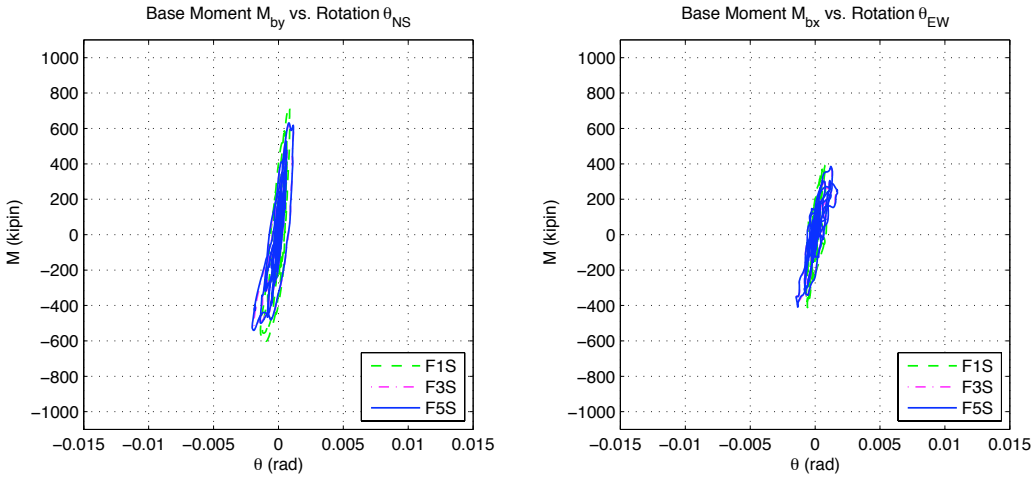

(c) FS – 1D-X, 2D-X+Y, 3D-X+Y+Z

Figure 4-30: Column Base Moment Footing Rotation Response (Tests AS, DS, FS)

4.6 Test Specimen with Design Axial Load and 5Dc x 3Dc Footing

The final test group widened the footing in one direction to $5D_c$ x $3D_c$ and the intensity of the motions were increased to the point where the column would be loaded into the inelastic range. For this test series, all three components of excitation were used for all runs. The test set AR includes all four tests conducted for Test Group 3. Only the Los Gatos record was used for testing. In the smaller footing dimension direction, rocking response was preferred over yielding in all cases. Section 4.7 will compare the applied vs. restoring moment to correlate the observations of increased inelastic demand and reduced uplift for the test set.

Time histories for global displacement, local response and force-displacement response are included in the following sections. Instrumentation described in Chapter 3 was again used to measure the global and local response. Positioning of the instruments was unchanged with the exception of the Novotechniks used to record footing uplift. The devices had to be repositioned to accommodate the wider footing direction, however the calculation of response was done in a similar manner.

The amplitude scale of ground motions was set at a level which would cause an elastic, yield, design and maximum displacement ductility response for the rocking system as determined by the column. The magnitude of scaling was 10%, 25%, 90%, and 120% of the original scale. A direct correlation on the effect of footing width on total response can be made between test A2R and D5S which both had a three-dimensional input excitation at 25% amplitude scale.

Only the first test run A1R was conducted in the elastic range of the column. All subsequent tests illustrated a nonlinear relationship of the lateral force-displacement response. Additionally permanent displacements occurred in the column due to the damage of nonlinear loading. This test group clearly shows that vertical restraint of the footing was unnecessary to develop the plastic hinge moment of the column and achieved the desired design goal. As determined by the Caltrans SDC, which is to confine damage in a bridge system to the plastic hinge region of the column. It also shows that it is prudent to detail columns to be ductile, even if they are expected to rock, due to the effects of bidirectional bending on the footing and column.

The results for Test Group 3 are presented in a similar fashion to those of Test Group 2 (Section 4.5).

4.6.1 Global Displacement

The global displacements of the system are described in this section. Three types of displacement are calculated to describe the response: (1) The total center of mass displacement is a combination of the rocking from rigid body translation due to footing uplift and the flexural displacement of the column due to inertial loading, (2) the uplift of the footing due to inertial loading, and (3) the rotation of the footing about a vertical axis due to uplift and simultaneous lateral loading.

4.6.1.1 Column Response

The set AR includes all four tests conducted for Test Group 3. Time histories of lateral displacement of the center of mass are presented in Figure 4-31 to Figure 4-34. The results for the wider footing suggest less rocking behavior in the orthogonal directions than for the smaller footing size of Test Group 2, and less total displacement for the elastic and yield level tests than the similar amplitude-scaled ground motions of group 2.

Test A2R and D5S both had three-dimensional input excitations scaled to 25% of the Los Gatos record. Figure 4-32 and Figure 4-11(c) show the response for each and suggest that the overall lateral displacement of the center of top mass is considerably smaller for the $3D_c$ x $5D_c$ footing than for the $3D_c$ x $3D_c$ footing in either direction. Little rocking was measured for the $3D_c$ x $5D_c$ case but rocking and uplift contributed to about half of the lateral displacement response for the $3D_c$ x $3D_c$ case. The response of the $3D_c$ x $5D_c$ footing is similar to that of the $3D_c$ x $3D_c$ if the rocking and uplift displacements are deducted. Comparison of Figure 4-32 and Figure 4-11(c) suggests that limiting rocking in one direction (by increasing the footing width to $5D_c$) can reduce its effect in the other direction.

During testing inelastic behavior occurred which can be seen, by recognizing the permanent later displacement, following test runs A3R and A4R (see Figure 4-33 and Figure 4-34). Following the A3R run there was approximately 1 inch of permanent displacement for the X and Y direction, respectively. Which was approximately a 1% permanent drift. The incremental permanent displacement for run A4R in the X and Y directions are about 9 and 13 inches, respectively; giving a cumulative residual displacement in the X and Y directions of 10 and 15 inches, respectively. Thus, even though the base was not restrained against rocking in either direction, and rocking would be expected on the basis of a simple one-dimensional analysis in the $3D_c$ direction, ductile yielding of the column dominated the response of the column with the $3D_c$ by $5D_c$ footing.

A comparison of peak total displacement and the contribution of rocking displacement to the total is shown in Figure 4-35(a) for tests A1R, A2R, A3R, and A4R. The bar on the left is the maximum lateral displacement of the center of mass and the bar on the right is the contribution of rocking to the maximum displacement. The ratio of rocking and flexural displacement to the total displacement is calculated by dividing the individual contribution to the total displacement and is shown in Figure 4-35(b). The assumption for these calculations is described in Section 4.5.1.1. The yield level test had the most amount of uplift and rocking. Approximately 25% and 10% for the short and wide footing directions, respectively. The design and elastic level tests each had no more than a peak of 10% uplift and rocking in either direction.

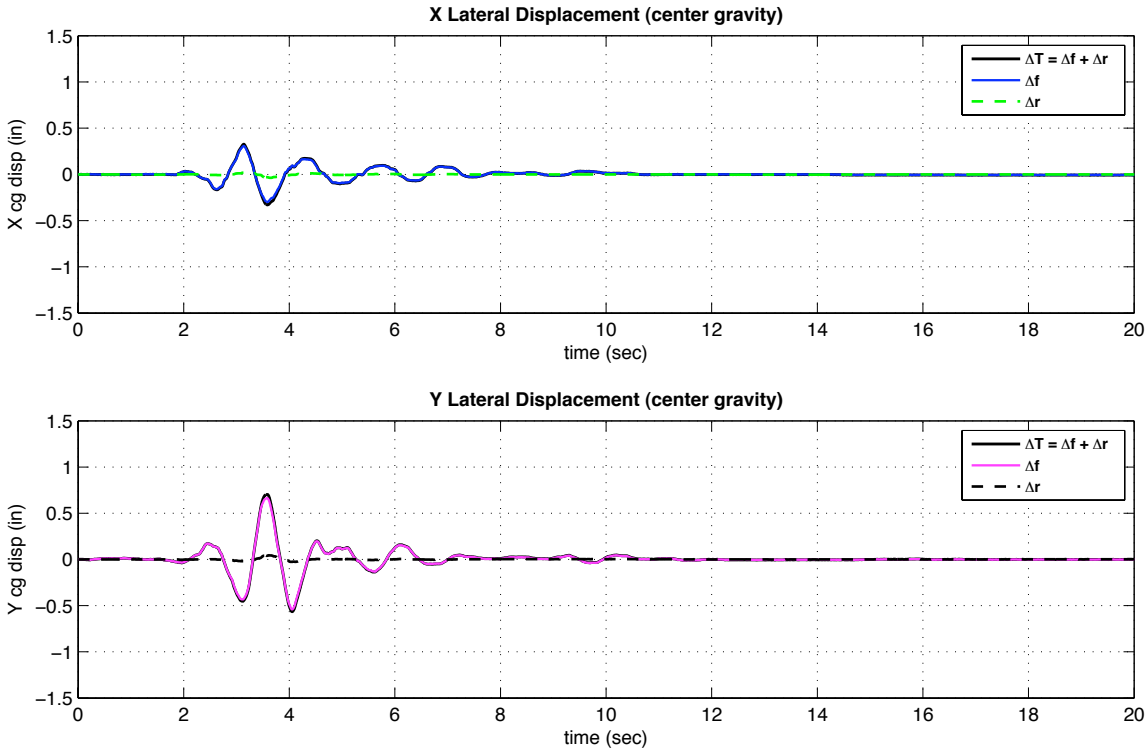

Figure 4-31: Elastic Level Test A1R Displacement Response

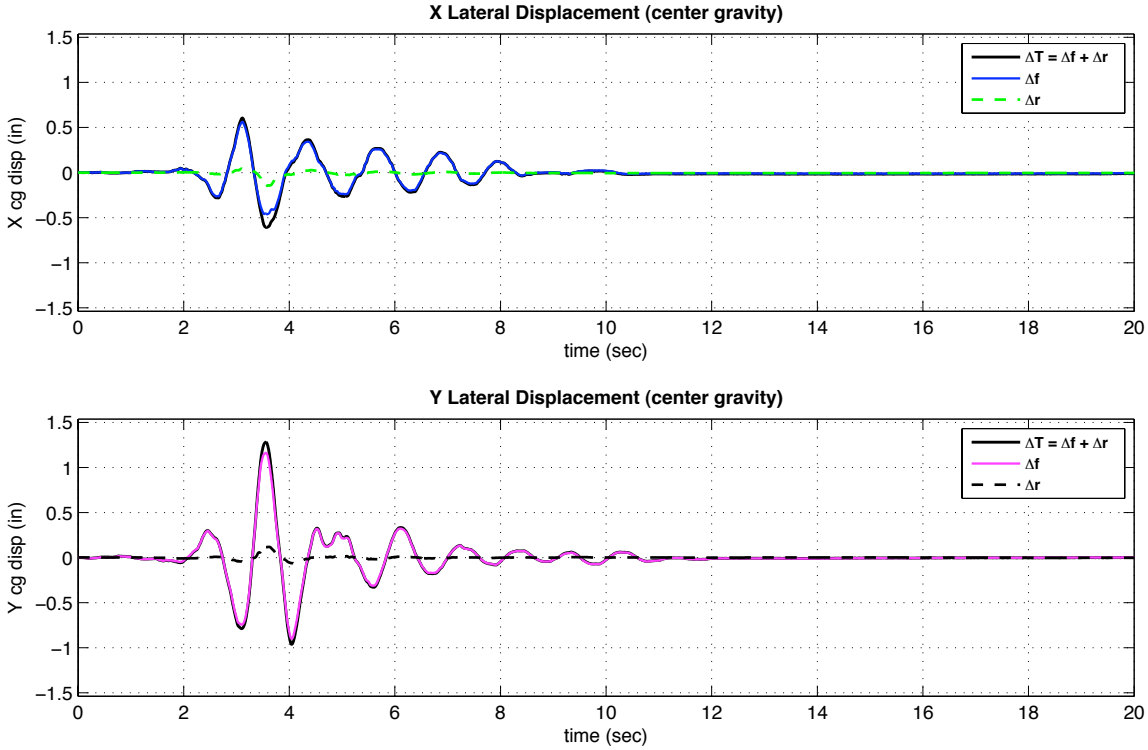

Figure 4-32: Yield Level Test A2R Displacement Response

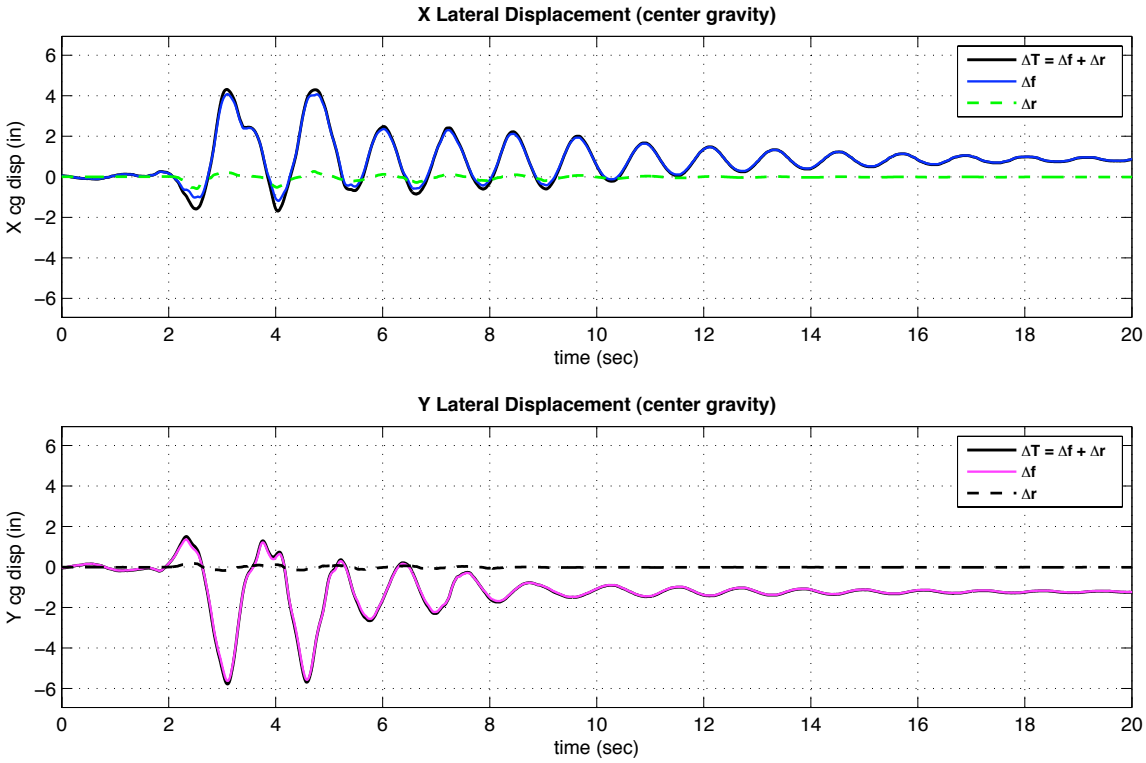

Figure 4-33: Design Level Test A3R Displacement Response

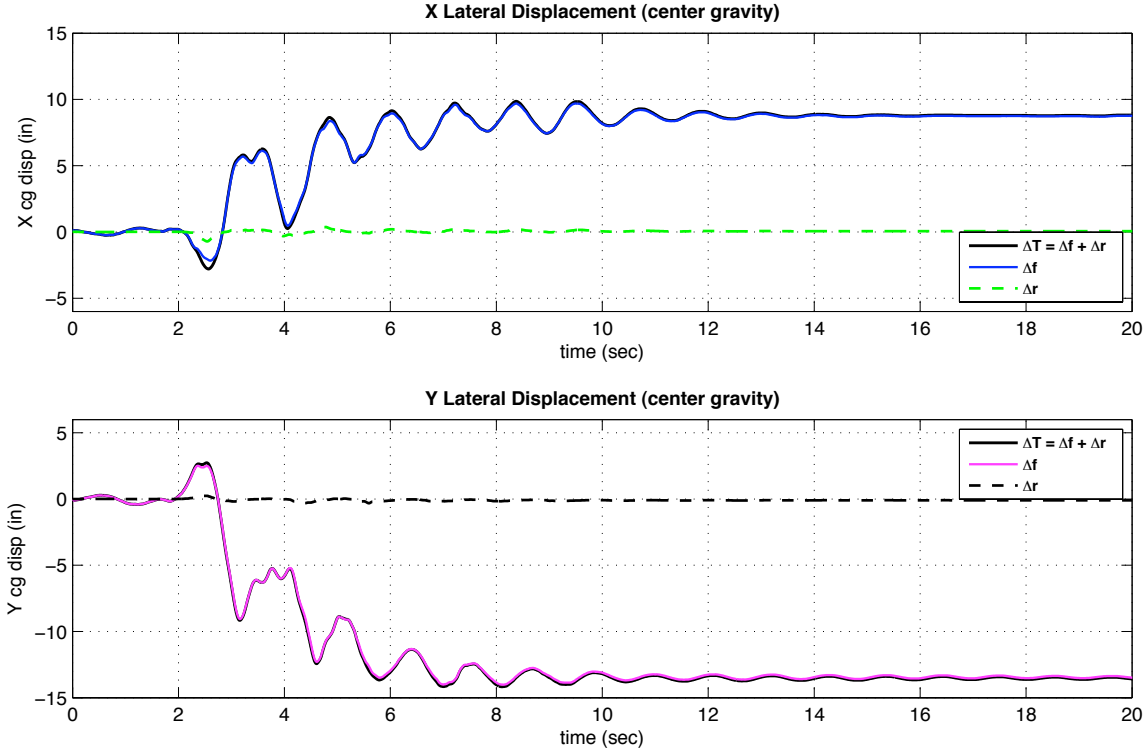

Figure 4-34: Maximum Level Test A4R Displacement Response

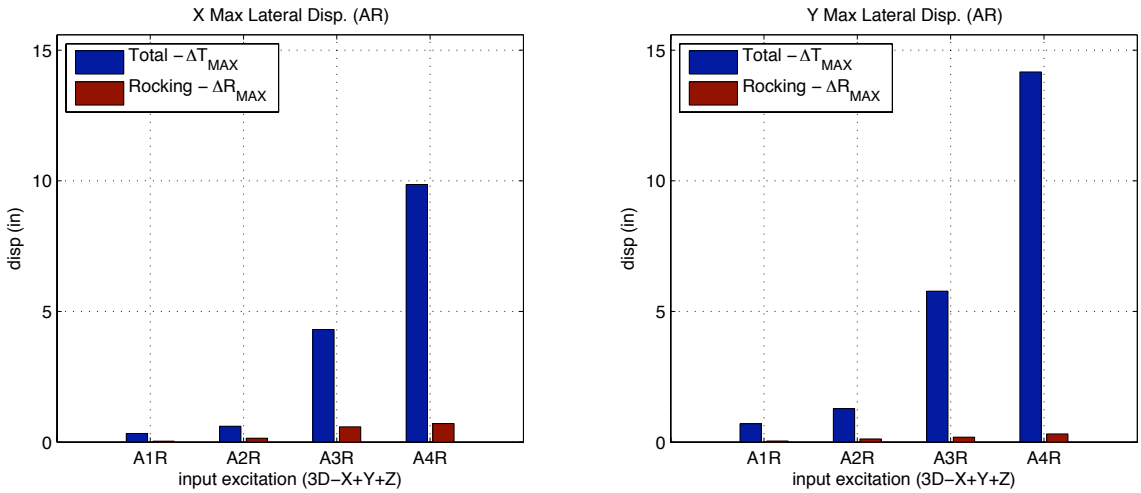

(a) Maximum Total vs. Rocking Displacement

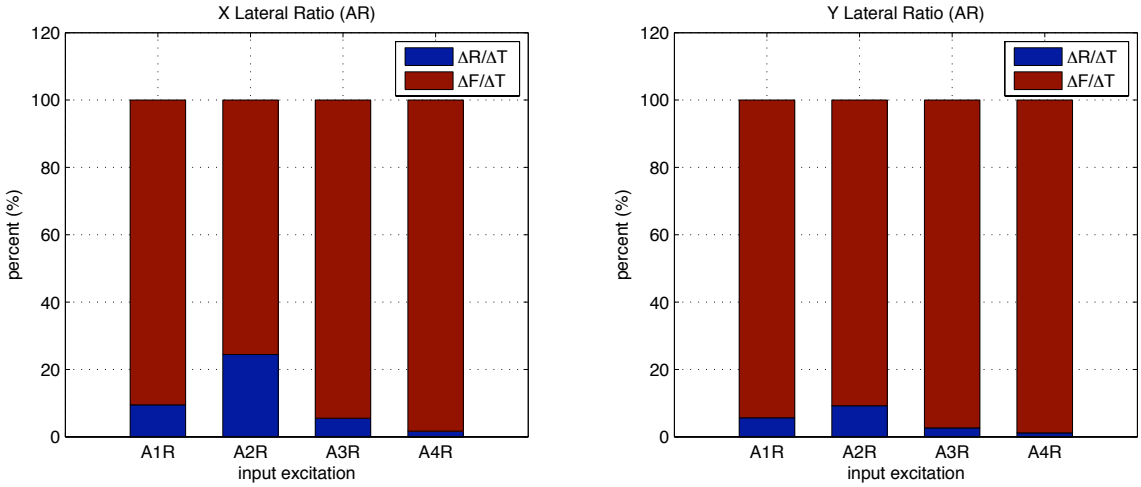

(b) Ratio of Rocking and Flexural Displacement to Maximum Total Displacement

Figure 4-35: AR Test Set Ratio of Rocking to Total Displacement

4.6.1.2 Footing Uplift

Footing uplift was determined by the procedures described in Section 4.2.1.2. The uplift response for Test Group 2 is described in Section 4.5.1.2 and some of the pertinent terminology for uplift is described in Figure 4-15. As described for the footing uplift of Test Group 2 the vertical displacement was calculated for the entire footing by assuming it was a rigid body. The vertical displacement of the footing can be described as uplift when the footing physically loses contact with the elastomeric pad or rocking when the footing remains in contact with the pad, but is rotating due to flexibility of the pad.

The results of center of top mass lateral displacement highlighted the fact that rocking contributed less than 25% of the total displacement for all four tests. In the X (North-South) direction the shorter footing dimension experienced more uplift as would be expected. However for even the larger tests of 90% and 120% of the original amplitude the amount of maximum uplift was small, approximately 0.2 inches. Which is

one-half of the measured 0.4 inches for the DS test. It is expected this is due to the bidirectional aspect of the response under tri-directional excitation, which leads to a larger effective footing width than assumed in a simple unidirectional analysis. Figure 4-38(c) supports this suggestion because it appears the dominant direction of uplift occurs along the diagonal axis.

For the $3D_c$ x $3D_c$ footing with the Los Gatos record scaled to 25%, the peak amount of uplift was measured to be approximately 0.4 inches. For Run A2R, the uplift was reduced to about 0.03 inches (Figure 4-36(a)) for the wider $5D_c$ direction and only 0.02 inches for the narrow $3D_c$ direction for this level of excitation. It interesting that for test A3R the amount of peak indentation into the elastomeric pad was greater than the amount of uplift. When the amplitude was increased, the amount of uplift increased moderately (to about 0.2 inches). In Figure 4-36(c), the last run A4R shows where the specimen retains a considerable permanent lateral displacement due to column yielding, the footing also has a permanent rocking and uplift at rest state due to the P-Δ moments created by the permanent lateral displacements.

The contour plots of peak uplift and indentation in Figure 4-38 are very useful in demonstrating the directional response of the footing while rocking and uplifting. Each individual test has different magnitudes of response, but a dominant direction is apparent along the diagonal from lower right to upper left (North-West footing corner to South-East corner).

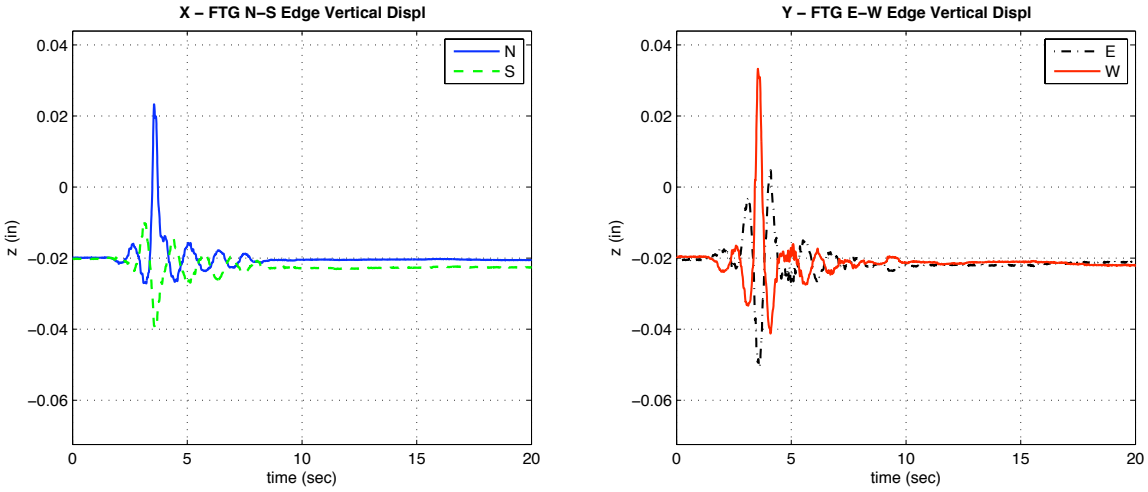

(a) A2R Yield Level

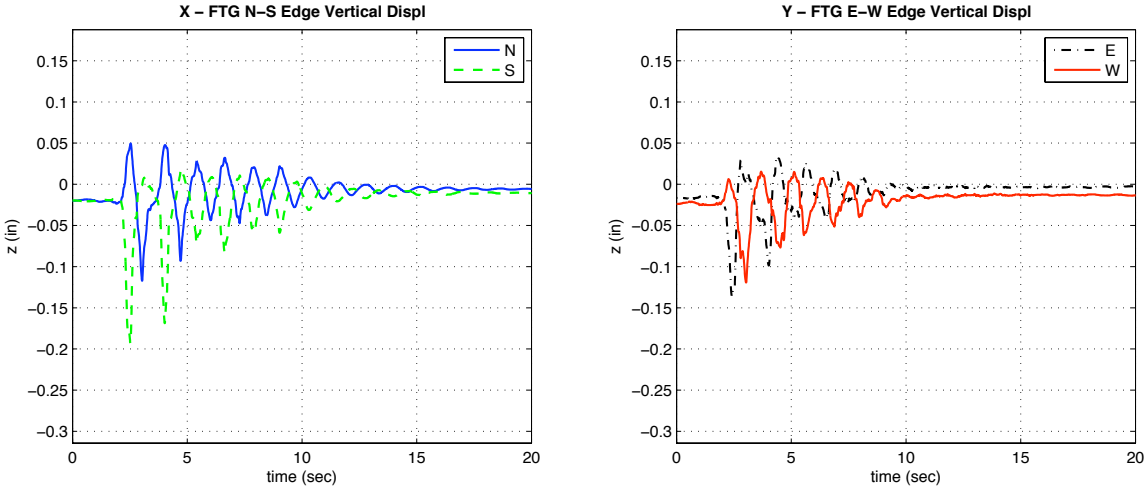

(b) A3R Design Level

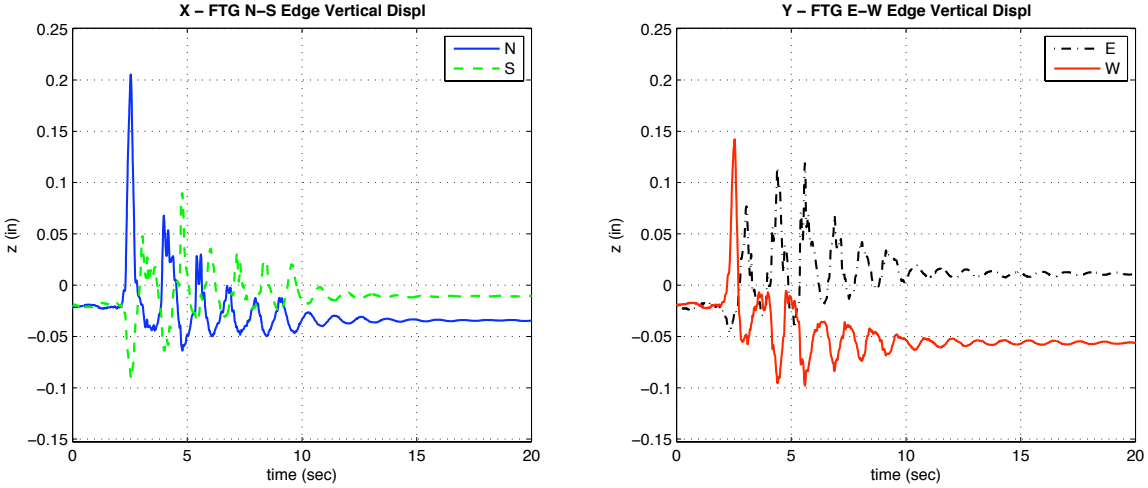

(c) A4R Maximum Level

Figure 4-36: AR Test Set - Footing Uplift Response (Centerline Edges)

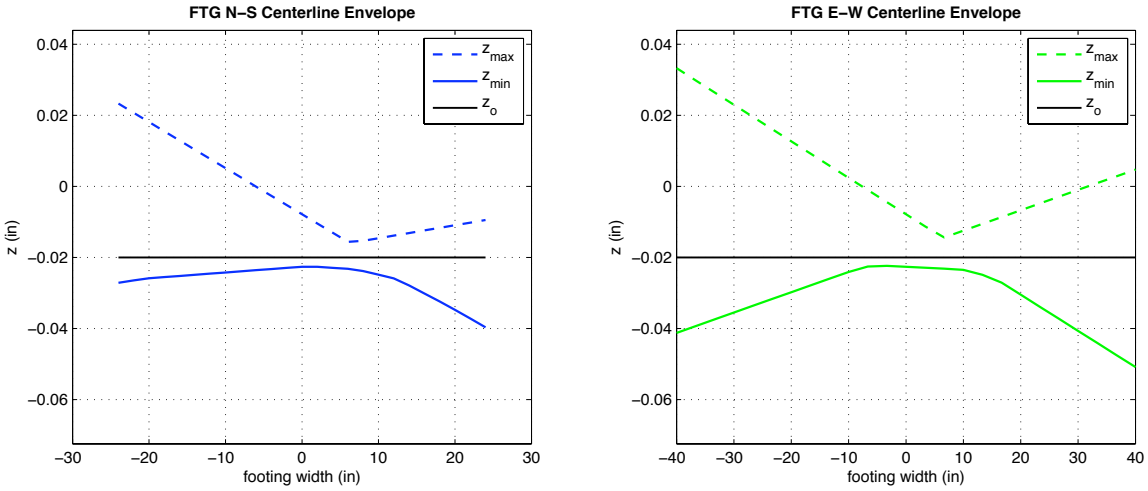

(a) A2R Yield Level

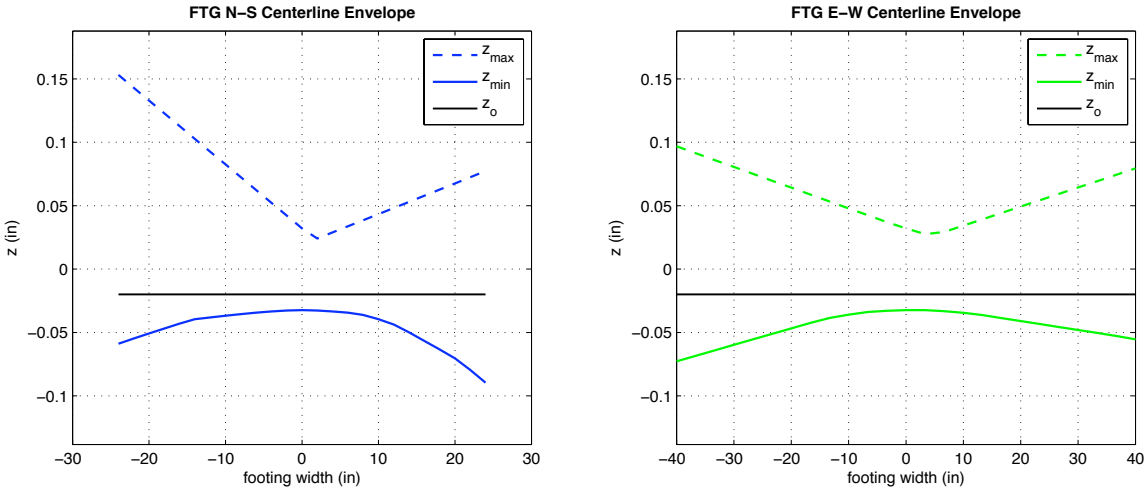

(b) A3R Design Level

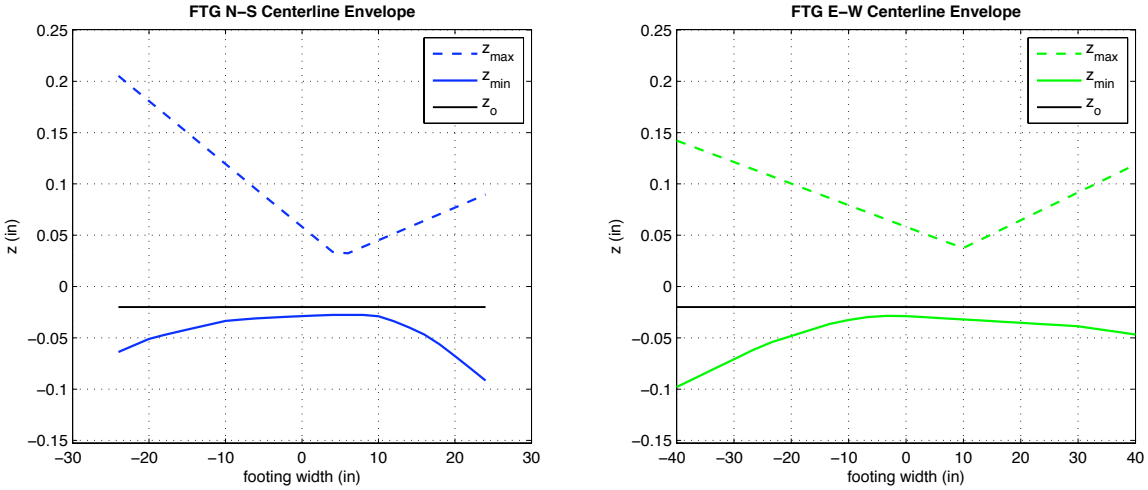

(c) A4R Maximum Level

Figure 4-37: AR Test Set – Envelope of Peak Footing Uplift (Centerlines)

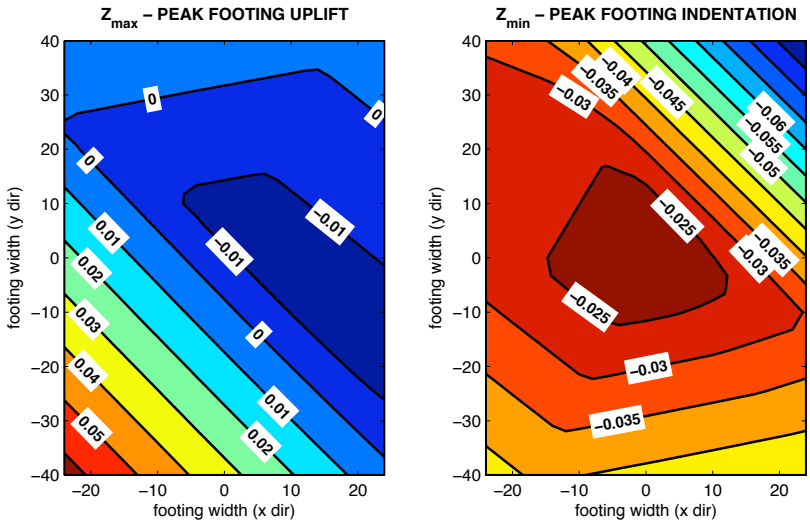

(a) A2RYield Level

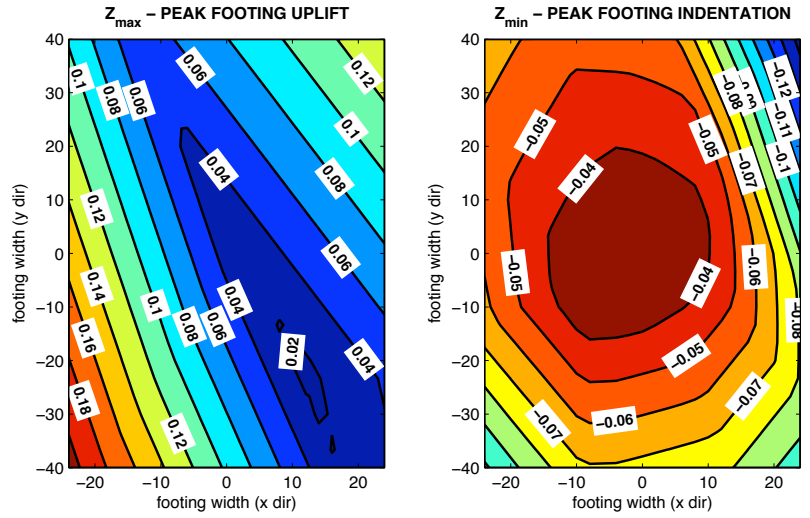

(b) A3R Design Level

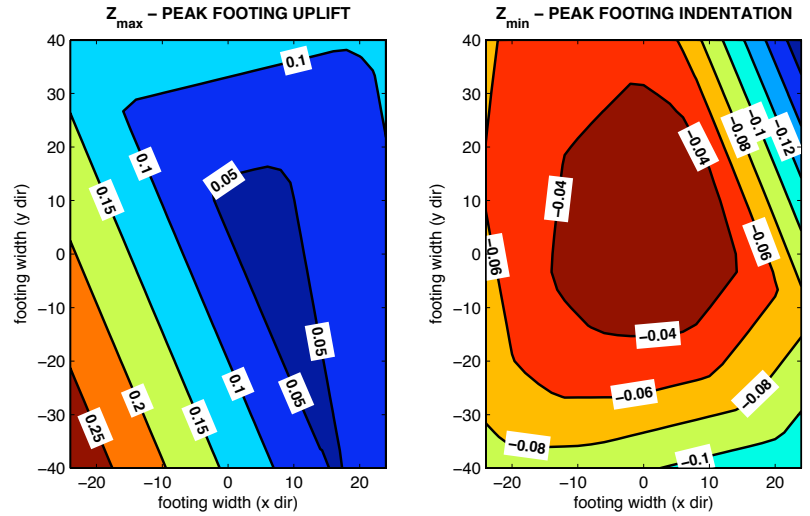

(c) A4R Maximum Level

Figure 4-38: AR Test Set – Contours of Max/Min Footing Uplift

4.6.1.3 Rotations about Vertical Axis

In Section 4.5.1.3 the propensity of the specimen to rotate about a vertical axis because of the lack of restraint was explained. As the footing is uplifting in one direction and experiencing an inertial load in the opposite direction it will want to rotate about the corner of footing still in contact. Less rocking and uplift occurred for Test Group 3 than Test Group 2, hence less rotation is expected. Figure 4-39 verifies that the rotation about the vertical axis occurred, especially for test A3R and A4R. The cumulative permanent displacement was estimated to be approximately 0.5 inches at the corners.

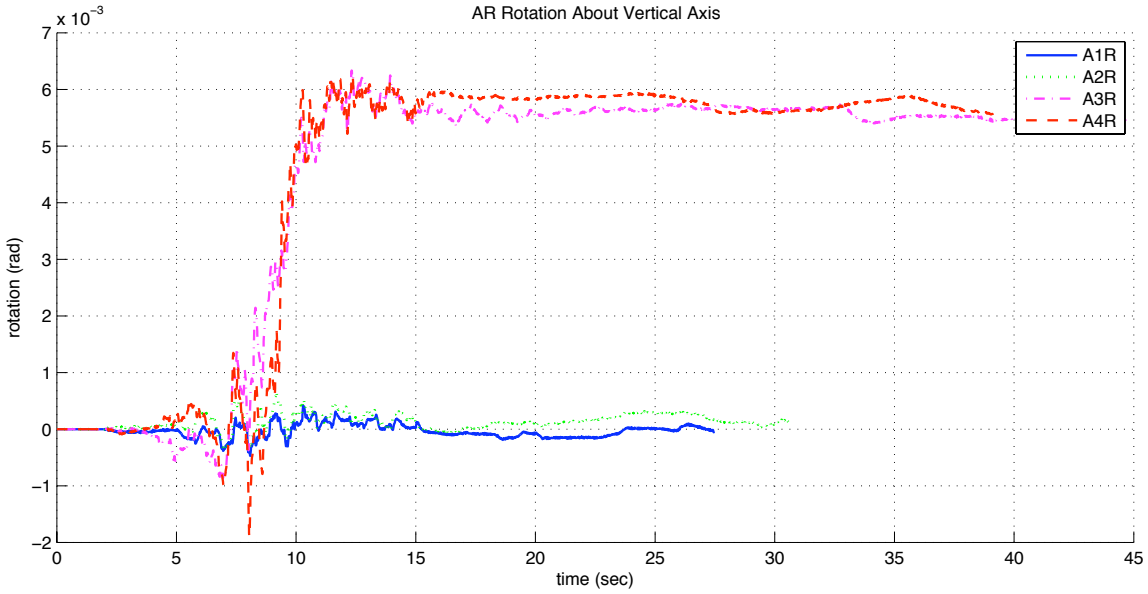

Figure 4-39: Test Set AR twisting about vertical axis.

4.6.2 Local Response

Test Group 3 experienced large inelastic displacements as well as significant permanent lateral displacements also as described in Section 4.6.1.1. The cause of permanent displacement was mostly due to damage in the plastic hinge region at the base of the column. The curvature demands and strains highlight the response of the specimen in this region.

4.6.2.1 Curvature Distribution

The calculation of average curvature and their characteristics, including bar pullout was described in Section 4.5.2.1. The curvature recordings for tests A3R and A4R are shown in Figure 4-40: Column Curvatures (Tests A3R & A4R)along both principal column directions. Following test A3R some permanent rotation was observation over regions 1, 2 and 3 which comprise the plastic hinge zone. At the conclusion of test A4R (the 120% maximum level) there was permanent curvature distribution along the column height which was not solely restricted to the plastic hinge region. Much of this permanent rotation above the plastic hinge region was due to P-D effects of the lateral displacement and not associated with inelastic response above the expected plastic hinge region. The peak curvature demand was in the y direction for test A4R and was approximately ϕ_{EWmax}=0.012 (1/in).

4.6.2.2 Strains

The strain gauges described in Section 4.5.2.2 were utilized for all of Test Group 3. The reliability and accuracy of the gauges used for testing is reduced when subjected to strains beyond the yield point. For this reason they are used only to determine when yielding in the bar and column has occurred and any results beyond this level are discounted.

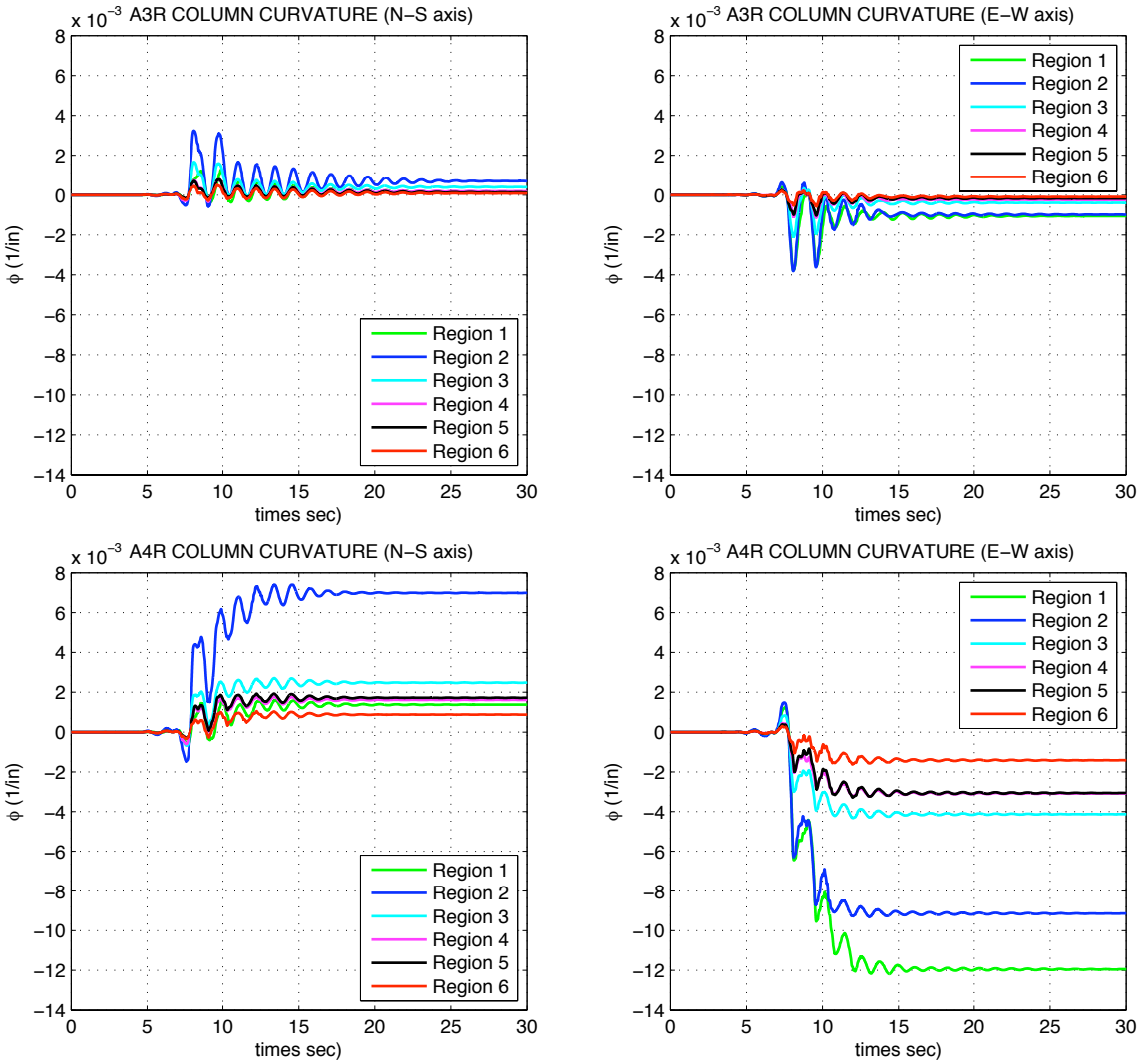

Figure 4-40: Column Curvatures (Tests A3R & A4R)

4.6.3 Force-Displacement Hysteresis Curves

The force-displacement relationship calculation method was described in Section 4.5.3. Test Group 3 was designed such that inelastic behavior would occur while the footing was simultaneously rocking and/or uplifting. The combination of the two was expected to produce an alternative method of energy dissipation to a column solely fixed at the base.

The behavior of the column while uplifting has several points of transition during the response, which affect the observed behavior. For the moment demand at the column base this includes the several points related to the footing displacement; moment at which rocking will occur (M_{rock}), first uplift of the footing (M_{up}), and total uplift of the footing so it is rotating about an edge pt (M_{edge}). For column displacement the moment values of interest are the curvatures at which yielding of the column occur (M_y) and the nominal strength level will be reached (M_n).

The lateral force versus lateral displacement hysteresis of the column base shear and center-of-mass of the top block is shown in Figure 4-41 for tests A2R, A3R, and A4R whose displacements are shown in Figure 4-32 through Figure 4-34. The plots for test levels A3R and A4R are very noisy, however they do illustrate the presence of nonlinear inelastic demands as well a significant amount of higher mode response as described by the noise in the plot.

4.6.3.1 Moment-Curvature Column Response

The nonlinearity of the column response and system can be best observed by looking at Figure 4-42. For Run A2R (25% of original amplitude) the column base moment-average curvature relation is nearly elastic especially for the direction associated with the $3D_c$ footing width. Significant hysteresis is noted for the column base for Run A3R (90% of original amplitude), especially for the direction parallel with the $5D_c$ footing dimension. For Run A4R (120% of original amplitude) the hysteresis for both directions is pronounced especially for the $5D_c$ footing direction. For the East-West (5Dc) direction, it is clear that there is a considerable P-Δ effect that results in a negative post-yield stiffness in the moment-average curvature relations for runs A3R and A4R.

During testing it was observed that at the yield displacement the moment demand was M_y= 1050 kip-in. The nominal strength at which the column response plateaued was approximately M_u= 1200 kip-in.

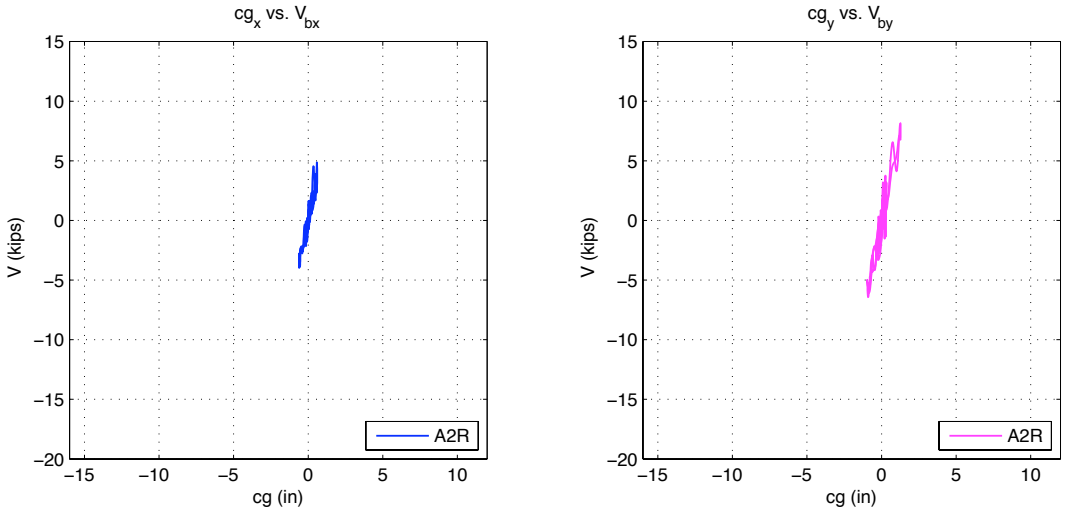

(a) Test A2R (Yield Level)

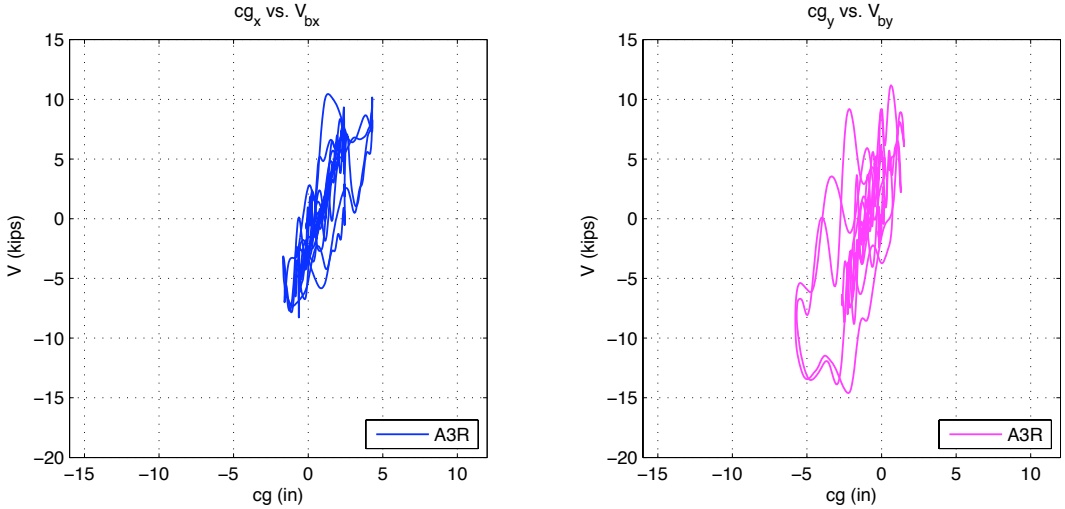

(b) Test A3R (Design Level)

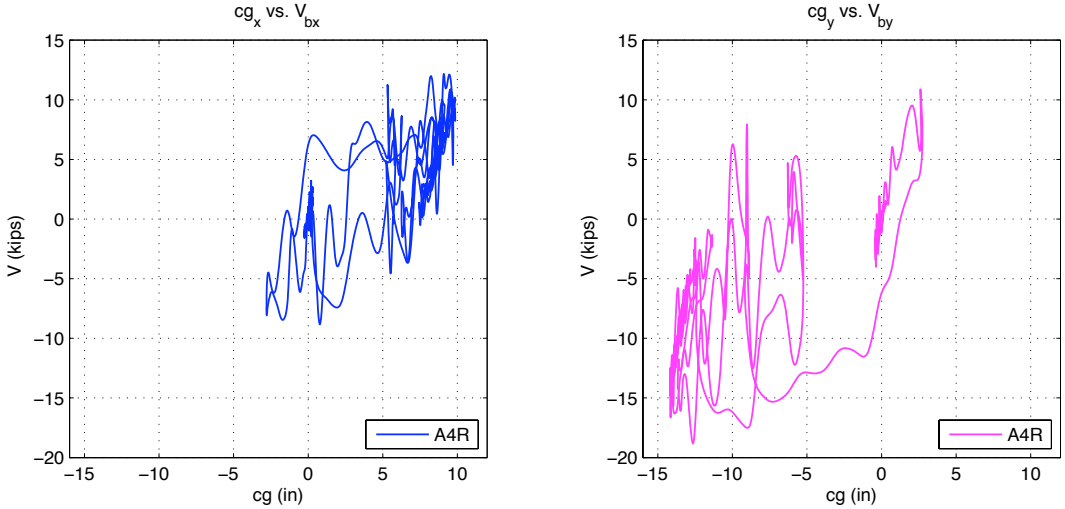

(c) Test A4R (Maximum Level)

Figure 4-41: Lateral Force vs. Lateral Displacement (Test A2R, A3R, A4R)

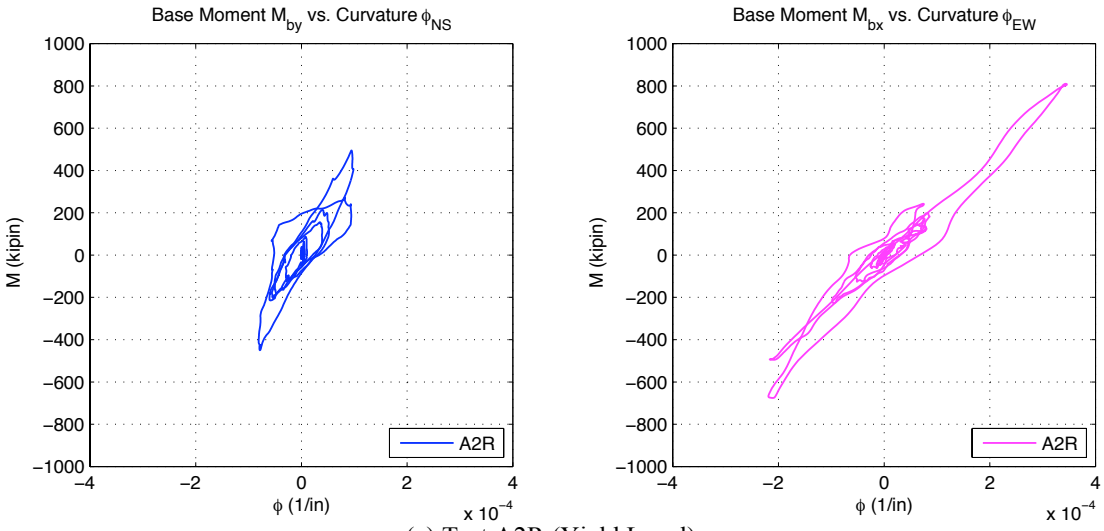

(a) Test A2R (Yield Level)

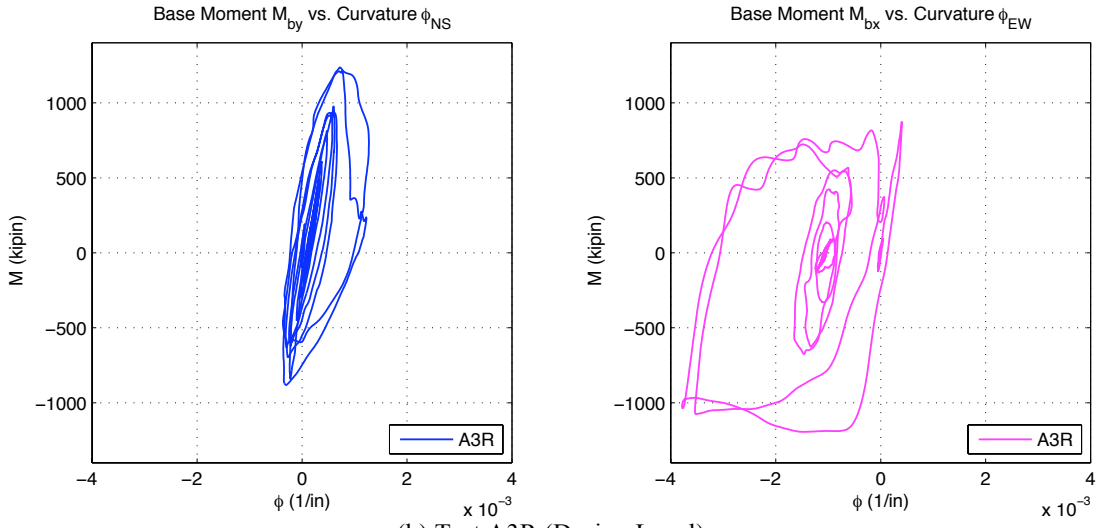

(b) Test A3R (Design Level)

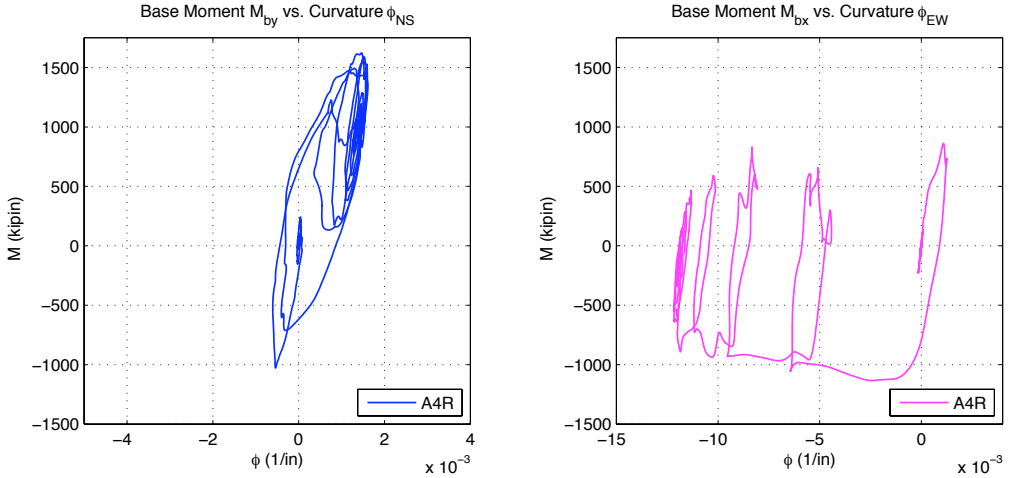

(c) Test A4R (Maximum Level)

Figure 4-42: Column Base Moment-Curvature Response (Test A2R, A3R, A4R)

4.6.3.2 Moment-Rotation Footing Response

The moment-rotation response of the footing can be observed in Figure 4-43. In spite of previous comments regarding the lower level of rocking and uplift for this column, it is clear from the plots of base moment-footing rotation that there is considerable energy dissipation at the footing elastomeric pad interface. Considerable moment-footing rotation nonlinearity is noted in the North-South ($3D_c$) direction, while there is little nonlinearity associated with uplift in the orthogonal direction. It is clear from Figure 4-42(b) and (c) that the forces developed in the base of the column in the North-South (3Dc) direction due to rocking are sufficient to initiate yielding in the column. In the East-West ($5D_c$) direction, the column yields before significant uplift can occur.

For Run A2R, Figure 4-43(b), as the footing starts to uplift (resulting in nonlinearity of the moment rotation relationship) prior to yielding of the column in the Y ($3D_c$) direction. The wider ($5D_c$) footing produces a greater restoring force in this direction, but it is still not sufficient to yield the column. However for run A3R (Figure 4-43 (c)), the strength of the column increases to the point where the column can yield slightly (under the effects of bi-directional excitation – the uni-directional yield capacity would be sufficient to prevent column yielding in this direction). For the other direction ($5D_c$), the column reaches its yield point before much rocking can occur. The effects of bi-directional excitation, stiffness deterioration, and P-Δ effects further weaken the column such that rocking/uplift is largely avoided in this direction as expected. The moment at footing uplift was measured M_{upNS}= 350 kip-in and M_{upEW} = 575 kip-in. The footing did not uplift enough to rotate about the outer edge.

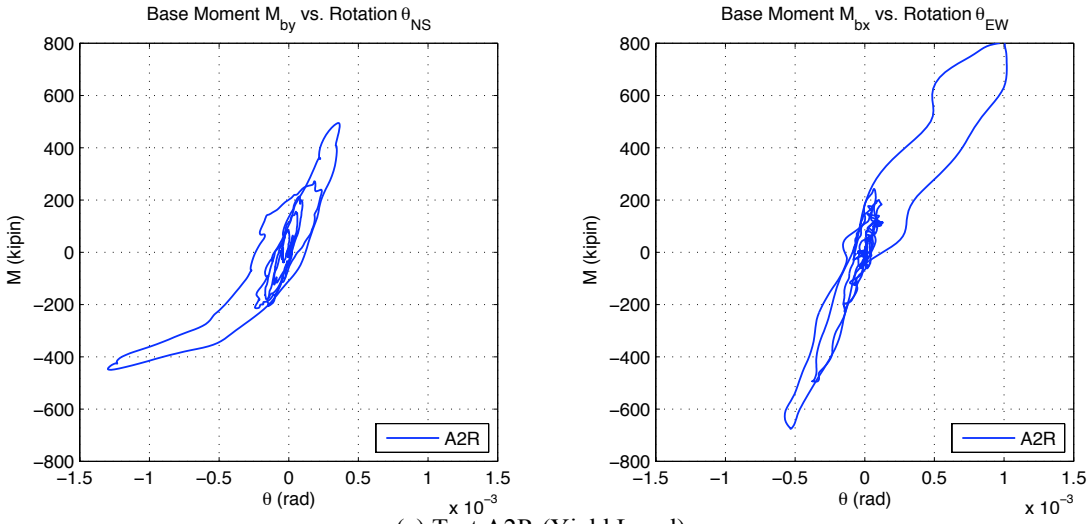

(a) Test A2R (Yield Level)

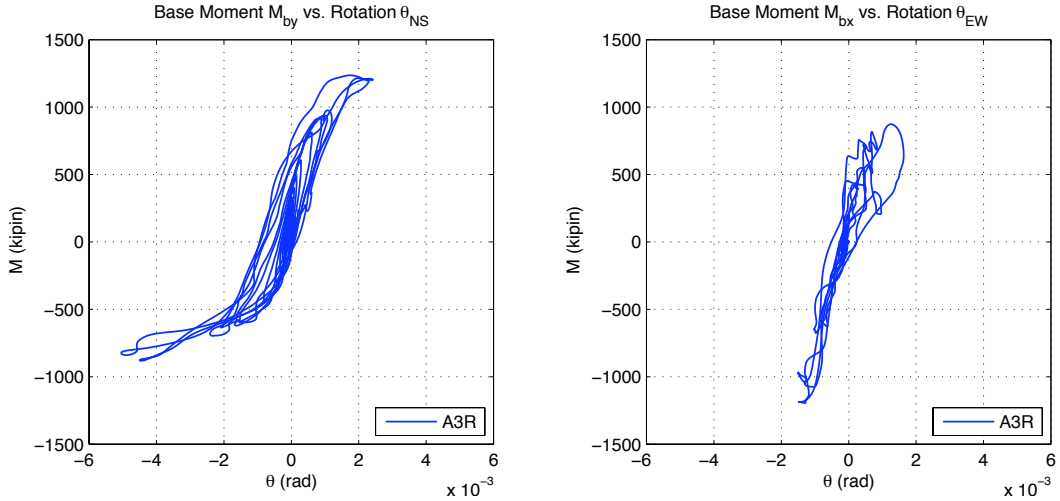

(b) Test A3R (Design Level)

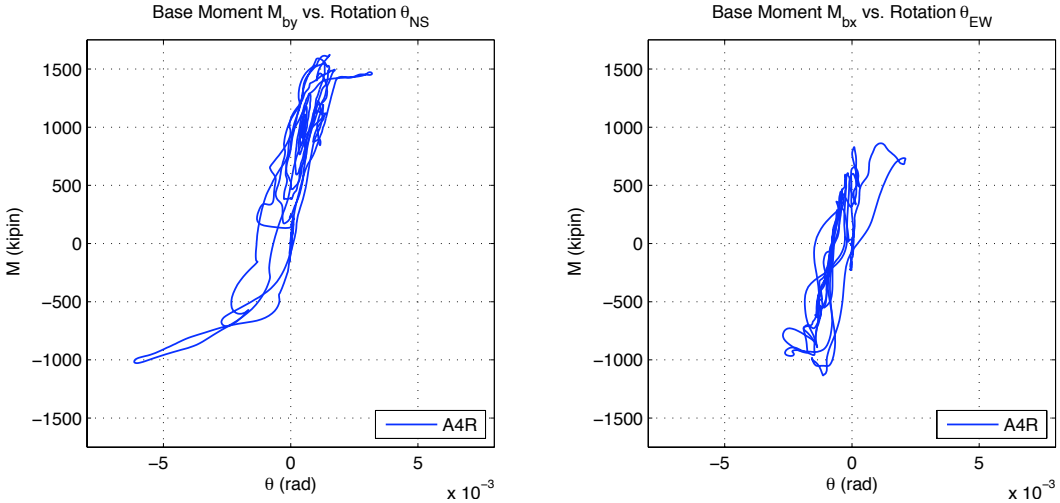

(c) Test A4R (Maximum Level)

Figure 4-43: Column Base Moment-Footing Rotation (Test A2R, A3R, A4R)

4.7 Applied Moment vs. Restoring Moment

A key parameter for assessing the likelihood of foundation rocking and uplift would be the ratio of applied moment to restoring moment due to gravity load. When the ratio of applied to restoring moment is greater than or equal to unity the footing of the column would be expected to uplift. Transition points in the moment deformation relationship of the column and footing have been described in Section 4.5.3. Key values of transition for the footing include the moment at which rocking, uplift, and uplift about the corner point occur. For the column relationship key values of response are described in Section 4.6.3 and include the yield moment, nominal strength, and ultimate moment. The moment values determined experimentally for the column and footing quantities are:

Table 4.4: Column and Footing Moment Characteristic Values

Column:	
My =	950 kip-in
Mn =	1050 kip-in
Mu =	1200 kip-in

Footing	**3Dc x 3Dc**		**3Dc x 5 Dc**	
	X (N-S)	Y (E-W)	X (N-S)	Y (E-W)
Mup	600 kip-in	600 kip in	350 kip-in	575 kip-in
Mupu	1100 kip-in	1100 kip-in	n/a	n/a

In Chapter 2 the lateral shear at incipient uplift of a cantilever column was described by Yim and Chopra (1984) for a two-spring model and a continuous Winkler foundation with uniform spring stiffness and spacing. The lateral shear applied to the top of a cantilever column at initiation of uplift is given for a two-spring model by Eqn. (4-14) as:

$$V_c = (m+mo)gb/h \qquad (4\text{-}14)$$

For a continuous Winkler foundation the load at incipient uplift changes to:

$$V_i = (m+mo)gb/(3h) \qquad (4\text{-}15)$$

The parameter β can be described as an indication of the tendency of the foundation to uplift due to the applied lateral shear Vcol. Insert value for general footing stiffness K_θ

$$\beta = V_{col}/ V_c \qquad (4\text{-}16)$$

Where M_{col} is the measured experimental column moment and h_{col} is column base to top mass center of mass height:

$$V_{col} = M_{col}/h_{col} \quad (4\text{-}17)$$

The columns considered here in have footing widths of 3Dc and 5Dc. The nominal column axial loads are 10%f'cAg for Test Groups 2 and 3 and 3%f'cAg for Test Group 1. Using the measured concrete strengths the calculated weights of Test Groups 1, 2 and 3 specimens are 0.027, 0.055 and 0.060 times f'_cA_g, respectively.

It is desirable to represent the likelihood of foundation uplift parameter β (4-16) to applied moment M_{col} in terms derived from the physical dimensions of the column and footing system. The gross area of the column A_g equals $\pi D_c^2/4$ and the axial load $(m+m_o)g$ equals $\gamma f'_cA_g$. The ratio of footing width to column width is $\rho = 2b/D_c$. Insert these values into the equations for V_c:

$$V_c = \gamma f'_cA\gamma\rho D_c/2h_{col} = \gamma\rho\pi D_c^3 f'_c/8h_{col} \quad (4\text{-}18)$$

Or V_i:

$$V_i = \gamma\rho\pi D_c^3 f'_c/24h_{col} \quad (4\text{-}19)$$

Thus the parameter β_c becomes:

$$\beta_c = 8M_{col}h_{col}/(\gamma\rho\pi D_c^3 f'_ch_{col}) = 8M_{col}/(\gamma\rho\pi D_c^3 f'_c) \quad (4\text{-}20)$$

and β_i is:

$$\beta_i = 24M_{col}h_{col}/(\gamma\rho\pi D_c^3 f'_ch_{col}) = 24M_{col}/(\gamma\rho\pi D_c^3 f'_c) \quad (4\text{-}21)$$

where M_{col} represents the moment induced by a particular earthquake (M_{eqk}), or the yield (M_y), nominal (M_n), or factored nominal (M_u) of the column.

Computed ratios for various tests are shown in Table 4.5, based on β_i for the column moment demand for each run (for the maximum component), and for the computed values of yield and nominal moment capacities of the column. If any of the values of β are greater than unity, the footing would be expected to uplift when M_{col} was developed during the earthquake. If the value of β_{eqk} is greater than β_y, the column would be expected to uplift before yielding could occur. If uplift occurs, the moment demand on the column will increase such that β increases up to β_c (the condition for which the footing is rotating about a corner point only). If β_n is less than β_c, the column might be expected to yield while uplifting. Note that some yielding during uplift may occur temporarily under bi-directional excitation since the effective width of the footing increases.

Table 4.5: Ratio of Applied to Restoring Moment (β Uplift Likelihood)

Test Group	ρ	γ	Record	Amplitude Scale	Time Scale	β_{eqk}	β_y	β_n
1	3	0.027	Los Gatos	0.08	2.12	0.56	3.90	4.56
1	3	0.027	Los Gatos	0.32	2.12	1.72	3.90	4.56
1	3	0.027	Los Gatos	0.32	1.50	0.56	3.90	4.56
1	3	0.027	Tabas	0.08	2.12	1.41	3.90	4.56
1	3	0.027	Tabas	0.32	2.12	1.32	3.90	4.56
1	3	0.027	Tabas	0.42	2.12	1.50	3.90	4.56
2	3	0.055	Los Gatos	0.15	1.50	1.44	1.98	2.30
2	3	0.055	Los Gatos	0.15	2.12	1.05	1.98	2.30
2	3	0.055	Los Gatos	0.25	2.12	1.54	1.98	2.30
2	3	0.055	Tabas	0.15	2.12	1.91	1.98	2.30
2	3	0.055	Tabas	0.25	2.12	1.96	1.98	2.30
2	3	0.055	Tabas	0.25	1.50	1.35	1.98	2.30
3	3 5	0.060	Los Gatos	0.10	2.12	0.49 0.54	1.82 1.09	2.11 1.26
3	3 5	0.060	Los Gatos	0.25	2.12	0.84 0.95	1.82 1.09	2.11 1.26
3	3 5	0.060	Los Gatos	0.90	2.12	1.54 1.40	1.82 1.09	2.11 1.26
3	3 5	0.060	Los Gatos	1.20	2.12	1.52 1.32	1.82 1.09	2.11 1.26

4.8 Interaction of Principal Displacements

The use of a square or rectangular footing raised the question of whether there would be interaction between the principal axis directions. This could be for lateral displacement of the top in the Y direction when the input excitation is restricted to 1D in the X direction. Evidence of this exists as highlighted in Section 4.5.1. See Figure 4-13 for a plot of peak rocking displacement vs. total displacement.

The results may be slightly influenced by rotation of the footing because of the lack of horizontal restraint. Investigation of the footing rotation during testing (Section 4.5.1.3 and 4.6.1.3) showed that there was a negligible amount compared to the overall displacements. However, it was difficult to perfectly align the specimen with the direction of excitation due to this rotation.

Figure 4-44 shows the peak displacement for the five directional load cases of each earthquake run for Test Group 1 and 2 ($3D_c$ x $3D_c$). These results are normalized to

the peak displacement of the 3D (X+Y+Z) loading case. If interaction were not an issue there would no response in the opposing direction for the 1D-X, 1D-Y, and 2D-X+Z input excitations. The figure clearly shows that there is a significant amount of displacement in the direction not being loaded.

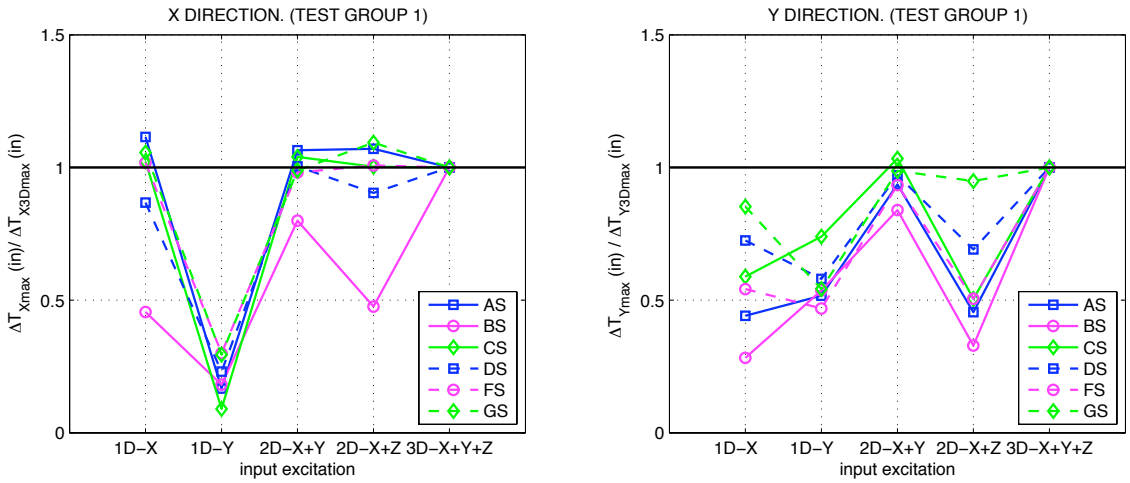

(a) Test Group 1

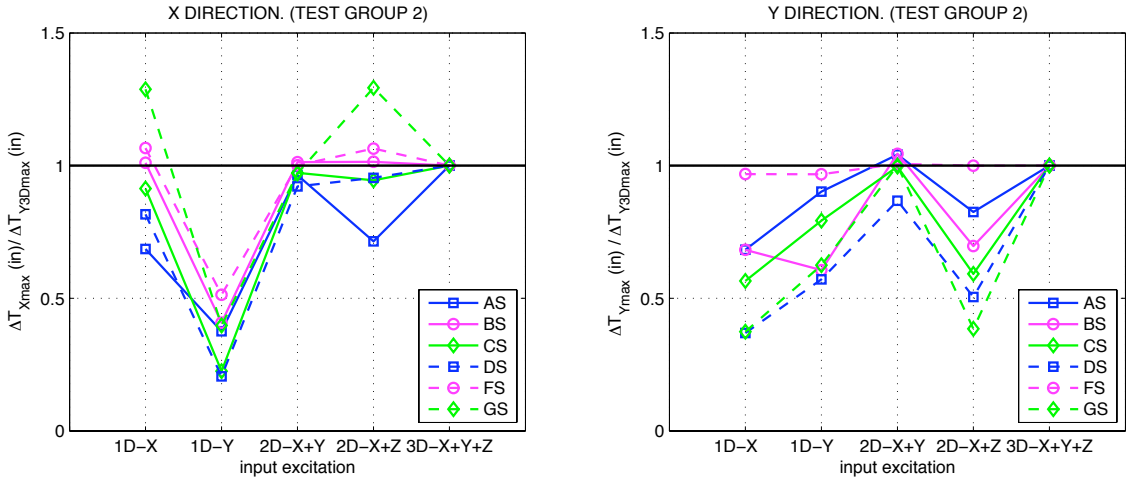

(b) Test Group 2

Figure 4-44: Normalized Interaction Displacements for Test Groups 1 and 2 ($3D_c$ x $3D_c$)

4.9 Natural Period and Damping

Prior to each test group the shaking table was blocked to prevent movement and a series of pullback tests were performed to estimate the free vibration characteristics of the specimen. The response to the free vibration was used to estimate the period of vibration and viscous damping properties at low amplitude motion. Pullback test were not performed between runs due to time and practical constraints. Instead the free vibration characteristics were determined during free vibration of the specimen (after earthquake excitation had ended) for each run. Both the natural period and damping were determined.

Table 4.6 shows the natural period and damping for the specimen at the listed phase. As expected at the conclusion of the elastic level tests the period change very little from beginning to end. Test Group 2 had approximately the same initial characteristics in each direction because of the equal footing dimensions. For the X and Y directions the fundamental period is approximately 0.9 sec. in each direction. Test Group 3 had a shorter period in the direction with the wider footing because it was more resistant to displacement. At the start of the test the natural period in the X and Y directions was approximately 0.8 and 0.7 sec, respectively. After the damage incurred during Test Group 3 the natural period was lengthened to approximately 1.2 and 1.1 sec. in the X and Y direction respectively.

The inclusion of a nonlinear elastic neoprene pad to represent the soil created nonlinear damping behavior for the system. Essentially there were two values of damping; that associated with significant footing rotation and was composed of elastomeric damping plus column damping and that associated with column damping only when the footing rotation was very small. The elastomeric pad damping of footing motion was predominant and only disappeared at the very end of the motions when the displacement amplitude was very small. At this point the motion was eliminated by the column damping qualities. For the test setup the damping value was approximately 8.0% and 2.5% for significant footing rotation and column damping only, respectively.

Table 4.6: Natural Period and Damping of Test Specimens

	T_{nx} (sec)	T_{ny} (sec)	ζ_{nx} (%)	ζ_{ny} (%)
Test Group 2 – Free Vibration	0.85	0.95	7.6	7.4
Test Group 2 – Conclusion	0.95	0.95	8.2	7.8
Test Group 3 – Free Vibration	0.9	0.75	8.1	7.8
Test A1R free vibration	0.82	0.76	7.6	7.9
Test A2R free vibration	0.82	0.70	7.9	8.1
Test A3R free vibration	1.16	1.06	8.2	7.6
Test A4R free vibration	1.12	1.08	8.1	7.9

4.10 Conclusions

Test Groups 1 and 2 were expected to remain elastic during all testing levels. Test Group 1 was an evaluation of the rocking setup and instrumentation so the axial load was one-third designed for load to avoid damaging the column. Five earthquake directional combinations were conducted at different earthquake intensity amplitudes: 1D-X, 1D-Y, 2D-X+Y, 2D-X+Z, and 3D-X+Y+Z. In total, approximately thirty runs were done for Test Group 1.

For Test Group 2, the footing size remained the same at three times the column diameter (3Dc) square. The axial load was increased to $0.057f'_cA_g$ and the column was

tested within the elastic range. Similar to the first test group approximately 5 types of earthquakes were run for five different input excitations. A total of approximately 30 runs were conducted again.

Test Group 3 was designed to have a wider footing in one direction, and be tested under simultaneous rocking and yielding. The interaction of fixed base behavior in one direction with rocking/uplifting behavior in the other direction was of interest. The footing was widened to 5Dc in one direction and the more intense component of shaking was oriented in that direction. The first earthquake run was 3D input at the elastic level. Next, the loading was increased to the yield and then design and maximum earthquake loading levels. At the conclusion of testing the column was significantly damaged and no further tests were feasible.

The measured base moment vs. footing rotation behavior for the footings generally followed the behavior expected based on simple analyses of Winkler foundation models of spread footing supported bridge piers. For sufficiently narrow footings uplift occurred, exhibiting a nonlinear elastic type hysteresis with some energy dissipation. In this case, the restoring capacity of the footing was less than the moment capacity of the column and the column responded elastically with no damage. The damage performance of the square footing with a width of $3D_c$ illustrated that flexural displacement demands may be reduced in comparison to a fixed column design and inelastic behavior confined to the footing soil interface.

It was also observed that rocking foundations lengthen the fundamental period of a system and can thereby reduce expected acceleration demands. However this can lead to larger total displacement demands for the system. Two and three components of excitation introduce more complex behavior where the footing may not rock as much as expected on the basis of analyses based on unidirectional excitations, and for the boundary conditions considered in these tests, the footing may twist about its vertical axis and translate from its initial position.

In Test Group 3, wider foundations and larger excitations were imposed such that yielding of the column would be expected slightly before uplift of the foundation in the direction of the 5Dc footing width. It was noted that bi-directional moments in the column reduced the effective moment capacity of the column in the narrow footing direction at various times so that column yielding occurred in this direction though it would not be expected on the basis of loading only in the narrow footing direction. Similarly, multi-directional response appears to increase the effective width of the footing (due to skew) and as such, rocking and uplift may not be again as much as expected. One important beneficial observation noted from Test Group 3 is the lack of need to tie-down the foundation where competent soils are available, the column has typical Caltrans axial loads applied, and the footing width is on the order of 3Dc or above. This can avoid the need to enlarge footings or install a pile foundation. The final test run of a maximum credible earthquake illustrated that the column was able to develop a full plastic hinge, dissipate earthquake energy, and remain stable and undergo small uplift without the need for a vertical restraint. These limited test runs show the design performance may be met with out added cost of piles or alternative methods.

However, in these shaking table tests, an elastomeric pad was used beneath the footing instead of soil. Consequently, the test results will be used subsequently to validate a numerical model for spread footings under multiple components of excitation, and these will be used in parametric studies to assess the behavior of bridge piers supported on footings resting on competent soil.

5 Validated Analysis of Experimental Results

5.1 Introduction

One of the primary objectives of this document is to develop analytical models, which can predict with reliable accuracy the seismic performance of reinforced concrete bridge piers allowed to uplift. In turn, these analytical models can be used to draw conclusions on an acceptable range of reinforced concrete columns, supporting soil, and seismic excitation. Design guideline development for bridge piers allowed to uplift can be created by considering the wide range of values for these parameters that are most relevant to bridge design. The validity of the guideline development depends on the accuracy of the analytic tools and modeling capabilities. A sample of the results described in the previous results sections are compared with analysis results obtained using several analysis methods and modeling approaches. Previous work in modeling guidelines for reinforced concrete bridge columns (Berry and Eberhard 2006) are used as an initial reference. Comparisons of the results in this chapter are done by using these initial recommendations and including a foundation Winkler spring model approach for the elastomeric pad and footing and by calibrating the response to the observed experimental data.

The analysis package Open System for Earthquake Engineering Simulation (OpenSees), was used to create the analytic models and perform linear and nonlinear dynamic analyses. OpenSees is an object-oriented framework that is open-source software used for structural and geotechnical earthquake analysis of structures. The analysis platform was developed by researchers at the Pacific Earthquake Engineering Research (PEER) center and collaborated on by many affiliated researchers. The open-source concept allows for easy additions and modifications to improve and enhancement material and element modeling analysis of structures.

To develop the analytic model, attention needs to be given to two phenomena observed during testing. The residual displacement from column damage was significant and must be addressed to accurately describe the simultaneously uplifting and yielding system. Also, the nonlinearity of the elastomeric pad affects the energy dissipation qualities of the system and will need to be addressed from the outset.

The analytic model begins with the material modeling assumptions which are described in Section 5.2. The material models considered include the reinforcing steel, concrete and elastomeric pad. The analytic model creation including column, footing and soil model assumptions are described in Section 5.3. The results of the linear and

nonlinear dynamic analysis performed using the soil, footing, and column specifications are compared to the experimental results and presented in Sections 5.5 and 5.6. Global response parameters including peak lateral displacement, residual displacements, footing rotation, peak lateral shear, overturning and restoring moments are presented in this section. The effect of varying the model for damping, soil, and column properties are also discussed in these sections. These effects include the damping value associated with elastomeric pad plus column viscous damping, soil spring rotational and vertical stiffness values, and values for the column concrete and reinforcing steel materials. A summary and conclusions of the modeling and results is presented in Section 5.7. This includes best practices for the soil structure interaction (SSI) with the footing and column for the elastomeric pad. With the experimentally validated models, a more broad range of bridge piers and underlying soil can be considered. Chapter 6 presents a parametric investigation using the validated models presented in this chapter. Varying the footing, column and soil properties in addition to the ground motion excitation will lead to a better understanding of bridge piers allowed to simultaneously uplift and yield. This more complete understanding of uplifting behavior will in turn lead to the development of guidelines for when uplifting of bridge piers is practical and beneficial in structural design philosophy.

5.2 Material Modeling

Accurate modeling of material stress-strain behavior is essential to predicting the observed member response. Hysteretic response, including under seismic loading, requires careful examination and replication of the unloading and reloading response of the materials in question. A brief discussion is presented here on the material models used in this study and their comparison to observed physical response of sample specimens. Materials used and modeled in this test program include concrete, steel, and neoprene.

5.2.1 Reinforcing Steel

Modeling of the mild longitudinal reinforcing steel was done using two different steel assumptions. The first was a Giuffre-Menegotto-Pinto (Taucer et al., 1991) constitutive model and the other was a model developed by Chang and Mander (1994).

Steel02

The material model **Steel02** is based on principles developed by Giuffre-Menegotto-Pinto. The model is a bilinear curve which transitions at the yield stress and strain but does not include the post yield plateau typically observed in the stress-strain relationship of mild steel. The model includes the Bauschinger effect, which is the contribution to the gradual stiffness degradation of reinforced concrete members under cyclic response. Figure 5-2(a) shows the coupon test data and the steel material model calibrated to the test data.

ReinforcingSteel

The **ReinforcingSteel** model uses a nonlinear backbone curve shifted as described by Chang and Mander (1994) to account for isotropic hardening. Several buckling options

are available for modeling using the material, however they were excluded because no buckling of the rebar was observed during testing. The complexity of the material model requires several inputs: yield stress, ultimate stress, initial elastic tangent, tangent at initial strain-hardening, and strain at peak stress. Figure 5-2(a) shows the response of the material calibrated to the observed coupon test. A very good correlation is shown between observed and predicted response.

5.2.2 Concrete

Two types of concrete behavior were modeled for this test program as unixaxial materials. They were confined concrete (core concrete) and unconfined concrete (cover concrete). The **Concrete02** model implemented by OpenSees uses the Kent-Park model to represent the concrete compressive stress-strain curve and linear behavior for the tension zone. Unloading in the compressive region is based on Karsan and Jirsa (1969). The material models are able to control the descending slope as well as the residual strength. Figure 5-2(b) shows the compressive strength of the cylinder tests compared to the material model for unconfined concrete. A reasonably good correlation is shown between the material model and the cylinder tests. The compressive behavior of the confined concrete was not directly measured. Instead the Mander equations for confined concrete were used as inputs to calibrate the confined concrete model. The ultimate stress and strain equations from Mander are shown in Equations (5-1) and (5-2). The stress-strain response of the material model for unconfined vs. confined concrete is shown in Figure 5-2(d). It is readily observed that the confined concrete offers much more strength in compression.

$$f'_{cc} = f'_{co}\left(-1.254 + 2.254\sqrt{1 + \frac{7.94 f'_l}{f'_{cc}}} - 2\frac{f'_{cc}}{f'_{co}}\right) \qquad (5\text{-}1)$$

$$\varepsilon_{cu} = 0.004 + \frac{1.4\rho_{sp} f_{yh} \varepsilon_{su}}{f'_{cc}} \qquad (5\text{-}2)$$

5.2.3 Elastomeric Pad

Modeling of the elastomeric pad was a challenge due to the lack of any materials explicitly developed in OpenSees for neoprene or rubber. The observed uniaxial test response of a sample 2 inch thick by 1 foot square piece of material showed an initial gap strain of 0.008 in/in followed by a linear elastic loading modulus of elasticity equal to 2.8 ksi. The material followed a nonlinear-elastic curve back to its origin and in the process dissipated some energy.

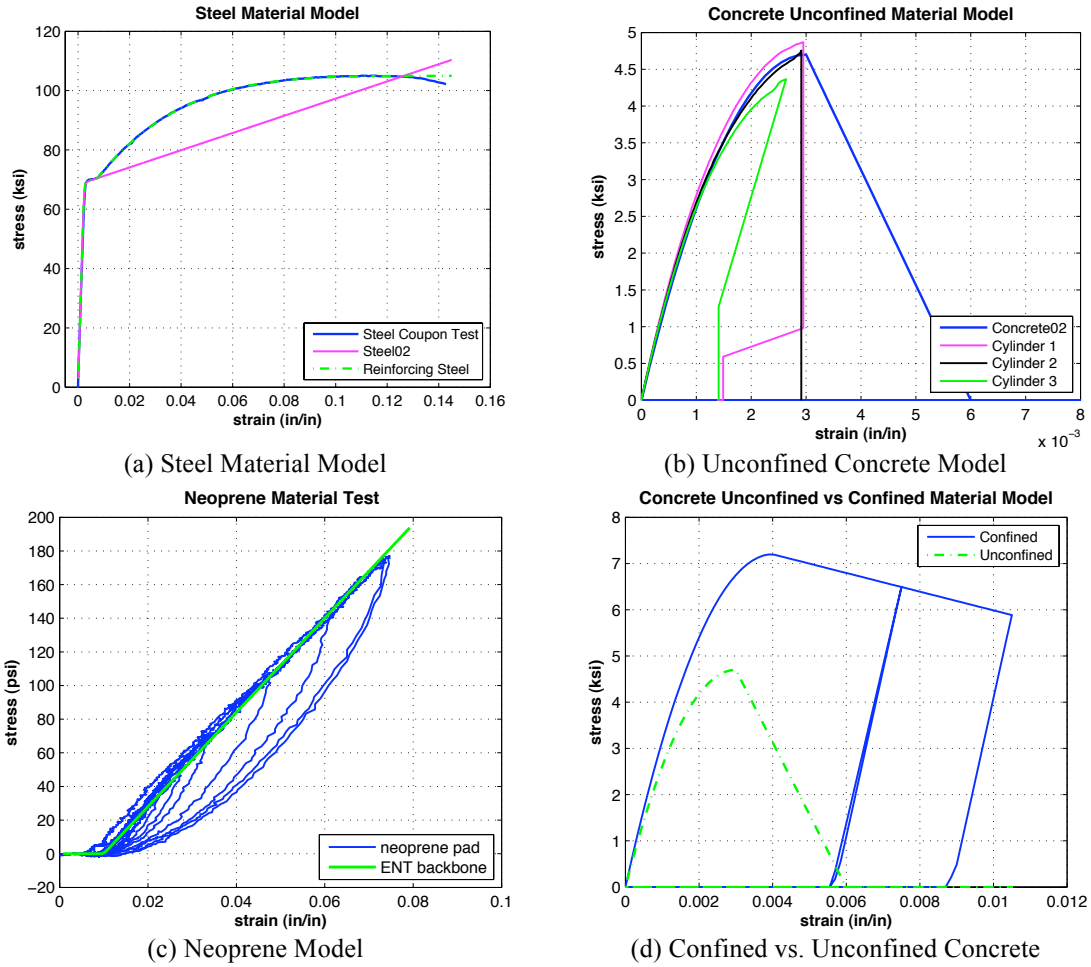

(a) Steel Material Model

(b) Unconfined Concrete Model

(c) Neoprene Model

(d) Confined vs. Unconfined Concrete

Figure 5-1: Analytic material modeling for analysis

Capturing the nonlinear elastic behavior proved to be a difficult task. To initially calibrate the model to the observed structure response, the damping qualities of the neoprene were omitted in the analysis. The backbone curve was modeled using a bi-linear elastic curve that loaded and unloaded along the same path. To do this a new material was created in OpenSees, which combined an **Elastic-No-Tension (ENT)** material with an initial gap strain. Figure 5-2(c) shows the recorded pad response compared to the OpenSees material backbone curve with no hysteretic qualities.

To better model the hysteretic energy dissipation of the neoprene using OpenSees a new material model **Neoprene** was developed. The material is Elastic-No-Tension and loads along the same backbone curve as the **ENT** material with a gap strain. During unloading the material follows a nonlinear elastic curve that is able to closely follow the measured unloading path before returning to the origin in an undamaged state.

Figure 5-2(a) shows the **Neoprene** material model response compared to the measured compressive behavior. When a compressive strain cycle is applied the **Neoprene** material closely follows the same loading path. During unloading the nonlinear curve is similar, however the material slightly under predicts the hysteretic

energy dissipation of the neoprene pad. Equally important is the material response when the material cycles through compressive and tensile loads. Figure 5-2 (b) illustrates the response of the material under this condition. Clearly, the **Neoprene** material is compression only. Finally, the material behavior for **Neoprene** is shown when it is loaded, partially unloaded, and then reloaded several times before the load is completely removed. See Figure 5-2 (c). In this case the reloading path is the initial stiffness. When the load is completely removed, the material returns to its original undamaged stress-strain state.

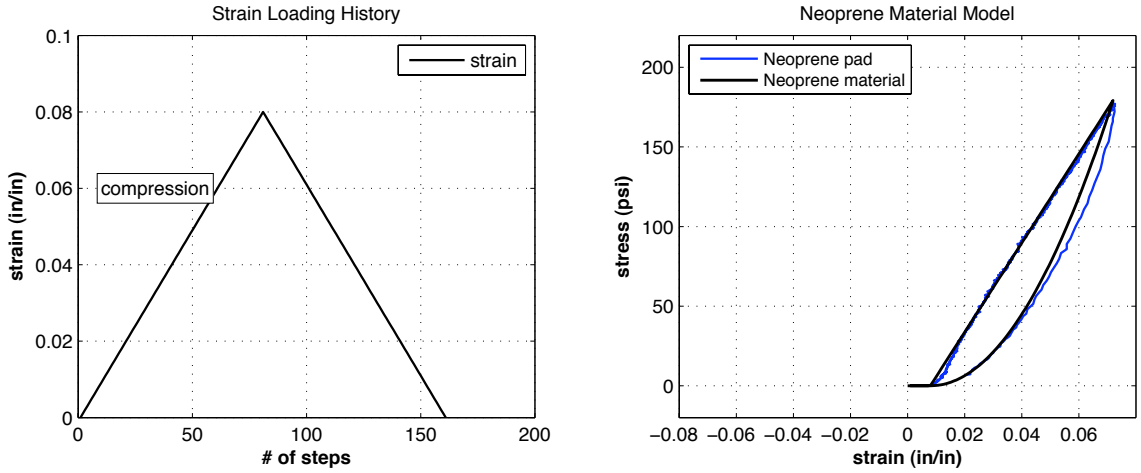

(a) One Compression Cycle Response

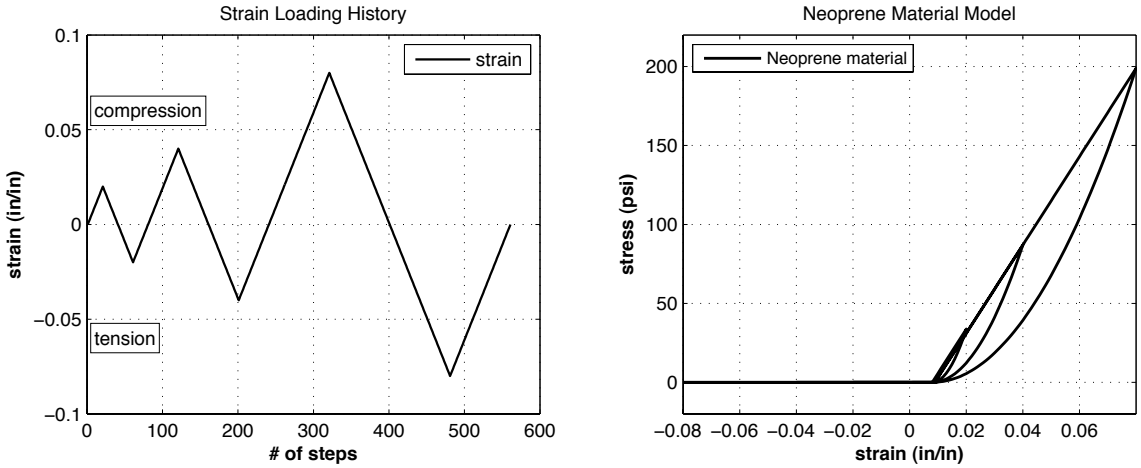

(b) Tension/Compression Cyclic Response

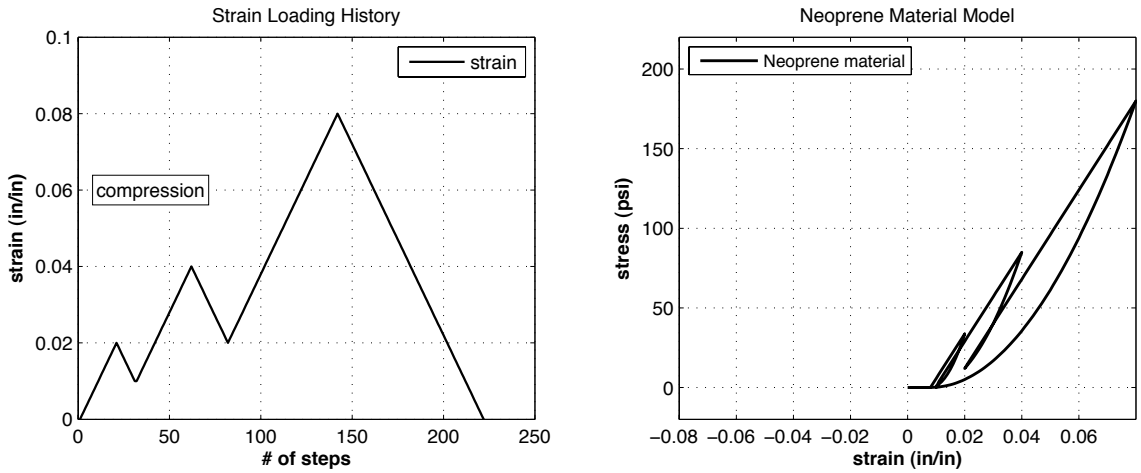

(c) Compressive Unloading/Reloading Response

Figure 5-2: OpenSees Neoprene Material Model Characteristic

5.3 Modeling of Reinforced Concrete Bridge Pier

Predicting the observed behavior of reinforced concrete bridges allowed to uplift is essential to furthering the understanding of uplifting bridge piers in general. The experimental results in Chapters 3 and 4 described the response of a single column with two footing sizes and varying multi-directional excitations. The type of analysis historically done to predict the demand response of uplifting bridge piers uses linear response spectrums and employs equivalent systems using static procedures. These methods use the physical footing and column dimensions but typically do not incorporate the soil characteristics or the potential inertial effects and yielding of the columns. To more accurately capture the behavior of uplifting bridge piers it is recommended to use dynamic time history analysis. Much dynamic time history analysis has been done to determine the response of uplifting systems (Kawashima et al., 2007). However not many research investigations have experimental data as a justification for the models. The analysis included herein attempts to fill the gap between the dynamic analysis research performed to date but which lacks the experimental data as verification of the behavior of uplifting systems.

Selecting the appropriate modeling technique involves several considerations. Care should be given to the complexity, reliability and accessibility of the analysis model. A priority in developing analytic models is to simplify where possible to make the model less complex and more obvious without sacrificing accuracy of the desired response quantities. Ideally a simple model that captured all of the relevant behavior modes of the system would be used. Equivalent static methods previously described do not accomplish this. For this research OpenSees has been selected as the analysis platform to conduct dynamic time history analyses. It is an open source model that allows many users to contribute various materials and elements. For this reason it is well suited to model uplifting bridge piers.

The column, footing and elastomeric pad can be represented using previously defined elements or user-specified elements when necessary. The modes of response for the uplifting bridge piers include elastic pad response, footing uplift, elastic footing response and both elastic and inelastic behavior of the column. The elastic column response levels can be utilized to determine the effect that uplift has on the system response without the complexity of simultaneous yielding of the column. The absence of yielding at these levels allows for a calibration of the footing response. With this understanding of uplifting behavior, attention can then be turned to the system response when the column is yielding concurrently with footing uplift.

The footing and pad response will be modeled using Beam-on-Nonlinear Winkler Foundation (BNWF) method. Response was nonlinear elastic for the pad and linear elastic for the footing. The pad is discretized into small rectangular sections whose vertical and rotational stiffness is simulated using a vertical spring at each sub-section. The footing behavior is assumed to be rigid elastic because of the very small footing flexural and shear deformations.

Fiber element modeling of reinforced concrete bridge column can be divided into two categories: elastic columns and inelastic columns. Both of these methods will use the

Beam-on-Nonlinear Winkler Foundation previously described. Elastic column models utilize the concept of effective sectional stiffness. The effect of cracking is estimated using the typical element formulation with an equivalent cracked stiffness under the axial load along the entire length of the column. Often the cracked stiffness of a section is estimated as one half of the gross section properties. In this case, it would be $EI_{eff} = EI_{gross}/2$. While useful for low level excitation with no yielding, this method will not capture the inelastic action of the column.

Inelastic action in the reinforced column can be modeled several ways. The choice here is to use fiber sections at discrete points along the column to represent the inelastic yielding behavior. Two fiber section approaches used here to model the columns are flexibility based beam-column elements:

- Distributed Plasticity Element – yielding may propagate along the column length. Each integration point is assigned a fiber section. Location of the integration points is important in modeling all of the observed inelastic behavior.
- Concentrated Plasticity Element – a region of finite length at each end of the element is assumed to contain all of the inelastic action. This region is known as the plastic hinge length. Each plastic hinge has two integration points at the ends with a fiber section model assigned. The rest of the element is assumed to be elastic with effective sectional properties.

Damping of the system will be carefully considered also. Systems allowed to uplift typically have more observed damping due to energy dissipation within the supporting soil during rocking and uplift. Commonly reinforced concrete columns use a mass and stiffness dependent Rayleigh approach for damping. The damping of the column will be modeled this way. The effect of a Rayleigh damping assumption for the footing and elastomeric pad will be investigated to see if appropriate or if there is a more suitable alternative.

In summary, a series of analyses will be done to determine the ability of three types of analytic models to predict observed response. Each of the models will use a Beam on Nonlinear Winkler Foundation to model the footing and elastomeric pad. The models are:

1. Elastic Column to predict system response for varying multi-directional excitations when no yielding occurs in the column.
2. Distributed Plasticity Column that allows for a progression of inelastic behavior along the column length with no restrictions.
3. Concentrated Plasticity Column that assumes inelastic behavior is restricted to the plastic hinge region at the ends of the column.

A comprehensive diagram of the analysis model showing the column and footing options is shown in Figure 5-12.

5.3.1 Fiber Element Modeling

Fiber section models will be used for sectional moment-curvature analysis and section assignment at integration points of flexibility based elements. Fiber models are used to predict the moment curvature relationship at the integration points over member lengths. The ability of fiber models to predict elastic or inelastic behavior allows for use of one element to model members, for example, which are yielding at the ends but behaving elastically in the center region.

A fiber model is built by dividing the cross-section of the desired member into a collection of fibers. Each fiber is assigned a uniaxial constitutive material model corresponding to the discretization location. For the experimental test program the column cross-section was discretized using confined concrete, unconfined concrete, and longitudinal steel. The uniaxial material models of the fibers are described in Section 5.2. The fiber section representation is shown in Figure 5-3. The section is comprised of 200 confined concrete fibers, 40 unconfined concrete fibers, and 12 longitudinal steel fibers. Figure 5-4 shows an example of a column element with 4 integration points and the associated fiber sections.

5.3.1.1 Moment-Curvature

Sectional analysis can be performed via OpenSees on the fiber section alone without having to build the entire model. This can serve useful in calibrating the analysis to the observed moment-curvature response during the testing. To perform a moment-curvature analysis, a moment is calculated based on an imposed curvature and axial load. This is accomplished by iterating on the neutral axis depth until axial load equilibrium is satisfied. Per the Bernoulli-Navier beam theory, plane sections are assumed to remain plane during deformation. For reinforced concrete structures, the confined concrete within the core is modeled using the enhanced properties as described in Section 5.2.2. The moment-curvature relationship used for these tests is shown in Figure 5-5. The analysis used the concrete properties described in Section 5.2.2 and varied the steel models as either the bilinear model Steel02 or the ReinforcingSteel model (Section 5.2.1).

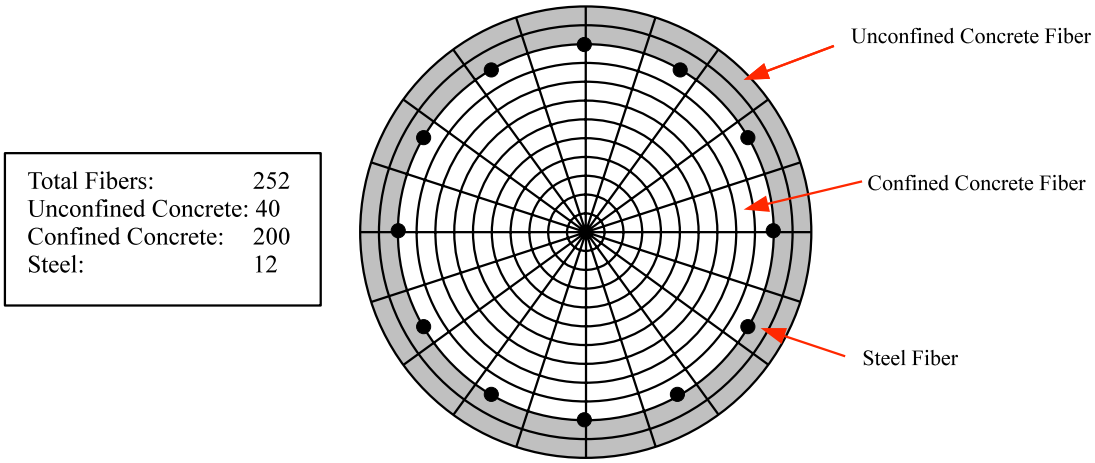

Figure 5-3: Fiber Section Representation of Column

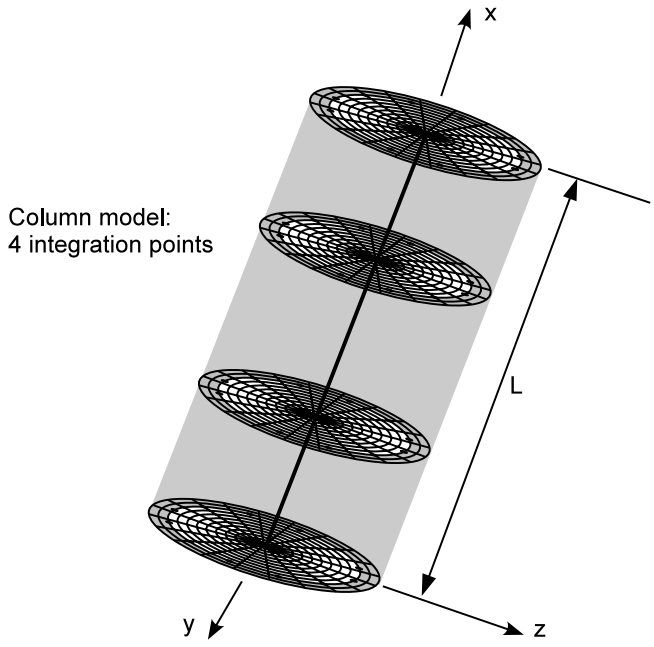

Figure 5-4: Column Element with Fiber Sections

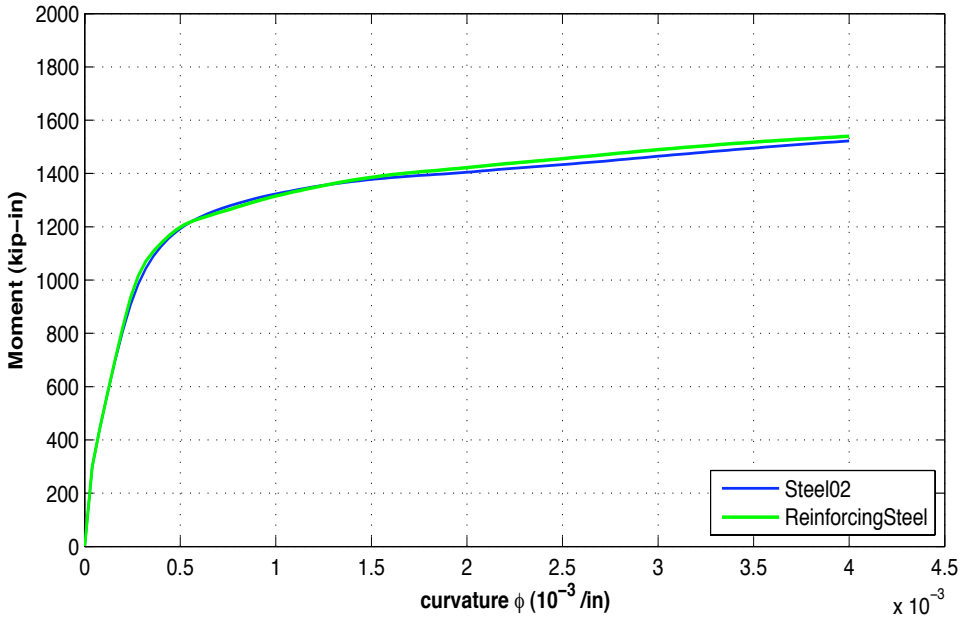

Figure 5-5: Moment-Curvature relationship of column section

5.3.2 Column

As described previously, three options are going to be used to model the reinforced concrete column. An elastic, distributed plasticity, or concentrated plasticity element. The elastic column model should only be used to predict the observed results when no yielding occurred. It utilizes effective section properties to predict observed response. The other two options are force-based beam column elements that can be used to model elastic or inelastic behavior. The distributed plasticity model has no restrictions on the spread of inelastic behavior over the member length. By comparison the concentrated plasticity model limits inelastic behavior to the ends of the column over a user specified length. This length is commonly known as the plastic hinge length. This section briefly describes the implementation of the column model assumption and the associated theory for each column type.

For each of the column models, the weight block assembly was modeled as a lumped mass with rotational mass moment of inertia specified at the center of gravity of the blocks. A rigid offset was used from the top of the column to the center of gravity of the blocks and at the base from the bottom of the footing to the bottom of the column. The lengths of the offsets were 56 inches and 18 inches respectively for the top and bottom. The P-Δ effects associated with gravity loads laterally displacing were also included for the system because measured P-Δ ratios were greater than $0.20M_u$ as specified by the Caltrans SDC.

In summary one column element with lumped mass and rotational mass moment of inertia at the center of gravity with rigid end offsets at both ends was used to model the reinforced concrete column for any of three column model assumptions. The idealized three-dimensional column model is depicted in Figure 5-8.

5.3.2.1 Elastic

The elastic column element is the simplest to implement typically in any type of analysis. In this case it is a three dimensional line element with uniform cross section properties along the length. The mechanical (E, G) and physical properties (L, A, I_y, I_z) are the specified from the outset. As mentioned, both ends have rigid end offsets. Figure 5-6 shows a depiction of the elastic column element.

The accuracy of linear elements response depends on the specified initial stiffness. It is common in design to assume the effective initial stiffness is $EI_{eff} = 0.5EI_g$. From the observed test results, it appears the effective stiffness ratio is closer to 0.2 - 0.3 EI_g.

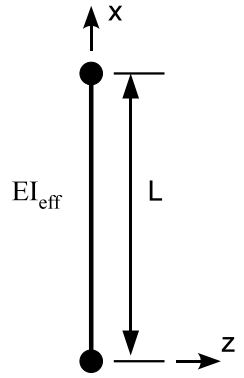

Figure 5-6: Elastic Column Model

5.3.2.2 Distributed Plasticity (NonlinearBeamColumn)

A distributed plasticity beam-column element is one of the two force-based flexibility elements used to model column response. It is implemented via OpenSees as a ***nonlinearBeamColumn*** element. The line element moment-curvature and axial load-deformation response is determined by the fiber sections assigned to each integration point. To predict the observed column response five integration points were used. Figure 5-7(a) shows the ***nonlinearBeamColumn*** element used in the analysis.

The flexibility based formulation estimates the inelastic behavior along the length of the member using integration points. A moment and axial force distribution, which is in equilibrium with the forces at the end of the member, is assumed along the member length. Curvatures and axial deformations are then estimated via iteration given the moment and axial load. Weighted integration of the section deformations at each integration point along the length (Taucer et al., 1991) is used to determine the column response. Because most of the inelastic action is expected to occur at the member ends, it is critical to have integration points there. The Gauss-Lobatto integration scheme places weighted integration points at the ends of the elements as well as along the column length when more than two integration points are used. For this scheme, the weights and

location of the integration points are predetermined. The user specifies only the number of integration points.

5.3.2.3 Concentrated Plasticity (BeamWithHinges)

The other force based flexibility element uses a concentrated plasticity beam-column element to model column response. It is implemented in OpenSees as ***beamWithHinges.*** The fiber based element has nonlinear constitutive behavior limited to user specified lengths at the ends known as plastic hinge lengths. Fiber sections are assigned to the integration points at the end of each plastic hinge. There are several methods available to estimate the plastic hinge length. Equation (5-3) shows the method by Priestly et al. (1996) to determine the plastic hinge length of a circular column. Away from the plastic hinge zones the element behaves linearly elastic with user specified effective stiffness properties EI_{eff}. Figure 5-7(b) shows the column modeled using a ***beamWithHinges*** approach. The cantilever column tested only had inelastic action at the base of the column; therefore a plastic hinge was specified only there. The estimated plastic hinge length was 13.0 inches.

$$l_p = 0.08L + 0.15 f_y d_b \qquad (5\text{-}3)$$

The concentrated plasticity element restricts the integration points to the hinge regions. By comparison the distributed plasticity element distributes integration points along the entire member length. Two integration points per hinge are used to model the curvature distribution. The formulation of the flexibility based element uses a modified Gauss-Radau quadrature rule for integrating element stiffness to eliminate objectivity in the nonlinear region while still maintaining the exact response under linear conditions. A full description of the element formulation can be found in Scott and Fenves (2006). The primary inputs for the column model are fiber sections, plastic hinge lengths, and effective stiffness of the elastic portion of the column.

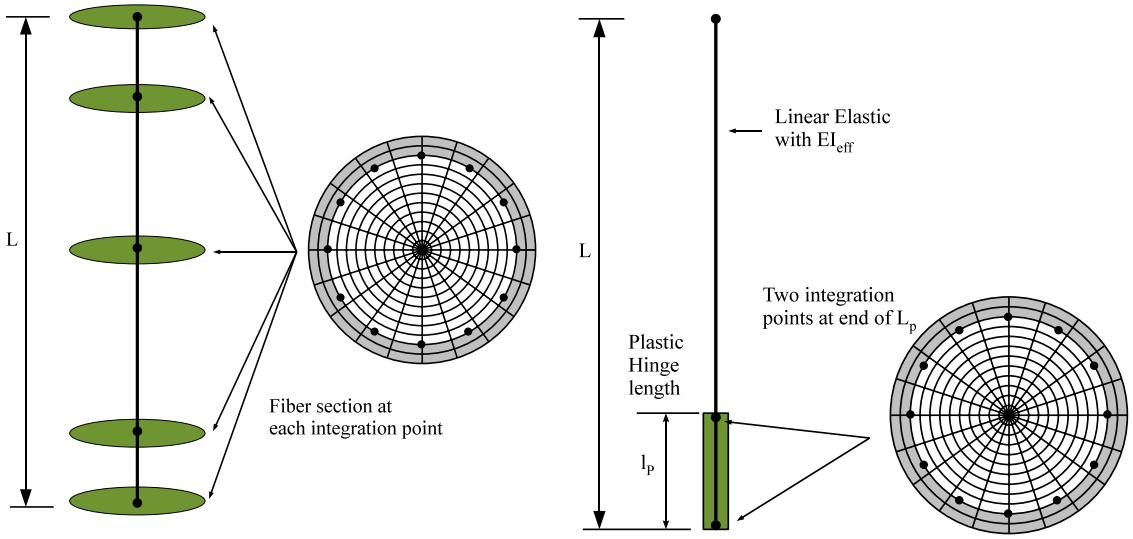

(a) NonlinearBeamColumn **(b) BeamWithHinges**

Figure 5-7: Force-Based Beam Column Models

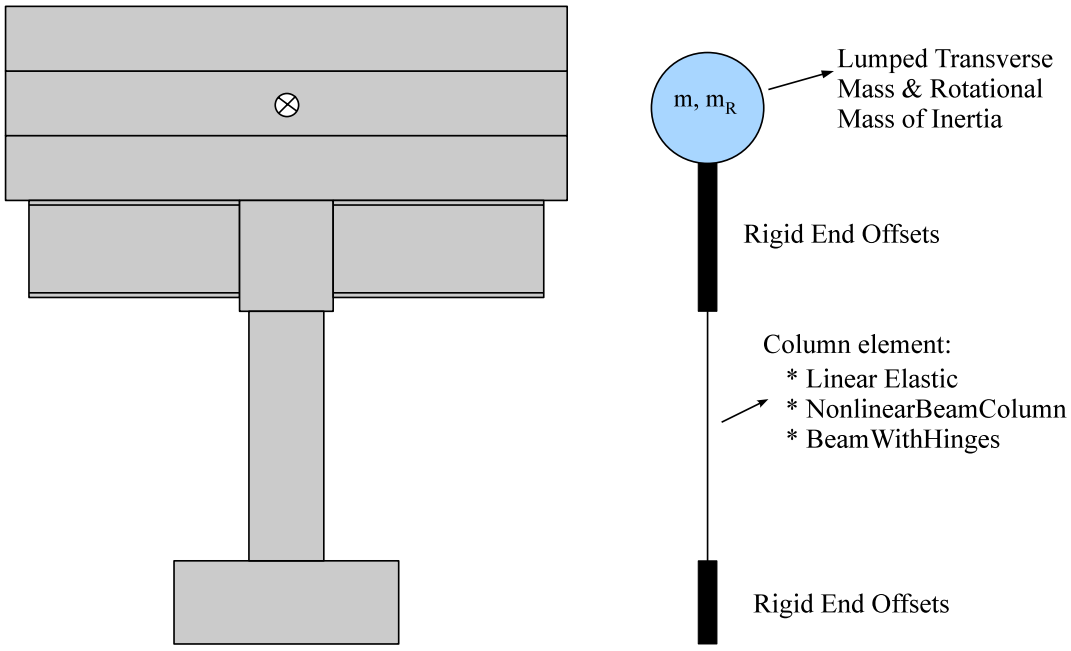

Figure 5-8: General Column Model

5.3.3 Footing - Soil Structure Interaction

Work by Harden et al (2005) illustrates that Winkler spring foundations may be able to provide results with a sufficient degree of accuracy. Because of the two- and three- dimensional character of excitations considered for the experimental testing program (Chapter 3 & 4), it was not viewed as suitable to use more simplified two-spring models or simplified methods based on rocking response of rigid blocks, such as those adapted from the procedures developed by Housner (1963). The model originally developed by Harden et al. (2005) was calibrated for two-dimensional analysis. This model is extended to consider three-dimensional response based on calibration to the experimental results.

The Winkler foundation model has several key parameters that affect the global response of the system. These include modeling of the rotation and vertical stiffness of the foundation. The rotational stiffness is calibrated by varying the stiffness of the end region springs and the length of the end region (Figure 5-9). The material used to represent elastic soil response for the specimens on the shake table was an elastomeric pad and is described in Section 5.2.3. The vertical stiffness characteristics of the padwere explicitly measured.

From the outset a few simplifying assumptions were made for the purposes of analysis. It was assumed that the footing was rigid, and that its horizontal translational movement on the pad was negligible. Some horizontal movement was detected, however it was very small in comparison to the overall lateral displacements of the specimen. Material damping of the elastomeric pads was also considered negligible, so the vertical dashpots were not included in the Winkler foundation model.

The Beam-on-Nonlinear-Winkler-Foundation (BNWF) model was chosen as the method to model the shallow spread footing response. Analytically it is simple to implement via OpenSees. The base of the column connects to the BNWF footing beam elements. The BNWF model links the footing and underlying soil response at each discretization point. Everywhere the footing is discretized the soil below is also discretized in the same size and shape. For the testing program the elastomeric pad beneath the sub-section is modeled using a vertical stiffness spring and a dashpot. The footing is modeled using rigid line elements. Figure 5-9 shows a two-dimensional cross section through the BNWF footing model. The footing elements are considered to be rigid-elastic. The springs and dashpots were modeled as a combination of linear and nonlinear elastic elements (Section 5.2.3). A plan view of the discretization scheme is shown in Figure 5-10. The spacing and number and nodes can be varied in each direction, which serves useful in calibrating the footing and pad response to observed results. Figure 5-11 shows the three-dimensional BNWF model used to predict the observed test results.

The physical properties needed to model the soil include ultimate bearing capacity (q_{ult}), soil type, vertical stiffness (K_z), rotational stiffness (K_θ), damping, etc. Modeling assumptions include the ratio of end length (Lend) to total length (L), the spacing of the springs for each region, and the spring stiffness in the middle and end regions. Also, the

type of uniaxial material hysteresis model to be used for the individual soil springs needs to be determined.

For the purposes of this research, the distribution of pressure for each spring across the foundation was assumed to be uniform. Appendix C contains the Tcl script for implementation of a shallow foundation allowed to uplift in the analysis framework OpenSees. The coding is such that for systems with more than one footing the command can be looped and called as many times as necessary. The resulting foundation model connects to the specified node of the superstructure and does not need spring or other coordinates to be implemented. For the analyses of the shaking table tests, the soil springs were assumed to be linear elastic and unable to resist tension.

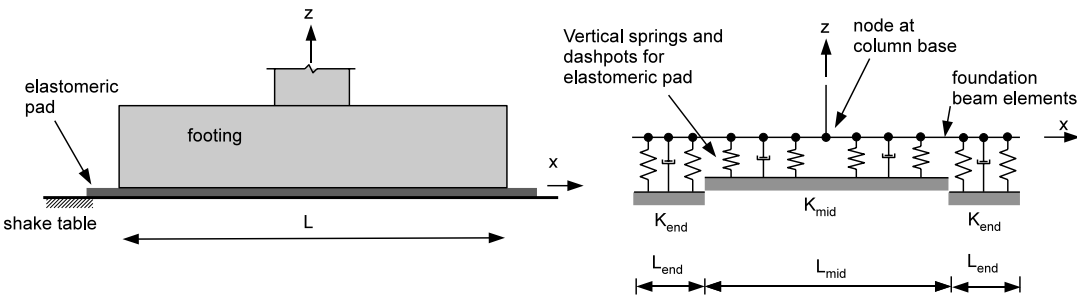

Figure 5-9: Beam on Nonlinear Winkler Foundation (BNWF) Model

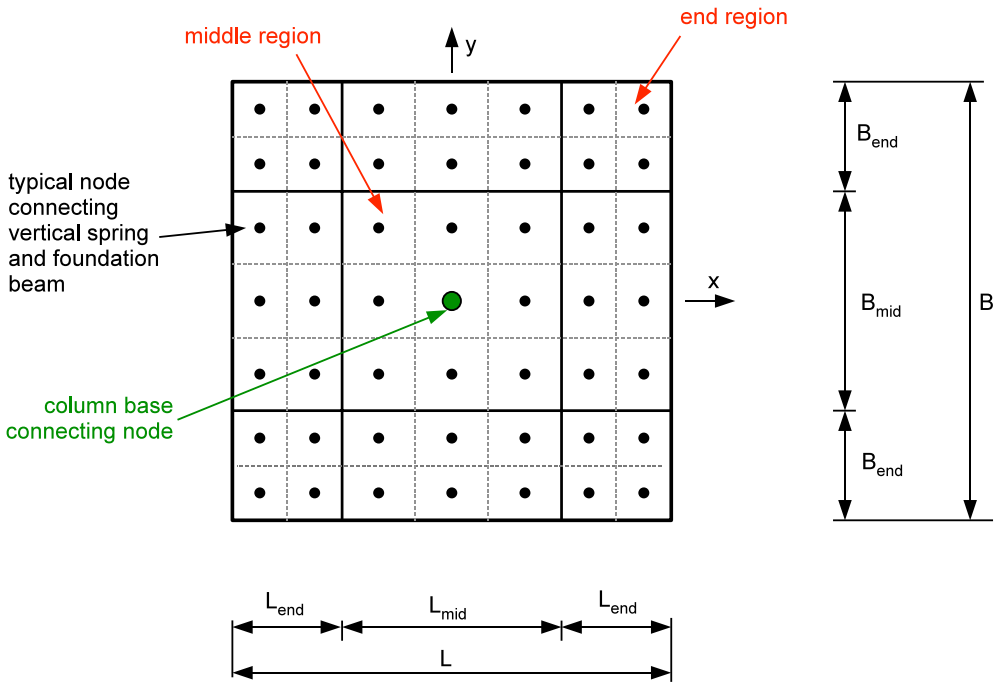

Figure 5-10: Discretization of 3D Footing Model

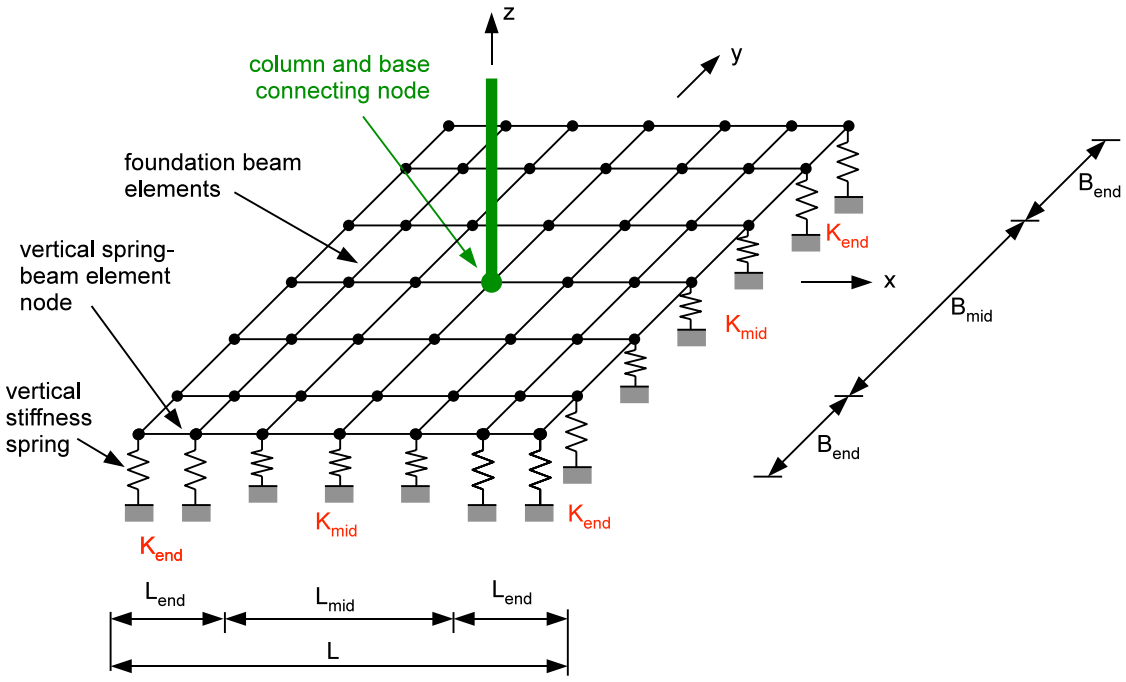

Figure 5-11: Beam-On-Nonlinear-Winkler-Foundation (BNWF) Three-Dimensional Model

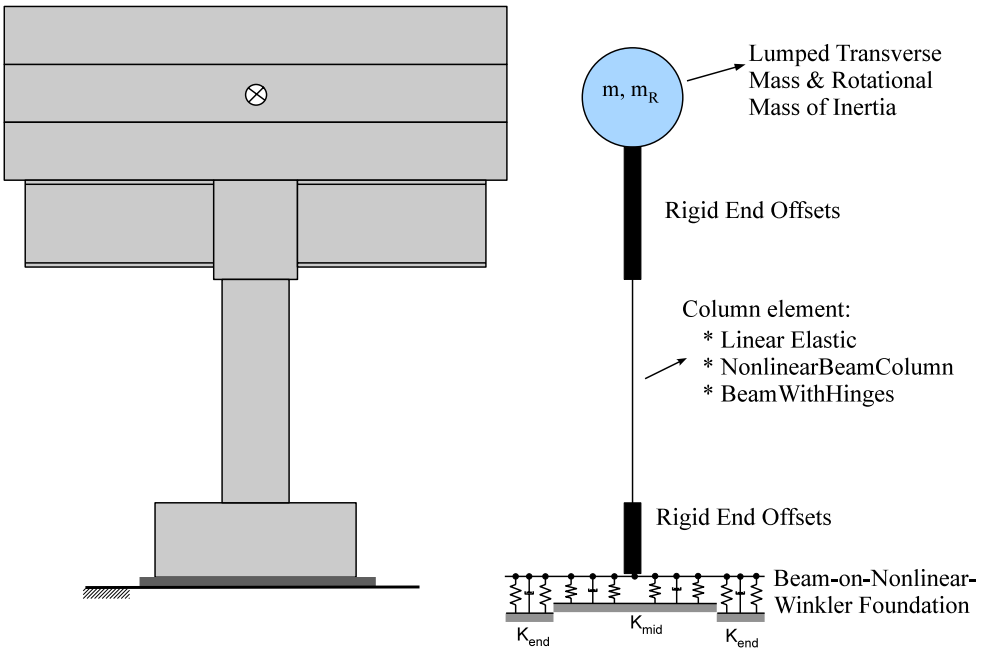

Figure 5-12: Analytic model of uplifting bridge pier system

5.3.4 Damping

Damping modes not associated with hysteretic energy dissipation are usually combined together and idealized as pure viscous damping. This may include soil-structure interaction, friction, material damping, and non-structural components. Rayleigh damping is often used for multi-degree of freedom structures because damping at two natural frequencies ω_i and ω_j may be specified. Damping is most conveniently expressed in terms of the ratio ξ defined as the damping coefficient c relative to the critical damping coefficient c_{cr}. Equation (5-4) shows the relationship for a single-degree-of-freedom structure.

$$\xi = \frac{c}{c_{cr}} = \frac{c}{2m\omega} \qquad (5\text{-}4)$$

For a multi-degree-of-freedom structure the damping matrix is computed as a linear combination of the mass and stiffness matrices (Equation (5-5)). The coefficients α and β are determined by solving the system of equations (Equation (5-6)). The estimation of damping can be mass proportional only, stiffness proportional only, or a combination of mass and stiffness damping.

$$c = \alpha \cdot m + \beta \cdot k_t \qquad (5\text{-}5)$$

$$\frac{1}{2}\begin{bmatrix} 1/\omega_i & \omega_i \\ 1/\omega_j & \omega_j \end{bmatrix} \cdot \begin{bmatrix} \alpha \\ \beta \end{bmatrix} = \begin{bmatrix} \xi_i \\ \xi_j \end{bmatrix} \qquad (5\text{-}6)$$

Damping ratios for reinforced concrete structures typically range from 3% to 7%. In design of structures, it is common to use 5%. However, this is for fixed base systems that do not include soil-structure interaction. The presence of soil deformation and yielding tends to increase the amount of damping in the system. The viscous damping associated with soil-structure interaction is a complex phenomenon that goes beyond the focus of this research work. A study by Housner (1963) determined the equivalent viscous damping of rigid blocks allowed to rock. Work by Chopra and Goel (1999) also may be useful in determine the equivalent viscous damping of an uplifting system.

For the purposes of this investigation, the effects of mass, stiffness and mass-stiffness proportional damping are investigated only. The analysis done also shows the effect that varying the damping ratio has on the damping force within the system. Based on the observed results (Chapter 4) of the shake table tests the initial Rayleigh damping parameters α and β were selected based on a damping ratio of 7.8%. The damping matrix was formed at each analysis step using the current tangent stiffness matrix.

5.4 Elastic Footing Analysis

Each of the analytic model options for the column is paired with an elastic footing model whose formulation is described in this section. Both footing sizes used in the test configurations are described here analytically. Best modeling values for the global vertical stiffness of the elastomeric pad and spring spacing are developed to most accurately capture the observed footing rotational stiffness and uplift. The footing analytic model is an approximation of the footing. More accuracy may be possible with smaller discretization segments of the footing, however this comes at the expense of more nodes and longer analysis run times. In general, decreasing the node spacing by a half (for example) increases the number of nodes by a power of 2. Damping of the elastomeric pad may be an additional source of uncertainty. The effects of the type of damping assumptions on footing response are described in the column analysis sections.

The footing analysis is accomplished by calibrating the analytic model to the observed moment-rotation relationship. Using the Beam-on-Nonlinear-Winkler-Foundation (BNWF) approach described in Section 5.3.3 several parameters need to be specified. The inputs for modeling are the middle region global stiffness K_{zm} and end region global stiffness K_{ze}. Additionally the footing length L, width B, end lengths and node spacing are specified.

The force deformation relationship can be formed as follows when assuming a rigid footing assumption supported on vertical springs. This is the method used by the BNWF footing mesh generator described in Section 5.3.3. The formulation method described here is based on a two-dimensional plane. However, the three-dimensional formulation is very similar. For all analysis cases the footing is restrained from translating laterally in the x or y axis direction. The footing is allowed to uplift in the z axis direction and rotate about all three axes. Using a rigid footing assumption the entire footing uplift along the length can be described by two degrees-of-freedom at the center node of the footing; the vertical displacement and the rotation about the centerline of the footing. Figure 5-13 shows a depiction of the footing, displacement degrees-of-freedom,

and generalized vertical spring stiffness and locations. The force deformation relationship is described by Equation (5-8) which is expressed in terms of vertical footing force and overturning moment as a function of footing displacement degrees of freedom. The uplift at a given spring location is determined by Equation (5-9).

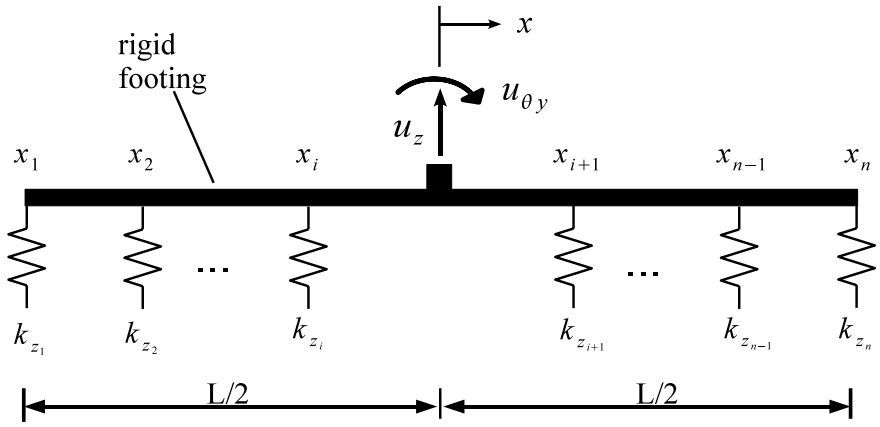

Figure 5-13: Footing Force Deformation Relationship Formulation

Footing Force Deformation Relationship:

$$F = K_{ftg} \cdot u \qquad (5\text{-}7)$$

Expressed in matrix form as individual forces and displacements:

$$\begin{bmatrix} F_z \\ M_{\theta_y} \end{bmatrix} = \begin{bmatrix} k_z & k_{z\theta} \\ k_{z\theta} & k_\theta \end{bmatrix} \cdot \begin{bmatrix} u_z \\ u_{\theta y} \end{bmatrix} \qquad (5\text{-}8)$$

Individual spring uplift displacement:

$$z_i = z_o + x_i \cdot \theta \qquad (5\text{-}9)$$

The general footing stiffness matrix is:

$$k_{ftg} = \begin{bmatrix} k_z & k_{z\theta} \\ k_{z\theta} & k_\theta \end{bmatrix} \qquad (5\text{-}10)$$

The individual components of the footing stiffness matrix as a function of the vertical spring stiffness and relative spring locations are given by Equations (5-11) through (5-13). The formulations as shown are for when no uplift of the footing at the springs has occurred.

$$k_z = \sum_{i=1}^{n} k_{zi} \qquad (5\text{-}11)$$

$$k_{z\theta} = \sum_{i=1}^{n} k_{zi} \cdot x_i \qquad (5\text{-}12)$$

$$k_{\theta} = \sum_{i=1}^{n} k_{zi} \cdot x_i^{\,2} \qquad (5\text{-}13)$$

The individual spring stiffness k_{zi} at each location x_i along the footing length L is the sum of the individual springs distributed along the width B of the footing at the x_i coordinate. In general the individual spring stiffness k_{zi} at x_i is the sum of each spring kz_{ij} for j=1:m. Where m = number of nodes in the y direction. The stiffness k_{zi} in the x direction can be expressed as Equation (5-15) for the middle region of the footing and Equation (5-16) for the end region of the footing. The procedure is the same for the y direction, however we substitute the width terms B, Bep, and fLy for length terms L, Lep, and fLx.

fLx = length of footing segment i (5-14)

The spring stiffness at middle footing region:

$$k_{zi} = \left[\frac{fL_x\left(1 - 2B_{ep}\right)}{L}\right] \cdot K_{zm} + \left[\frac{fL_x B_{ep}}{L}\right] \cdot K_{ze} \qquad (5\text{-}15)$$

The spring stiffness at end footing region:

$$k_{zi} = \left[\frac{fL_x}{L}\right] \cdot K_{ze} \qquad (5\text{-}16)$$

Under a static vertical load with zero rotation the footing stiffness matrix is uncoupled owing to the symmetry of the springs locations and stiffness values. The force-deformation relationship simplifies to:

$$\begin{bmatrix} F_z \\ M_{\theta_y} \end{bmatrix} = \begin{bmatrix} k_z & 0 \\ 0 & k_{\theta} \end{bmatrix} \cdot \begin{bmatrix} u_z \\ u_{\theta y} \end{bmatrix} \qquad (5\text{-}17)$$

The initial static displacement of all the springs under a vertical load with no rotation is:

$$u_z = z_o = \frac{F_z}{k_z} = \frac{F_z}{\sum_{i=1}^{n} k_{zi}} \qquad (5\text{-}18)$$

The rotation of the footing and the corresponding moment when the first spring loses contact with the footing is:

$$\theta_{up1} = \frac{u_z}{x_1} = \frac{z_o}{x_1} \qquad (5\text{-}19)$$

$$M_{\theta up1} = k_\theta \cdot \theta_{up1} = \left[\sum_{i=1}^{n} k_{zi} \cdot x_i^{\,2}\right] \cdot \frac{z_o}{x_1} \qquad (5\text{-}20)$$

The footing stiffness while rocking, when no uplift occurs along the footing length at the springs, can be described by Equation (5-17). As the footing uplifts with increasing rotation the footing stiffness matrix will be redefined as subsequent springs lose contact with the footing. The moment-rotational stiffness relationship will be a multi-linear curve with transition points defined by the uplift of individual springs. In reality as the footing continues to uplift there is a continuous decrease in the length of footing resisting the uplift and therefore a continuous change in the vertical and rotational stiffness, whether it be small or large magnitude, which results in a smooth moment-rotation relationship. The individual components of the footing stiffness matrix $\mathbf{K_{ftg}}$ as footing uplift occurs can be described by modifying the Equations (5-11) through (5-13). When uplift occurs at the first spring i=1, the force is eliminated and the individual spring stiffness k_{z1} is removed from the determination of $\mathbf{k_z}$, $\mathbf{k_{z\theta}}$ and $\mathbf{k_\theta}$. As the footing loses contact with the spring at location x_i, the footing stiffness components are a function of the spring stiffnesses from $\mathbf{k_{zi}}$ for **i= i+1:n** (Equations (5-21) to (5-23)). This is the case until the next spring uplifts, when the footing stiffness matrix is recalculated for contributing springs $\mathbf{k_{zi}}$ for **i= i+2:n**.

The individual footing stiffness $\mathbf{K_{ftg}}$ components when uplift has occurred at spring location x_i are:

$$k_z = \sum_{i=i+1}^{n} k_{zi} \qquad (5\text{-}21)$$

$$k_{z\theta} = \sum_{i=i+1}^{n} k_{zi} \cdot x_i \qquad (5\text{-}22)$$

$$k_\theta = \sum_{i=i+1}^{n} k_{zi} \cdot x_i^{\,2} \qquad (5\text{-}23)$$

The representative moment rotation relationship for a footing with dimensions L long and B wide are shown in Figure 5-14. The applied rotation θ is one full cycle from zero to $+\theta_{max}$ to $-\theta_{max}$ and back to zero. The M-θ relationship is for the two vertical spring

analysis options; Elastic No Tension (Fig. 5-14a) and Neoprene (Fig. 5-14b). The end length ratios $\mathbf{L_{ep}}$ and $\mathbf{B_{ep}}$ and global vertical stiffness $\mathbf{K_{zm}}$ and $\mathbf{K_{ze}}$ are specified and the node spacing is set so there is 6 nodes in each direction (symmetric about the centerlines). Before first uplift the footing rotational stiffness $\mathbf{K_\theta}$ may be calculated by Equation (5-17). At first uplift the corresponding moment is $\mathbf{M_{up1}}$ as given by Equation (5-20). As the footing rotation increases the footing loses contact with the vertical springs and the rotational stiffness decreases. The plots show the transitions in rotational stiffness as each subsequent vertical spring loses contact with the footing. During unloading the Elastic No Tension springs follow the same path, while the Neoprene springs dissipate some energy as described in Section 5.2.3.

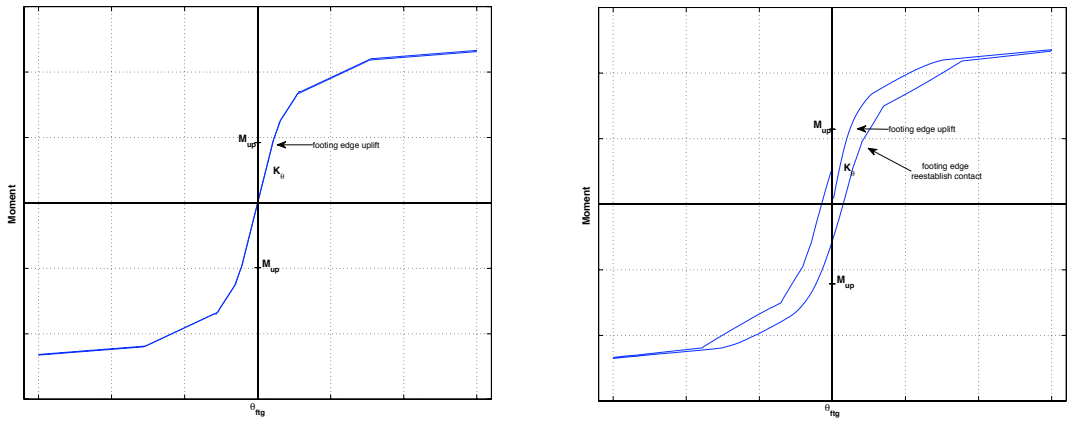

(a) Elastic-No-Tension (ENT) Springs (b) Neoprene Springs

Figure 5-14: Analytic Model Moment Rotation Relationship of Footing (ENT springs)

The methods described above can be used to calibrate the footing stiffness and spring spacing to best match the observed response. The comparison of results is focused on the two footing configurations when the column had a nominal design axial load applied. The less than design axial load experimental test was used to assess the viability of rocking systems and is not investigated further. The first test group was the $3D_c$ x $3D_c$ square footing configuration, which had only elastic response of the column. The second test group was the $5D_c$ x $3D_c$ rectangular footing configuration that had elastic and inelastic response of the column.

5.4.1.1 $3D_c$ x $3D_c$ Square Footing Configuration

The best values of global vertical stiffness for the square configuration footing are in the range of $\mathbf{K_{zm}}$ = 600-800 kip/in for the middle region and $\mathbf{K_{ze}}$ = 2000-2200 kip/in for the end region. When using the neoprene vertical spring material the stiffness needs to be slightly higher than the elastic no tension material due to the gap strain which creates more deflection with less force on the footing springs. The range of end length ratio for the $3D_c$ square footing configuration is approximately L_{ep}, B_{ep} = 0.20-0.30. Figure 5-15 shows the moment – rotation envelope from an applied cyclic rotation using Elastic-No-Tension (ENT) springs for the $3D_c$ square footing compared to the recorded DS test group data (3D X+Y+Z input) which had the most significant uplift. Dynamic effects are not included in this envelope analysis. The recorded FS test group data (3D X+Y+Z input) is shown Figure 5-16 for the ENT springs. The response using Neoprene springs

and an applied cyclic rotation are very similar to that shown for the ENT springs with the addition of energy dissipation during unloading as shown in Figure 5-17 and Figure 5-18 for the 3D-X+Y+Z input of the DS and FS experimental tests.

The ranges of $\mathbf{K_{zm}}$ and $\mathbf{K_{ze}}$ best match the recorded vertical displacement $\Delta_z=z_o$ under static load, the initial rotational stiffness K_θ, the moment at first uplift M_{up1}, and an approximation of the softening of the footing rotational stiffness as the footing uplifts with increasing rotation. The values of global vertical stiffness and end length ratio, which best approximated the vertical and rotational stiffness of the $3D_c$ x $3D_c$ footing for all experimental tests of the square footing are given in Table 5.1. The square configuration does not have identical rotational stiffness and first uplift moment about the X and Y axes because of the variable spring spacing in each direction.

Table 5.1: Footing Vertical Stiffness Values

	$3D_c$ x $3D_c$		$3D_c$ x $5D_c$	
	ENT Spring	**Neoprene Spring**	**ENT Spring**	**Neoprene Spring**
$\mathbf{K_{zm}}$ (kip/in)	600	600	600	600
$\mathbf{K_{ze}}$ (kip/in)	2200	2200	2200	2200
L_{ep}	0.24	0.24	0.24	0.24
B_{ep}	0.26	0.26	0.26	0.26
z_o (in)	0.033	0.041	0.033	0.04
$K_{\theta Y}$ (kip-in)	427,750	427,750	312,680	427,745
$K_{\theta X}$ (kip-in)	438,900	438,900	890,430	1,219,170
M_{up1Y} (kip-in)	580.0	720.0	594.0	730
M_{up1X} (kip-in)	595.0	740.0	1095.0	1260

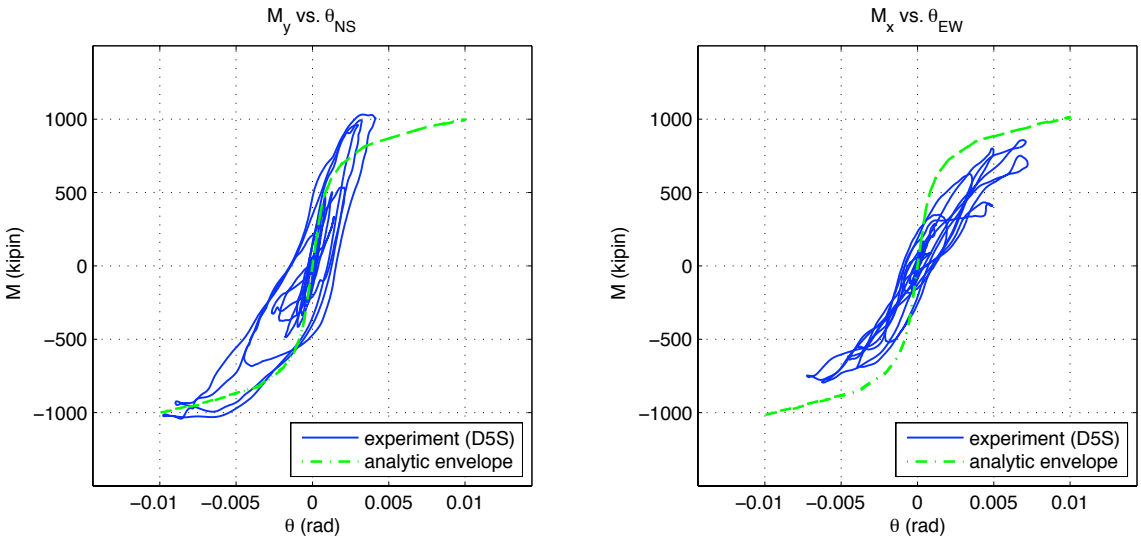

Figure 5-15: M-θ Analytic Envelope of 3Dc Square Footing (Test D5S ENT springs)

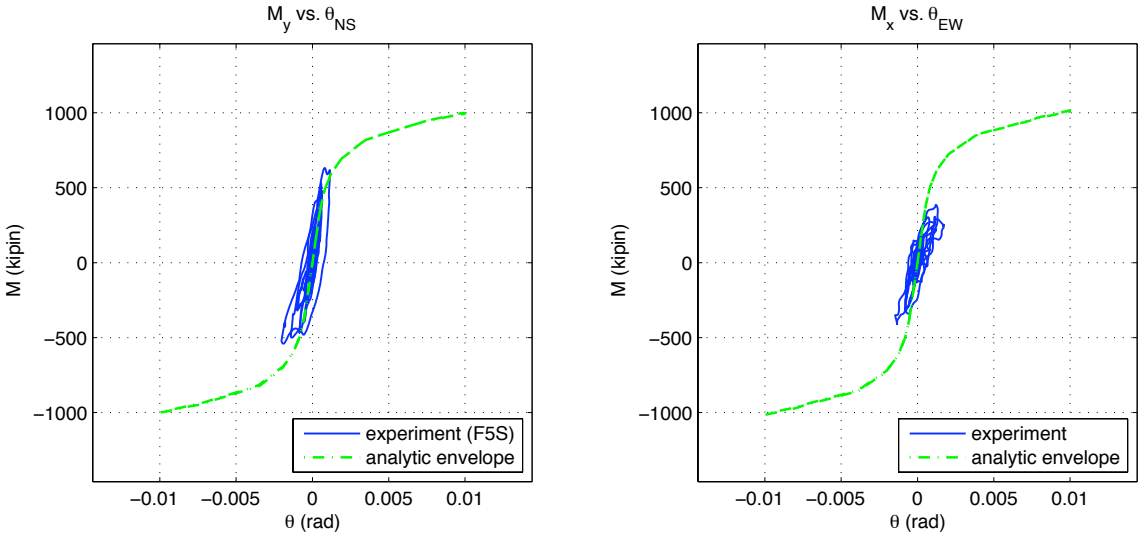

Figure 5-16: M-θ Analytic Envelope of 3Dc Square Footing (Test F5S ENT springs)

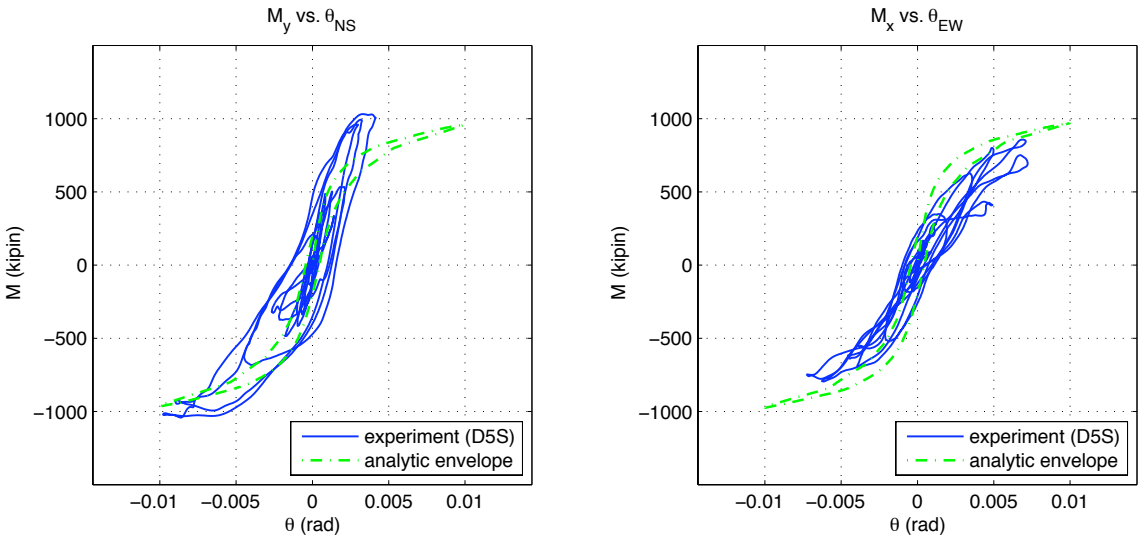

Figure 5-17: M-θ Analytic Envelope 3Dc Square Footing (Test D5S Neoprene springs)

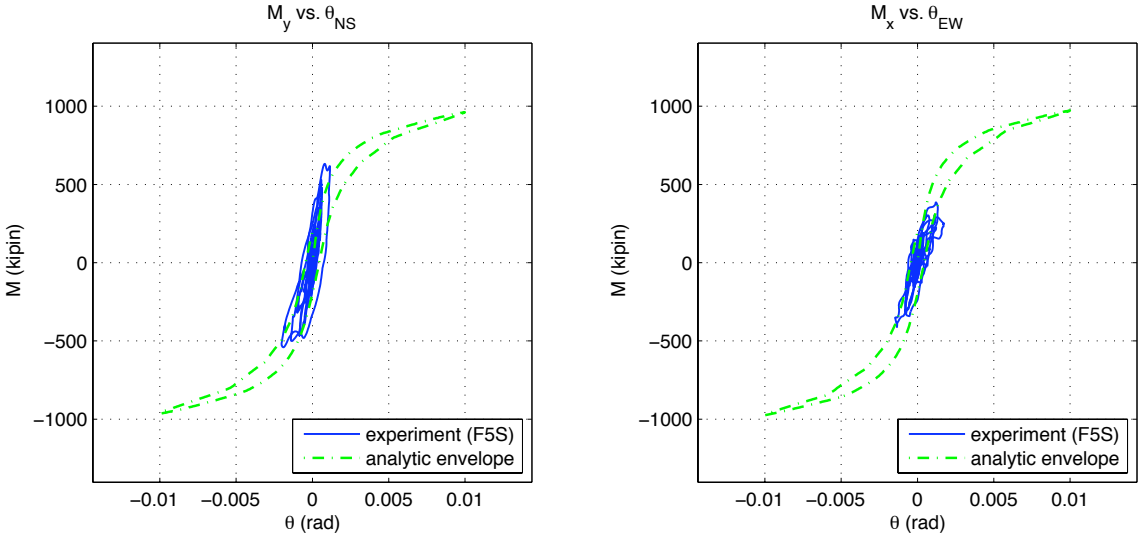

Figure 5-18: M-θ Analytic Envelope of 3Dc Square Footing (Test F5S Neoprene springs)

5.4.1.2 5D_c x 3D_c Square Footing Configuration

The best values of global vertical stiffness for the rectangular configuration footing are in the range of $\mathbf{K_{zm}}$ = 600-800 kip/in for the middle region and $\mathbf{K_{ze}}$ = 2000-2200 kip/in for the end region. The range of end length ratio for the 3D_c (X) direction and the 5D_c (Y) direction is approximately L_{ep}, B_{ep} = 0.20-0.30, respectively. Figure 5-19 and Figure 5-20 show the moment – rotation envelope from an applied cyclic rotation using Elastic-No-Tension (ENT) springs and Neoprene springs (NEO) for the 3D_c x 5D_c rectangular footing compared to the recorded A2R test group data (3D X+Y+Z input), which had some uplift and is not influenced by residual displacements which cause a shifted moment-rotation origin due to permanent overturning moment. Dynamic effects

are not included in this envelope analysis. The footing values of $\mathbf{K_{zm}}$ and $\mathbf{K_{ze}}$ which best match the initial displacement z_o, rotational stiffness K_θ, the moment at first uplift M_{up1}, and an approximation of the softening of the footing rotational stiffness as the footing uplifts with increasing rotation are given are in Table 5.1.

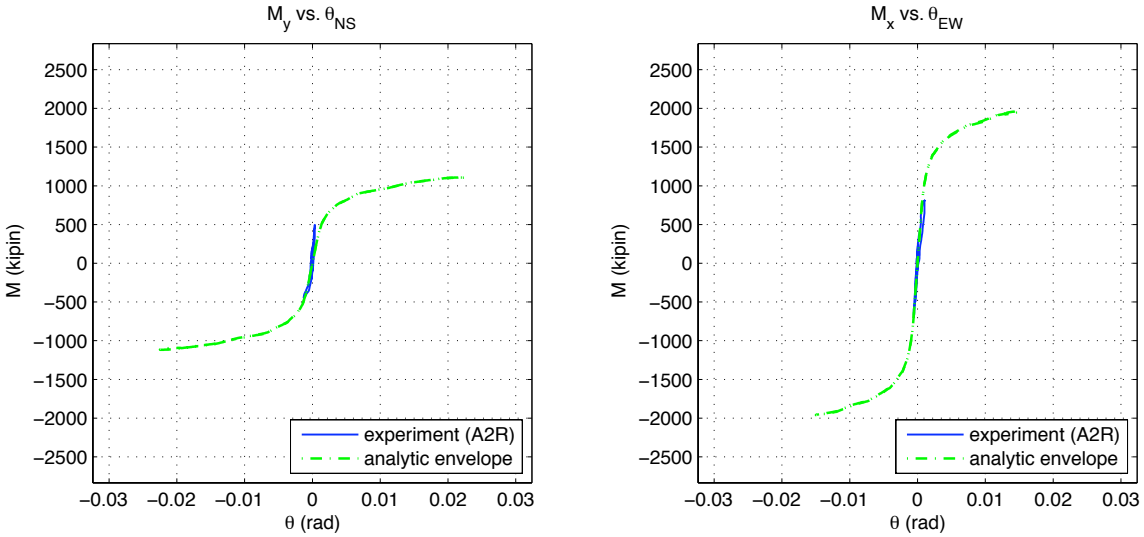

Figure 5-19: M-θ Analytic Envelope $3D_c$ x $5D_c$Footing (A2R ENT springs)

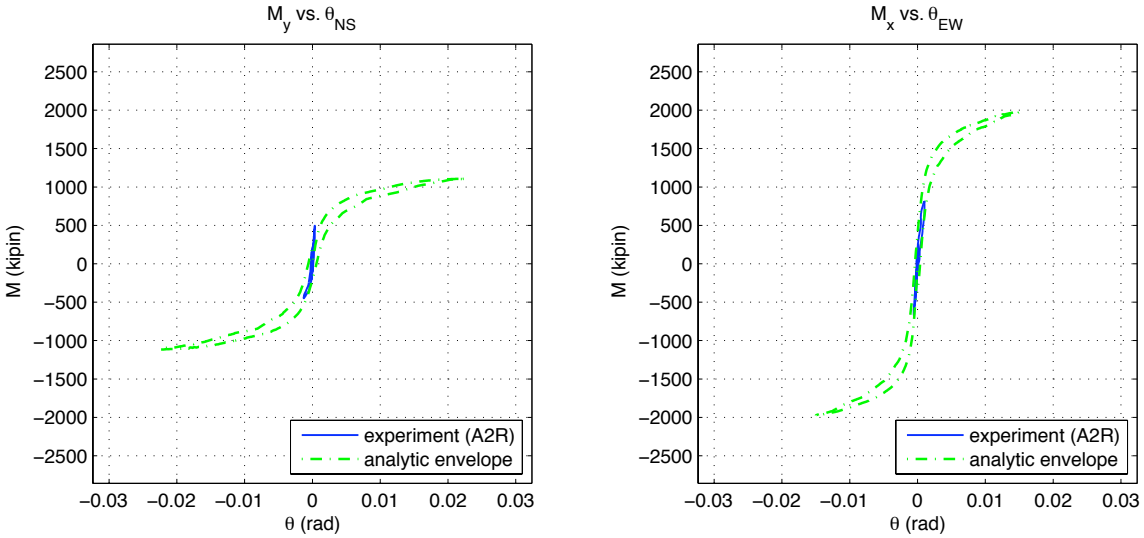

Figure 5-20: M-θ Analytic Envelope of $3D_c$ x $5D_c$Footing (A2R NEO springs)

5.5 Comparison of Linear Analysis and Experimental Results

Several analysis models will be evaluated for their ability to predict the observed specimen response. The analysis models considered have elastic footing response and column response that is linear or nonlinear. The tests performed were monitored for displacement, acceleration, and strains, which are used to validate the analysis models. The recorded natural modes of vibration, damping values of the system, and material properties were used to calibrate and conduct the analysis. See Chapter 4 for a summary of the experimental results.

The material modeling assumptions for concrete, steel, and neoprene are described in Section 5.2. Element modeling options and assumptions for the neoprene pad, footing, column and superstructure weight blocks are described in Section 5.3.

The quantities of interest that will be compared describe the key response parameters of an uplifting bridge system. The displacement quantities of interest include the footing uplift (or footing rotation) and the column center of mass displacement. The acceleration response of the center of mass is compared. Force quantities include the lateral force at center of mass, moment-curvature response at the column base and the moment-footing rotation response.

The two ground motions used in the testing program varied combinations of the amplitude, time scale, and input directions. In addition footing widths were also varied. A comprehensive list of all the test runs can be found in Appendix A. The volume of test results is too vast to present here in the analysis section. Instead, the most relevant test runs and analytic comparisons are shown. For all analysis cases the input accelerations used are those recorded by the shaking table instrumentation and directly felt by the uplifting bridge pier system.

To begin, the simplest possible model is considered, which is the linear column coupled with the elastic footing model. Upon comparison and calibration of the footing and column for linear response the model is enhanced to include nonlinear column response. The footing response is modeled as elastic for all column model assumptions and is described in Section 5.4. Linear column analysis for the two column footing width test groups ($3D_c$ x $3D_c$ and $5D_c$ x $3D_c$) is described in Sections 5.5.1 and 5.5.2. Nonlinear column analysis is described in Section 5.6 for the $5D_c$ x $3D_c$ footing width test group. Summaries and conclusions on the various column and footing analysis models are described in Section 5.7.

5.5.1 Design Axial Load and 3Dc x 3Dc Footing

The linear column response analysis compares analytic model predictions to experimental tests when the column behaved linearly. This includes all of the tests using a square footing configuration. In this section the best model properties will be determined which capture displacements, forces, and accelerations. The modeling options include the column type, which may be elastic, concentrated plasticity, or distributed plasticity models and either an elastic-no-tension or neoprene vertical spring model for

the footings. To calibrate the models to the observed response the effective column stiffness, damping ratios, and spring spacing will be adjusted.

In the following section, the analytic results are compared to the experimental results for the DS and FS test groups. The two groups exhibit the largest magnitudes of elastic column response for the Los Gatos and Tabas input earthquake excitations, respectively. Three types of input acceleration are compared: 1D-X, 2D-X+Y, and 3D-X+Y+Z. The center of mass and footing displacements are compared in Section 5.5.1.1. A comparison of the center of mass acceleration is presented in Section 5.5.1.2. The comparison of the column moment curvature response and footing moment rotations is described Section 5.7.

The initial model used had an elastic column assumption, with elastic no tension vertical springs for the footing. Table 5.2 summarizes the combinations of models used for the uplifting system when in the elastic range.

Table 5.2: Linear Analysis Modeling Options

Column	**Footing Vertical Springs**	**Materials**
Elastic	Elastic-No-Tension (ENT) Neoprene (NEO)	-
Distributed Plasticity (DIST)	Elastic-No-Tension (ENT) Neoprene (NEO)	Concrete02 Steel02 Reinforcing Steel
Concentrated Plasticity (BWH)	Elastic-No-Tension (ENT) Neoprene (NEO)	Concrete02 Steel02 Reinforcing Steel

5.5.1.1 Displacements

The linear analysis displacement histories are compared to measured displacement for the square configuration footing subjected to the one dimensional input excitation for the Los Gatos (D1S) and Tabas (F1S) test runs. Figure 5-21 and Figure 5-22 show the center-of-mass displacement response for an elastic column model with elastic-no-tension or Neoprene vertical springs subjected to D1S. The center-of-mass displacement response for an elastic column model with elastic-no-tension or neoprene vertical springs are presented in Figure 5-23 and Figure 5-24 for F1S.

The analysis was repeated using the alternate distributed plasticity or lumped plasticity column model assumptions. Figure 5-25 and Figure 5-26 show the center of mass displacement of test D1S using a distributed plasticity column model with either vertical spring material. This analysis was repeated using the lumped plasticity column model. Figure 5-27 and Figure 5-28 show the corresponding center of mass displacement for test D1S. Test F1S results varying the column models are not shown here to limit the

amount of information displayed. The response in general is very similar to that shown for D1S.

Inspection of the one-dimensional input excitation results shows the elastic column model approximates the observed center of mass displacement response very well as does the lumped plasticity column model which is expected since the behavior of the column was elastic. The distributed plasticity model does not predict the observed response as well due to difficulty in matching the initial stiffness of the column. The contribution of column total displacement due to flexural and rocking was not shown in the column modeling and vertical spring material comparisons to simplify the presentation. In general the accuracy of the various column models and vertical spring materials on flexure and rocking column displacement is in agreement with the observed center of mass displacements accuracies. The ability to predict the flexural and rocking column displacement was investigated thoroughly for all combinations of column and vertical spring options presented in this discussion and used as an evaluator.

Upon review of the relevant response quantities it was found for modeling the elastic response of the test system for 1D input excitation the best model available is an elastic column model assumption with a Neoprene (NEO) vertical spring material. The elastic column model and lumped plasticity column model yielded similar results, but the elastic option is preferred because of its analytic simplicity. The hysteretic damping qualities of the neoprene vertical spring made it the preferred option because of its ability to capture observed damping of the neoprene pad. The analytic damping options which best predicted the column and footing response was Rayleigh *mass proportional only* with 5-6% damping ratio.

The relevant displacement results for the one-dimensional input excitation D1S using the best model available are presented in Figure 5-29. The total center of mass displacement is shown in Figure 5-29(a). The contribution of column flexural displacement is shown in Figure 5-29(b). The lateral displacement of the center of mass due to rocking will be represented by the footing rotation since they are analogous as described in Section 4.2 and by Equation (4-3). For test D1S, the comparison is shown in Figure 5-29(c). The initial stiffness and free vibration phase at the end of the signal track reasonably well as shown in Figure 5-29. As does the damping which is indicated by the signal attenuating after the forced vibration phase ends. The peak column displacements seem to track reasonably well given the complexity of the uplifting and deforming column system. The peak total displacement, flexural displacement and rocking displacement all occur at the peaks as those recorded. Their magnitude is within 15%, 27%, and 26%, respectively, of the recorded results. The acceleration and moment-deformation results are discussed in Section 5.5.1.2 and 5.5.2.3. They, too, reasonably approximate the observed response.

Using the best model developed for the 1D input analytic comparisons the column model was investigated for 2D and 3D input excitation. The center of mass displacement results for the Los Gatos tests are shown in Figure 5-30(a)-(c) for the 2D input excitation test D3S and Figure 5-31(a)-(c) for the 3D input excitation test D5S. Inspection of the results shows that test D3S approximates the results reasonably well. The peaks occur at the same time and are within 22%, 20%, and 20% for the peak column total, flexural, and

rocking displacement. The forced vibration phase tracks very well and begins to deviate during the free vibration phase (approximately 15 seconds and beyond). It appears the system is slightly over damped for the 2D input excitation. However, attempts to reduce the damping and lengthen the period in the free vibration phase negatively affected the peak displacements. It appears the test results indicated the two-directional input excitation affects the natural period of the system along the diagonal.

Inspection of the results for test D5S show the analysis predicts the peak displacements reasonably well. Within 15%, 9%, and 11% for the peak column total displacement, flexural displacement, and rocking displacement. The stiffness of the system during the forced vibration phase of the signal tracks reasonably well also. However the analytic model is over damped during the free vibration phase. Again, attempting to reduce the damping overestimates the peak displacements significantly for the 3D input excitation.

Comparison of the analytic vs experimental displacement results are give in Figure 5-36 using the best column model. The peak column displacements are within 17%, 5%, and 11% of the observed column total, flexural and rocking values. In the Y direction the analytic prediction deviates from the observed response. This is due mostly to filtering of the recorded input signal for high frequency content. When using the original signal the analysis tracks well. However, the noise generated in the analytic prediction is significant and affects the ability to evaluate the model. For this reason, the results using the filtered signal are presented, because the overall clarity outweighs the distorted signal at this time step.

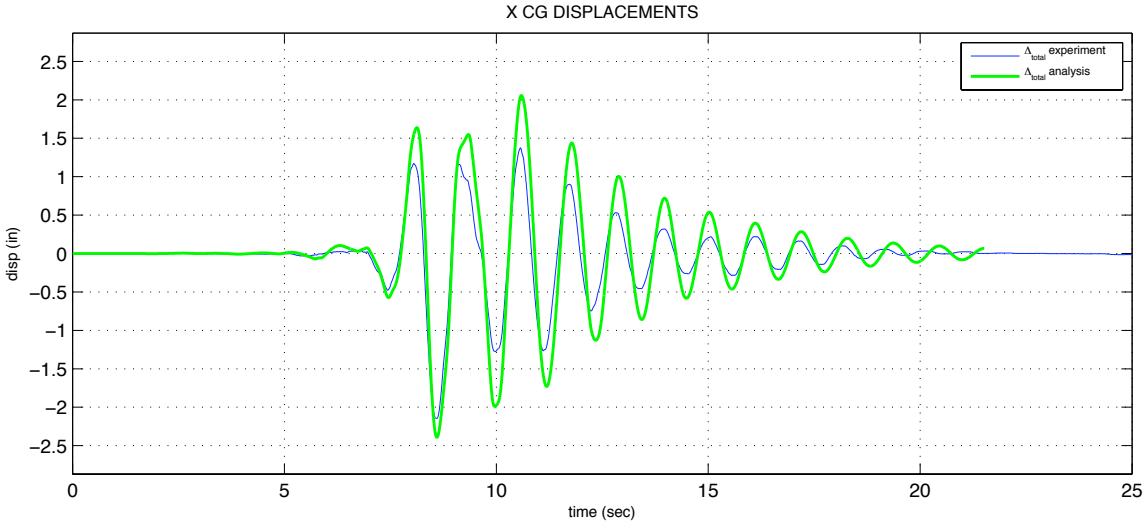

Figure 5-21: Center Mass Displacement – Elastic Column ENT Springs (D1S)

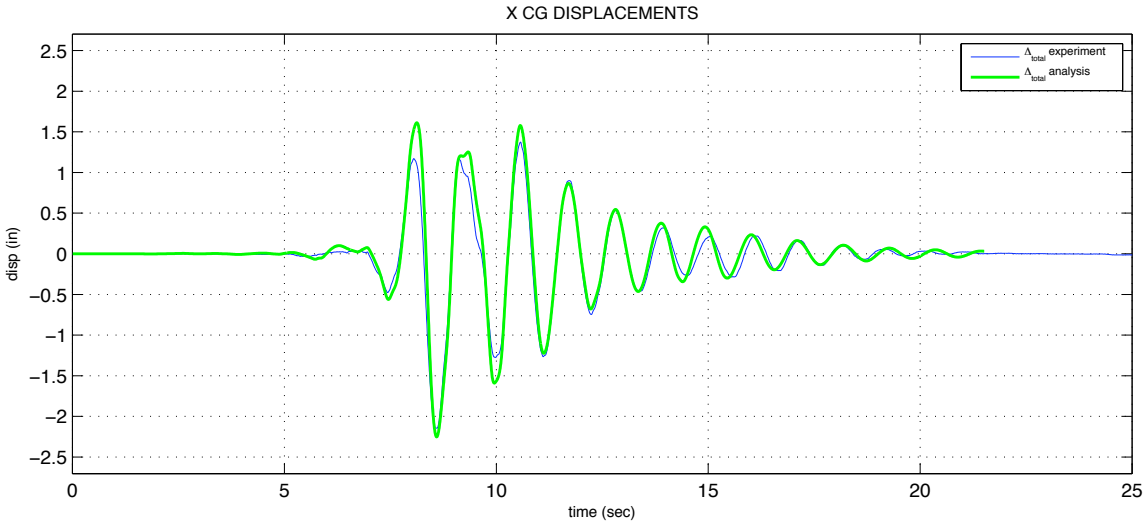

Figure 5-22: Center Mass Displacement – Elastic Column NEO Springs (D1S)

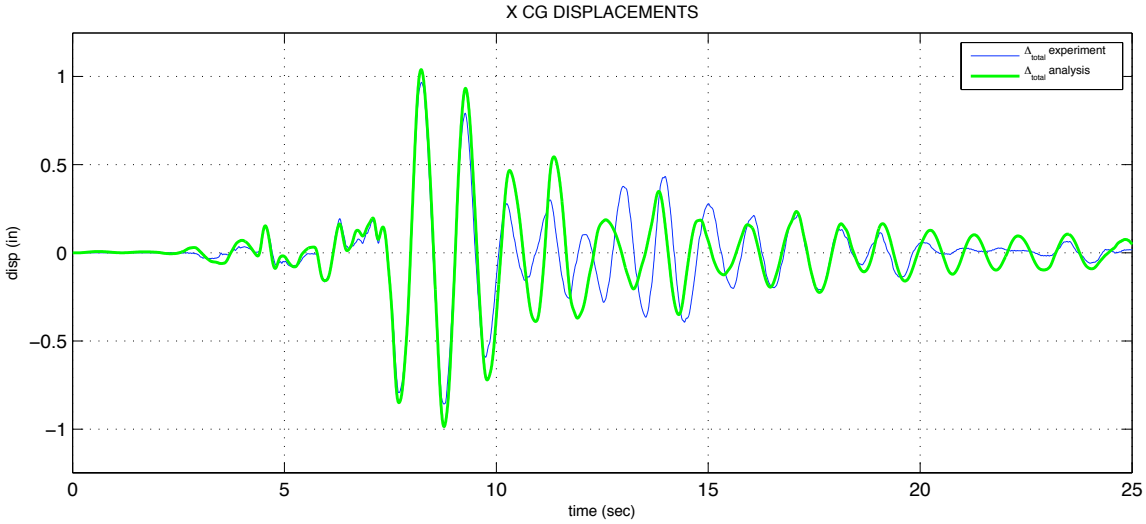

Figure 5-23: Center Mass Displacement – Elastic Column ENT Springs (F1S)

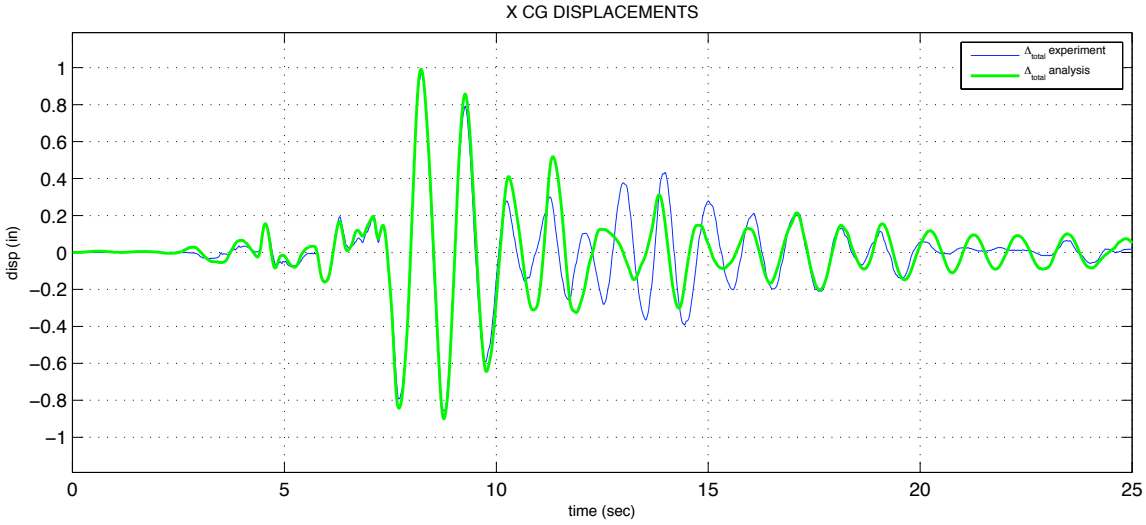

Figure 5-24: Center Mass Displacement – Elastic Column NEO Springs (F1S)

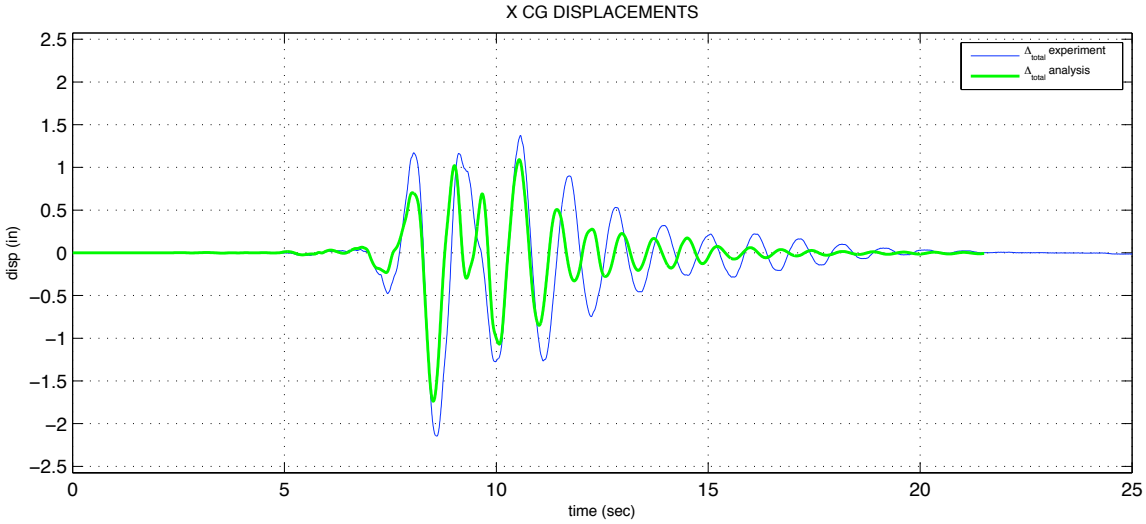

Figure 5-25: Center Mass Displacement – Distributed Plasticity Column ENT Springs (D1S)

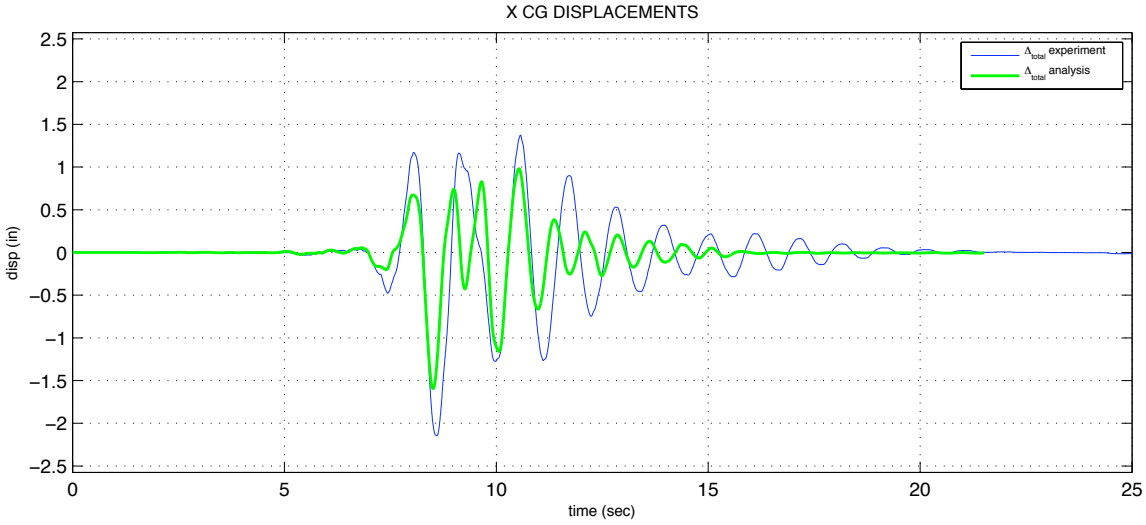

Figure 5-26: Center Mass Displacement – Distributed Plasticity Column NEO Springs (D1S)

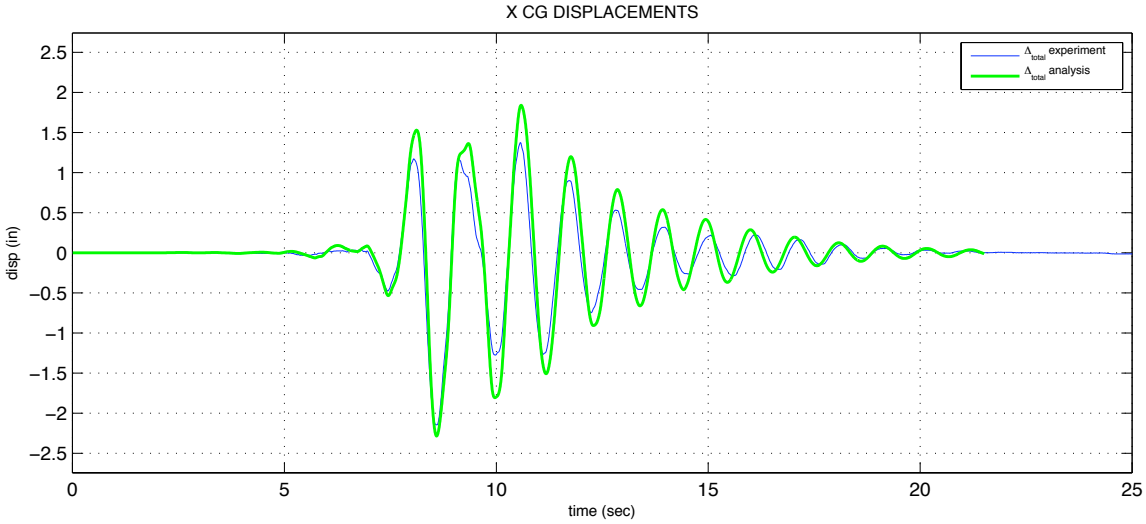

Figure 5-27: Center Mass Displacement – Lumped Plasticity Column ENT Springs (D1S)

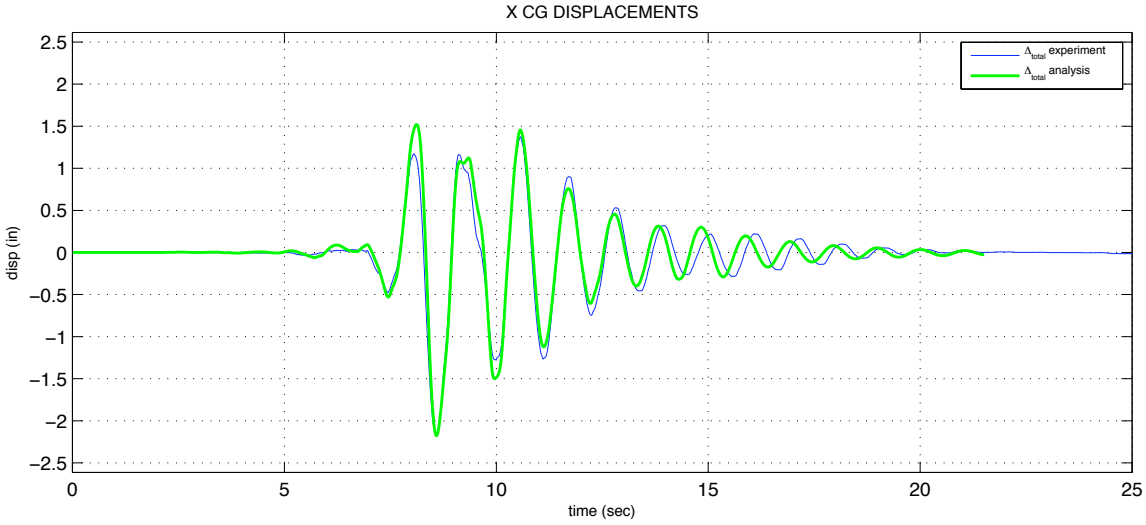

Figure 5-28: Center Mass Displacement – Lumped Plasticity Column NEO Springs (D1S)

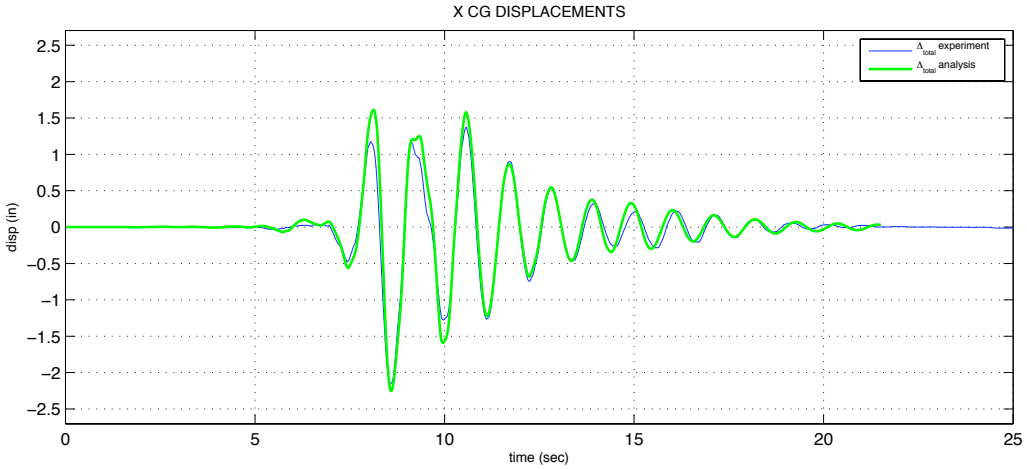

(a) Column Total Center of Mass Displacements

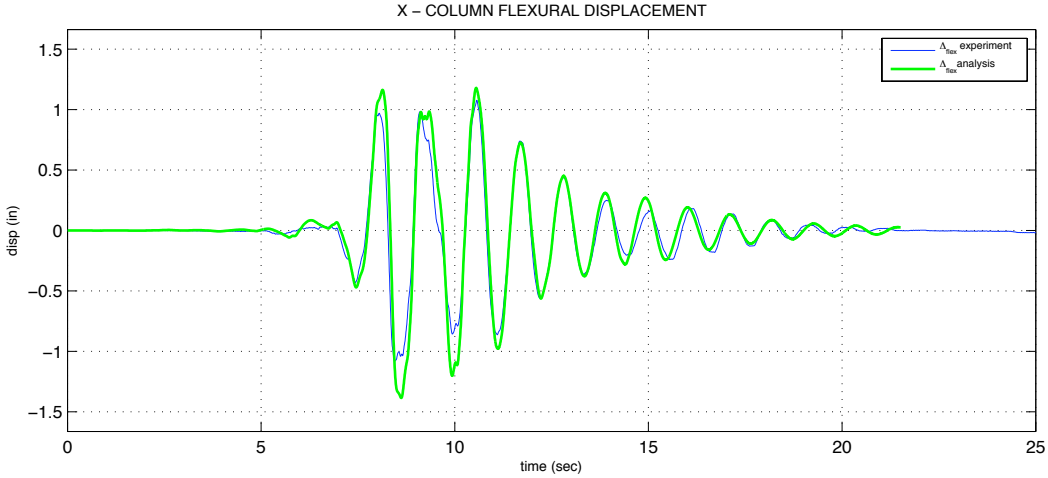

(b) Column Flexural Displacements

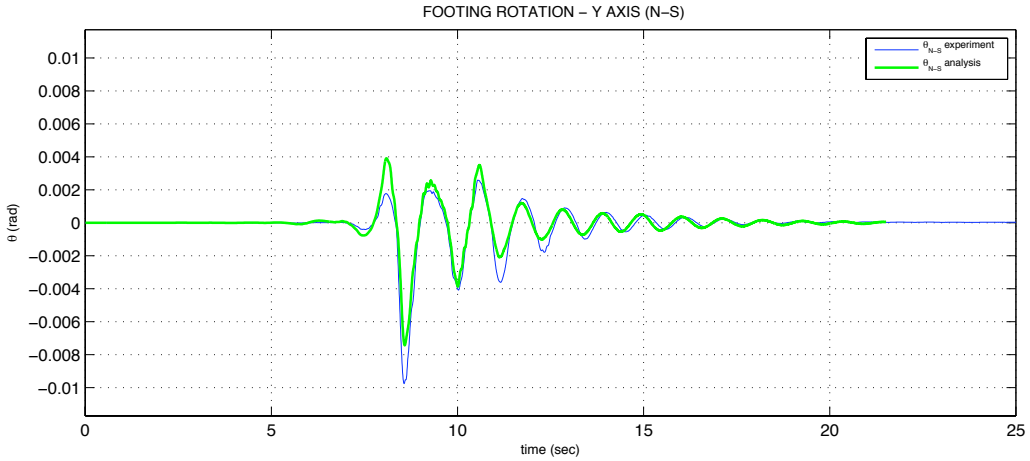

(c) Footing Rotation

Figure 5-29: Elastic Column NEO Springs – Displacements Comparison (D1S)

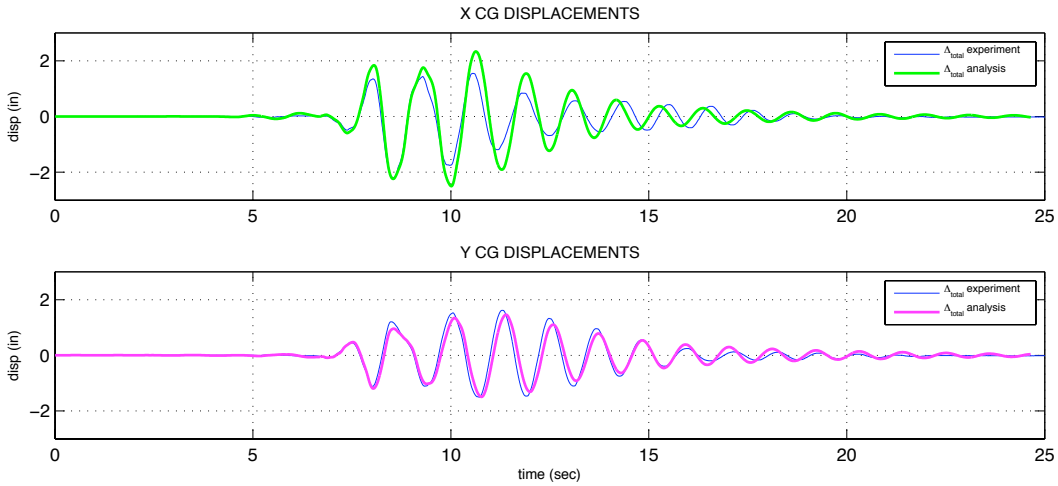

(a) Column Total Center of Mass Displacements

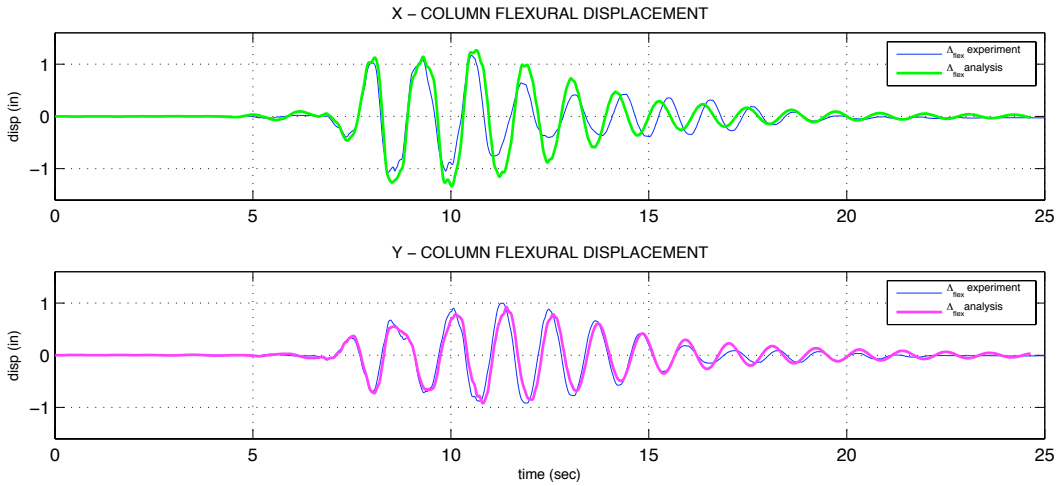

(b) Column Flexural Displacements

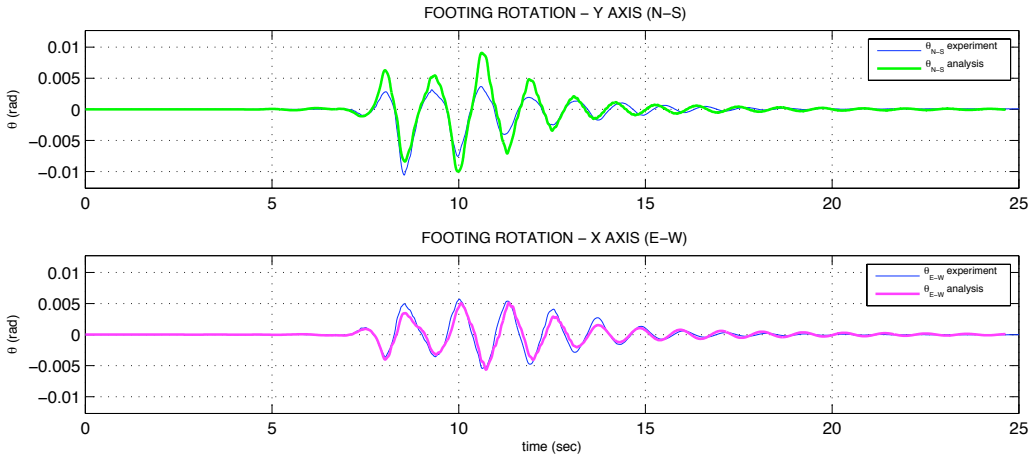

(c) Footing Rotation

Figure 5-30: Elastic Column NEO Springs – Displacements Comparison (D3S)

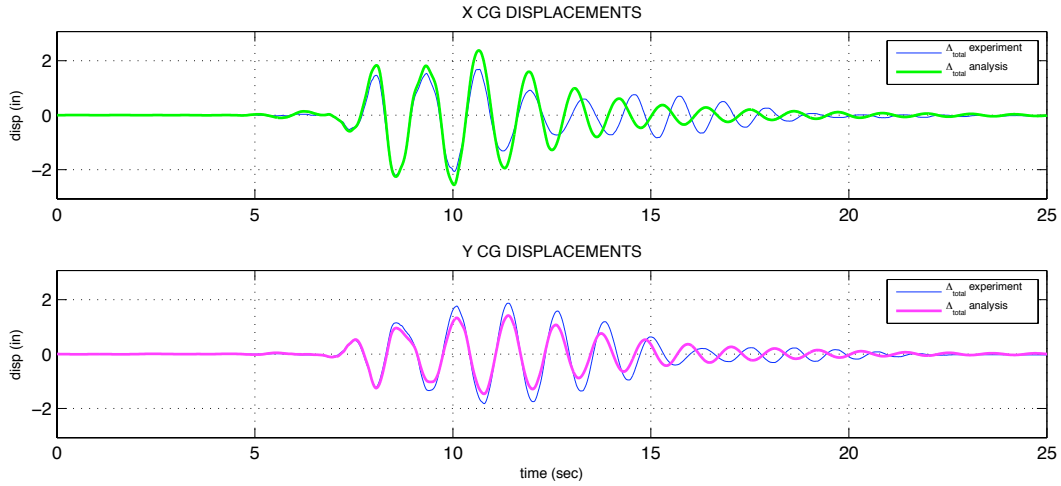

(a) Column Total Center of Mass Displacements

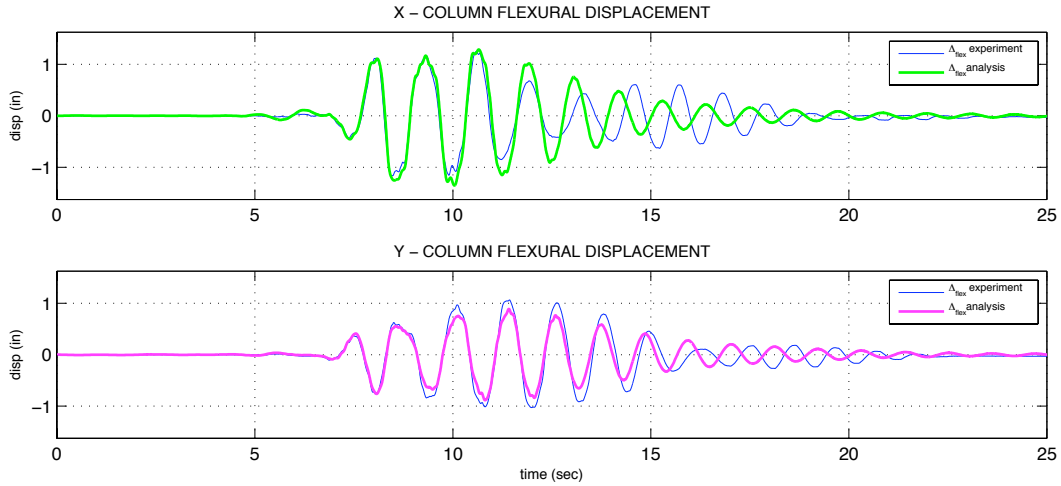

(b) Column Flexural Displacements

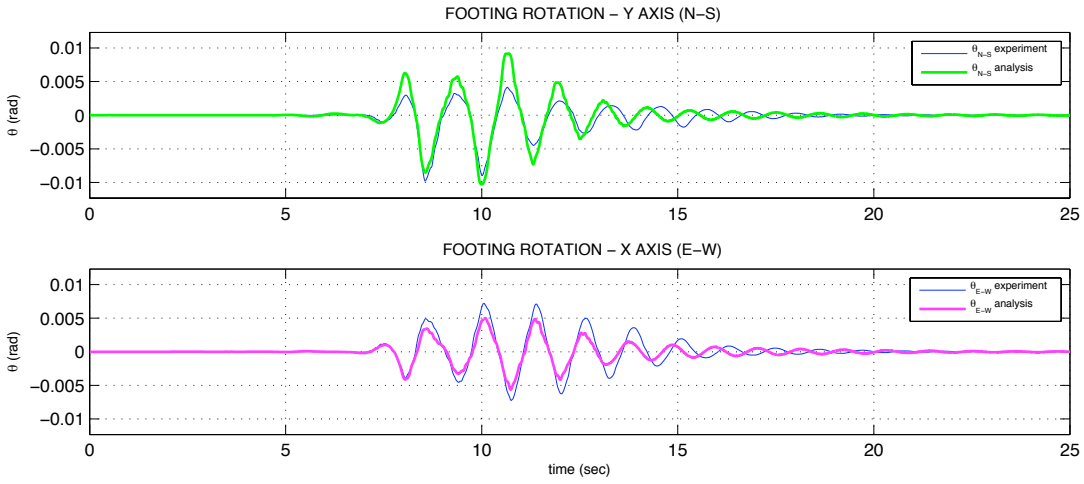

(c) Footing Rotation

Figure 5-31: Elastic Column NEO Springs – Displacements Comparison (D5S)

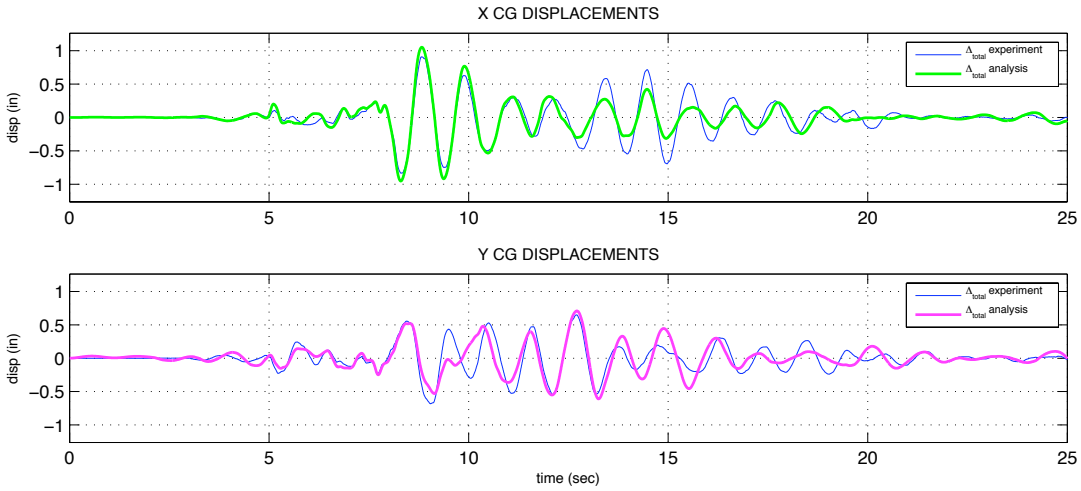

(a) Column Total Center of Mass Displacements

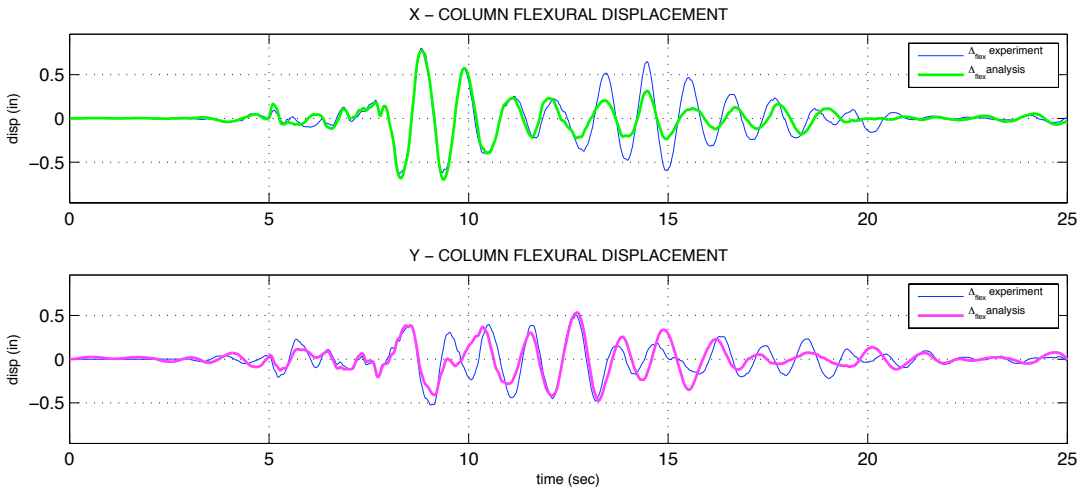

(b) Column Flexural Displacements

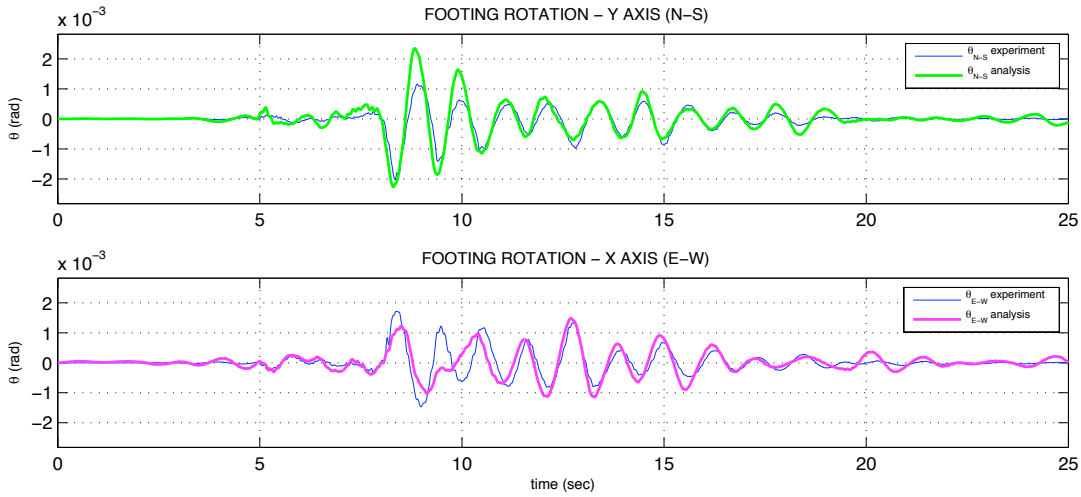

(c) Footing Rotation

Figure 5-32: Elastic Column NEO Springs – Displacements Comparison (F5S)

5.5.1.2 Accelerations

The acceleration time histories for the relevant test comparisons described in the displacement evaluations (Section 5.5.1.1) are shown in the following plots. Figure 5-33, through Figure 5-36 show the comparison for tests D1S, D3S, D5S, and F5S, respectively.

In general the accuracy of the analytic predictions seems to track very well. The peak values appear to occur at the same cycle and are within 25% of the recorded values. For test D3S and D5S the signal deviates during the free vibration phase as discussed in the displacement comparison section. Test F5S tracks reasonably well and again deviates from the observed response in the Y direction around the 9 second mark.

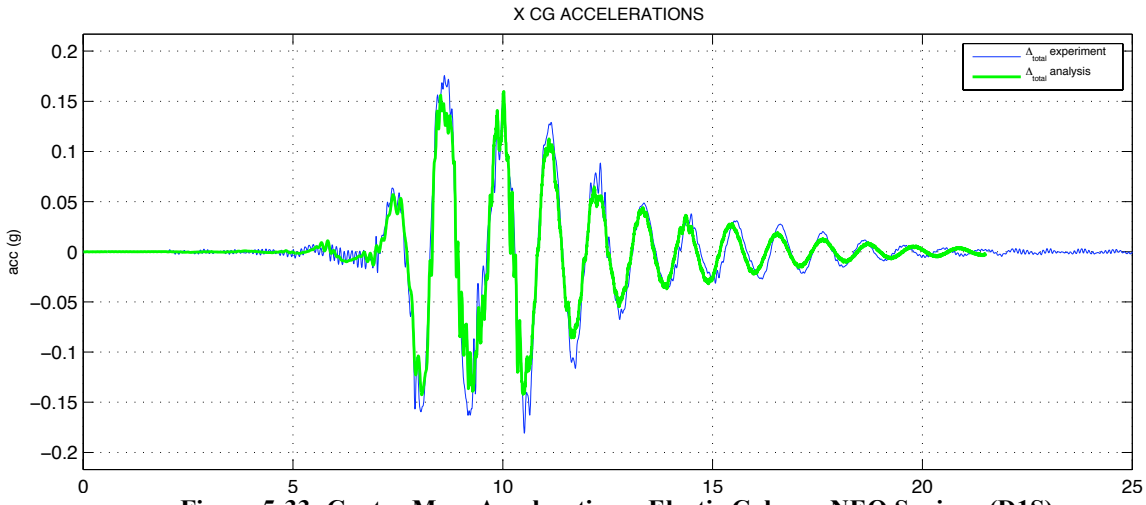

Figure 5-33: Center Mass Acceleration – Elastic Column NEO Springs (D1S)

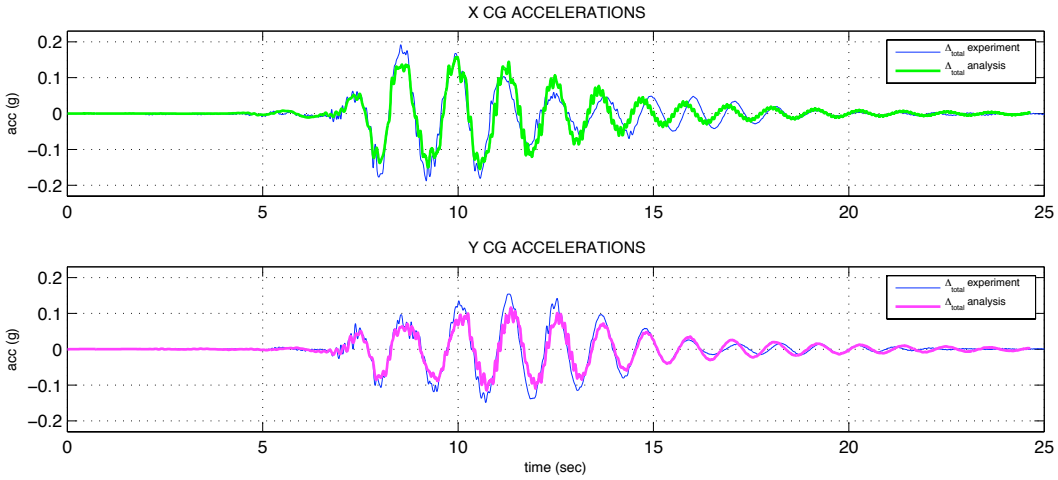

Figure 5-34: Center Mass Acceleration – Elastic Column NEO Springs (D3S)

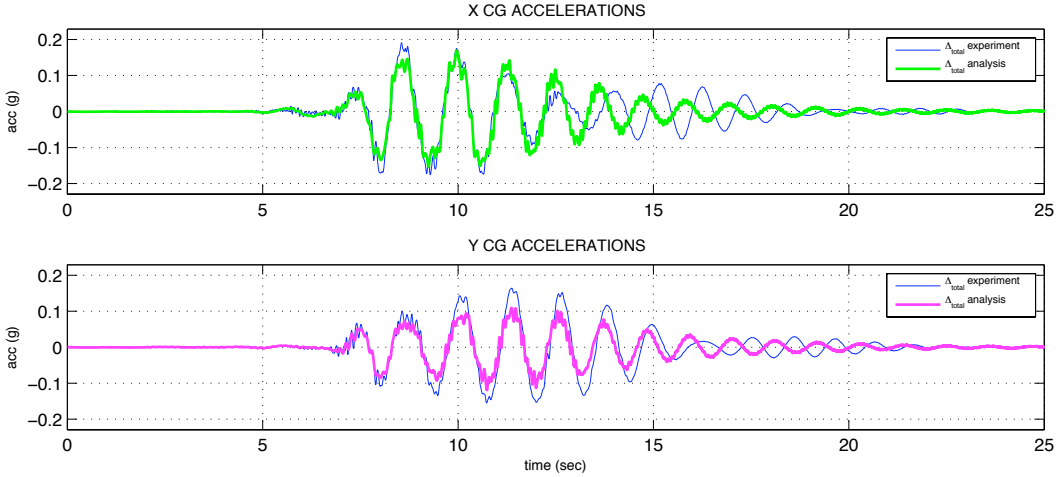

Figure 5-35: Center Mass Acceleration – Elastic Column NEO Springs (D5S)

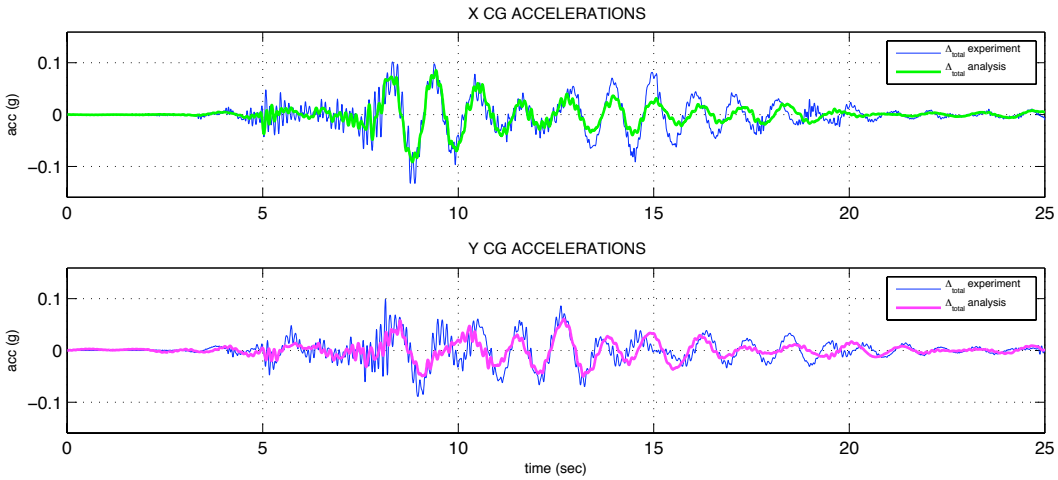

Figure 5-36: Center Mass Acceleration – Elastic Column NEO Springs (F5S)

5.5.1.3 Forces & Moments

Column base moment vs. curvature (M-ϕ) and column base moment vs. footing rotation (M-θ) comparisons are presented for the relevant tests described in the displacement analysis (Section 5.5.1.1) for the best model developed. The base shear vs. center of mass displacement is not shown here.

Column Moment-Curvature

The column base moment curvature best analytic models are compared to the observed response in Figure 5-37 – Figure 5-40 for the tests D1S, D3S, D5S, and F5S. In general the prediction is reasonably good including the peak values of moment and curvature, which appear to match.

Column Moment- Footing Rotation

The column base moment footing rotation analytic prediction is compared to the experimental results using the best model and is shown in Figure 5-41 through Figure 5-44 for the tests D1S, D3S, D5S, and F5S. In general the prediction agrees with what was observed in the displacement comparison, which is reasonably good including the peak values of moment and curvature, which appear to match. It should be noted that the observed rotational stiffness of the footing for F5S is higher than that predicted by the model. It is unclear if this is an aberration in the calculated results or a discrepancy in the model.

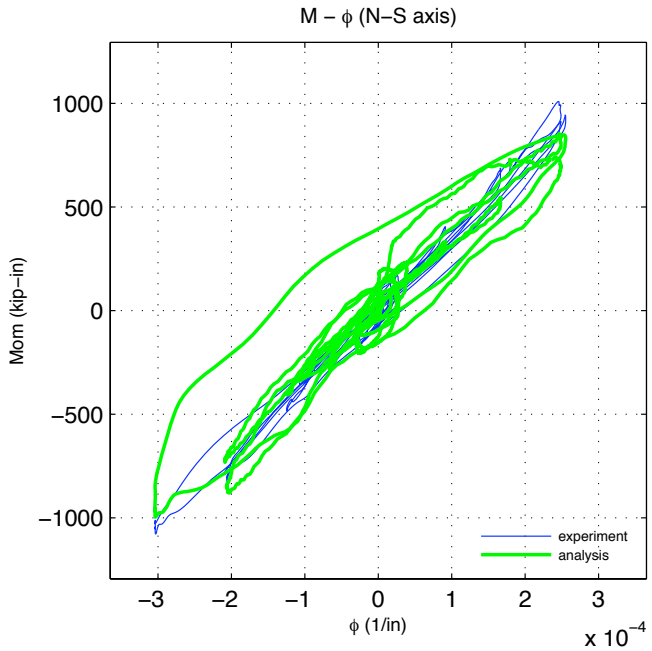

Figure 5-37: Column Base M-ϕ – Elastic Column NEO Springs (D1S)

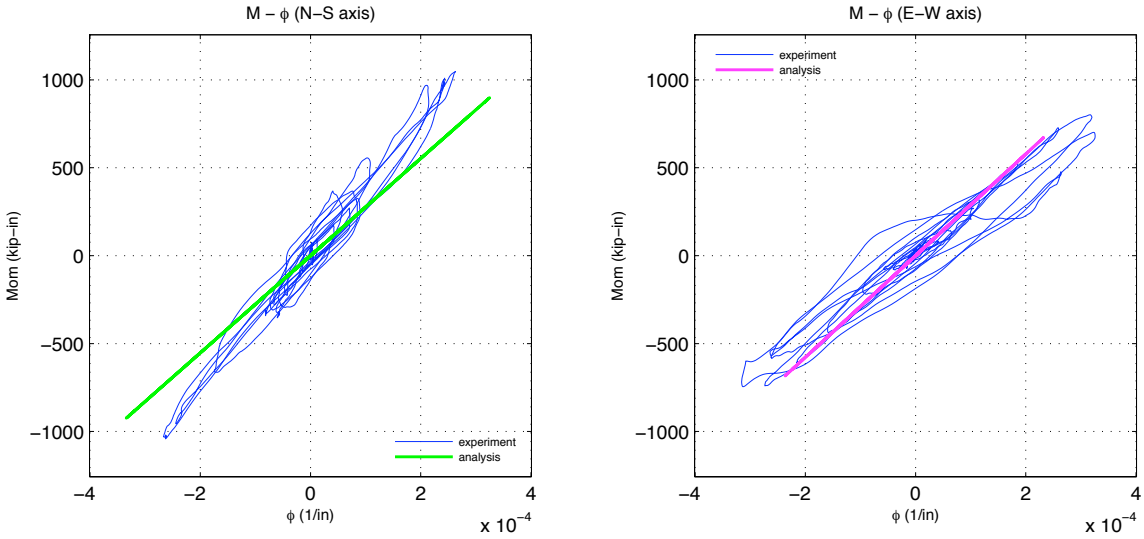

Figure 5-38: Column Base M-ϕ – Elastic Column NEO Springs (D3S)

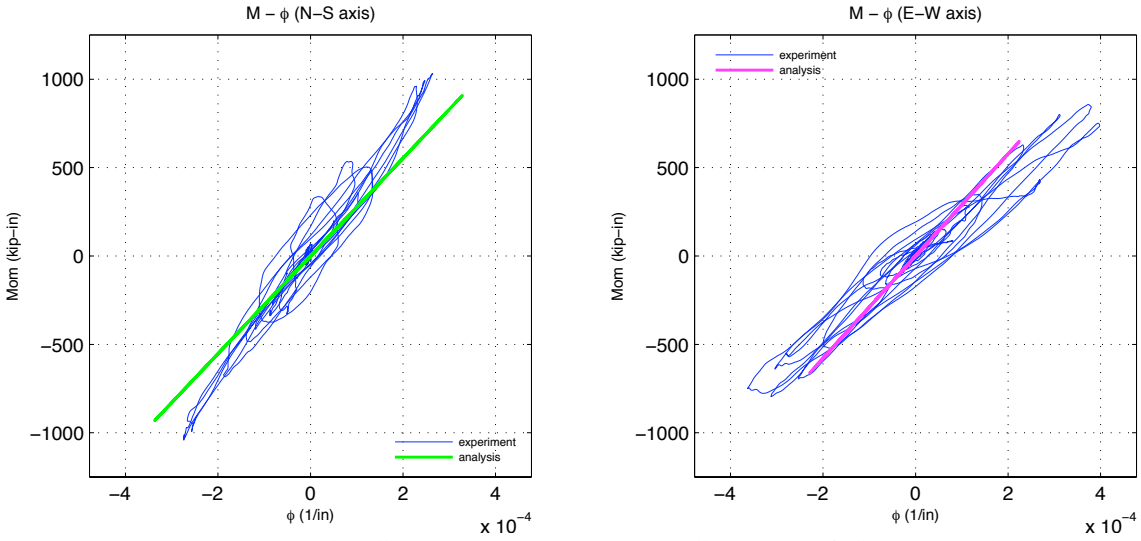

Figure 5-39: Column Base M-ϕ – Elastic Column NEO Springs (D5S)

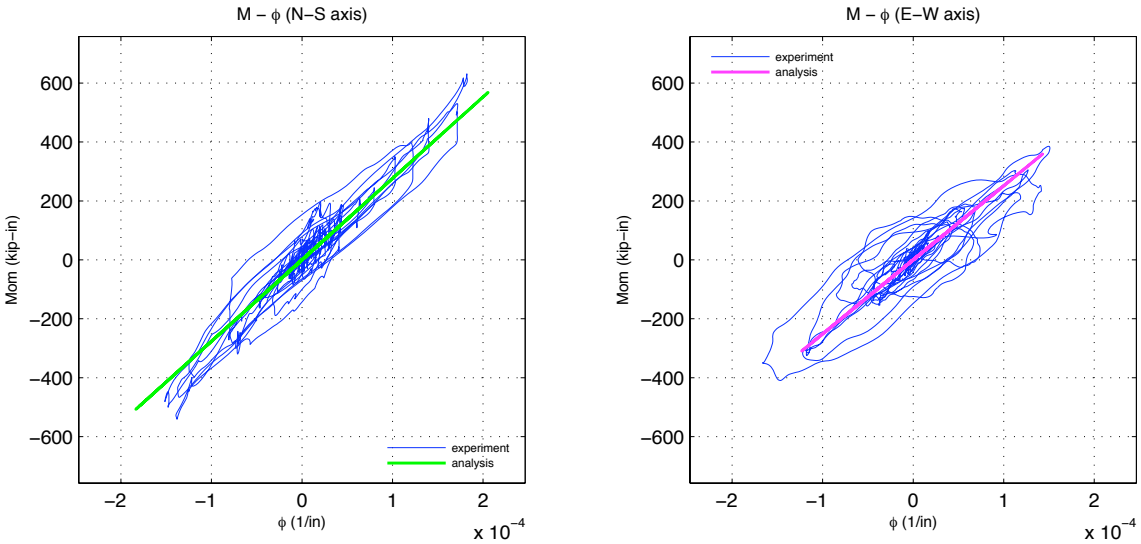

Figure 5-40: Column Base M-ϕ – Elastic Column NEO Springs (F5S)

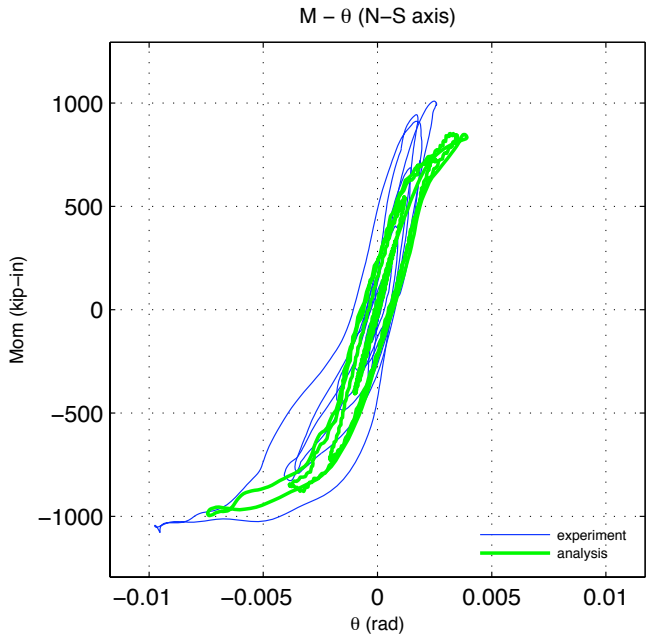

Figure 5-41: Footing Moment Rotation M-θ – Elastic Column NEO Springs (D1S)

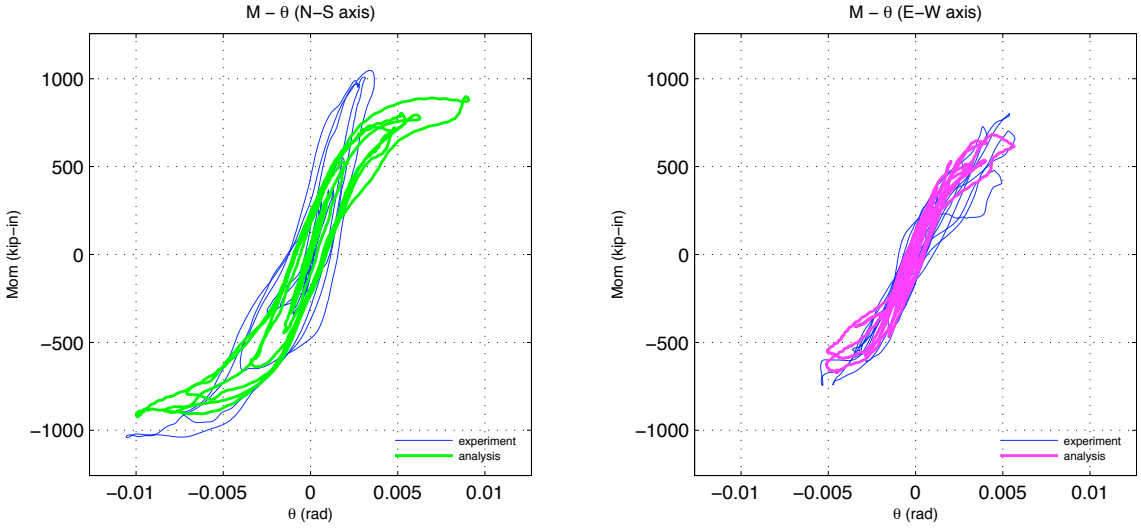

Figure 5-42: Footing Moment Rotation M-θ – Elastic Column NEO Springs (D3S)

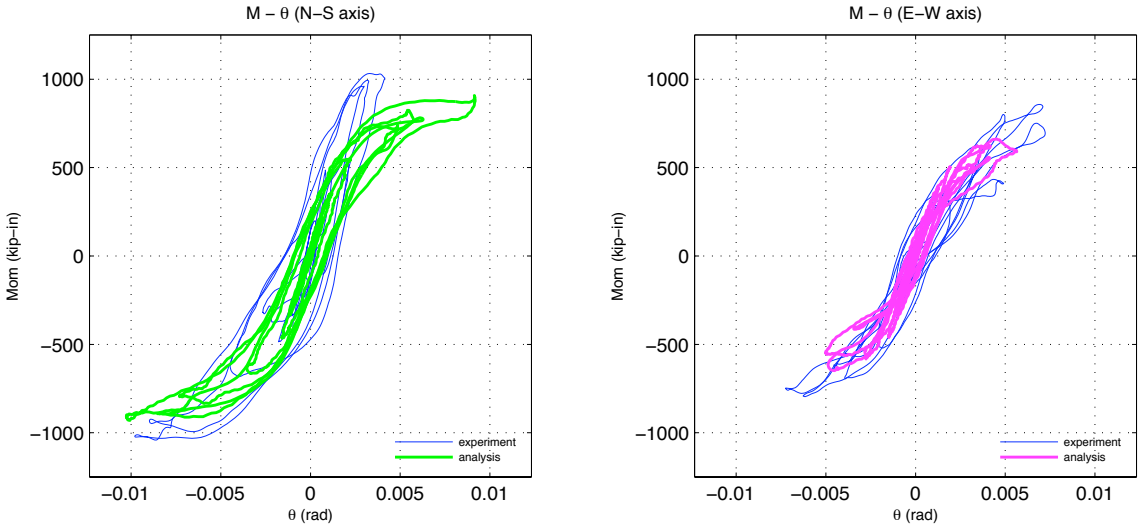

Figure 5-43: Footing Moment Rotation M-θ – Elastic Column NEO Springs (D5S)

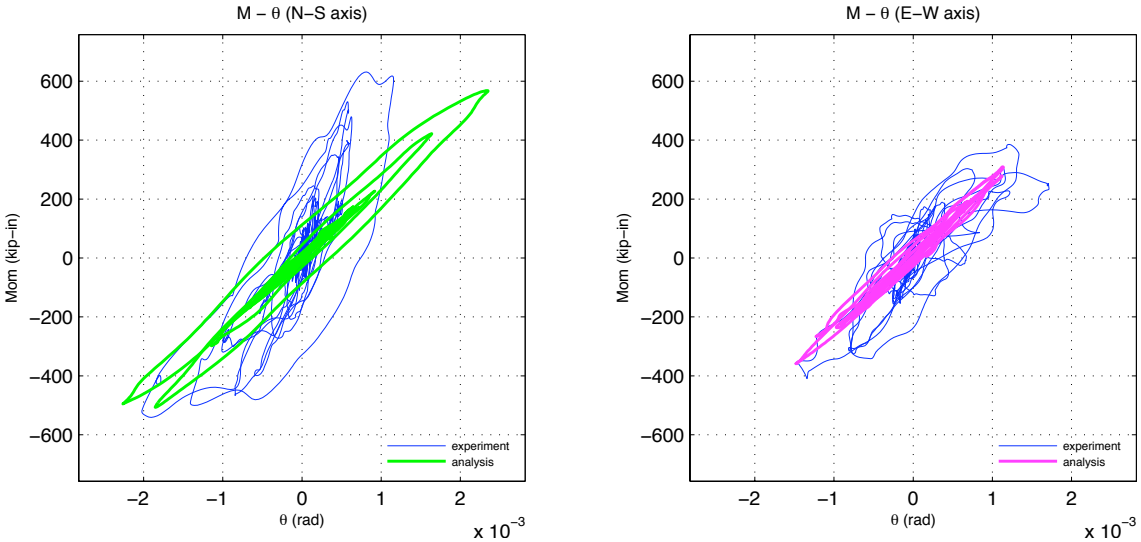

Figure 5-44: Footing Moment Rotation M-θ – Elastic Column NEO Springs (F5S)

5.5.2 Design Axial Load and 5Dc x 3Dc Footing

The test group AR has the widened footing as described in Section 5.4.1.2. The analytic results presented here use the best model developed and described in Section 5.5.2.1. This test group had a widened footing in the Y direction ($5D_c$ width) while the X direction remained the same ($3D_c$ width). A discussion of the results for displacement, acceleration and moment-deformation response is presented below. Of the two elastic tests done for this footing configuration only A2R is presented since it contains more significant column and footing response.

5.5.2.1 Displacements

Using the best model developed the uplifting bridge analytic prediction is shown here for test A2R which tested the column to incipient yielding. In general the analytic models seems to predict the experimental results very well. The column total displacements, flexural displacements and footing rotation are shown in Figure 5-45, Figure 5-46, and Figure 5-47. The peak values were within 5%, 5%, and 27% of the observed peak total, flexural and rotational column displacements. The stiffness and damping appear to match the observed response well during the forced and free vibration phase of the bridge pier system.

5.5.2.2 Accelerations

The accelerations comparison using the best column model developed in Section 5.5.1.1 are presented in Figure 5-48. In general the peaks and natural periods appear to match very well. The analytic model prediction is within 20% of the observed peak values.

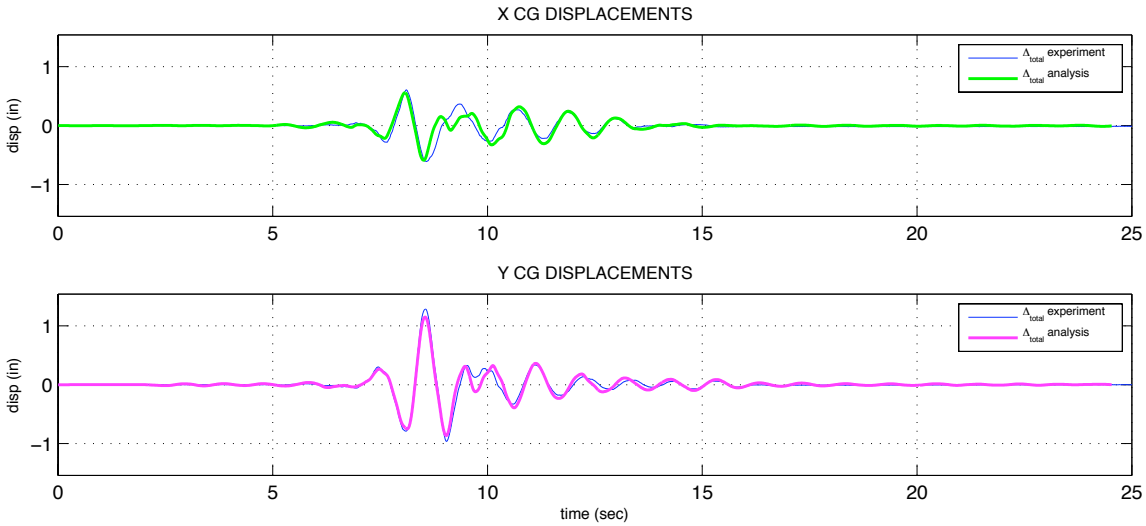

Figure 5-45: Center Mass Total Displacement – Elastic Column NEO Springs (A2R)

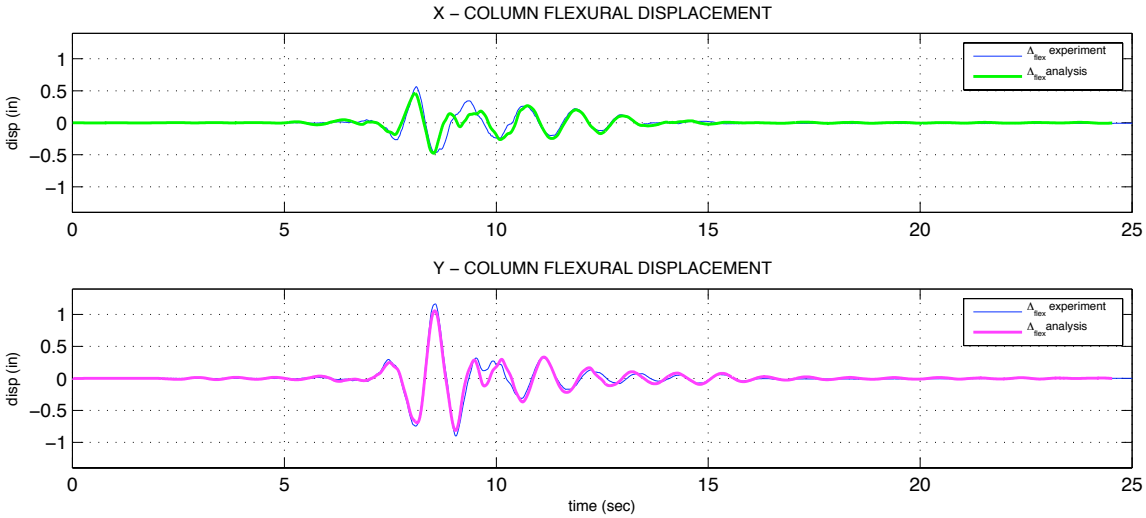

Figure 5-46: Center Mass Flexural Displacement – Elastic Column NEO Springs (A2R)

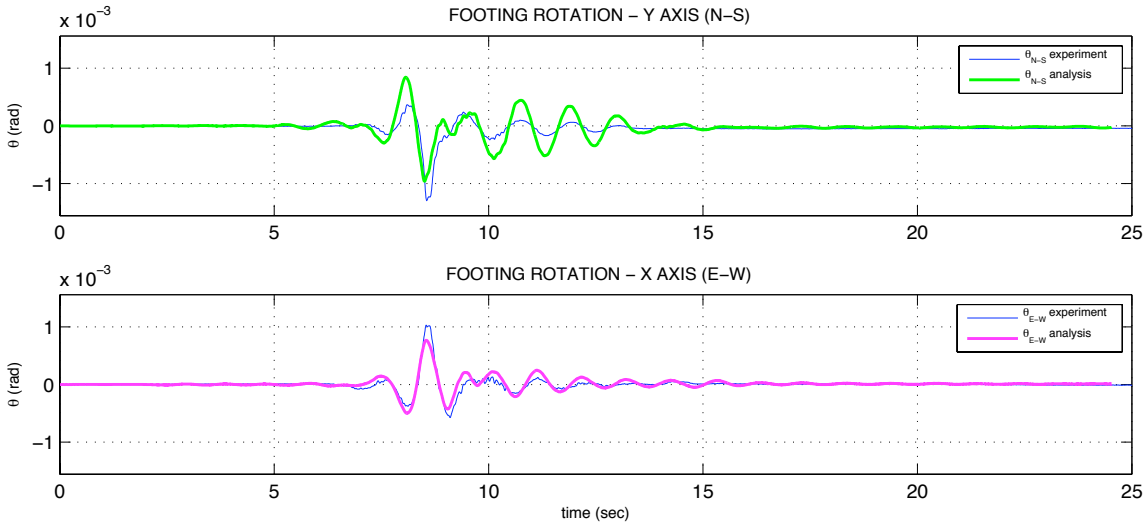

Figure 5-47: Footing Rotation – Elastic Column NEO Springs (A2R)

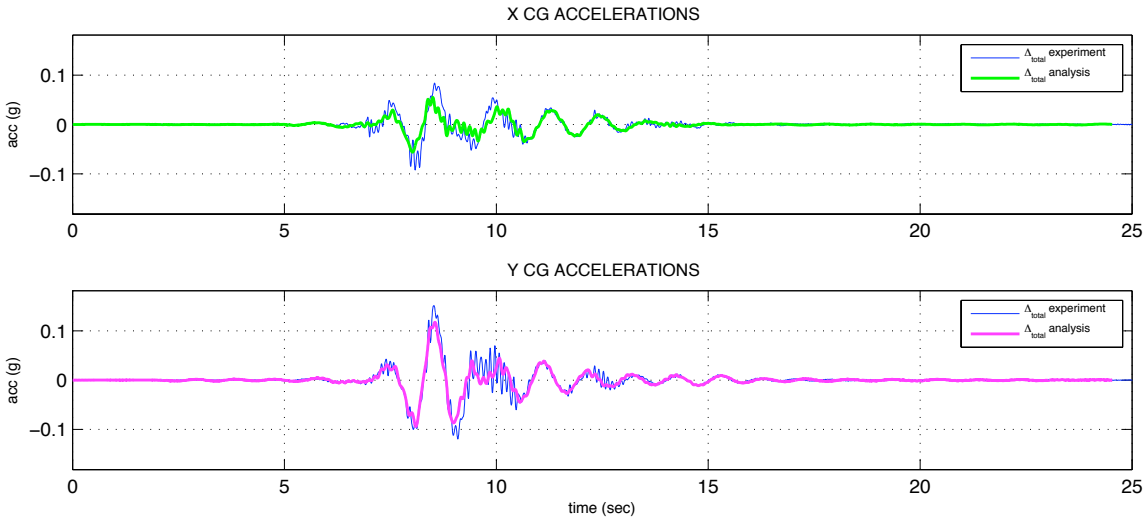

Figure 5-48: Center Mass Acceleration – Elastic Column ENT Springs (A2R)

5.5.2.3 Forces & Moments

Column base moment vs. curvature (M-ϕ) and column base moment vs. footing rotation (M-θ) comparisons are presented for the best model described in the displacement analysis (Section 5.5.1.1)

Column Moment-Curvature

The column base moment curvature best analytic model is compared to the observed response for test A2R in Figure 5-49. In general the prediction is reasonably good including the peak values of moment and curvature, which appear to match. The elastic column does not capture the cycle where a small amount of inelastic action occurs in the E-W direction, which is to be expected.

Column Moment- Footing Rotation

The column base moment footing rotation analytic prediction is compared to the experimental results using the best model and is shown in Figure 5-50 for test A2R. In the N-S narrow footing direction ($3D_c$) the experimental response is rotationally stiffer than the analytic prediction. In the wider footing direction the observed and analytic models appear to agree reasonably well.

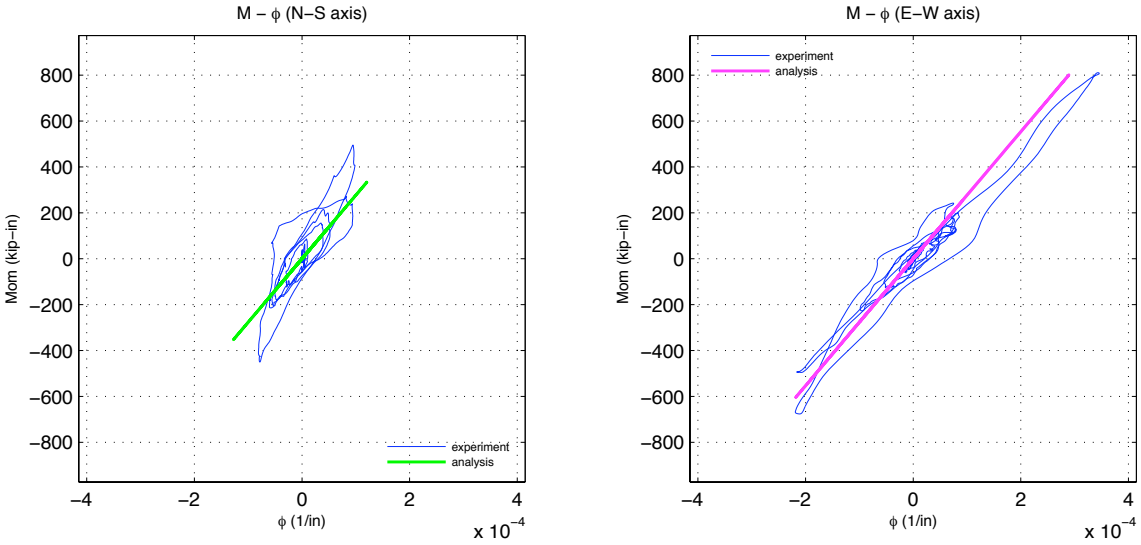

Figure 5-49: Column Base M-ϕ – Elastic Column ENT Springs (A2R)

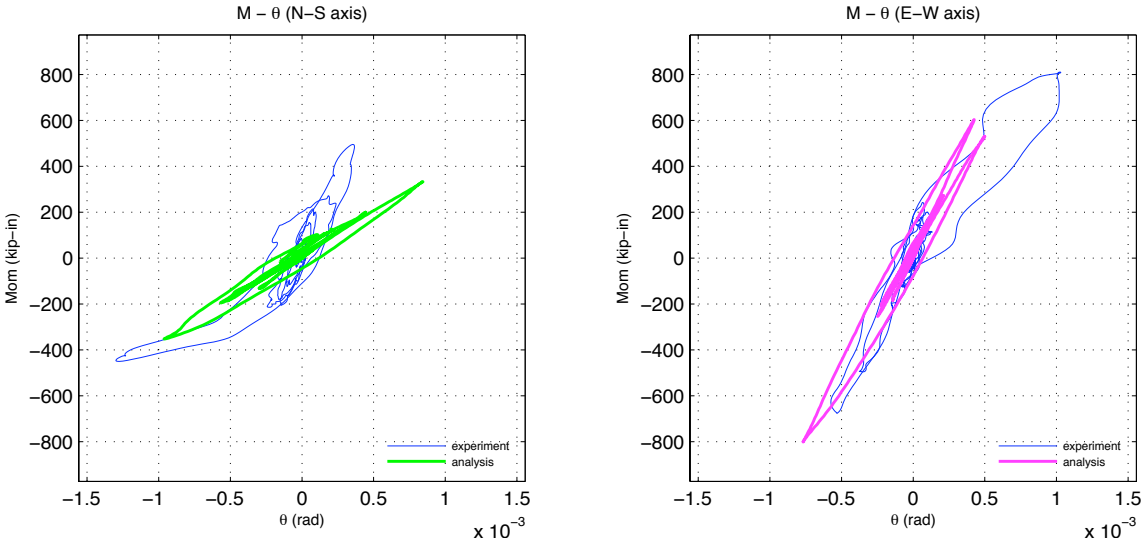

Figure 5-50: Footing Moment Rotation M-θ – Elastic Column ENT Springs (A2R)

5.6 Comparison of Nonlinear Analysis and Experimental Results

5.6.1 Design Axial Load and 5Dx x 3Dc Footing

Several models will be evaluated for their ability to analytically predict the inelastic specimen response. The analysis models considered here have the ability to respond inelastically with an elastic footing and supporting soil. The goal is to model a column footing system which has simultaneous footing uplift and column yielding. The inelastic yielding of the column includes crushing of the core and cover concrete and/or yielding and fracture of the steel reinforcing bars. These combinations often lead to permanent drifts or residual displacements of the column center of mass. As noted inelastic column response was observed during the test programs for runs A3R and A4R. The column model options for inelastic response are described in Section 5.3.2. In the experimental program the footing uplifted but remained elastic and is modeled here as described in Section 5.4.

Initial efforts to model column yielding have focused on using fiber sections with distributed plasticity column elements. Eberhard and Berry (2006) as well as Jeong et al. (2008) have a discussion on this approach. Results have shown there is a limited ability to accurately predict peak and residual displacements unless the initial stiffness accurately matches the observed initial stiffness. Even under these conditions the magnitude of residual displacement is difficult to match. Recent work by Jeong et al. (2008) has shown the improved prediction capabilities when using a concentrated plasticity column model that has fiber sections over a finite plastic hinge length at the column ends and elastic column response in between. The author has shown this column model calibrated to the observed initial stiffness with a bilinear steel model or nonlinear backbone curve.

Properties of Nonlinear Column Models

The nonlinear models described each use an elastic footing and soil model with a column model that uses fiber sections. The uplifting footing and column model with modeling options is shown in Figure 5-12.

1. Footing and Soil is modeled using Beam-on-Nonlinear-Winkler-Foundation (BNWF)
2. Concrete using Kent-Park model with tension
3. Steel modeled using bilinear or nonlinear backbone curve.
4. Fiber element model with distributed plasticity column model and five integration points along the column length.
5. Fiber element model with concentrated plasticity column model. One finite length plastic hinge at column base with two integration points. Remainder of column is elastic with effective column properties EI_{eff}.

Each of the models described was used to predict the response of the specimen. The recorded three dimensional (X+Y+Z) shaking table accelerations were used as input ground motions. During the discussion of results the peak and residual displacements reported refer to the incremental change measured from the start of the given test run.

5.6.1.1 Displacements

Figure 5-51 to Figure 5-59 compare the analytical displacement time histories to experimental for the multi-direction input accelerations of the center of mass and footing uplift, which is described here via the footing rotation. The accuracy of the different models in predicting the column response and the footing uplift response is evaluated.

The base model used is the distributed plasticity column model (Nonlinear Beam Column) with a bilinear steel model option (Steel02) concrete modeled using Concrete02 and neoprene springs (NEO). Using the measured material properties the center of mass displacements are shown in Figure 5-51 for this model. The analysis of the design level earthquake (A3R) is repeated three times while varying either the column plasticity or steel model assumption. Results are shown in Figure 5-52 through Figure 5-54. Each model was reviewed and investigated to achieve best agreement possible between analysis and observed results. Evaluation was based on the initial stiffness, total displacement, column flexural and rocking displacements at center of mass, footing uplift, and corresponding force deformation relationships.

Ultimately, the lumped plasticity column model with reinforcing steel provided the best approximation of the observed results. For the design level earthquake (A3R) column flexural displacements are shown in Figure 5-55 and footing rotation displacements are presented in Figure 5-56. Center of mass displacements, using the best analytic model, for the maximum level earthquake (A4R) are presented in Figure 5-57. The column flexural displacements are presented in Figure 5-58. The corresponding footing rotation displacements are given in Figure 5-59. Damping was observed to be low for this system (approximately 3.0%).

The residual displacements for the design level earthquake (A3R) were approximately ½ ” and 1” in the X and Y directions, respectively. The design level earthquake had a flexural ductility of approximately 6 ($\mu=u_{flex}/u_{yield}$). The analytic model predicted ¼” and ½” respectively in the X and Y directions. Considering the complexity of rocking system and large displacements this seems to be a reasonable approximation of the observed behavior. The maximum level earthquake (A4R) with a residual displacement of 9” and 12” was more difficult to model for residual displacements. The best model chosen predicted approximately 4” and 6”. Several options were investigated to better capture the residual displacements including modifying the concrete descending region, steel hardening ratio, and the damping ratio. At this time no modifications shown were able to better capture the residual displacements while maintaining the observed current stiffness and damping qualities. Further work is warranted.

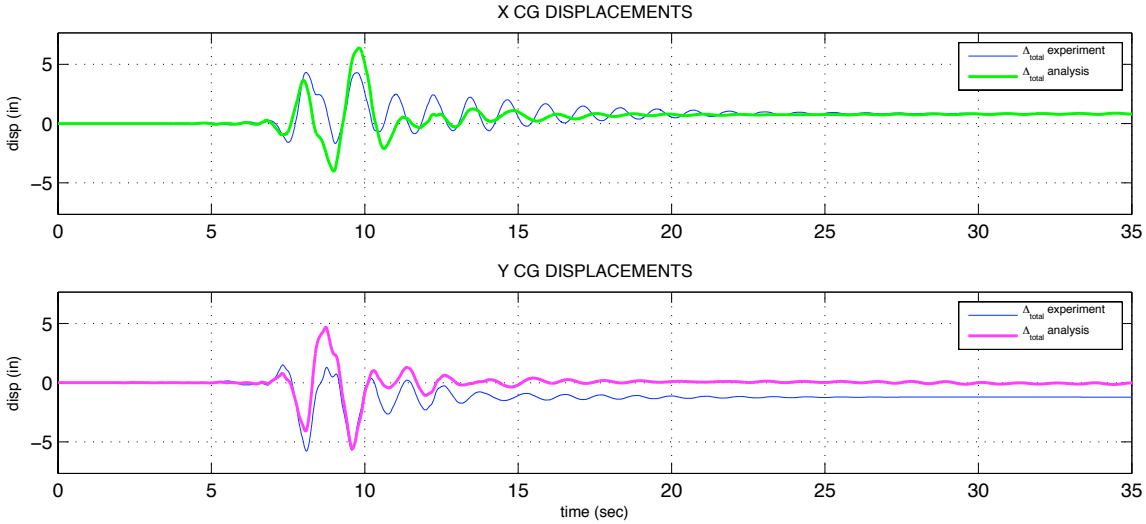

Figure 5-51: Design Level Earthquake - Distributed Plasticity Column with NEO Springs CG Displacements, Bilinear Steel (A3R)

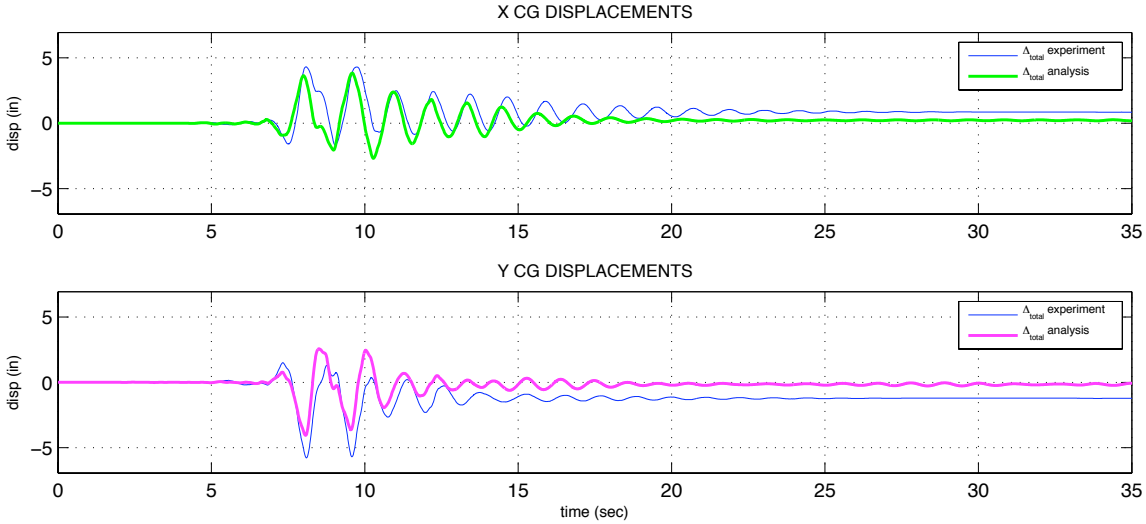

Figure 5-52: Design Level Earthquake - Distributed Plasticity Column with NEO Springs CG Displacements, Reinforcing Steel (A3R)

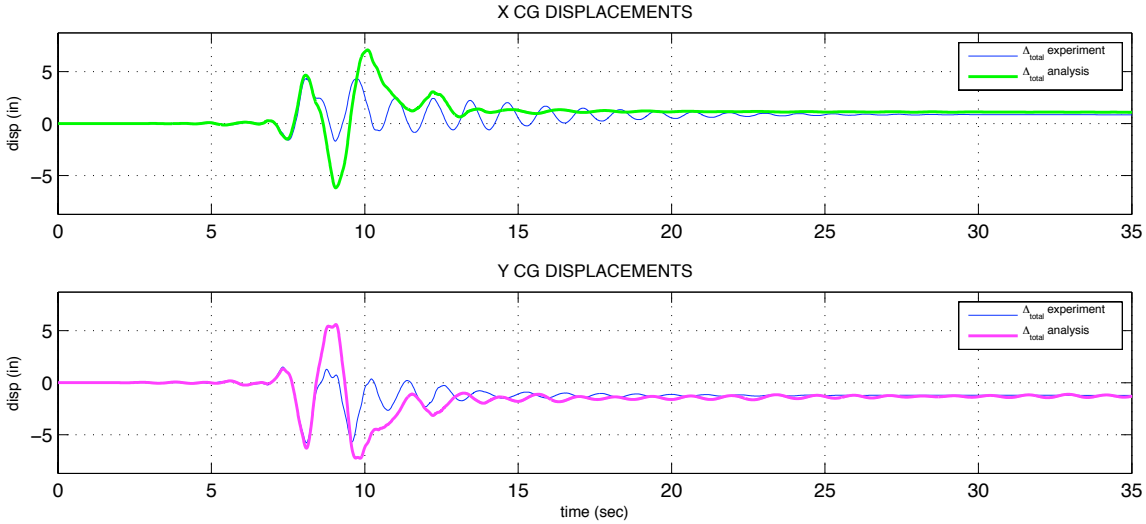

Figure 5-53: Design Level Earthquake Concentrated Plasticity Column with NEO springs CG Displacements, Bilinear Steel (A3R)

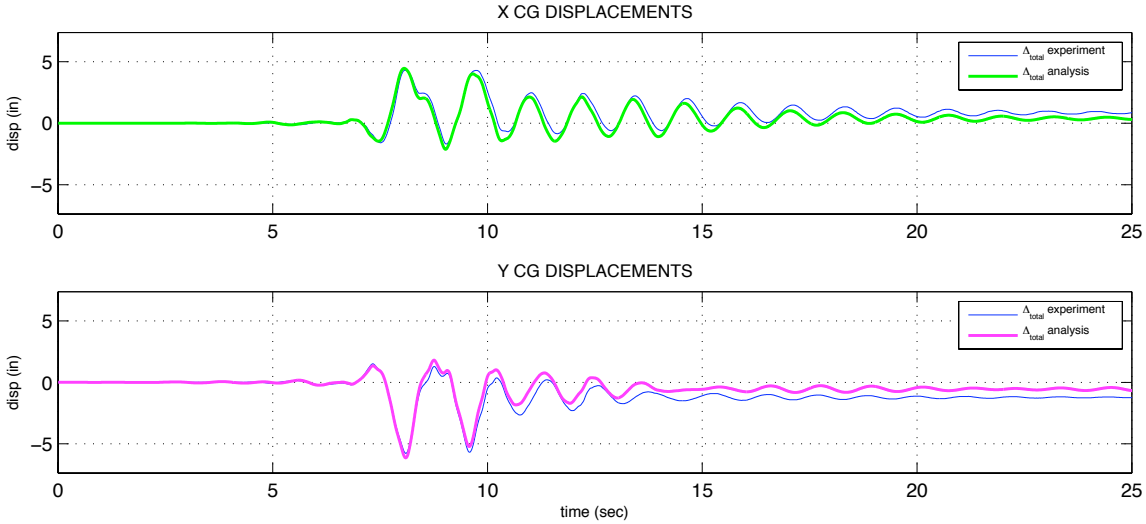

Figure 5-54: Design Level Earthquake Concentrated Plasticity Column with NEO springs CG Displacements, Reinforcing Steel (A3R)

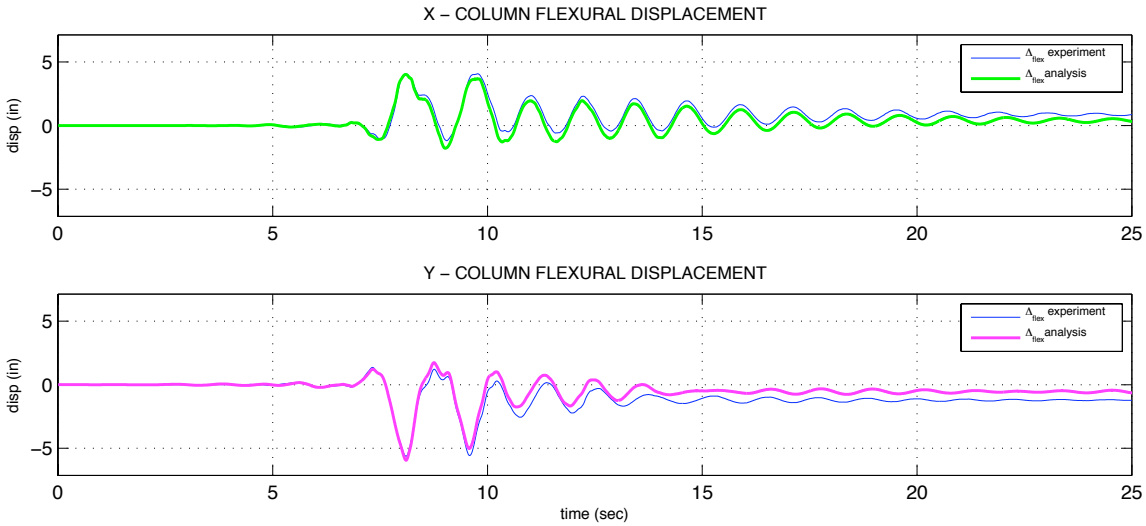

Figure 5-55: Design Level Earthquake Concentrated Plasticity Column with NEO springs Column Flexural Displacements (A3R)

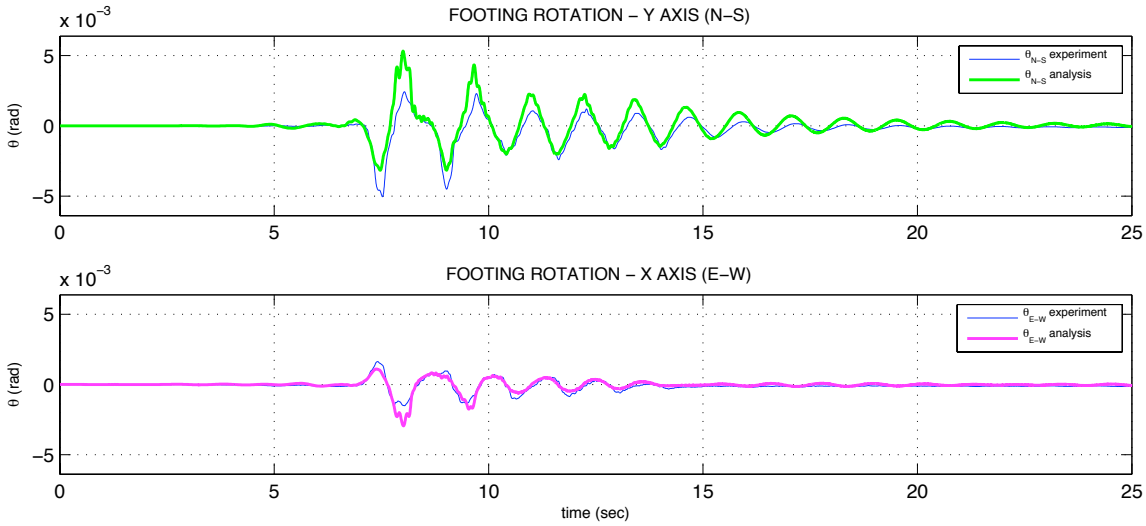

Figure 5-56: Design Level Earthquake Concentrated Plasticity Column with NEO springs Footing Rotation (A3R)

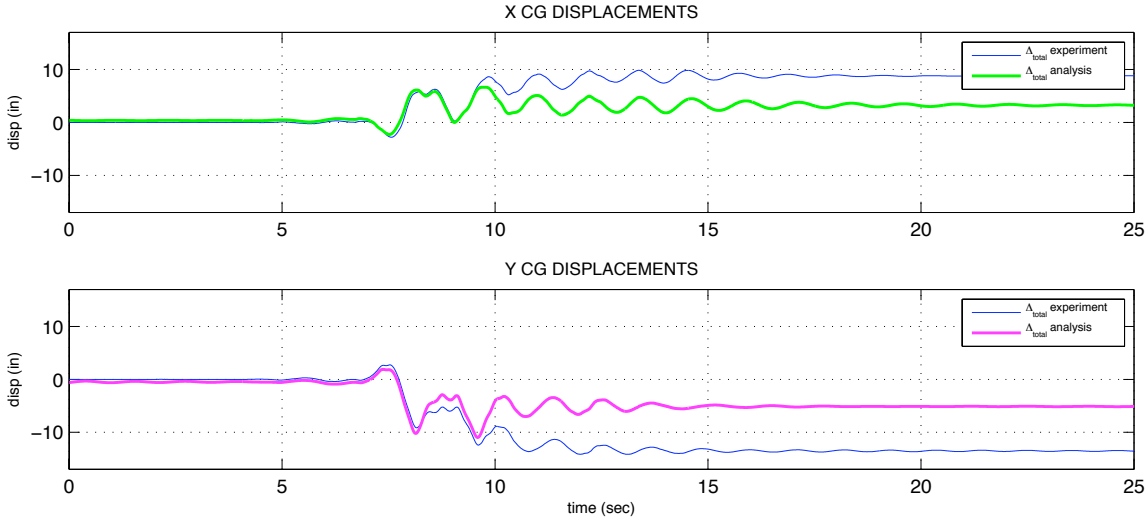

Figure 5-57: Maximum Level Earthquake Concentrated Plasticity Column with NEO springs CGDisplacements (A4R)

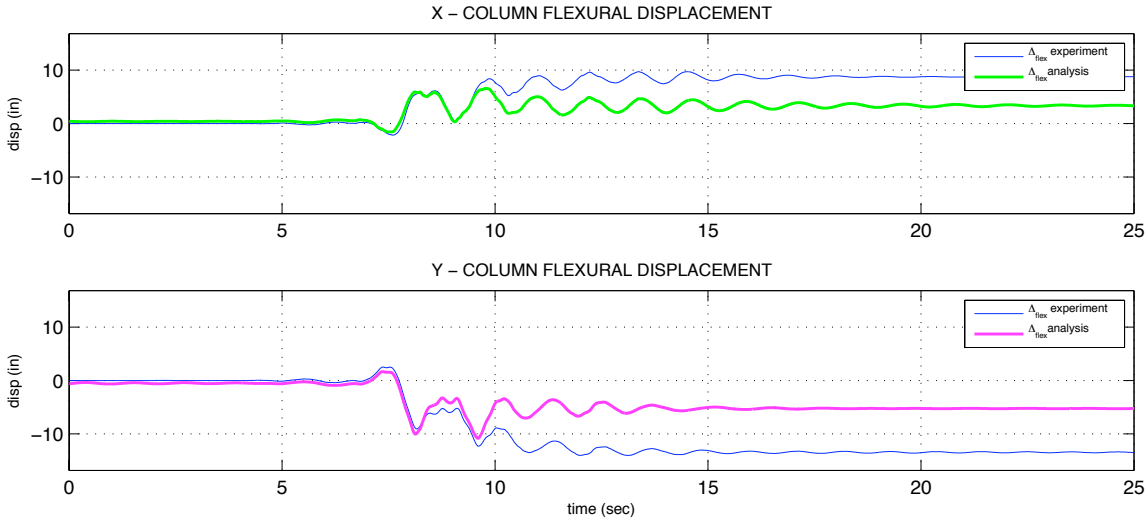

Figure 5-58: Maximum Level Earthquake Concentrated Plasticity Column with NEO springs Column Flexural Displacements (A4R)

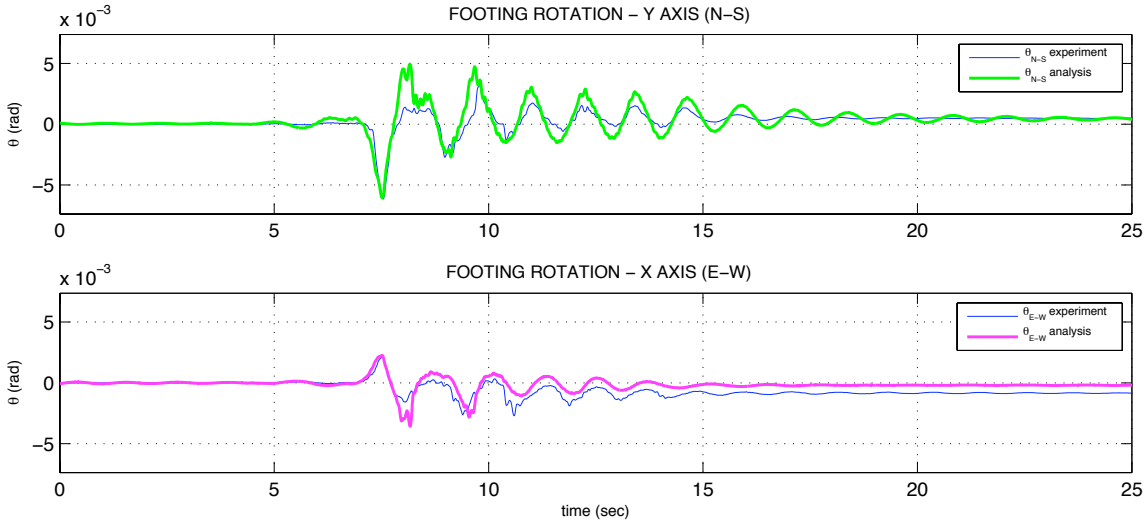

Figure 5-59: Maximum Level Earthquake Concentrated Plasticity Column with NEO springs Footing Rotation (A4R)

5.6.1.2 Accelerations

From the comparison of displacement response for the experiment and analysis it was shown that the Concentrated Plasticity column model with Reinforcing Steel provided the best approximation of the observed response. This best approximation is limited to the column and footing models discussed herein. The accelerations responses shown are for the best model approximation only to limit the amount of information. Figure 5-60 shows the acceleration time history comparison for the design level test A3R. The peak value magnitudes are approximately the same. Figure 5-61 shows the acceleration time history for the maximum level test A4R. The magnitudes of accelerations do not track well once the column has significant inelastic action. (See Section 5.6.1.1 for a discussion on modeling the inelastic response.) The residual acceleration of the experiment is not an observed behavior but rather a by-product of the accelerometer recording method.

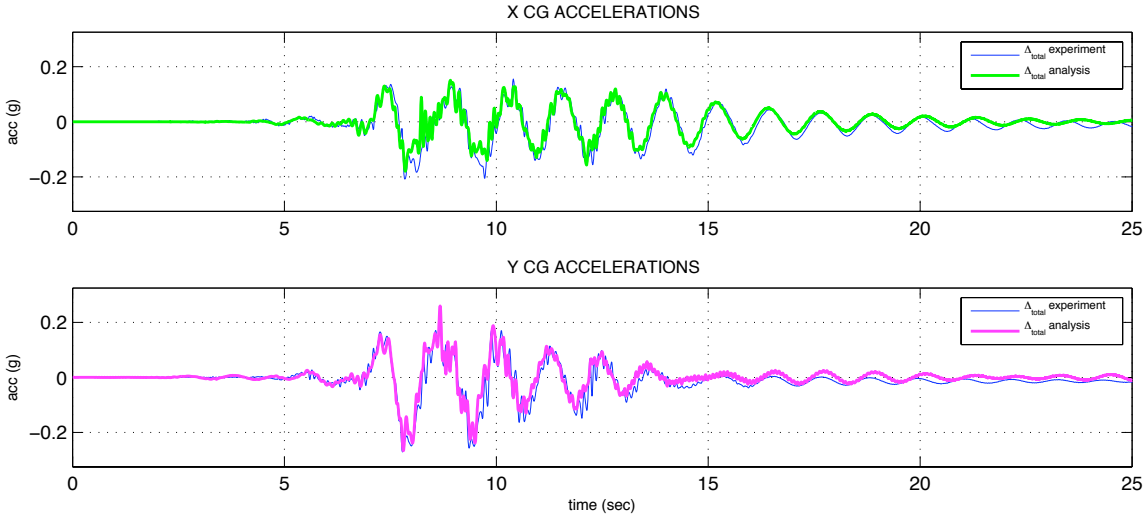

Figure 5-60: Design Level Earthquake Concentrated Plasticity Column with NEO springs CG Accelerations (A3R)

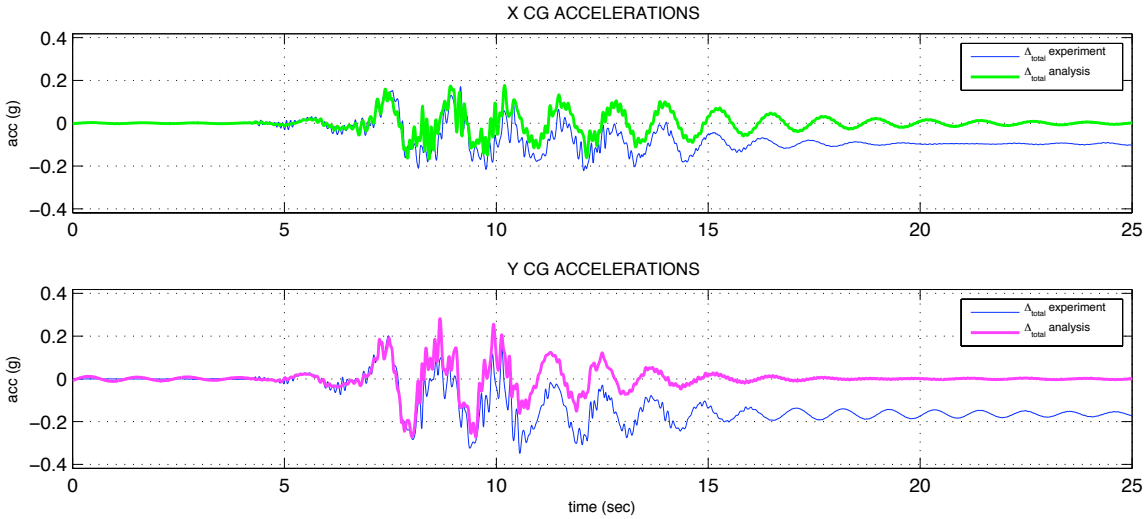

Figure 5-61: Maximum Level Earthquake Concentrated Plasticity Column with NEO springs CG Accelerations (A4R)

5.6.1.3 Forces & Moments

The inelastic response relationship of the column base moment to column base curvature and the footing rotation are shown in the following figures. Experimental test A3R set to the design level acceleration and A4R was set to the maximum level acceleration. From the comparison of displacement response for the experiment and analysis it was shown that the Concentrated Plasticity column model with Reinforcing Steel provided the best approximation of the observed response. Modeling of the inelastic response is especially complex when considering uplifting of the footing. It requires accurately capturing the stress-strain relationships that results in concrete crushing, reinforcement yielding, strain hardening, and buckling. Secondary P-Δ effects are significant in this case due to the large displacements of the center of mass.

The lumped plasticity column model with ReinforcingSteel material is the best option for modeling the column behavior because it allows for calibrating the column stiffness to the observed stiffness using effective properties. The distributed plasticity model does not allow for an adjustment of the observed effective column properties caused by cracks developed by among other things small level earthquakes experienced by the system. The ReinforcingSteel option better captures the nonlinear behavior of yielding steel than the bilinear Steel02 uniaxial material.

Column Moment-Curvature

The column base moment vs curvature response for the Design level test (A3R) is presented in Figure 5-62. The E-W axis has the more significant inelastic response during testing was captured relatively well by the lumped plasticity column model assumption with reinforcing steel assumption. This includes the peak moment and peak curvature values. The moment at the column base due to residual displacement of the center of mass was not captured well by the analytic model. For that reason the experimental and analytic are centered on differing values of M-ϕ and the end of the test. The N-S axis tracks relatively well, however there is some inelastic response in the analytic model which was not observed in the experimental test. The Maximum level test (A4R) moment curvature response is presented in Figure 5-63. The analytic vs experiment comparisons diverge due to the significant residual displacement observed for this test which were not captured by the analytic model.

Footing Moment-Rotation

The comparison of column base moment to footing rotation is presented in Figure 5-64 for the Design level test (A3R) and Figure 5-65 for the Maximum level test (A4R). The responses track reasonably well. However, they are affected by the inability of the analytic model to capture the residual displacement. The residual displacement affects the column base moment calculation, which fundamentally alters the moment-footing rotation relationship.

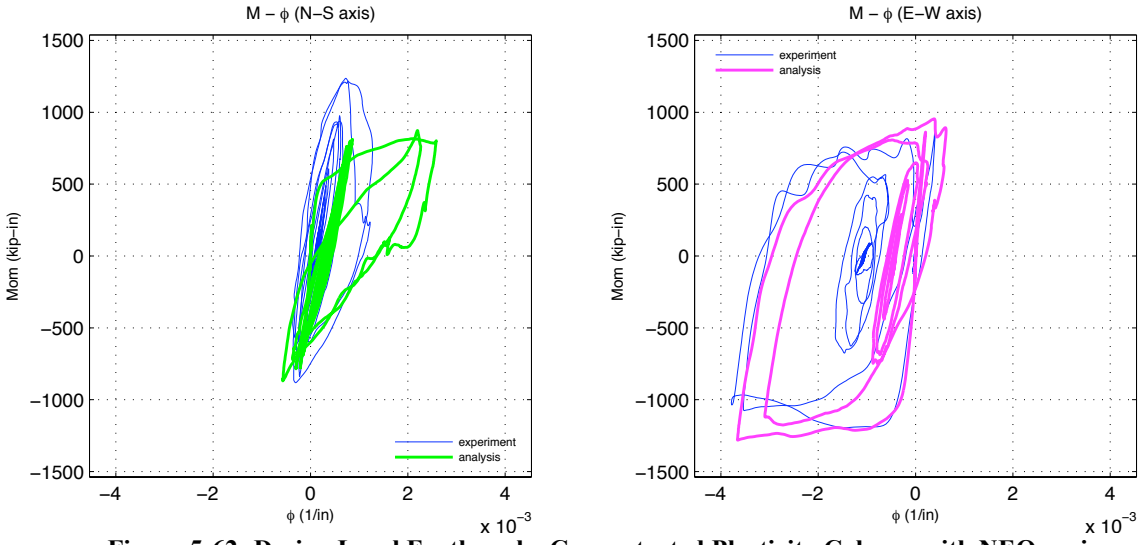

Figure 5-62: Design Level Earthquake Concentrated Plasticity Column with NEO springs Column Base M-ϕ (A3R)

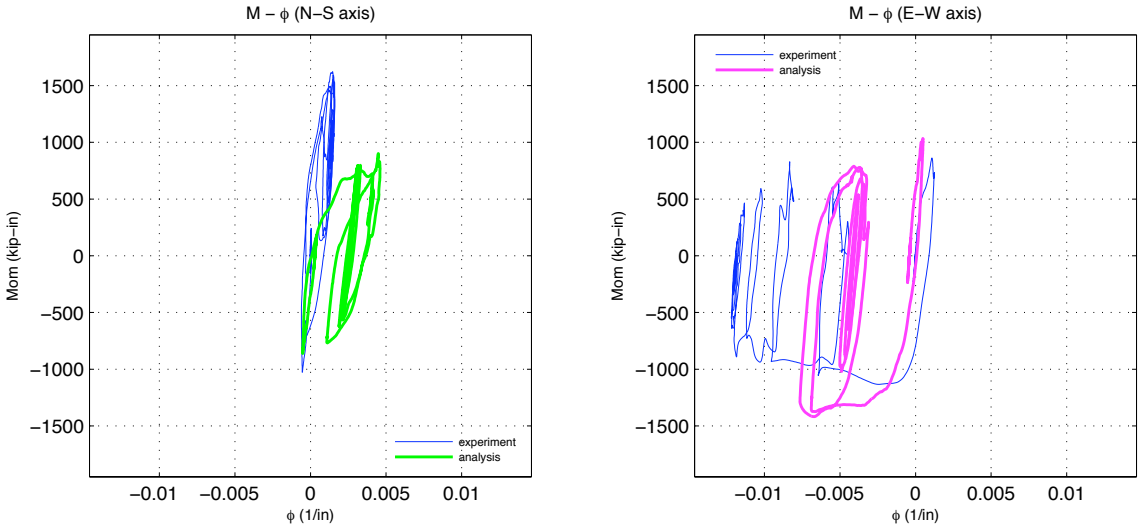

Figure 5-63: Maximum Level Earthquake Concentrated Plasticity Column with NEO springs Column Base M-ϕ (A4R)

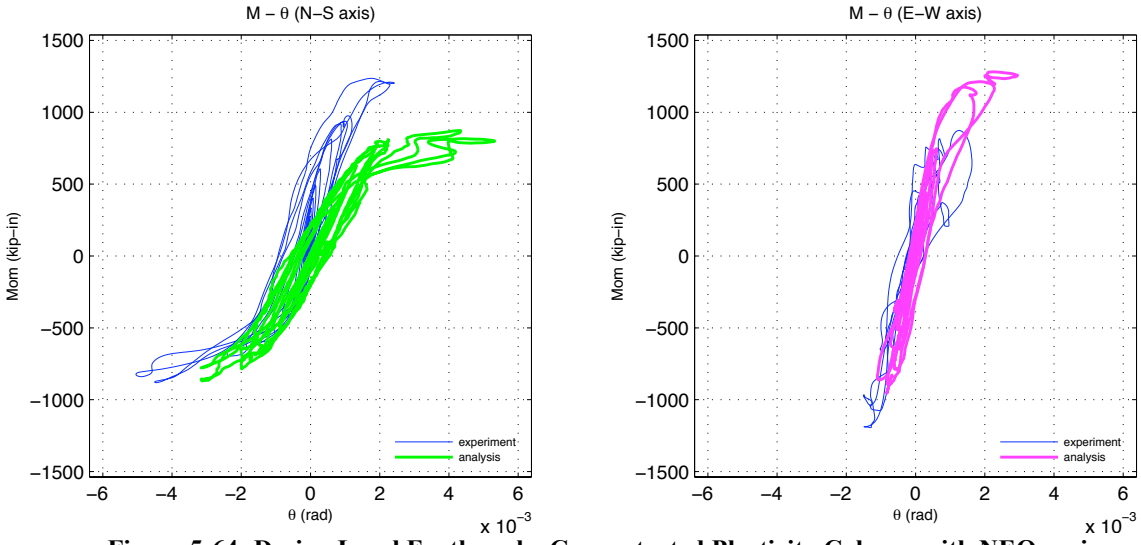

Figure 5-64: Design Level Earthquake Concentrated Plasticity Column with NEO springs Footing Moment Rotation M-θ (A3R)

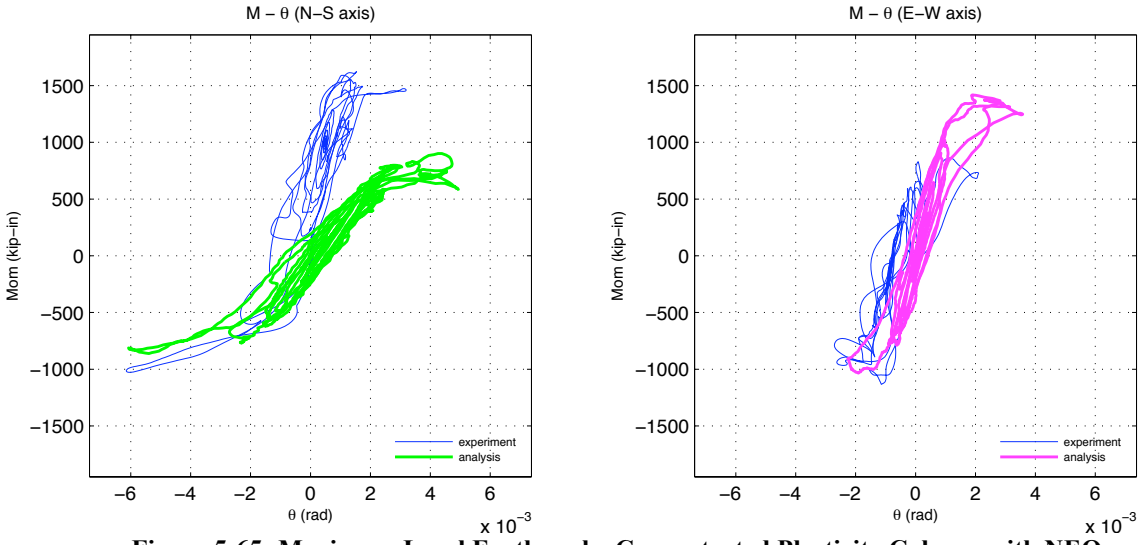

Figure 5-65: Maximum Level Earthquake Concentrated Plasticity Column with NEO springs Footing Moment Rotation M-θ (A4R)

5.7 Summary and Conclusions

A comparison of analytic models with observed response was performed to reliably predict the seismic performance of reinforced concrete bridge piers allowed to uplift. Global and local response parameters were compared to the observed displacements, accelerations, and force deformation relationships of the uplifting system. The open-source structural analysis platform OpenSees was used to conduct both linear and nonlinear analysis. A summary of the analysis performed is given in Section 5.7.1. Conclusions about the analytic models are presented in Section 5.7.2.

5.7.1 Summary

Several analytic models were developed and calibrated to the observed specimen characteristics. These models varied the column type, soil spring type, soil spring spacing, and column reinforcement type to match the column initial stiffness, footing rotational stiffness, footing vertical stiffness, footing uplift relationship, etc. Only experimental test runs with significant displacement and/or uplift response were presented in this chapter. Response parameters compared include column total displacement and the contribution of flexural column displacement and lateral translation due to footing rocking to the total displacement. As well as column accelerations, column moment curvature and footing moment rotation relationships.

Column

- The Distributed Plasticity option did not model system response well, because of the inability to model effective section properties of concrete columns. The elastic and lumped plasticity options both were adequate for modelling the elastic response of the system. The lumped plasticity model is a valid option for modelling the inelastic response of the system.
- Using a plastic hinge length calculated using the Priestley method for estimating the plastic hinge length, provided reasonable results on the yielding of the column.

Footing

- Elastic-No-Tension (ENT) and Neoprene (NEO) soil springs were able to adequately model the observed rotational and vertical stiffness of the footing.
- The number of springs used for the best model comparison was a 6 x 6 grid (36 total). More refined grids were unwarranted, because they provided a small improvement in accuracy at a significant increased computational expense.

Materials

- Column Steel Reinforcement -- The ReinforcingSteel model was the better option for modeling the inelastic response of the column. In part because it better captures the post-yield behavior of the reinforcement.
- Soil Springs: The ENT and NEO material both are able to model the vertical and rotational stiffness of the footing. The NEO material is the better option because of the hysteretic damping properties that are similar to the observed elastomeric pad response.

Damping

- Rayleigh damping applied to the entire system was used for the analytic modelling. At significant levels of uplift the analytic damping level was 5-6%. When there was less uplift, lower values of damping, approximately 3%, were warranted.

5.7.2 Conclusions

It was shown that analytic models have the capability to reasonably predict the seismic response of uplifting bridge pier systems with the use of the open-source structural analysis platform OpenSees. The analytic models were idealizations of the superstructure mass, column, footing, and elastomeric pad the footing rested upon. The evaluation criteria, was based on observed results of natural properties and dynamic response to multi-directional input earthquake accelerations. Linear and nonlinear models were used based on the observed system response.

The linear models used were able to predict the peak displacements to within 20-25% for the square configuration footing ($3D_c$ x $3D_c$) tests with nominal design axial load ($10\%f'_cA_g$) and the rectangular footing ($3D_c$ x $5D_c$) tests with the equal design axial load. In general the linear models used were able to predict the observed response with a high degree of confidence.

The nonlinear models used were able to predict the design level (flexural ductility μ=6) test peak displacements to within 20% of the observed values. The residual displacements were under-predicted by approximately 100%. However, given the small value of residual displacements (less than 1") the best model predicted the amount of rocking and uplifting, column flexural displacements and column total displacements very well for the design level earthquake. For the maximum level earthquake (μ=8) the analytic model predicted the initial cycles of displacement well but deviated once the column experienced significant residual displacements. When discounting the effect residual displacements had on total displacement the model was still able to reasonably predicting the peak displacements which occurred at approximately a column flexural ductility of 10. Additionally, the model still was able to predict approximately 50% of the observed residual displacement and appeared to have similar post-yield stiffness response despite not having the same amount of yielding.

The column center of mass accelerations were predicted to within 25% for the linear and nonlinear analysis models. The column base moment curvature prediction for the linear response was predicted reasonably well. The nonlinear analytic model performed reasonably well for the design level earthquake but did not completely predict the residual displacements observed as discussed. Because of this the analytic model moment-curvature relationship does not show the shift in origin due to the residual displacements of the column. The analytic model needs further refinement for the maximum level test in part because of its inability to capture the residual displacements. The permanent column offset creates a shift in the origin that affects the system displacement and thus acceleration and moment response.

The footing rotational stiffness and subsequent softening during uplift were predicted reasonably well by the numerical models for the linear analysis cases. The

neoprene springs for the elastomeric pad provided good approximations of the static displacement, rotational stiffness, moment and rotation at first footing edge uplift and the softening behavior. The footing response under nonlinear analysis was affected by the discrepancy in predicted residual displacements, which caused a permanent shift in the origin of the footing moment rotation relationship.

The more uplift that is expected in a system the higher the value of Rayleigh damping that should be used. Analytic models showed 5-6% damping should be used for systems with significant uplift and approximately 3-4% for yielding systems with less uplift.

Based on these comparisons, the recommended analysis models for the uplifting bridge pier system have sufficient accuracy to predict the global responses of linear uplifting systems and design and maximum level uplifting systems. Additional research is needed to improved modeling of the free vibration phase of uplifting systems subjected to multi-directional input excitation and residual displacements in columns allowed to uplift.

6 Parametric Investigation of Uplifting Bridge Piers

6.1 Introduction

The experimental and analytic work presented in this report is intended to support the development of guidelines for design of traditional reinforced bridge columns that may uplift on competent soil. As noted in Chapter 1, much analytic work and some experimental work has been done in the past to devise simplified guidelines. Considerable research, including that carried out in this study, demonstrates that rocking and uplift may provide a useful form of seismic isolation for bridge piers supported on narrow foundations. Further, narrow foundations may be sufficient to develop yielding in the column plastic hinge region. However, few studies have developed guidelines that could be integrated within existing design methods for bridge footings and superstructures. The methodology proposed by Priestly et al. (1996) is perhaps the most widely referenced, including within the Federal Highway Administration Bridge Design Manual. However, as noted previously, it has a number of important limitations, and may be difficult to apply to more general multi-directional excitations.

From past experimental tests and analytic research, it was found that there are a few important parameters that control the characteristics of a rocking bridge pier system. These include the dimensions of the footing, ratio of superstructure height to footing width, the weight acting on the footing, allowable bearing pressure of the soil, the fixed base period of the pier, and the effective period of the pier resulting from the flexibility of the supporting soil. Simplified theories such as those by Yim and Chopra (1983) and Meek (1975) appear to be adequate to predict whether a foundation will uplift, However, these early studies focused on the beneficial effects of uplift on reducing base shear, rather than on predicting the lateral displacement of the system and the amount of uplift required. Methods such as those by Priestley et al. appear based on available evidence (Harden et al., 2005) to result in significantly over or under-conservative estimates of lateral displacements.

The uplifting system parameters of investigation are discussed in Section 6.3. These include analytic assumptions for the superstructure, column, footings, soil, soil springs, and effective natural period. Sections 6.4 through 6.7 describe the parametric investigation of uplifting systems and spectral acceleration and displacement. Section 6.8 compares the response of fixed base and uplifting systems. Guideline development, based on the parametric investigation, including observed characteristics of uplifting systems and potential benefits and negative consequences of allowing uplift is described in Section 6.9.

6.2 Summary of Objectives

An assessment is made here to determine the benefits of designing a bridge which would normally be fixed base via large spread footings instead as a spread footing foundation allowed to uplift. The concept to expand on is if allowing a footing to uplift provides a reliable and appreciable seismic isolation mechanism and/or energy dissipation, such that demand levels for design earthquakes would be significantly reduced to below inelastic levels or a reduced damage state. Criteria to determine if global instability would be likely to occur by allowing uplift are also needed.

The previous chapters have shown that allowing bridge piers to uplift is a valid mode of response for the column system considered. However, the experimental testing was limited in scope to a single column, with two footing configurations, and one soil medium considered. Analytic models developed in Chapter 5 will be used to perform the parametric investigation. The purpose is to determine the response of a wide variety of bridge pier systems allowed to uplift and to compare to a traditional fixed base bridge pier design. The parameterization includes the natural period of the pier, column response type, footing width, soil response, ground motions, allowable soil pressure, and column displacement demands vs. capacity. Uplifting systems have been seen to act as seismic isolators of sorts, with a noticeable elongation of the natural period directly correlated to the footing and soil stiffness. The parametric investigation will illustrate the differences between fixed and uplifting systems by plotting the response variable of interest for the uplifting systems against the corresponding fixed base response.

The second objective is to assess the benefits and drawbacks of allowing traditional bridge piers to uplift in design. This is accomplished by evaluating traditional design metrics including total displacement, acceleration, local demands on deformation and forces. A comparison of existing design methods for columns allowed to uplift is performed and compared to the dynamic time history method used herein.

6.3 Uplifting Bridge Pier System

The uplifting bridge pier system is designed according to the criteria described in the Caltrans Bridge Design Specifications (BDS) and the Seismic Design Criteria (SDC). The focus of this study is on piers resting on competent soil that allows for the use of spread footings. A traditional fixed base design would select footing dimension sufficient to prevent measurable uplift compared to the column displacement and also maintain soil pressures well below the allowable limits. Figure 6-1 illustrates the uplifting bridge pier model and the parameters of interest. The following sections described the notation used to describe the uplifting system and the analytic modeling of the various components.

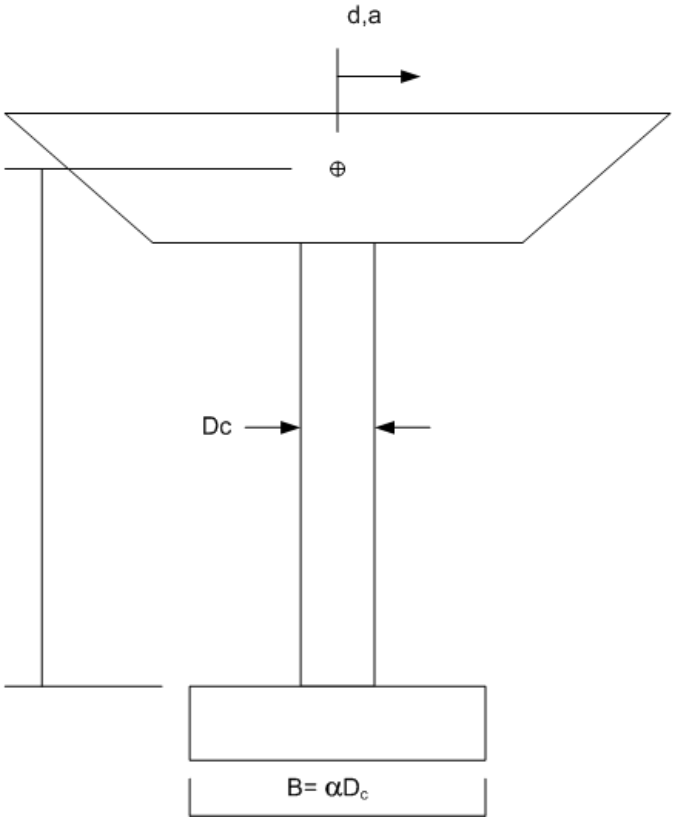

Figure 6-1: Prototype Column

6.3.1 Notation

Below is a description of the parameters used in the parametric investigation as well as response variables used to describe the uplifting system. Some of these are repeated from Chapter 4.

D_c = column diameter

α = ratio of footing length to column diameter

T_{nf} = fundamental period of fixed base system

T_{nr} = fundamental period of uplifting system

S_{AF} = a_{max} fixed base system at column center of mass

S_{AR} = a_{max} uplifting system at column center of mass

S_{DF} = d_{max} fixed base pier at column center of mass

S_{DR} = d_{max} of uplifting system at column center of mass

= $d_f + d_r$

S_{DRF} = peak column flexural displacement of uplifting system at column center of mass

S_{DRR} = peak column translation displacement of uplifting system at column center of mass due to footing rotation

6.3.2 Column and Superstructure

The prototype column and superstructure were designed according to Caltrans BDS. The column was modeled for both elastic and inelastic response for the parametric investigation. Superstructure mass was idealized as a lumped mass for this inverted pendulum parametric model investigation.

The column was modeled as a reinforced concrete section with a fixed column diameter of 6 ft (72 in). The reinforcement ratio was selected to 1.5% for longitudinal reinforcing and 0.6% for the volumetric spiral reinforcement. Longitudinal bars were selected to be No. 7 and the spiral reinforcement was selected as No. 5 bars. The concrete was assumed to have a compressive strength of f'c = 4 ksi. Steel reinforcing tensile yield strength was assumed to be f_y = 60 ksi. The column height measured from top of footing to center of column mass varied to provide a range of periods from 0.1 secs to 3.0 secs for the fixed base system. The axial dead load was assumed to be 10% of f'_cA_g.

The column was modeled as either an elastic beam-column element or a nonlinear beam-column element. Effective section properties as recommended by the Caltrans SDC were used in modifying the concrete flexural stiffness. For nonlinear response the column plastic hinge length was estimated using the Priestly equation (Eqn. 7.25) in the SDC.

6.3.3 Footing

The footing is assumed to be rigid relative to the column and soil response during rocking and uplifting. It is assumed to be square with dimensions B = L determined by the column to footing width ratio $\alpha = B/D_c = L/D_c$. Footing width ratios of 3, 4, 5, and 6 were used for the analysis. Footing ratios less than 3 tend to have bearing pressures much larger than allowable. Footing width ratios larger than 6 tend to be too conservative for design when considering effective fixed base response and bearing pressures

When considering uplifting systems the footing depth is not negligible because the footing uplifts about the bottom of the footing face which affects the effective column height. The amount of footing height is small though compared to the column heights used for this investigation and is not considered.

Embedment and lateral translation were not considered in the investigation. The purpose was to remove any negligible response mode that might distort the affect of uplift on the column response. The analytic model allows the footing to translate vertically and rotate about the two horizontal axes as shown in Figure 5-11.

6.3.4 Soil

The focus of this investigation is on footings resting on competent soil. A representative sandy medium dense soil was selected to model the soil of a system allowed to uplift. Several sources are available to determine appropriate soil engineering properties including allowable bearing pressure, shear modulus, friction angle of sand, and soil factor of safety. The study by Harden et al. (2005), ASCE 41 and the Caltrans BDS were consulted to determine suitable soil engineering properties.

The representative medium dense sandy soil was selected to have the properties ϕ=35 degrees, unit weight of 130 pcf, poisson's ration of 0.3, and a shear wave velocity of 600 ft/sec, which is comparable to a NEHRP soil site class *D*. Allowable bearing pressure design values for spread footings are listed in the Caltrans BDS Table 4.11.4.1.4-1 and ASCE 41 (Table 4-2), for medium dense sands Caltrans recommends allowable bearing pressures of 4.0-6.0 ksf and ASCE 41 recommends approximately 3-4 ksf. A representative value of q_{allow} was selected based on the Caltrans recommendation. Factor of safety for soil bearing pressure were selected to be FS_v = 3.0. which is the BDS recommended value.

The shear modulus (G) estimation is determined by procedures in ASCE 41 Shallow Bearing Foundations methods (4.4.2.1). Using the recommended effective modulus ratio G/G_o = 0.5, the calculated initial shear modulus G_o = 662 ksf the effective shear modulus used was G=331 ksf. The soil properties are listed in Table 6.1

6.3.5 Soil Springs

Soil springs for modeling the footing as a Beam on Nonlinear Winkler Foundation were implemented as described in Section 5.3.3. Global vertical and rotational stiffness of the footing needs to be established prior to discretizing the footing into middle and end regions with associated spring stiffnesses. The ASCE 41 recommended method by Gazetas (1991), used in Harden et al. (2005) with modifications, for modeling shallow bearing foundations with rigid footings and flexible soil was used here to estimate the global vertical and rotational stiffness. The Gazetas method calculates the vertical and rotational stiffness of a footing B x L as a function of dimensions, shear modulus, and poisson's ratio. Table 6.1 lists the calculations for vertical and rotational stiffness. The recommended embedment correction factors were not used because the footing embedment effects are not considered in this study.

As expected for a uniform soil the vertical and rotational stiffness increase as the footing dimensions increases. The discretized middle and end region spring stiffness are calculated as described in Section 5.3.3. Table 6.1 lists the relative soil spring information.

Table 6.1: Parametric Soil Spring Model Parameters

Column-Footing Width Ratio	$\alpha = 3, 4, 5, 6$
Footing Width	$L = \alpha D_c$
Footing Length	$B = \alpha D_c$
Effective Shear Modulus Ratio	$G/G_o = 0.5$
Initial Shear Modulus	$G_o = 662$ ksf
Allowable Bearing Pressure	$q_{allow} = 5.0$ ksf
Global Vertical Stiffness	$K_z = \frac{GB}{1-v}\left[1.55\left(\frac{L}{B}\right)^{0.75} + 0.8\right]$
Global Rotational Stiffness	$K_{\theta x} = \frac{GB^3}{1-v}\left[0.4\left(\frac{L}{B}\right) + 0.1\right]$ $K_{\theta y} = \frac{GB^3}{1-v}\left[0.47\left(\frac{L}{B}\right)^{2.4} + 0.034\right]$

6.3.6 Natural Period

The natural period of elastic response can be calculated using the methods described in Chapter 5. The initial fundamental period of the uplifting system before uplift is a function of the column fixed base fundamental period T_{nf} and a factor related inversely to the footing rotational stiffness. As the footing width increases in this study, the rotational stiffness increases given the consistent soil assumption. Consequently, the fundamental period of uplifting decreases until is reaches the asymptote defined by the fixed base fundamental period. The fundamental period of uplifting system is repeated here in Equation (6-1).

$$T_{nr} = T_{nf}\sqrt{1 + \frac{k_{col} \cdot H_{col}^{\ 2}}{K_\theta}} \qquad (6\text{-}1)$$

6.3.7 Damping

Damping for uplifting system was estimated using the methods described in ASCE 41. The uplifting system has damping from hysteretic response of the column and the radiation damping from the footing interacting with the underlying soil. The fixed base system has damping from the hysteretic column response only.

The hysteretic damping of the column was assumed to be $\xi_o = 5\%$. This is the typical value used for elastic response spectra analysis. The uplifting system damping ξ is calculated as a function of the column damping and soil radiation damping ξ_f. Equation (6-2) below shows the calculation for system damping for soil-structure interaction.

$$\xi = \xi_f + \frac{\xi_o}{\left(T_{nr}/T_{nf}\right)^3} \quad (6\text{-}2)$$

The range of damping for uplifting systems is 5% to 7.5% using the soils and footing configurations described above.

6.3.8 Ground Motions

Ground motions for the investigation of uplifting systems were selected based on relevant criteria used to design fixed base bridge piers, in order to facilitate a direct comparison between the two systems. The ground motions were selected from the PEER Transportation System Ground Motion Studies program (Baker et al., 2011). One set considered the directivity effects from near-fault earthquakes and the other considered site specific target hazard levels.

Near-fault records chosen have significant velocity pulses in the fault normal component of the record. In most cases, the fault parallel component had a noticeable velocity pulse with smaller velocity. In general, the range of periods of velocity pulses for the motions considered is from 0-5 seconds. None of the ground motions were amplitude scaled. All were recorded within 11km of the fault rupture.

Three site specific hazards levels typically used for design of structures were selected for analyzing uplifting systems. They correspond to 2%, 10%, and 50% in 50 year probabilities of exceedance. The site specific ground motions used are for the I880 Testbed program in Oakland, CA (37.803N, 122.287W) described in Baker et al. The target PGA for the three hazard levels are 0.94g, 0.60g, and 0.27g for the 2%, 10% and 50% probabilities of exceedance. Some of the ground motions considered had directivity effects like velocity pulses due to their proximity to the Hayward fault line.

For each of the four groups described above 10 ground motions were selected for analysis of uplifting and fixed base systems. Ground motions selected were not scaled beyond that described in the Baker et al report. Table 6.2 list the ground motions used in the parametric investigation.

Table 6.2: Parametric Investigation Ground Motions

No.	Hazard Level	Name[1]	Record
1	2% in 50yr	Oak_2_50_1	Imperial Valley-02 (1940)
2	2% in 50yr	Oak_2_50_2	Imperial Valley-06 (1979)
3	2% in 50yr	Oak_2_50_3	Chalfant Valley-02 Bishop (1986)
4	2% in 50yr	Oak_2_50_4	Superstition Hills-02 (1987)
5	2% in 50yr	Oak_2_50_5	Loma Prieta-Gilroy (1989)
6	2% in 50yr	Oak_2_50_6	Erzican, Turkey (1992)
7	2% in 50yr	Oak_2_50_7	Northridge-01 Sylmar (1994)
8	2% in 50yr	Oak_2_50_8	Kobe (1995)
9	2% in 50yr	Oak_2_50_9	Duzce, Turkey (1999)
10	2% in 50yr	Oak_2_50_10	Chi-Chi, Taiwan (1999)
11	10% in 50yr	Oak_10_50_1	Imperial Valley-02 (1940)
12	10% in 50yr	Oak_10_50_2	Victoria, Mexico (1980)
13	10% in 50yr	Oak_10_50_3	Westmoreland (1981)
14	10% in 50yr	Oak_10_50_4	Chalfant Valley-02 Bishop (1986)
15	10% in 50yr	Oak_10_50_5	Superstition Hills-02 (1987)
16	10% in 50yr	Oak_10_50_6	Loma Prieta-Gilroy (1989)
17	10% in 50yr	Oak_10_50_7	Northridge-01 Sepulveda (1994)
18	10% in 50yr	Oak_10_50_8	Northridge-01 Sylmar (1994)
19	10% in 50yr	Oak_10_50_9	Duzce, Turkey (1999)
20	10% in 50yr	Oak_10_50_10	Chi-Chi, Taiwan (1999)
21	50% in 50yr	Oak_50_50_1	Imperial Valley-02 (1940)
22	50% in 50yr	Oak_50_50_2	San Fernando (1971)
23	50% in 50yr	Oak_50_50_3	Imperial Valley-06 (1979)
24	50% in 50yr	Oak_50_50_4	Chalfant Valley-02 Bishop (1986)
25	50% in 50yr	Oak_50_50_5	Superstition Hills-02 (1987)
26	50% in 50yr	Oak_50_50_6	Loma Prieta-Gilroy (1989)
27	50% in 50yr	Oak_50_50_7	Landers (1992)
28	50% in 50yr	Oak_50_50_8	Northridge-01 Sepulveda (1994)
29	50% in 50yr	Oak_50_50_9	Duzce, Turkey (1999)
30	50% in 50yr	Oak_50_50_10	Chi-Chi, Taiwan (1999)
31	Near Fault	PL_1	Imperial Valley-06 (1979)
32	Near Fault	PL_2	Morgan Hill (1984)
33	Near Fault	PL_3	Loma Prieta-LGPC (1989)
34	Near Fault	PL_4	Landers-Lucerne (1992)
35	Near Fault	PL_5	Northridge-01 Newhall (1994)
36	Near Fault	PL_6	Northridge-01 Sylmar (1994)
37	Near Fault	PL_7	Kobe (1995)
38	Near Fault	PL_8	Kocaeli, Turkey (1999)
39	Near Fault	PL_9	Chi-Chi, Taiwan (1999)
40	Near Fault	PL_10	Chi-Chi, Taiwan (1999)

[1] Ten files selected for each group from Baker et al. were renumbered from 1-10. Do not match original numbering

6.4 Performance Evaluation of Uplifting Bridge Pier System

The rocking system column response and its components were described in Section 4.2. The relationship of column displacement is repeated in Equation (6-3).

$$\Delta_T = \Delta_{flex} + \Delta_{rock} \qquad (6\text{-}3)$$

{or}

$$d = d_f + d_r$$

A representative system with a fixed base natural period equal to 1.0 second is used to evaluate the performance of a system allowed to uplift. The representative ground motion was selected based on seismic design requirements of reinforced concrete columns. For this system a ground motion was selected to reach the target ductility for a design level earthquake (10% in 50 year probability of exceedance).

Three types of analysis are performed to evaluate the system: pushover, dynamic, and spectral analysis. Three combinations of column and footing modeling assumptions are presented: elastic column and soil, nonlinear column and elastic soil, and nonlinear column and soil. The same column characteristics were used for all systems. The footing width was chosen as 3, 4, 5 or 6 times the column diameter.

As shown in this section, a footing to column width of 5 has a significant amount of yielding. For this system to realize the benefits of rocking, the footing/column ratio needs to be less than 5. In particular, the footing to column width of 4 also has a displacement contribution from yielding. To reduce the amount of inelastic response the footing needs to be approximately 3 to 4 times the column diameter.

6.4.1 Pushover Analysis

A pushover analysis of uplifting systems provides an enveloped response of systems allowed to uplift. It also facilitates a relative comparison of design variables and their sensitivity on key response parameters such as total column displacement. This section describes and illustrates the pushover response of the three types of modeling assumptions used.

Some of the key response parameters include: footing uplift, column yield, soil yield, column shear, column base moment, total column displacement, and column displacement from flexure. These parameters will be compared to the fixed base system response of the same column to gauge the performance of uplifting systems.

6.4.1.1 Column Force Displacement

The applied lateral force versus total column displacement is shown in Figure 6-2(a) for an elastic column - soil modeling assumption. The three curves show the force vs. column displacement for the fixed column, and uplifting columns with footing-to-column width ratios of 3 and 5. As expected the footing uplifts at larger applied loads for

increasing footing widths. The applied force to uplift a footing with α=3 is approximately one-half that of the α=5 assumption.

Figure 6-2(b) shows the system response assuming a nonlinear column - elastic soil for the fixed column, α=3, and α=5 assumptions. The yield displacement of the fixed base column is approximately 3.5 in. The figure shows α=3 footing uplifts before it yields and α=5 footing yields before it uplifts. The α=3 footing uplifts at total displacement of 2.8 in. and yields at 8.6 in. The α=5 footing uplifts at 10.6 in and yields at 4.1 in. Table 6.3 lists some of the values for these uplifting systems. This indicates that the α=3 footing will uplift well before it yields and that the total displacement at yield will be approximately 2.5 times larger than that of the fixed base column. This shows there should be a reduction in nonlinear behavior for the α=3 footing. The α=5 footing will yield before it uplifts and the displacement at uplift will be approximately 3.0 times that of the yield displacement. Hence the column will have an approximate displacement ductility of 3 before the footing uplifts. Figure 6-3 shows the response of the system assuming a nonlinear column and soil model. As stated previously, it was assumed that the yield soil bearing pressure is three times greater than the system vertical bearing pressure. The α=3 soil yields before the column reaches the yield point which is evident in the figure by the negatives slope. The α=5 does not reach soil yield until well after the column has yielded.

Table 6.3: Uplifting System Response Values

Response Parameter	α=3		α=5		Fixed
	Elastic	Nonlinear	Elastic	Nonlinear	
u_{up} (in)	2.8	2.8	3.1	10.6	-
u_{flex} at u_{up} (in)	1.3	1.4	2.5	10.0	-
θ_{up} (rad)	0.0042	0.0042	0.0017	0.0017	-
F_{up} (kip)	222	209	425	376	-
M_{up} (k-ft)	6,490	6500	12,405	12,406	-
u_{yield} (in)	-	8.6	-	4.1	3.51
M_{yield} (k-ft)	-	11,400	-	11,400	11,400
F_{yield} (kip)	-	351	-	372	374

(a) Elastic Column – Elastic Soil

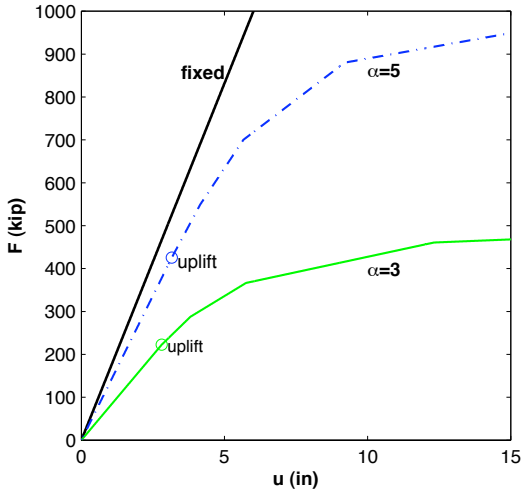

(b) Nonlinear Column – Elastic Soil

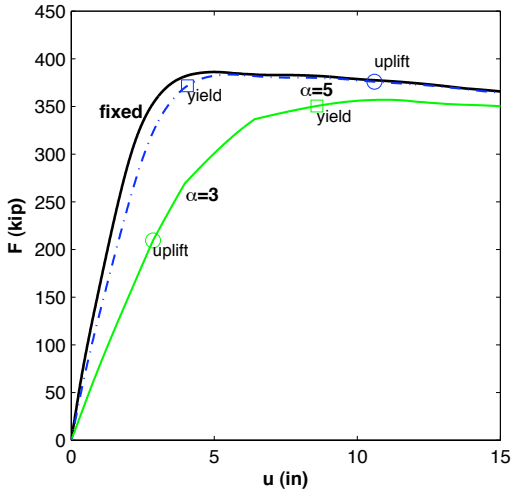

Figure 6-2: Pushover Analysis (Elastic or Nonlinear Column – Elastic Soil)

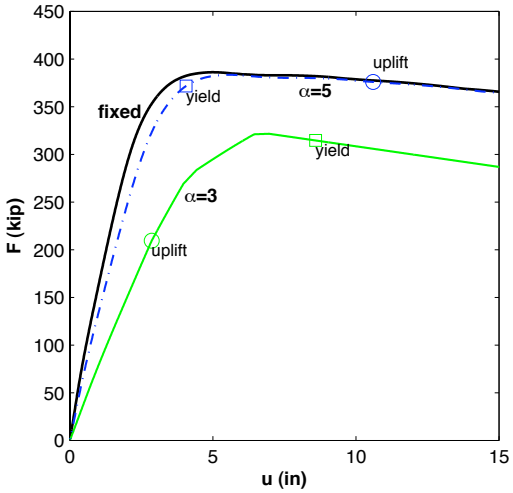

Figure 6-3: Pushover Analysis (Nonlinear Column-Soil)

6.4.1.2 Footing Moment Rotation

The footing moment rotation response for the same modeling assumptions discussed in the column force displacement section is shown in this section. Figure 6-4 shows the elastic column-soil model and nonlinear column-elastic soil model moment rotation response of the footing. The nonlinear column-soil model response is shown in Figure 6-5. The relationship between the various modeling assumptions is very similar to the column force-displacement curves.

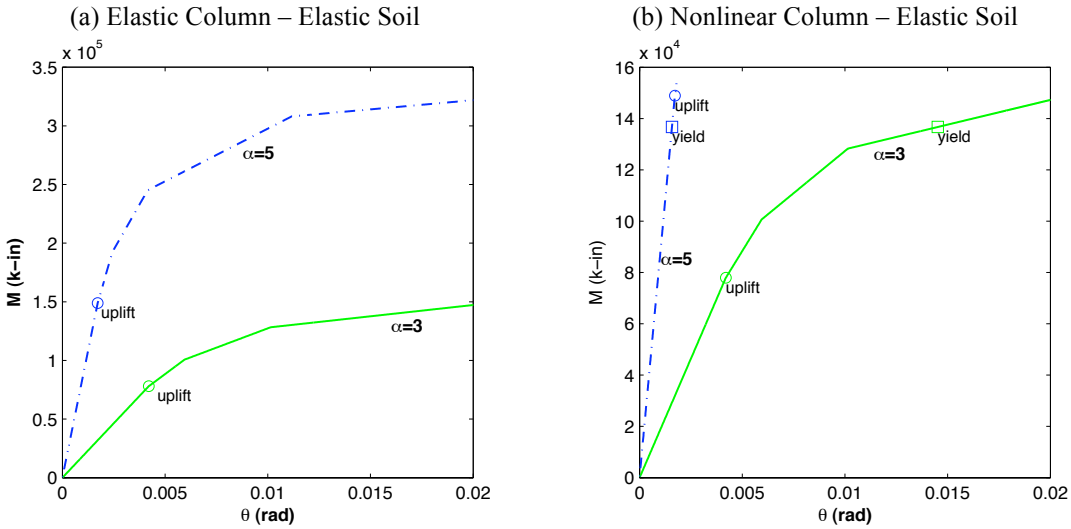

Figure 6-4: Footing Moment Rotation (Elastic or Nonlinear Column – Elastic Soil)

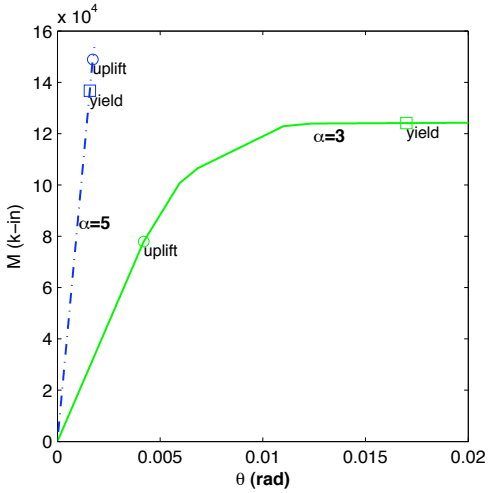

Figure 6-5: Footing Moment Rotation (Nonlinear Column-Soil)

6.4.1.3 Moment-Curvature Relationship

The moment-curvature response is similar for the nonlinear column assumptions because the axial load is relatively uniform. See Section 6.4.2.5 for the dynamic response of column moment curvature which is more informative.

6.4.1.4 Soil Springs

The soil spring bearing pressure vs. footing rotation is shown in Figure 6-6 for the elastic column-soil and nonlinear column-elastic soil model assumptions. The nonlinear column-soil model is shown in Figure 6-7.

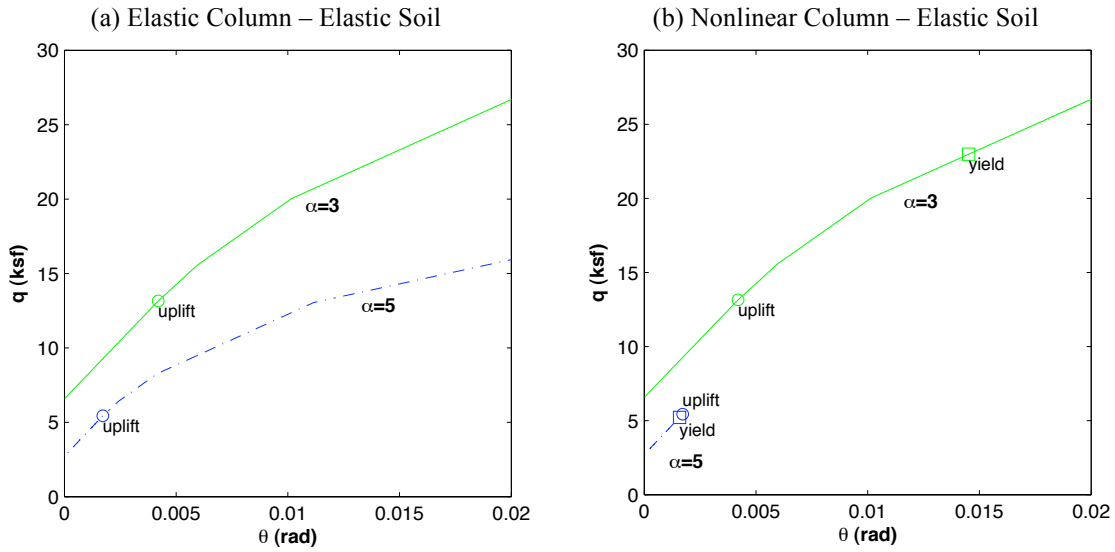

Figure 6-6: Soil Springs vs. Rotation (Elastic or Nonlinear Column – Elastic Soil)

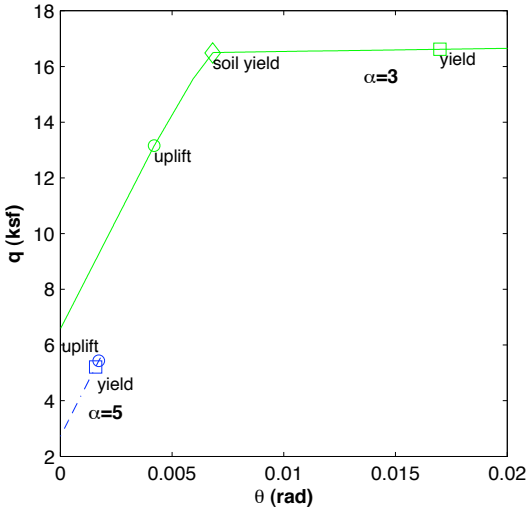

Figure 6-7: Soil Springs vs. Rotation (Nonlinear Column-Soil)

6.4.2 Dynamic Analysis

The dynamic response of the fixed base and uplifting system are compared to illustrate the relative differences between the assumptions. The ground motion, fixed base natural period and footing widths are the same as those described in the previous section. Time histories of acceleration, total displacement, column flexural displacement, and moment are compared, as are the force deformation relationships for column base moment vs. footing rotation and column base moment vs. column curvature.

6.4.2.1 Acceleration

The fixed base column acceleration is compared to the uplifting system in Figure 6-8 for the elastic column and soil model assumption. Figure 6-8 (a) shows the acceleration of α=3 footing width is consistently smaller than the fixed base response and longer period of motion. The peak acceleration of the uplifting system is approximately 90% the fixed base response. The α=5 footing width has a similar acceleration response as α=3 footing width. The peak acceleration of the uplifting system is approximately 95% of the fixed base response.

For the nonlinear column and elastic soil the acceleration response of the uplifting and fixed based systems are similar. Figure 6-9(a) shows the α=3 footing width response. Figure 6-9(b) shows the α=5 footing width response. For both footings the accelerations are very similar especially after the column reaches yield. Essentially the uplifting and fixed base response are identical once the column reaches the yield point.

(a) α=3 (b) α=5

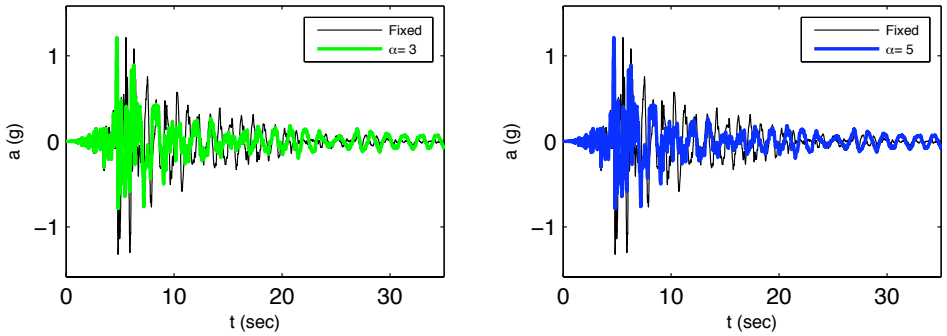

Figure 6-8: Acceleration Time History (Elastic Column & Soil)

(a) α=3 (b) α=5

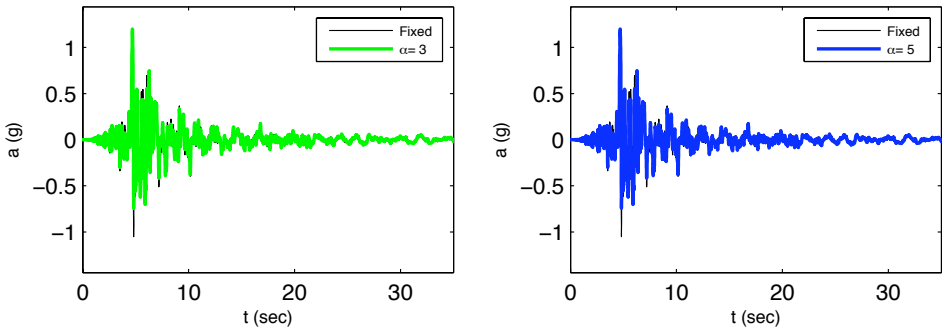

Figure 6-9: Acceleration Time History (Nonlinear Column-Elastic Soil)

6.4.2.2 Displacement

The displacement time history of the uplifting footing is shown in the following plots. To illustrate the general displacement response of uplifting systems the total displacement and column flexural displacement are shown. The column displacement due to rocking is not presented for simplicity. The quantity of uplift can be inferred from the difference between total and column flexural displacement. Figure 6-10 shows the displacement time history of the elastic column-soil system. For the α=3 footing width the peak total displacement and column flexural displacement are approximately 14.3 inches and 3.0 inches. For the α=5 footing width the peak total displacement and column flexural displacement are approximately 9.2 inches and 5.5 inches. The fixed base response peak is 7.6 in. This indicates that for the smaller footing width there is a significant contribution from rocking and that from the larger footing width uplifting occurs, but it is less pronounced.

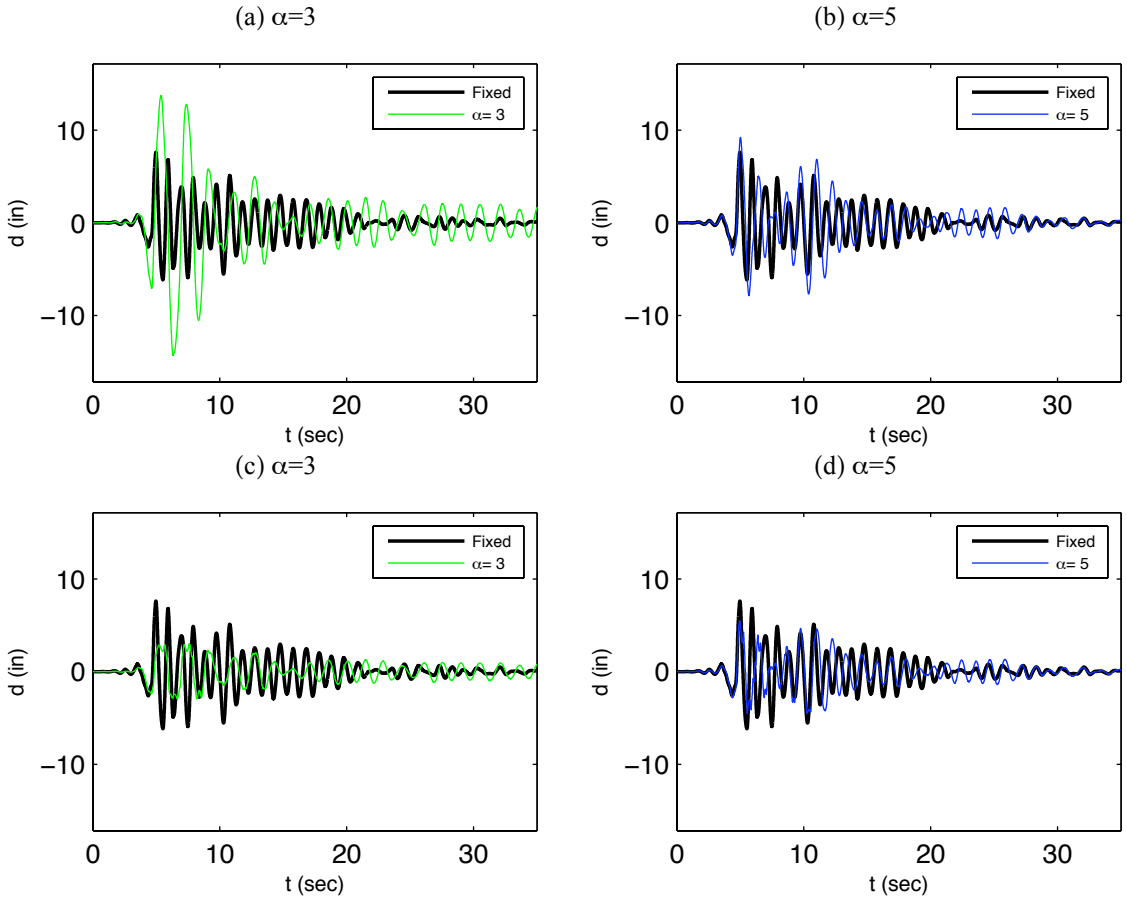

Figure 6-10: Displacement Time History (Elastic Column & Soil)

(a) α=3

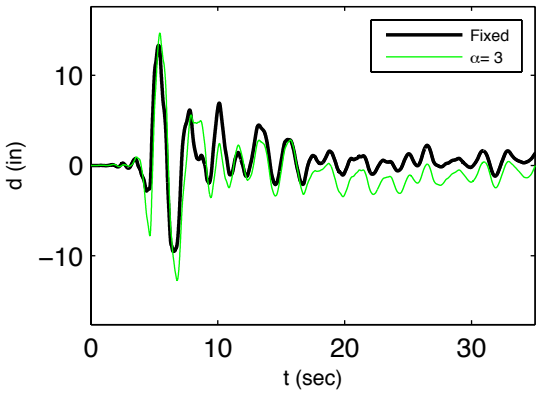

(b) α=5

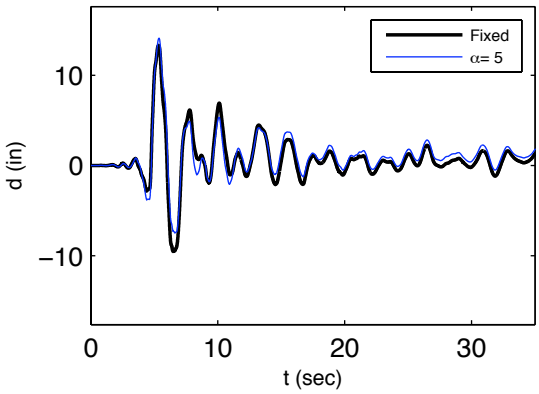

(c) α=3

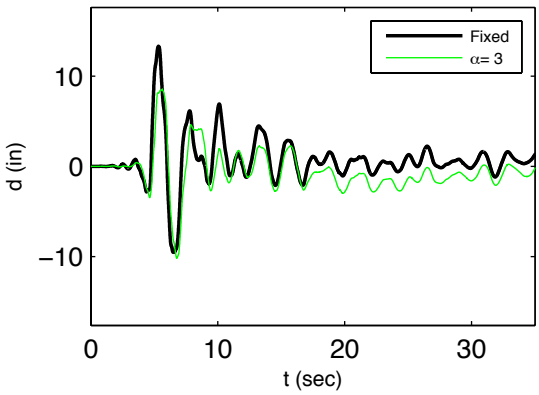

(d) α=5

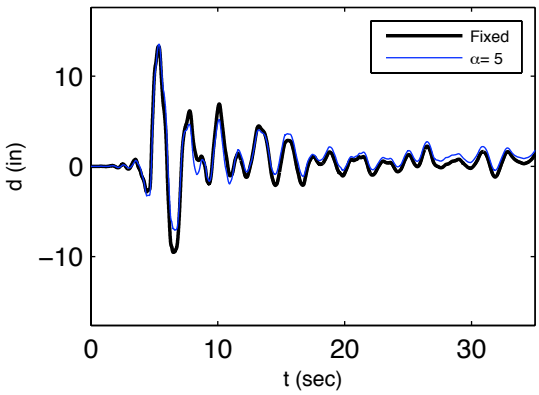

Figure 6-11: Displacement Time History (Nonlinear Column-Elastic Soil)

6.4.2.3 Moment

The moment time histories for the elastic column-soil models are presented in Figure 6-12. The α=3 footing has consistently smaller moment demands compared to the fixed base response while the α=5 footing is very similar to the fixed base response. The ratios of uplifting system peak moment to fixed base systems are 0.40 and 0.72, respectively.

Nonlinear column-elastic soil model time histories are presented in Figure 6-13. The moment demands for the uplifting and fixed base responses are very similar. This is due to the nonlinear response of the column. The ratios of uplifting system peak moment to fixed base systems are 0.96 and 0.97, respectively. The column demands for uplifting and fixed systems both reach yield during excitation.

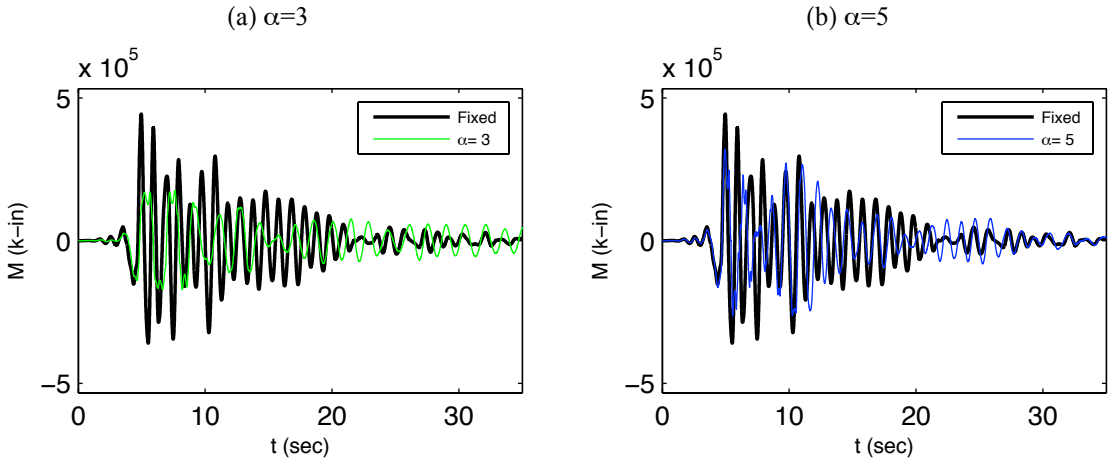

Figure 6-12: Moment Time History (Elastic Column & Soil)

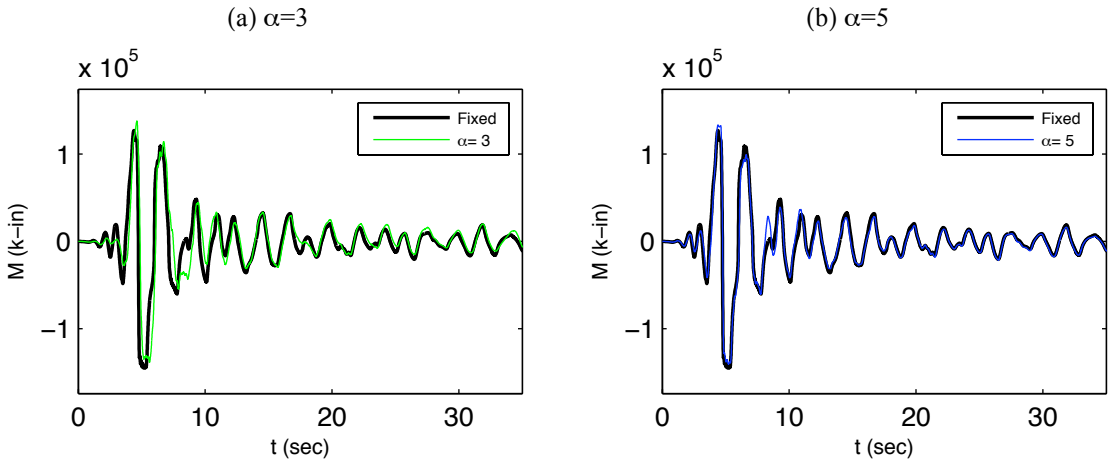

Figure 6-13: Moment Time History (Nonlinear Column-Elastic Soil)

6.4.2.4 Moment-Rotation

Footing moment-rotation response for the elastic column-soil model assumption is presented in Figure 6-14. The figure shows that uplift occurs for both footings but that the α=3 has much more uplift than the α=5 footing. The footing moment-rotation response of the nonlinear column model is presented in Figure 6-14. For this case the α=3 footing uplifts, however the total rotation is smaller and the number of cycles of uplift is less. The footing uplifts before the column yields, however once uplift occurs the column yields and does not significantly uplift subsequently. The α=5 footing does not uplift for the nonlinear column-elastic soil model. In this case the column yields before uplift and the moment required to uplift to footing does not occur.

6.4.2.5 Moment Curvature

For the nonlinear column-elastic soil model assumption the moment curvature response of the column is presented in Figure 6-15. The α=3 footing and the α =5 footing both experience nonlinear response however the amount of nonlinearity is smaller for the α =3 footing. Which indicates a benefit by allowing the footing to uplift.

The ductility demands can also be estimated by the curvature values, which are more representative of system response since they are the result of moment demand, which includes P-Δ effects. The ratios of peak curvatures for the two footings are 0.76 and 1.02 respectively. For the α=3 and α=5 footing widths the ductility demands $\mu=\phi_r/\phi_f$ are 4.7 and 6.3, respectively. Which are similar, but not exactly the same as the calculated displacement ductility demand in Section 6.4.2.2.

(a) Elastic Column-Soil

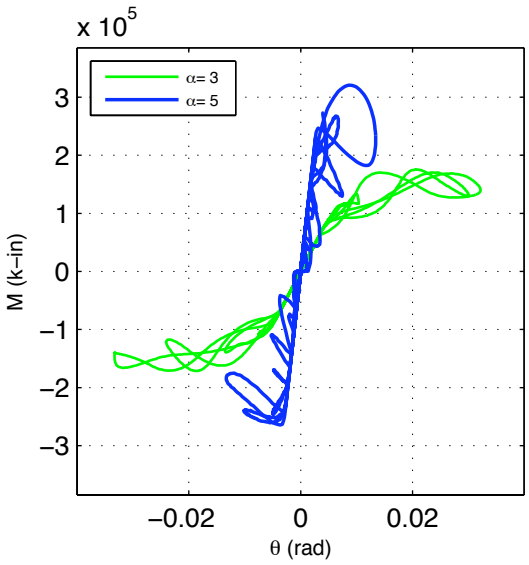

(a) Nonlinear Column-Elastic Soil

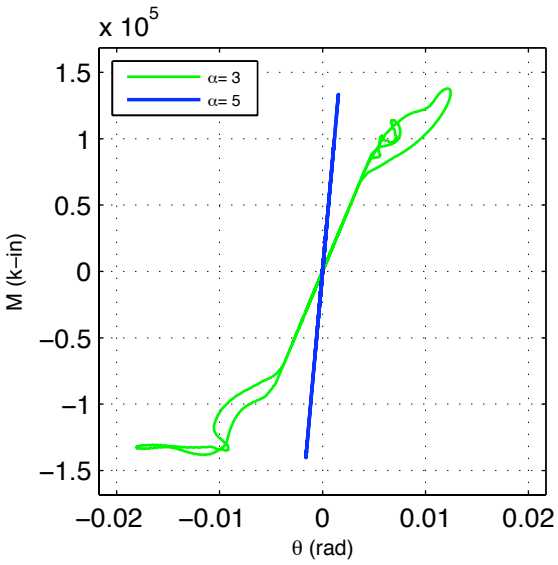

Figure 6-14: Moment-Footing Rotation (Elastic Column & Soil)

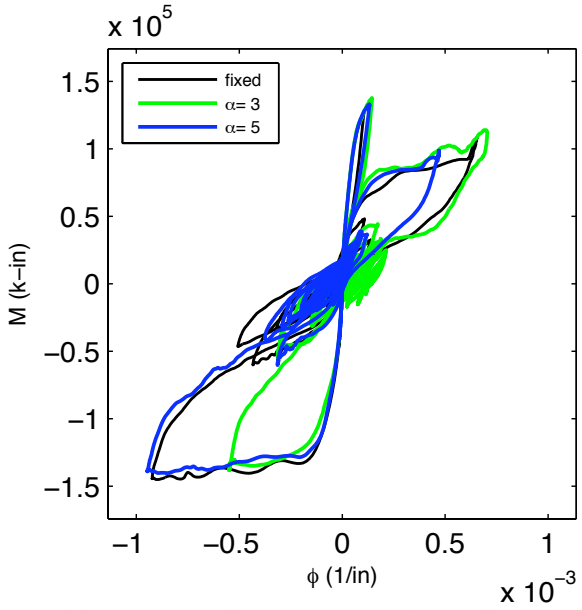

Figure 6-15: Moment Curvature (Nonlinear Column-Elastic Soil)

6.4.3 Spectral Analysis

For the single ground motion considered, the spectral response of an uplifting column is plotted for two footing widths and compared to the fixed base response. All spectral response quantities of the uplifting systems are plotted using the corresponding cantilever column fixed base period T_{nf}, not the effective rocking period T_{nr}. For example, the spectral acceleration of an uplifting system is plotted as a function of T_{nf} and S_{AR}. Spectral accelerations, total spectral displacement and column flexure spectral displacement response are compared to the fixed base response. The two modeling assumptions presented are elastic column-soil and nonlinear column and elastic soil. Only the one-dimensional directional excitation is shown for illustrative purposes.

6.4.3.1 Acceleration

Elastic column and soil spectral acceleration response to the selected ground motion is show in Figure 6-16. A narrow footing width (α= 3) shows peak accelerations consistently smaller than the fixed base period system (Figure 6-16a). For the same ground motion and a larger footing width (α= 5), the response more closely represents that of a fixed base system. However, the total acceleration is still less than the fixed base response. For both systems the predicted peak acceleration is less than or equal to the fixed base response.

The nonlinear column and elastic soil spectral acceleration response to the selected ground motion is show in Figure 6-17. A narrow footing width (α= 3) shows peak accelerations are approximately equal for all periods considered except the short period range. For natural periods less than approximately 0.25 sec. the peak acceleration exceeds that of the fixed base system (Figure 6-17a). The larger footing width (α=5) has a spectral response almost identical to the fixed base response for the nonlinear column and elastic soil model. Except for the very short period range in which the uplifting response is much larger.

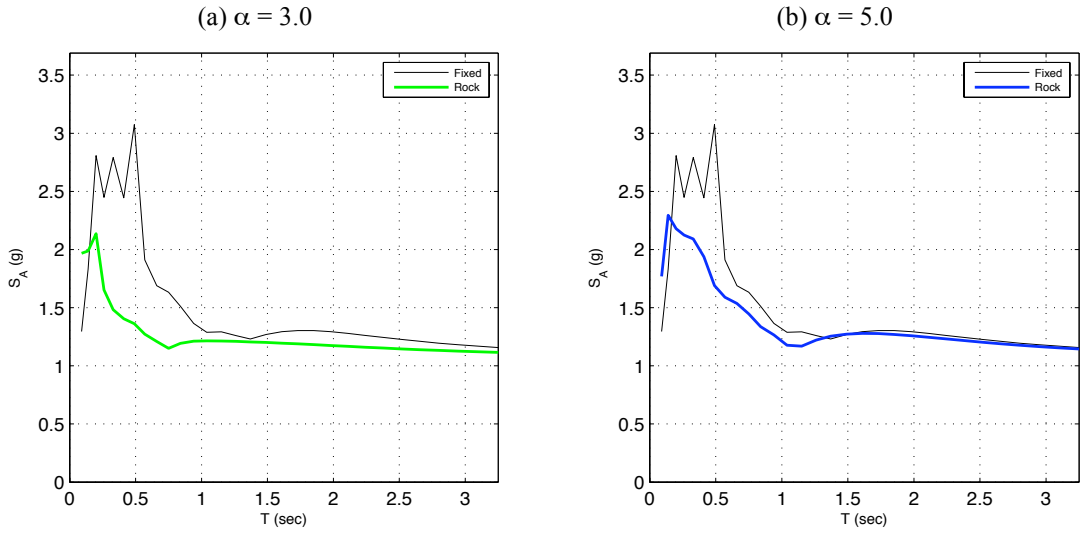

Figure 6-16: Spectral Acceleration. Elastic Column and Soil. 1D excitation. (Oak_10_50_6)

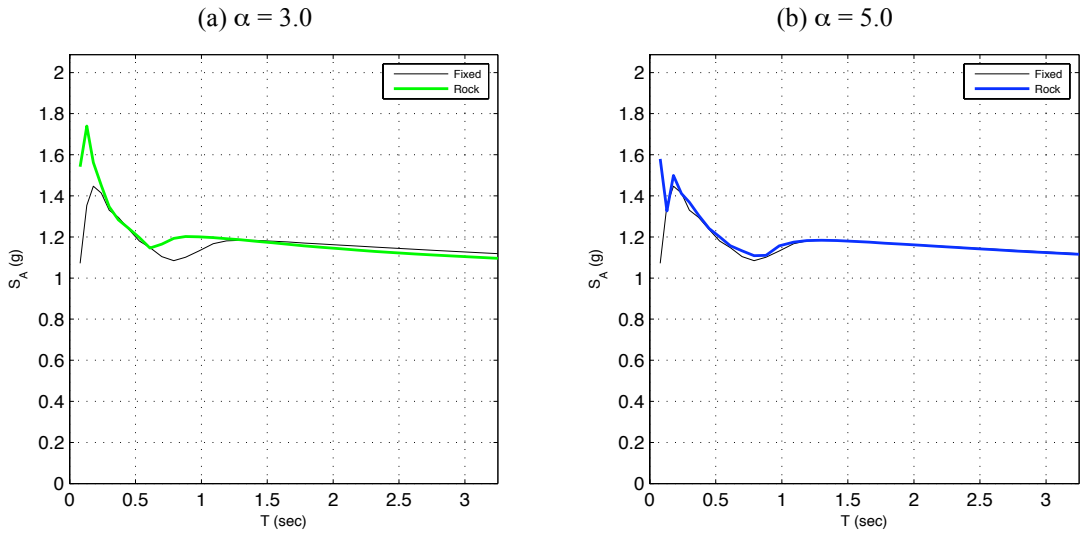

Figure 6-17: Spectral Acceleration. Nonlinear column-Elastic Soil. 1D excitation. (Oak_10_50_6)

6.4.3.2 Displacement

Figure 6-18 and Figure 6-19 show the displacement spectral response of the uplifting system vs. the rocking system. Response of the two footing widths for total rocking displacement, column flexural displacement, and fixed base displacement response are shown.

The elastic column-soil model spectral displacement is shown in Figure 6-18. Figure 6-18(a) shows the fixed base response vs. the total uplifting column displacement for α = 3.0 and Figure 6-18 (b) shows the same response for α =5.0. The fixed base response vs. column flexural displacement component is shown in Figure 6-18 (c) for α =3.0 and Figure 6-18 (d) for α =5.0.

In general for the period ranges considered the α=3 footing width has larger total displacements for T_{nf} < 1.5 secs. At a natural period of 0.8 sec the ratio of total column displacement for rocking vs. fixed is a maximum of 2.0. Everywhere else it is less. However inspection of the rocking column flexural displacement shows this component is about one-half the fixed base response. Indicating that the system will not have significant flexural response while uplifting when in the elastic range.

The nonlinear column-soil model spectral displacement is shown in Figure 6-19. The fixed base response vs. the total uplifting column displacement for α = 3.0 is shown in Figure 6-19(a) and Figure 6-19 (b) for α =5.0. The fixed base response vs. column flexural displacement component is shown in Figure 6-19(c) for α =3.0 and Figure 6-19(d) for α =5.0.

Total displacements for the α= 3 footing width are greater for Tn < 1.0 sec and then become smaller for larger periods compared to the fixed base nonlinear column response. The column flexural response is approximately the same as the fixed base response for T_{nf} less than or equal to 0.75 sec and then significantly less. The α=5 footing is very similar to the fixed base response for total and column flexural displacements. Indicating there is not significant rocking response for this footing width. Except for periods larger than 1 sec when there is a slight reduction.

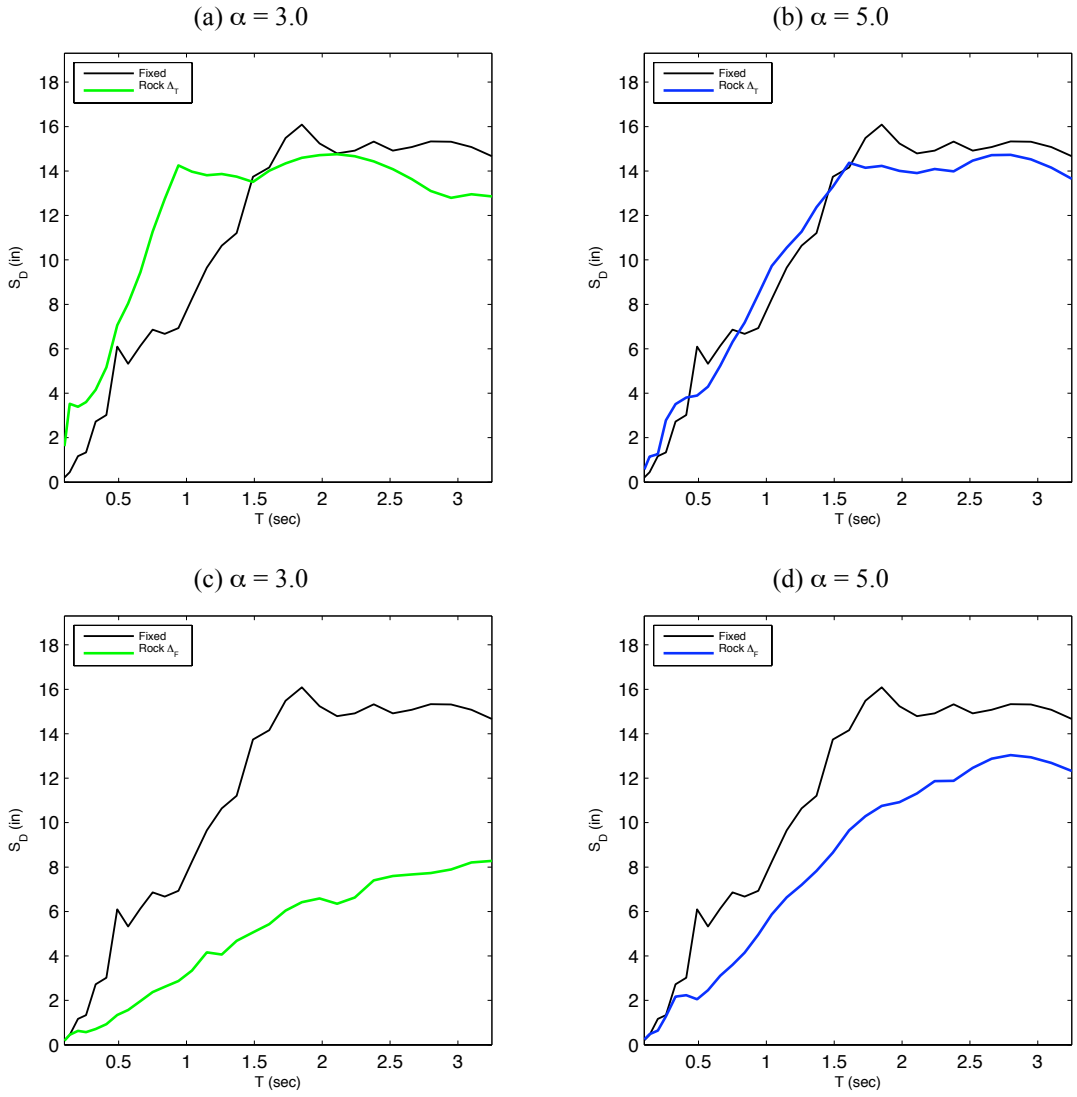

Figure 6-18: Spectral Displacement. Elastic Column-Soil. 1D excitation. (Oak_10_50_6)

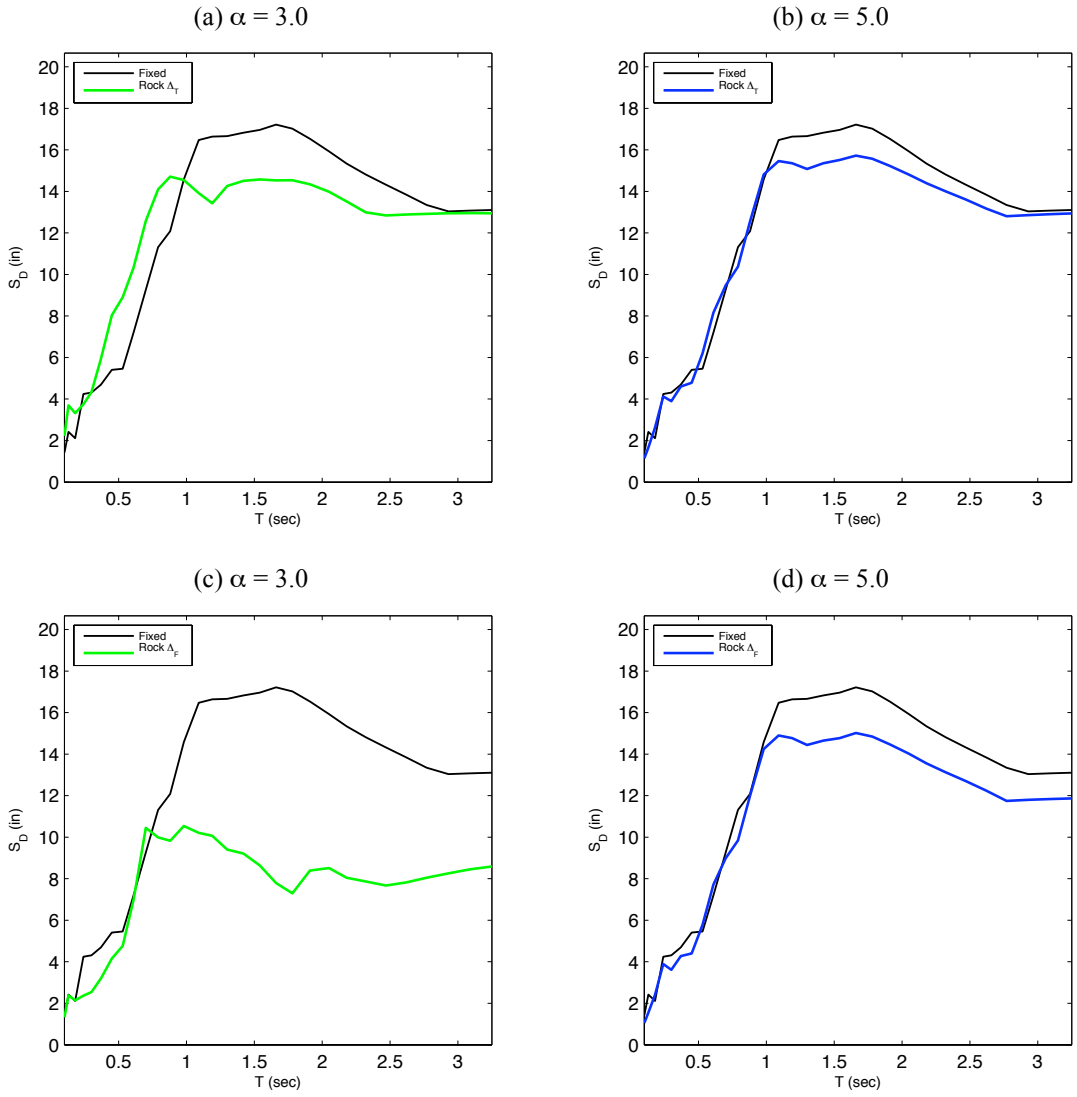

Figure 6-19: Spectral Displacement. Nonlinear Column-Elastic Soil. 1D excitation. (Oak_10_50_6)

6.5 Spectral Acceleration Response of Uplifting Bridge Pier System

The spectral acceleration response of uplifting bridge pier systems is presented in this section. The response for two combinations of analytic assumptions for column and soil are presented here. The first is elastic column and soil where there is no yielding in either element (Section 6.5.1). The second is a nonlinear column assumption with elastic soil. In this case the column may yield while the footing uplifts (Section 6.5.2). The nonlinear column-soil is not presented since significant yielding was found for only α=4 footing widths or smaller. The goal of this investigation is to compare a variety of uplifting systems to fixed base response. Future work on this topic is warranted. The spectral acceleration response quantity is measured at the center of mass of the superstructure for both x and y directions of the cantilevered system.

Ground motions used are those presented in Section 6.3.8. A more thorough description of the spectral response variables was given in Section 6.4.3 for a single ground motion. This section presents the median response for all hazard levels and ground motions considered. The following sections discuss the two types of uplifting systems analytic models subjected to one-dimensional and three-dimensional input excitation. To assess the spectral response of uplifting systems the mean response for each group of ground motions is presented. The mean response for spectral acceleration is plotted against individual dynamic test runs to illustrate the group response for a select ground motion group initially before displaying all mean group responses.

6.5.1 Elastic Column and Soil

The spectral acceleration response of uplifting bridge piers assuming elastic column and soil response is presented in the following sections. The total acceleration of the uplifting and corresponding fixed based systems are plotted to illustrate the amplification or reduction of the peak column acceleration as a function of column natural period.

Figure 6-20 illustrates the individual ground motion spectral acceleration mean responses and the response of the ten motions for the 10% in 50 year probability of exceedance 1D ground motions. Fixed base response is shown in (a) and uplifting system response with a footing to column width ratio of 3.0 as an example is shown in (b).

The mean responses for the four ground motion groups are compared to the fixed base response in Figure 6-21 through Figure 6-25. Each group has four associated footing widths related to uplifting footings.

(a) Fixed Base

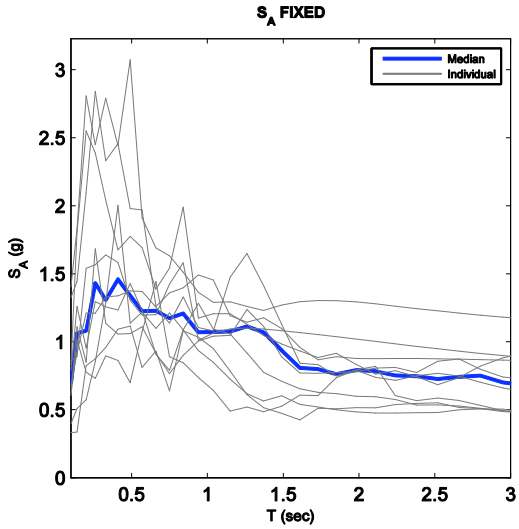

(b) Uplifting system α =3.0

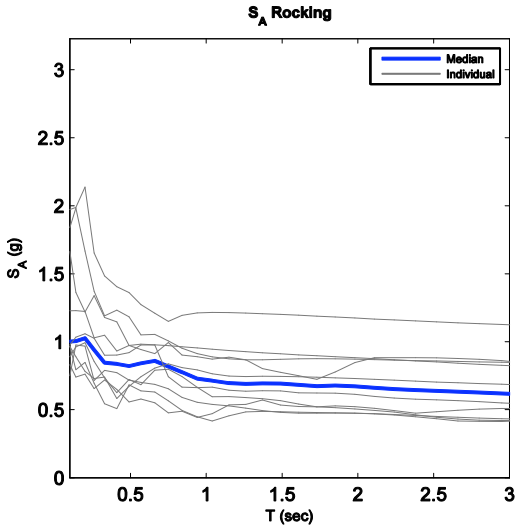

Figure 6-20: S_A Representative Mean Response. (10% in 50 years 1D)

6.5.1.1 1D Excitation

The spectral acceleration response of the single-degree-of-freedom system fixed at the base and allowed to uplift is presented in Figure 6-21. The ground motions evaluated are the X component of the four groups described in Section 6.3.8. Typically, the magnitude of acceleration is smaller, across all groups, for smaller footing widths. As footing size decreases, the reduction in acceleration relative to fixed-base response increases. This observation does not hold for very short period, stiff structures ranges. The near fault, 2% in 50, 10% in 50, and 50% in 50 year probability of exceedance groups all have accelerations larger than the fixed base at 0.25 secs or less (Figure 6-21 (a) – (d)).

The uplifting system amplifies the acceleration in the short period range. For longer period structures (T_{nf} = 2.0 secs.), the uplifting response approaches the fixed base response. As the footing width increases, the reduction in acceleration decreases. However, even for large footing widths (α=6) where there is not significant uplift the rocking motion of the system still dissipates some of the energy. The figures show that as the magnitude of the input excitation increases the amount of acceleration reduction is increased.

6.5.1.2 3D Excitation

The spectral acceleration response of the single-degree-of-freedom system to three-dimensional input accelerations of the four ground motion groups is presented in Figure 6-22 through Figure 6-25. Typically, allowing the footing to uplift reduces the peak accelerations, the smaller the footing the more the amount of reduction. As shown for the 1D input excitation at periods less than approximately 0.25 seconds, the acceleration of uplifting systems is actually larger. At periods of approximately 2.0 secs or longer, the uplifting response approaches the fixed base response.

Figure 6-22 illustrates the X and Y response of the near fault inputs. In the X direction there appears to be more acceleration reduction than the Y direction. However they both present acceleration reductions when allowed to uplift. For example, at T=1.0 secs for the α=3 footing the X and Y acceleration reduction is 1.3g/0.8g = 1.6 and 1.0g/0.6g = 1.67, respectively. In this case, the magnitudes of reduction are actually quite similar. The 1D X response (Figure 6-21(a)) and 3D X response are very similar, which indicates there may be little interaction for the near fault records.

The 2% in 50 acceleration response to 3D input is shown in Figure 6-23. There is a significant reduction in acceleration when allowing the footing to uplift especially for the α=3 footing. The 10 in 50 acceleration response is shown in Figure 6-24. The 50 in 50 is shown in Figure 6-25. The 3D input excitation does not seem to significantly alter the X direction magnitudes (Figure 6-21) for the elastic column-soil assumption.

See Section 6.8 for a discussion on the ratio of amplification of uplifting footings to fixed base response.

(a) Near Fault

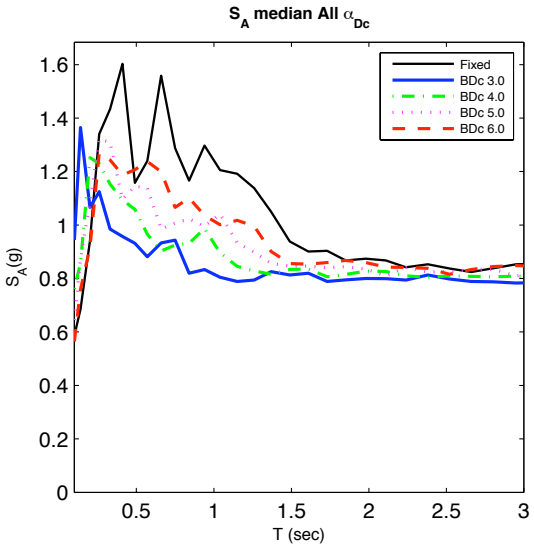

(b) 2 in 50

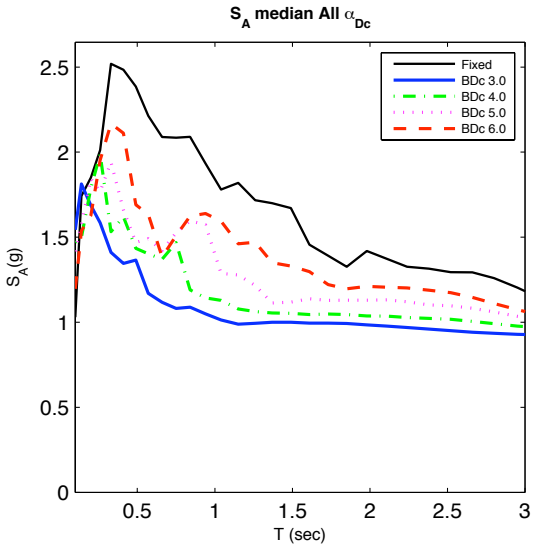

(c) 10 in 50

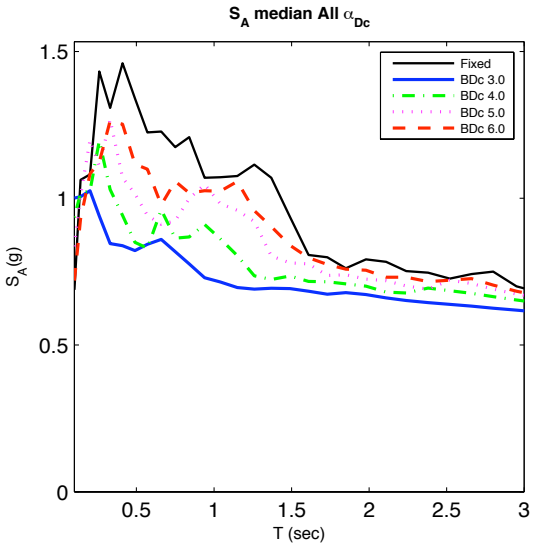

(d) 50 in 50

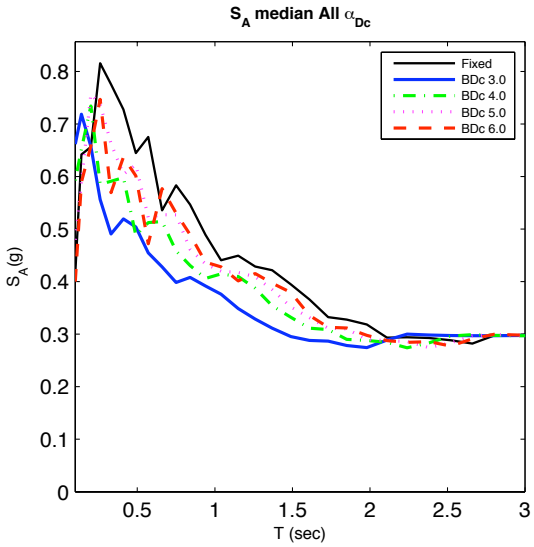

Figure 6-21: S_A Mean Response. Elastic Column-Soil. (All Ground Motions 1D)

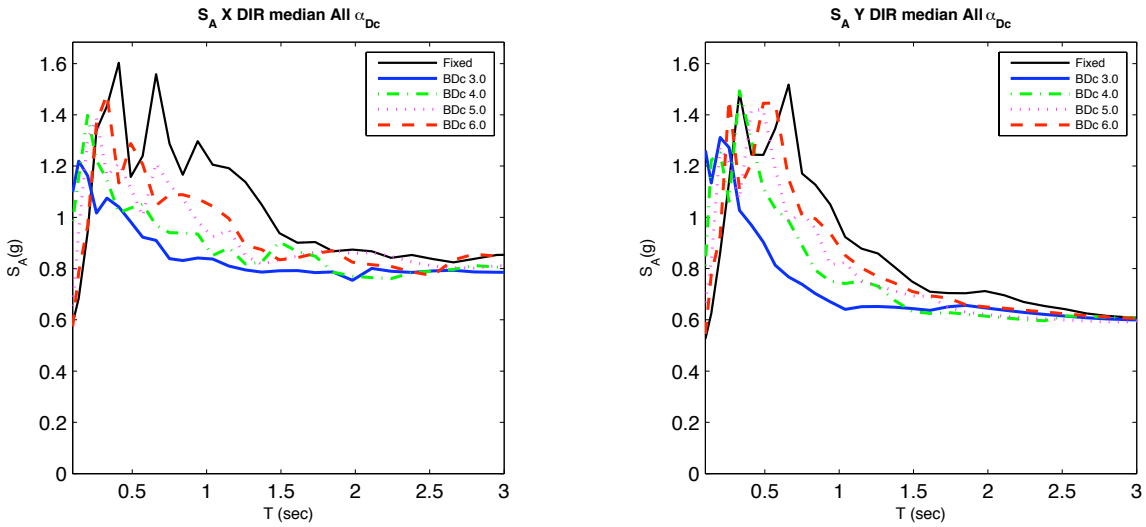

Figure 6-22: S_A Mean Response. Elastic Column-Soil. (Near Fault 3D)

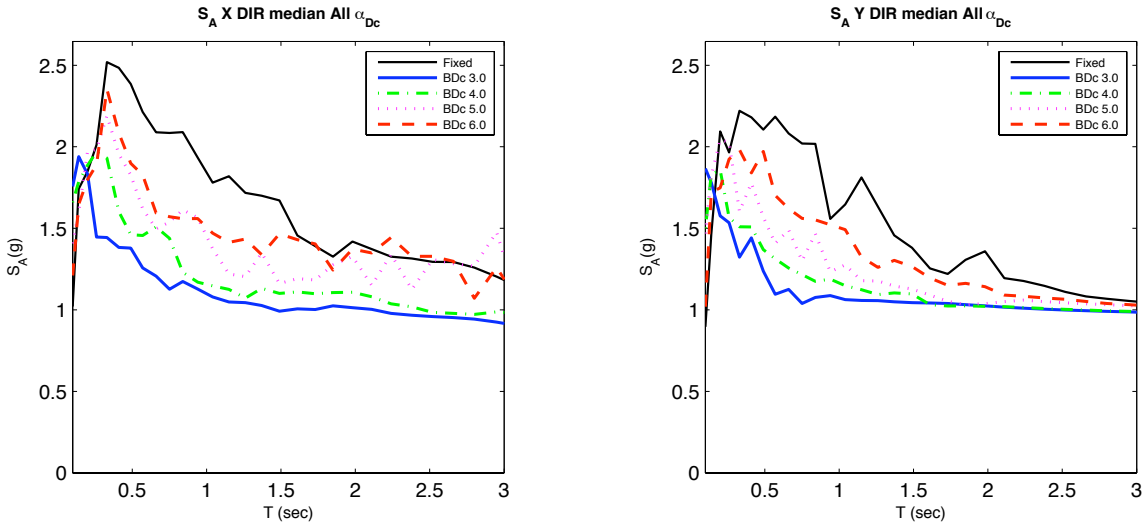

Figure 6-23: S_A Mean Response. Elastic Column-Soil. (2% in 50 years 3D)

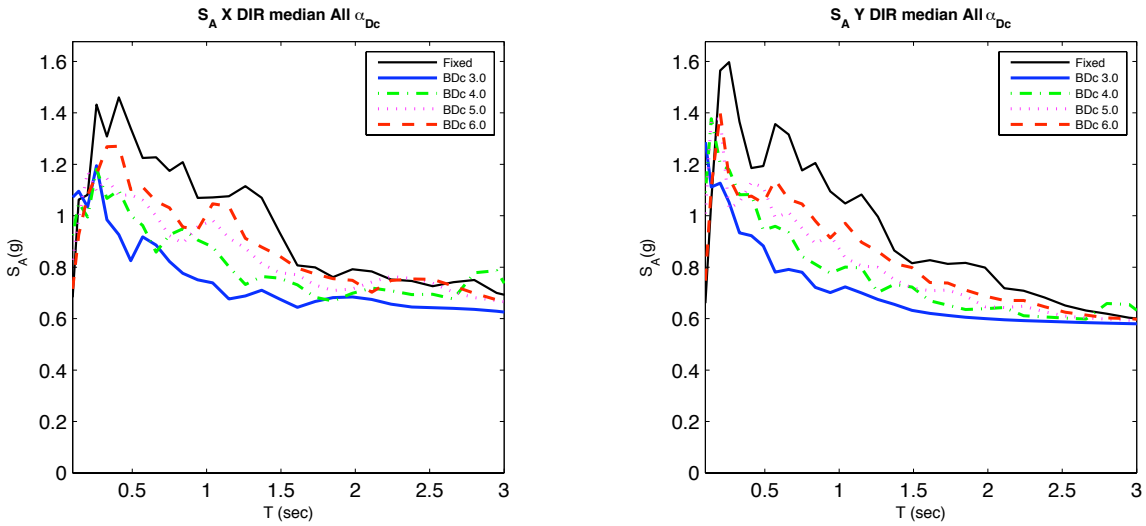

Figure 6-24: S_A Mean Response. Elastic Column-Soil. (10% in 50 years 3D)

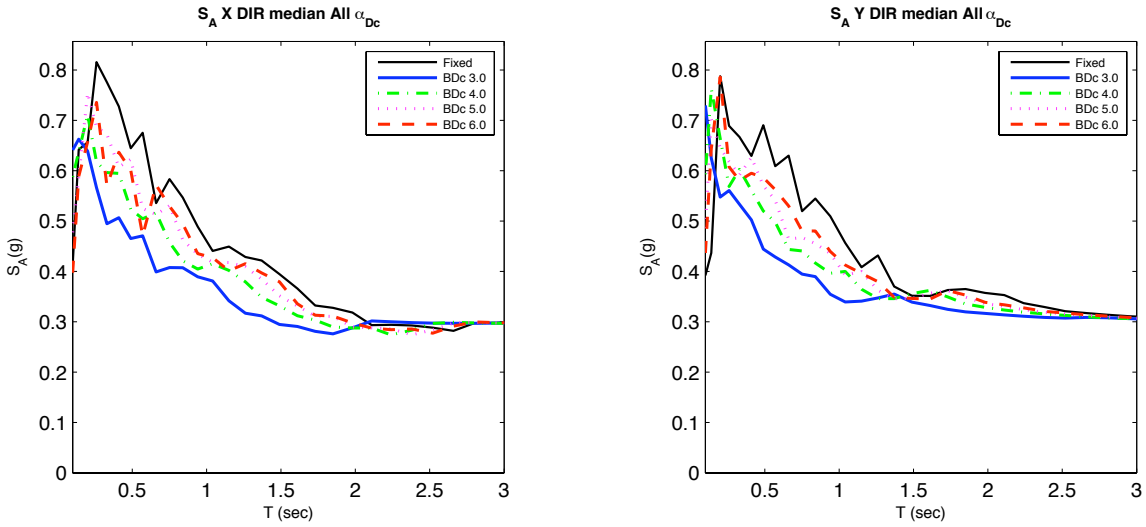

Figure 6-25: S_A Mean Response. Elastic Column-Soil. (50% in 50 years 3D)

6.5.2 Inelastic Column and Elastic Soil

Spectral acceleration response of the single degree of freedom system with nonlinear column and elastic soil model assumption is presented in this section. Figure 6-26 through Figure 6-29 show the 1D and 3D input excitation response for the three ground motion groups and the three footing widths. The 50% in 50 year probability of exceedance motions were not presented in this section, because the magnitude of nonlinear behavior was small. The α=6 footing width group is not presented either because the footing essentially acts as a fixed base system when nonlinear response is evaluated. The total displacements, moment-curvature and base shear are all very similar to the fixed base response for this footing width.

6.5.2.1 1D Excitation

The 1D spectral acceleration response for nonlinear column and soil is presented in Figure 6-26. The plots (a)-(c) show the Near Fault, 2 in 50, and 10 in 50 acceleration responses. Typically, these footings all have identical acceleration at periods of 1.0 sec or larger. Which differs from the elastic column-soil assumption (Section 6.5.1). It can be inferred that the uplifting systems are reaching the acceleration at which yield occurs and no more force is being developed in the system.

For period ranges less than 1.0 seconds typically the uplifting systems are developing slightly larger accelerations, especially for the α=3 footing widths. The α=4 and 5 footing widths approach the fixed base response. The increase in this range is on the order of 30-100%. While these are relatively large percentage increases, they may be small for the system. A refined analysis which includes displacements of the system for this period range will assist in answering if uplifting of nonlinear columns-elastic soil is viable. See Section 6.8 for more discussion.

6.5.2.2 3D Excitation

The acceleration response of the nonlinear column-elastic soil model subjected to 3D input excitation is presented in Figure 6-27 through Figure 6-29 for the three ground motion groups. Typically, the fixed base and uplifting systems have very similar response for the periods of 1.0 secs or larger. At less than 1.0 secs, the uplifting systems have slightly larger accelerations. The peak percentage increase is approximately 20-30% for the 3D input excitation, which is less than the 1D input excitation. The α=3 footing width appears to have the largest increase relative to the fixed base. The α=4 and 5 widths more close resemble the fixed base. When compared to the 1D input excitation the magnitude of acceleration is reduced, indicating the Y component affects the response of the column. This is likely due to more inelastic response occurring in the Y direction and further dissipating the input energy.

It appears that in both directions of input for the three ground motion groups the column is reaching the acceleration at which yield occurs and developing no further acceleration. This does not answer how much inelastic action occurs, only that there is some. The amount of inelasticity may better be answered by evaluating displacements of the system. For example, the ductility of the uplifting and fixed base systems may be

different. See Section 6.8 and 6.9 for a discussion of displacement response for uplifting and fixed base systems.

(a) Near Fault

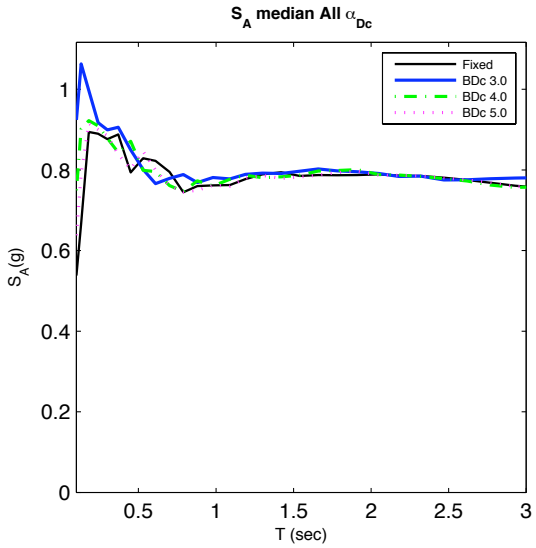

(b) 2 in 50

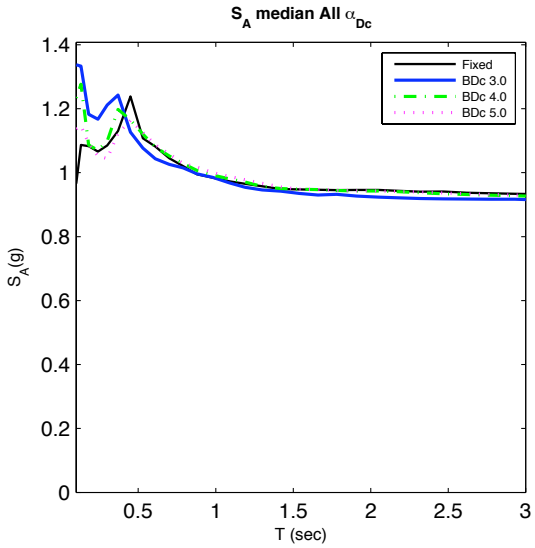

(c) 10 in 50

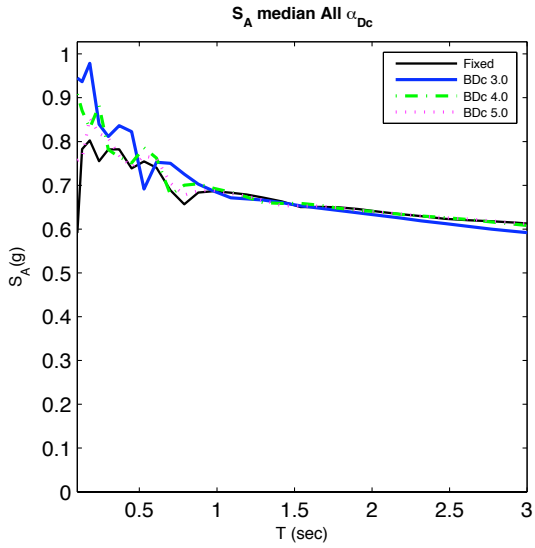

Figure 6-26: S_A Mean Response. Nonlinear Column-Elastic Soil. (All Ground Motions 3D)

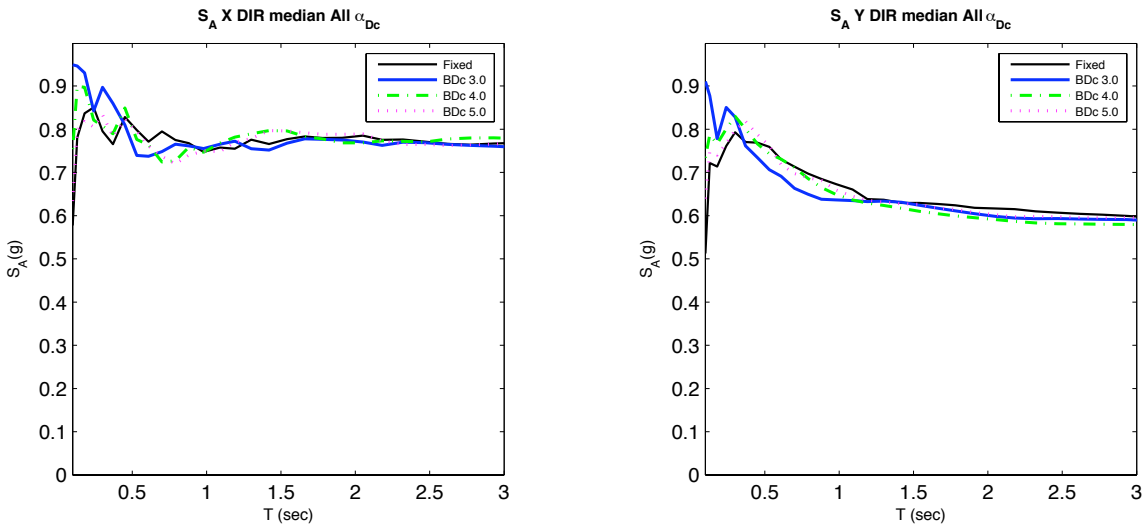

Figure 6-27: S_A Mean Response. Nonlinear Column-Elastic Soil. (Near Fault 3D)

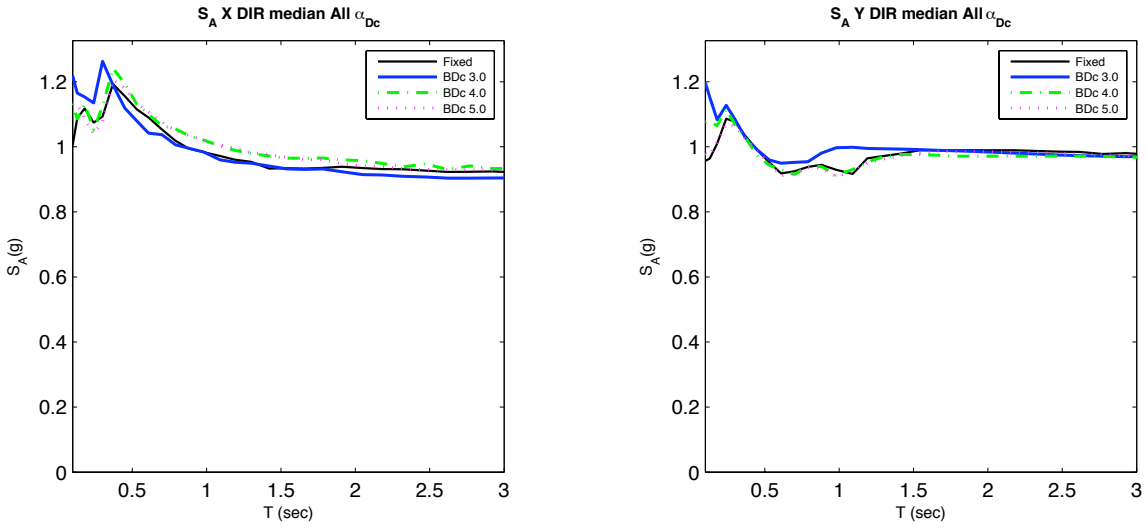

Figure 6-28: S_A Mean Response. Nonlinear Column-Elastic Soil. (2% in 50 years 3D)

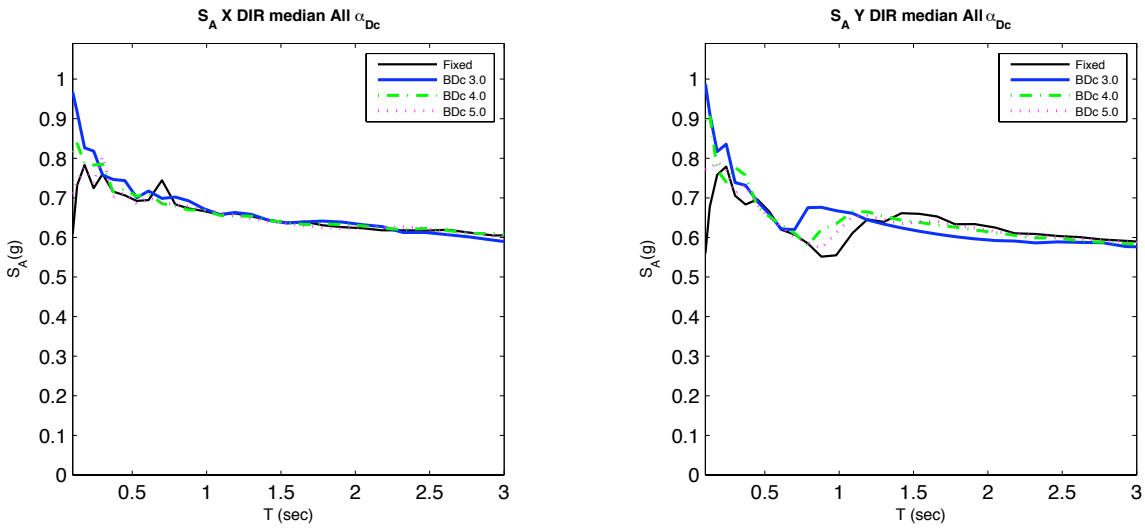

Figure 6-29: S_A Mean Response. Nonlinear Column-Elastic Soil. (10% in 50 years 3D)

6.6 Spectral Displacement Response of Uplifting Bridge Pier System

The spectral displacement response of the uplifting system for the two analytic column and soil combinations considered is presented in the following sections. As described in the representative case in Section 6.4.3, the two types of column displacement of uplifting systems are presented against the fixed base response.

The intent is to illustrate the relative response between the uplifting and fixed base response and highlight benefits and drawbacks. As is expected, the rocking response will approach the fixed base response as the footing width increases. To simplify the presentation, only the total and flexural rocking components will be shown compared to the fixed base. The rocking component of response may be inferred from the total and flexural column displacement presented. Also the response for each footing width will be presented on one plot for each ground motion group to assist in presentation.

6.6.1 Elastic Column and Soil

Figure 6-30 shows the mean response determination for the 10% in 50 year probability of exceedence group assuming a footing to column width ratio of 3.0. The plot in (a) shows the fixed base response, (b) the total rocking response, (c) the flexural component of total rocking response, and (d) the rocking component of total rocking response. It should be noted the amount of flexural column displacement for uplift is very uniform despite the wide variance of total rocking displacement and column displacement from footing uplift.

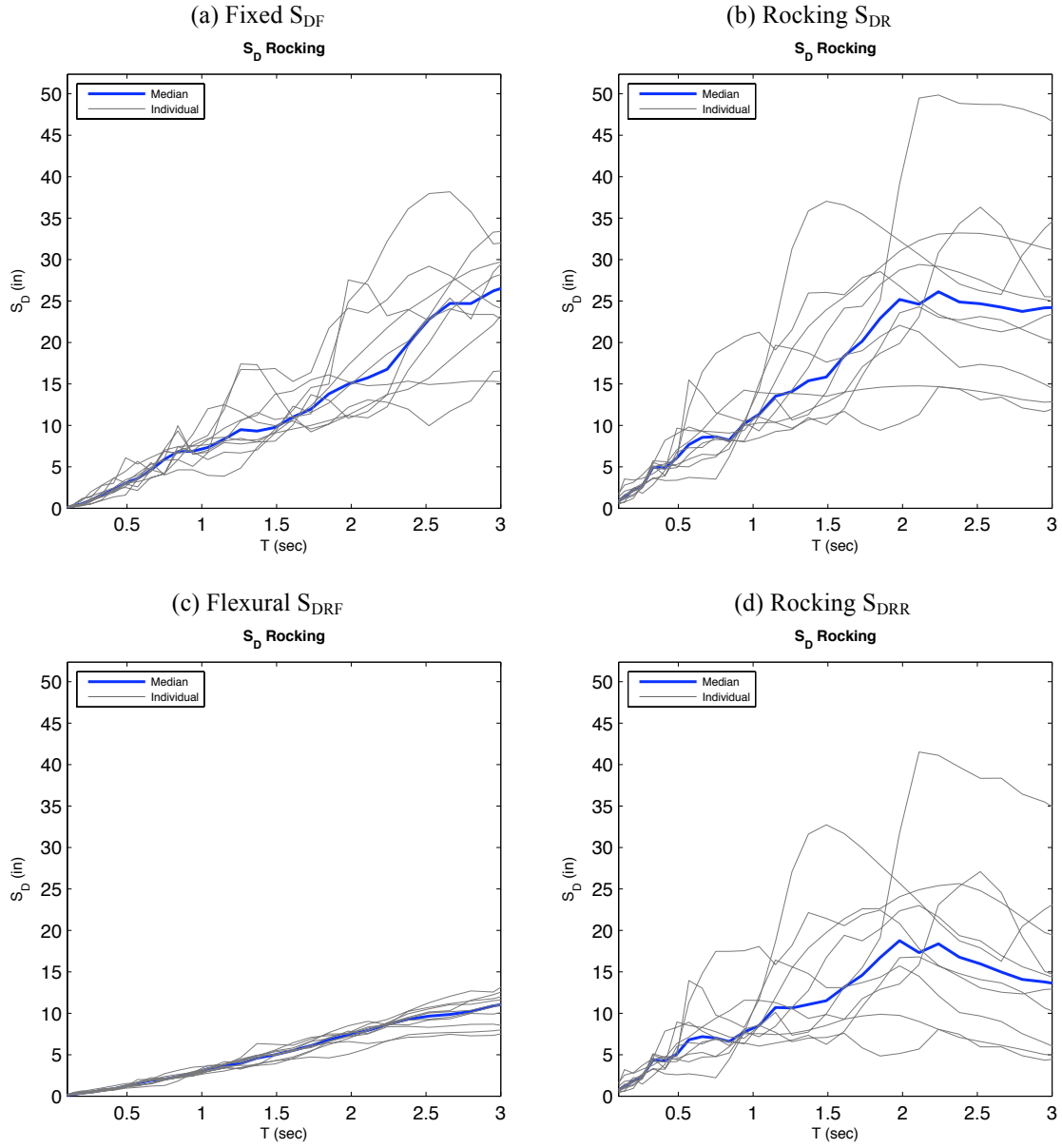

Figure 6-30: S_D Representative Mean Response. (10% in 50 years 1D)

6.6.1.1 1D Excitation

The uplifting system displacement response for the four ground motion groups subject to the 1D X input excitation is presented in Figure 6-31 through Figure 6-34. The total displacements are compared in the (a) figure and the column flexural displacements are presented in the (b) figure.

Total column displacements of the uplifting systems are typically larger than the fixed base response. Figure 6-31(a) shows the Near Fault ground motion group. The α=3 footing is larger for the period range shown while the α=6 is approximately the same as

fixed base. The 2% in 50 year response also has larger total displacements than the fixed base however they converge at approximately 2.5 secs and larger and become smaller magnitude. The 10% in 50 and 50% in 50 year also have larger uplifting response. For a structure with T_{nf}=1.5 secs, the ratio of uplifting to fixed base total displacement for α=3 is approximately 1.18-2.31, for the four footing groups as an example. As the footing width increases, all total displacements approach the fixed base response.

The amount of column flexural displacement is consistently less than the fixed base response. Indicating allowing uplift reduces the amount of column flexural displacement and likely the inelastic response for a wide range of footing widths. This shows that if the fixed base system can accommodate the total predicted displacement when uplifting there is a likely benefit in reduced column response.

See Section 6.8 for the comparison of rocking displacement to fixed base ratios as a function of period.

6.6.1.2 3D Excitation

The spectral displacement response to the 3D input excitation for the four ground motion groups is presented in Figure 6-35 through Figure 6-38. The (a) plot shows the X and Y total displacements and the (b) plots shows the X and Y column flexural displacements.

Typically, the total displacement of uplifting systems is greater than the fixed base response. As was shown in the 1D discussion of displacements the α=3 footing has more total displacement than the α=6 footing for all ground motions. The amount of displacement amplification appears to be similar to the 1D response; on the order of 1-2 times larger. Column flexural displacement is consistently less than the fixed base response, indicating less flexural demand on the column and a likely reduction in inelastic response.

The interaction of displacements from multi-directional input is not readily apparent. It appears that the 1D and 3D X response are relatively similar. The comparison of the ratios of uplift to fixed base displacements in Section 6.8 will further discuss the relationship. It appears that the smaller the excitation the less the amount of uplift that occurs. The 2% in 50 year results appear to have more uplift than the 10% in 50 year ones, which in turn has more than the 50% in 50 year response. The near fault motions seem to have larger rocking response in the period range matching the pulse period of the near fault motions.

(a) S_{DR} (b) S_{DRF}

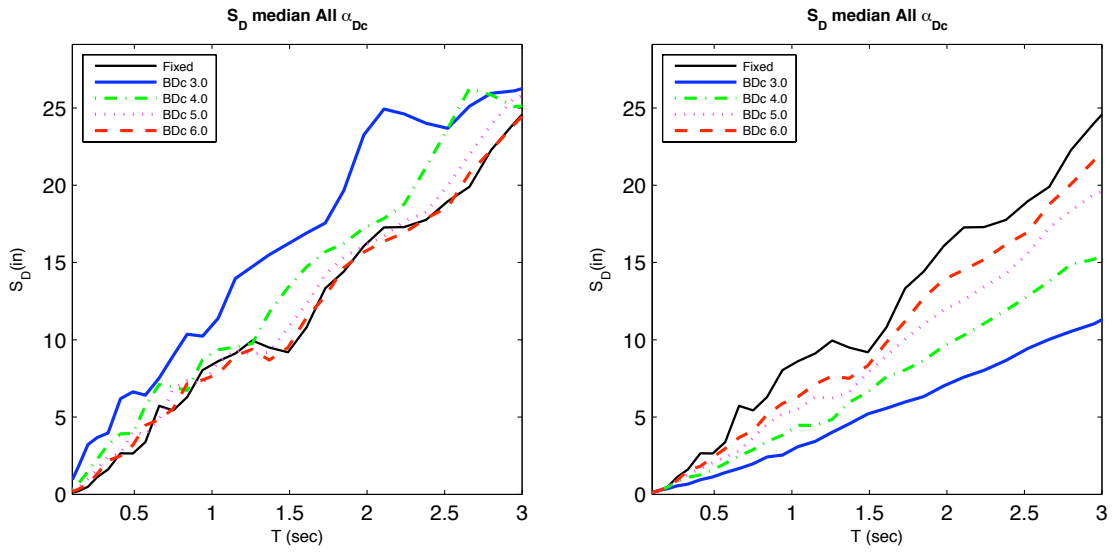

Figure 6-31: S_D Mean Response. Elastic Column-Soil. (Near Fault 1D)

(a) S_{DR} (b) S_{DRF}

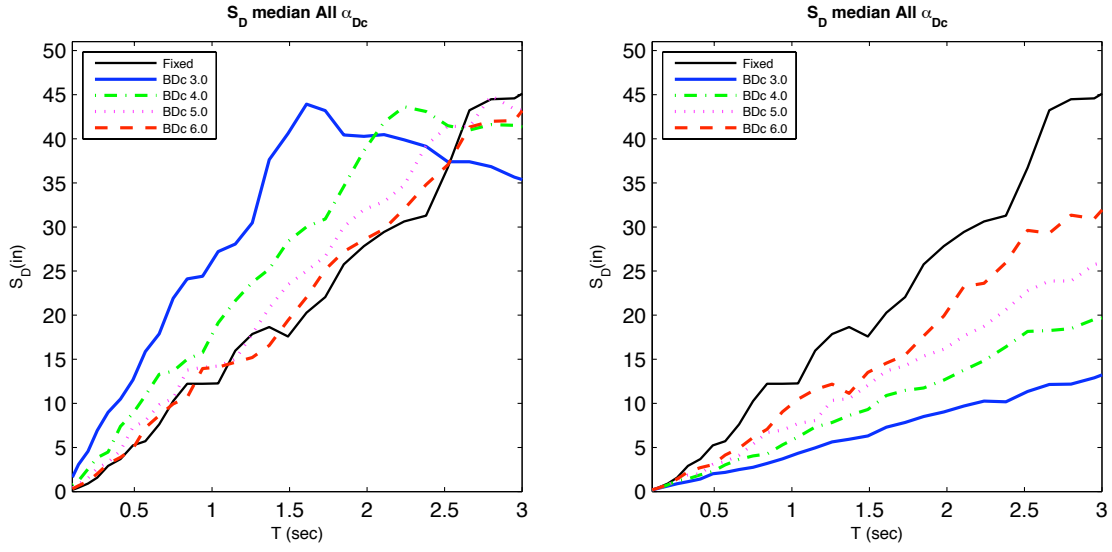

Figure 6-32: S_D Mean Response. Elastic Column-Soil. (2% in 50 years 1D)

(a) S_{DR} (b) S_{DRF}

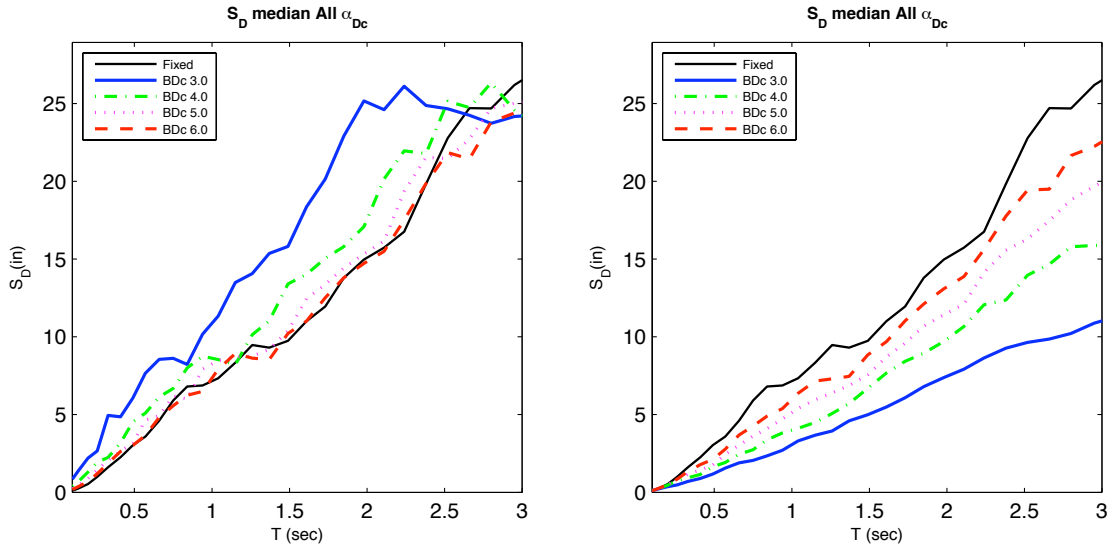

Figure 6-33: S_D Mean Response. Elastic Column-Soil. (10% in 50 years 1D)

(a) S_{DR} (b) S_{DRF}

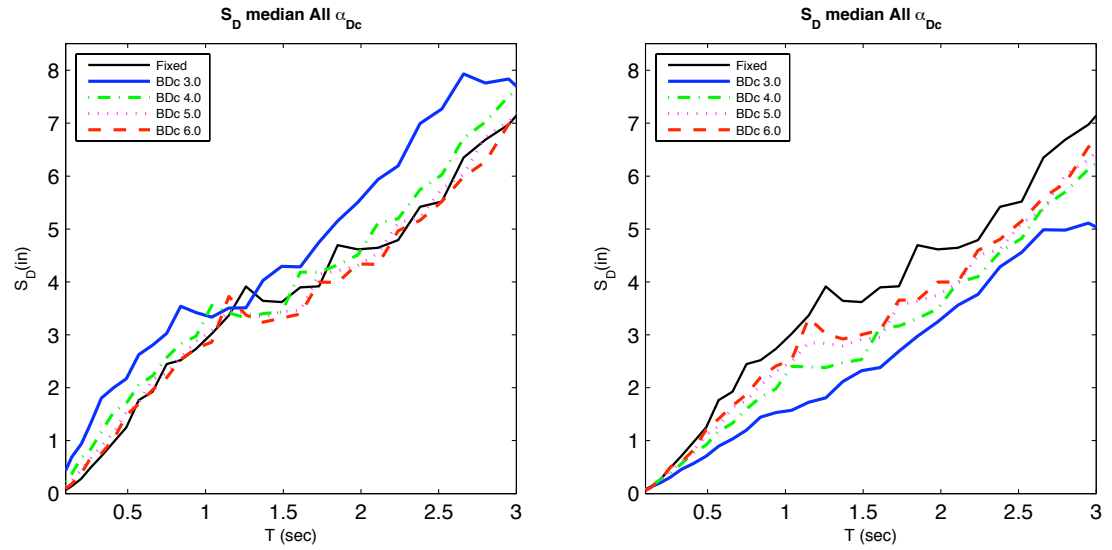

Figure 6-34: S_D Mean Response. Elastic Column-Soil. (50% in 50 years 1D)

(a) S_{DR}

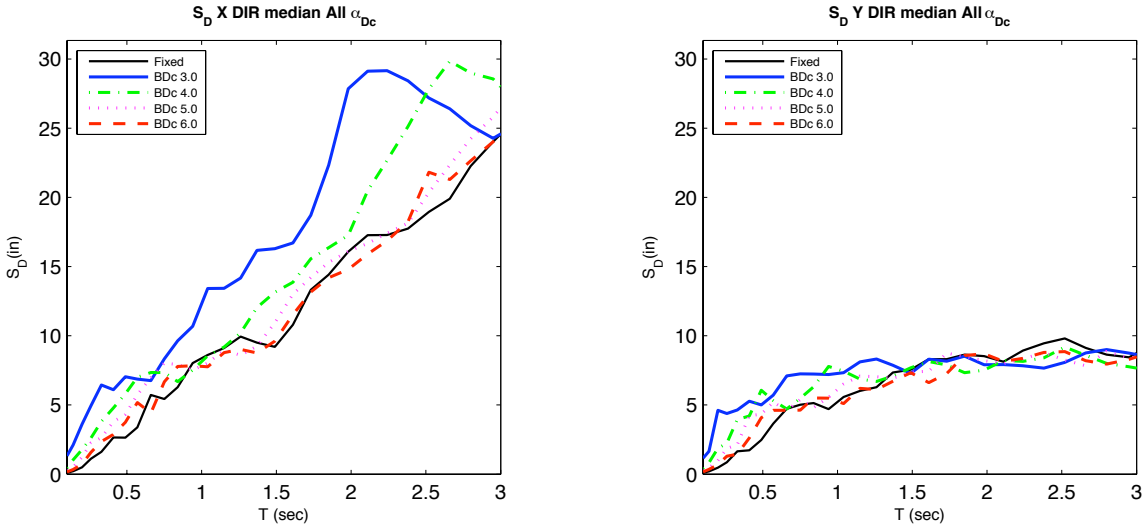

(b) S_{DRF}

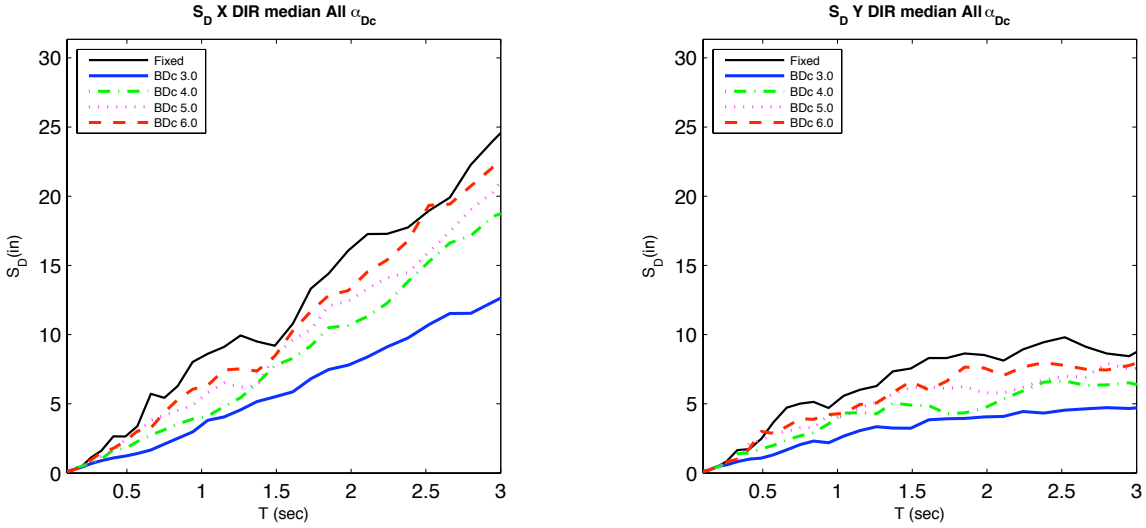

Figure 6-35: S_D Mean Response. Elastic Column-Soil. (Near Fault 3D)

(a) S_{DR}

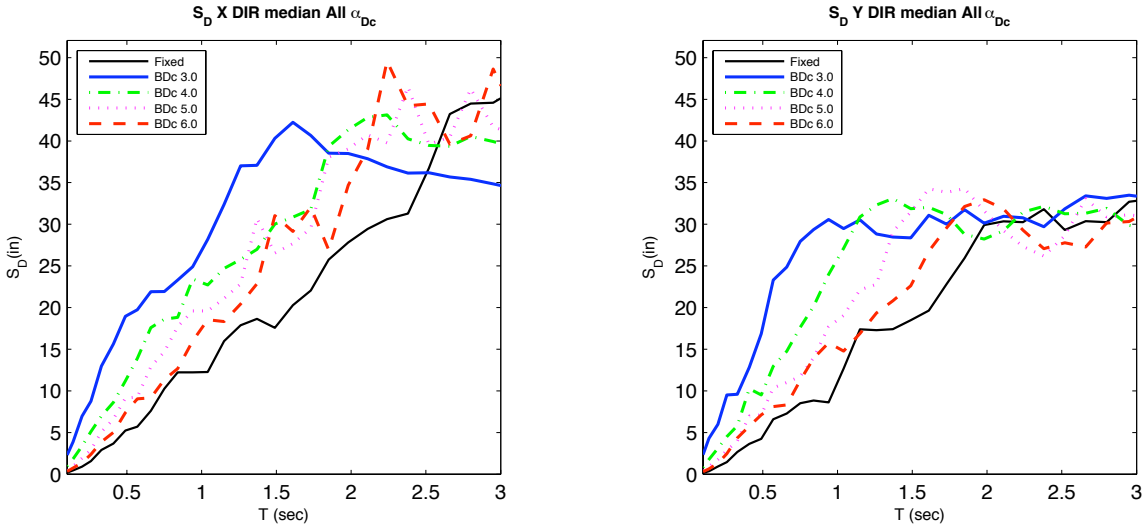

(b) S_{DRF}

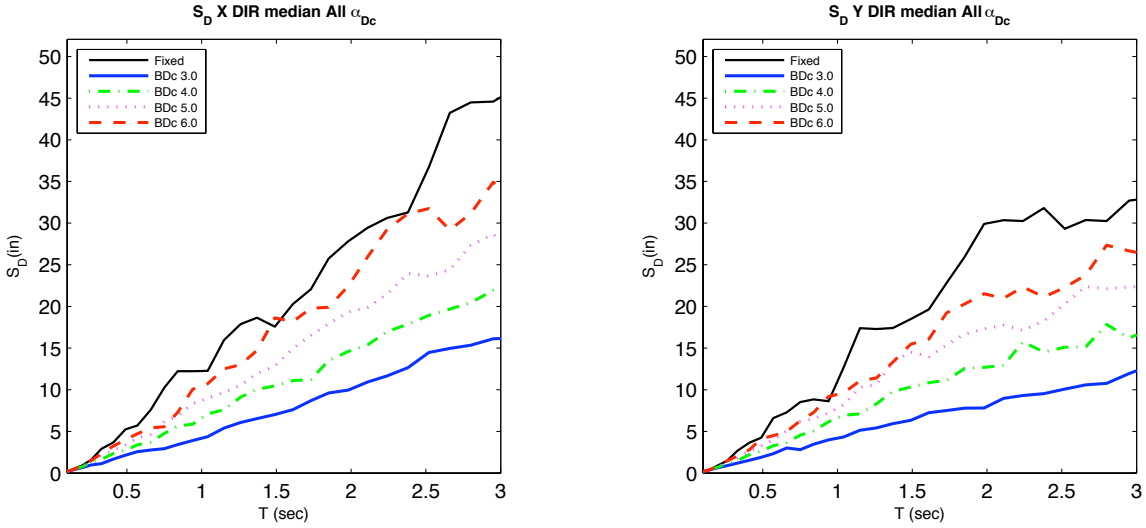

Figure 6-36: S_D Mean Response. Elastic Column-Soil. (2% in 50 years 3D)

(a) S_{DR}

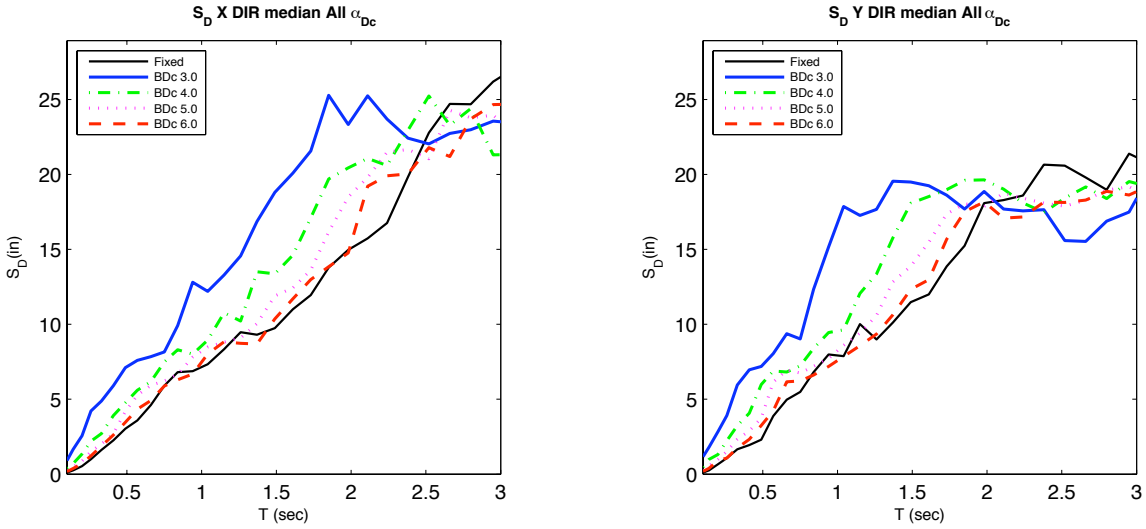

(b) S_{DRF}

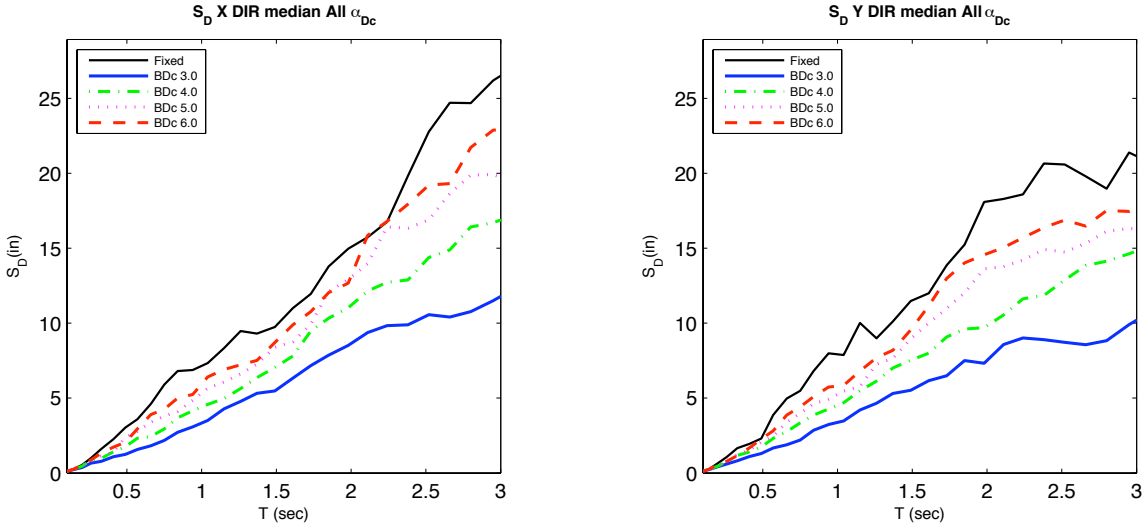

Figure 6-37: S_D Mean Response. Elastic Column-Soil. (10% in 50 years 3D)

(a) S_{DR}

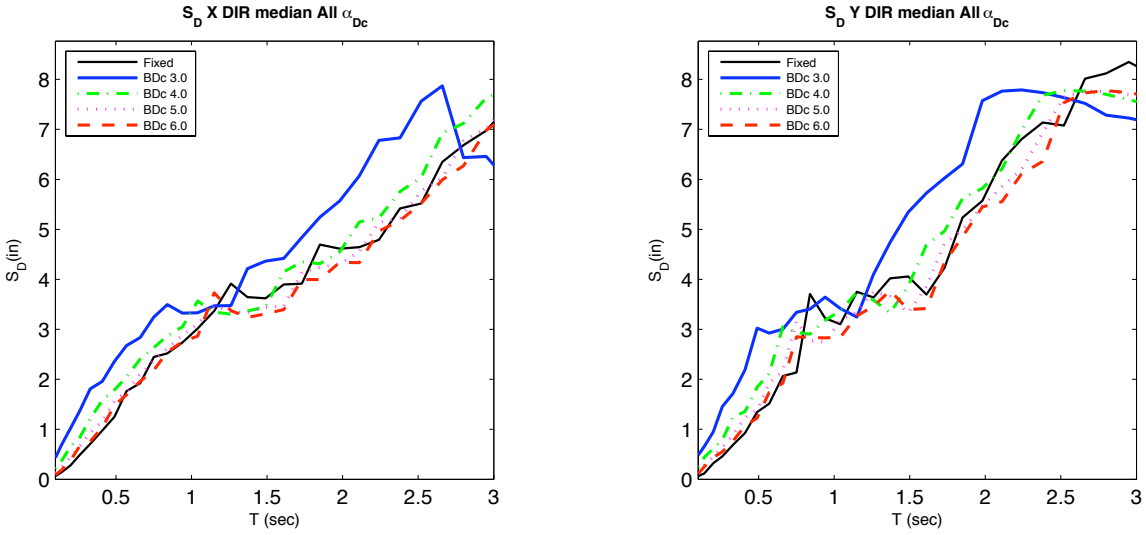

(b) S_{DRF}

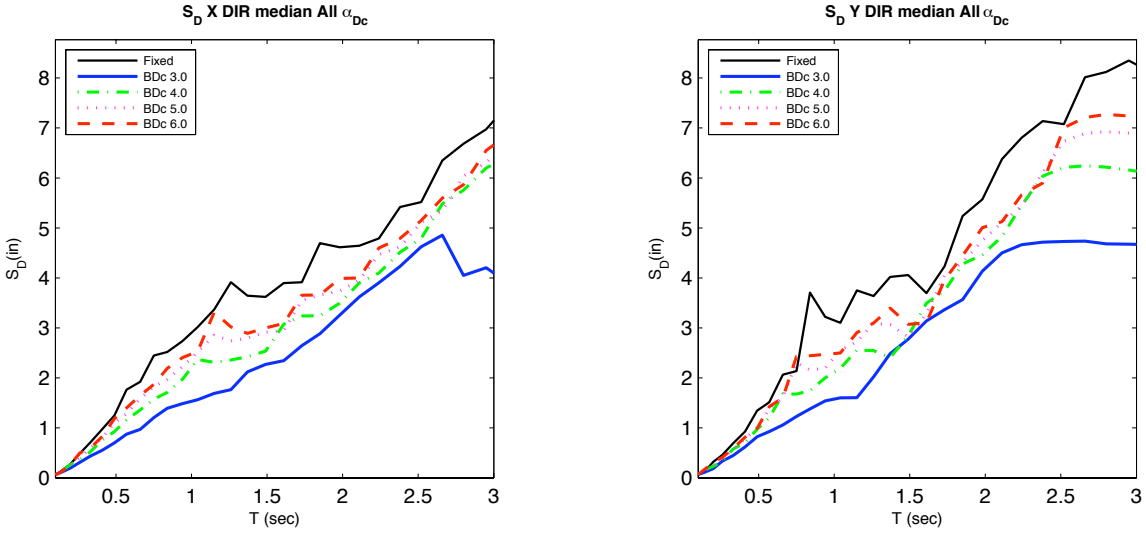

Figure 6-38: S_D Mean Response. Elastic Column-Soil. (50% in 50 years 3D)

6.6.2 Inelastic Column and Elastic Soil

The response of uplifting footings assuming nonlinear column and elastic soil model assumption is presented in the following section. The ground motions used are the same as described in the Section 6.6.1. The total and column flexural displacements of uplifting systems are plotted against the fixed base response. As was discussed in Section 6.5.2.2, the 50% in 50 year ground motion is not presented and the α=6 footing width is excluded.

6.6.2.1 1D Excitation

Displacement response of the uplifting system to 1D X input excitation is presented in Figure 6-39 through Figure 6-41. The consideration of inelastic action appears to alter the response of the total displacement, which is shown in plot (a). For each ground motion group the total displacements are approximately equal for the 0 to 1.5 second range. However, for the 2% in 50 year and 10% in 50 year motions, the total displacement of uplifting systems is less than the fixed base response at periods greater than 1.5 seconds.

The column flexural displacements are also very similar for periods less than or equal to 1.5 seconds. As shown in the (b) plots. At periods larger than 1.5 seconds the amount of column displacement is less than the fixed base response, indicating a reduction in inelastic action at this range. In general, the α=3 footings have the smallest column flexural displacements and get progressively larger as the footing width increase. However they do not reach the level of fixed base response for these footing widths.

Section 6.7 presents the ductility response of uplifting columns and Section 6.8 presents the ratio of displacements for uplifting and fixed base response.

6.6.2.2 3D Excitation

The displacement response of uplifting footing to 3D input excitation is presented in Figure 6-42 through Figure 6-44. The (a) plots show the total response and the (b) plots show the column flexural displacement. The X and Y components of displacement are presented for each ground motion group.

The total displacements are similar for the X and Y direction for the fixed base and the three footing widths considered. Typically the α=3 footing width had smaller displacements but not significantly smaller than the other footing widths and fixed base response. The exception is the Y direction of the 2% in 50 year group which had a larger discrepancy compared to fixed base response than the others.

The column flexural displacements in the X direction are similar to the 1D excitation response. The fixed base and uplifting systems are approximately the same for 0 to 1.5 second period structures. At periods larger than 1.5 seconds, the uplifting footing systems have smaller displacements. The Y direction is similar. However, the amount of reduction at 1.5 secs appears to be less. This may be due to smaller excitation accelerations in the Y direction. This result is also observed for the difference between ground motion groups 2%, 10%, and 50% probability of exceedance.

Sections 6.8 and 6.9 have further discussion on the relationship between displacement demands of uplifting and fixed base systems.

(a) S_{DR} (b) S_{DRF}

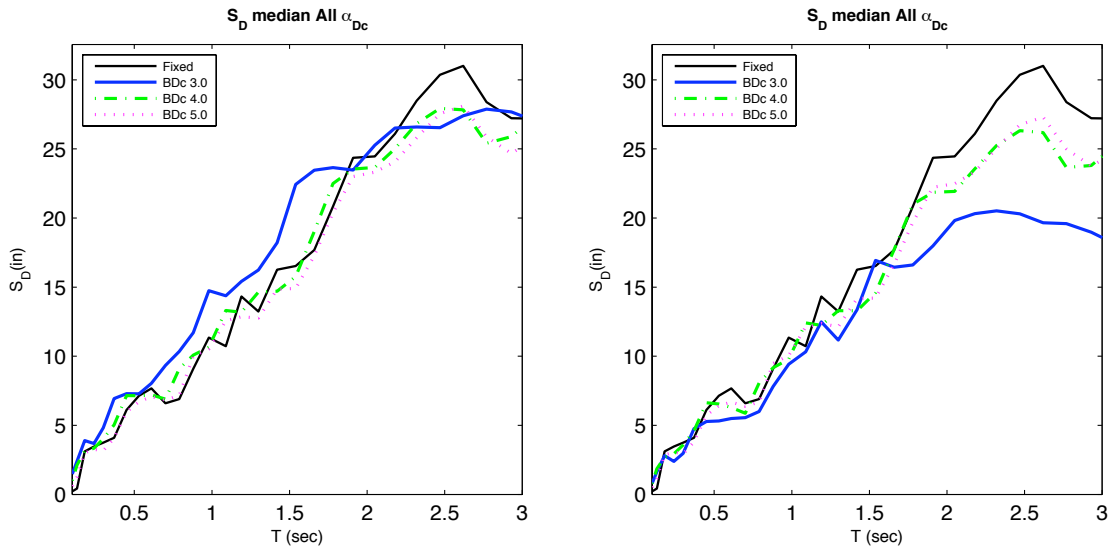

Figure 6-39: S_D Mean Response. Nonlinear Column-Elastic Soil. (Near Fault 1D)

(a) S_{DR} (b) S_{DRF}

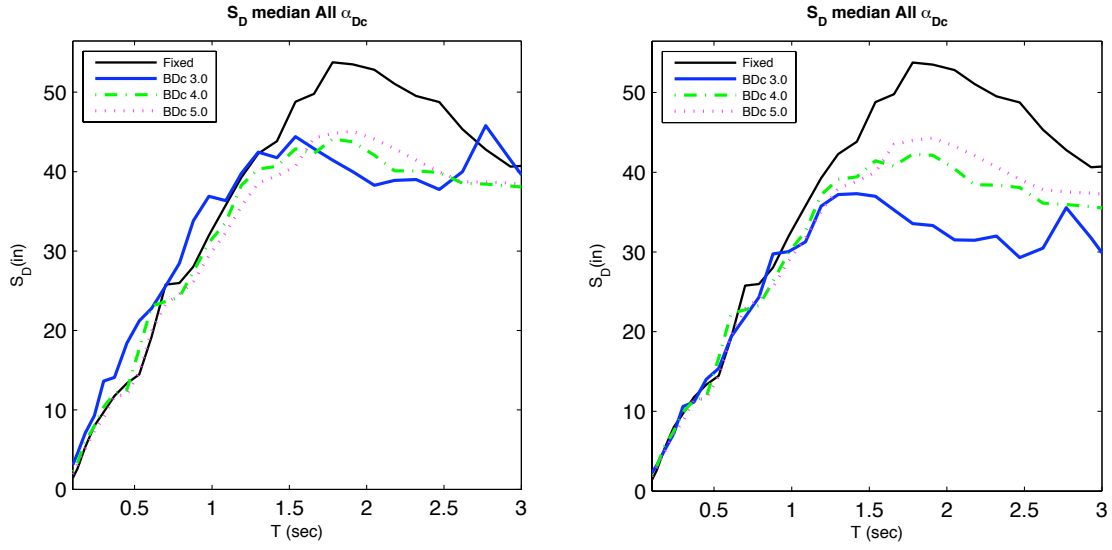

Figure 6-40: S_D Mean Response. Nonlinear Column-Elastic Soil. (2% in 50 years 1D)

(a) S_{DR} (b) S_{DRF}

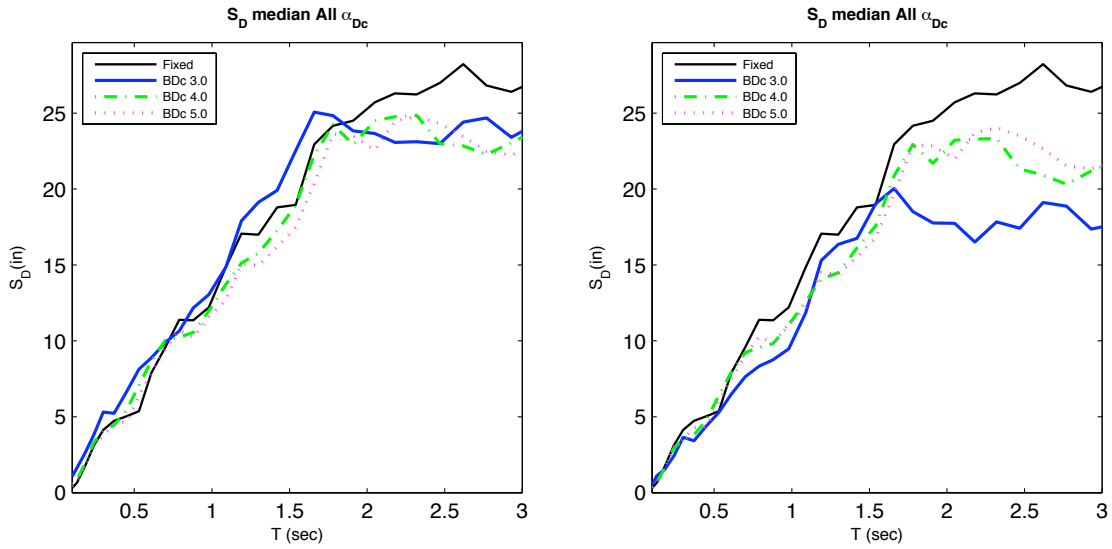

Figure 6-41: S_D Mean Response. Nonlinear Column-Elastic Soil. (10% in 50 years 1D)

(a) S_{DR}

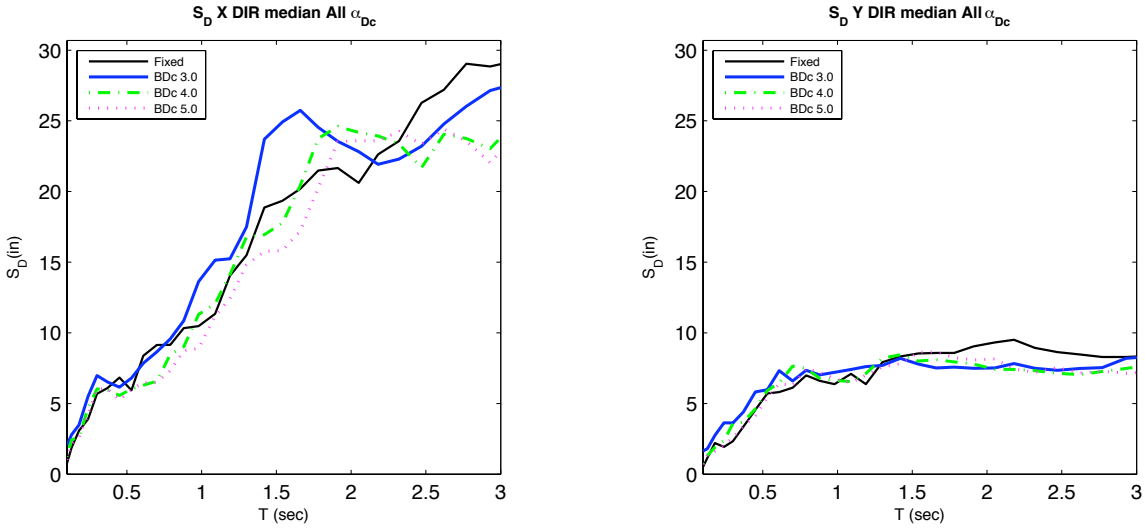

(b) S_{DRF}

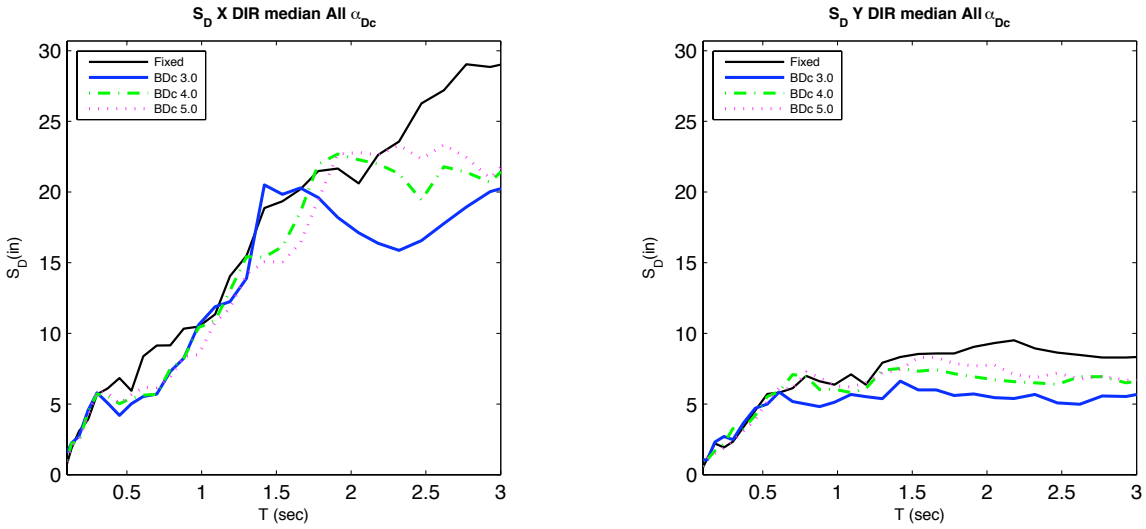

Figure 6-42: S_D Mean Response. Nonlinear Column-Elastic Soil. (Near Fault 3D)

(a) S_{DR}

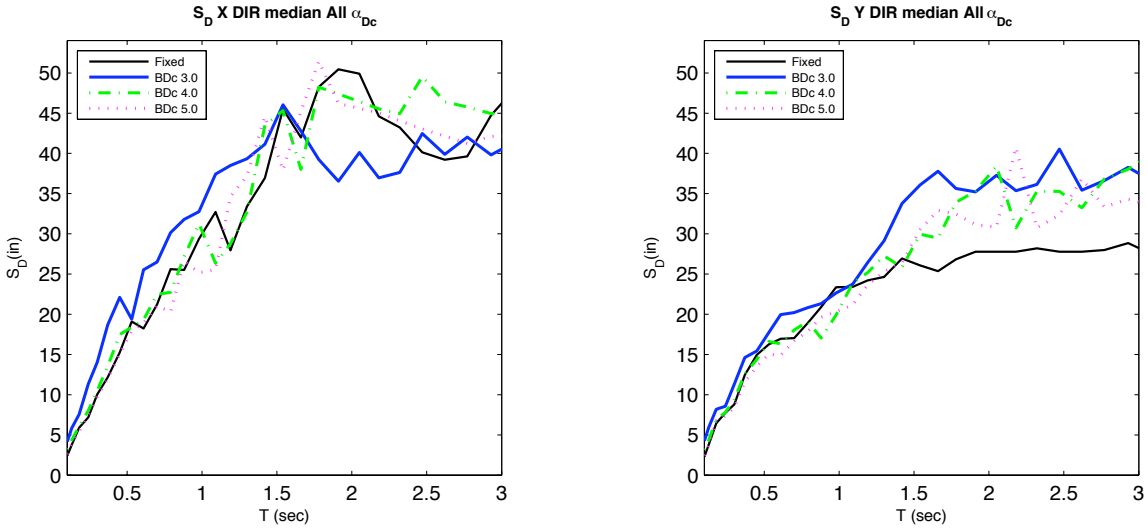

(b) S_{DRF}

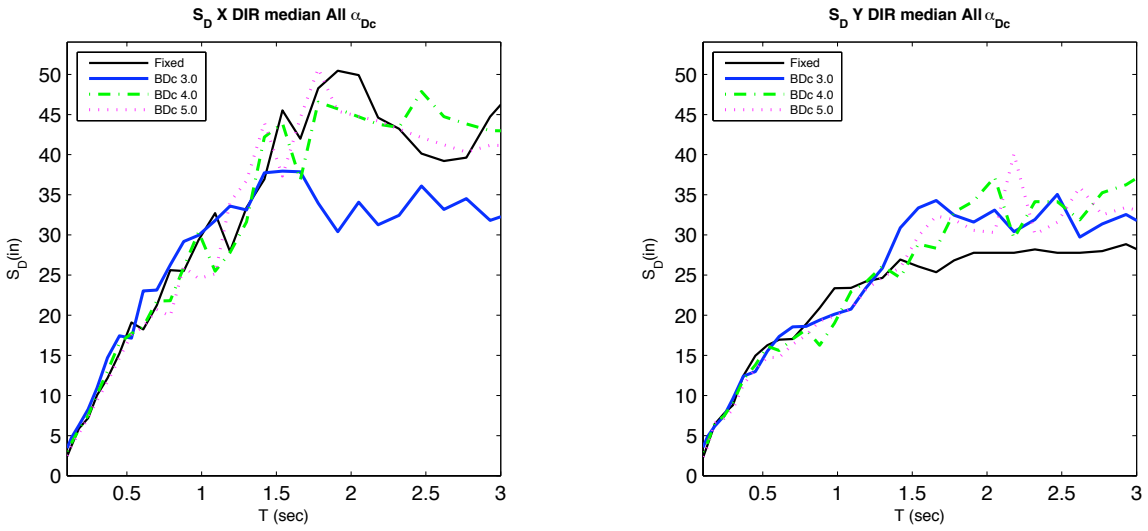

Figure 6-43: S_D Mean Response. Nonlinear Column-Elastic Soil. (2% in 50 years 3D)

(a) S_{DR}

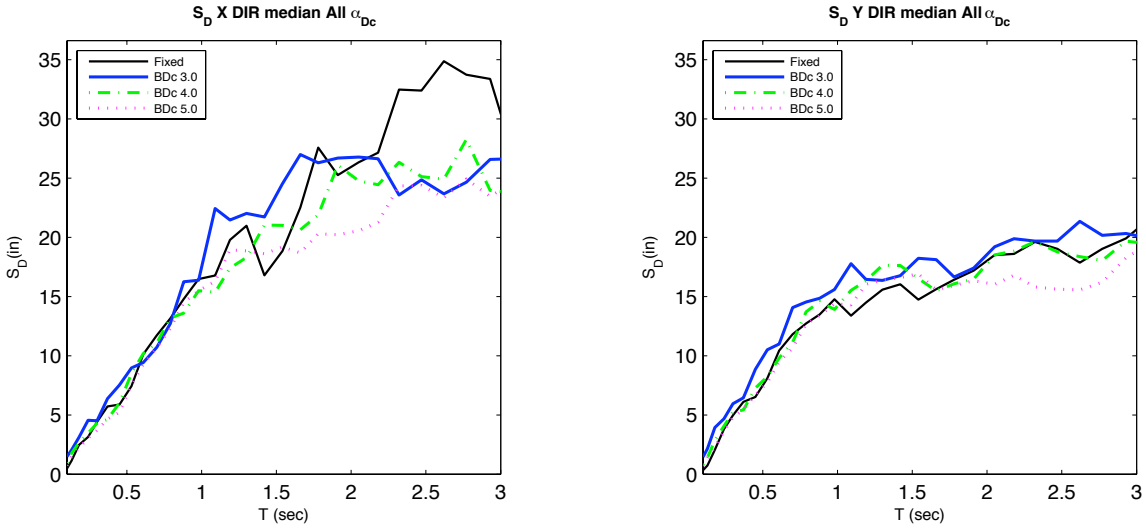

(b) S_{DRF}

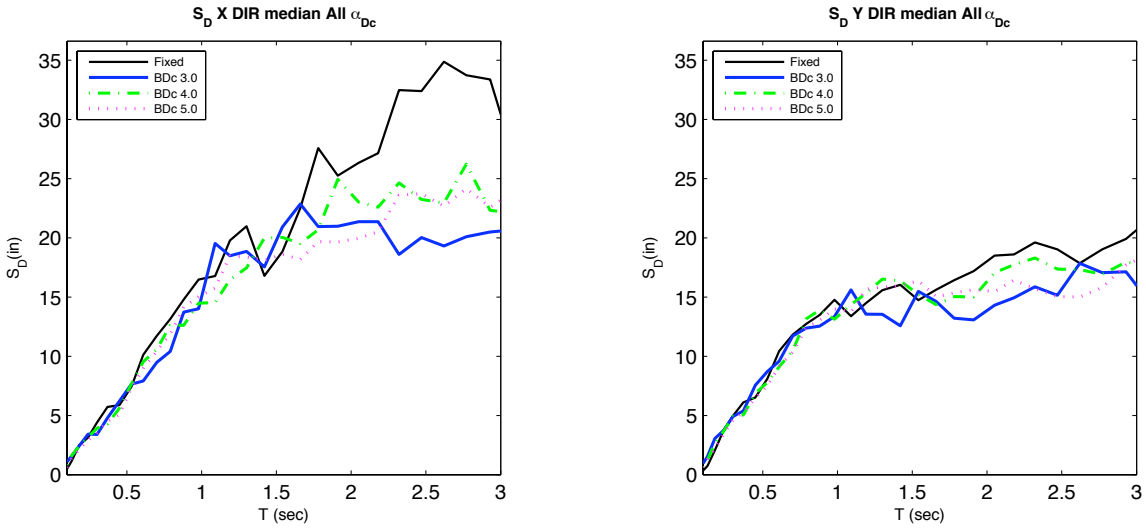

Figure 6-44: S_D Mean Response. Nonlinear Column-Elastic Soil. (10% in 50 years 3D)

6.7 Displacement Ductility Response of Uplifting Bridge Pier System

Ductility response of the uplifting and fixed column bases are compared in this section for the nonlinear column - elastic soil model. Ductility values for the three ground motion groups and footing widths are plotted in Figure 6-45 based on the mean spectral displacement presented in Section 6.7.

The displacement ductility of the fixed base column is calculated using the standard ratio of total column displacement to column yield displacement (Eqn. (6-4)).

$$\mu = \frac{u_{total}}{u_{yield}} \qquad (6\text{-}4)$$

The uplifting system displacement ductility is estimated in Eqn. (6-5). as the ratio of column flexural displacement to column yield displacement. It is more accurate to use the column curvature deformation ductility (Eqn. (6-6)) since it accurately captures the moment and resulting curvature demand for the uplifting system with earthquake loading and overturning P-Δ effects. In this case, the uplifting system column displacement ductility will under-predict the ductility value, but the difference is on the order of 10%. This is a reasonable approximation for this comparison.

$$\mu = \frac{u_{flexural}}{u_{yield}} \qquad (6\text{-}5)$$

$$\mu_{\phi} = \frac{\phi_u}{\phi_y} \qquad (6\text{-}6)$$

Figure 6-45 (a)-(c) shows the ductility demands for the Near Fault group for the 1D X and 3D X and Y components. Figure 6-45 (d)-(f) shows the ductility demands for the 2% in 50 group for the 1D X and 3D X and Y components. Figure 6-45 (g)-(i) shows the ductility demands for the 2% in 50 group for the 1D X and 3D X and Y components.

Inspection of the plots shows that there is not a significant difference in ductility between the fixed base system and any of the uplifting footing systems. All of the ground motion groups are very similar in the short and medium period range. At the long period ranges, a select number of the α=3 footing widths have smaller ductilities than the fixed base response, particularly for periods greater than 1.5 seconds. The ratio of ductilities in Section 6.8.3 provides more critique of the demand ductilities of uplifting systems.

NEAR FAULT

(a) 1D - X (b) 3D - X (c) 3D - Y

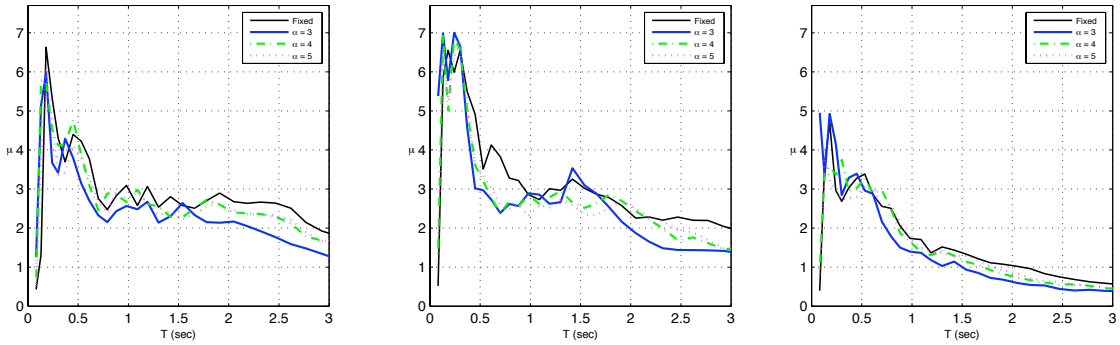

2% IN 50 YEARS

(d) 1D - X (e) 3D - X (f) 3D - Y

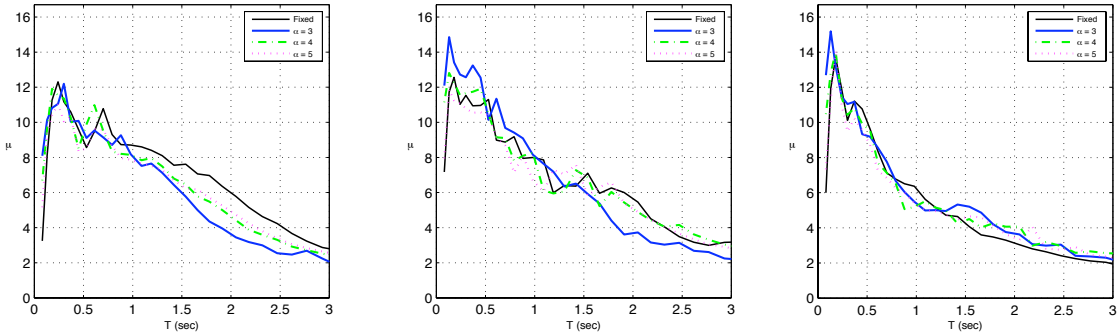

10% IN 50 YEARS

(g) 1D - X (h) 3D - X (i) 3D - Y

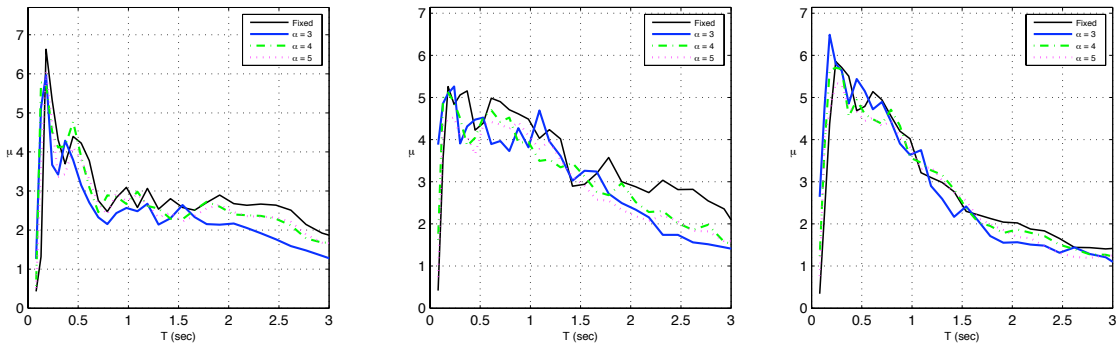

Figure 6-45: Displacement Ductility Response

6.8 Spectral Relationship of Uplifting to Fixed Base Systems

The spectral analysis of Sections 6.5 to 6.7 are used to compare uplifting and fixed base systems and evaluate the benefits and drawbacks of uplifting systems. Periods of all systems are plotted as a function of the corresponding fixed base period.

6.8.1 Acceleration

The ratio of fixed base to uplifting peak accelerations is calculated as R_R using Eqn. (6-7). For values of $R_R > 1$ the uplifting systems have a reduced acceleration. Values of $R_R < 1$ indicate the uplifting systems amplify the peak acceleration. Figure 6-46 shows the elastic column-elastic soil R_R values. Mean responses of the 1DX, 3DX, and 3DY input motions are plotted for each footing width and ground motion group. Figure 6-47 shows the R_R values for the nonlinear column-elastic soil.

$$R_R = \frac{S_{A\,fixed}}{S_{A\,uplift}} \qquad (6\text{-}7)$$

Elastic column-soil uplifting models have reduced accelerations in the medium period range from 0.5 to 1.5 seconds. It is shown that narrower footing widths have a more significant reduction in acceleration. Also larger magnitude excitations tend to have a larger reduction in accelerations. For the shorter period range, less than 0.5 secs, the uplifting systems amplify the acceleration relative to fixed base response. For longer period structures the ratio of uplifting to fixed response converge towards unity. Nonlinear column-elastic soil uplifting accelerations are virtually identical to fixed base response (R_R=1) for periods of 0.5 secs or greater. This indicates the nonlinear uplifting systems reach the same yield acceleration as the fixed base system. At the short period range, the uplifting systems also amplify the peak accelerations.

6.8.2 Displacement

The ratio of uplifting total column and flexural column displacement to fixed base displacement is calculated as γ_R (Eqn. (6-8)) and γ_{RF} (Eqn. (6-9)). Magnitudes < 1 indicate a reduction in displacement for the uplifting system and values > 1 indicate amplification in uplifting systems.

$$\gamma_R = \frac{S_{DR\,total}}{S_{D\,fixed}} \qquad (6\text{-}8)$$

$$\gamma_{RF} = \frac{S_{DR\,ColFlexural}}{S_{D\,fixed}} \qquad (6\text{-}9)$$

Figure 6-48 and Figure 6-49 show the elastic column-soil and nonlinear column-elastic soil displacement amplification ratios. The elastic column-soil models show that narrower footing widths tend to have larger total displacements however the amount of column flexural displacement is typically about one-half the fixed base displacement.

Typically, the greater the magnitude of excitation the greater the displacement of the uplifting system. At very short periods both the total and column flexural displacement of uplifting systems is larger than the fixed base. Longer period structures (> 2.0 secs) tend to have similar displacements indicated by displacement amplification ratios converging on 1.0. Nonlinear column-elastic soil displacement amplification ratios are approximately 1.0 for the larger footing widths (α=4 and 5), except for the very stiff structures with T < 0.25 secs. The narrow footing width (α=3) has a slight increase in total displacement and a reduction in column flexural displacement, especially for longer period ranges. Short period structures have significant displacement amplification.

6.8.3 Ductility

Ratio of displacement ductilities for uplifting to fixed base systems is calculated as μ_R (Eqn. (6-10)). Values < 1 indicated a reduction in ductility demand of uplifting systems and >1 indicated an increase in ductility. Rocking can be beneficial or neutral when μ_R is less than or equal to 1, which means reduced inelastic action.

$$\mu_R = \frac{\mu_{uplift}}{\mu_{fixed}} \qquad (6\text{-}10)$$

Figure 6-50 shows the ductility amplification ratio. For the footing widths and ground motion groups shown there is a reduction in the ductility demand for medium and long period ranges. Short periods have a significant increase in the ductility demand. The narrow footing width (α=3) has approximately a 25% reduction in the ductility demand for medium and long periods. Wider footings α=4 and 5 have approximately a 10% reduction.

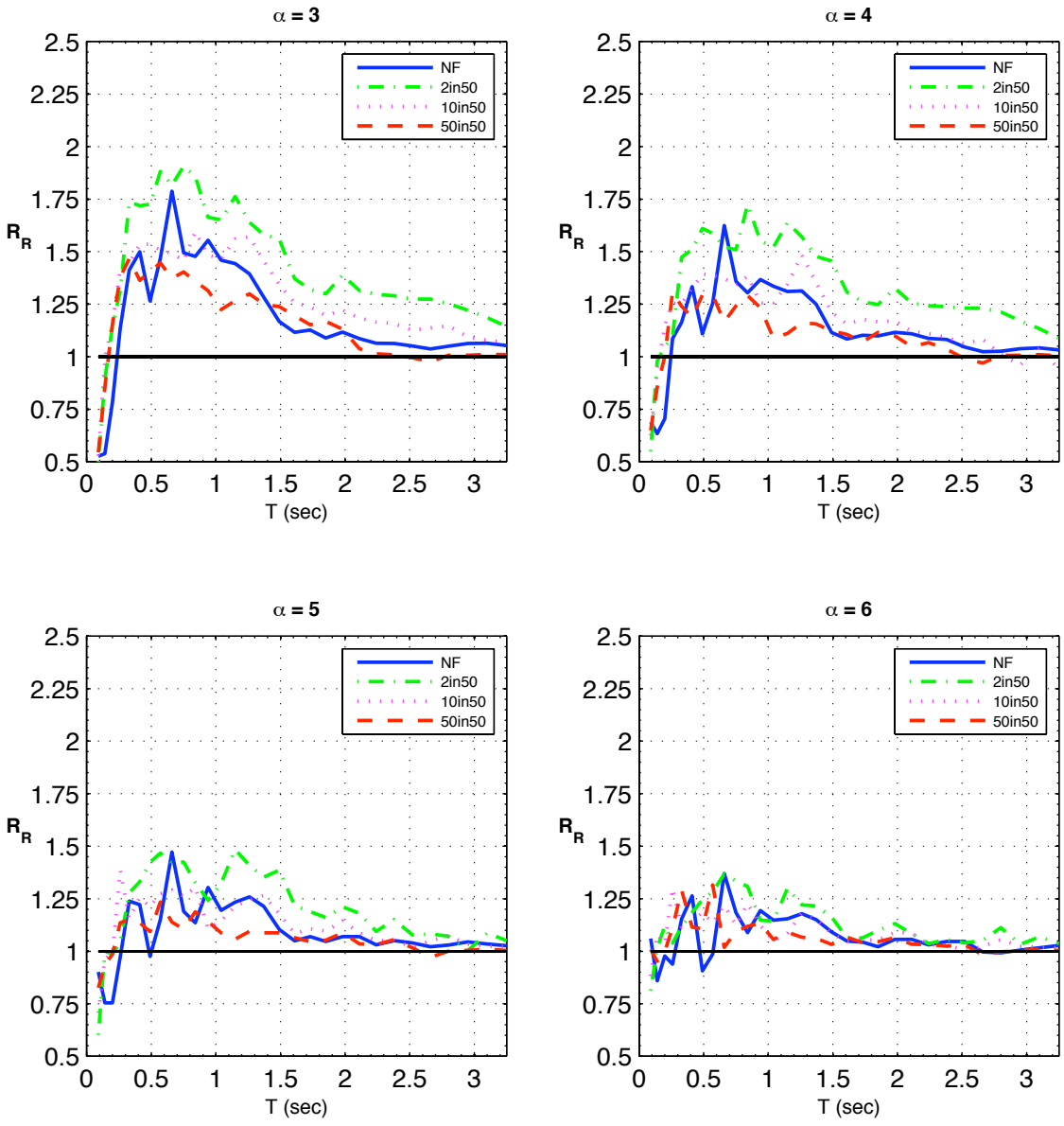

Figure 6-46: R_R Elastic Column-Elastic Soil

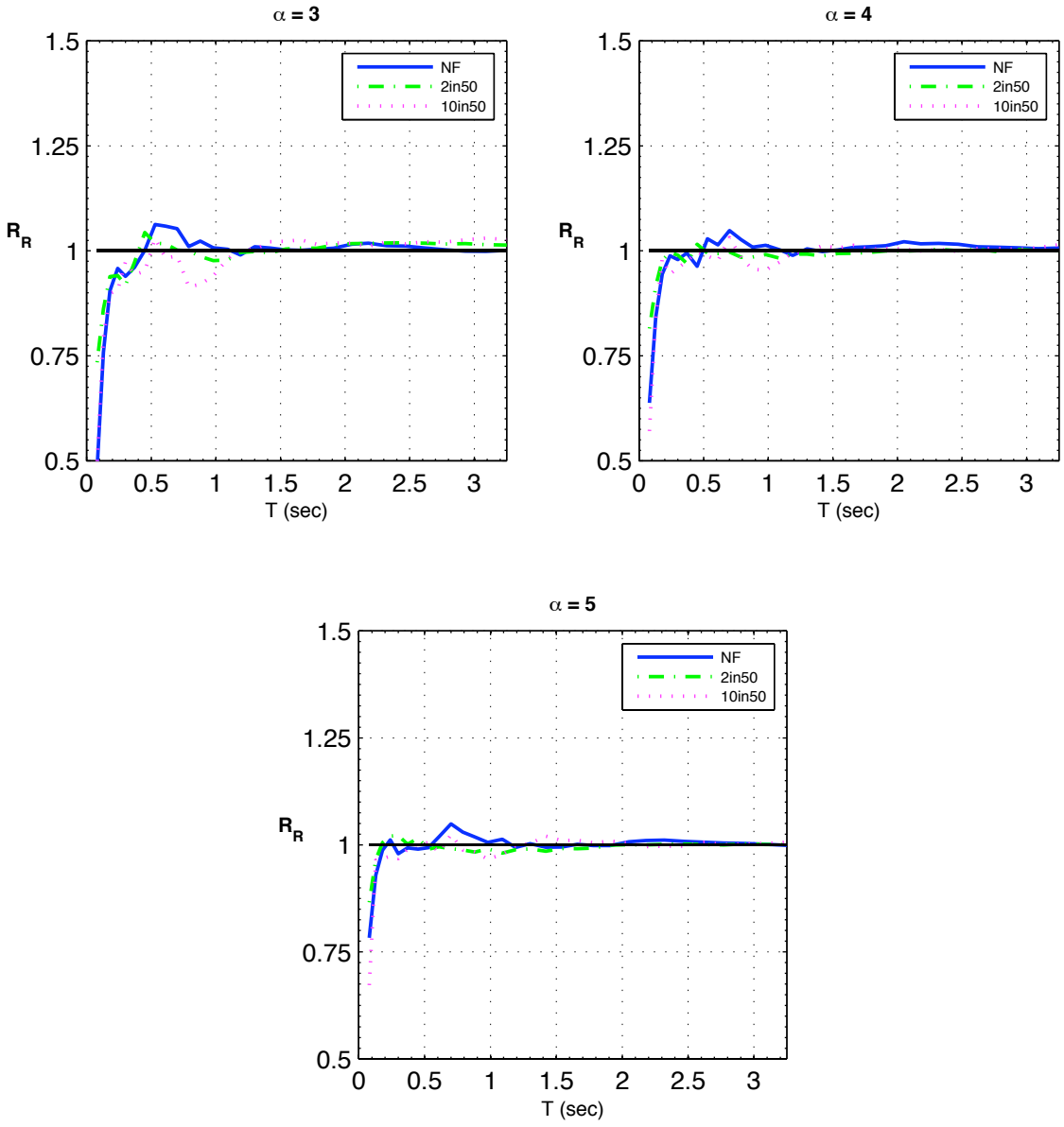

Figure 6-47: R_R Nonlinear Column-Elastic Soil

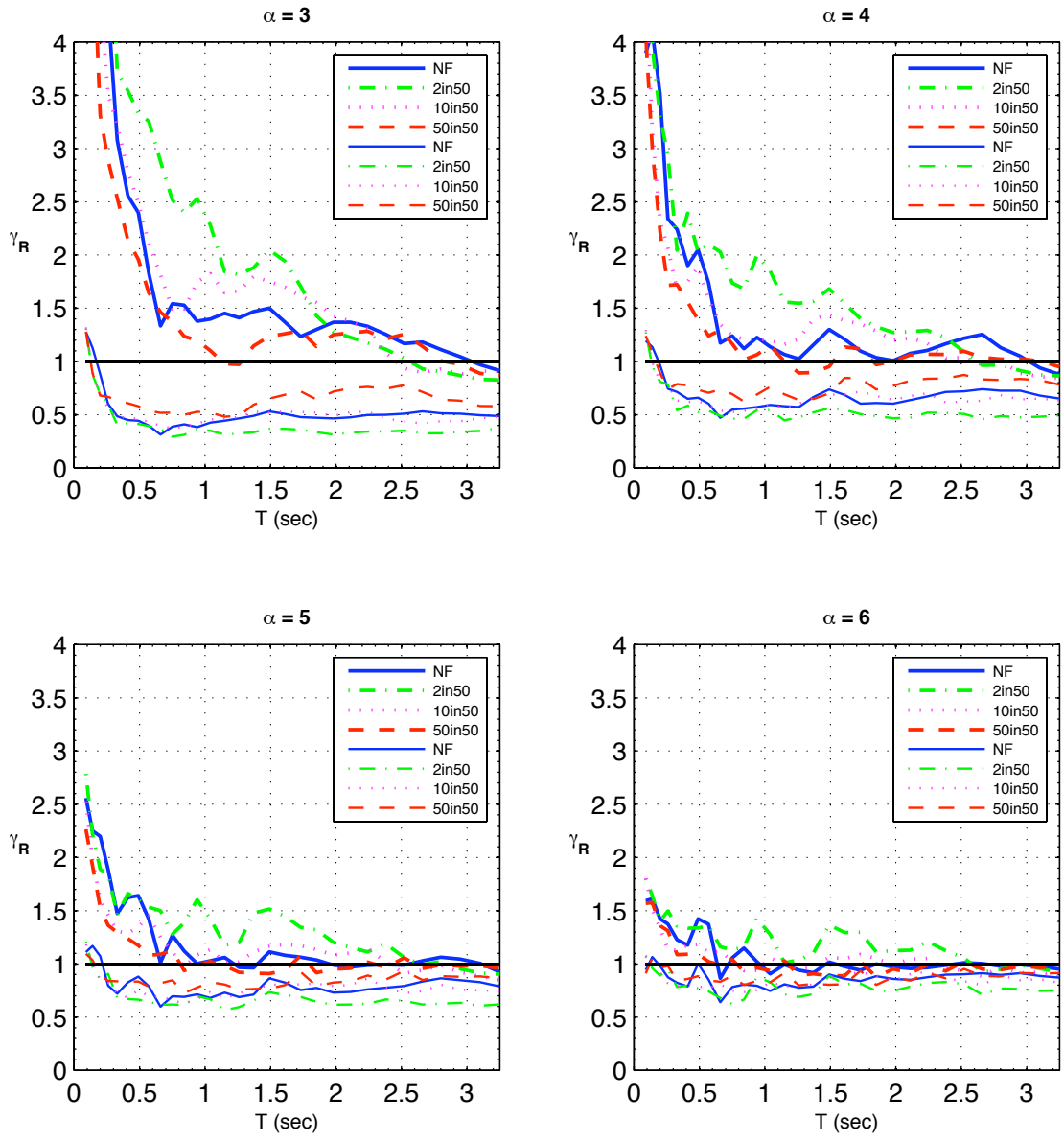

Figure 6-48: γ_R and γ_{RF} Elastic Column-Elastic Soil

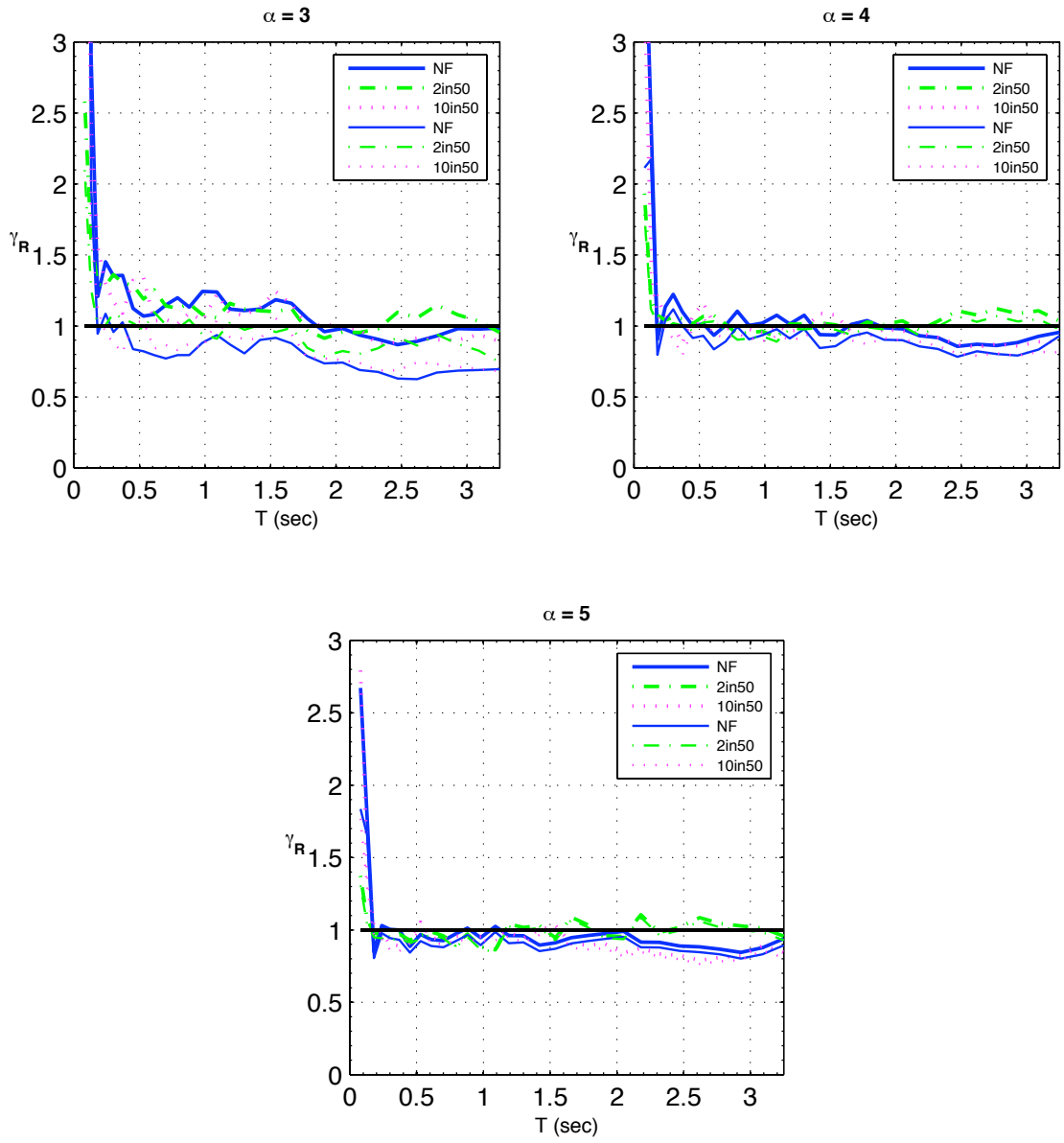

Figure 6-49: γ_R and γ_{RF} Nonlinear Column-Elastic Soil

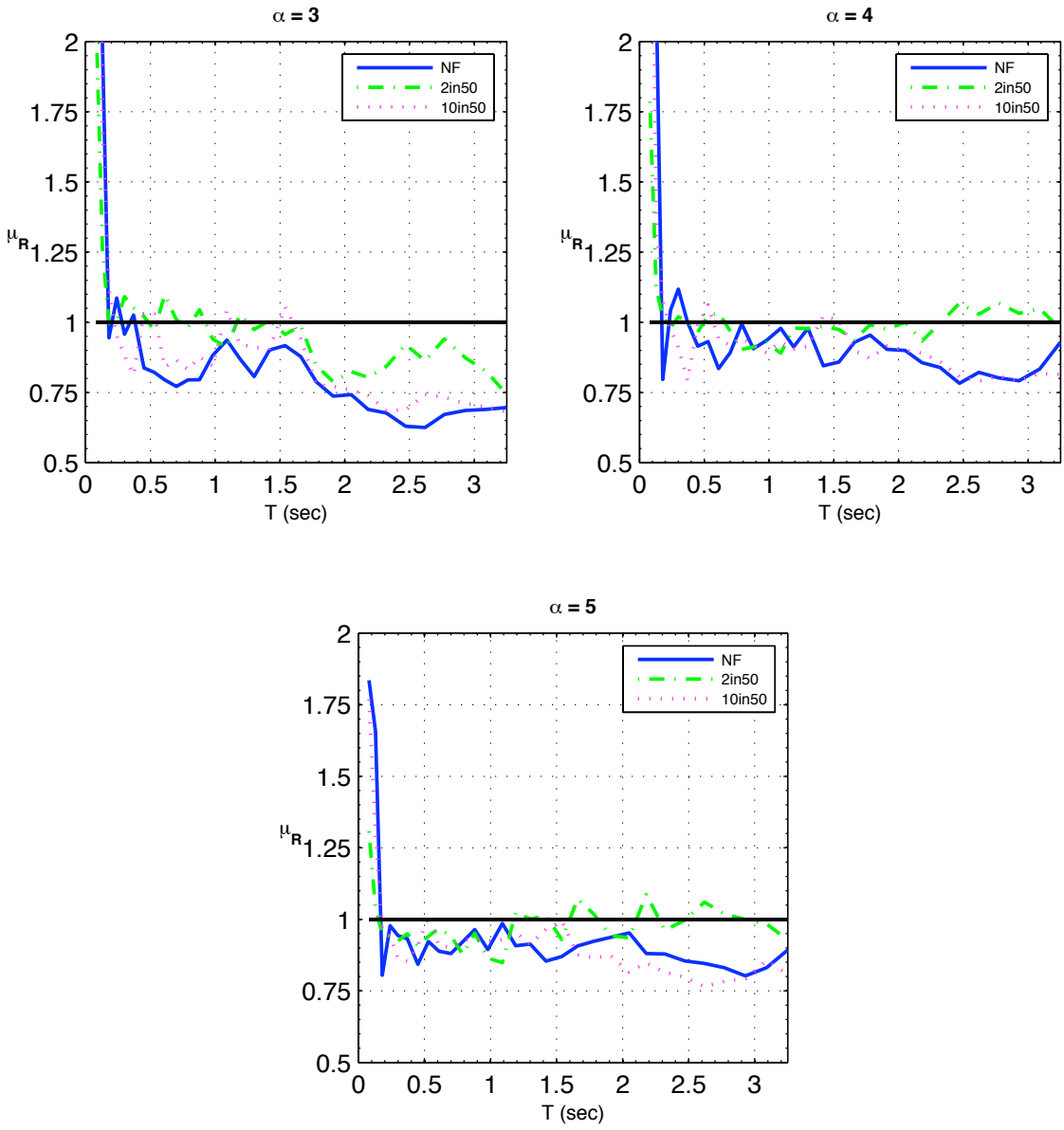

Figure 6-50: μ_R Ductility Ratio

6.9 Uplifting Bridge Pier Guideline Recommendations

Design of bridge piers is evaluated for systems allowed to uplifting using the predictions developed for when uplift will occur and the resulting effects of uplift on column accelerations, displacements, and inelastic response. These are compared to the traditional fixed base design methods. Design guidance, benefits, drawbacks, and a comparison to existing methods are provided in this section.

6.9.1 Design Guidance

Use of spread footings to support new bridge piers is a viable, economical approach in many situations. Agencies such as Caltrans will typically use spread footings where the soil has a high bearing capacity and is not susceptible to consolidation. Footings are designed as capacity protected elements with widths selected so that plastic hinging occurs in the base of the column. The influence of foundation uplift on seismic response raises sufficient concerns that design engineers often provide wider footings or even piles to provide assurance that uplift cannot occur. The parametric investigation conduct here has attempted to show that allowing uplift may reduced inelastic response or at the least identify that plastic hinging will occur in the column base in-spite of uplifting footings.

From the analytic and experimental work provided herein it appears that basic equations can be used with confidence to predict the lateral force on the column at the onset of uplift. Thus, the ratio β of the moment capacity of the column to the gravity load restoring moment can be used to determine whether uplift will occur. Eqn. (6-11) is repeated from Chapter 4.

$$\beta_i = \frac{M_{col}}{M_i} = \frac{3M_{n\,col}}{(W + W_o)b} \qquad (6\text{-}11)$$

Where W is the weight of the inertial mass of the system and W_o represents the weight of the footing, surcharge, and other loads acting on the footing not associated with the inertial mass of the bridge deck. If $\beta < 1$ when M_n is used for the column moment, the column would be expected to develop its full nominal moment capacity prior to uplift.

6.9.2 Benefits

As presented in the experimental investigation and parametric study, uplift can have a beneficial effect on the behavior of a bridge, by providing a means of seismic isolation. Also it has been shown that plastic hinging in column bases can occur for smaller footing widths than typically considered in design. The overall displacement of the structure may be increased depending on the degree of energy dissipation in the soil that accompanies the uplift, and the damage in the column may be reduced. Designing for uplift may not necessarily be beneficial because in certain configurations there may be amplification or displacement demands when compared to fixed base analysis.

If the total displacements are acceptable, or contained by abutments or other restraints, the fact that the piers are supported on spread footings that uplift might not mean that the expected performance is inadequate. Reduction of damaged to the column, and the tendency of narrow footings to re-center following an earthquake when situated on soils with high gravity load factors of safety may result in superior performance.

Retrofit strategies of existing bridge piers have been undertaken to increase the footing width and ensure plastic hinging occurs in the column base. In situations where the total displacements are acceptable and soils have sufficient strength against bearing failure the parametric investigation has shown that the hinge can occur at the column base for narrow footing widths of α=3 and 4. This may prevent the need to incur costly retrofit schemes to widen the footings.

Table 6.4 provides the ratios of column acceleration, total displacement, column flexural displacement and ductilities for the uplifting to fixed base systems. In general $R_R > 1$ indicated a reduction in peak acceleration which is desired and $R_R < 1.0$ indicates an increase. Displacement and ductility values < 1.0 indicate a reduction in uplifting system response. The shaded regions of the table indicate that period ranges where the uplifting response is amplified relative to the fixed base response.

Table 6.4: Uplifting System Ratios of Response Parameters

Period	Elastic Column-Soil			Nonlinear Column-Elastic Soil			
	R_R	γ_R	γ_{RF}	R_R	γ_R	γ_{RF}	μ_R
Short T < 0.5 s	< 1.0	1.5-4.0	0.5-1.25	< 1.0	1.0-4.0	0.9-3.0	1.0-3.0
Medium T= 0.5-1.5 s	1.0- 1.80	1.5-3.0	0.5-1.0	1.0-1.08	0.8-1.4	0.8-1.0	0.75-1.0
Long T > 1.5 s	1.0- 1.25	1.0-1.5	0.5-1.0	1.0	1.0-1.2	0.7-1.0	0.65-1.0

6.9.3 Negative Consequences

In evaluating the potential use of uplift in bridge pier seismic design the consideration is based on a neutral or reduced response compared to fixed base systems. Or a small increase in some response parameters where appropriate. The comparison of response parameters shown in Section 6.8 provides guidance on negative effects of uplift. Table 6.4 in the previous section provides a summary of the ratios of uplifting to fixed base response and the ranges where uplift significantly amplifies response.

In general acceleration amplification occurs for uplifting systems with corresponding fixed base periods, T_{nf}, less than 0.5 seconds when considering elastic or nonlinear column modeling response (Figure 6-46 and Figure 6-47). Total displacements of uplifting systems are increased for short period fixed based structures (T_{nf} < 0.3 sec.) even though column flexural displacements of the uplifting systems in question are less

than fixed base response (Figure 6-48 and Figure 6-49). The amount of total displacement amplification increases as the footing width becomes narrower. For example, the total displacement of the α=3 footings, for periods less than 1.0 secs, for the elastic systems is 2.0 times greater than the fixed base response. For the nonlinear system, with α=3, the total displacements are up to 1.25 times greater than the fixed base response.

Where uplift is not desired, several checks should be done. The effect of realistic material properties and deformation hardening should be considered in evaluation of M_n. Solution of Eqn. (6-11) should be based on ϕM_n or alternately M_u obtained from a section analysis of the column based on material properties and detailing. Soil properties should be checked to determine if soil would be overstressed due to footing rotation loading and vertical bearing pressures. Finally, the rotational and translational stiffness of the footing should be determined and used to assess the effect of the footing flexibility on the effective period and dynamic response of the pier. Lastly, the column and footing should be designed and detailed in accordance with standard Caltrans practices.

6.9.4 Recommendations

The Winkler spring foundation models presented in Chapter 5 and 6 give a reasonable prediction of response consistent with emerging trends in bridge analysis practice. Performing nonlinear column and soil analysis via the foundation model and fiber sections for the column appears to give reasonable predictions. Recommendations and conclusions can be made for bridge piers designed to uplift on the basis of the analytical and parametric investigations performed.

The following conclusions on typical response parameters of bridge pier design are helpful in making the accompanying recommendations for when uplift should and should not be considered:

1. Similarly to fixed base response, larger ground motion excitations tend to create more displacement response of uplifting systems when compared to smaller motions for similar structures. Rocking and uplifting, as a percentage of the total displacement response, increased as the magnitude of excitation increased. This indicates, allowing uplift for smaller magnitude design earthquakes does not increase instability of the system because the amount of uplift is small.
2. Footing rotations were found to increase for similar magnitude earthquakes as the footing size is reduced. Increasing footing rotation leads to greater possibility of soil yielding and a subsequent reduced effective footing width post-seismic event. Hence, effective footing sizes may be less than desired, for footings designed with minimum dimensions, which may decrease system stability.

From the parametric investigation it was found that certain uplift bridge pier design ranges (noted by the corresponding fixed base period) had harmful response compared to traditional fixed base piers. For these ranges, this indicates uplift should be prevented:

3. The displacement, acceleration and ductility demands for short period columns supported on footings that uplift tend to be significantly amplified. The short period range is for columns with fixed base natural periods as $T_{nf} < 0.5$ sec. Uplift should not be considered unless detailed nonlinear dynamic analyses are undertaken.

Using the parametric investigation and above discussion on uplifting bridge piers, the following recommendations are made on when uplift should be considered as a potential benefit in the design and response of traditional fixed base bridge piers:

4. Design of bridge piers in low seismicity regions should be considered because; while the amount of rocking is small it can still prove beneficial. And the overall stability of the system has been shown in the parametric study to be sufficient.
5. Given the observed response, retrofit schemes for widening footings that do not consider uplift, should be revisited after detailed nonlinear dynamic analysis of uplifting footings has been performed. The analysis should determine if the plastic hinge can be formed and if the total displacements are acceptable for uplifting response.
6. Acceptable uplifting behavior was observed both experimentally on the shaking table and numerically for the parametric investigation for footing sizes $3D_c$ or larger. This is for competent soils with gravity load factors of safety 3 or larger. Uplift should be considered for footings meeting these conditions.
7. Uplifting systems tend to have larger global displacements, as such, clearances between columns and the surrounding environment should be sufficiently designed to accommodate anticipated displacement amplification. For the cases considered herein with fixed bases periods greater than 0.5 secs the amplification ranged from 1.0 to 3.0.
8. In spite of the potential benefit of reduced moments and damage in columns of uplifting systems, it is recommended that columns and footings be detailed for ductile behavior with a plastic hinge occurring at the base of the column. Skewed bending and bidirectional loading of the column into the inelastic range can increase the uplift resistance of the footing, and reduce the moment capacity of the column. Which may result in column yielding not anticipated based on uni-directional excitation analysis. Also, uplift resistance may be increased by construction of roadways, barriers, and other structures over a footing. As such, use of ductile details and capacity design on the basis of a fixed footing condition is considered prudent unless special efforts are taken to mitigate these conditions.

7 Conclusions

The seismic response of traditional reinforced concrete bridge piers supported on shallow foundations allowed to uplift during seismic events has been evaluated as part of a research program to determine the response and potential benefits of uplifting foundations. Research has been conducted through an experimental program, development of analytic models, and parametric investigation based on the validated analytic models. The intent is to identify traditional fixed base piers which may benefit from the consideration of uplift during seismic events.

The specific research objectives were to develop and validate analytic models of bridge piers on shallow foundations allowed to uplift. Typically the fixed base design approach would yield significant inelastic response during seismic events and corresponding displacement ductilities demands. The benefit of uplifting systems is that the mode of uplift may dissipate energy thereby reducing inelastic demands and damage related to seismic events. The experimental and analytic validation program focused on two footing configurations and two earthquake excitations. The parametric investigation built upon the analytic models to consider a wide range of ground motions, column height to diameter ratios, footing widths, and elastic and inelastic response.

7.1 Experimental Investigation of Uplifting Systems

A bridge pier typically designed as a fixed based system was tested through a series of shaking table tests to evaluate the response of bridge piers uplifting during seismic events. The specific objective was to validate that rocking is a valid mode of response and that the rocking motion dissipates some of the energy typically associated with inelastic response thereby reducing plastic deformations. The single column system modelled was a conventional reinforced concrete column with typical axial load and a footing smaller than typical design dimensions would require. The footing was designed to be expandable and also as a capacity protected element to ensure plastic behavior occurred at the column base.

Three test groups were conducted to assess the response of uplifting systems. Groups 1 and 2 had footing to column width ratios of 3 and axial loads of 33% and 100% of the design axial load. Test group 3 had a footing width of 5 by 3 column diameters with 100% of the column design axial load.

Test groups 1 and 2 each were tested using motions scaled to keep the column in the elastic demand level range. Various combinations of 1D, 2D, and 3D excitations were

input. Test group 3 was tested using motions which were scaled to achieve column yield and displacement ductility demands of 1, 4, and 6-8 which correspond to yield, design and maximum credible earthquake loading levels. At the conclusion of the maximum credible earthquake the column was significantly damaged and no further testing was feasible.

Measured base moment vs. footing rotation behavior typically followed the response predicted by the simple analysis model using a Winkler foundation. For the sufficiently narrow footings, uplift occurred and exhibited a nonlinear elastic type hysteresis with some energy dissipation from the supporting elastomeric pad. In this case the overturning moment exceeded the restoring capacity of the footing and the column behaved elastically illustrating the potential benefits of allowing uplift. The comparison of 1D, 2D, and 3D input excitations revealed that interaction may reduce the amount of uplift.

The wider footing and larger excitations of Test Group 3 were expected to induce yielding of the column prior to uplift of the foundation in the $5D_c$ footing width direction. It was observed that bi-directional moments in the column reduced the effective moment capacity of the column in the narrow footing direction such that yielding occurred earlier than expected on the basis of the uni-directional excitation. Multi-directional response appeared to increase the effective width of the footing (due to skew), which resulted in less rocking and uplift than expected. It should be noted that for Test Group 3 the column plastic hinge occurred in spite of the smaller than typical footing dimensions. For design applications it appears where competent soils are available a column with footing dimension $3D_c$ or larger and typical axial load, no tie-downs or footing increase is necessary to induce energy dissipation through plastic hinging of the column. The final test run at the maximum credible earthquake illustrated the column was able to develop a full plastic hinge, dissipate earthquake energy and remain stable without the need for vertical restraint.

In conclusion the limited run of experimental testing shows the design performance of traditional fixed base bridge piers may be met when rocking and uplift occur without the added cost of piles or alternative methods. However for these shaking table tests an elastomeric pad was used beneath the footing in place of soil. Consequently the tests were used to validate a numerical model for spread footings resting on competent soil.

7.2 Analytical Modelling of Uplifting Systems

Analytic models have the capability to reasonably predict the seismic response of uplifting bridge pier systems with the use of the open-source structural analysis platform OpenSees. Idealizations of the superstructure mass, column, footing, and elastomeric pad were used in the analytic models. Evaluation of the analytic models through linear and nonlinear model assumptions was based on the observed dynamic response to multi-direction input earthquake accelerations and natural properties of the systems.

Linear models used to model the elastic response behavior of the uplifting systems were able to predict the observed response with a high degree of confidence. The

models were found to predict peak displacements to within 25% for the uplifting systems with design axial load ($10\%f'_cA_g$) and square ($3D_c$ x $3D_c$) or rectangular ($5D_c$ x $3D_c$) footings.

Nonlinear models were able to predict the design level (μ=6) test peak displacements to within 20% of the observed response. Residual displacements were under-predicted by 100% however the observed magnitude was small (less than 1"). Given this response the observed model predicted the amount of rock, uplift, column flexural displacements, and column total displacements very well for the design level earthquake. For the maximum level earthquake (μ=8), the analytical model predicted initial cycles of displacement well, but deviated once the column experienced significant residual displacements. In-spite of this the model was still able to reasonably predict the peak displacements which occurred at a column flexural displacement ductility of μ=10. Also the model was able to predict approximately 50% of the observed residual displacement and had a similar post-yield stiffness to the observed response.

Column center of mass accelerations are predicted to within 25% for the linear and nonlinear analytic models. For the linear response the column base moment curvature prediction was reasonable. For the nonlinear analytic model the design level earthquake moment-curvature response is reasonable but does not show the shift in origin due to residual displacements that cause a permanent overturning moment at the column base. This permanent column offset creates a shift in the origin that affects the system displacement and corresponding acceleration and moment response.

The footing rotational stiffness was modeled reasonably well by the numerical models for the linear analysis cases. The Winkler foundation used to model the neoprene springs provided a good approximation of the static displacement, rotational stiffness, moment and rotation at initial footing uplift and the softening behavior as the footing uplifts. Nonlinear response predicted by the analysis was affected by the discrepancy in residual displacements, which caused a permanent shift in the origin of the footing moment-rotation relationship. Analytic models showed 5-6% Rayleigh damping was effective for systems with significant uplift and 3-4% was effective for yielding systems with less uplift.

Based on these comparisons the analytic models of uplifting bridge pier systems on shallow foundations using linear and nonlinear column assumptions and a Winkler spring foundation have sufficient accuracy to predict the global response of linear uplifting systems and yielding systems tested to design and maximum earthquake levels.

7.3 Parametric Study

Using the uplifting analytical model developed in the analytical validation, parametric studies were performed to evaluate the effects of different ground motions, footing widths, column height to diameter ratios, and column model assumptions. Accelerations, displacement and displacement ductility responses were determined for various combinations of these uplifting systems and compared to fixed base response.

The following observations and conclusions, on typical response parameters used in the design of fixed base bridge piers, for uplifting bridge piers are drawn:

- The amount of uplift and rocking varies based on the magnitude of excitation. For smaller magnitude seismic events, such as 50% in 50 year probability of exceedance, the rocking and fixed base responses were similar. Larger events such as the 2% in 50 year probability of exceedance caused larger rocking response. In general the percentage of rocking displacement relative to the total displacement increased as the seismic excitation increased.
- The observed accelerations of elastic column and soil models were reduced for uplifting systems relative to the similar fixed base systems. With the exception of the short period range, $T_{nf} < 0.5$ secs, where the response was amplified. The medium period range of 0.5-1.5 secs had the most significant reduction. At longer periods the uplifting response tended to be similar to the fixed based, however the magnitude was still greater.
- The observed accelerations of the nonlinear column and elastic soil models were approximately equal for periods typically greater than 0.5 seconds. Inspection of the results showed that the uplifting systems reached the acceleration at which column yield occurs for the Near Fault, 2% in 50 year and 10% in 50 year events. This was observed for all footing widths used in the nonlinear column and elastic soil model parametric investigation (i.e. $3D_c$ to $5D_c$). At periods less than 0.5 seconds the observed accelerations of the uplifting systems were much greater than the corresponding fixed base acceleration.
- Elastic column and soil model total displacements were typically larger than the fixed base response. In the medium and long period ranges, previously described, the increase varied by footing width. In general the amount of increase was 1 to 3 times larger. The short period ranges significantly amplified the motion, by up as much as 4 times. The associated column flexural displacement component, for these ranges, of the total displacement was typically less than the fixed base response which indicates the rocking response was primarily responsible for the total displacement increase. This suggests short period structures whose design is sensitive to total displacement should not consider rocking in design evaluation.
- Total displacements of the nonlinear column and elastic soil models were typically equal for the short and medium period ranges. Uplift was observed for these model assumptions, which indicates that the total flexural displacement on the column is reduced when allowing uplift. At longer period ranges of 2.0 seconds or greater the uplifting system total displacements were slightly less.
- The displacement ductility demands of uplifting systems are an indicator of the amount of inelastic action and response that occurs during seismic excitation. For the nonlinear column and elastic soil models, the ductility demands were typically less than the fixed base system for structural fixed base periods greater than 0.5 seconds. The amount of reduction was up to 25% less than the fixed base response. In the short period range the ductility

demands on the uplifting bridge pier were significantly increased relative to the fixed base period structures. The range was 1.0 to 3.0 times as much. For these expected ductility demands, bridge piers designed to uplift would need to be reassessed to ensure that adequate detailing for ductile response was provided.

- A reduction in column inelastic action is observed based on the parametric investigation and the comparison on ductility demands described in the previous note. Reduction by up to 25% of the displacement ductility demands gives an indication that the permanent displacements in the system may be reduced compared to a fixed base system, which can be very beneficial in the function of bridge piers following seismic events. However, allowing uplift did not eliminate inelastic column response relative to corresponding fixed base bridge piers.

Allowing uplift on bridge piers typically designed as fixed based appears to have a beneficial or neutral response when compared to fixed base systems. The exception is short period fixed base structures allowed to uplift where the system response is amplified. The neutral or beneficial behavior was observed for a wide variety of footing widths, column natural periods, and ground motions. Based on the observed parametric investigation results described above the following conclusions and recommendations are made for when to allow bridge piers, typically designed as fixed base to prevent uplift, to uplift so as to utilize potential damage reduction characteristics:

- Current practice evaluates existing bridges for increasing seismic demands and determines if retrofits of footings are necessary to prevent uplift and ensure plastic hinging can be confined to the column base. Given the observed response, these footing widening schemes, should be revisited after detailed nonlinear dynamic analysis of uplifting footings has been performed to determine if the plastic hinge can be formed and if the total displacements are acceptable for the bridge pier response.
- Uplift should be considered for footing sizes $3D_c$ or larger supported by competent soils with gravity load factors of safety 3 or larger. These uplifting systems were found to have acceptable uplifting behavior on traditional fixed base bridge pier design metrics.
- For systems where uplift is to be utilized in design, clearances between columns and the surrounding environment should be sufficiently designed to accommodate anticipated displacement amplification. For the cases considered herein with fixed bases periods greater than 0.5 secs the amplification ranged from 1.0 to 3.0.
- Columns and footings should be detailed for ductile behavior, in spite of the potential benefit of reduced inelastic column response of uplifting systems. Columns should be detailed such that a plastic hinge occurs at the base of the column. The reason being a variety of factors including skewed bending and bidirectional loading of the column into the inelastic range which can increase the uplift resistance of the footing, and reduce the moment capacity of the column. Also, uplift resistance may be increased by construction of roadways, barriers, and other structures over

a footing. Hence, use of ductile details and capacity design on the basis of a fixed footing condition is considered prudent unless special efforts are taken to mitigate these conditions.

7.4 Future Research

This study has provided insight on the seismic response of uplifting bridge piers and has developed analytic models. There are additional items, which require further investigation in order to apply to the design of bridge piers allowed to uplift:

1. More extensive parametric studies to examine a broader range of soil conditions should be conducted. The parametric studies undertaken herein should be expanded to consider a broader range of soil types and mechanical characteristics.
2. Additional parametric studies on the bridge pier response when soil yields during excitation are warranted. In particular focus should be paid to the amount of yielding and the effective footing width following yield due to both unidirectional and multidirectional excitation. Which will have an effect on post-seismic event footing stiffness (rotational and translational).
3. Residual displacements of uplifting footings are an important design consideration for bridge pier design. Further work is warranted to assess the magnitude of residual displacements compared to fixed base design.
4. For locations of poorer soil conditions, some of the benefits of possible reduced damage to the column and re-centering of the bridge system may be achieved by supporting the pier footing on piles, where the pile cap is allowed to uplift from the pier. An option would be to place the pile into a socket cast on the bottom of the pile cap so that lateral load can be transferred from the pile cap to the pile during uplift. Elastomeric pads or some type of yielding device might be installed in the socket between the pile cap and the pile so that energy is dissipated during uplift and reseating.
5. Bridge systems should be evaluated where the effect of the vertical movement of the column associated with rocking is considered. Uplift behavior will cause the bridge deck to raise and lower on opposite ends. For cases where restraints are provide to prevent this uplift movement, the uplift behavior may be prevented or greater soil yielding may be produce. For example, the bridge deck may be vertically restrained at the abutments, and a stiff bridge deck will tend to resist the upward movement of the deck associated with uplift of the footings. Similarly, where columns of different length support a bridge, or the individual footings have different widths, the amount of vertical movement during uplift will differ. As such, the resistance of the footing to vertical movement at the column lines will result in different vertical forces in each column, and as such, the rocking and uplift behavior will differ from what is observed here. In the case of curved or skewed bridges, the different principal axes of the footings may result in behaviour not considered herein. Thus it is strongly recommended that this work be extended to consider bridge systems having columns supported on spread footings susceptible to uplift. Testing on

a geotechnical centrifuge and shaking table would be desirable, as would numerical simulations.

REFERENCES

Alameddine, F. and Imbsen, R. (2002). "Rocking of Bridge Piers Under Earthquake Loading," *Proceedings,* Third National Seismic Conference & Workshop on Bridges and Highways.

Algie, T.B., Deng, L., Erduran, E., Kutter, B.L., Kunnath, S. (2008). "Centrifuge Modeling of Innovative Foundation Systems to Optimize Seismic Behavior of Bridge Structures." *Proceedings*, 14th World Conference on Earthquake Engineering: Innovation Practice Safety, Beijing, China. Oct. 12-17 2008.

ASCE 41, (2007). *Seismic Rehabilitation of Existing Buildings*, American Society of Civil Engineers. Reston, Virginia.

Baker, J.W., Lin, T., Shahi, S.K., Jayaram, N. (2011). "New Ground Motion Selection Procedures and Selected Motions for the PEER Transportation Research Program," *Technical Report PEER 2011/03,* Pacific Earthquake Engineering Research Center, University of California, Berkeley, CA.

Berry, M. P., and Eberhard, M. O. (2006). "Modeling of reinforced concrete bridge columns." Presentation at the PEER annual meeting, San Francisco, California.

Boulanger, R. W., Curras, C. J., Kutter, B. L., Wilson, D. W., and Abghari, A. (1999). "Seismic Soil-Pile Structure Interaction Experiments and Analyses," *Journal of Geotechnical and GeoEnvironmental Engineering,* ASCE, Vol. 125, No. 9.

Caltrans (2004). *Seismic Design Criteria,* Version 1.4, California Department of Transportation, Sacramento, CA.

Caltrans (2004). *Bridge Design Specifications,* Version 1.4, California Department of Transportation, Sacramento, CA.

Chang, G., and Mander, J. (1994). *Seismic energy-based fatigue damage analysis of bridge columns: part I – evaluation of seismic capacity*. Report No. NCEER-94-0006, Department of Civil and Environmental Engineering, State University of New York at Buffalo, NY.

Ciampoli, M. and Pinto, P. (1995). Effects of soil-structure interaction on inelastic seismic response of bridge piers, *Journal of Structural Engineering,* ASCE, Vol. 121 (5), pp. 806-814.

Chopra, A. K. and Yim, C., (1983). "Simplified Earthquake Analysis of Structures with Foundation Uplift." *Journal of Structural Engineering,* ASCE, Vol. 111, No. 4, April 1985.

Chopra, A.K. and Goel, R. K. (1999). "Capacity-demand-diagram methods for estimating seismic deformation of inelastic structures: SDF systems," *Technical Report PEER-1999/02,* Pacific Earthquake Engineering Research Center, University of California, Berkeley, 1999-04, 67 pages

Chopra, A.K. (2001). Introduction to Structural Dynamics and Earthquake Engineering, Prentice Hall.

D'Amico, A.; Cimini, V.; Valente, G. (1999). "Seismic response of a prestressed concrete bridge pier with stepping," *Proceedings,* Fourth European Conference on Structural Dynamics, EURODYN '99; pp. 1217-1222.

Deng, L., Kutter, B. L., Kunnath, S., and Algie, T. (2010). "Centrifuge modeling of bridge system with rocking footings." *Proceedings.* Intl. Conf. on Physical Modeling in Geotechnics, Zurich, Switzerland. A.A. Balkema Publishers, Rotterdam, Netherlands

Deng, L. and Kutter, B. L. (2011), "Characterization of rocking shallow foundations using centrifuge model tests." *Earthquake Engineering & Structural Dynamics*. doi: 10.1002/eqe.1181

Donikian, Roupen R. (1998). "Seismic Modeling and Analysis of the Richmond-San Rafael Bridge," *Structural Engineering World Wide 1998,* pp. Paper T170-5.

Espinoza, A., Mahin, S., Jeremic, B., Kutter, B., and Ugalde, J. (2005). "Rocking of bridge piers subjected to multi-directional earthquake loading," *Proceedings,* Caltrans Bridge Research Conference: Oct. 31-Nov. 1, 2005, Sacramento.

Espinoza, A. and Mahin, S. (2006). "Rocking of bridge piers subjected to mulit-directional earthquake loading," *Technical Memorandum,* the Public Works Research Institute, Tsukuba, Japan.

Espinoza, A. and Mahin, S. (2006). "Rocking of bridge piers subjected to mulit-directional earthquake loading," *Proceedings,* 100th Anniversary Earthquake Conference, EERI, held in San Francisco, CA during 18-22 Apr. 2006.

FEMA 356 (2000). *Prestandard and Commentary for the Seismic Rehabilitation of Buildings,* prepared by the American Society of Civil Engineers for the Federal Emergency Management Agency, Washington, D. C. (FEMA Publication No. 356).

Gajan S, Phalen JD, Kutter BL, Hutchinson TC, and Martin, G (2005). "Centrifuge modeling of the load deformation behavior of rocking shallow foundations," *Journal of Soil Dynamics and Earthquake Engineering,* 25, 773–783.

Gajan S (2006). "Physical and Numerical Modeling of Nonlinear Cyclic Load-Deformation Behavior of Shallow Foundations Supporting Rocking Shear Walls," *Ph.D. Thesis,* University of California at Davis, College of Engineering.

Gajan, S., Kutter, B.L. (2009). "Effects of Moment-to-Shear Ratio on Combined Cyclic Load-Displacement Behavior of Shallow Foundations from Centrifuge Experiments." *Journal of Geotechnical and GeoEnvironmental Engineering*, ASCE, Vol. 135, No. 8, pp 1044-1055, August 2009.

Gazetas, G. (1991), "Displacement and Soil-Structure Interaction Under Dynamic and Cyclic Loading," Proceedings of the Tenth European Conference on Soil Mechanics and Foundation Engineering, Florence, May 1991.

Faccioli E, Paolucci R, and Vivero G (2001). Investigation of seismic soil-footing interaction by large-scale cyclic tests and analytical models, *Proceedings,* Fourth International Conference on Recent Advances in Geotechnical Earthquake Engineering and Soil Dynamics, San Diego, March 26-31.

Hachem, M., Mahin, S. and Moehle, J. (2003). "Performance of Circular Reinforced Concrete Bridge Columns Under Bidirectional Earthquake Loading," *Technical Report PEER 2003/06,* Pacific Earthquake Engineering Research Center, UC Berkeley.

Harden, C., Hutchinson, T., Martin, G. and Kutter, B. (2005). "Numerical Modeling of the Nonlinear Cyclic Response of Shallow Foundations," *Technical Report PEER 2005/04,* Pacific Earthquake Engineering Research Center, University of California, Berkeley, CA.

Housner GW (1963). "The Behavior of Inverted Pendulum Structures During Earthquakes," *Bulletin of the Seismological Society of American,* Vol. 53, No.2, pp. 403-417.

Hu, Z.-J. (2006), "Rocking of Foundations: A Numerical Analysis Using OPENSEES," *M.S. Thesis,* Department of Civil and Environmental Engineering, University of California, Davis, pp 142.

Huckelbridge, A. Jr. and Clough, R. W. (1978)."Seismic Response Of Uplifting Building Frame," *Journal of the Structural Division,* ASCE. Vol. 104, no. ST8, pp. 1211-1229. Aug. 1978

Hutchinson, T.C., Raychowdhury, P. (2009). "Performance Evaluation of a Nonlinear Winkler-Based Shallow Foundation Model using Centrifuge Test Results." *Earthquake Engineering and Structural Dynamics.* Vol 38, Issue 5, March 2009, p g 679-698.

Jeong, H., Sakai, J., Mahin, S.A. (2008). "Shaking Table Tests and Numerical Investigation of Self-Centering Reinforced Concrete Bridge Columns," *Technical Report PEER 2008/06,* Pacific Earthquake Engineering Research Center, UC Berkeley, May 2008.

Karsan, I. D., and Jirsa, J. O. (1969). “Behavior of concrete under compressive loading.” *ASCE J. Structural Division*, 95(ST-12).

Kawashima, K. and Hosoiri, K. (2003). "Rocking Response of Bridge Columns on Direct Foundations," *Proceedings,* Symposium on Concrete Structures in Seismic Regions, Paper No. 118, FIB, Athens.

Kawashima, K. Nagai, T. and Sakellaraki, D. (2007). “Rocking Seismic Isolation of Bridges Supported by Spread Foundations,” *Proceedings,* 2nd Japan-Greece Workshop on Seismic Design, Observation and Retrofit of Foundations, pp. 254-265, Japan Society of Civil Engineers, Tokyo, Japan, 2007

Kelly, J. and Tsztoo, D. (1977). “Earthquake Simulation Testing Of A Stepping Frame With Energy-Absorbing Devices,” *Technical Report,* Earthquake Engineering Research Center, University of California, 1977. 53 pages

Kelly, T.E. (2009). "Tentative Seismic Design Guidelines for Rocking Structures." *Bulletin of the New Zealand Society for Earthquake Engineering,* Vol 42, no. 4, pp. 239-274. December 2009.

Krawinkler, H., and Moncarz, P. D. (1982). “Similitude Requirements for Dynamic Models.” *Dynamic Modeling of Concrete Structures, ACI SP 73-1*, Detroit, MI, 1–22.

Ko, E., Chambers, L., Field, C., Wenger, C., and Mole, A. (2006). “Seismic Design Allowing Foundation Uplift (Rocking) For The California Academy Of Sciences Building, San Francisco,” *Proceedings,* 100th Anniversary Earthquake Conference, EERI, San Francisco, CA.

Kutter BL (1995). "Recent Advances in Centrifuge Modeling of Seismic Shaking" State-of-the-Art Paper, *Proceedings,* Third International Conference on Recent Advances in Geotechnical Earthquake Engineering and Soil Dynamics, St. Louis, MO, Vol.2, pp. 927-942, April.

Lam, I.P. and Fenves, G. (1998). “Effects of Footing Rotation on Earthquake Behavior of Pile Supported Bridge Piers,” *Report to NCEER,* Task Number 106-E-4.1, State University of New York at Buffalo.

Lipscombe, P.R.; Pellegrino, S. (1993). Free Rocking of Prismatic Blocks,” *Journal of Engineering Mechanics,* Vol. 119, no. 7, July, pp. 1387-1410.

Meek, J. (1975). Effects of Foundation Tipping on Dynamic Response,” *Journal of the Structural Division,* ASCE, Vol. 101, No. ST7, pp 1297-1311.

Mergos, P. and Kawashima, K. (2005). “Rocking Isolation Of A Typical Bridge Pier On Spread Foundation,” *Journal of Earthquake Engineering,* Vol. 9, Special Issue 2 (2005) 395–414

Miranda, E. and Ruiz-Garcia, J. (2002). “Evaluation of approximate methods to estimate maximum inelastic displacement demands,” *Earthquake Engng Struct. Dyn*., 31, pp 539–560.

Nagai, T. and Kawashima, K. (2006). “Effect of Bilateral Excitation on the Rocking Seismic Isolation of Foundations,” *Journal of Structural Engineering,* Vol. 52, No.2, pp. 499-509.

Newmark, N. and Rosenblueth, E. (1971). *Fundamentals of Earthquake Engineering*, Prentice Hall, New York, NY.

Opensees Development Team (Open Source Project). "OpenSees: open system for the earthquake engineering simulations" http://opensees.berkeley.edu/, 1998-2003.

Phalen, J. D. (2003). “Physical Modeling of the Soil-Foundation Interaction of Spread Footings Subjected to Lateral Cyclic Loading,” *M.S. Thesis,* University of California, Davis

Pollino, M P C; Bruneau, M. (2007). “Seismic Retrofit of Bridge Steel Truss Piers Using a Controlled Rocking Approach,” *Journal of Bridge Engineering*, No. 5, pp. 600-610. Sept. 2007.

Pollino, M., Bruneau, M. (2008). "Dynamic Seismic Response of Controlled Rocking Bridge Steel-Truss Piers," *Engineering Structures.*" Vol 30, No. 6, pp. 1667-1676, June 2008.

Pollino, M., Bruneau, M. (2010a). "Bidirectional Seismic Behavior of Controlled Rocking Four-Legged Bridge Steel Truss Piers." *Journal of Structural Engineering*, ASCE, Vol. 136, No. 12, pp 1512-1522, December 2010.

Pollino, M., Bruneau, M. (2010b). "Seismic Testing of a Bridge Steel Truss Pier Designed for Controlled Rocking." *Journal of Structural Engineering*, ASCE, Vol. 136, No. 12, pp 1523-1532, December 2010.

Priestley, N.M.J., Evison, R.J. and Carr, A.J. (1978). “Seismic Response of Structures Free to Rock on their Foundations,” *Bulletin of the New Zealand National Society for Earthquake Engineering*, Vol. 11, No. 3, Sept. pp. 141-150.

Priestley, N.M.J. and Seible, F. (1991). “Seismic Assessment and Retrofit of Bridges,” *Technical Report SSRP-91/03,* University of California, San Diego.

Priestley, N.M.J, Seible, F. and Calvi, G.M. (1996). *Seismic design and retrofit of bridges,* John Wiley & Sons, 1996.

Psycharis, I. N.; Jennings, P. C. (1983). “Rocking of slender rigid bodies allowed to uplift,” *Earthquake Engineering & Structural Dynamics,* Vol. 11, no. 1, pp. 57-76. Jan.-Feb. 1983

Psycharis, I. N.; Jennings, P. C. (1984). “Rocking, tipping and upthrow of simple structures by horizontal motion,” *Proceedings,* Eighth World Conference on Earthquake Engineering; pp. 291-298.

Rosebrook, K. R. (2001), “Moment Loading on Shallow Foundations: Centrifuge Test Data Archives," *M.S. Thesis,* University of California, Davis.

Rutenberg, A., Jennings, P.C. and Housner, G.W. (1982). “The response of Veterans Hospital Building 41 in the San Fernando Earthquake.” *Earthquake Engineering and Structural Dynamics*. Vol. 10.

SAC Steel Project (2006). Impulsive Near-Field Earthquake Ground Motions http://nisee.berkeley.edu/data /strong_motion/sacsteel/motions/nearfault.html

Sakai, J., and Mahin, S. A. (2006). *Earthquake simulation tests on reducing residual displacements of reinforced concrete bridge columns*. PEER Report (in preparation), Pacific Earthquake Engineering Resource Center, University of California, Berkeley, CA.

Sakellaraki, D., Watanabe, G. and Kawashima, K. (2005). “Experimental Rocking Response of Direct Foundations of Bridges,” *Proceedings, ”*2nd Int. Conf. on Urban Earthquake Engineering, March 7-8, 2005, Tokyo Inst. of Technology, Tokyo, Japan.

Sakellaraki, D. and Kawashima, K. (2006). “Effectiveness of Seismic Rocking Isolation of Bridges based on Shake Table Test,” *Proceedings,* First European Conference on Earthquake Engineering and Seismology, Paper No. 364, 1-10, Geneva, Switzerland, 2006.

Scott, M. H., and Fenves, G. L. (2006). “Plastic hinge integration methods for force-based beam-column elements." *ASCE J. of Structural Engineering*, 132(2): 244 –252.

Spanos, P. D.; Koh, A.-S.; Roesset, J. M. (1986). “Seismic uplifting of structures on flexible foundation,” *Proceedings*, 8th European Conference on Earthquake Engineering; pp. 5.6/25-32. 1986

Taucer, F. F., Spacone, E., and Filippou, F. C. (1991). *A fiber beam-column element for seismic response analysis of reinforced concrete structures*. Report No. UCB/EERC-91/17, Pacific Earthquake Engineering Research Center, University of California, Berkeley, CA.

Taylor PW, Bartlett PE, and Weissing PR (1981). "Foundation rocking under earthquake loading." *Proceedings,* 10th International Conference on Soil Mechanics and Foundation Engineering, Vol. 3. 313–322.

Ugalde , J.A., Kutter, B.L., Jeremic, B. and Gajan, S. (2007). "Centrifuge Modelling Of Rocking Behaviour Of Bridges On Shallow Foundations," *Proceedings,* 4th International Conference on Earthquake Geotechnical Engineering June 25-28, 2007, Paper No. 1484, 12pp.

Wang, S., Kutter, B. L., Chacko, J. M., Wilson, D. W., Boulanger, R. W. and Abghari, A. (1998). "Nonlinear Seismic Soil-Pile Structure Interaction" *Earthquake Spectra,* Volume 14, No. 2.

WINROCK: Computer program to estimate displacement of bridge piers allowed to rock on their foundations, Caltrans (Version 1.1.2 – 5/25/05)

Yim, C.-S.; Chopra, A. K.; Penzien, J. (1980). "Rocking response of rigid blocks to earthquakes," *Earthquake Engineering & Structural Dynamics,* Vol. 8, no. 6, pp. 565-587. Nov.-Dec.

Yim, C-S. and Chopra, A. (1983). "Effects of Transient Foundation Uplift on Earthquake Response of Structures," *Report no. UCB/EERC-83/09,* Earthquake Engineering Research Center, UC Berkeley, June, pp134

Yim, C.-S., Chopra, A. K. (1984a). "Dynamics of structures on two-spring foundation allowed to uplift," *Journal of Engineering Mechanics,* Vol. 110, no. 7, pp. 1124-1146. July 1984

Yim, C.-S., Chopra, A. K.(1984b). "Earthquake response of structures with partial uplift on Winkler foundation," *Earthquake Engineering & Structural Dynamics,* Vol. 12, no. 2, pp. 263-281. Mar.-Apr.

Werner, S.D, Nisar, A., Beck, J.L. (1992). "Assessment of UBC Seismic Design Provisions Using Recorded Building Motions," *Proceedings*, Earthquake Engineering, Tenth World Conference, Vol 10.5723-5728

Zhang, J., Tang, Y. (2009). "Dimensional Analysis of Structures with Translating and Rocking Foundations Under Near-Fault Ground Motions," *Soil Dynamics and Earthquake Engineering,* Vol 29, Issue 10, October 2009, pp. 1330-134.

Appendix A Experimental Test Schedule

Three test groups were run on the shaking table. Each of the test groups had several variations of loading direction, earthquake, and excitation amplitude or time scaling. The test schedule including run identification numbers is outlined in this Appendix.

Test Group	Test	Level[1]	Earthquake	Amplitude Scale	Loading Input	$dt=dt_o/\sqrt{S_d}$
1 (nominal $3\%f'_cA_g$ & $3D_c$ x $3D_{c)}$	A1	Elastic	Los Gatos	8%	1D-X	$0.02/\sqrt{(4.5)}$
	A2	Elastic	Los Gatos	8%	1D-Y	$0.02/\sqrt{(4.5)}$
	A3	Elastic	Los Gatos	8%	2D-X+Y	$0.02/\sqrt{(4.5)}$
	A4	Elastic	Los Gatos	8%	2D-X+Z	$0.02/\sqrt{(4.5)}$
	A5	Elastic	Los Gatos	8%	3D-X+Y+Z	$0.02/\sqrt{(4.5)}$
	B1	Elastic	Los Gatos	32%	1D-X	$0.02/\sqrt{(4.5)}$
	B2	Elastic	Los Gatos	32%	1D-Y	$0.02/\sqrt{(4.5)}$
	B3	Elastic	Los Gatos	32%	2D-X+Y	$0.02/\sqrt{(4.5)}$
	B4	Elastic	Los Gatos	32%	2D-X+Z	$0.02/\sqrt{(4.5)}$
	B5	Elastic	Los Gatos	32%	3D-X+Y+Z	$0.02/\sqrt{(4.5)}$
	C1	Elastic	Tabas	8%	1D-X	$0.01/\sqrt{(4.5)}$
	C2	Elastic	Tabas	8%	1D-Y	$0.01/\sqrt{(4.5)}$
	C3	Elastic	Tabas	8%	2D-X+Y	$0.01/\sqrt{(4.5)}$
	C4	Elastic	Tabas	8%	2D-X+Z	$0.01/\sqrt{(4.5)}$
	C5	Elastic	Tabas	8%	3D-X+Y+Z	$0.01/\sqrt{(4.5)}$
	D1	Elastic	Tabas	32%	1D-X	$0.01/\sqrt{(4.5)}$
	D2	Elastic	Tabas	32%	1D-Y	$0.01/\sqrt{(4.5)}$
	D3	Elastic	Tabas	32%	2D-X+Y	$0.01/\sqrt{(4.5)}$
	D4	Elastic	Tabas	32%	2D-X+Z	$0.01/\sqrt{(4.5)}$
	D5	Elastic	Tabas	32%	3D-X+Y+Z	$0.01/\sqrt{(4.5)}$
	E1	Elastic	Los Gatos	32%	1D-X	$\sqrt{(2)}*0.02/\sqrt{(4.5)}$
	E2	Elastic	Los Gatos	32%	1D-Y	$\sqrt{(2)}*0.02/\sqrt{(4.5)}$
	E3	Elastic	Los Gatos	32%	2D-X+Y	$\sqrt{(2)}*0.02/\sqrt{(4.5)}$
	E4	Elastic	Los Gatos	32%	2D-X+Z	$\sqrt{(2)}*0.02/\sqrt{(4.5)}$
	E5	Elastic	Los Gatos	32%	3D-X+Y+Z	$\sqrt{(2)}*0.02/\sqrt{(4.5)}$
	F1	Elastic	Tabas	42%	1D-X	$0.01/\sqrt{(4.5)}$
	F2	Elastic	Tabas	42%	1D-Y	$0.01/\sqrt{(4.5)}$
	F3	Elastic	Tabas	42%	2D-X+Y	$0.01/\sqrt{(4.5)}$
	F4	Elastic	Tabas	42%	2D-X+Z	$0.01/\sqrt{(4.5)}$
	F5	Elastic	Tabas	42%	3D-X+Y+Z	$0.01/\sqrt{(4.5)}$
2 (nominal $10\%f'_cA_g$ & $3D_c$ x $3D_{c)}$	A1S	Elastic	Los Gatos	15%	1D-X	$\sqrt{(2)}*0.02/\sqrt{(4.5)}$
	A2S	Elastic	Los Gatos	15%	1D-Y	$\sqrt{(2)}*0.02/\sqrt{(4.5)}$
	A3S	Elastic	Los Gatos	15%	2D-X+Y	$\sqrt{(2)}*0.02/\sqrt{(4.5)}$
	A4S	Elastic	Los Gatos	15%	2D-X+Z	$\sqrt{(2)}*0.02/\sqrt{(4.5)}$
	A5S	Elastic	Los Gatos	15%	3D-X+Y+Z	$\sqrt{(2)}*0.02/\sqrt{(4.5)}$
	B1S	Elastic	Tabas	15%	1D-X	$0.01/\sqrt{(4.5)}$
	B2S	Elastic	Tabas	15%	1D-Y	$0.01/\sqrt{(4.5)}$
	B3S	Elastic	Tabas	15%	2D-X+Y	$0.01/\sqrt{(4.5)}$
	B4S	Elastic	Tabas	15%	2D-X+Z	$0.01/\sqrt{(4.5)}$
	B5S	Elastic	Tabas	15%	3D-X+Y+Z	$0.01/\sqrt{(4.5)}$
	C1S	Elastic	Los Gatos	15%	1D-X	$0.02/\sqrt{(4.5)}$
	C2S	Elastic	Los Gatos	15%	1D-Y	$0.02/\sqrt{(4.5)}$
	C3S	Elastic	Los Gatos	15%	2D-X+Y	$0.02/\sqrt{(4.5)}$
	C4S	Elastic	Los Gatos	15%	2D-X+Z	$0.02/\sqrt{(4.5)}$
	C5S	Elastic	Los Gatos	15%	3D-X+Y+Z	$0.02/\sqrt{(4.5)}$
	D1S	Elastic	Los Gatos	25%	1D-X	$0.02/\sqrt{(4.5)}$
	D2S	Elastic	Los Gatos	25%	1D-Y	$0.02/\sqrt{(4.5)}$

	D3S	Elastic	Los Gatos	25%	2D-X+Y	0.02/√(4.5)
	D4S	Elastic	Los Gatos	25%	2D-X+Z	0.02/√(4.5)
	D5S	Elastic	Los Gatos	25%	3D-X+Y+Z	0.02/√(4.5)
	E1S	Elastic	Los Gatos	15%	3D-X+Y+Z	0.02/√(4.5)
	E2S	Elastic	Los Gatos	25%	3D-X+Y+Z	0.02/√(4.5)
	F1S	Elastic	Tabas	25%	1D-X	0.01/√(4.5)
	F2S	Elastic	Tabas	25%	1D-Y	0.01/√(4.5)
	F3S	Elastic	Tabas	25%	2D-X+Y	0.01/√(4.5)
	F4S	Elastic	Tabas	25%	2D-X+Z	0.01/√(4.5)
	F5S	Elastic	Tabas	25%	3D-X+Y+Z	0.01/√(4.5)
	G1S	Elastic	Tabas	25%	1D-X	√(2)*0.01/√(4.5)
	G2S	Elastic	Tabas	25%	1D-Y	√(2)*0.01/√(4.5)
	G3S	Elastic	Tabas	25%	2D-X+Y	√(2)*0.01/√(4.5)
	G4S	Elastic	Tabas	25%	2D-X+Z	√(2)*0.01/√(4.5)
	G5S	Elastic	Tabas	25%	3D-X+Y+Z	√(2)*0.01/√(4.5)
	H1S	Elastic	Los Gatos	25%	1D-X	0.02/√(4.5)
	H2S	Elastic	Los Gatos	25%	3D-X+Y+Z	0.02/√(4.5)
3 (nominal $10\%f'_cA_g$ $5D_cx3D_c$)	A1R	Elastic	Los Gatos	10%	3D-X+Y+Z	0.02/√(4.5)
	A2R	Yield	Los Gatos	25%	3D-X+Y+Z	0.02/√(4.5)
	A3R	Design	Los Gatos	90%	3D-X+Y+Z	0.02/√(4.5)
	A4R	MCE	Los Gatos	120%	3D-X+Y+Z	0.02/√(4.5)

[1]loading level defined by flexural ductility demands

Appendix B Experimental Test Results

Some of the experimental results from selected tests listed in Appendix A are displayed on the following pages. The general behavior of a system allowed to uplift are shown. Plots presented include the center of mass translational components, footing uplift displacement, the moment demand at base of column vs. the rotation of the footing and the column base moment vs. average curvature demands.

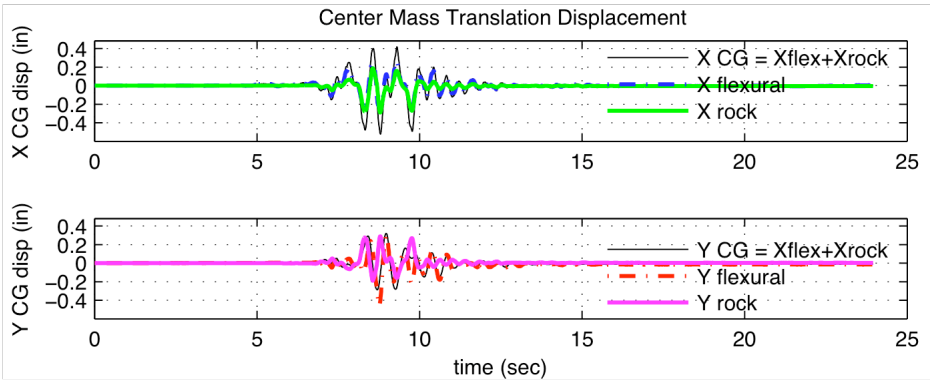

(a) X center mass translation (b) Y center mass translations

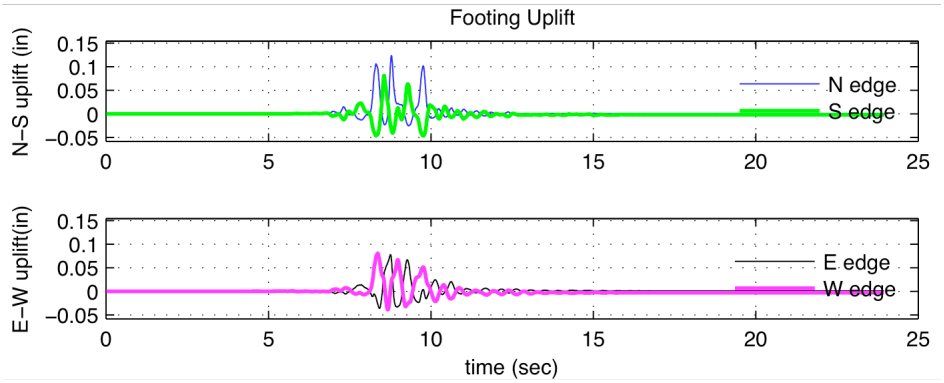

(c) N-S footing uplift (d) E-W footing uplift

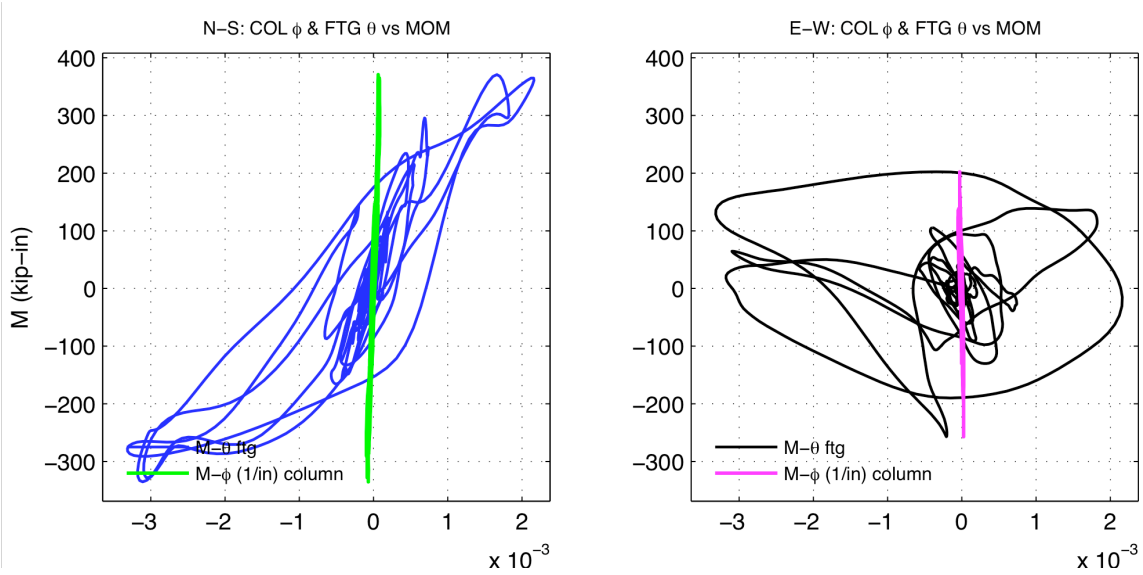

(e) N-S: Mom. vs Col ϕ (1/in) and FTG θ (f) E-W: Mom. vs Col ϕ (1/in) and FTG

Figure B-1: B1 Experimental Results

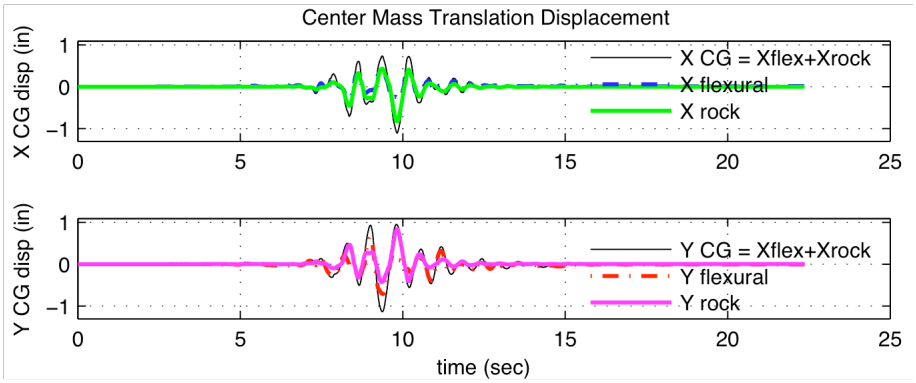

(a) X center mass translation (b) Y center mass translations

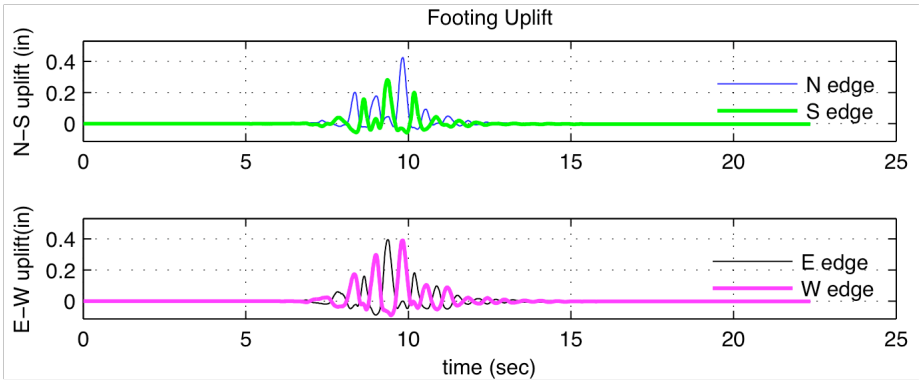

(c) N-S footing uplift (d) E-W footing uplift

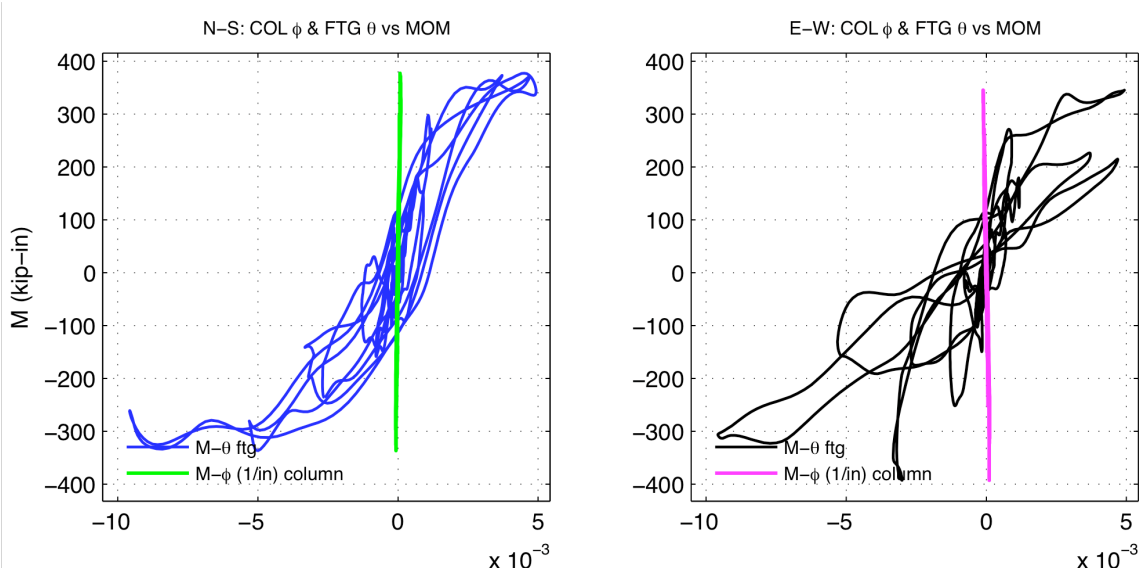

(e) N-S: Mom. vs Col ϕ (1/in) and FTG θ (f) E-W: Mom. vs Col ϕ (1/in) and FTG

Figure B-2: B3 Experimental Results

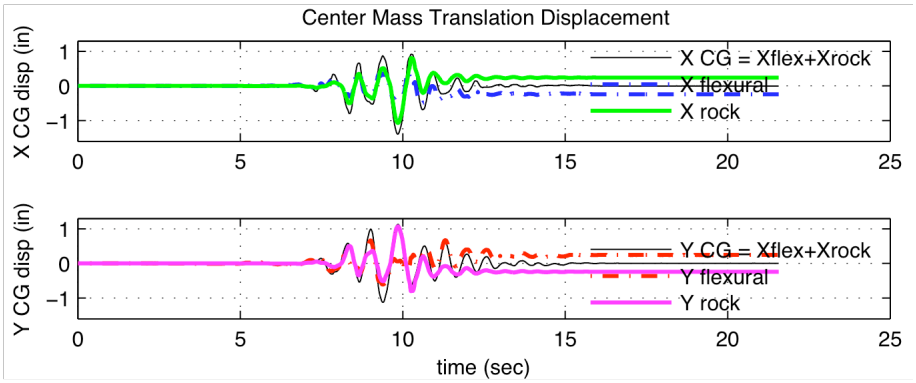

(a) X center mass translation (b) Y center mass translations

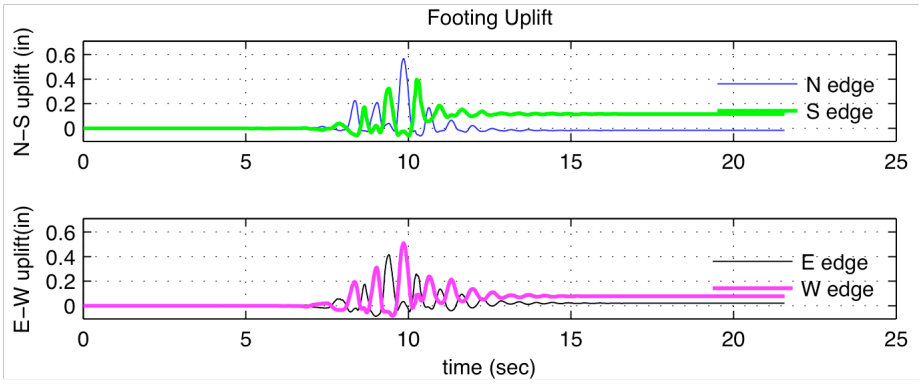

(c) N-S footing uplift (d) E-W footing uplift

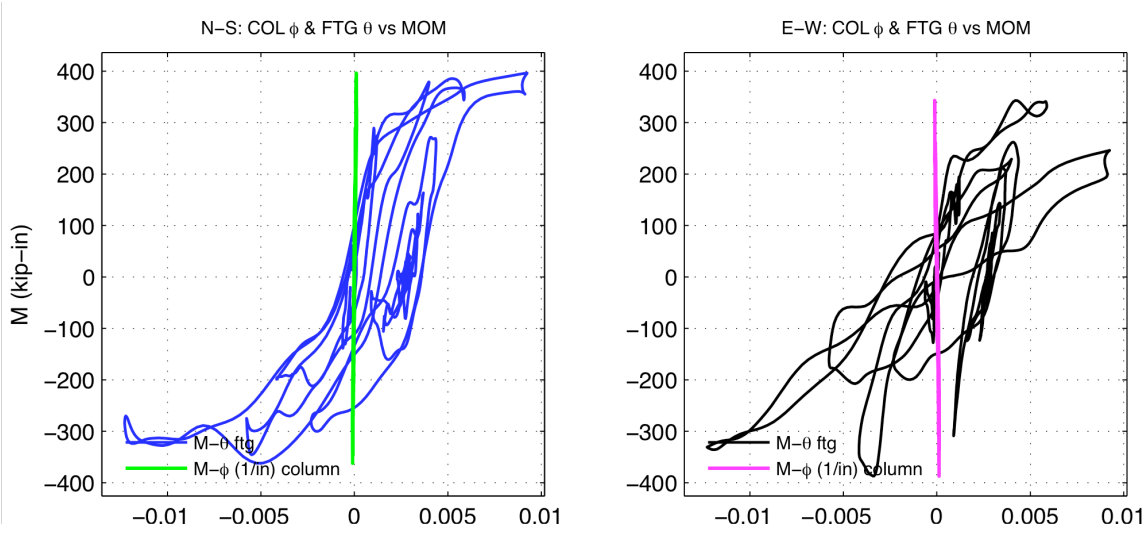

(e) N-S: Mom. vs Col ϕ (1/in) and FTG θ (f) E-W: Mom. vs Col ϕ (1/in) and FTG

Figure B-3: B5 Experimental Results

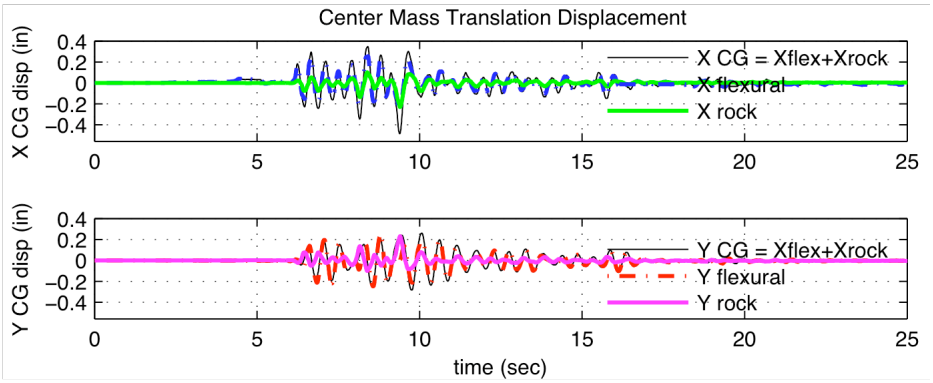

(a) X center mass translation (b) Y center mass translations

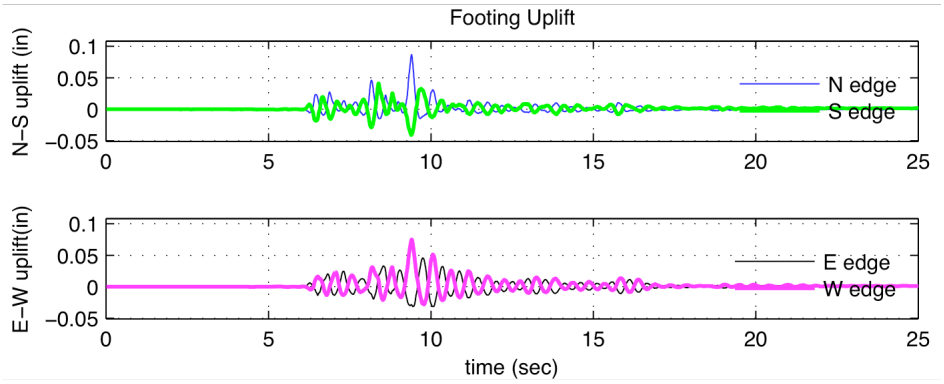

(c) N-S footing uplift (d) E-W footing uplift

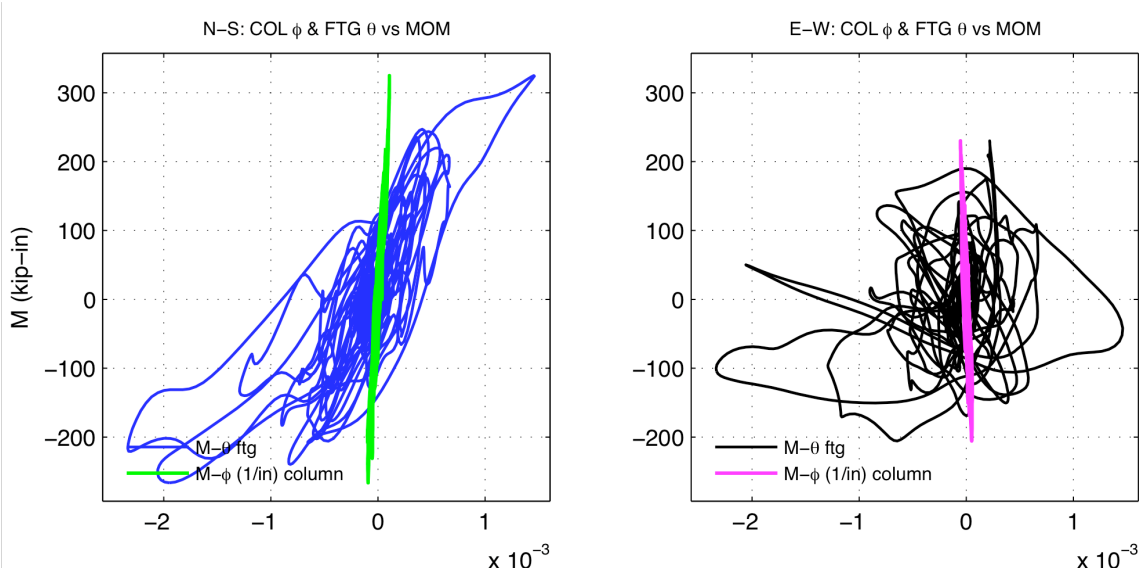

(e) N-S: Mom. vs Col ϕ (1/in) and FTG θ (f) E-W: Mom. vs Col ϕ (1/in) and FTG

Figure B-4: D1 Experimental Results

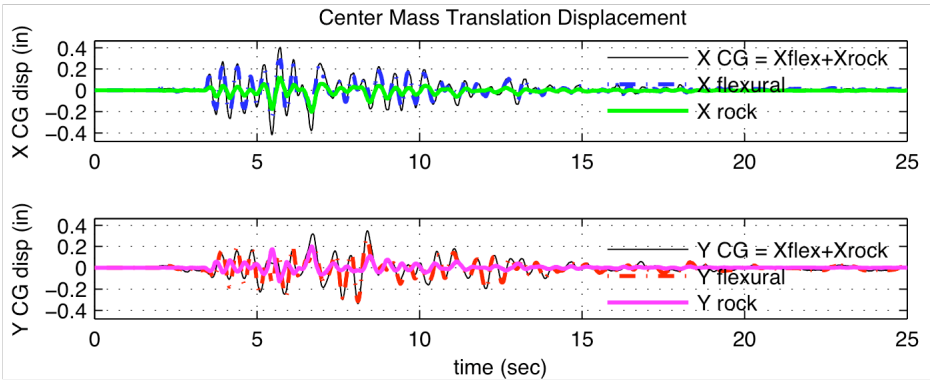

(a) X center mass translation (b) Y center mass translations

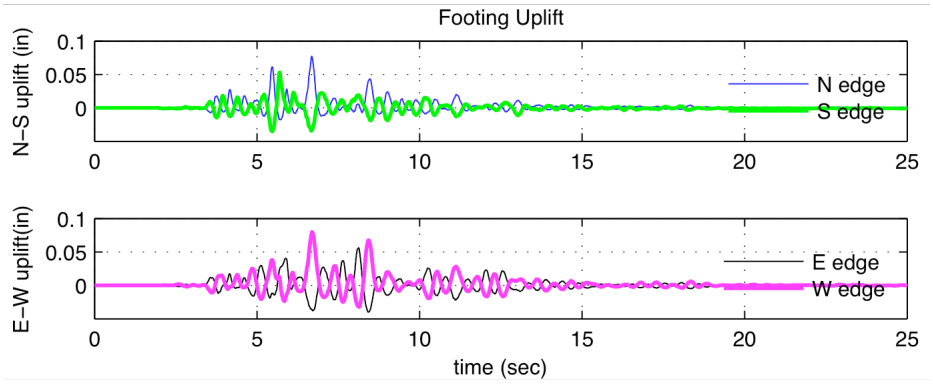

(c) N-S footing uplift (d) E-W footing uplift

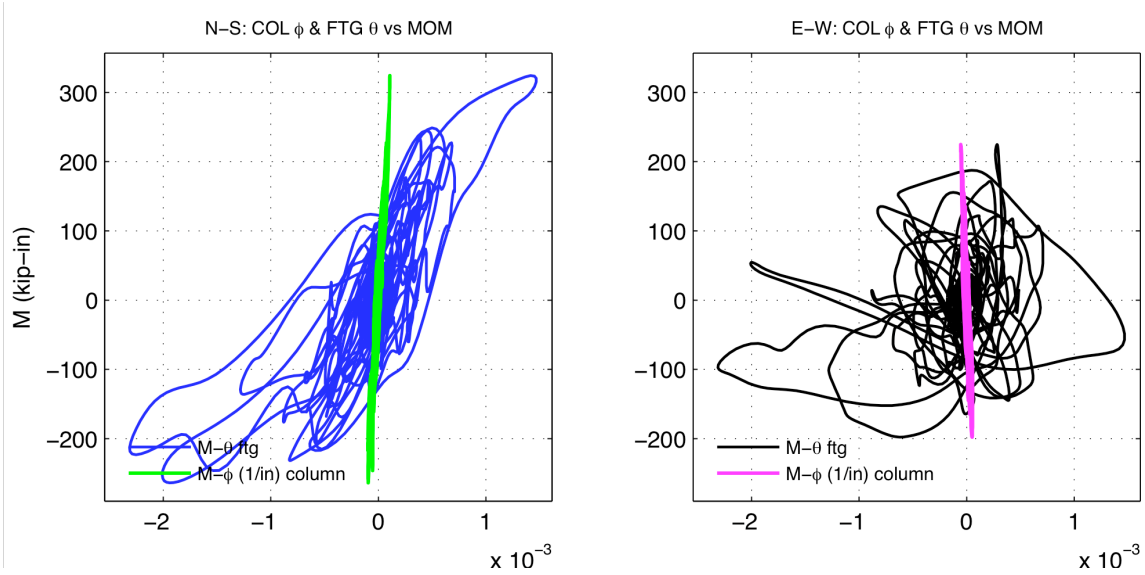

(e) N-S: Mom. vs Col ϕ (1/in) and FTG θ (f) E-W: Mom. vs Col ϕ (1/in) and FTG

Figure B-5: D3 Experimental Results

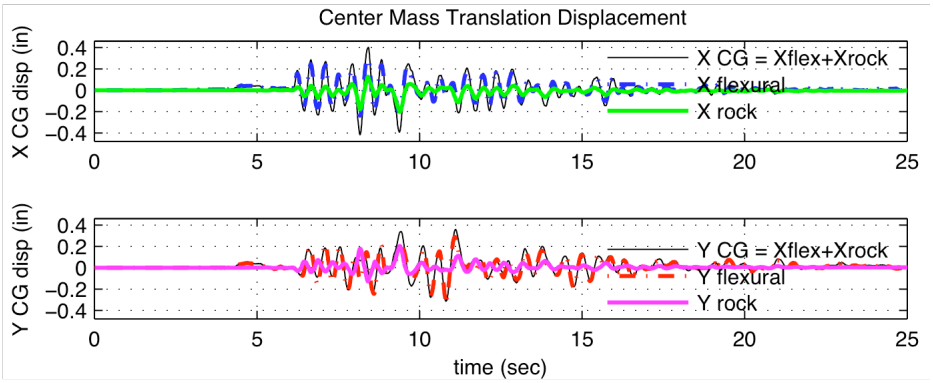

(a) X center mass translation (b) Y center mass translations

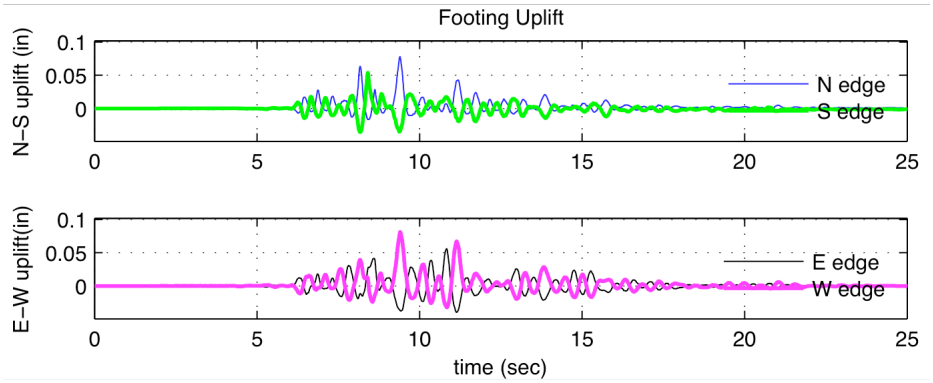

(c) N-S footing uplift (d) E-W footing uplift

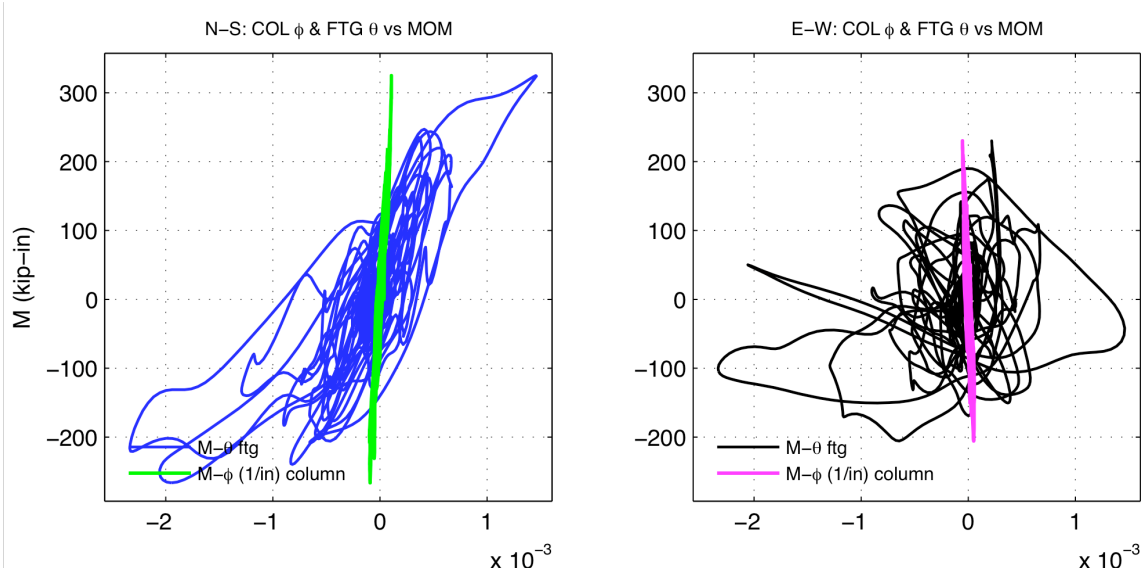

(e) N-S: Mom. vs Col ϕ (1/in) and FTG θ (f) E-W: Mom. vs Col ϕ (1/in) and FTG

Figure B-6: D5 Experimental Results

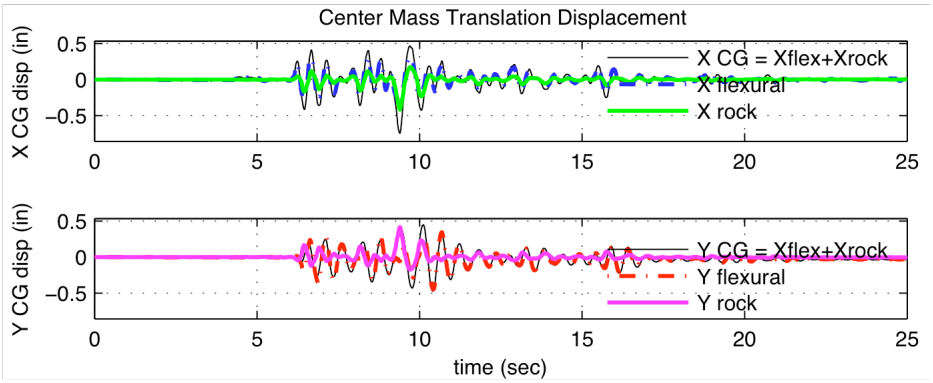

(a) X center mass translation (b) Y center mass translations

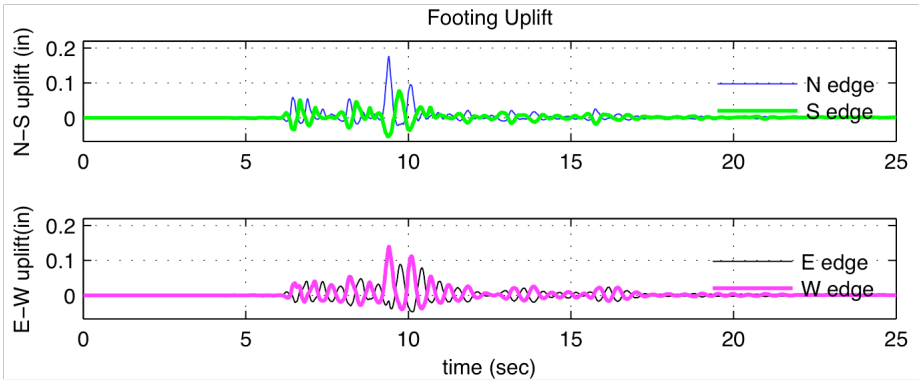

(c) N-S footing uplift (d) E-W footing uplift

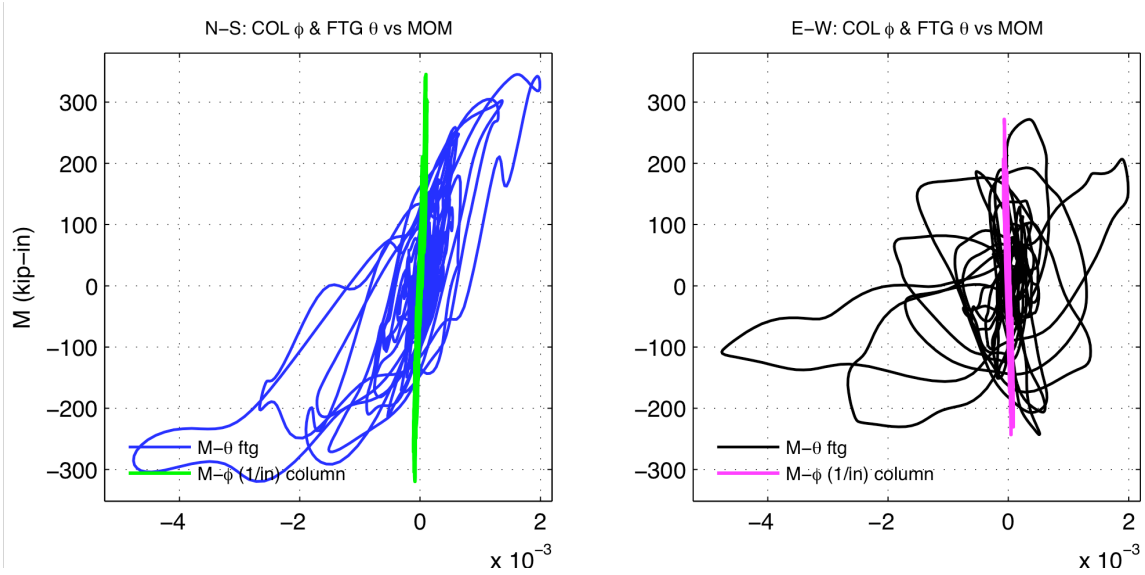

(e) N-S: Mom. vs Col ϕ (1/in) and FTG θ (f) E-W: Mom. vs Col ϕ (1/in) and FTG

Figure B-7: F1 Experimental Results

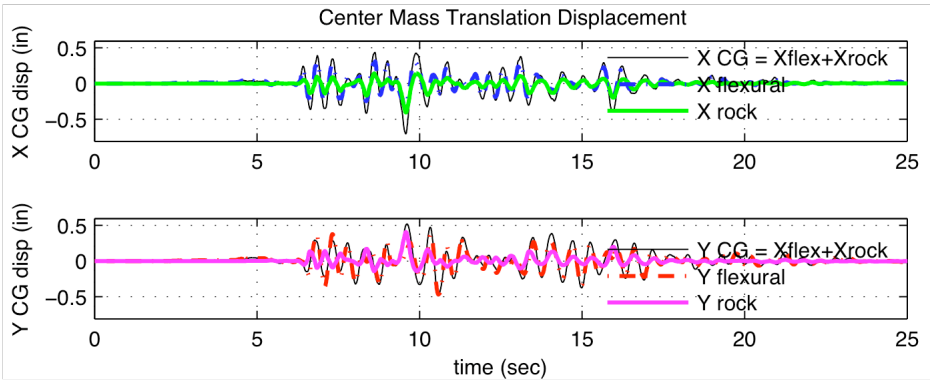

(a) X center mass translation (b) Y center mass translations

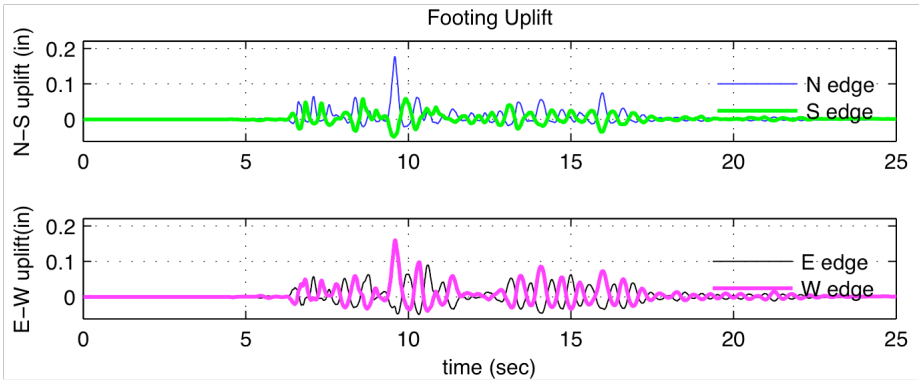

(c) N-S footing uplift (d) E-W footing uplift

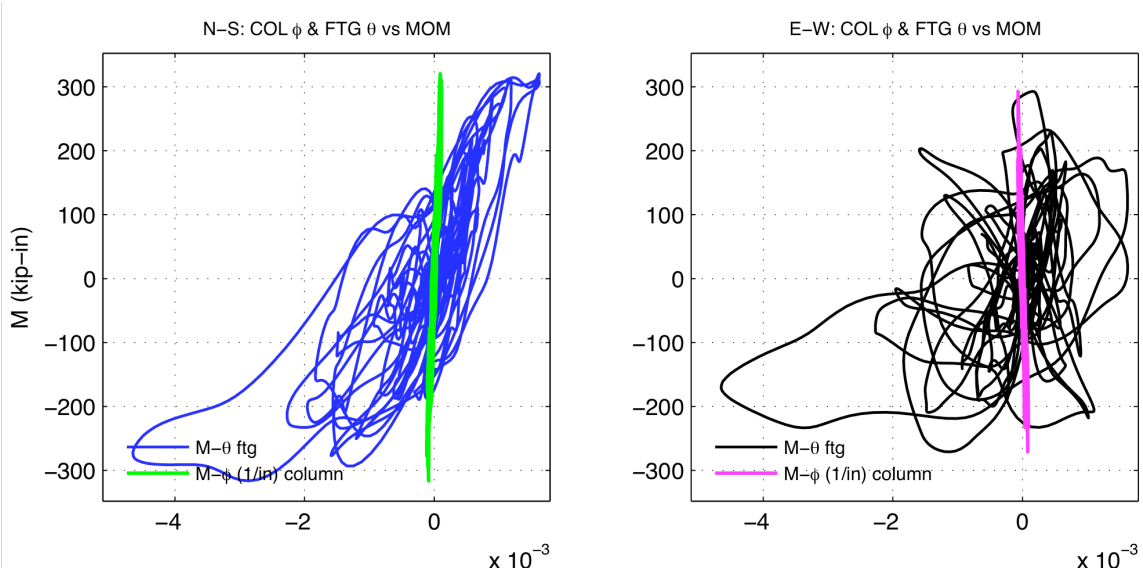

(e) N-S: Mom. vs Col ϕ (1/in) and FTG θ (f) E-W: Mom. vs Col ϕ (1/in) and FTG

Figure B-8: F3 Experimental Results

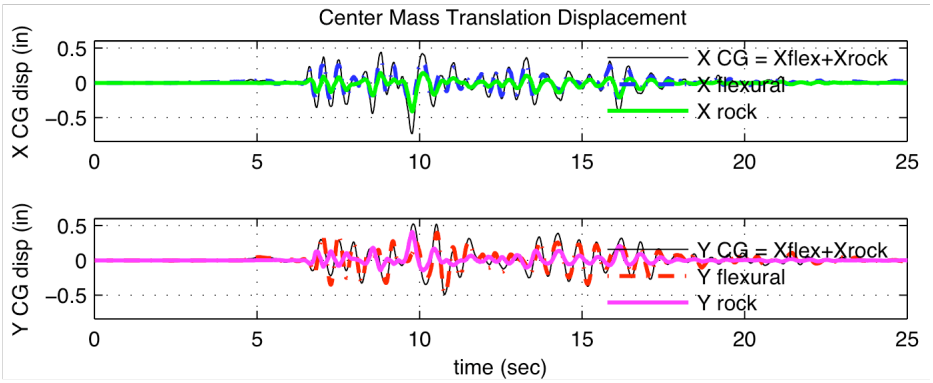

(a) X center mass translation (b) Y center mass translations

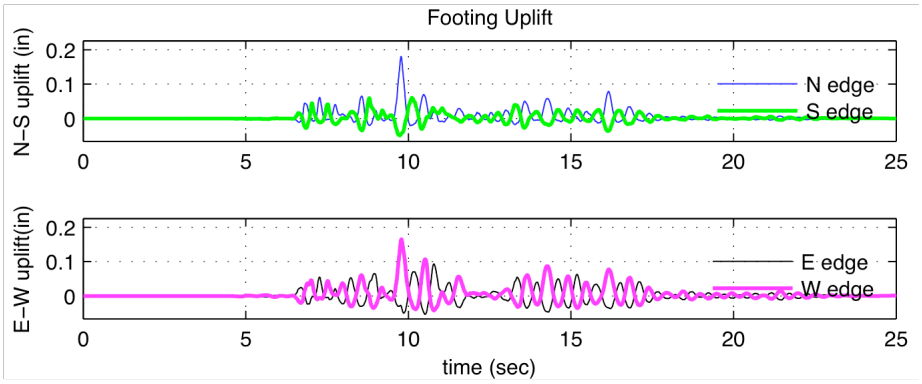

(c) N-S footing uplift (d) E-W footing uplift

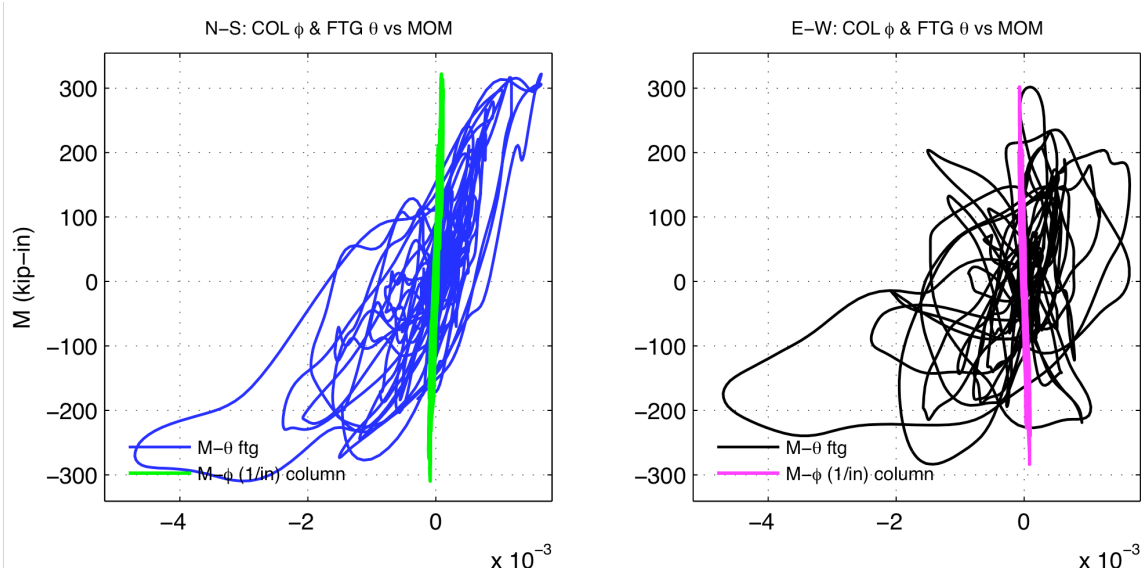

(e) N-S: Mom. vs Col ϕ (1/in) and FTG θ (f) E-W: Mom. vs Col ϕ (1/in) and FTG

Figure B-9: F5 Experimental Results

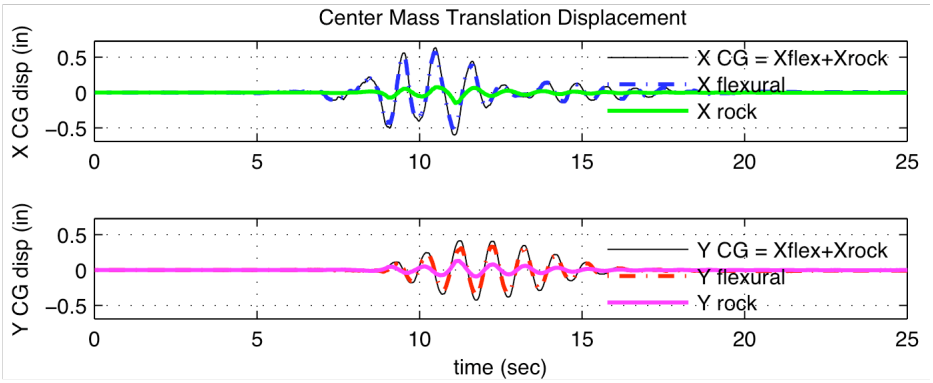

(a) X center mass translation (b) Y center mass translations

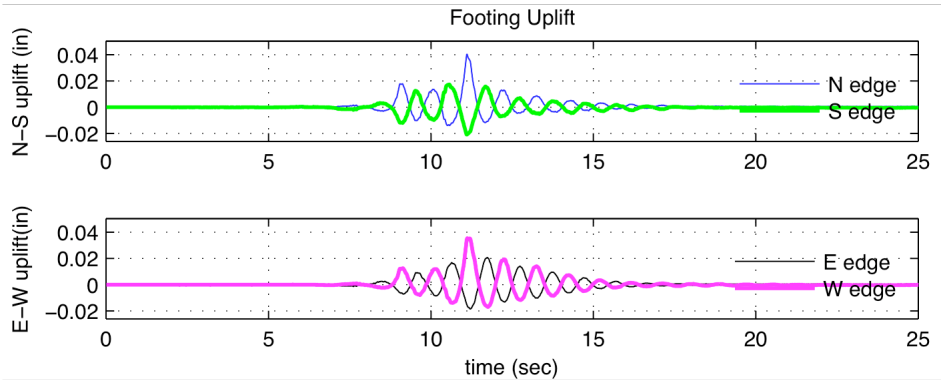

(c) N-S footing uplift (d) E-W footing uplift

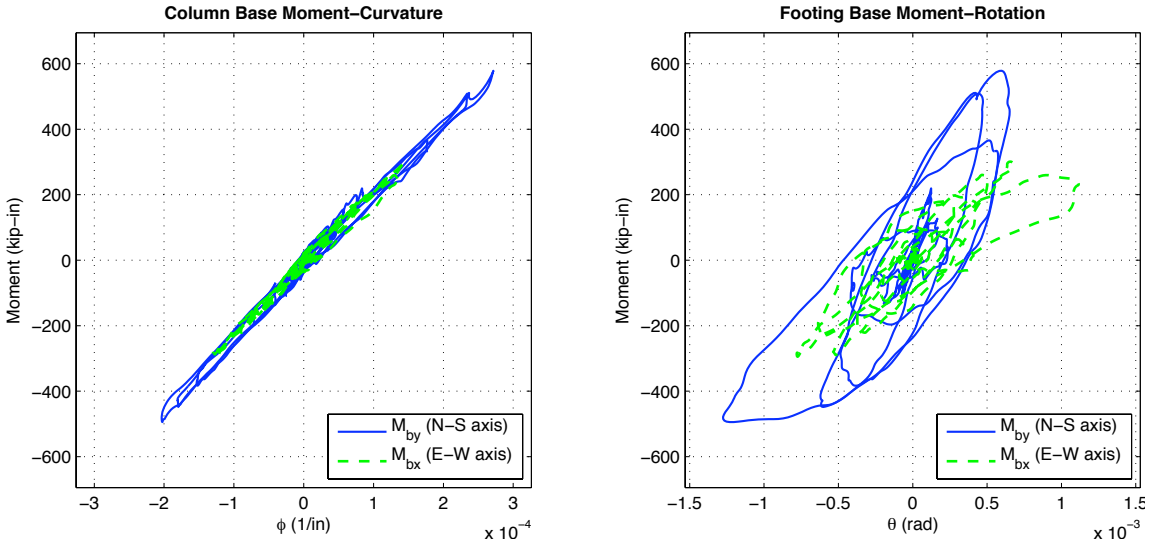

(e) Mom. vs Col ϕ (1/in) (f) Mom. vs FTG θ (rad)

Figure B-10: A1S Experimental Results

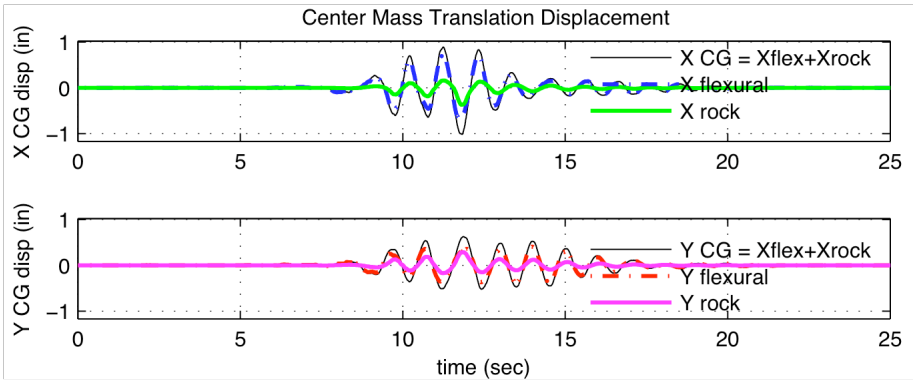

(a) X center mass translation (b) Y center mass translations

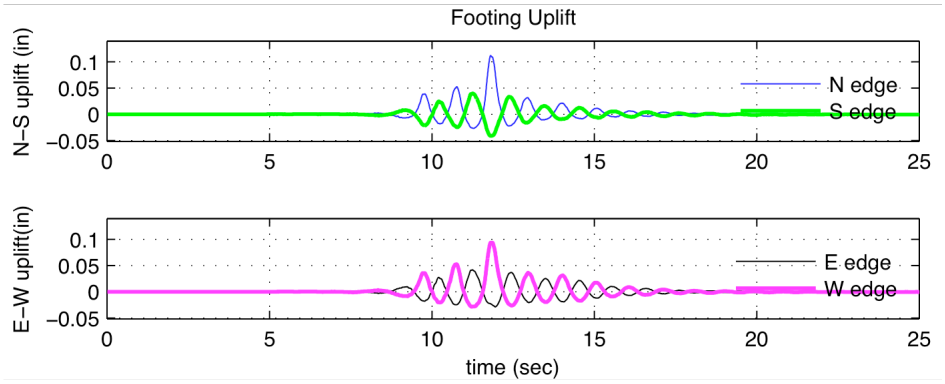

(c) N-S footing uplift (d) E-W footing uplift

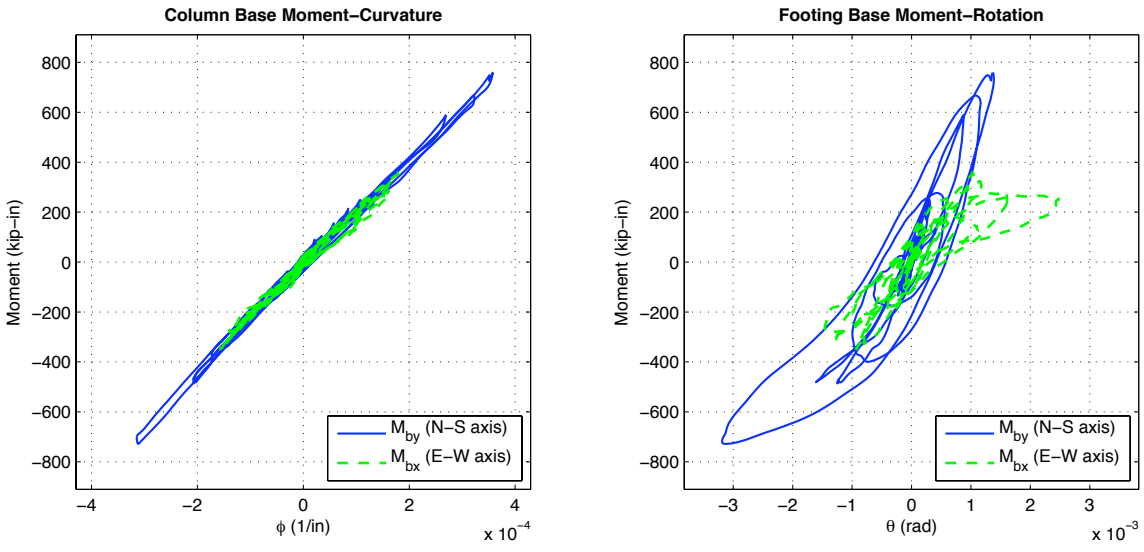

(e) Mom. vs Col ϕ (1/in) (f) Mom. vs FTG θ (rad)

Figure B-11: A3S Experimental Results

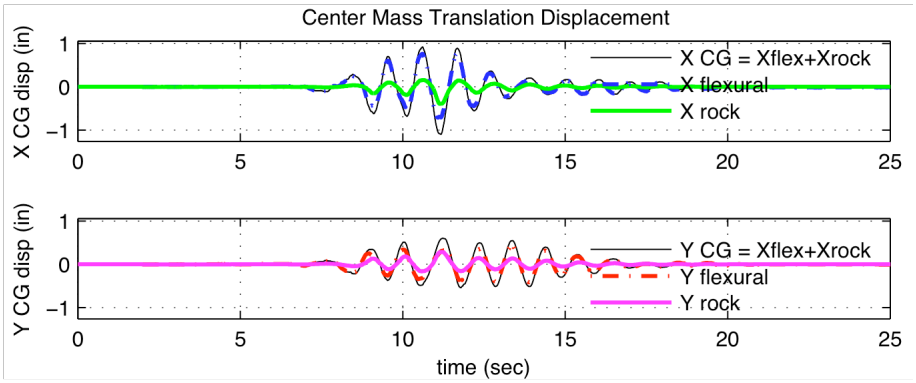

(a) X center mass translation (b) Y center mass translations

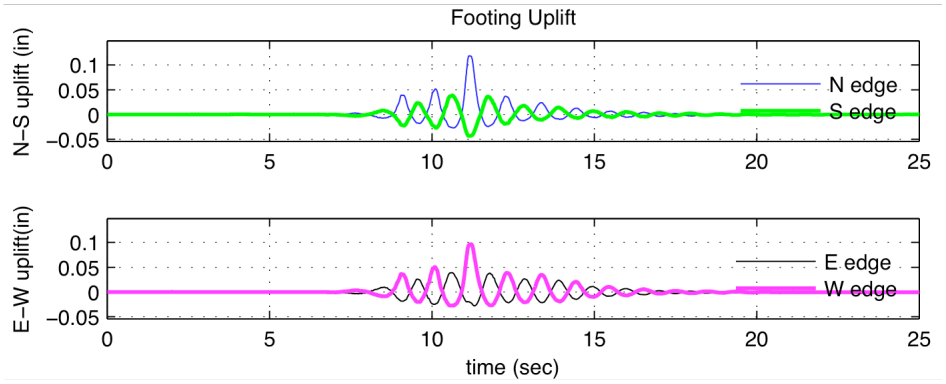

(c) N-S footing uplift (d) E-W footing uplift

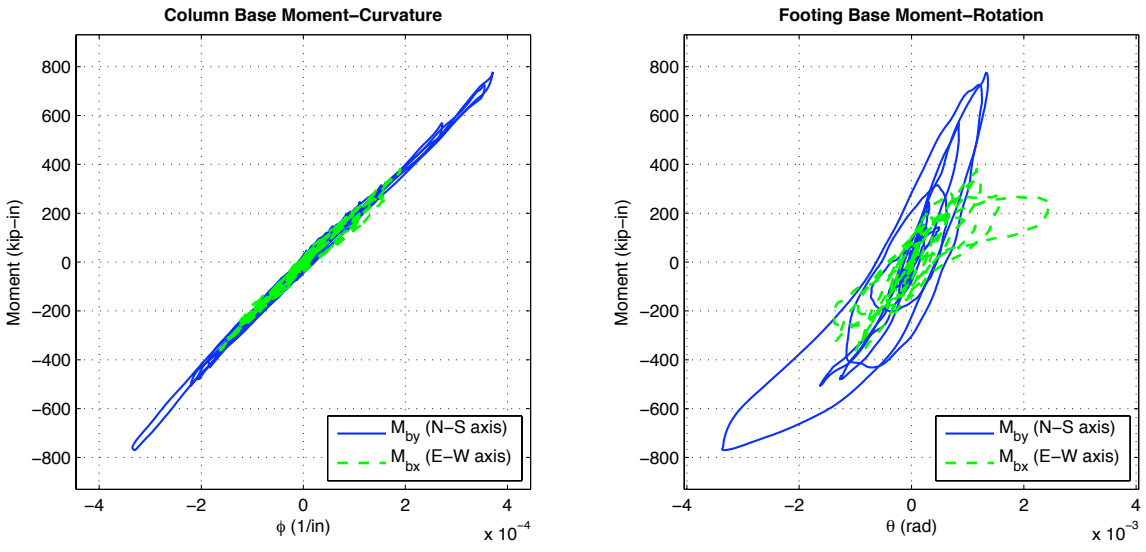

(e) Mom. vs Col ϕ (1/in) (f) Mom. vs FTG θ (rad)

Figure B-12: A5S Experimental Results

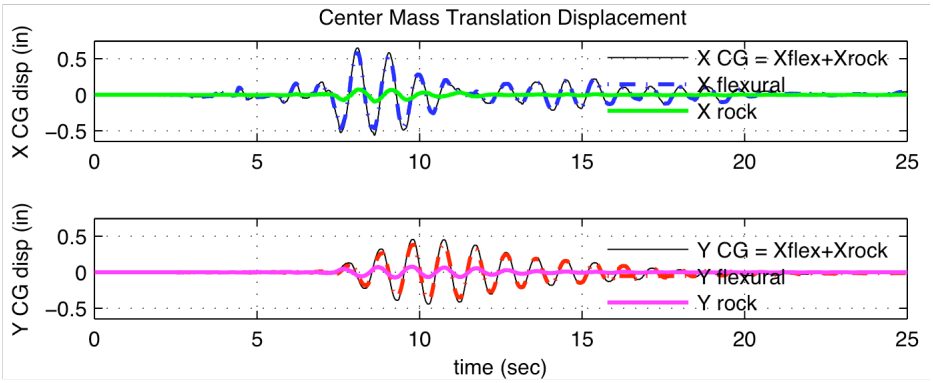

(a) X center mass translation (b) Y center mass translations

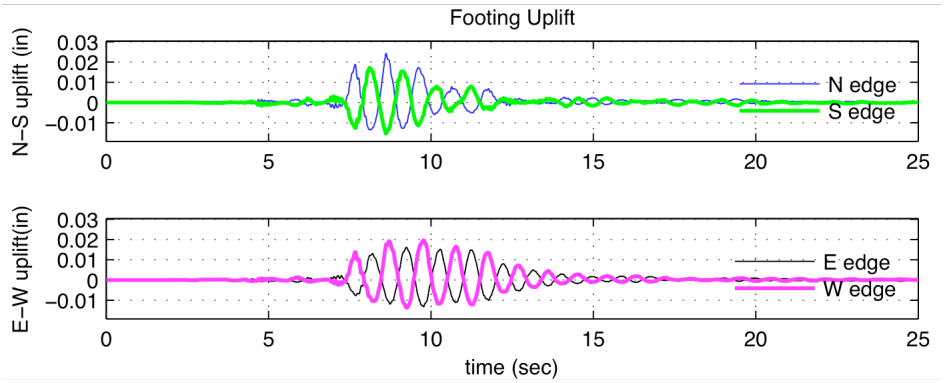

(c) N-S footing uplift (d) E-W footing uplift

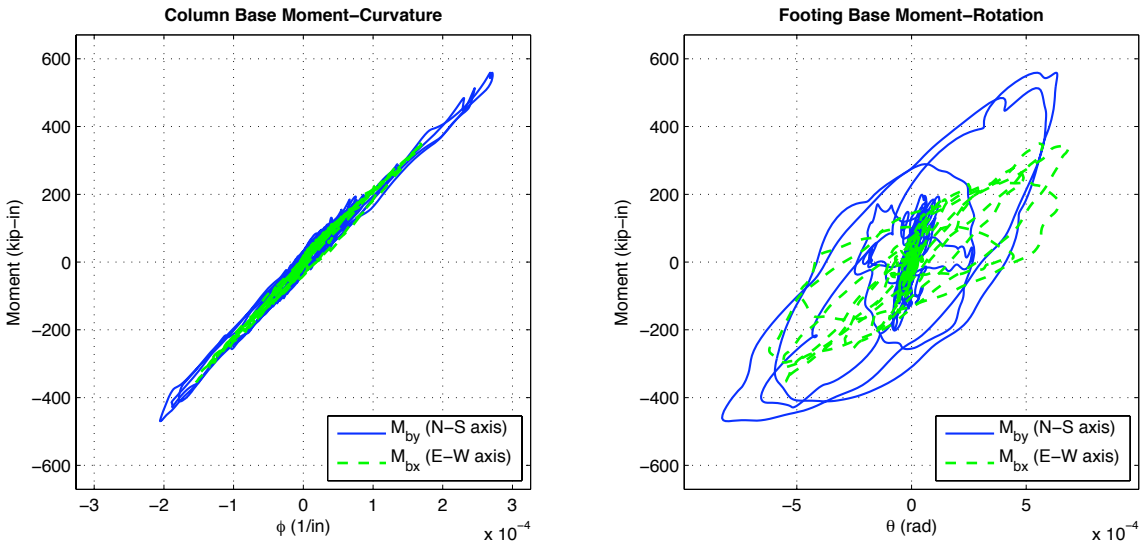

(e) Mom. vs Col ϕ (1/in) (f) Mom. vs FTG θ (rad)

Figure B-13: B1S Experimental Results

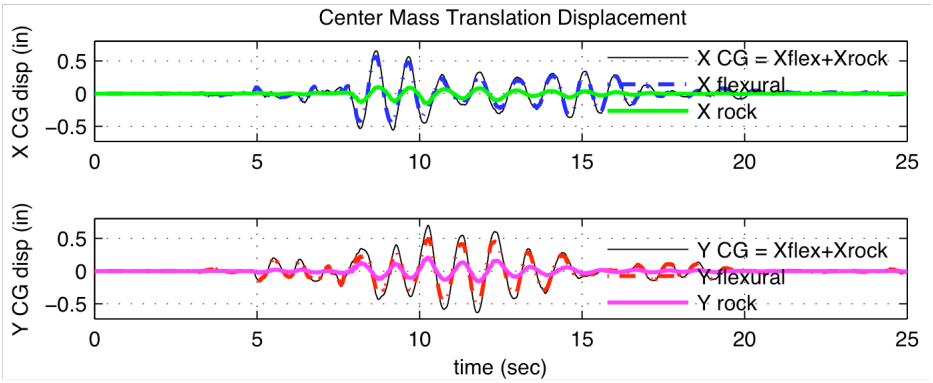

(a) X center mass translation (b) Y center mass translations

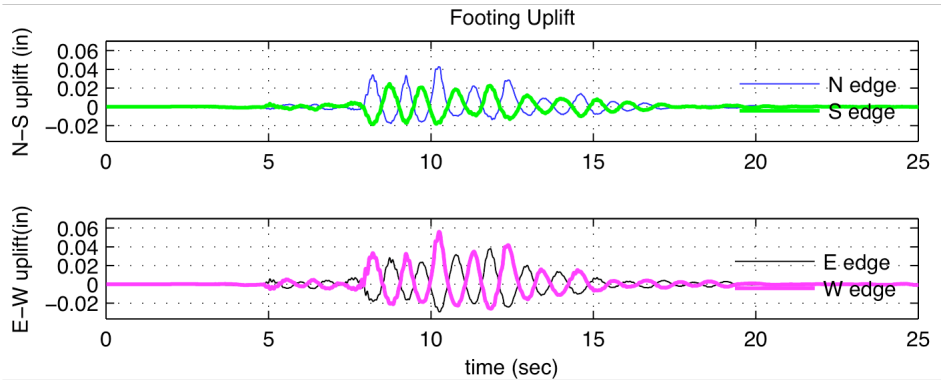

(c) N-S footing uplift (d) E-W footing uplift

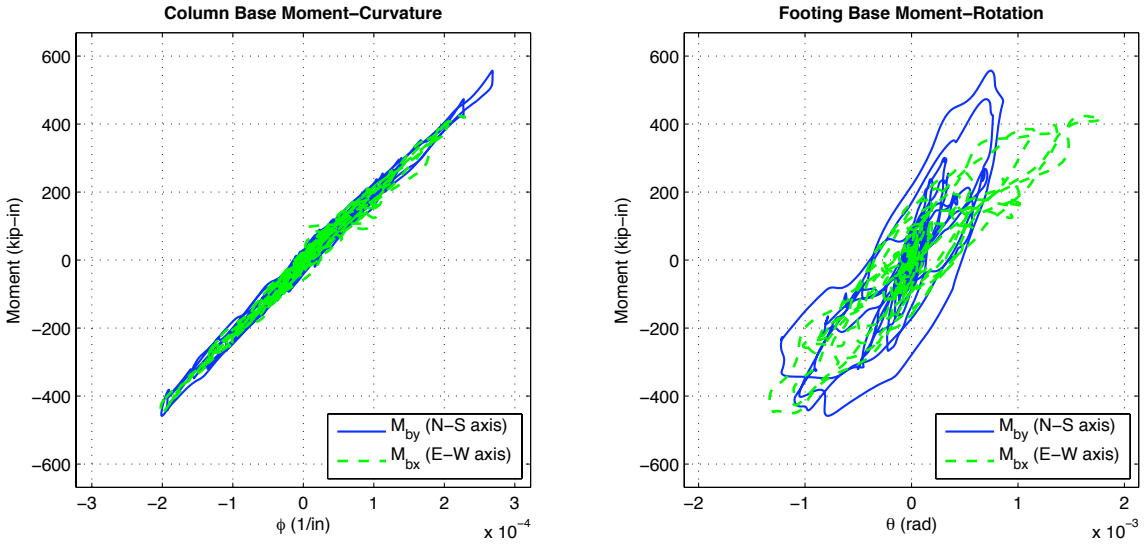

(e) Mom. vs Col ϕ (1/in) (f) Mom. vs FTG θ (rad)

Figure B-14: B3S Experimental Results

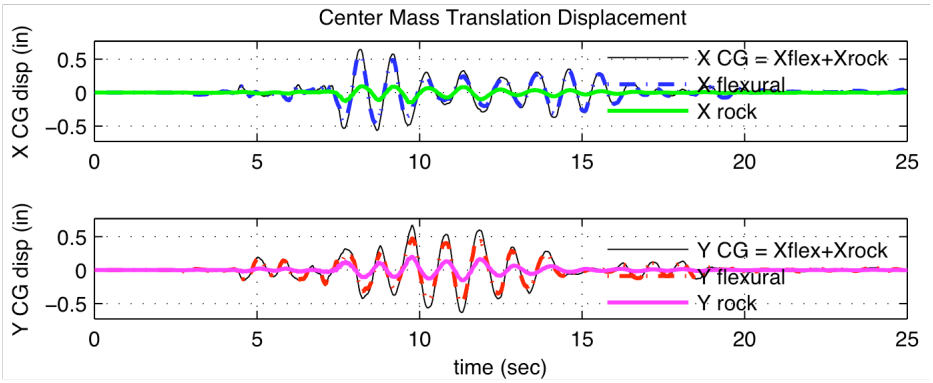

(a) X center mass translation (b) Y center mass translations

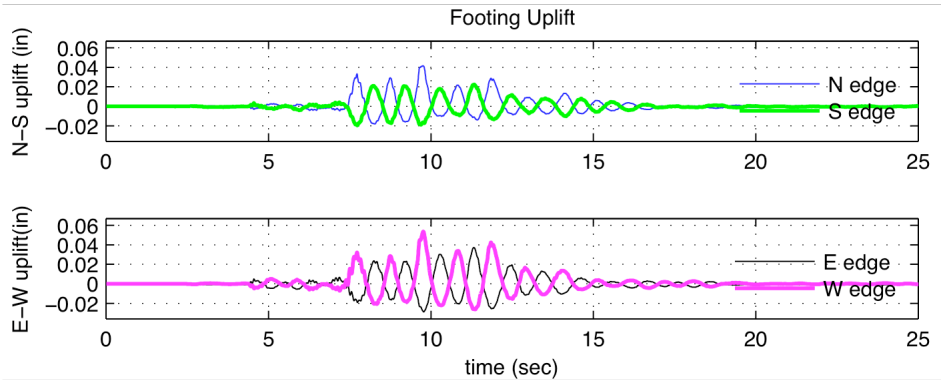

(c) N-S footing uplift (d) E-W footing uplift

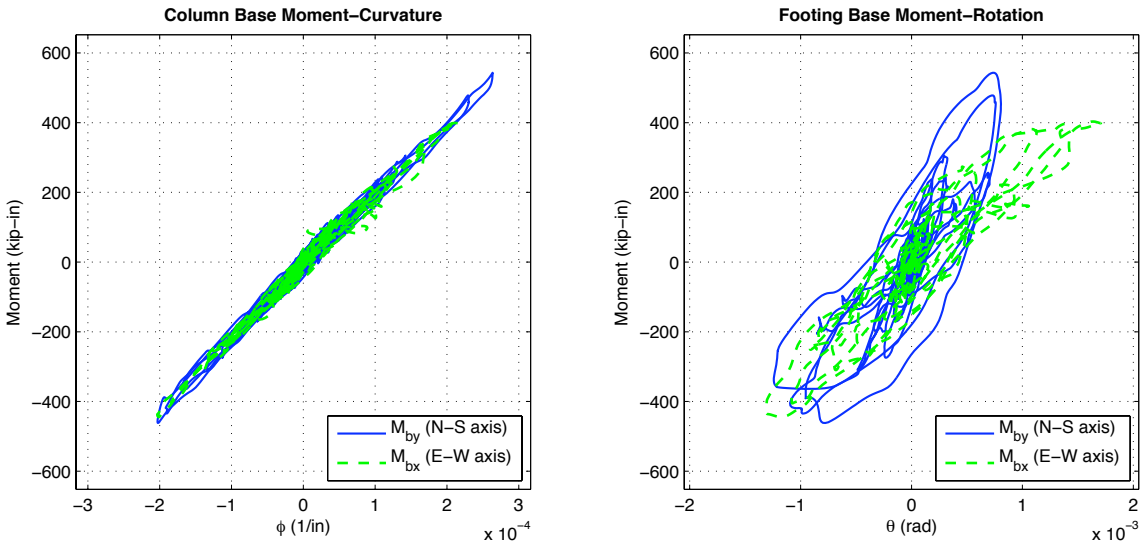

(e) Mom. vs Col ϕ (1/in) (f) Mom. vs FTG θ (rad)

Figure B-15: B5S Experimental Results

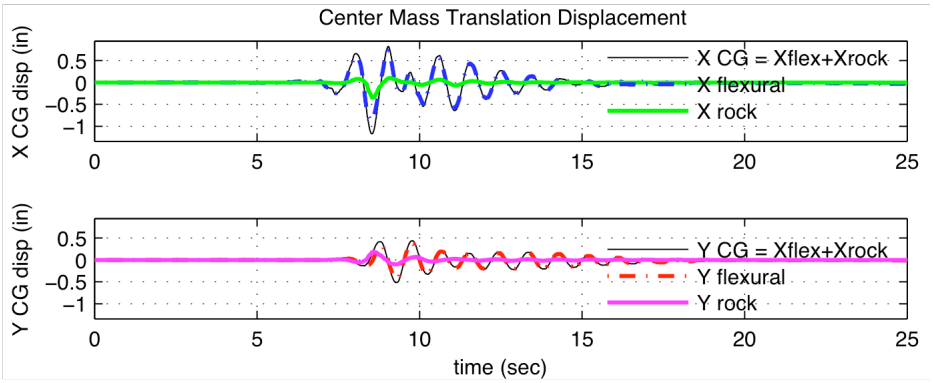

(a) X center mass translation (b) Y center mass translations

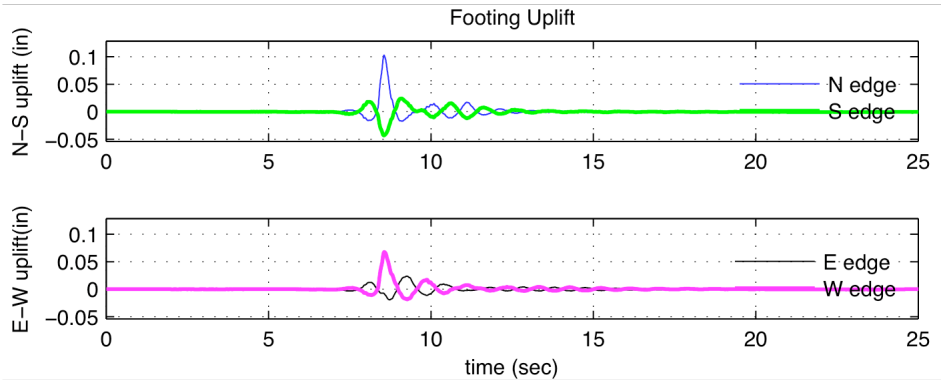

(c) N-S footing uplift (d) E-W footing uplift

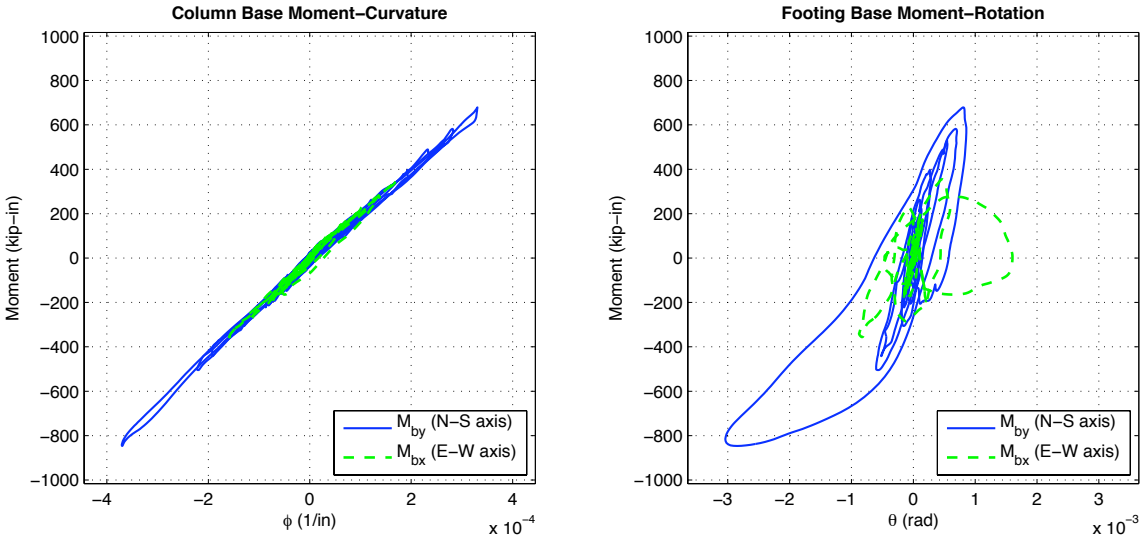

(e) Mom. vs Col ϕ (1/in) (f) Mom. vs FTG θ (rad)

Figure B-16: C1S Experimental Results

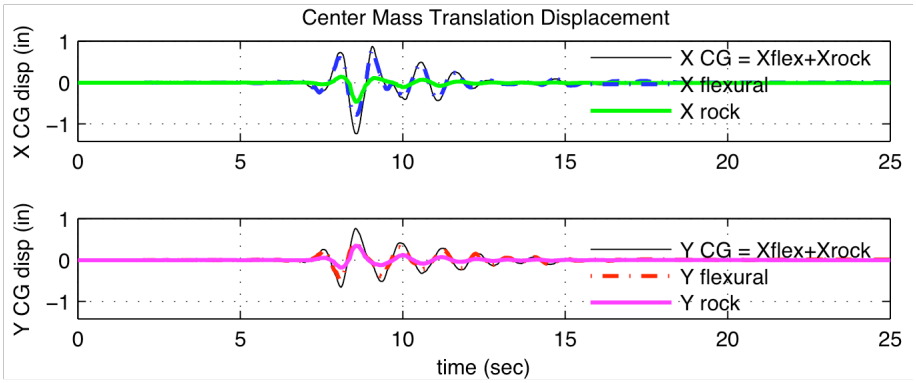

(a) X center mass translation (b) Y center mass translations

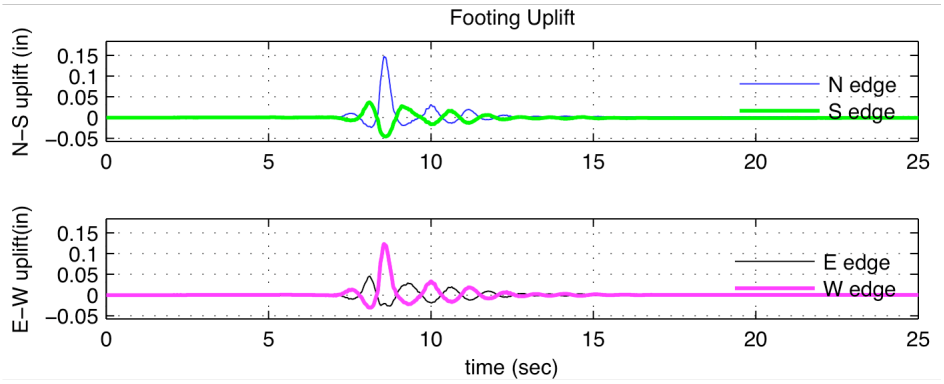

(c) N-S footing uplift (d) E-W footing uplift

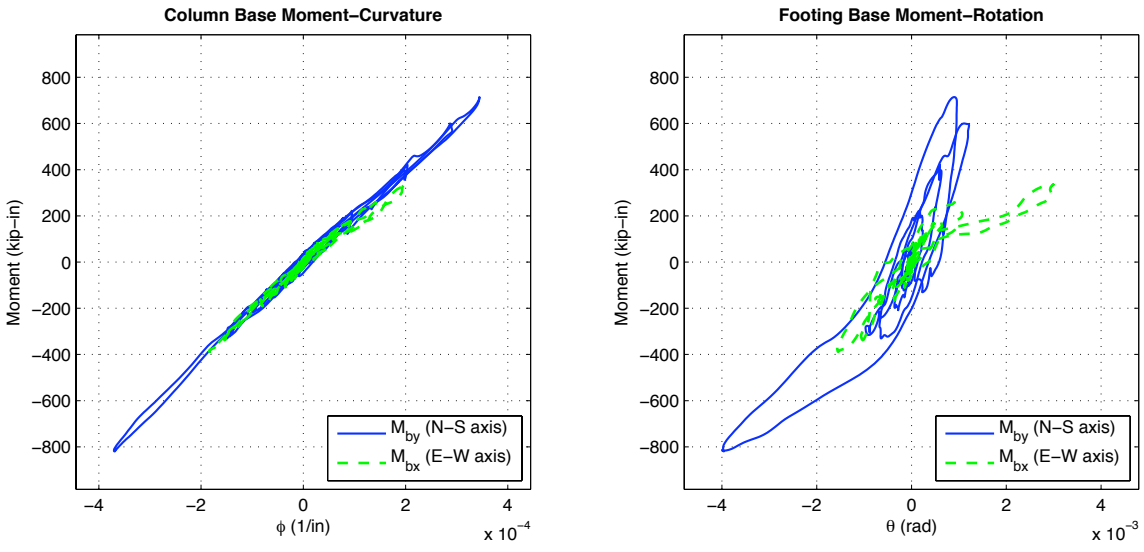

(e) Mom. vs Col ϕ (1/in) (f) Mom. vs FTG θ (rad)

Figure B-17: C3S Experimental Results

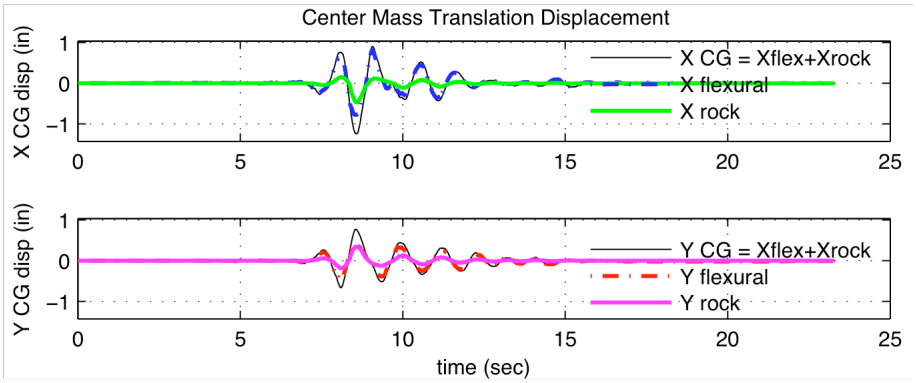

(a) X center mass translation (b) Y center mass translations

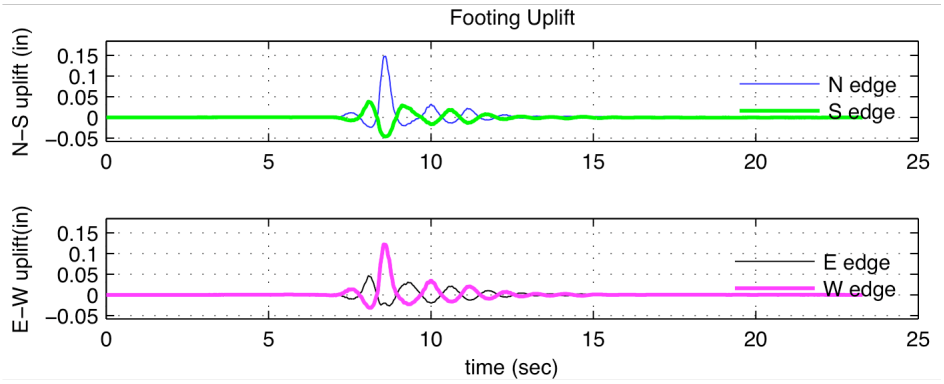

(c) N-S footing uplift (d) E-W footing uplift

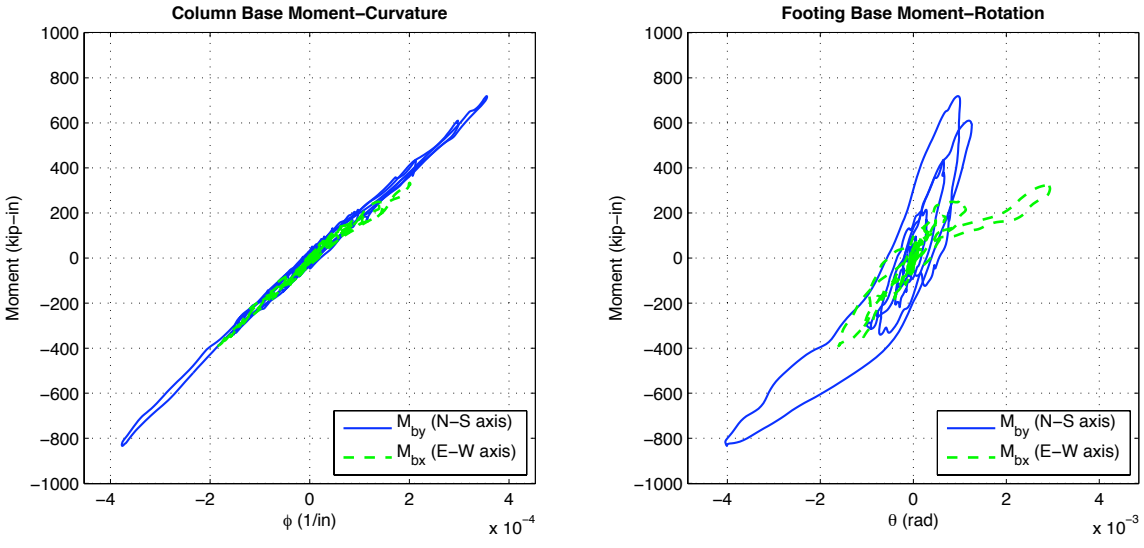

(e) Mom. vs Col ϕ (1/in) (f) Mom. vs FTG θ (rad)

Figure B-18: C5S Experimental Results

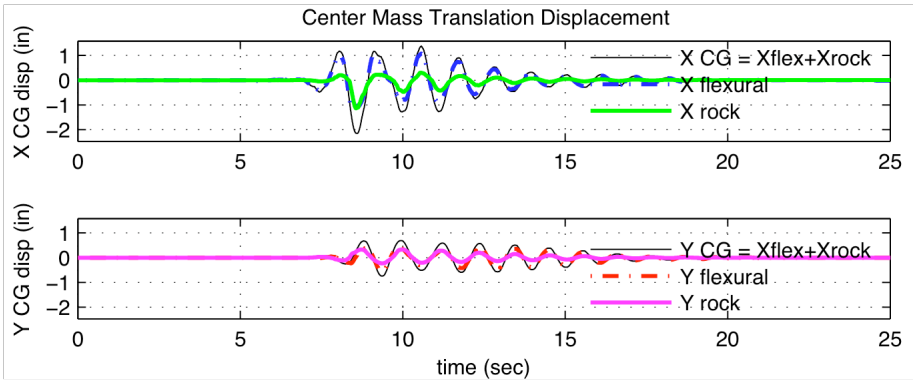

(a) X center mass translation (b) Y center mass translations

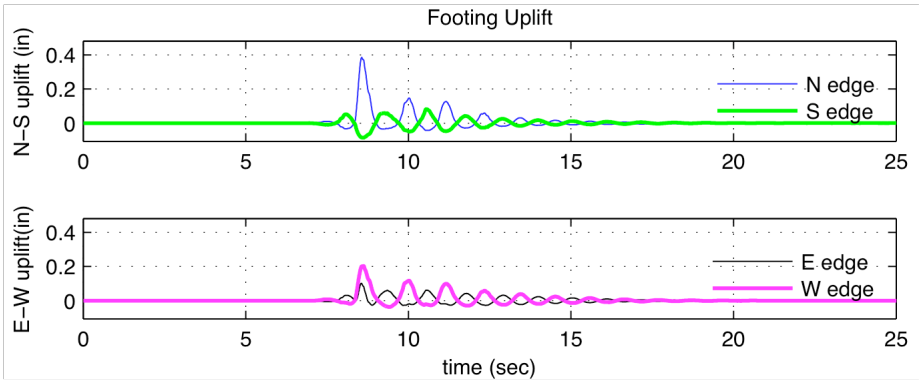

(c) N-S footing uplift (d) E-W footing uplift

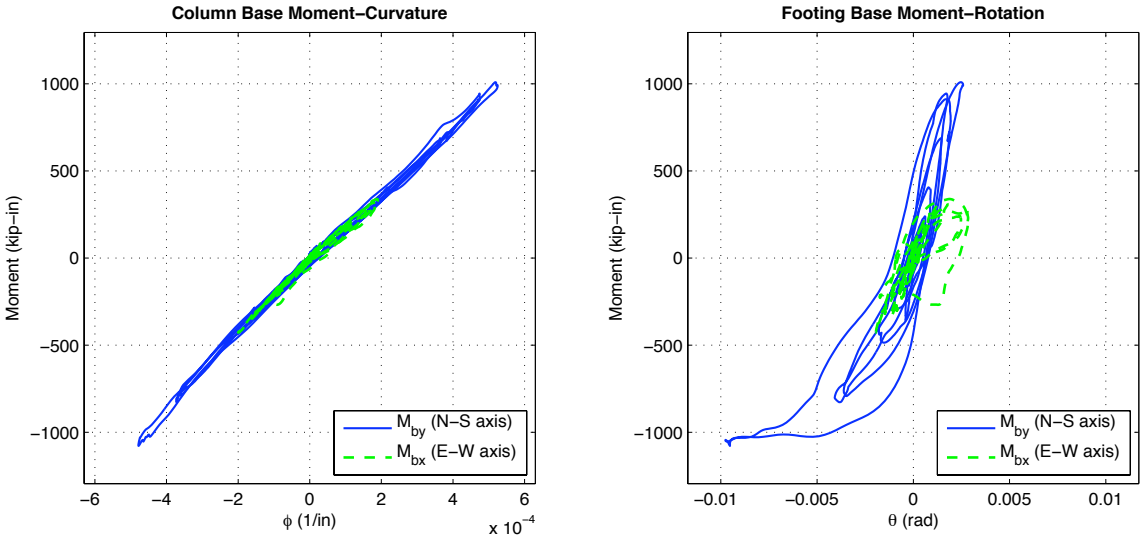

(e) Mom. vs Col ϕ (1/in) (f) Mom. vs FTG θ (rad)

Figure B-19: D1S Experimental Results

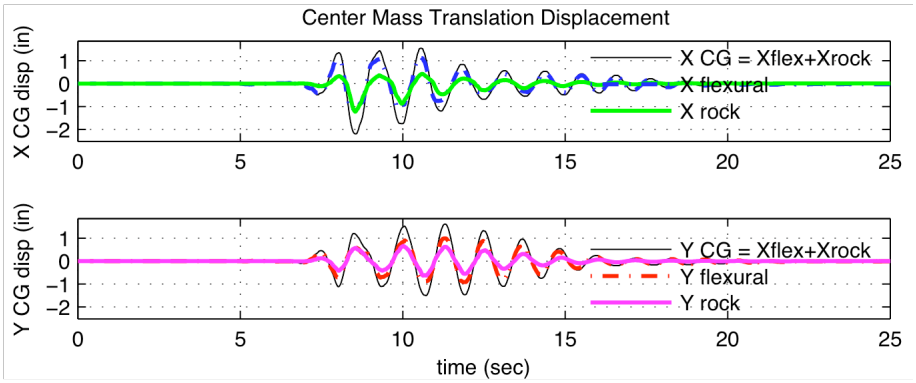

(a) X center mass translation (b) Y center mass translations

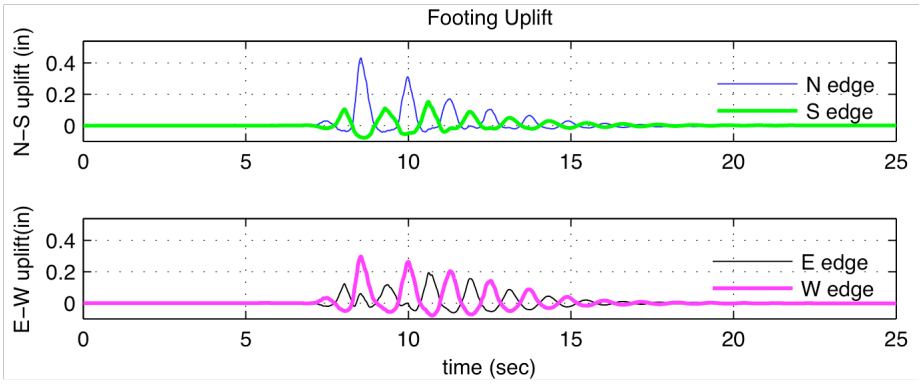

(c) N-S footing uplift (d) E-W footing uplift

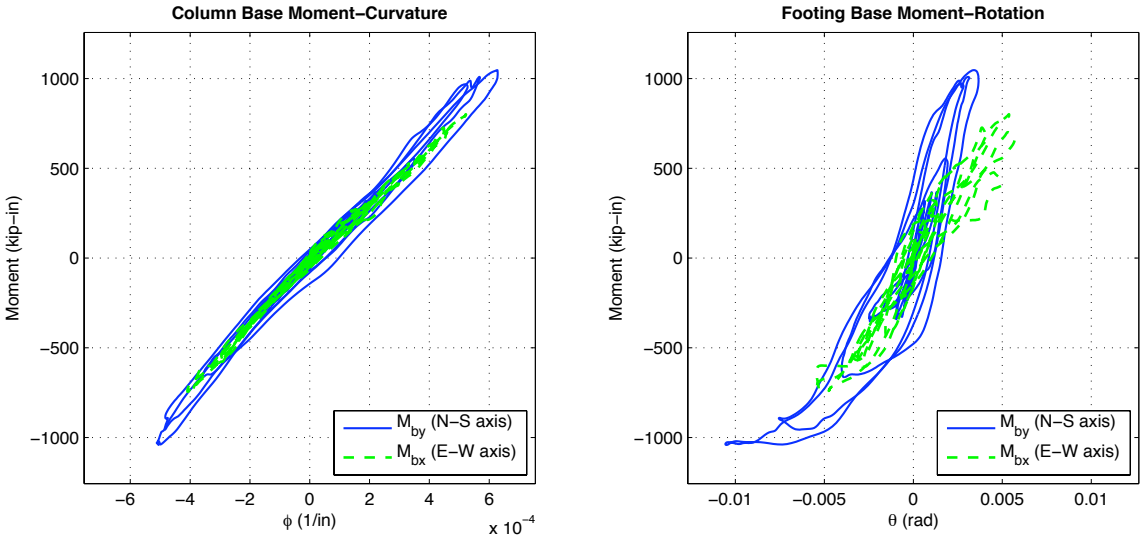

(e) Mom. vs Col ϕ (1/in) (f) Mom. vs FTG θ (rad)

Figure B-20: D3S Experimental Results

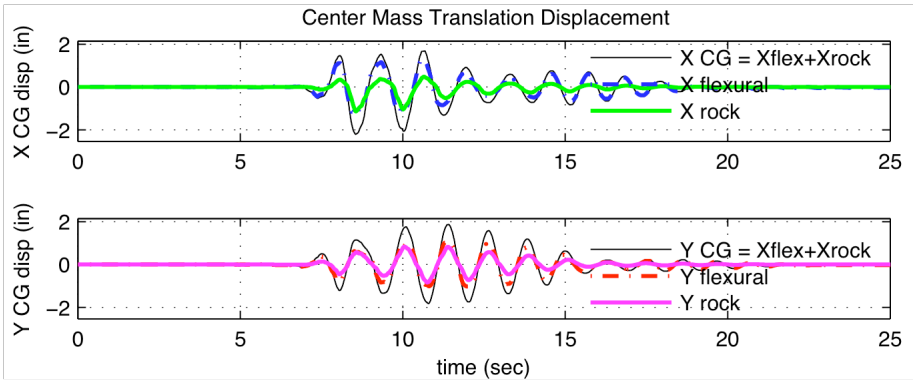

(a) X center mass translation (b) Y center mass translations

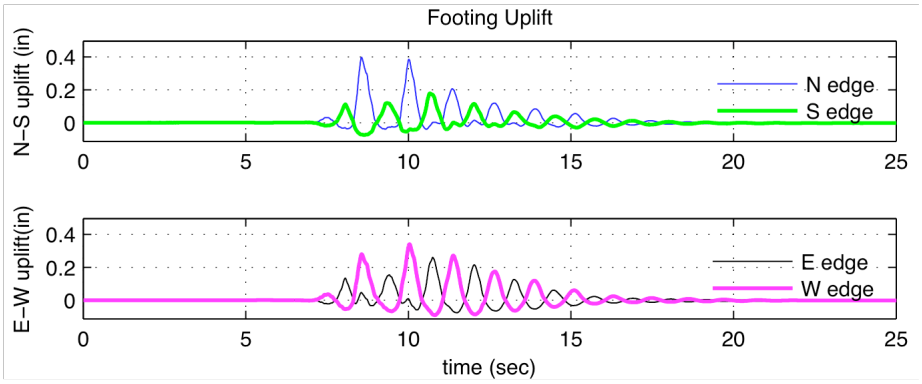

(c) N-S footing uplift (d) E-W footing uplift

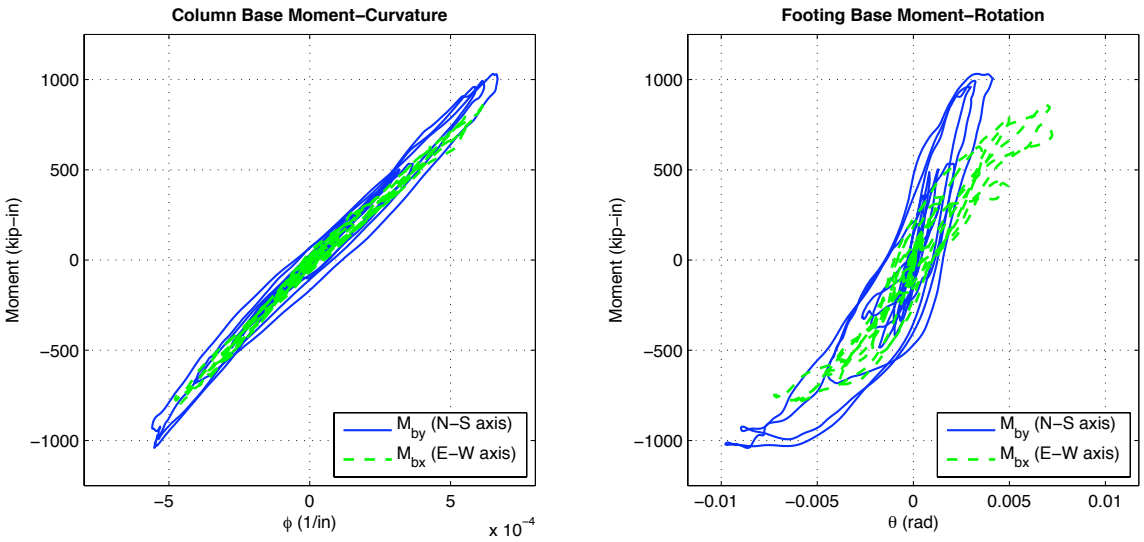

(e) Mom. vs Col ϕ (1/in) (f) Mom. vs FTG θ (rad)

Figure B-21: D5S Experimental Results

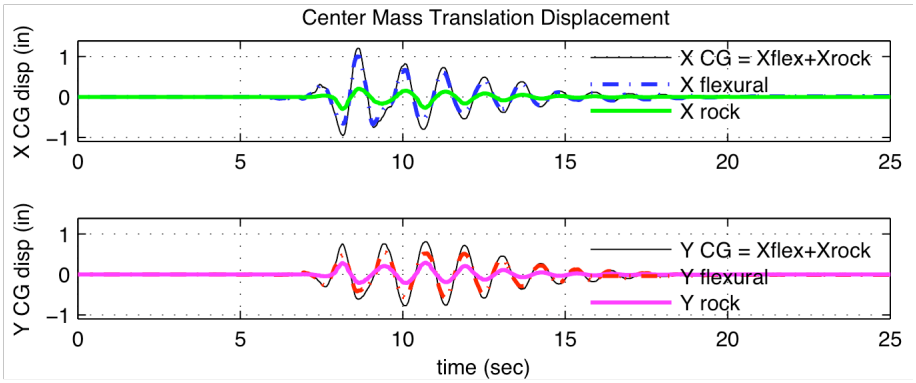

(a) X center mass translation (b) Y center mass translations

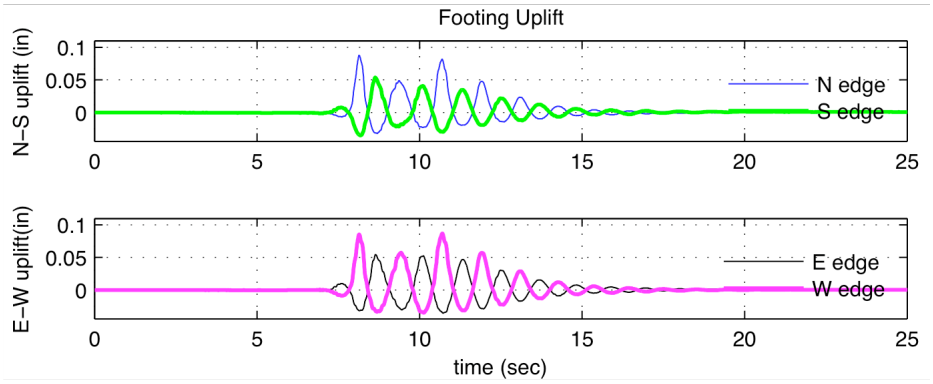

(c) N-S footing uplift (d) E-W footing uplift

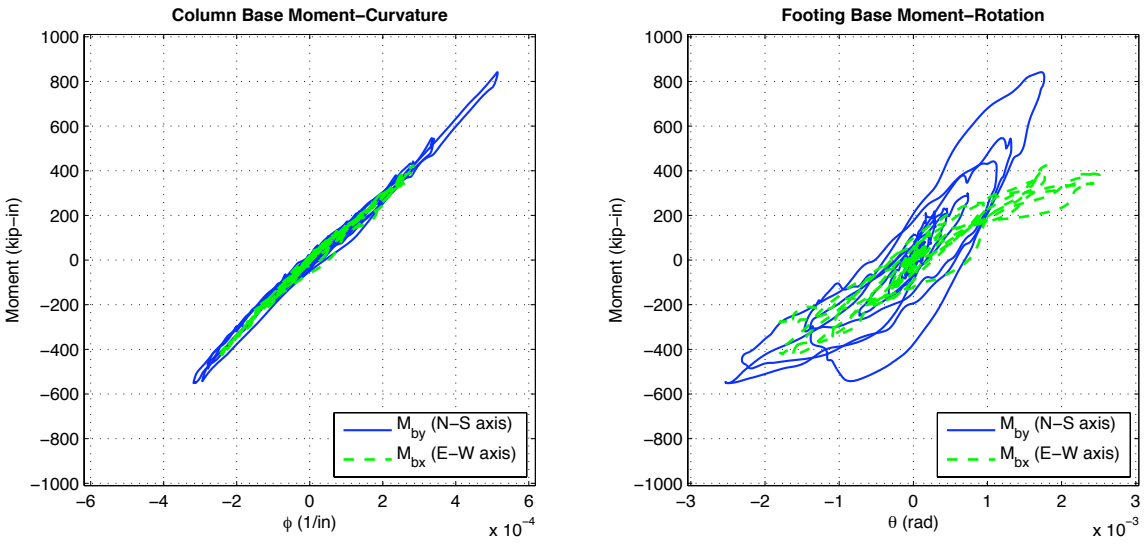

(e) Mom. vs Col ϕ (1/in) (f) Mom. vs FTG θ (rad)

Figure B-22: E1S Experimental Results

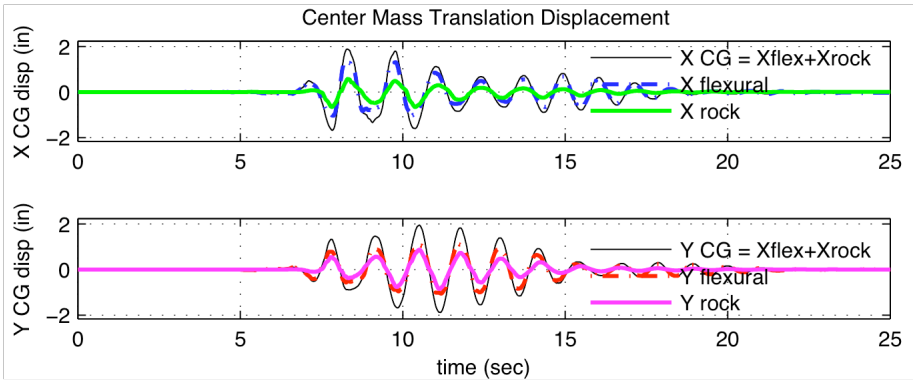

(a) X center mass translation (b) Y center mass translations

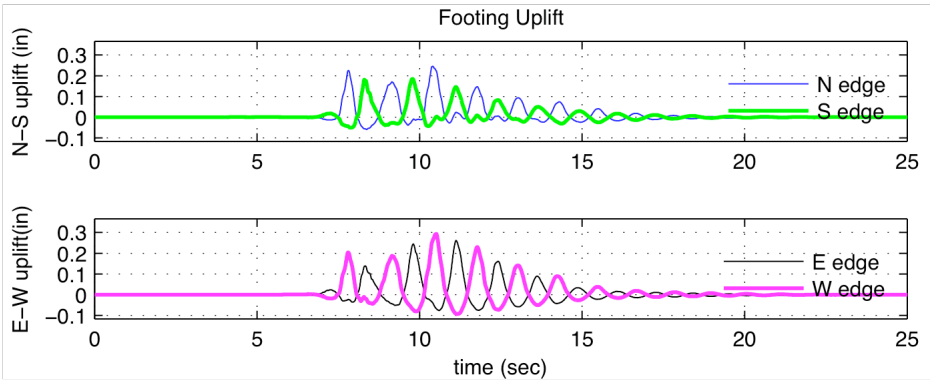

(c) N-S footing uplift (d) E-W footing uplift

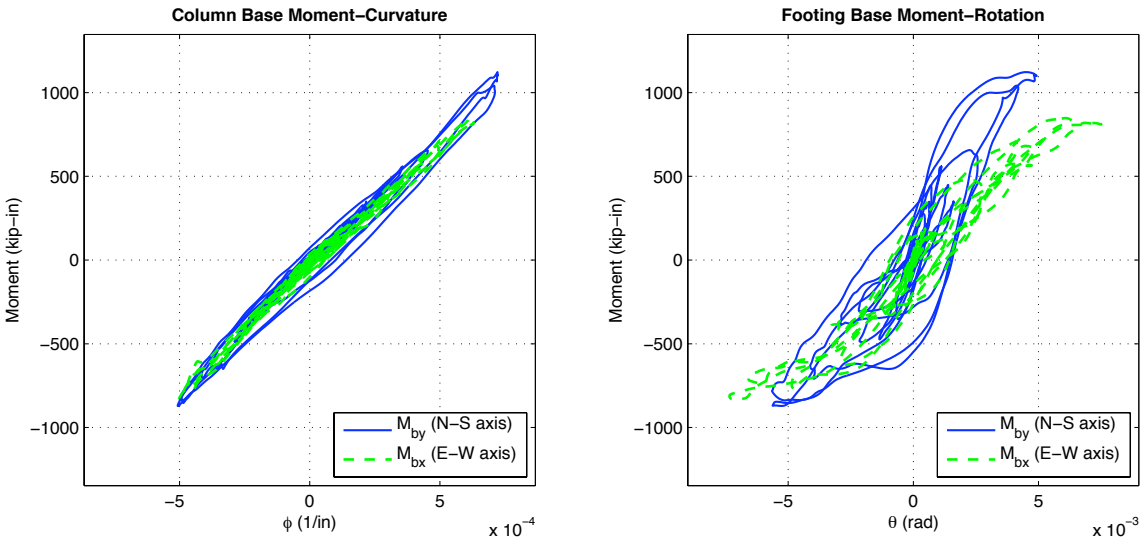

(e) Mom. vs Col ϕ (1/in) (f) Mom. vs FTG θ (rad)

Figure B-23: E2S Experimental Results

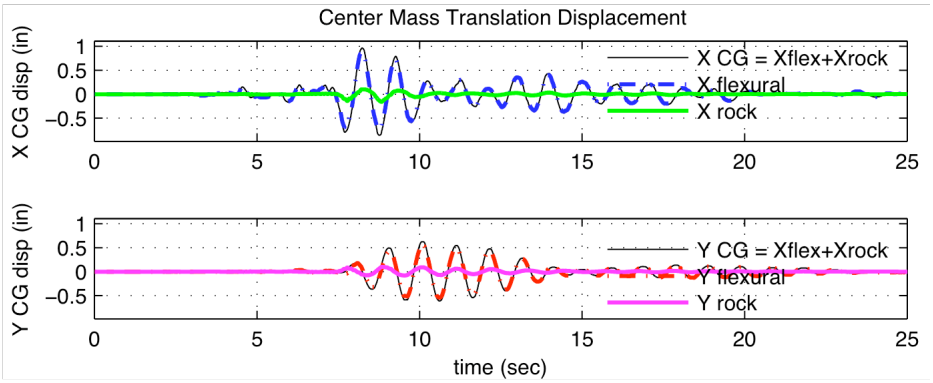

(a) X center mass translation (b) Y center mass translations

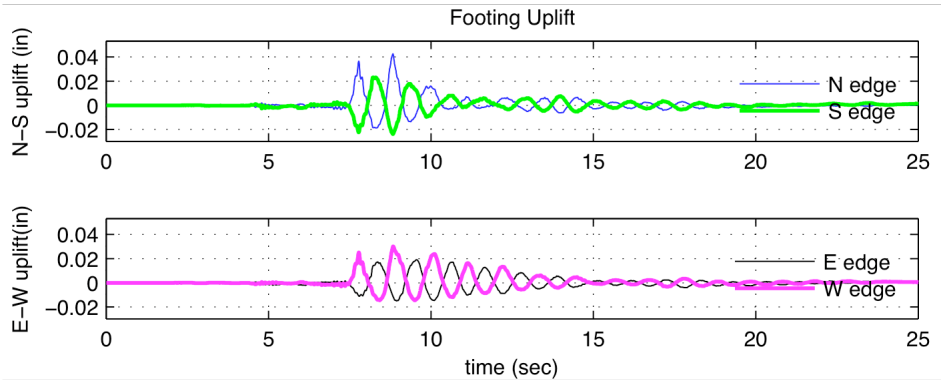

(c) N-S footing uplift (d) E-W footing uplift

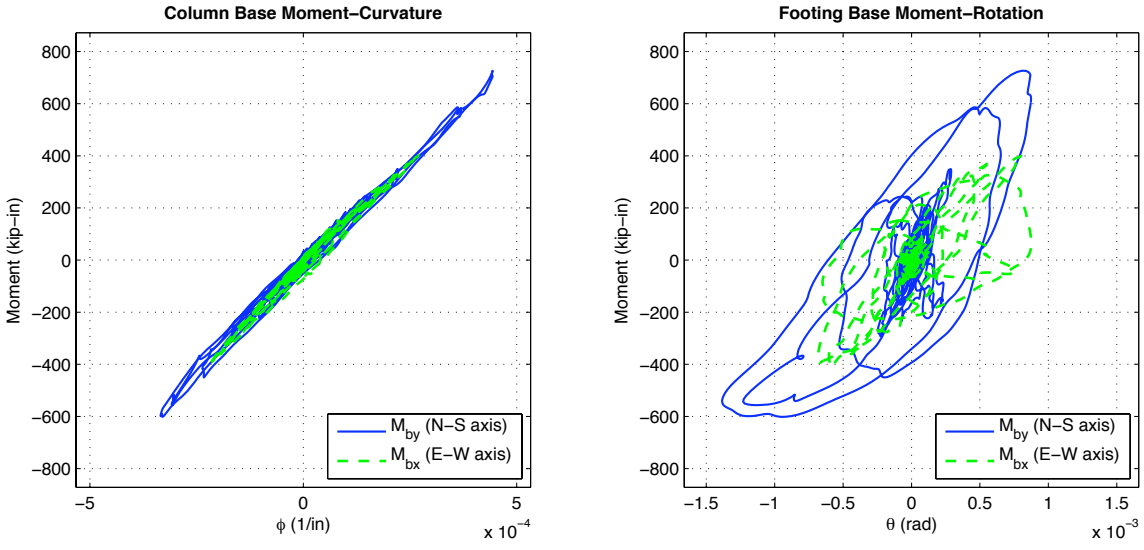

(e) Mom. vs Col ϕ (1/in) (f) Mom. vs FTG θ (rad)

Figure B-24: F1S Experimental Results

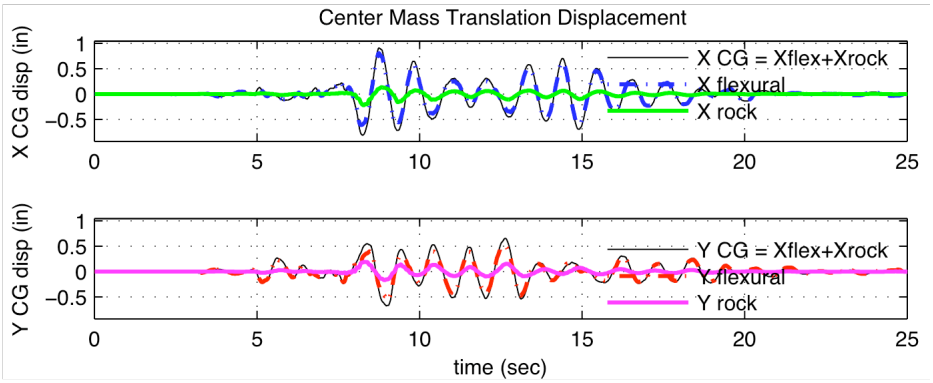

(a) X center mass translation (b) Y center mass translations

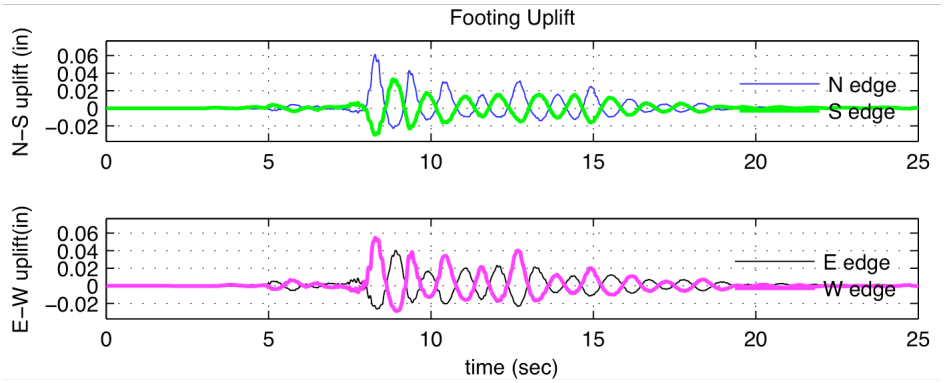

(c) N-S footing uplift (d) E-W footing uplift

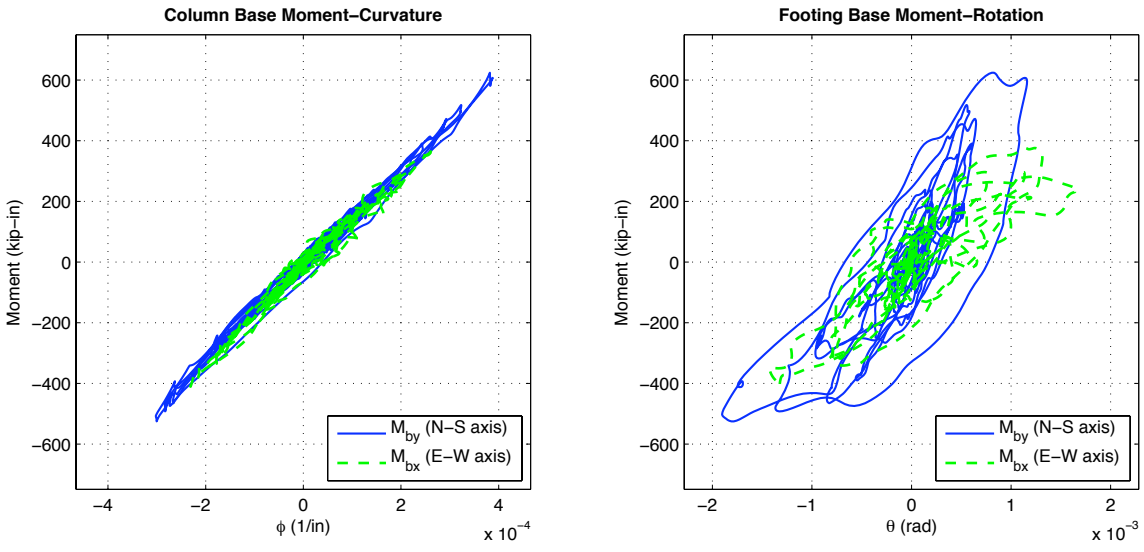

(e) Mom. vs Col ϕ (1/in) (f) Mom. vs FTG θ (rad)

Figure B-25: F3S Experimental Results

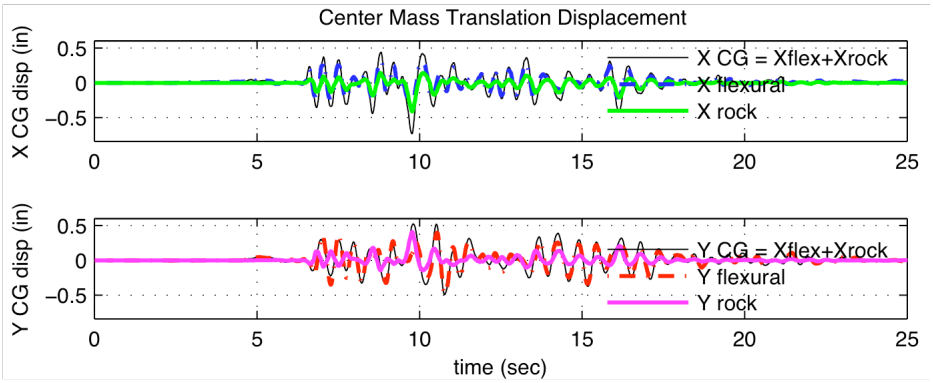

(a) X center mass translation (b) Y center mass translations

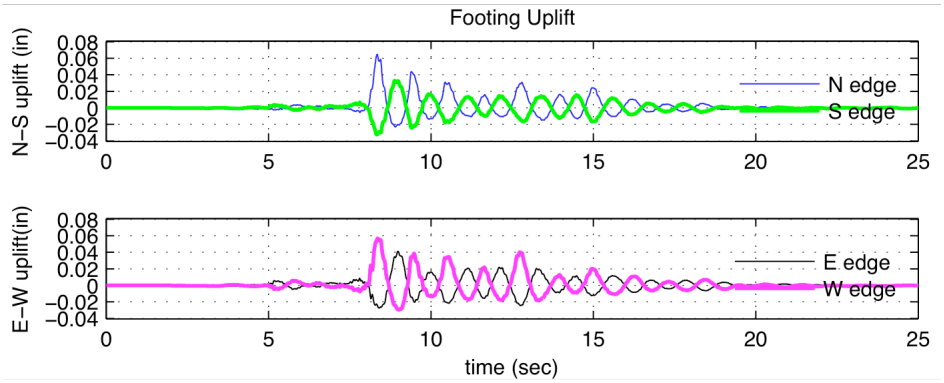

(c) N-S footing uplift (d) E-W footing uplift

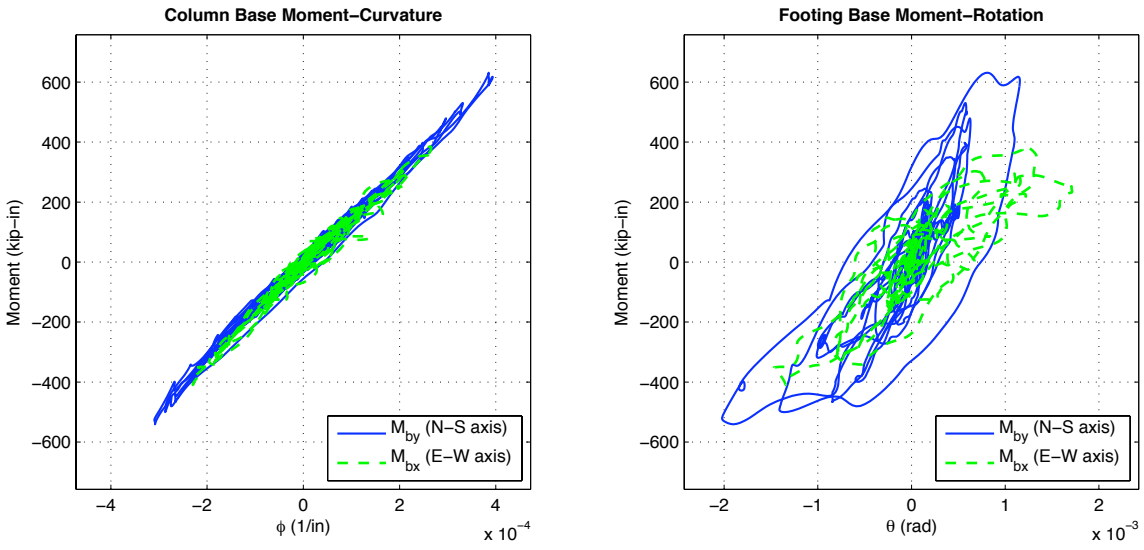

(e) Mom. vs Col ϕ (1/in) (f) Mom. vs FTG θ (rad)

Figure B-26: F5S Experimental Results

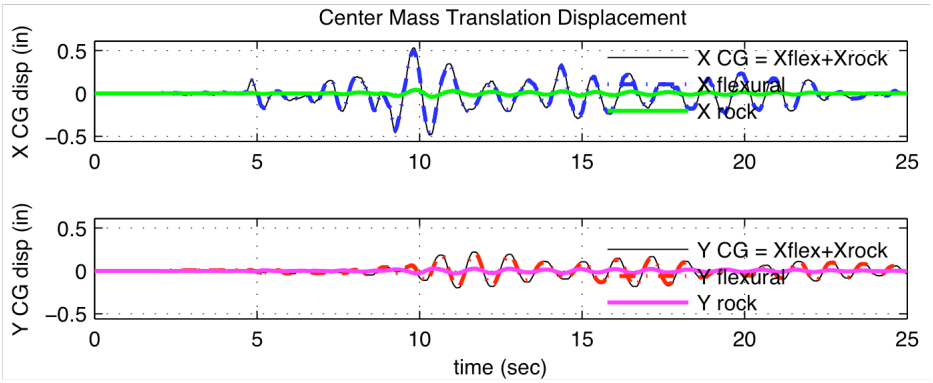

(a) X center mass translation (b) Y center mass translations

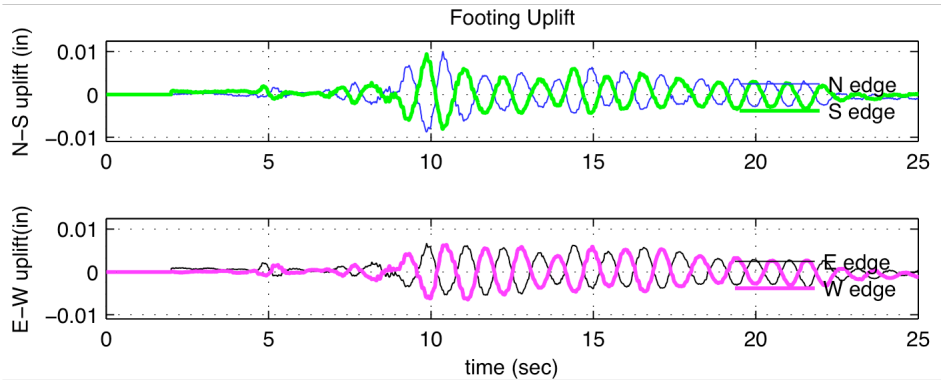

(c) N-S footing uplift (d) E-W footing uplift

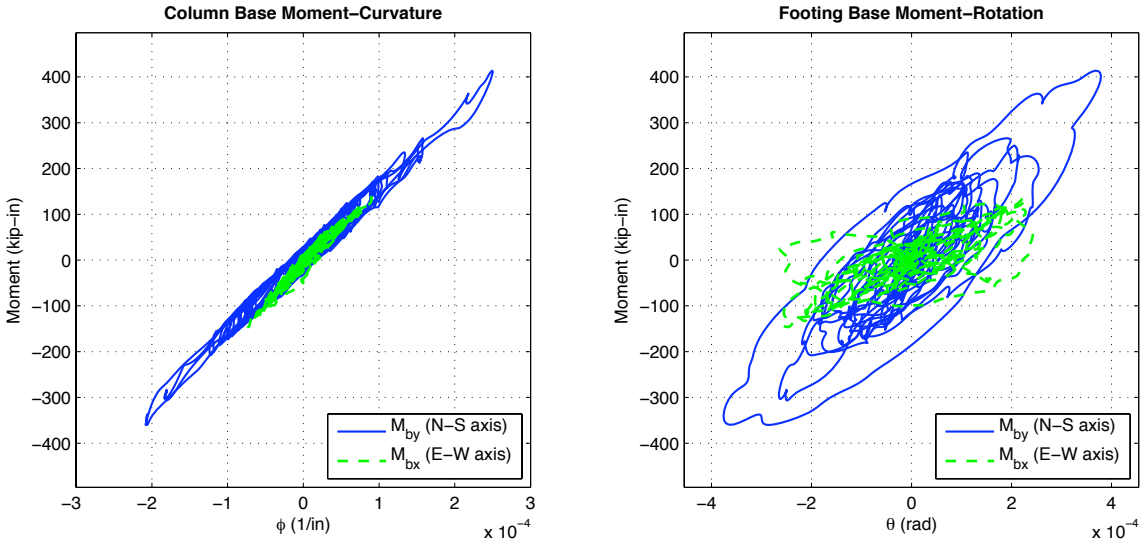

(e) Mom. vs Col ϕ (1/in) (f) Mom. vs FTG θ (rad)

Figure B-27: G1S Experimental Results

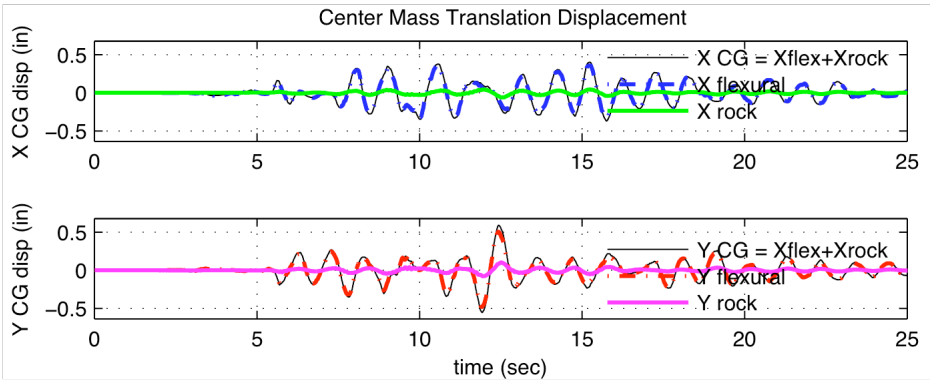

(a) X center mass translation (b) Y center mass translations

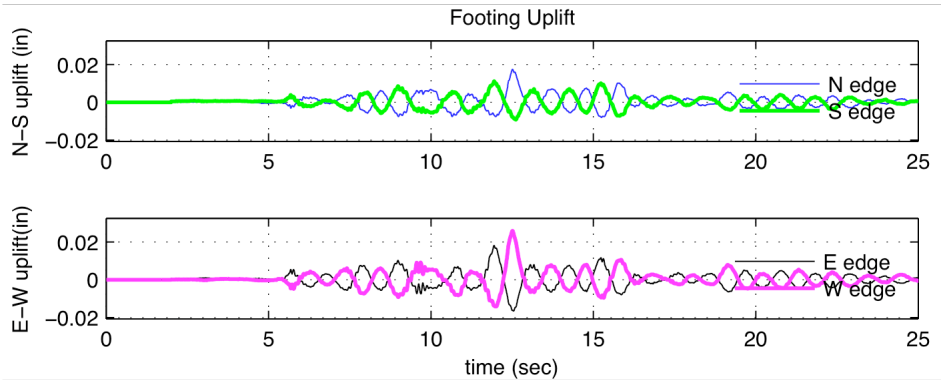

(c) N-S footing uplift (d) E-W footing uplift

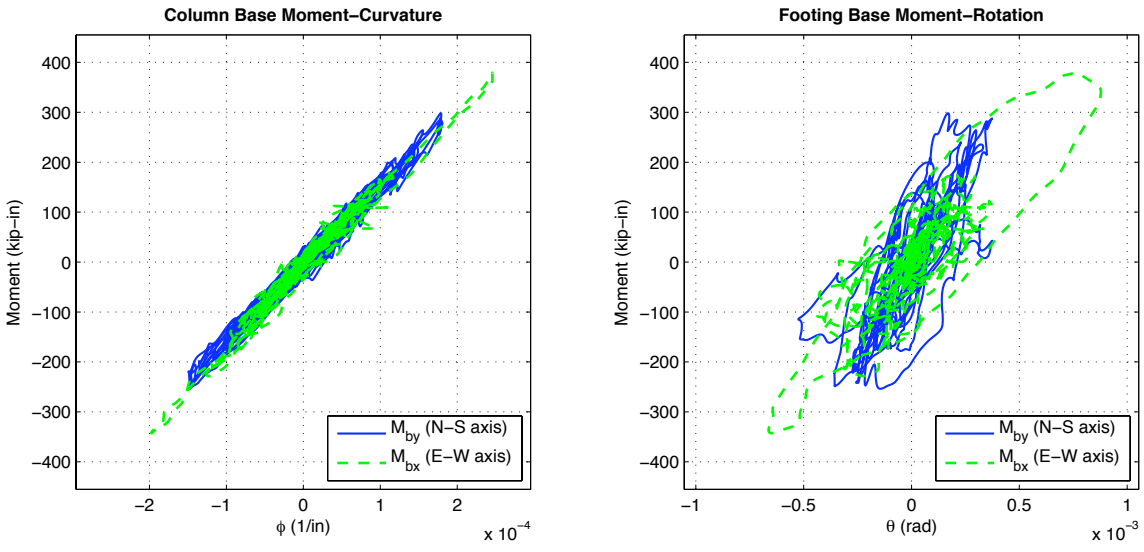

(e) Mom. vs Col ϕ (1/in) (f) Mom. vs FTG θ (rad)

Figure B-28: G3S Experimental Results

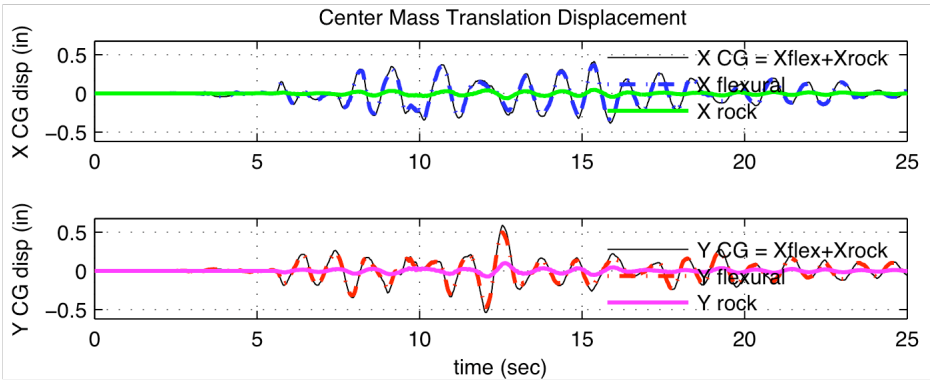

(a) X center mass translation (b) Y center mass translations

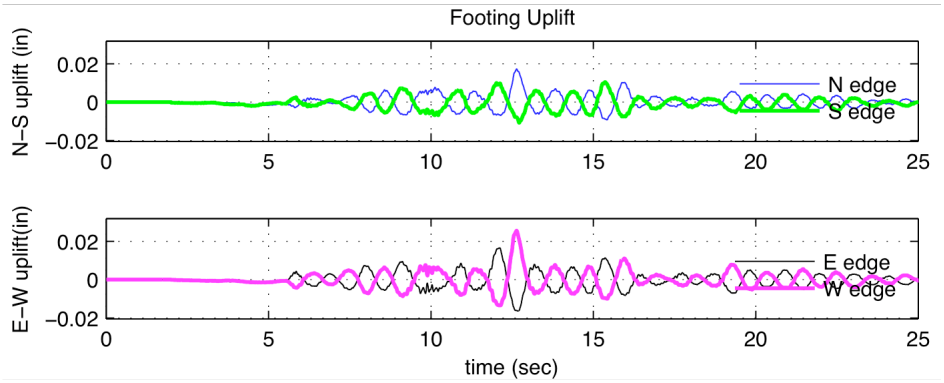

(c) N-S footing uplift (d) E-W footing uplift

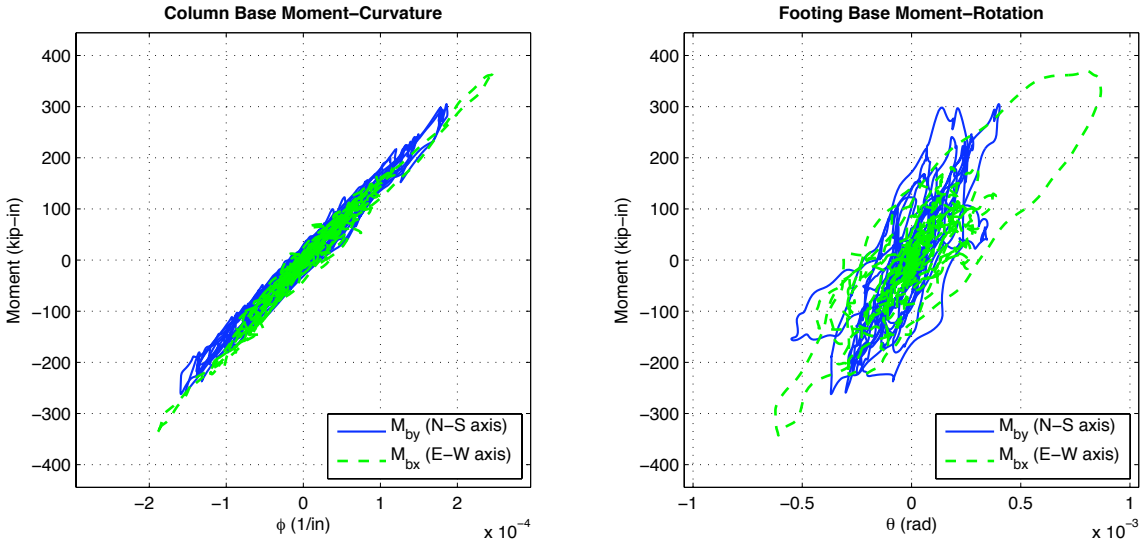

(e) Mom. vs Col ϕ (1/in) (f) Mom. vs FTG θ (rad)

Figure B-29: G5S Experimental Results

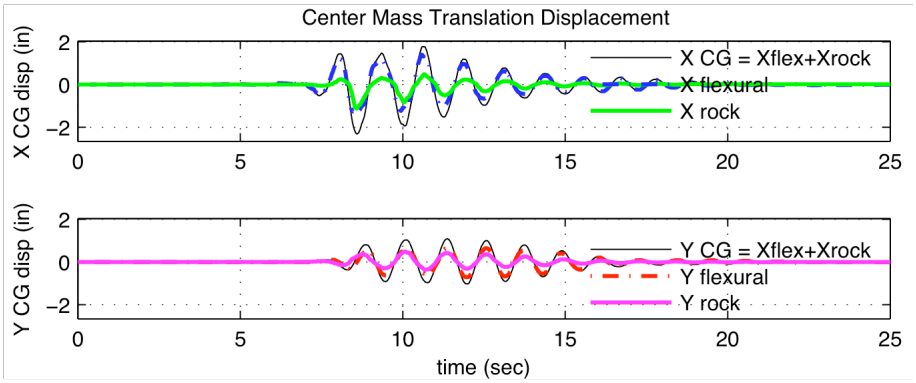

(a) X center mass translation (b) Y center mass translations

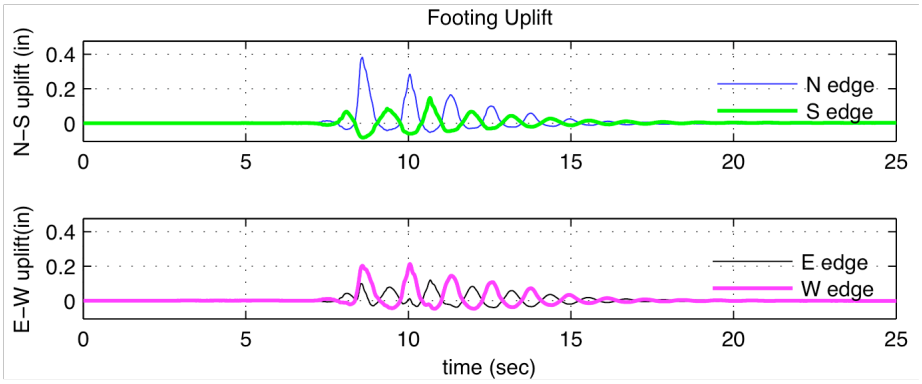

(c) N-S footing uplift (d) E-W footing uplift

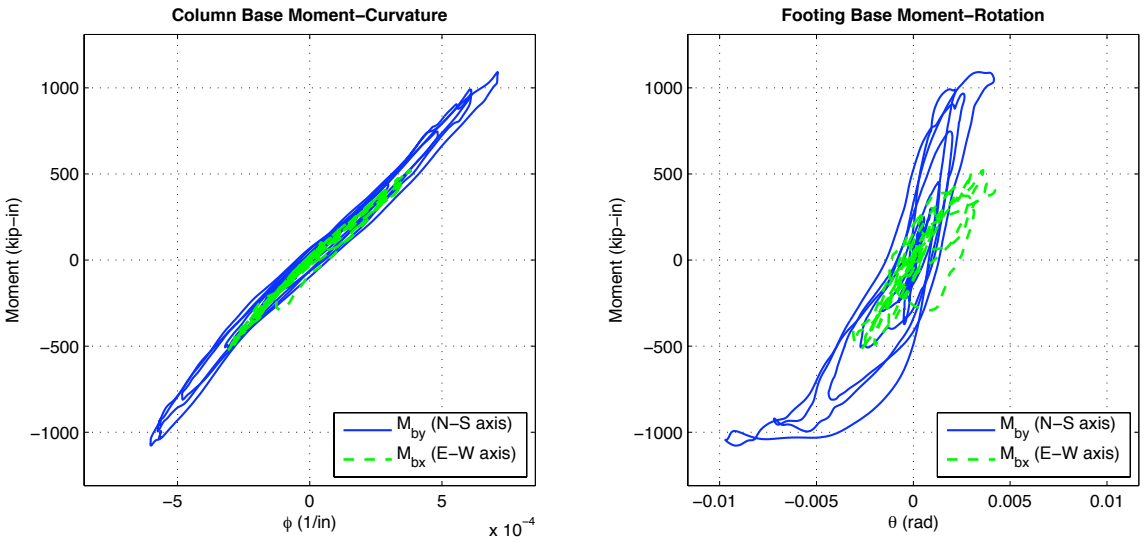

(e) Mom. vs Col ϕ (1/in) (f) Mom. vs FTG θ (rad)

Figure B-30: H1S Experimental Results

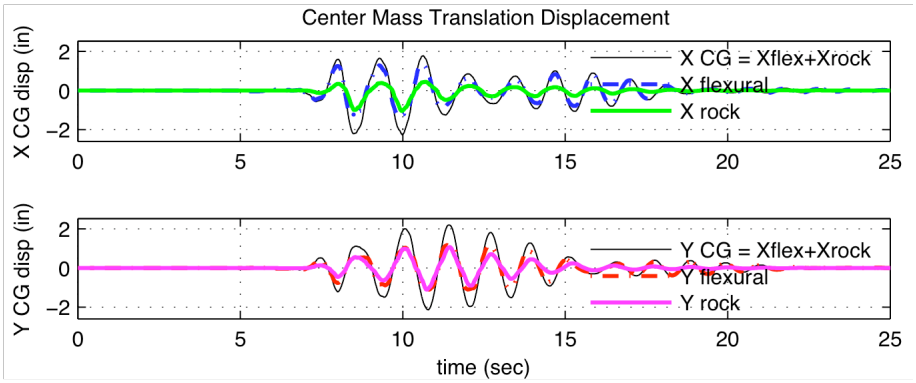

(a) X center mass translation (b) Y center mass translations

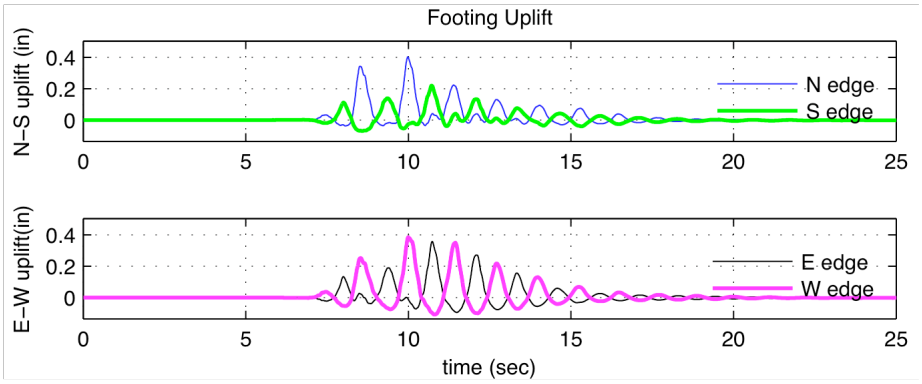

(c) N-S footing uplift (d) E-W footing uplift

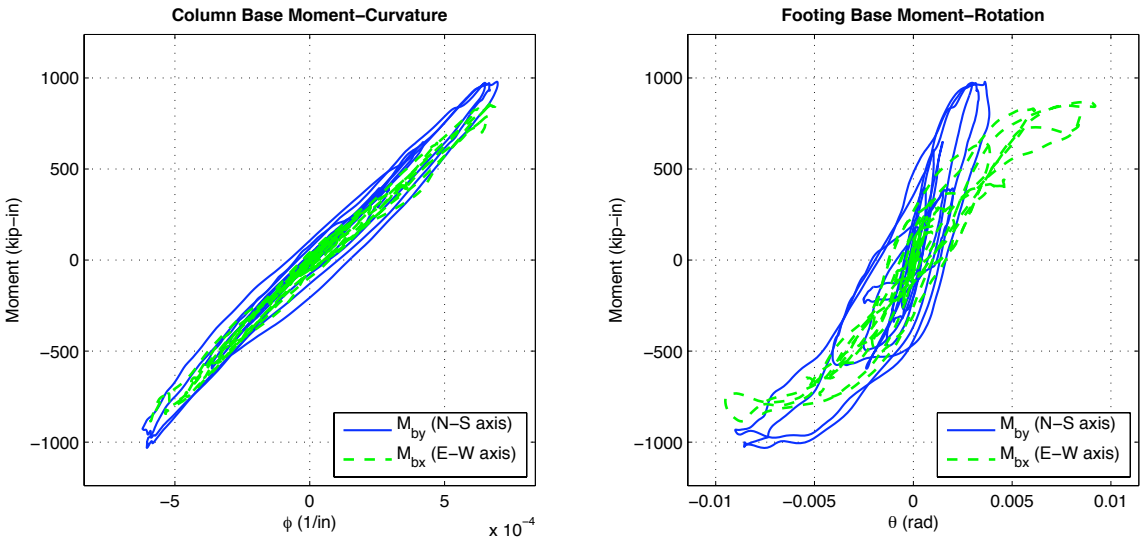

(e) Mom. vs Col ϕ (1/in) (f) Mom. vs FTG θ (rad)

Figure B-31: H2S Experimental Results

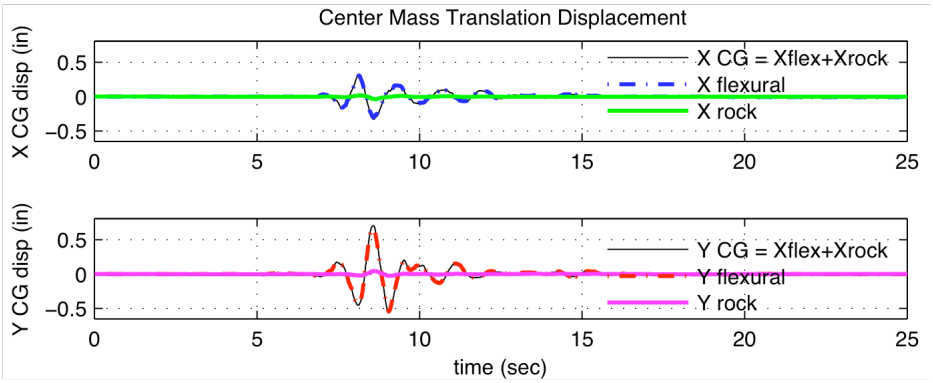

(a) X center mass translation (b) Y center mass translations

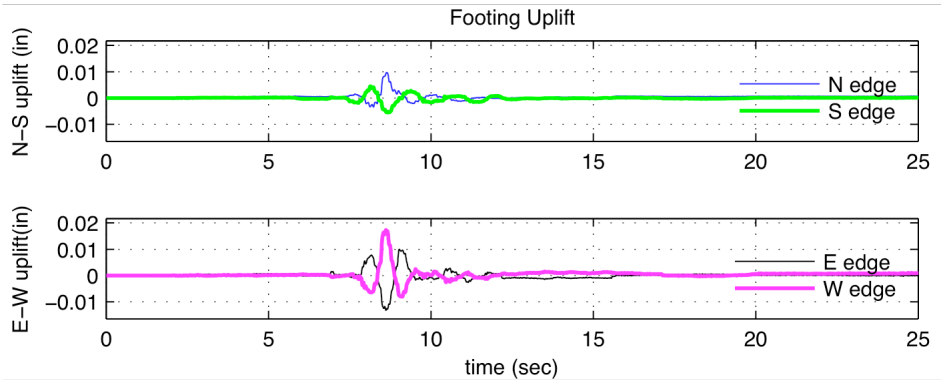

(c) N-S footing uplift (d) E-W footing uplift

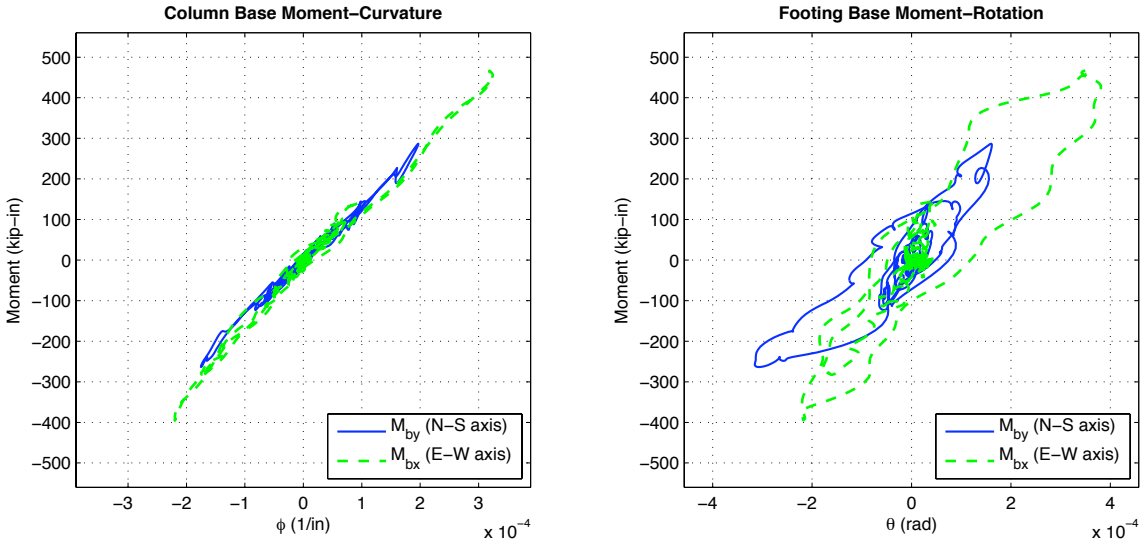

(e) Mom. vs Col ϕ (1/in) (f) Mom. vs FTG θ (rad)

Figure B-32: A1R Experimental Results

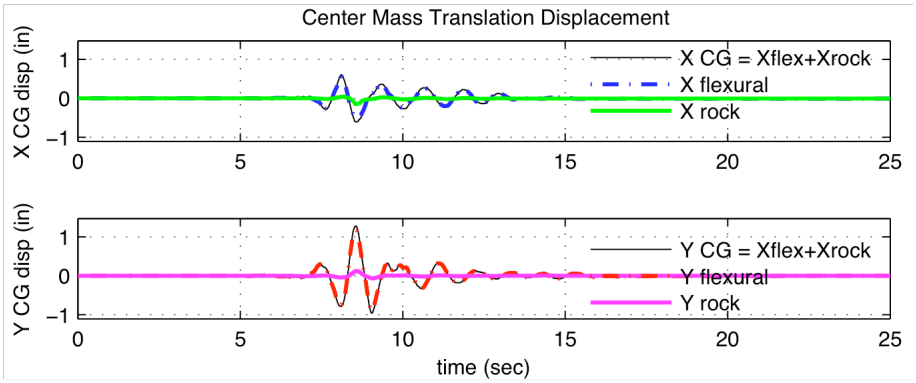

(a) X center mass translation (b) Y center mass translations

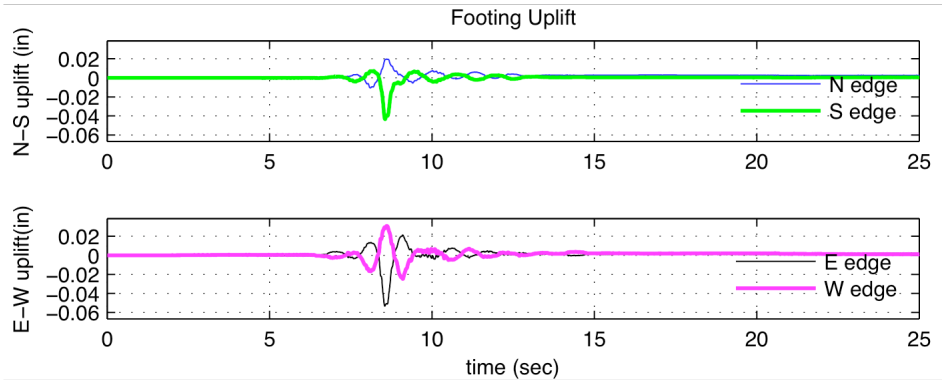

(c) N-S footing uplift (d) E-W footing uplift

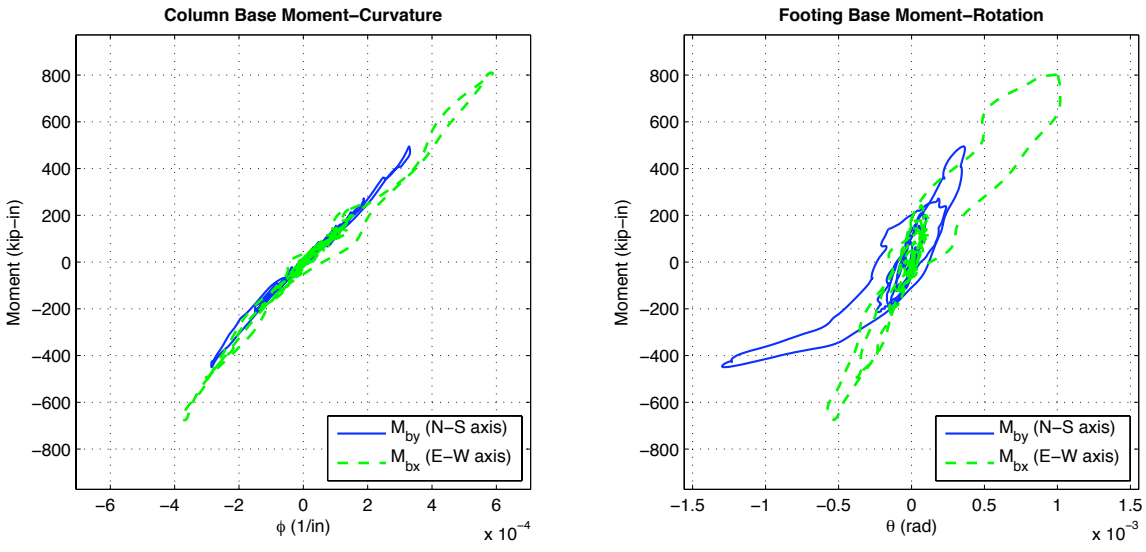

(e) Mom. vs Col ϕ (1/in) (f) Mom. vs FTG θ (rad)

Figure B-33: A2R Experimental Results

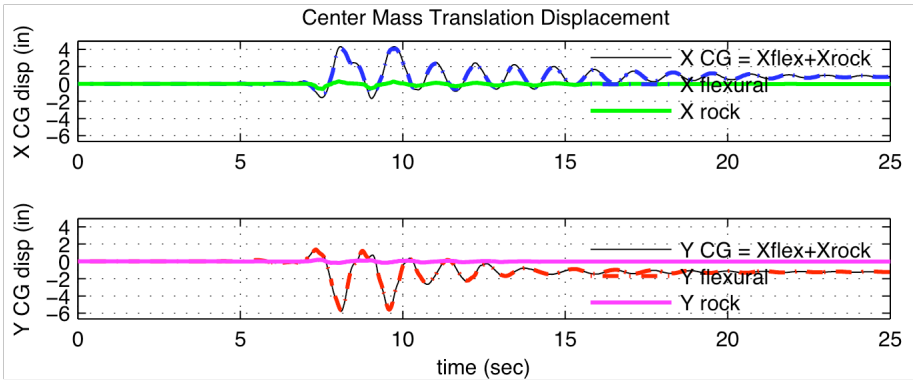

(a) X center mass translation (b) Y center mass translations

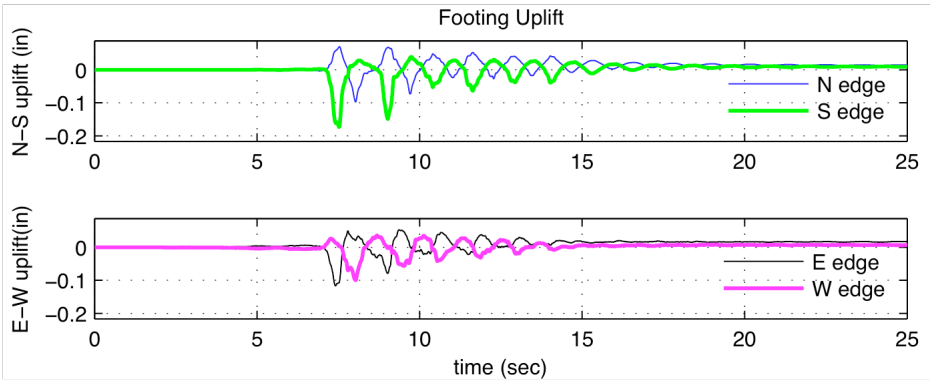

(c) N-S footing uplift (d) E-W footing uplift

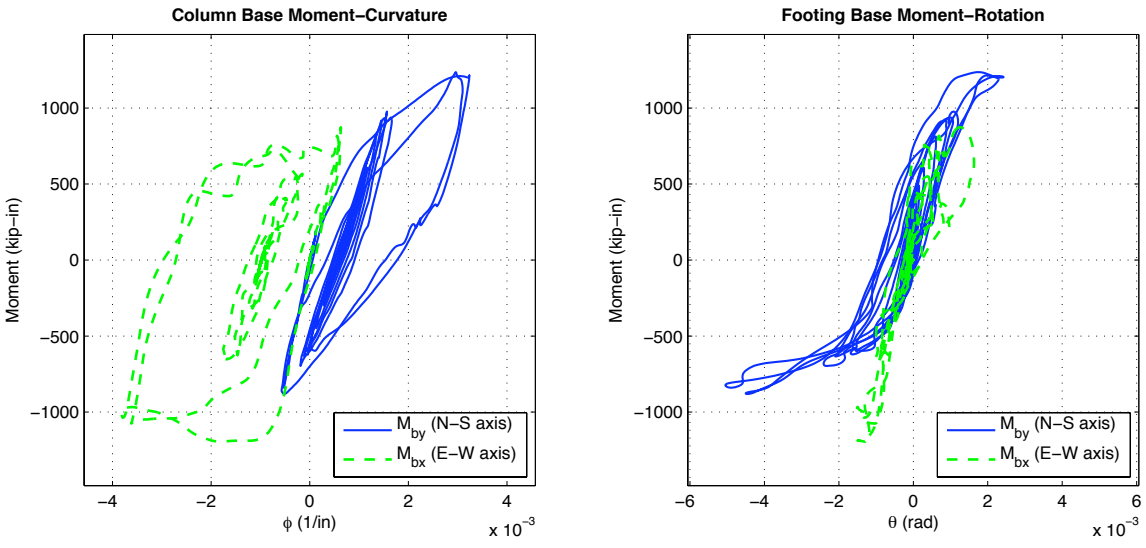

(e) Mom. vs Col ϕ (1/in) (f) Mom. vs FTG θ (rad)

Figure B-34: A3R Experimental Results

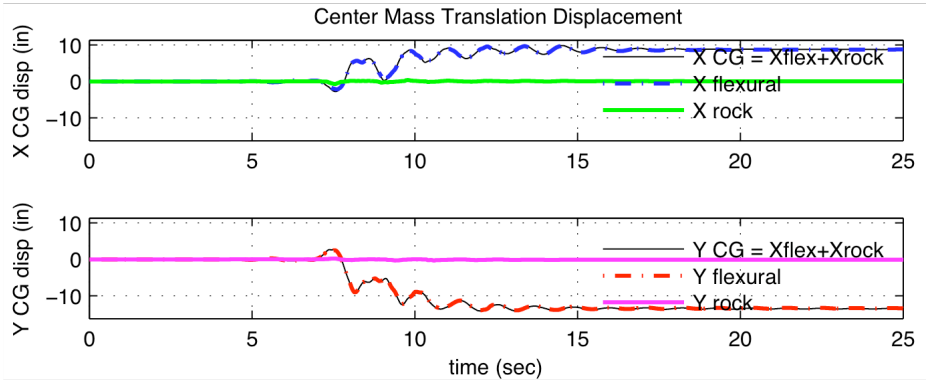

(a) X center mass translation (b) Y center mass translations

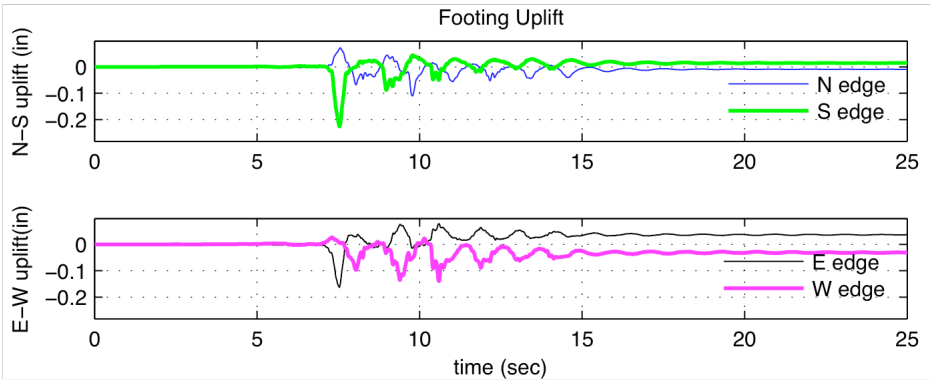

(c) N-S footing uplift (d) E-W footing uplift

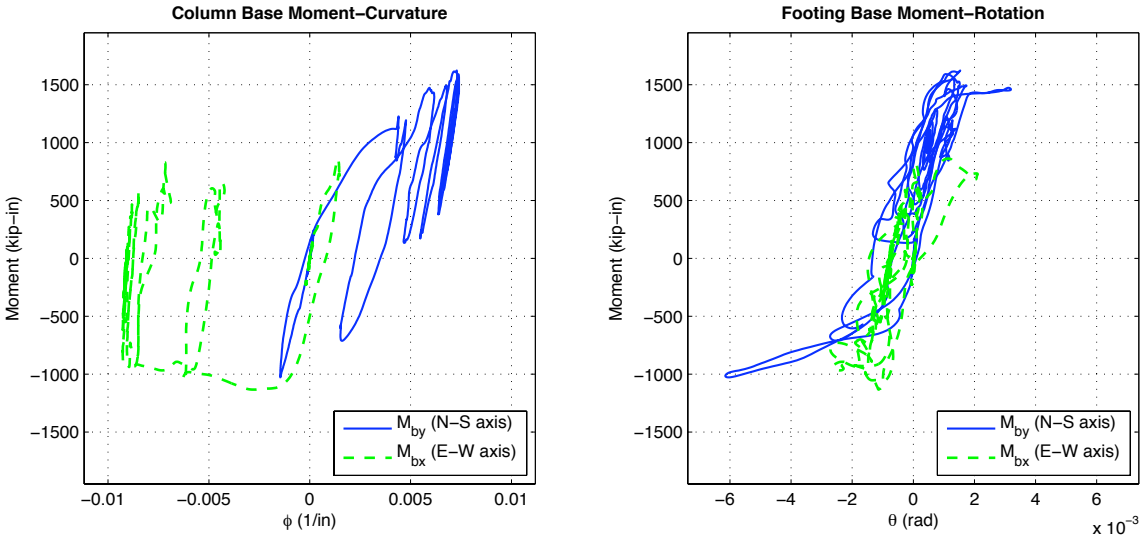

(e) Mom. vs Col ϕ (1/in) (f) Mom. vs FTG θ (rad)

Figure B-35: A4R Experimental Results

Appendix C Tcl Code – 3D Shallow Foundations Allowed to Uplift

The script included here is intended for use with the tcl based structural and geotechnical analysis platform OpenSees (Open System for Earthquake Engineering Simulation). The purpose is to model a spread footing on flexible underlying soil that is allowed to uplift. The footing is modeled as a three-dimensional Nonlinear Winkler Beam Foundation (NWBF) with springs and dashpots. The code builds the physical representation of the footing and calls a second sequence that assigns material properties to each spring being created.

```
##########################################################################################
##  BUILDFOUNDATION_F.tcl
##
##  Developed by Andres Espinoza ,Ph.D. Candidate at the Univ. of California, Berkeley.
##  Work supported by Caltrans under a grant for Development of Design Guidelines for Foundation Uplift
##
##  Coding was derived from work done by :
##  Harden et al. (2005) PEER Report 2005/04
## "Numerical Modeling of the Nonlinear Cyclic Response of Shallow Foundation"
##########################################################################################

proc BuildFOUNDATION_F { sn tn qult Kzm Kze Kr L B Lep Bep rmx rmy rex rey type FEmat soiltype
gap qip z50 Cr crad Kf Qf KPEP QPEP VISC VC Valpha FSECTION Wf TP} {

  variable node1
  variable node2
  variable node3
  variable node4

  set depth 0.0
  set matdir 3

# CALCULATION FOR SPRING SPACING
  ###################################

          if {$rmx > 0.5}  {set $rmx 0.5; puts "RATIOMX TOO LARGE -- RESET TO O.5"}
          if {$rmy > 0.5}  {set $rmy 0.5; puts "RATIOMY TOO LARGE -- RESET TO O.5"}
          if {$rex > 0.5}  {set $rex 0.5; puts "RATIOEX TOO LARGE -- RESET TO O.5"}
          if {$rey > 0.5}  {set $rey 0.5; puts "RATIOEY TOO LARGE -- RESET TO O.5"}

  set Lmp         [expr 1-2*$Lep]
  set Lmid        [expr $Lmp*$L]
  set Lend        [expr $Lep*$L]

  set Bmp         [expr 1-2*$Bep]
  set Bmid        [expr $Bmp*$B]
  set Bend        [expr $Bep*$B]

  set nmx         [expr int(pow($rmx,-1))]
  set nmy         [expr int(pow($rmy,-1))]

  if {$Lend != 0} {
    set nex         [expr int(pow($rex,-1))]
    set ney         [expr int(pow($rey,-1))]
  } elseif {$Lend == 0} {
    set nex 0;
    set ney 0
  }


          # CHECK FOR ODD NUMBER OF  NODES
          # CHANGE TO EVEN IF NECESSARY
          ###################################
          set rtmx [expr $nmx*0.5 - int($nmx*0.5)]
          set rtmy [expr $nmy*0.5 - int($nmy*0.5)]
          set rtex [expr $nex*0.5 - int($nex*0.5)]
```

```
        set rtey [expr $ney*0.5 - int($ney*0.5)]

        if {$rtmx == 0.5} {set nmx [expr $nmx+1]}; puts "NODESMX = $nmx"
        if {$rtmy == 0.5} {set nmy [expr $nmy+1]}; puts "NODESMY = $nmy"
        if {$rtex == 0.5} {set nex [expr $nex+1]}; puts "NODESEX = $nex"
        if {$rtey == 0.5} {set ney [expr $ney+1]}; puts "NODESEY = $ney"


set rmx [expr 1.0/$nmx];  puts "RATIOMX = $rmx"
set rmy [expr 1.0/$nmy];  puts "RATIOMY = $rmy"
if {$Lend != 0} {
  set rex [expr 1.0/$nex];  puts "RATIOEX = $rex"
  set rey [expr 1.0/$ney];  puts "RATIOEY = $rey"
} elseif {$Lend == 0} {
  set rex 0
  set rey 0
}

set Aratiom       [expr $rmx*$rmy*$Lmid*$Bmid/$L/$B]; puts "Aratiom  = $Aratiom"
set Aratioe  [expr $rex*$rey*$Lend*$Bend/$L/$B]; puts "Aratioe  = $Aratioe"
set AratioXe [expr $rex*$rmy*$Lend*$Bmid/$L/$B]; puts "AratioXe = $AratioXe"
set AratioYe [expr $rmx*$rey*$Lmid*$Bend/$L/$B]; puts "AratioYe = $AratioYe"

set nodesx [expr $nmx + 2*$nex] ; puts "NODESX = $nodesx"
set nodesy [expr $nmy + 2*$ney] ; puts "NODESY = $nodesy"
set nodes  [expr $nodesx*$nodesy]             ; puts "NODES  = $nodes"

## FOUNDATION SECTION
if {$FSECTION == 0} {
        set Efoundation [expr 1.0e10]
        section Elastic 100 $Efoundation [expr pow($L,2)] [expr pow($L,3)]
        set FSECTION 100
}


### CREATE NODES AND ELEMENTS FROM CENTER TO EDGES
### OVER ALL Y FOR EACH X STRIP
set a(1) 1;   set a(2) -1;  set a(3)  1;  set a(4) -1;  # toggle axis postion
set b(1) 1;   set b(2)  1;  set b(3) -1;  set b(4) -1;  # for symmetric nodes

set Aratio          $Aratiom
set kzi $Kzm

set fLx  [expr $Lmid/$nmx]
set fLy  [expr $Bmid/$nmy]

set x    [expr $fLx*0.5]
set y    [expr $fLy*0.5]
set mc   1000

        ## OPEN FILE TO RECORD NODE COORDINATES & SPRING CONSTANTS
        set h1       [open "NODEXYZ.txt" w]
        set h2    [open "ELEMENTid.txt" w]
        set h3       [open "ELEMENTxy.txt" w]
        puts $h1  [format "iNODE \t Xi \t Yi \t Zi \t jNODE \t Xj \t Yj \t Zj \t Aratio \t kzi"]
```

```
puts $h1  [format "%4.0f  %6.2f  %6.2f  %6.2f  %4.0f  %6.2f  %6.2f  %6.2f  %6.4f\
                                %6.2f"  $sn 0 0 0 $sn 0 0 $depth 0 0]
puts $h2  [format "ELEMENT\tiNODE\tjNODE\tTYPE (0=zeroLength\, 1=ElasticBeam)\tX\tY "]


  set node0   [expr $tn+1]
  set Atotal  0.0

  set node4    [expr $tn+2*$nodes-1]
  set node3    [expr $node4-2]
  set node2    [expr $node3-2]
  set node1    [expr $node2-2]

  set mF              [expr $Wf/$nodes/386.4]

  ## VISCOUS DAMPING MATERIAL
  if {$VISC == 1} {
    set matVISC $nodes
    uniaxialMaterial Viscous $matVISC $VC $Valpha
  }


  ## START LOOPING OVER ALL NODES
  for {set j 1} {$j <= [expr 0.5*$nodesy]} {incr j} {
    for {set i 1} {$i <= [expr 0.5*$nodesx]} {incr i} {

               source BUILD_MAT_F.tcl;       # CALL MATERIAL CONSTANTS
# FOR 4 SYMMETRIC NODES

            for {set k 1} {$k <=4} {incr k} {
              node [expr $node0]    [expr $a($k)*$x] [expr $b($k)*$y] $depth
              node [expr $node0+1]  [expr $a($k)*$x] [expr $b($k)*$y] $depth
              fix  [expr $node0+1] 1 1 1 1 1 1

              mass $node0 $mF $mF $mF 1e-6 1e-6 1e-6

              element zeroLength $mc  [expr $node0+1] [expr $node0] -mat $mati -dir $matdir

 if {$VISC == 1} {
    puts "ADDING VISCOUS MATERIAL -- VC=$VC  Valpha=$Valpha"
    element zeroLength [expr $mc+10*$nodes] [expr $node0+1] [expr $node0] -mat $matVISC -dir $matdir
 }

  puts $h1 [format "%4.0f    %6.2f    %6.2f    %6.2f    %4.0f    %6.2f    %6.2f    %6.2f  %6.4f  %6.2f" \
    $node0 [expr $a($k)*$x] [expr $b($k)*$y] $depth [expr $node0+1] [expr $a($k)*$x] \   [expr
$b($k)*$y] $depth $Aratio $Ki ]

  puts  $h2 [format "%d\t%d\t%d\t%d" $mc [expr $node0] [expr $node0+1] 0 ]
  puts $h3 [format "%d\t%d\t%d\t%6.4f\t%6.4f" $mc [expr $node0] [expr $node0+1] [expr $a($k)*$x] \
    [expr $b($k)*$y]]

 set mc    [expr $mc+1]
 set node0 [expr $node0+2]

}
```

```
set Atotal [expr $Atotal + 4*$Aratio]

set x [expr $x+$fLx]

 if {$Lend != 0} {
 if {$i == [expr int($nmx*0.5)]} {

   set fLx [expr $Lend/$nex]
              set x     [expr 0.5*$Lmid+$fLx*0.5]

    if {$j <= 0.5*$nmy} {set Aratio $AratioXe;     set kzi    $Kze       }
              if {$j >  0.5*$nmy} {set Aratio $Aratioe;          set kzi    $Kze       }
 }
 }

};   # END OF LOOP OVER i

     if {$j < 0.5*$nmy}   {set Aratio $Aratiom;       set kzi    $Kzm        }
     if {$j >= 0.5*$nmy}  {set Aratio $AratioYe;    set kzi    $Kze        }

     set fLx   [expr $Lmid/$nmx]
     set x       [expr 0.5*$fLx];

     set y [expr $y+$fLy];
     if {$Bend != 0 } {
     if {$j == [expr int($nmy*0.5)]} {

           set fLy [expr $Bend/$ney]
           set y     [expr 0.5*$Bmid+$fLy*0.5]

     }
     }
  }; # END OF LOOP OVER j

  puts "ATOTAL = $Atotal"


  ################################################
  ## BUILD ELASTIC BEAMS AND CONNECT            ##
  ## TO SPECIFIED SPRING LOCATIONS              ##
  ################################################
  set xTf  50;
  set yTf  [expr $xTf+1];

  geomTransf Linear $xTf  0 0 1
  geomTransf Linear $yTf  0 0 1


  set Af  1e10;
  set Ef  1e12;    set Gf  1e8;
  set Jf  1e8;   set Iyf 1e6;   set Izf 1e6;
```

```
  set node0 [expr $tn+1];


  # CONNECT STARTING NODE SN TO FOUNDATION
  ########################################

 for {set k 1} {$k <= 4 } {incr k} {

    set iN $sn;
    set jN [expr $node0];

    element elasticBeamColumn $mc $iN $jN $Af $Ef $Gf $Jf $Iyf $Izf $xTf

    puts $h2 [format "%d\t%d\t%d\t%d" $mc $iN $jN 1]

    set mc    [expr $mc+1]
              set node0 [expr $node0+2]
 }


 # LOOP OVER ALL X AND Y NODES TO CREATE
 # ELASTIC BEAM ELEMENTS
 #######################################
 set node0 [expr $tn+1]

# BUILD BEAMS IN X DIRECTION
############################

for {set j 1} {$j<=0.5*$nodesy} {incr j} {

 set nc [expr 4*$nodesx*($j-1)]

 for {set i 1} {$i<= 0.5*$nodesx-1} {incr i} {

          if {$i==1} {
            set ap 0

           for {set k 1} {$k <= 2} {incr k} {
       set iN [expr $node0+$nc+ $ap   ]
       set jN [expr $node0+$nc+ $ap +2]

                 element elasticBeamColumn $mc $iN $jN $Af $Ef $Gf $Jf $Iyf $Izf $xTf

       puts $h2 [format "%d\t%d\t%d\t%d" $mc $iN $jN 1]

       set mc [expr $mc+1]
                 set ap [expr $ap+4]

           }
   }


  for {set k 1} {$k <= 4} {incr k} {
       set iN [expr $node0+$nc+8*($i-1)+2*($k-1) ]
        set jN [expr $node0+$nc+8*($i)  +2*($k-1) ]
```

```
            element elasticBeamColumn $mc $iN $jN $Af $Ef $Gf $Jf $Iyf $Izf $xTf

             puts $h2 [format "%d\t%d\t%d\t%d" $mc $iN $jN 1]

          set mc [expr $mc+1]
 }

}
}


# BUILD BEAMS IN Y DIRECTION
############################

for {set i 1} {$i<=0.5*$nodesx} {incr i} {
    set nc  [expr 8*($i-1)]

    for {set j 1} {$j<= 0.5*$nodesy-1} {incr j} {
        set nc2 [expr $nc+4*$nodesx*($j-1)]
        set nc3 [expr $nc+4*$nodesx*($j)]

if {$j==1} {
   set ap 0
   for {set k 1} {$k <= 2} {incr k} {
          set iN [expr $node0+$nc+ $ap   ];
          set jN [expr $node0+$nc+ $ap +4];

          element elasticBeamColumn $mc $iN $jN $Af $Ef $Gf $Jf $Iyf $Izf $yTf

          puts $h2 [format "%d\t%d\t%d\t%d" $mc $iN $jN 1]

          set mc [expr $mc+1]
          set ap [expr $ap+2]
  }
          }

         for {set k 1} {$k <= 4} {incr k} {
 set iN [expr $node0+$nc2+2*($k-1) ]
 set jN [expr $node0+$nc3+2*($k-1) ]

            element elasticBeamColumn $mc $iN $jN $Af $Ef $Gf $Jf $Iyf $Izf $xTf

            puts $h2 [format "%d\t%d\t%d\t%d" $mc $iN $jN 1]

 set mc [expr $mc+1]
       }
    }
  }
 ##############################################

 close $h1
 close $h2
 close $h3

};  # END OF PROCEDURE....BUILDFOUNDATION_F.tcl
```

```
##############################################################################################
##  BUILD_MAT_F.tcl
##
## Source code for subgrade reaction elements. Zerolength springs of varied materials.
## Either linear elastic or nonlinear
##
##          Written:
##             Andres Espinoza
##             AUGUST 2006;  based on work done by Harden et al. (2005) PEER REPORT 2005/04
##############################################################################################


set qi [expr $qip*$qult]


##   PRESSURE DISTRIBUTION SPECIFICATION
#####################################################
 if {$type == 1} {              ;# Uniform Pressure Distribution
   set qx $qult
 }
 if {$type ==2} { ;# Triangular Distribution
   # nothing for this yet
 }
if {$type ==3} {  ;# Trapezoidal Distribution
    # nothing for this yet
 }
 if {$type ==4} { ;# Parabolic Distribution
    # nothing for this yet
 }
 if {$type ==5} { ;# Inverse Distribution
     # nothing for this yet
 }
#####################################################


            ## CHECK FOR ZER0/NEGATIVE qx
            ###################################
            if {$qx == 0} {
              set qx 0.0001;  puts "qx zero, set=0.0001 for material $mati"
            }
            if {$qx < 0.0} {
              set qx 0.0001;  puts "qx negative, set=0.0001 for material $mati"
            }
            ###################################


# CALCULATE ULTIMATE BEARING FORCE/NODE FOR WHEN REQ'D
set Qultx [expr $L*$B*$Aratio*$qx]



## SOIL FOUNDATION SPRINGS MODEL SELECTION
#############################################

set Ki [expr $kzi*$Aratio]
```

```
if {$FEmat == 8} {                                          ;## ELASTIC NO TENSION SPRINGS
  set mati [expr $mc+1000]
  uniaxialMaterial ENT $mati $Ki
 }

if {$FEmat == 9} {                                           ; ## ELASTIC SPRINGS
  set mati [expr $mc+1000]
  uniaxialMaterial Elastic $mati $Ki
 }

    ###############################
    ##  QZ CONSTANTS           ##
    ###############################
    if {$soiltype == 1} {;  #clay soil
          set qzType 1;
       set c 0.35
          set n 1.2
       set Kfar 0.525
    }
    if {$soiltype == 2} {;  #sand soil
       set qzType 2;
       set c 12.3
          set n  5.5
       set Kfar 1.39
     }

if {$FEmat == 10} {                                          ; ## QzSimple1 SPRING
  set mati [expr $mc+1000]

  set QultQZ [expr $Qultx]
  set z50i   [expr $Kfar*$Qultx*pow($Ki,-1)]

  uniaxialMaterial QzSimple1 $mati $qzType $QultQZ $z50i $TP $crad
 }

if {$FEmat == 11} {                                          ; ## PySimple1 SPRING
  set mati [expr $mc+1000]

  set QultPy [expr $Qultx]
  set y50i [expr $Kfar*$Qultx*pow($Ki,-1)]

  uniaxialMaterial PySimple1 $mati $qzType $QultPy $y50i $TP $crad
 }

if {$FEmat == 12} {                                          ; ## ELASTICPPGAP SPRINGS
  set mati [expr $mc+1000]
  uniaxialMaterial ElasticPPGap $mati $Ki -$Qultx -$gap  0.01 damage
 }
```